

Naval Research Laboratory

Monterey, CA 93943-5502



2

NRL/PU/7541-92-0001

AD-A277 993



Forecasters Handbook for the Philippine Islands and Surrounding Waters

FORREST R. WILLIAMS AND GLENN H. JUNG

*Department of Meteorology
Naval Postgraduate School.
Monterey, CA 93943-5000*

RONALD E. ENGLEBRETSON

*Science Applications International Corporation
Monterey, CA 93940*

*Prepared for:
Forecast Support Branch
Marine Meteorology Division*

December 1993

DTIC QUALITY INSPECTED 3

Approved for public release; distribution unlimited.

35796 94-10813



94 4 8 016

REPORT DOCUMENTATION PAGE

Form Approved
OMB No. 0704-0188

Public reporting burden for this collection of information is estimated to average 1 hour per response, including the time for reviewing instructions, searching existing data sources, gathering and maintaining the data needed, and completing and reviewing the collection of information. Send comments regarding this burden or any other aspect of this collection of information, including suggestions for reducing this burden, to Washington Headquarters Service, Directorate for Information Operations and Reports, 1215 Jefferson Davis Highway, Suite 1204, Arlington, VA 22202-4302, and to the Office of Management and Budget, Paperwork Reduction Project (0704-0188), Washington, DC 20503.

1. Agency Use Only (Leave blank).		2. Report Date. December 1993	3. Report Type and Dates Covered. Final	
4. Title and Subtitle. Forecasters Handbook for the Philippine Islands and Surrounding Waters			5. Funding Numbers. PE O&M,N AN DN656794	
6. Author(s). Forrest R. Williams, Glenn H. Jung, Ronald E. Englebretson*				
7. Performing Organization Name(s) and Address(es). Naval Postgraduate School Department of Meteorology Monterey, CA 93943-5000			8. Performing Organization Report Number.	
9. Sponsoring/Monitoring Agency Name(s) and Address(es). Naval Oceanography Command, Stennis Space Center, MS 39529-5000; Naval Research Laboratory, Marine Meteorology Division, Monterey, CA 93943-5502; Naval Postgraduate School, Monterey, CA 93943-5000			10. Sponsoring/Monitoring Agency Report Number. NRL/PU/7541--92-0001	
11. Supplementary Notes. NRL Monterey monitor: Dennis C. Perryman, Forecast Support Branch, code 7541. *Third author affiliation: Science Applications International Corp., Monterey CA 93940				
12a. Distribution/Availability Statement. Approved for public release; distribution unlimited.			12b. Distribution Code.	
13. Abstract (Maximum 200 words). The analysis and forecasting of atmospheric and oceanic conditions important to air/sea operations in the Philippine Islands area are described. The area covered includes the islands -- Luzon, the Visayas (the central islands) and Mindanao -- from about 4.7°N to 21.5°N and 117°E to 127°E; and the Philippine Sea, Luzon Strait, South China Sea, and Sulu Sea. Seasonal climatologies of the southwest and northeast monsoons and tradewind regime, plus electromagnetic and ducting conditions, are presented. Appendices provide additional climatologies, a study of tropical cyclone characteristics, climatic normals for 60 Philippine stations, and percent frequencies of wave heights. Five case studies examine current accuracy of the Navy Operational Global Atmospheric Prediction System (NOGAPS) model analyses and prognoses. Tropical cyclone bulletins issued by the Joint Typhoon Warning Center, Guam, are identified and described; forecast philosophies are discussed. Interaction of Typhoon Yunya and the eruption of Mount Pinatubo volcano in June 1991 is described, and the dangers posed to aviation by volcanic ash are discussed.				
14. Subject Terms. Philippine meteorology Philippine oceanography			Monsoon Tropical cyclone	Typhoon
			15. Number of Pages. 358	
			16. Price Code.	
17. Security Classification of Report. UNCLASSIFIED	18. Security Classification of This Page. UNCLASSIFIED	19. Security Classification of Abstract. UNCLASSIFIED	20. Limitation of Abstract. Same as report	

Contents

Foreword	v
Preface	vii
Acknowledgments	viii
Record of Changes	ix
1 The Philippine Islands	1-1
1.1 General Introduction	1-1
1.2 Philippine Geography and Topography	1-2
1.3 Meteorological Stations of the Philippine Islands	1-4
2 Seasonal Climatology	2-1
2.1 Introduction	2-1
2.2 Southwest Monsoon	2-4
2.2.1 June–November (Months of Heavier Precipitation)	2-7
2.3 Tropical Cyclones	2-10
2.3.1 Introduction	2-10
2.3.2 Tropical Cyclone “Thumb Rules”	2-11
2.4 Northeast Monsoon and the Trade Wind Regime	2-14
2.4.1 December–May (Months of Lighter Precipitation)	2-17
3 Typhoon (and other) Forecasting	3-1
3.1 The Danger of Volcanic Ash to Aviation	3-1
3.2 JTWC Bulletins	3-4
3.3 Forecasting Philosophies	3-7
3.3.1 Formation	3-7
3.3.2 Movement	3-7
3.3.3 Intensity	3-10
3.4 Recent Tropical Cyclones Striking the Philippine Islands	3-14
3.4.1 Typhoons striking Luzon	3-14
3.4.2 Tropical Storm and Super Typhoon striking Visayas	3-26
3.4.3 Tropical Cyclones striking Mindanao	3-33
3.5 Case Studies using NOGAPS	3-35
3.5.1 Typhoon Eli, 9–13 July 1992	3-36
3.5.2 Typhoon Bobbie, 23-27 June 1992	3-71
3.5.3 An Atypical Southwest Monsoon Surge, 8-18 August 1992	3-85
3.5.4 Southwest Monsoon Surge “Snapshot”, 4 September 1992	3-115
3.5.5 Northeast Monsoon Cold Surge, 6–8 February 1992	3-122
3.5.6 Lessons Learned while preparing Case Studies	3-144

4	Geological Structure and Physical Oceanography	4-1
4.1	Geological Structure	4-1
4.2	Ocean Parameters	4-9
4.2.1	Introduction	4-9
4.2.2	Ocean Parameters by Region	4-10
4.2.2.A	Western Philippine Sea	4-10
4.2.2.B	South China Sea (northern portion)	4-49
4.2.2.C	Sulu Sea	4-64
4.2.2.D	Luzon Strait (Bashi Channel)	4-76
4.2.2.E	Shallow Seas (between islands)	4-87
5	Oceanic Aspects of Operational Weather Forecasting	5-1
5.1	Introduction	5-1
5.2	Seasonal and Regional Variations	5-2
5.3	Ocean Currents and Associated Fronts	5-3
5.4	Marine Planetary Boundary Layer	5-5
5.5	Introduction to Electro-Optical and Electromagnetic Conditions	5-5
5.5.1	E-O and the Atmosphere as a Medium	5-5
5.5.2	Comments on E-O/EM and Atmospheric Interactions	5-7
5.5.3	High Energy Laser	5-8
5.5.4	Forward Looking Infrared	5-8
5.5.5	Radar and Microwave	5-10
5.5.6	Elevated and/or Surface Based Ducts	5-10
5.5.7	Forecast Aids for Elevated and/or Surface Based Ducts	5-12
5.6	Regional Atmospheric Circulation Patterns	5-16
5.6.1	Northeast Monsoon	5-16
5.6.2	Shear Lines	5-17
5.6.3	Tropical Waves (or Waves in the Easterlies)	5-17
5.6.4	Southwest Monsoon	5-18
5.6.5	Cloudiness	5-19
5.6.6	Visibility	5-19
5.6.7	Thunderstorms	5-19
5.6.8	Turbulence	5-20
5.7	Forecast Aids for Oceanic Areas East of the Philippines	5-20
5.7.1	Forecasting Movement of Shear Lines	5-20
5.7.2	Intertropical Convergence Zone	5-21
5.7.3	Tropical Waves (or Waves in the Easterlies)	5-21

REFERENCES	R-1
-------------------	------------

APPENDICES

A	Comprehensive Ocean-Atmosphere Data Set	A-1
B	Characteristics of Tropical Cyclones Affecting the PI	B-1
C	Climatic Normals of the Philippines (1951-1985)	C-1
D	Percent Frequencies of Wave Heights	D-1

FOREWORD

The Forecasters Handbook for the Philippine Islands and Surrounding Waters was developed under the continuing effort of the Naval Research Laboratory (NRL) Monterey to improve the quality of operational weather forecasting support in all parts of the world.

While several sources address the environment in the vicinity of the Philippine Islands, the purpose of this document is to accumulate and suitably present the most pertinent information available for use by Fleet forecasters who are unfamiliar with the region.

Additionally, the handbook includes case studies to examine the analytic and prognostic skill of the current (1992) Navy Operational Global Atmospheric Prediction System (NOGAPS 3.3) in the vicinity of the Philippine Islands. The NOGAPS products, prepared by Fleet Numerical Oceanography Center (FNOC), Monterey, California, were received via the Navy Oceanographic Data Distribution System (NODDS) software on a personal computer, in *real time*.

It is intended that this document be responsive to current requirements of U. S. Navy operating forces; therefore, it has been assembled in loose-leaf form. Users are urged to submit to this Command their comments and suggestions regarding its contents.

The Forecasters Handbook for the Philippine Islands and Surrounding Waters was prepared by Adjunct Professor Forrest R. Williams (CDR, USN, retired) of the Meteorology Department of the Naval Postgraduate School (NPS), Monterey, California, with Dr. Glenn H. Jung, Professor Emeritus of the Oceanography Department, NPS, who wrote the Geological Structure and Physical Oceanography Section and Ronald E. Englebretson of Science Applications International Corporation, Monterey, California, who wrote the Oceanic Aspects of Operational Weather Forecasting Section. Mr. Dennis Perryman (NRL Monterey) served as Project Coordinator. The project leading to the development of this handbook was sponsored by the Naval Postgraduate School, the Naval Oceanography Command, Stennis Space Center, MS and the Naval Research Laboratory Monterey.

Accession For	
NTIS CRA&I	<input checked="" type="checkbox"/>
DTIC TAB	<input type="checkbox"/>
Unannounced	<input type="checkbox"/>
Justification	
By	
Distribution /	
Availability Codes	
Dist	Avail and/or Special
A-1	

PREFACE

This handbook is published to provide meteorological and oceanographic guidance, as well as regional familiarization, to naval personnel embarked in Fleet units or ashore supporting naval operations in the vicinity of the Philippine Islands, including the South China Sea and the Philippine Sea.

In the event of limited planning or preparation time prior to operations, it is recommended that the forecaster first read Section 2 "Seasonal Climatology", including the relevant monsoon season, but concentrating on Subsection 2.3 "Tropical Cyclones", regardless of season. Next read Section 5 which describes electromagnetic conditions including standard and anomalous propagation in ducts, plus forecast aids for relevant atmospheric circulation patterns. Equally important, the forecaster quickly should become familiar with Subsection 3.2 "JTWC Bulletins" to ensure their accurate interpretation in command tropical cyclone briefings.

Subsection 3.4 describes forecasts and history of certain catastrophic tropical cyclones during the last two years, e.g., Super Typhoon Mike (1990) and Tropical Storm Thelma (1991), as well as the interaction of Typhoon Yunya with the eruption of Mount Pinatubo (1991). Subsection 3.5 presents case studies describing the performance of the current NOGAPS model (3.3) during typhoons, surges in the southwest monsoon and a cold surge during the northeast monsoon affecting the Philippine Islands in 1992. Descriptions of both atmospheric and oceanographic conditions are included in the analyses and prognoses presented in the case studies.

If possible, Fleet units should acquire the following publications before deployment—(see References for publishers):

1. Climatology of North Pacific Tropical Cyclone Tracks,
2. U.S. Navy Regional Climatic Study of the Central East Asian Coast and Associated Waters,
3. Forecaster's Handbook of the Naval Oceanography Command Facility, Cubi Point, PI, and
4. Typhoon Forecasters Handbook (currently, in preparation by NRL Monterey).

Little needs to be said to alert forecasters to the potential threat of tropical cyclones. Both East and West have witnessed the destructive power demonstrated in 1992 by Hurricanes Andrew and Iniki and Typhoon Omar. A subsection describing aviation forecasting in the vicinity of volcanic ash plumes is also included.

ACKNOWLEDGMENTS

A very special thanks to Lt. Col. Charles Guard, USAF, Director of the Joint Typhoon Warning Center (JTWC) for both his advice and his detailed review of the handbook. Thanks also to LCDR Nicholas Gural, USN, and especially to Mr. Frank Wells, who briefed the author on the operations of JTWC and provided DMSP transparencies.

Sincere appreciation is extended to CDR William Johnson, USN, Commanding Officer, Naval Oceanography Command Facility, Cubi Point for his hospitality and assistance during the author's visit to the Philippine Islands. Thanks to ENS Scott Oswalt, USN, who provided photographs of the Mount Pinatubo eruption, and to AGC Stephen Smith, USN, and Mr. Silverio Torio, who answered weekly queries by phone. Thanks also to Lt. Col. James Woessner, of Detachment 5, 20th Weather Squadron, Clark AB, RP.

Appreciation is extended to Dr. Roman Kintanar, Director of the Philippine Atmospheric, Geophysical and Astronomical Services Administration for provision of the climatological normals for 60 Philippine weather observing stations.

The case studies could not have been prepared without the continuous, reliable model runs and transmissions from Fleet Numerical Oceanography Center, Monterey, CA. Thanks to the staff and especially to Mr. Ralph Loveless who advised on the use of NODDS. Thanks also to the Naval Oceanographic Office, Stennis Space Center, MS for supplying the chart depicting the bathymetry surrounding the Philippine Islands.

Appreciation is also extended to Dr. Mark Lander, University of Guam and to Dr. Johnny Chan, City Polytechnic of Hong Kong for sharing their expertise.

Thanks also to Meteorology Department personnel at NPS: Professors Robert Renard, Robert Haney, Carlyle Wash and Philip Durkee for their assistance and encouragement; Jim Cowie for his continual assistance in the maintenance of computer hardware and software; Dr. Jeng-Ming Chen for programming assistance; Professor Russell Elsberry, Professor Chih-Pei Chang, LCDR Lester Carr, USN, and LCDR George Dunnavan, USN, for sharing their tropical expertise; Professor Wendell Nuss for assistance in plotting programs; and Russell Schwanz, Ben Borelli, Sandy Huddleston, Penny Jones, Mark Boothe and David Woody for their assistance and genuine interest in the project.

Thanks to Dennis Perryman and LT Richard Jeffries, USN, of NRL Monterey and to Kenneth Richards, Science Applications International Corporations, Monterey, California for proofreading the handbook. Finally, last but not least, a sincere thanks to the Naval Postgraduate School and the Naval Oceanography Command for funding the project.

RECORD OF CHANGES

Change Number	Date of Change	Date Entered	Page Number	Entered By	Notes

1. THE PHILIPPINE ISLANDS

1.1 General Introduction

This handbook describes the analysis and forecasting of atmospheric conditions important to air/sea operations near the Philippine Islands. Following the presentation of geography and topography in this section, Section 2 presents seasonal climatologies for the Philippine Islands. Case studies for respective seasons, using Navy products, are presented in Section 3, while oceanographic and geological aspects are presented in Sections 4 and 5. Finally, a variety of appendixes, presenting relevant climatologies from unique sources, serves to make the handbook a self-sufficient document.

While the vulnerability of the Philippines to tropical cyclones is universally appreciated, the last decade of the twentieth century has commenced with a variety of natural disasters. In 1990, a deadly earthquake struck the mountains of northern Luzon. The eruption of Mount Pinatubo in June 1991 wreaked added destruction to the island of Luzon, forcing the closure of Clark Air Base and threatening the globe with debris carried for months in the stratosphere. In November 1991, Tropical Storm Thelma—despite its unimpressive satellite signature—made landfall in the central Philippines causing flooding that killed an estimated 6000 people on the island of Leyte.

Improved computer programming, better satellite imagery and interactive graphics techniques are currently providing operational forecasters with better tools for performing their tasks. Additionally, it is likely that tropical cyclone (TC) research, as described by Elsberry et al. (1987) and elsewhere, will provide improved TC forecasting techniques in the near future. However, this handbook will emphasize the effects on the Philippine Islands (PI) of the alternating monsoons. During much of the Northern Hemisphere summer, the southwest¹ monsoon dominates over the PI in the lower troposphere. While the northeast monsoon dominates during the Northern Hemisphere winter. Intrinsicly included within this discussion will be the attendant reversal of the upper-level flow, as well as the embedded tropical cyclones and air-mass surges.

¹Meteorological convention dictates that wind direction is the direction from which the wind is blowing, i.e., southwest winds blow from the southwest (toward the northeast).

1.2 Philippine Geography and Topography

A knowledge of the geography and topography of the Philippines assists in the understanding of climatology, as well as atmospheric or oceanographic processes. The Philippine Islands are located in the western North Pacific Ocean, just off the southeastern portion of the Asian continent. Lying in a near north to south orientation, the islands extend from about 4.7°N to 21.5°N and 117°E to 127°E (Fig. 1.1). The Philippines consist of more than 7,000 islands, having an area of about 300,000 km² (90,000 nm²). The islands are grouped into three regions: the **Luzon Region** in the north (composed of Luzon Island and small islands in its vicinity); the **Visayas Region** (composed of many islands near the center, the largest being, Palawan, Mindoro, Panay, Masbate, Negros, Cebu, Bohol, Leyte and Samar); and the **Mindanao Region** (composed of Mindanao Island and small islands in its vicinity). Only the islands of Luzon and Mindanao have areas of more than 80,000 km² (23,000 nm²).

The Philippine Islands are surrounded by large bodies of water. They are bounded on the west by the South China Sea, on the north by the Luzon Strait separating the Philippine Islands from Taiwan, on the east by the Philippine Sea (and the Pacific Ocean), on the south by the Celebes Sea, and on the southwest by the Sulu Sea separating the Philippine Islands from Borneo.

Many of the larger islands have narrow coastal plains, generally less than 15 km (8 nm) in width, and interior highland plains and mountain ranges. Many of the ranges, generally oriented north and south, cover almost the entire length of the islands. Most of the mountain ranges have heights of more than 500 m (1600 ft), with large areas having heights above 1,000 m (3300 ft), and a small number having heights above 2,000 m (6600 ft).

On the largest island, Luzon, several mountain ranges with heights above 500 m (1600 ft) cover almost one-half of the entire island. On the east coast of north and central Luzon, lies the Sierra Madre Range. The Ilocos Range (not depicted on Fig. 1.1) runs along the extreme western coast of the northern Luzon, with the Cordillera Central Range (the longest on the figure) lying between the Sierra Madre Range and the Ilocos Range. The Zambales Range located along the western coast of central Luzon contains Mount Pinatubo (Point "P" on Fig. 1.1) near its southern extremity. Many of the larger islands of the Visayas have mountain ranges extending most of their entire length, with elevations greater than 500 m (1600 ft). Mindanao has extensive mountain ranges along its eastern coast, in its central section and along the western coast, with elevations above 500 m (1600 ft). Similar to those of Luzon, the ranges of Mindanao cover about one-half of the island (Flores and Balagot 1969).

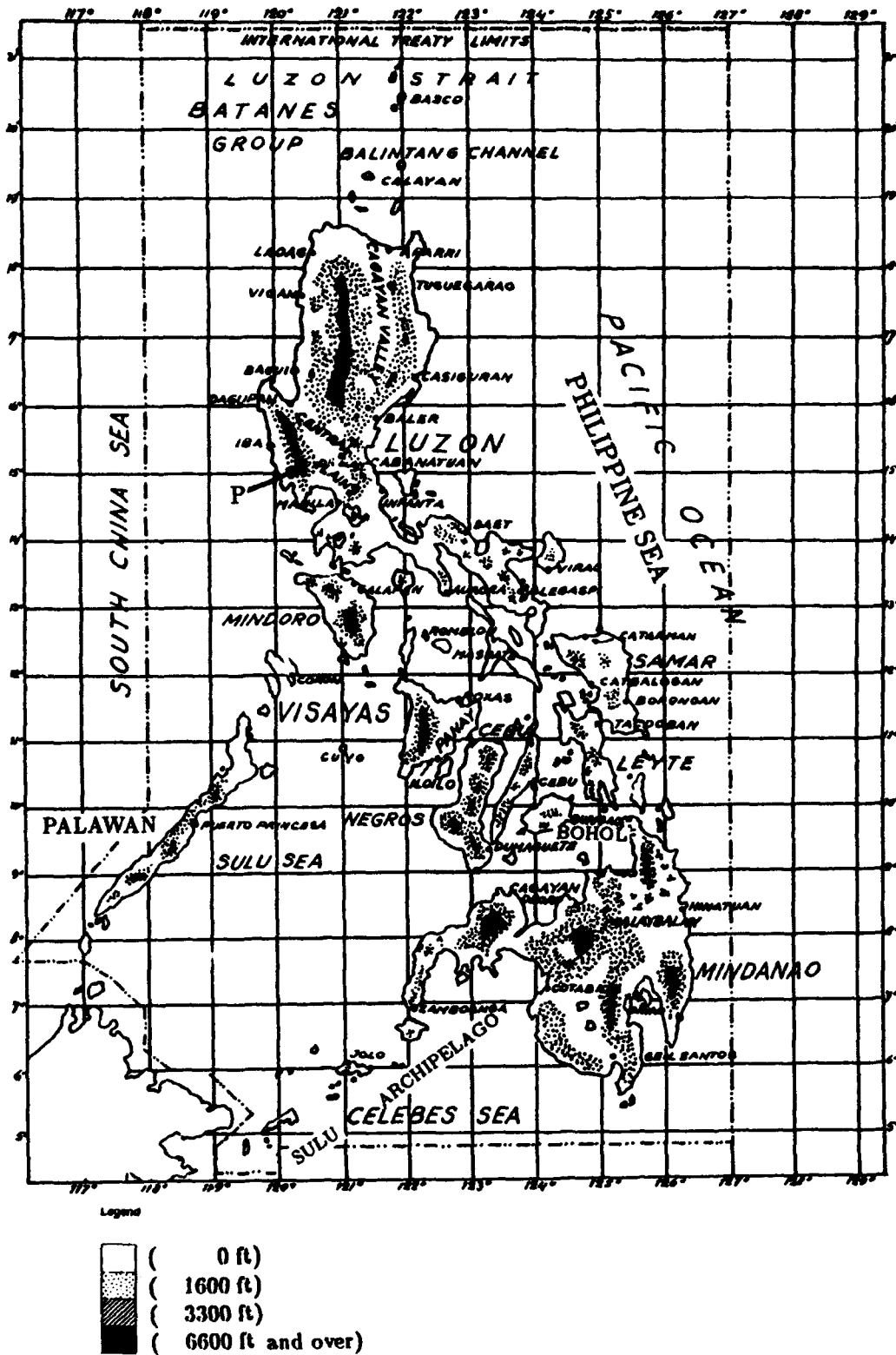


Figure 1.1: Geographical and Topographical Chart of the Philippine Islands. Mount Pinatubo indicated by "P" (adapted from Flores and Balagot (1969)).

1.3 Meteorological Stations of the Philippine Islands

Stations reporting meteorological observations are identified in Table 1.1. The table includes the international four-letter location indicator (where available) and the World Meteorological Organization (WMO) block number/international station number. Station locations are plotted on Fig. 1.2, and a more complete map of the country is found in Fig. 1.3. Ocean bathymetry is depicted in Section 4 on Fig. 4.7.

Table 1.1: Meteorological Stations in the Philippine Islands

STATION	LETTER CODE	BLOCK & STA. #	STATION	LETTER CODE	BLOCK & STA. #
Basco *	RPUO	98135	Coron *		98526
Vigan *	RPUQ	98222	San Jose *	RPUH	98531
Laoag *	RPML	98223	Romblon *	RPMR	98536
Aparri *	RPUA	98232	Roxas *	RPVR	98538
Tuguegarao *	RPUT	98233	Masbate *	RPVM	98543
Iba *	RPUI	98324	Catarman *		98546
Dagupan *		98325	Catbalogan *		98548
Baguio *	RPUB	98328	Tacloban *	RPVA	98550
Munoz *		98329	Guiuan *	RPVG	98558
Cabanatuan *		98330	Puerto Princesa *	RPVP	98618
Baler *	RPUR	98333	Cuyo *		98630
Casiguran *		98336	Iloilo *	RPVI	98637
Manila		98425	Dumaguete *	RPVD	98642
Cubi Point NAS	RPMB	98426	Tagbilaran *	RPVT	98644
Tayabas *		98427	Mactan Intl. *	RPMT	98646
Sangley Point *	RPMS	98428	Surigao	RPWS	98653
Manila Intl. *	RPMM	98429	Dipolog *	RPWG	98741
Science Garden *		98430	Cotabato *	RPWC	98746
Calapan *	RPUK	98431	Lumbia *		98747
Ambulong *		98432	Cagayan De Oro *	RPWL	98748
Infanta *		98434	Malaybalay *	RPWY	98751
Alabat *	RPXT	98435	Butuan *	RPWE	98752
Daet *	RPUD	98440	Davao *	RPWD	98753
Legaspi *	RPMP	98444	Hinatuan *		98755
Virac *	RPUV	98446	Zamboanga *	RPMZ	98836
Catanduanes Radar		98447	General Santos *	RPWB	98851

* Appendix C contains climatic normals for stations marked with an asterisk in Table 1.1.

X Basco

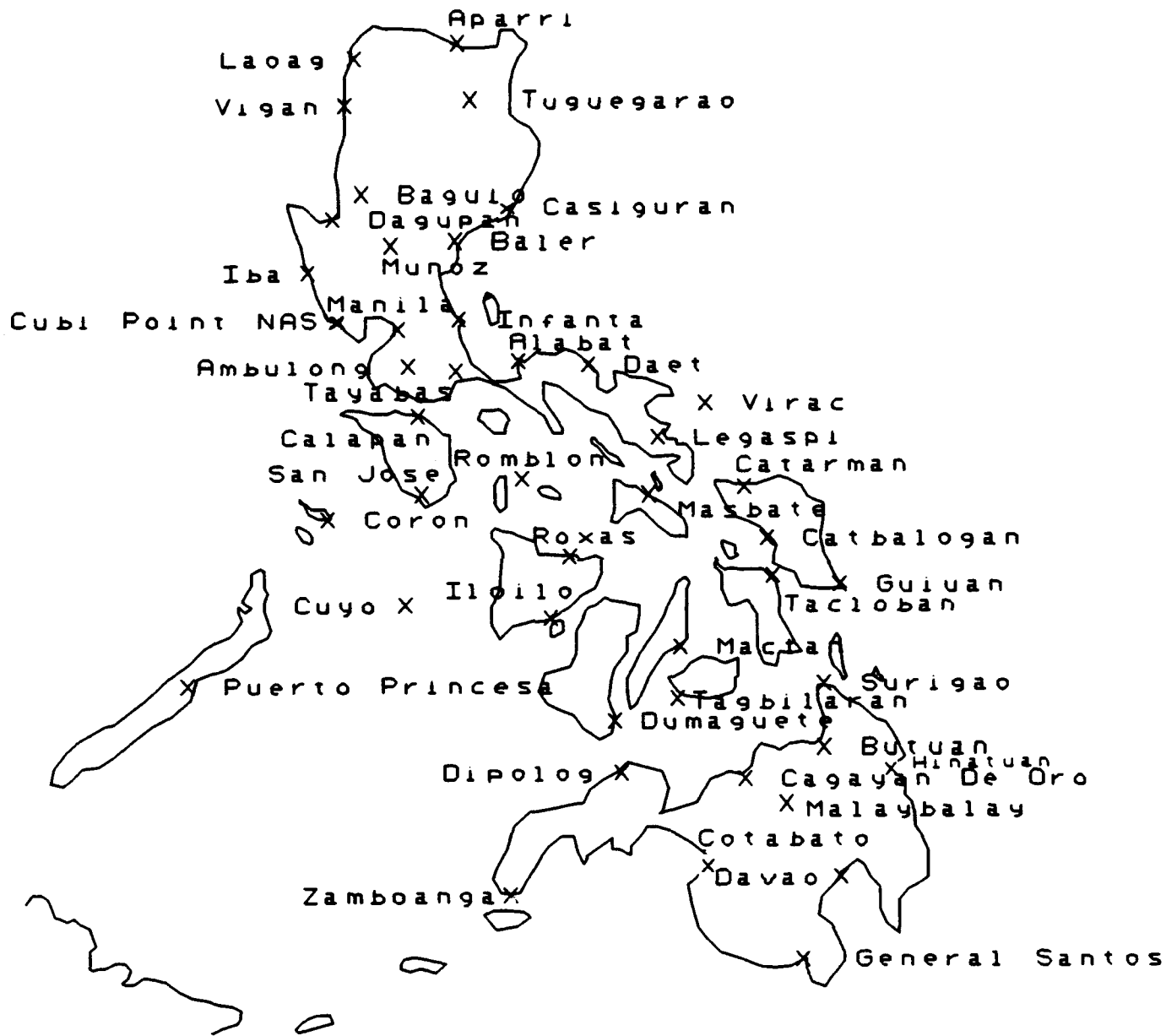


Figure 1.2: Meteorological Stations of the Philippine Islands. Station positions are identified by "X". (Note: **Cabanatuan**—SE of Munoz; **Sangley Pt.**—SW of Manila; **Manila Intl. Airport**—S of Manila; **Science Garden**—N of Manila; **Catanduanes Radar**—N of Virac; **Lumbia**—S of Cagayan De Oro.)

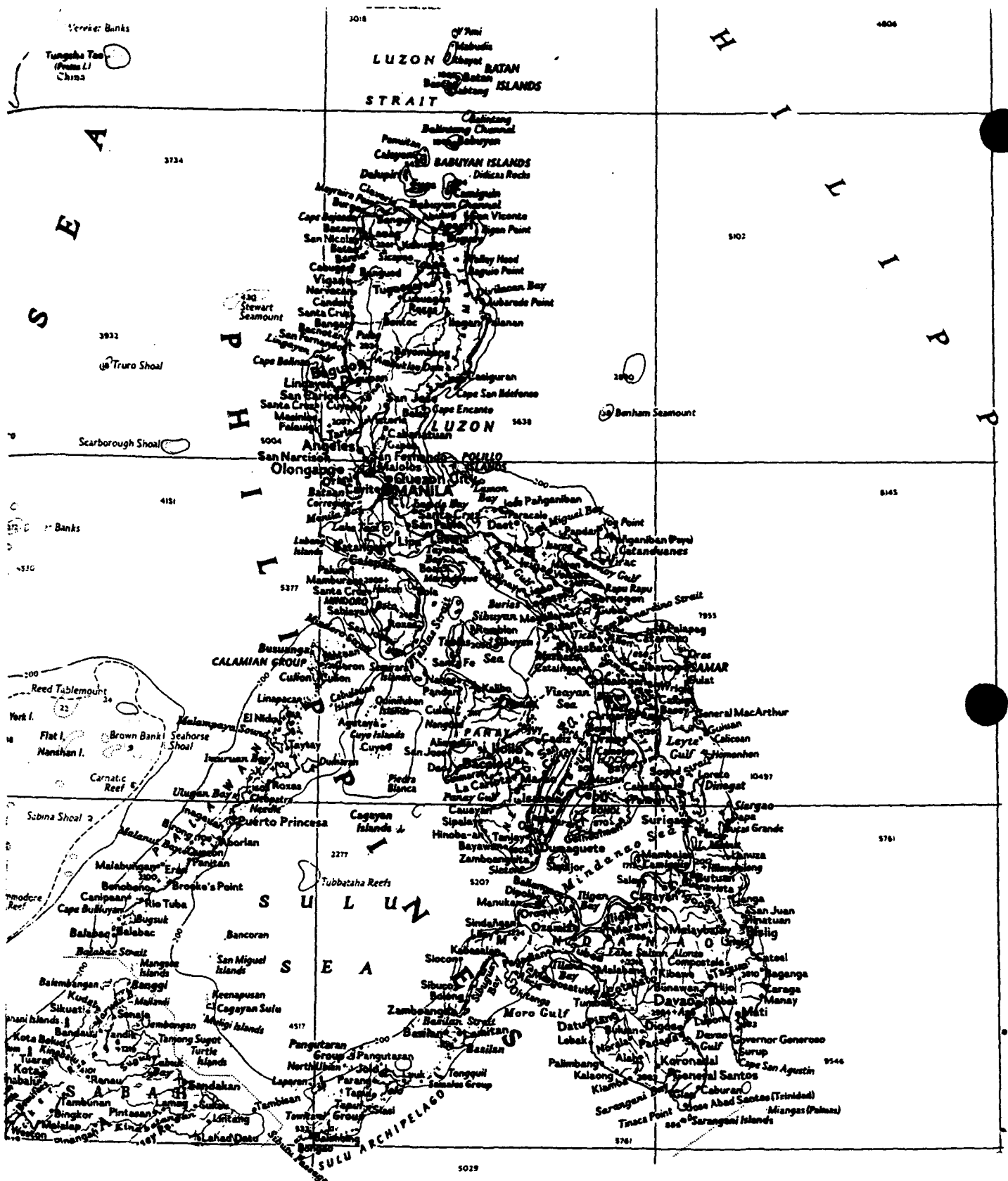


Figure 1.3: Map of the Philippine Islands (adapted from National Geographic Society (1981)).

2. SEASONAL CLIMATOLOGY

2.1 Introduction

This section of the handbook describes the large-scale circulations dominating the Philippine Islands during the northeast and southwest monsoons. As shown in Table 2.1, sources often disagree as to the months constituting each seasonal regime of the Philippines. Table 2.2 (Ramage 1971) shows the monsoon seasons of continental Asia.

Table 2.1: Seasons of the Philippines

First Weather Wing, 1987

TRANSITION III	NE MONSOON	TRANSITION I	TRADE WIND SEASON	TRANSITION II	SOUTHWEST MONSOON
Oct-Nov	Dec-Jan	Feb-Mar	April	May-June	Jul-Aug-Sep

Commander, Naval Oceanography Command, 1990

INTER-MONSOON PERIOD	NE MONSOON FORMATION	NE MONSOON or TRADE WIND	NORTH PACIFIC TRADE WIND	INTER-MONSOON PERIOD	SW MONSOON FORMATION	SW MONSOON (SUMMER)
Oct-Nov	Sep-mid Oct	Nov-Apr	March	Apr-May	Mar-Jun	Jun-Oct

Table 2.2: Monsoon Seasons of Continental Asia (Ramage 1971)

AUTUMN TRANSITION	WINTER	SPRING TRANSITION	EARLY SUM. TRANSITION	ADVANCE OF SUMMER	HEIGHT OF SUMMER AND ITS WANE
Oct-Nov	Dec-Feb	Mar-April	May	Jun-mid July	Mid Jul-Sep

The Indian Ocean and the western tropical Pacific Ocean are dominated by monsoonal flow. That is, during the northern hemisphere winter, relatively cold air flows equatorward from the Himalayas toward the relative warmth of the Indian Ocean and the South China Sea. With rare exceptions the characteristics of this continental air mass are moderated as the air mass passes over water before reaching the Philippine Islands. The Coriolis force deflects this flow to the right (in the Northern Hemisphere) giving birth to the northeast monsoon, before it is deflected to the left as it enters the Southern Hemisphere, see Fig. 2.1(a). The reverse is found during the northern hemisphere summer when relatively cool air flows toward the warmer Indian subcontinent and southern China and is deflected to the right by the Coriolis force to create the southwest monsoon, before flowing into the heat low created over India and China, see Fig. 2.1(b).

An example of a feature important to weather development to the Philippine Islands is depicted at Point "A" to the southeast of the PI on Fig. 2.1(b). There, the interaction between the easterly (or northeasterly) flow coming from the central North Pacific and the southwesterly flow coming from the Southern Hemisphere establishes the monsoon trough identified by the dash-dot line. Further to the east near "B" on Fig. 2.1 is found the trade-wind trough where the trade winds from the respective hemispheres converge—in the eastern Pacific Ocean and Atlantic Ocean this convergence line is known as the Intertropical Convergence Zone (ITCZ).

The large-scale Hadley cell circulation (perceptible in monthly or seasonal averages) as shown in Fig. 2.2 supports the low- and upper-level flow during the two monsoon periods. Viewing the Hadley cell from the winter hemisphere provides a perspective of the respective monsoonal circulation. That is, as shown in the upper frame of Fig. 2.2 (DECEMBER-FEBRUARY) during the Northern Hemisphere winter, the Hadley cell (centered near 10°N) displays average descending motion between 10°N – 25°N near the 400 mb level. Especially note the northerly component of flow, near the surface, from near 25°N to the equator, supporting the northeast monsoon regime. Mass is returned poleward on upper-level pressure surfaces between 300 mb and 100 mb. In a contrasting manner, when the Hadley cell moves into the Southern Hemisphere, during that hemisphere's winter (JUNE-AUGUST) as shown in the lower frame of Fig. 2.2, a southerly wind component, near the surface, is found from south of the equator to a latitude north of the Philippines, supporting the southwest monsoon regime.

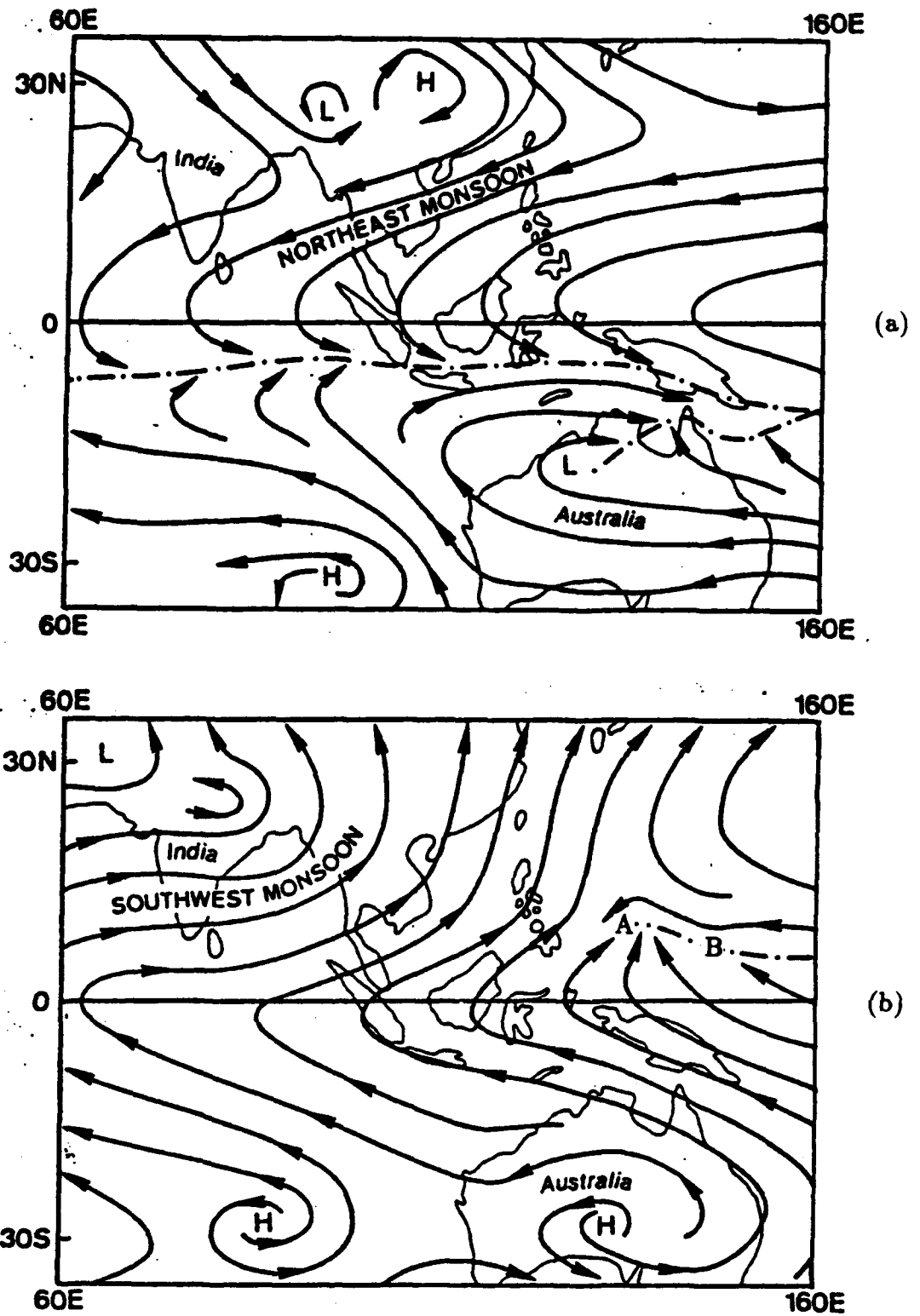


Figure 2.1: Low Level Flow in the Western Pacific and Indian Oceans during (a) January and (b) July.

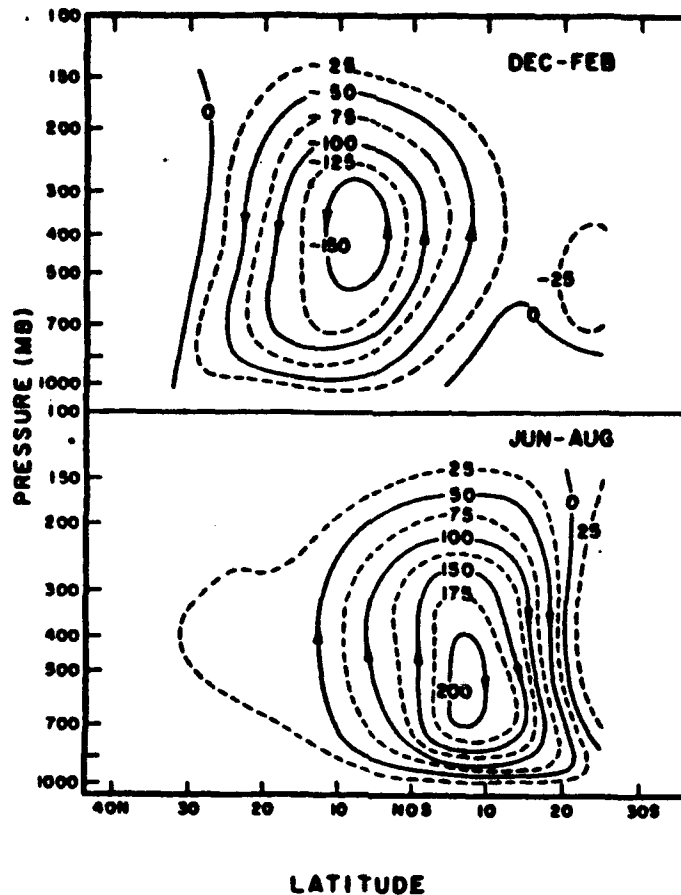


Figure 2.2: Seasonal Mean Meridional Circulation in the Tropics in Terms of Mass Flow (10^{12} grams/second) Streamlines (adapted from Atkinson (1971)).

The following sections describe the characteristics of the two surface monsoon regimes, i.e., the northeast monsoon and the southwest monsoon; plus the well-defined spring intermonsoon transition season or trade wind regime. Also presented is a climatology section on the tropical cyclone, without which the chapter would be incomplete. Again, while the disagreement in the particular months associated with each season is acknowledged, the monthly mean charts for January and August will be used in describing the characteristics of the respective monsoon seasons. (Appendix A presents the average surface flow over the Philippines for each month of the year. Appendix A also includes the average sea-level pressure and sea-surface temperature for each month.)

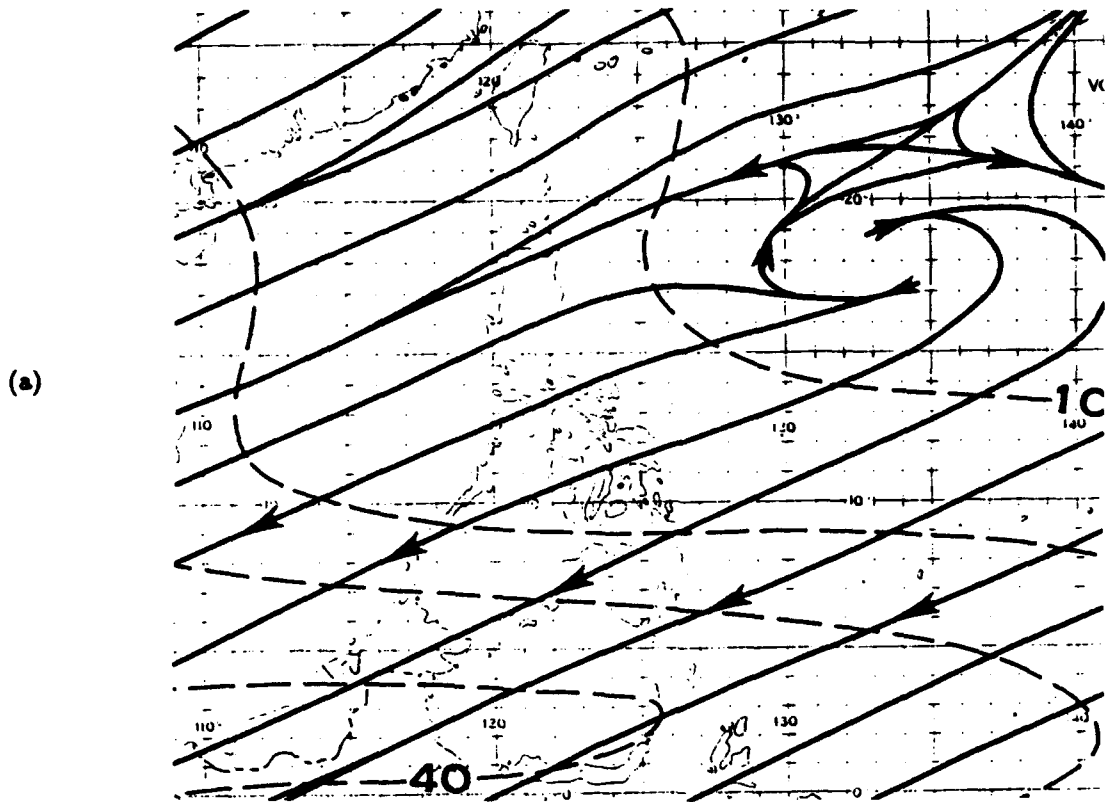
2.2 Southwest Monsoon

While many manuals place their discussion of the northeast monsoon first—since it can be associated with January, the first month of the year—the southwest monsoon is presented first in this handbook. Since the author began closely observing and monitoring the Philippine Islands (PI) nearly three years ago, it has been obvious that the southwest monsoon regime presents much more interesting and challenging weather for the Philippines. In particular, during a 10-day visit during January 1990, the author found most of Luzon devoid of any rainfall, with daytime temperatures in the 80's (°F) and comfortably-low humidity. The likelihood of a tropical cyclone (TC) striking the PI during January (and other months during the northeast monsoon) is small and will be discussed in Section 2.3.

Figure 2.3 displays the average 200-mb and surface wind flow patterns during August¹. As the northern hemisphere summer months approach, the warming of the Asian continent (with the commensurate increase of thickness in the lower and middle troposphere), establishes a high pressure center over Nepal and Tibet at 200 mb, with its associated tropical easterly jet over southern India and Sri Lanka (not shown). Fig. 2.3(a) shows the dominant northeasterly flow aloft over the PI during the southwest monsoon regime, with the neutral point (near 22°N, 134°E) identifying the western extension of the tropical upper tropospheric trough (TUTT), often extending from western Canada southwestward to the western Pacific Ocean in the upper troposphere. While the subtropical ridge at 200 mb is poleward (off the chart in Fig. 2.3(a)), the sub-equatorial ridge, with its associated divergence, is present just south of the TUTT. Its existence is supported by the release of latent heat in the monsoon trough below. At the surface, land station wind speeds may approach zero during the night and early morning hours. Figure 2.3(b) displays the typical compensating southwesterly surface wind. As displayed in the monthly progression of Appendix A, high surface pressure over Asia commences to weaken as the land heats up, during April and May. Then as lower surface pressure is established over China (Fig. 2.4(a)) and the surface pressure ridge recedes northward and eastward over the Pacific Ocean, the southwesterlies are established during July and August. Additionally, the sea surface temperature (SST) (Fig. 2.4(b)) is everywhere far above 26.5°C, generally accepted as the SST required to support tropical cyclone genesis (Elsberry et al. 1987).

While there is no exact date for the commencement of the surface southwest monsoon flow in the South China Sea and Philippine Islands, Appendix A displays the normal progression from northeasterly surface winds in April, becoming southeasterly during May, southerly in June and finally southwesterly in July, August and September. During 1991 and 1992, the southwest monsoon regime commenced early (in June). The commencement of the southwest monsoon regime in 1991 was coincident with the eruption of Mount Pinatubo and is discussed in Section 3.4.1.

¹Often typical of months June through early November—except at 200 mb over Luzon, where the northeasterly flow is replaced by the subtropical ridge during October and November.



(a)

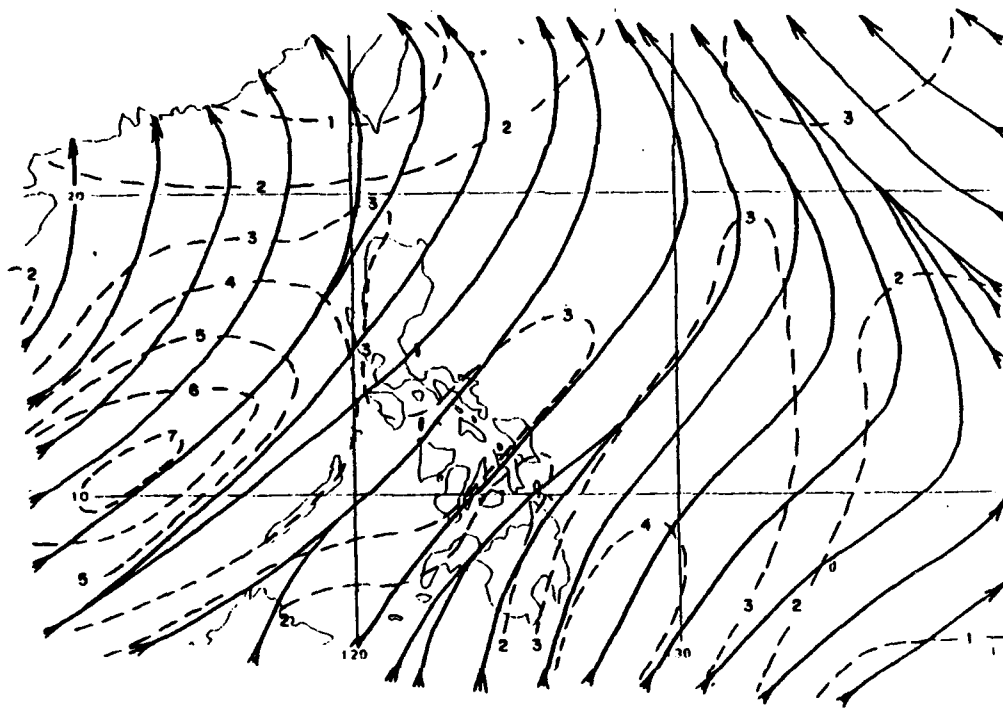
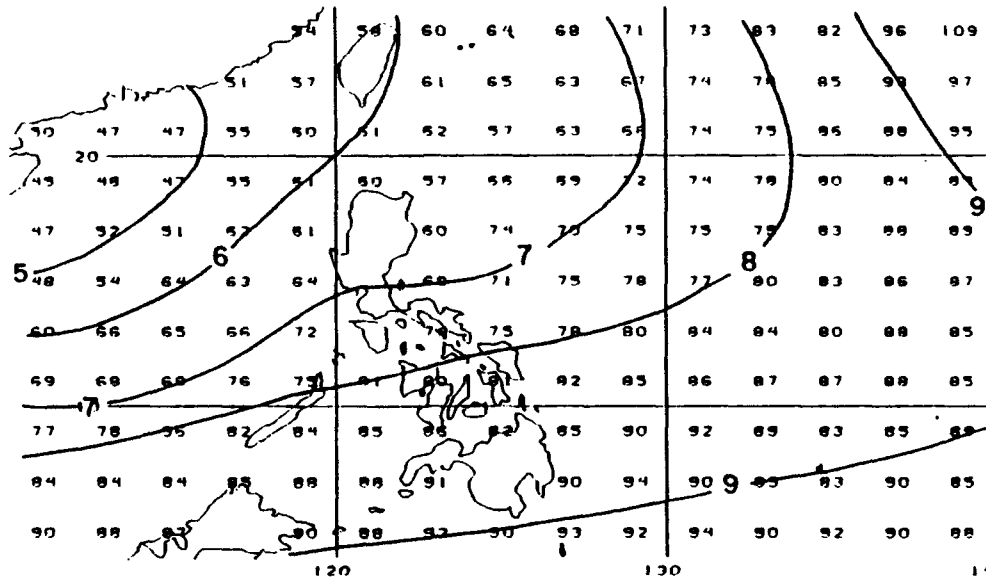
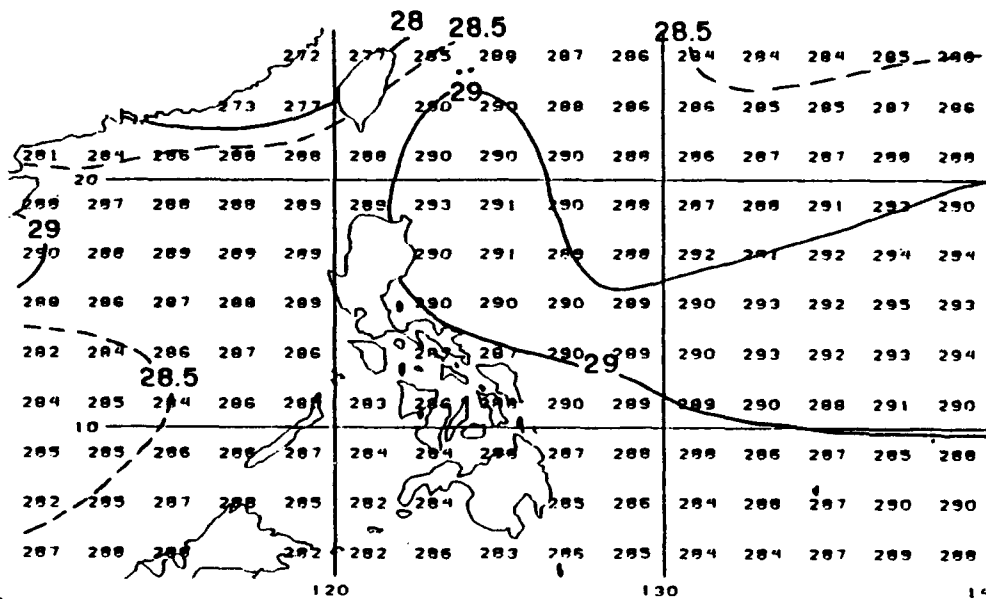


Figure 2.3: (a) Mean 200 mb Flow, August (Sadler and Wann 1984) Streamlines (solid, with arrow indicating direction of flow) and isotachs (dashed) in knots

(b) Surface Wind Flow, August (adapted from Sadler et al. 1987a and 1987b) Streamlines (solid, with arrow indicating direction of flow) and isotachs (dashed) in m/sec



(a)



(b)

Figure 2.4: (a) Mean Sea-level Pressure, August
The isobars are labeled in millibars (or hectopascals (hPa)) with the leading 100 omitted.

(b) Sea-surface Temperature (SST) in °C, August (adapted from Sadler et al. 1987a and 1987b)

2.2.1 June–November (Months of Heavier Precipitation)

General

June–August

Many references classify June as a transition month or a southwest monsoon formation month; however, this handbook presents June with the following two months. While Fig. 2.3(b) indicates that the flow is generally from the southwest during August², the wind direction may vary, e.g., westerly, southerly, or even southeasterly. During periods of weak southwest monsoon flow, onshore (sea breeze) and offshore (land breeze) winds may dominate. The air mass may be classified as maritime equatorial, often extending to 10 km. The southwest monsoon may appear as early as May, attaining its maximum intensity by July or August (Flores and Balagot 1969).

The southwest monsoon is cloudy³, hot, humid and wet. Surface temperature maxima vary from the mid 80's to the 90's (°F), while the temperature minima range from 65° (probably during an early onset of the NE monsoon) to 75° (see the table of Manila statistics on page 2-10). Relative humidities are high, though varying diurnally. Their average of 60–80% during the afternoon increases to 85–95% or more during the early morning. Cool temperatures only occur due to prolonged lack of insolation; however, the presence of deep moisture (with its back radiation) keeps nighttime temperatures warm.

The absence of pronounced temperature inversions and the presence of large water vapor magnitudes aloft combine with temperature lapse rates near saturated adiabatic to produce frequent convective activity. While the air stream is fairly constant, the presence of a large tropical cyclone to the north (e.g., near the Luzon Strait or approaching Taiwan) may enhance the magnitude of the southwesterly wind. Such a condition may persist for a week or longer with an associated increase in rainfall and is one cause of a surge in the southwest monsoon (see case studies in Sections 3.5.3 and 3.5.4). Although the June–August rainfall is high (see the table on page 2-10), it varies widely, from 4–10 inches a month to 20–45 inches a month. The greatest rainfall occurs at western locations in the northern Philippines (with rain occurring 20–28 days during a month), while only 10–20 days elsewhere. Thunderstorms occur on 5–20 days per month. Gale force winds, though rare, can last for 5–10 minutes during thunderstorms, or longer during passage of a tropical cyclone—although gale force wind may be intermittent for several days during a deep surge (USAFETAC 1985).

This period is the cloudiest for the Philippines, and the mean cloud cover varies from 60 to 95%. This increase in cloudiness is partially attributed to the monsoon trough moving northward during the period. The location of the trough is displayed in Appendix A, extending from northeastern Luzon toward the southeast during July (Fig. A-8(b)), and then extending from the Luzon Strait toward the east-southeast during August (Figure A-9(b)). As discussed in Section 2.3, tropical cyclones are often spawned within the monsoon trough and then move westward to affect the Philippine Islands.

²See Appendix A for monthly climatological wind directions

³Clear = 0/10 sky cover, partly cloudy = 1/10–5/10, cloudy = 6/10–9/10 and overcast = 10/10.

September–November

As described for the previous three months, the surface wind direction may deviate from the monthly averages displayed in Appendix A. Recognizing the effects or superposition of sea breezes and land breezes, the monthly surface winds change from southwesterly in September, when the monsoon trough is over northern Luzon (Fig. A-10(b)) to northeasterly in November, when the monsoon trough has returned south to Mindanao (Fig. A-12(b)).

While the weather during September is dominated by the southwest monsoon, that of October and November experiences less of its effects, as attested by the decrease of Manila rainfall (see table on page 2-10). The normal disappearance of the southwest monsoon during October, is followed, on the average, by the appearance of northeasterly flow in the northern Philippines (north of 13°N) during November. However, occasionally the southwest monsoon may persist even until December (Flores and Balagot 1969). As mentioned earlier, the monsoon trough passes over the PI moving southward during this period providing cloudy, hot, humid and wet weather. However, the mean cloud cover decreases from 60–95% in September to 50–85% in November. Mean daily maximum temperatures are much like the previous three months: 80°F to 90°F, with mean minima decreasing somewhat: 60–75°F. Relative humidity remains high: 85–95% during the early morning, decreasing to 65–80% in the afternoon. While precipitation varies widely from 2 to 25 inches a month within the PI, rainfall increases on the windward northeastern coasts. In November, rainfall occurring only 5–10 days a month in western Luzon is contrasted to 20–25 days a month at northeastern locations. Thunderstorm activity decreases in frequency from 4–15 days a month in September to 1–9 days in November. As in the previous three months (if tropical cyclones are omitted), gale force winds are rare except during thunderstorms when they are common and can last for 5–10 minutes (USAFETAC 1985).

Flying Weather (USAFETAC 1985)

June–August

- Good, but conditions are poor in the mountains.
- Ceilings and visibilities⁴ ≤ 5000/6 occur up to 30% of the time.
- < 1500/3: up to 20% of the time.
- < 500/1: about 2% of the time.

⁴ceiling/visibility, e.g., 5000/6 indicates "ceiling of 5000 feet and/or visibility of 6 miles."

September–November

- Good.
- Ceilings and visibilities $\leq 5000/6$ occur from less than 5 to 30% of the time.
- $< 1500/3$: less than 20% of the time.
- $< 500/1$: about 2% of the time.

Terminal Weather, Manila (USAFETAC 1985)

June–August

Good. Ceiling/visibility $\leq 300/1$ occurs less than 1% of the time. Thunderstorms occur 5–10 days of the month. Prevailing surface wind directions vary greatly, easterly through westerly, at 5–10 kt or less.

September–November

Good. Ceiling/visibility $\leq 300/1$ occurs less than 1% of the time. Thunderstorms occur on 8 days in September and 2 days in November. Surface winds are light from the north or northeast.

Monthly temperature, precipitation, thunderstorms & twilight (USAFETAC, 1985)

(See Appendix C for Climatic Normals compiled by PAGASA (Philippine Atmospheric, Geophysical and Astronomical Services Administration) for 60 Philippine stations other than Manila.)

MANILA	JUN	JUL	AUG	SEP	OCT	NOV
TEMPERATURE (°F)						
Absolute maximum	99	97	95	96	95	94
Mean maximum	90	88	87	87	88	87
Mean minimum	75	75	75	75	74	72
Absolute minimum	71	69	69	69	67	60
MEAN PRECIPITATION (INCHES)	9.9	16.3	17.2	13.9	7.7	5.4
MEAN NUMBER OF DAYS						
Precipitation	17	24	23	22	19	14
Thunderstorms	8	9	8	8	6	2
CIVIL TWILIGHT (15th of month)						
First light (local standard time)	0503	0512	0520	0523	0525	0534
Last light (local standard time)	1850	1852	1841	1819	1758	1747

2.3 Tropical Cyclones

2.3.1 Introduction

Tropical cyclones can affect the Philippine Islands during almost any month⁵. The Climatology of North Pacific Tropical Cyclone Tracks (Miller et al. 1988) presents the tracks and statistics of tropical cyclones that have occurred in the entire North Pacific Ocean during the years 1945–1987. While this voluminous document will not be duplicated here, Thumb Rules from Shoemaker (1991) for forecasting tropical cyclones specifically over the PI will be presented. Before forecasting in or around the Philippine Islands, the reader should review the condensation of Shoemaker's PI study contained in Appendix B.

A review is also recommended of the last several issues of the Annual Tropical Cyclone Report (ATCR) published by JTWC, if available. The tracks of all recent TCs striking the PI and the verification of various forecasting aids during similar flow patterns should be studied. The 1991 ATCR (U. S. NOCC/JTWC 1992) reveals that during 1991, the Navy Operational Global Atmospheric Prediction System (NOGAPS) Vortex Tracking Routine (NGPS)⁶ aid improved (relative to other objective aids discussed in Chapter 3) for the longer forecast periods, i.e., 48-h and 72-h. The 1991 ATCR reports that during the period 1959–1991 the average number of tropical cyclones in the entire western North Pacific Ocean was 31. The year 1991 was an above average year with 32 tropical cyclones: 2 tropical depressions (TDs), 10 tropical storms (TSs) and 20 typhoons (TYs), of which 5 were super typhoons (STYs).

Table 2.3, below, shows the comparison of the 1991 JTWC forecast errors⁷ with the average JTWC errors during the last 14 years.

Table 2.3: JTWC Mean Forecast Errors (JTWC 1992)

FORECAST INTERVAL	YEAR 1991	YEARS 1978–1991
24-h	96 nm	116 nm
48-h	185 nm	229 nm
72-h	287 nm	347 nm

⁵See Fig. 2.6 which shows that from 1970 to 1989 the PI did not experience a tropical cyclone in February. In fact no February TCs were recorded from 1945 through 1989. This is likely due to the strong vertical shear of the northeast monsoon.

⁶NGPS identifies the TC forecast position from the Navy's NOGAPS model.

⁷Obviously, 1991 was an outstanding year for average position forecast errors.

For nearly three years, the effects of tropical cyclones upon the Philippine Islands have been under surveillance by the author. An average of 31 tropical cyclones occurs in the western North Pacific Ocean each year. While it is a highly speculative concept—and the author is not an expert on ENSO⁸ theory—, it was suspected that 1992 might be a year of fewer than normal tropical cyclones for the western North Pacific Ocean, following the ENSO episode of warmer SST, in the east, during 1991/1992. This is based on the observation that fewer than normal tropical cyclones occurred during the typhoon seasons following the 1976/1977 and the 1982/1983 ENSO episodes. However, C. P. Guard (1992, personal communication) theorizes that an ENSO episode may delay onset of (early) typhoons, but does not necessarily reduce the total number of typhoons.

While the above theory addresses the entire western North Pacific Ocean, Shoemaker (1991) discusses only tropical cyclones affecting the Philippine Islands. His study shows that during the 20-year period (1970–1989), an average⁹ of 6.5 TCs struck the PI per year. However, the Philippine Atmospheric, Geophysical and Astronomical Services Administration (PAGASA) reports an average >10 per year.

2.3.2 Tropical Cyclone “Thumb Rules”

The following rules (Shoemaker 1991) must be applied judiciously to each given situation. They may help “fine tune” a forecast, but are seldom forecasts in themselves. As will be shown, the rules are not irrefutable!

1. If a TC is forecast to be moving 320°– 360° when approaching the east coast of the PI, forecast recurvature rather than a PI transit (see Fig. 2.5).
2. Do not forecast February, March, or April Philippine Sea TCs to strike the PI (see Fig. 2.6).
3. Consider September–November as the most favorable period for TCs to hit the PI. The June–July period is next most favorable. The monthly number of TCs (Fig. 2.6) is bimodal in consonance with the sun passing over the PI twice per year. (During late July–early September storms generally move north or northeast of Luzon, inducing a monsoon surge.)

⁸The El Nino/Southern Oscillation (ENSO) phenomenon exists when an anomalous pressure gradient exists across the tropical Pacific Ocean, i.e., the magnitude of the near-surface easterly trade winds decreases, and nearly simultaneously a thicker, warmer upper-ocean layer forms in the central, then in the eastern, Pacific Ocean. With the anomalous eastward transport of Pacific Ocean near surface water, upwelling along the west coast of South America is inhibited and sea surface temperature (SST) increases. The increased SST leads to increased atmospheric convection over the central and eastern Pacific with its associated upward atmospheric motion. This is accompanied by a large scale downward (sinking) atmospheric motion over the western tropical Pacific which tends to inhibit the strength of the convection otherwise expected to occur within the vicinity of the monsoon trough of the western Pacific. It logically follows that any decrease in convective activity within the monsoon trough should lessen the likelihood of TC formation in the western Pacific.

⁹See Page B-2 of Appendix B.

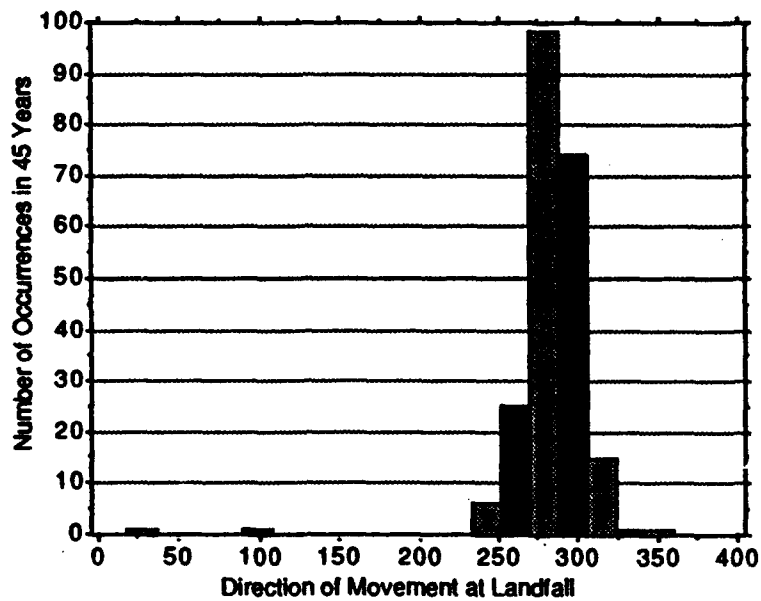


Figure 2.5: Frequency Distribution of Tropical Cyclone Direction at Landfall (adapted from Shoemaker 1991)

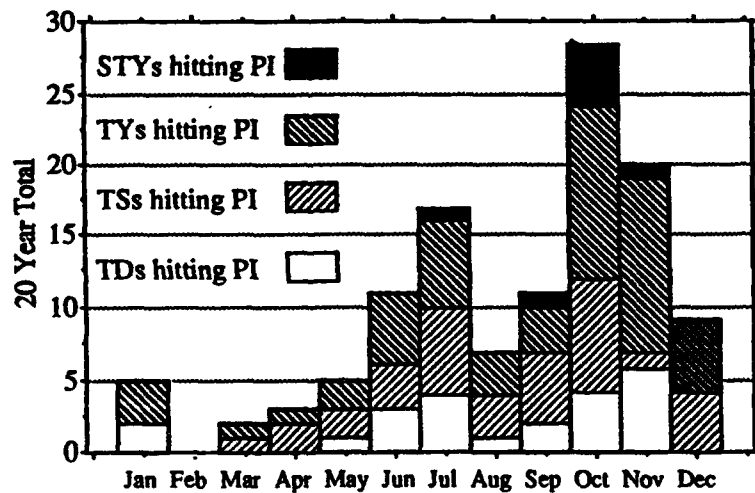


Figure 2.6: TCs hitting the PI during the 20 Years 1970-1989 (adapted from Shoemaker 1991)

4. Only forecast super typhoon intensity prior to landfall in October.
5. Expect typhoon intensity to weaken as typhoons cross the PI¹⁰. However do not expect TCs with intensity less than 50 knots at landfall to weaken significantly. The amount of weakening is proportional to intensity, and weakening is less for TCs south of 14.5°. (However, according to C. P. Guard (1992, personal communication), TCs crossing the Visayas or extreme southern Luzon may maintain up to 65 kt intensity without weakening.)
6. Do not forecast west-southwest movement for more than 24 hours. This movement is generally caused by a transiting environmental factor, such as an extratropical trough passage to the north¹¹.
7. Expect TCs approaching the PI moving southwestward to move more westward (as they make landfall).
8. Expect a slight northward direction bias for stronger tropical cyclones (>50 knots) when compared to weaker TCs.
9. As the winter monsoon season approaches in the South China Sea, expect the low-level center to move more southward than it had previously moved, even if the deep cloud signature moves more northward. (The system may shear apart.)
10. For TCs moving 300°– 320° just prior to landfall, consider forecasting a more westward movement while transiting land; then resume west-northwestward movement.
11. According to C. P. Guard (1992, personal communication) if the TC, approaching northern Luzon from the east, has:
 - (a) a greater westward than northward component, the TC will cross PI.
 - (b) a greater northward than westward component, the TC will tend to follow orientation of Sierra Madres, then resume a more westward movement.
12. For all tropical cyclones moving 8 kt or faster, and especially for those faster than 17 kt, consider a slowing trend after they enter the South China Sea.
13. Consider EVERYTHING!!!

¹⁰See Section 3.5 for a possible exception (Typhoon Eli 1992)

¹¹See Section 3.4 for a possible exception (TS Thelma 1991)

2.4 Northeast Monsoon and the Trade Wind Regime

During two recent northeast monsoon seasons (1990/91 and 1991/92), major Asian cold-surge events had little effect upon the Philippine Islands. These major cold-surges (see Boyle and Chen 1987), emanating from near Lake Baikal in the Russian Republic, moved eastward over Korea and toward Japan, with little perceived effect upon the PI.

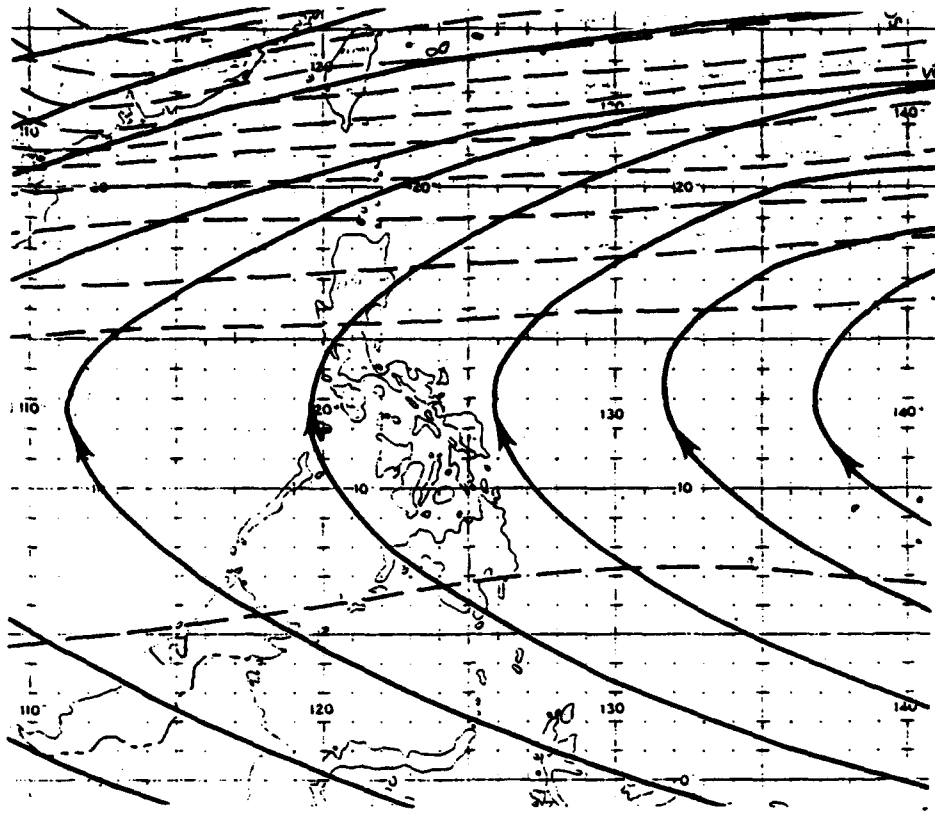
Figure 2.7 displays the average 200-mb and surface flow pattern during January¹². In Fig. 2.7(a) at 200 mb, the subtropical ridge has been displaced equatorward by the strong westerlies associated with the polar front jet, which averages 140 kt, to the north near 30°N (not shown). This streamline pattern provides the general poleward mass transport aloft. Figure 2.7(b) then shows the near-surface equatorward return flow, the northeast monsoon regime, described earlier in the introduction. The intermittent passage of cold fronts or weaker shear lines, near the surface, are masked by the more prevalent northeasterly flow. That is, the southwesterly flow ahead of the cold surges—normally weak by the time they reach Luzon—is not visible in the mean flow depicted in Fig. 2.7(b). Cold fronts frequently pass over Hong Kong and Taiwan through May—even later into June. While they typically penetrated no further south than the Luzon Strait during the most recent season, forecasters should expect weak cold fronts (or shear lines), with their associated cloudiness and light showers, to make several penetrations into Luzon during the northeast monsoon regime. The shear lines may move south, even into the Visayas, and then move back over Luzon, with their persistent broken cloudiness, before dissipating (CNOG 1990).

Figure 2.8(a) for January shows the reversal of sea-level pressure gradient over the PI compared with that of August (Fig. 2.4(a)). The lower surface pressure over mainland China during August has now been replaced by high pressure (near 1021 hPa or mb) (Fig. 2.8(a)) associated with the very cold, dense winter air mass. The January SST surrounding the Philippine Islands (Fig. 2.8(b)) is now 1–5 °C colder than in August, with the temperature required for TC genesis (26.5°C) restricted to the general vicinity of the Visayas and Mindanao.

During April and May, the Philippine Sea was monitored for tropical waves moving westward toward the PI. Although several very weak convective centers were detected moving westward toward the Visayas, they were of no significant impact—quite different from the frequent convective tropical waves, with their associated precipitation, moving from the North Atlantic Ocean westward into the Caribbean Sea (Williams et al. 1989). If they existed farther equatorward, they may have moved westward over Mindanao, but were probably masked by persistent cloudiness so near to the equator. Also, by late May, the monsoon trough commences its return at the surface (see Appendix A, Fig. A-6(b)), and any convective clusters east of Mindanao can become tropical cyclones.

¹²The 200-mb flow is typical of months December through April. The subtropical ridge then moves northward to the Luzon Strait during May. The surface flow is typical of December through March. The surface patterns for April and May are presented Fig. 2.9.

(a)



(b)

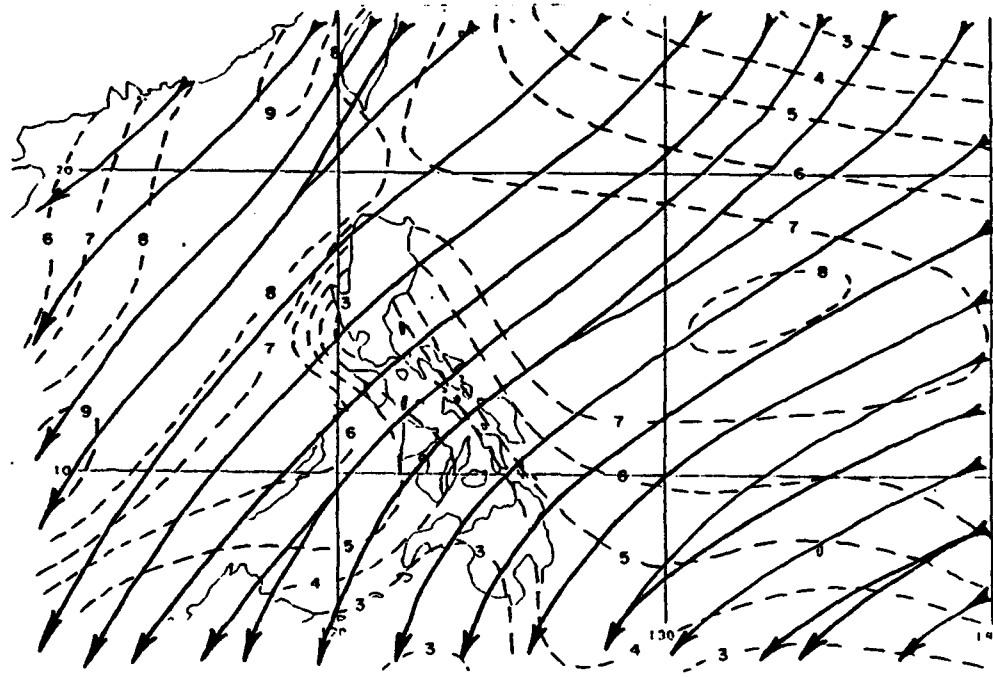
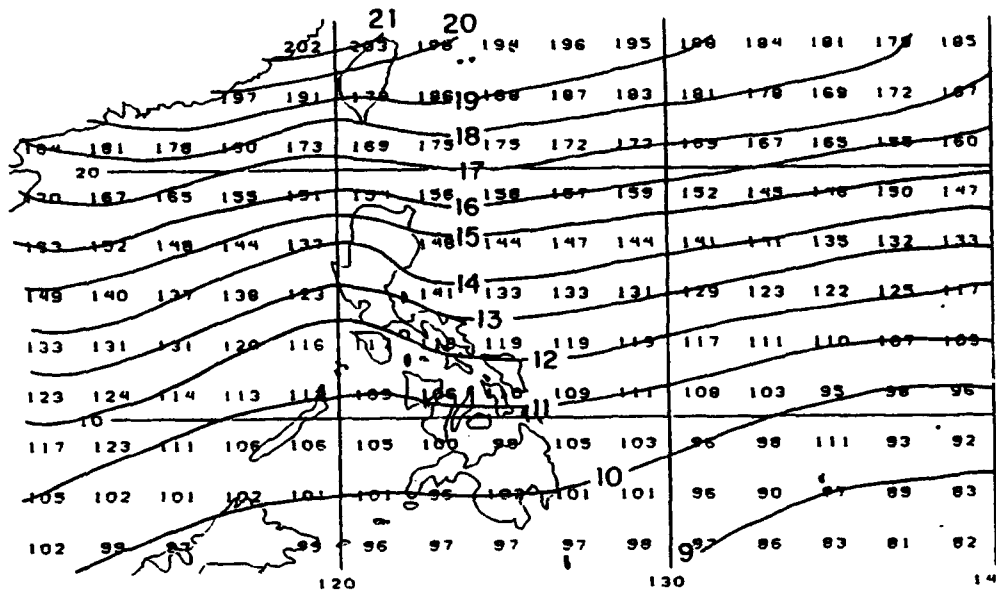
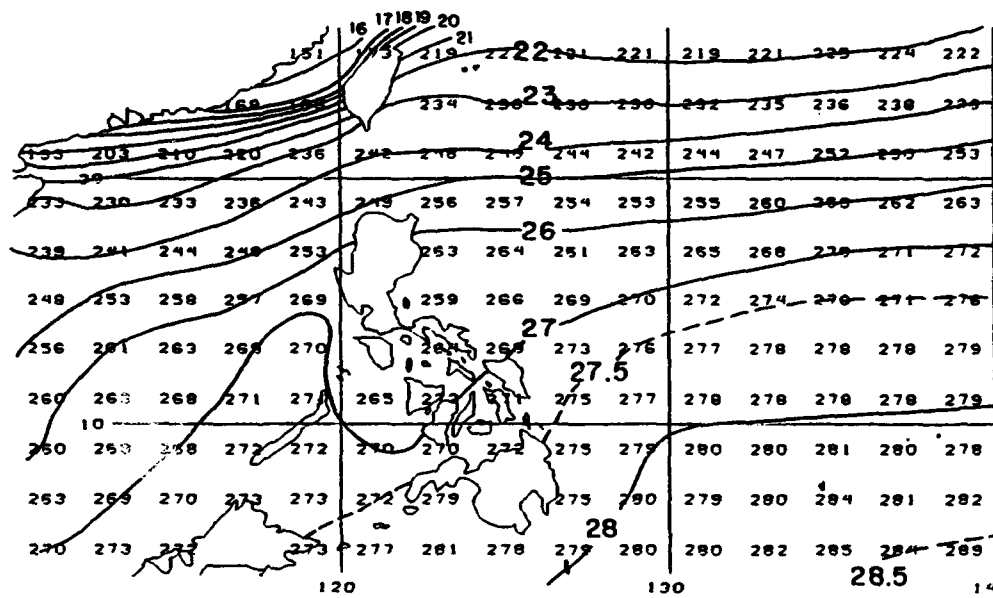


Figure 2.7: (a) Mean 200 mb Flow, January (Sadler and Wann 1984) Streamlines (solid, with arrow indicating direction of flow) and isotachs (dashed) in knots
(b) Surface Wind Flow, January (adapted from Sadler et al. 1987a and 1987b) Streamlines (solid, with arrow indicating direction of flow) and isotachs (dashed) in m/sec



(a)



(b)

Figure 2.8: (a) Mean Sea-level Pressure, January
 The isobars are labeled in millibars (or hectopascals (hPa)) with the leading 10 omitted.
 (b) Sea-surface Temperature (SST) in °C, January (adapted from Sadler et al. 1987a and 1987b)

2.4.1 December–May (Months of Lighter Precipitation)

General

December–March

Figure 2.7(b) shows the steady northeast surface flow associated with the northeast monsoon, although at times it may pulsate in surges. This air stream, originating in the cold, intense Asiatic winter anticyclone, follows a path across Japan or the Ryukyu Islands (the island chain containing Okinawa). As the air mass finally reaches the PI, it may come from a northerly through easterly direction. During periods with weaker synoptic winds, the sea breeze or land breeze component may dominate. In fact, the northeast monsoon may start as early as October, attain maximum strength in January, weaken in March and disappear in April.

Commencing as a continental polar air mass with temperature near -5°F and a mixing ratio ($\sim 0.5\text{ g/kg}$) near the surface, the air mass is transformed into a maritime polar air mass as it passes over the northwestern Pacific Ocean. Finally arriving over the Philippine Islands as a maritime sub-tropical air mass, the air mass has a surface temperature of about 77°F and a mixing ratio near 12 g/kg .

The air stream has a moderate temperature inversion at about 5000 ft, with most of the water content in the layer below the inversion. The northeast monsoon is relatively shallow, rarely exceeding 8000 ft in depth. Aloft, it normally is overlaid by extratropical (or temperate zone) westerlies over northern Luzon and by North Pacific trades over the remainder of the PI. Typically the northeast trades are characterized by heavy stratocumulus clouds, with isolated showers or drizzle. While clear conditions exist aloft in the upper-level extratropical westerlies, an upper-level trade regime will bring both middle and high clouds (Flores and Balagot 1969).

The northeast monsoon is partly cloudy to cloudy, less humid than the southwest monsoon regime, but sometimes hot. The mean cloudiness varies between 50 and 85%; however, some locations on the west coast (lee side) of Luzon, experience cloudiness of only 25 to 50%. Mean relative humidity, somewhat lower through January, still averages 60–80% in the afternoon and 85–95% in the early morning at coastal areas, but less inland where subsidence over the mountains helps dry the atmosphere. While mean daily maximum temperatures range from low 80's ($^{\circ}\text{F}$) to the low 90's, the mean daily minima are 65–75° (see Manila statistics on page 2-22). Temperatures at mountain sites are about 10° lower. Throughout the PI, temperatures rarely go below 55° or above 100° . As will be noted at the 60 stations in Appendix C, precipitation varies considerably throughout the PI. During this period, the smallest rainfall amounts are found along the west coast of Luzon, with the largest, on the northeast coast along the Sierra Madre mountain range, where the orographic effects produce ≥ 20 inches. Similarly, the number of days per month with precipitation varies from ≤ 5 to 25 days, and the mean number of days a month with thunderstorms, from 0 to 9 days. Gale force winds are rare during this regime, but do occur near thunderstorms, lasting 5–10 minutes (USAFETAC 1985).

Frequent tropical disturbances may drop considerable precipitation on Mindanao during

this period, but they seldom develop into TCs. Gales are also common in the Luzon Strait during NE surges.

April-May

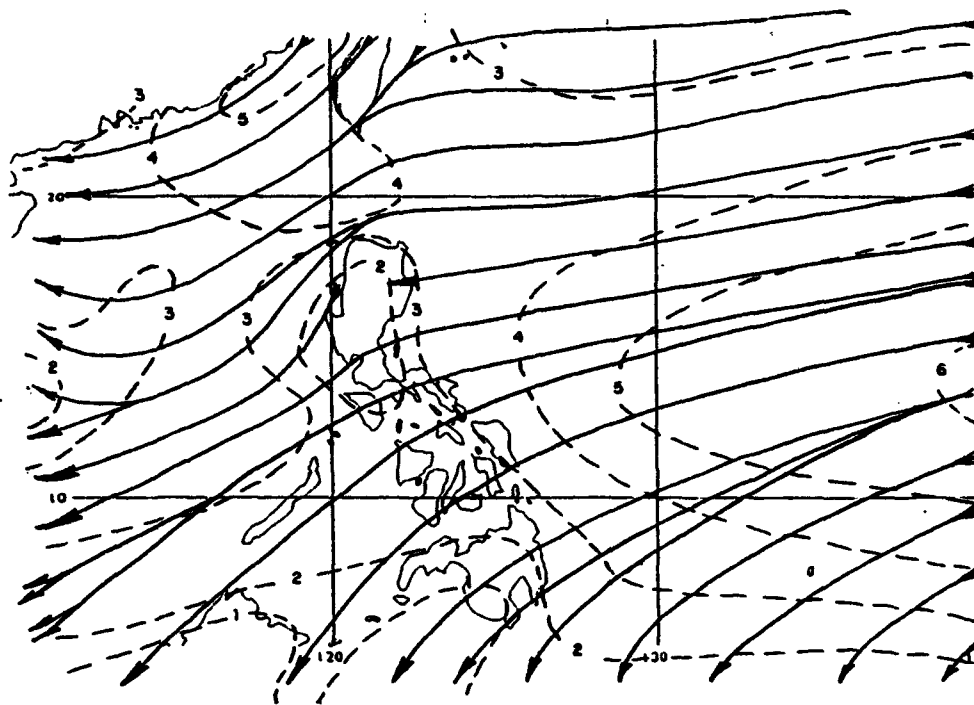
This period is classified as the trade wind or transition season. The monthly mean streamlines for April and May (Figs. 2.9(a) & (b)) demonstrate graphically the evolution of this transition. The North Pacific trades air stream is the southern portion of the North Pacific anticyclone and is thus classified as a maritime tropical air mass. Traveling over a vast expanse of the ocean, the air stream arrives at the Philippine Islands from varying directions, generally northeast, east or southeast, but sometimes south, or even southwest. The trade winds are generally dominant over the entire PI in April and early May. As mentioned in the previous section, they usually overlie the northeast monsoon, especially over eastern portions of the Philippine Islands.

As seen in the following statistics for Manila, this trade wind regime is the warmest to affect the PI. The air mass has a lapse rate slightly greater than saturated adiabatic, with a weak trade wind inversion at about 5000 ft elevation. The moisture content below the inversion is moderate, but very dry above the inversion where the relative humidity is generally <25%. While these vertical temperature and moisture profiles make the air mass normally both conditionally and potentially (or convectively) unstable, the relatively dry upper layers and the general subsidence from the nearby large-scale anticyclone prevent the occurrence of intense convective activity. Most cloudiness is limited to cumulus humilis (fair weather cumulus) and stratocumulus, except where orographic enhancements lead to towering cumulus and showers (Flores and Balagot 1969).

While May commences with the Philippine Islands under the domination of the trade winds, May, nevertheless, is part of the southwest monsoon formation season. The monsoon trough begins its northeastward movement across the PI from the southwest (see Appendix A, Fig. A-6(b)). Mean cloudiness during this season varies from 50-80%, except along the western coastal areas of Luzon, where it is 25-50%. Relative humidity remains much like February and March averaging 60-80%, afternoons, to 85-95%, mornings, but more humid over the eastern PI while drier inland. As mentioned earlier, these are the warmest months in the Philippine Islands with mean daily maximum temperatures ranging from the low 80's to the mid 90's. Mean minimum temperatures range from the mid 60's to the upper 70's. Yet, temperatures are very rarely below 55° or above 100°. As the formation of the southwest monsoon commences, rainfall increases along the southwest coasts, and decreases along the northeast coasts. While rainfall occurs 5-20 days a month, the thunderstorm activity increases with the approach of the monsoon trough. Gale force winds are rare except during thunderstorms (USAFETAC 1985).

This is the season for severe, inland thunderstorms. In April the sun is directly overhead, skies are relatively clear and surface heating creates very active convection. Dry air above 5-8000 ft results in strong evaporative cooling and strong thunderstorm downdrafts. Additionally, a strong sea breeze front frequently sets up between Manila Bay and Lingayen Gulf, creating thunderstorms with tops in excess of 55,000 ft.

(a)



(b)

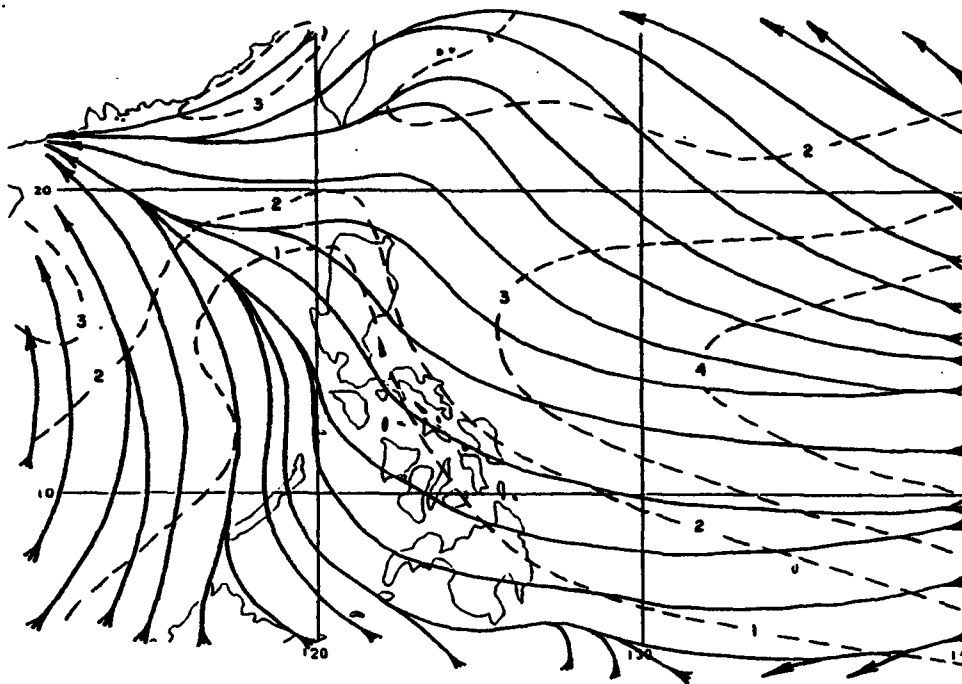


Figure 2.9: Surface Wind Flow, (a) April & (b) May (adapted from Sadler et al. 1987a and 1987b) Streamlines (solid, with arrow indicating direction of flow) and isotachs (dashed) in m/sec

Flying Weather (USAFETAC 1985)

December-March

- Fair to good.
- Ceilings and visibilities $\leq 5000/6$:
 1. Less than 10% of the time along the west coast of Luzon.
 2. Up to 33% of the time at eastern locations.
- $< 1500/3$: From less than 1 to 20% of the time.
- $< 500/1$: Less than 2% of the time.

April-May

- Good.
- Ceilings and visibilities $\leq 5000/6$ occur 5-20% of the time.
- $< 1500/3$: Less than 12% of the time.
- $< 500/1$: Less than 1% of the time.

Terminal Weather, Manila (USAFETAC 1985)

December-March

Good. Ceiling/visibility $\leq 300/1$ occurs less than 1% of the time. Surface winds are northeasterly through southeasterly, 5-15 kt.

April-May

Good. Ceiling/visibility $\leq 300/1$ occurs less than 1% of the time. Thunderstorms occur on less than 10 days a month. Surface winds are easterly through southeasterly, 5-15 kt.

Monthly temperature, precipitation, thunderstorms & twilight (USAFETAC, 1985)
 (See Appendix C for Climatic Normals of 60 additional stations.)

MANILA	DEC	JAN	FEB	MAR	APR	MAY
TEMPERATURE (°F)						
Absolute maximum	94	95	96	98	100	100
Mean maximum	86	86	88	91	93	93
Mean minimum	70	69	69	70	73	75
Absolute minimum	58	58	60	61	63	68
MEAN PRECIPITATION (INCHES)	2.7	0.9	0.4	0.7	1.3	5.1
MEAN NUMBER OF DAYS						
Precipitation	11	6	3	2	2	8
Thunderstorms	1	0	0	0	1	6
CIVIL TWILIGHT (15th of month)						
First light (local standard time)	0549	0601	0558	0542	0520	0506
Last light (local standard time)	1753	1809	1822	1828	1832	1839

TYPHOON (AND OTHER) FORECASTING

3.1 The Danger of Volcanic Ash to Aviation

The 1989–90 eruption of Redoubt Volcano in Alaska and the June 1991 eruption of Mount Pinatubo in the Philippines have resulted in over 16 aircraft damaged; mostly 747 series commercial aircraft. The following is quoted from Hufford (1991) reporting items of interest to aviation forecasters from the First International Symposium on Volcanic Ash and Aviation Safety, held in Seattle, Washington 9–11 July 1991.

It is the forecaster who has the ultimate responsibility to accurately forecast and issue timely advisories on the movement of airborne volcanic debris. It was the experience of the forecasters in the Anchorage WSFO that there were deficiencies in information that greatly hampered their response. The forecaster had no information on (1) ash particle size and concentration; (2) initial height and horizontal extent of the ash plume into the atmosphere; (3) real-time vertical profile of the winds near and downstream of the volcano; and (4) rapid access to volcanic ash trajectory models.

Volcanoes and Ash

Volcanic eruptions that involve release of volcanic ash in the atmosphere have some common characteristics. The first portion of the eruptive cloud column just above the volcano is called the gas thrust and protrudes 3000–6000 ft into the atmosphere. This section of the column is a jet of material leaving the volcano vent. It is characterized by rapid deceleration and loss of coarse volcanic debris. The second portion of the column is called the convective thrust zone characterized by acceleration of the gases and small particles due to the heat energy. The ash/gas cloud ceases to accelerate vertically when the temperature of the cloud equals the ambient temperature of the air. The final portion of the eruptive column is called the umbrella and it can push out horizontally upwind as well as downwind. In the case of Mt. St. Helens, the umbrella pushed 40 km upwind—even farther upwind, for Mt. Pinatubo. It is important that the forecaster recognizes that volcanic ash can be upwind of the

volcano and includes this area in the advisory. There is no known technology at this time that can be used to provide a reasonable estimate of the ash in the eruptive column. Thus the concentration and particle size of the ash in an eruptive column is unknown.

Aircraft Damage

It is of interest to the forecaster to understand the damage airborne volcanic ash can do to a jet engine. The following types of damage are listed in order of importance:

1. Glassification of the ash and deposition on hot section components of the engine.
2. Erosion of compressor and turbine components by the ash.
3. Deposition on fuel nozzles and cooling parts (clogging).
4. Windshield crazing causing loss of visibility.
5. Deterioration of engine control system by electrical shorting, clogging of sensors, etc.

The most critical problem is glassification of the ash. The modern jet engine runs at temperatures approaching 2000°F. This is well above the melting point of silicate, a major component of ash. The ash enters the engine, melts and coats the inside of the engine, covering nozzles, air vents, and other critical components. The engine quits running. Depending on concentration, this shutdown can occur as quickly as 1 minute (the case of the KLM 747 incident 150 km from Redoubt) or as long as 29 minutes (the recent case of a 747 1200 km from Pinatubo).

The forecaster must be aware of the location and presence of ash in the atmosphere regardless of particle size. Concentration is more important. It was the conclusion of the air industry at the symposium that these areas must simply be avoided at all costs. At this time there are no sensors onboard the aircraft to detect ash during flight. The only warning to the pilot is the presence of St. Elmo's fire around the windshield, wing tips and engines. This fire-like glow occurs because of the static charge associated with each ash particle. If ash concentration is high, the notice of St. Elmo's fire by the pilot may be too late for the pilot to take evasive action and save the engines from damage.

Ash Detection

The technologies identified as most important in detecting, monitoring and tracking of airborne volcanic ash were satellite imagery, radar, doppler wind profilers and aviation reports (ACARS). Techniques have been developed to utilize NOAA AVHRR imagery to detect volcanic eruptive clouds in a variety of weather, and both day and night. The techniques use multiple infrared

channels (bands 4 and 5) in the algorithms. In addition the imagery can be used to track the eruptive clouds as they move downwind. The use of weather radar (5 cm) to detect ash in the eruptive cloud has been established though there are some limitations; once the ash becomes dispersed and it consists of very small particles, the radar is unable to detect it. The radar's use is best near the volcano.

The wind profiler is an instrument that provides real-time winds near the volcano and at sites downwind. The air industry would like to see critical volcanoes instrumented with wind profilers along with other sensing equipment. Ready access to aircraft winds and temperature (ACARS) are critical in providing the forecaster with information on the wind field in the atmosphere and the ultimate movement of volcanic ash. The airlines are now aware of the importance of these data and are willing to make it available to the NWS in areas where it is not presently available.

Ash Trajectory Forecasting

NOAA's Forecast Systems Laboratory has developed a Mesoscale Analysis and Prediction System (MAPS) for assimilating surface and tropospheric data every three hours and providing nowcasting. It uses isentropic coordinates in the free atmosphere and terrain-following coordinates near the ground. Isentropic coordinates are well suited for trajectory calculations because air remains on these surfaces in adiabatic flow. MAPS has been adapted for use in Alaska...

To provide for larger scale and longer term trajectories, the Air Resources Laboratory is developing a model to simulate ash transport. MAPS will provide the initial conditions and short-term forecast data. The larger scale and longer term meteorological data will come from the NMC models. Dispersion and wet and dry deposition is included in the model. Output describes the ash cloud in both space and time. This model should be available to Alaskan forecasters this winter.

Just before publication of this Handbook, it was learned that the NOAA Air Resources Laboratory (ARL) had developed a Volcanic Ash Forecast Transport and Dispersion (VAFTAD) model (Western Region Headquarters 1992). If the user supplies the name of the volcano, its location, time of the eruption and the height (in feet) of the volcanic ash cloud, the ash cloud is advected by a computer model on an IBM RISC System/6000 computer located at NOAA ARL in Silver Spring, MD. Gridded forecast data (from the National Meteorological Center (NMC) Global Spectral Model (AVN)) out to 48-h (in 6-h intervals) are used to advect the ash cloud. The graphical product will be "faxed" to the requester providing concentration of ash, in four layers from the surface to 50,000 feet. Until model runs become regular NMC products (estimated during the later part of 1993), direct any operational requests, to the appropriate regional Naval Oceanography Center of the Naval Oceanography Command. The center will provide support via the appropriate laboratory or the Navy's own model.

3.2 JTWC Bulletins (U. S. NOCC/JTWC 1992)

While the tropical maritime climate of the Philippines can produce heavy convection, especially during the southwest monsoon, a tropical cyclone greatly enhances the intensity and the length of time of the rainfall, as well as the magnitude of the winds. To limit both property and human life losses, local and regional planning dictates that the best forecasts that modern technology permits must be provided. This section describes the bulletins promulgated by the U. S. Naval Oceanography Command Center/Joint Typhoon Warning Center (JTWC) in Guam. Following the presentation of TC forecasting philosophies, case histories of recent tropical cyclones are presented.

In a following section, on case studies, graphical products available to units within the Department of Defense (DoD) via the Naval Oceanography Data Distribution System (NODDS) are described. However, forecasters should know the bulletin headings used by JTWC to deliver alphanumeric messages regarding tropical cyclones¹. In particular, Naval Oceanography Command (NOC) personnel should be prepared to interpret and explain the bulletins to the commands supported. The possibility of random behavior of tropical cyclone movement dictates that JTWC issue timely alerts and warnings to support the Fleet, other units of DoD, U. S. territories, and, indirectly, other affected nations and islands in the western Pacific. Table 3.1 from U. S. NOCC/JTWC (1992) lists the relevant messages issued by JTWC useful in supporting operations in the Philippine Islands and the western North Pacific Ocean.

The **Significant Tropical Weather Advisory**, issued by 0600Z daily, describes the latest tropical cyclone warnings, if any, as well as all tropical disturbances and their potential for further development. This advisory may be reissued if the situation warrants. The potential for further development of each suspect area is described by:

- Poor – Meteorological conditions are currently unfavorable for development.
- Fair – Meteorological conditions are favorable for development, but significant development has not commenced or is not expected to occur in the next 24 hours.
- Good – Potential for development of a disturbance is covered by an alert.

¹Tropical Cyclones are classified as follows: Tropical depression (TD) <34 kt, tropical storm (TS) 34–63 kt, typhoon (TY) 64–129 kt and *super typhoon* (ST) ≥130 kt. (Winds are 1-minute averaged sustained winds.)

The Tropical Cyclone Formation Alert (TCFA) is issued whenever interpretation of satellite imagery or other meteorological data indicates that formation of a tropical cyclone is likely. The alert is valid for a period not to exceed 24 hours and must be canceled, reissued or superseded by a warning prior to expiration.

Table 3.1: JTWC Tropical Cyclone Positions, Alerts, Warnings, etc.

U. S. NOCC/JTWC, 1992

BULLETIN HEADING	TITLE	ISSUANCE	FORECAST PERIOD
ABPW10 PGTW	SIGNIFICANT TROPICAL WEATHER ADVISORY FOR THE WESTERN PACIFIC OCEAN	24 h	24 h
WTPN21 PGTW	TROPICAL CYCLONE FORMATION ALERT	WHEN APPLICABLE	24 h
WTPN31 PGTW	TROPICAL CYCLONE (OR DEPRESSION) WARNING	TC (6 h) TD (12 h)	TC (72 h) TD (36 h)
WDPN31 PGTW	PROGNOSTIC REASONING MESSAGE	12 h	TC (72 h)
TPPN10 PGTW	TROPICAL CYCLONE (OR DEPRESSION) POSITION	WHEN APPLICABLE	N/A

Note: Consult the latest JTWC Annual Tropical Cyclone Report for changes after 1992. The existence of multiple TCs at the same time are covered by bulletins WTPN31-36 and WDPN31-36, while multiple alerts are identified by bulletins WTPN21-26. Tropical Cyclone Position bulletins (based on satellite analysis) routinely are issued by PGTW (JTWC); however, TPPNs may also be issued by Hickam AFB, Hawaii; Kadena AB, Okinawa, Japan; Osan AB, Republic of Korea; the Air Force Global Weather Central, Offutt AFB, Nebraska; as well as by Navy ships equipped for direct satellite readout.

The **Tropical Cyclone Warning** is issued when a closed circulation is evident and maximum sustained winds are forecast to reach 34 kt within 48 hours, or when the TC is in such a position that life or property may be endangered. Each tropical cyclone warning is numbered sequentially and includes the following:

- Current position of the surface center
- An estimate of the position accuracy and the supporting reconnaissance (fix) platforms
- The direction and speed of movement during the past six hours
- The intensity and radial extent of over 35-, 50- and 100-kt surface winds, when applicable².
- At forecast intervals of 12, 24, 36, 48 and 72 hours, information on the TC's anticipated position, intensity and wind radii³
- Vectors indicating the mean direction and mean speed between forecast positions
- Additionally, a 3-hour extrapolated position is provided in the remarks section.

The **Tropical Depression (TD) Warning** is issued for TDs that are not expected to reach the criteria for tropical cyclone warnings, as mentioned above. It contains the same information as a tropical cyclone warning except the TD warning is issued every 12 hours and extends only to the 36-hour forecast.

The **Prognostic Reasoning Message (WDPN)** provides meteorologists with the rationale for the forecasts. Importantly, they also discuss alternate⁴ forecast scenarios. NOC personnel can present more descriptive briefings by using the material presented in this message. These bulletins are required every 12 hours for western North Pacific tropical cyclones, but are frequently provided every 6 hours (Guard et al. 1992).

The **Tropical Cyclone "Satellite" Position (TPPN)** is transmitted between the formal warnings and alerts. NOC personnel may find this bulletin useful in perceiving the evolution of the intensity, track and wind radii of respective tropical cyclones, even before receiving the official warning from JTWC.

²A 30-kt radius (vice 35-kt radius) was used before 1992.

³Before 1992, the 36 hour forecast was omitted.

⁴Several objective aids are available to the the Typhoon Duty Officers at JTWC for use in preparing the final official forecast. At times the climatology-based and the dynamically-based objective aids differ.

3.3 JTWC Forecasting Philosophies

Forecasters in the Philippine Islands and at JTWC are deeply interested in the formation, movement and intensity of tropical cyclones. The environmental conditions used to forecast these three features are now described.

3.3.1 Formation

Using satellite and conventional data, the forecaster can anticipate the formation of a tropical cyclone by being alert to the existence of the following necessary, but not sufficient conditions (Elsberry et al. 1987):

- Sea surface temperature $\geq 26.5^{\circ}\text{C}$.
- Large sustained cloud clusters identified by satellite, indicating weak vertical wind shear and large mid-level moisture.
- Low-level cyclonic circulation, identified by synoptic reports or satellite imagery.
 1. This feature is enhanced by the commencement of the Southern Hemisphere winter which provides low-level cross-equatorial southerly winds which are deflected to the right to become the westerly flow providing the cyclonic shear with the easterly trade winds located to the north. The area identified by this cyclonic shear is commonly called the monsoon trough.
 2. Residual cyclonic shear associated with an equatorward moving front (or shear line) may also provide the low-level circulation or cyclonic shear.
- Mean upward motion in the vicinity of the disturbance. This condition may be identified by anticyclonically curved cirrus on satellite imagery. As identified in the southwest monsoon section, the tropical upper tropospheric trough (TUTT) is often present over the Pacific Ocean near 200 mb. Cyclonic centers, "cells", within the TUTT, often have diffuent flow, immediately to their east, providing the needed divergence aloft.

3.3.2 Movement

The task of separating the tropical cyclones that move straight toward the west or northwest before making landfall in Asia from the tropical cyclones that recurve⁵ toward the northeast (i.e., come under the steering of the mid-latitude "westerlies") is a very difficult task, indeed.

⁵Convention dictates that TCs undergoing even their first change of direction into the mid-latitude westerlies, i.e., their direction of movement changes from NW to N to NE (poleward of the axis of the mid-tropospheric subtropical ridge), be called "recurvers".

- Most TCs have their genesis within the monsoon or near-equatorial trough, and are initially transported (or steered) in a generally westward or north-westward direction. This drift toward the northwest can be shown to be the result of the variation of the Coriolis Parameter⁶ with latitude (known as the “beta”-effect⁷), but will not be discussed here.
- However, as the TC drifts farther poleward, it crosses the axis of the subtropical ridge or moves around the western periphery of the subtropical ridge, and then is steered (or advected) by the flow in the mid-tropospheric “westerlies”.
- Whenever synoptic-scale troughs from the mid-latitudes (or extratropics) extend equatorward (or disrupts the dominance of the subtropical ridge), then the embedded TC is expected to be steered—at least initially—more northward, and eventually with an eastward component. The approach of an extratropical trough (normally from the west) can be forecast by synoptic experience, judgement, and satellite interpretation, but most often the forecaster relies upon the prognoses of numerical models to predict the position of the troughs, especially in 36, 48 and 72 hours .
- Even in the absence of an identifiable approaching upper-level trough, the forecaster is often presented with a prognosis of a numerical model which depicts the retreat of the subtropical ridge to the east (a condition that might prompt the forecast of “recurvature”) or of the penetration of the subtropical ridge farther westward (a condition that would suggest that the TC follows a straighter track).
- As discussed in the formation section above, TCs often form within the monsoon trough. This trough normally lies on an axis from near the central Philippines (the Visayas) extending toward the southeast. Subsequently, vortices developing along this axis typically move toward the northwest, in the direction of the PI. However, during the northern hemisphere summer there are periods when the monsoon axis rotates counterclockwise, and thus lies on an axis extending northeastward from the Visayas. Tropical cyclones developing in this anomalously oriented monsoon trough frequently move initially toward the northeast, and thus are often to the north of the PI before commencing their movement toward the northwest (Mark Lander (1990, personal communication)). In addition, in August the monsoon trough generally moves northward with the sun, leading to cyclone development north of the Philippine Islands.
- The Typhoon Duty Officers (TDOs) at JTWC are provided with movement objective aids displayed in Table 3.2. In combination with the β -effect, the last three aids in the table provide the option of using steering from deep or shallow layers.

⁶Coriolis Parameter, $f = 2 \cdot \Omega \cdot \sin\phi$ where: Ω = Earth's rotation rate and ϕ = °Latitude.

⁷Beta = $\beta = \partial f / \partial y$.

Table 3.2: Summary of JTWC Objective Aids.(U. S. NOCC/JTWC, 1992)

TYPE	NAME	DESCRIPTION
Persistence Climatology	XTRP	Extrapolation based on past 12-h motion.
	CLIM	Average storm motion based on all storms within seasonal and spatial windows.
Half Persistence and Climatology Analog	HPAC	Simple interpolaton between forecast position of XTRP and CLIM.
	TOTL	Average of XTRPs for all tropical cyclones matching current tropical cyclone with respect to position, time of year, past motion, and current intensity.
Analog Statistical	RECR	Same as TOTL, except only for recurring TC.
	CLIP	Regression equations based on persistence and climatology.
Statistical- Dynamic	CSUM	Regression equations for 24-h motion using surface pressure, 500- and 200-hPa heights at various positions relative to the tropical cyclone as predictors. Separate equations for tropical cyclone motion based on the recent direction of track.
Dynamic	OTCM	Primitive equation numerical model with three layers, 205-km grid, and one-way influence boundary conditions provided at 12-h interval from NOGAPS prognostic fields.
Dynamic	FBAM	NOGAPS deep-layer mean steering (1000-100 hPa) plus empirically derived propagation due to the beta effect.
Dynamic	MBAM	Same as FBAM, but with steering computed over 850-500-hPa layer.
Dynamic	SBAM	Same as FBAM, but with steering computed over 850-700-hPa layer.

NOTE: (1) The pressure unit "hPa" stands for hecto-Pascal (100 Pascal) and is equal to a millibar (mb). (2) NOGAPS (Navy Operational Global Atmospheric Prediction System) will be discussed in following section. (3) After 1992, refer to the latest JTWC Annual Tropical Cyclone Report for newly-developed objective aids.

- There is a documented reaction between tropical cyclones that are ≤ 750 n.mi. apart. This effect, known as the Fujiwhara effect, and more recently as binary interaction, is often visible as the weaker tropical cyclone is steered cyclonically around the stronger. The effect upon equally strong TCs is more easily perceived when their positions are plotted relative to the mid-point (or "centroid") on the line connecting the two tropical cyclones. Both TCs will then exhibit a component of motion cyclonically around the centroid. (JTWC has developed a computer program to calculate the degree of the Fujiwhara effect and to provide a CLIPER-like forecast of the resultant typhoon track.)
- Unfortunately, the forecasters of tropical cyclone motion must accept the existence of TCs that exhibit large directional changes in motion over short periods of time. These cyclones represent a small percentage of the total; however, they may change direction or loop, often several times. Fortunately, the subtropical ridge is typically located north of the Philippine Islands, providing TC movement in a general westward direction. However, this does not negate the possibility of a loop over the Luzon Strait, the South China Sea or wherever!

3.3.3 Intensity

The evolution of the intensity (maximum one-minute sustained winds) of a tropical cyclone, while often "normal" in its developing or weakening, can also be erratic and difficult to forecast, as well as to analyze. Since the U. S. Air Force ceased aircraft reconnaissance flights in 1987 (the U. S. Navy had ceased its operations in 1971), JTWC must primarily use satellite imagery to determine tropical cyclone intensity. (Satellite imagery is also the primary tool for determining location, although limited radar reports and synoptic observations provide a minimal, but important, contribution.)

- Forecasters having satellite imagery—preferably enhanced infrared (IR) imagery—available can perform their own wind analysis/forecast using the Dvorak technique. The technique uses both visible and IR cloud feature measurements and rules based on a model of tropical cyclone development to arrive at the current and 24-hour intensity of the TC. For example, the model would describe a normally developing tropical cyclone as having a T-number (Tropical number) T1 on day one, T2 on day two, etc. After the analyst has determined the final T-number, rules assist the analyst in the determination of a Current Intensity (CI) number (see Table 3.3 for the empirical relationship between the Current Intensity number (CI) and the maximum wind speed (MWS) for tropical cyclones in the western North Pacific Ocean). The Dvorak technique dictates that the T-number and CI number be the same for developing or steady TCs. However, the CI is held higher than the T-number while a cyclone is weakening. This scheme is used because a lag is observed between the time a TC pattern indicates that weakening has begun and the time when the storm's intensity has actually decreased, i.e., the sur-

face wind (spin or momentum) of the TC continues at the higher magnitude, even though the satellite signature (from above) indicates its initial weakening. In practice, the CI number is not lowered until the T-number has shown weakening for at least 12 hours. The Dvorak technique uses many features of the TC's satellite signature: Enhanced IR image (EIR): the spiral arc distance of the curved band surrounding the center, temperature of the eye and of the surrounding cloud tops, the presence of an upper-level "shear" cloud signature, the presence of a "central cold cover" pattern, etc. Visible image: the spiral arc distance of the surrounding curved band, the embedded distance of the eye, the presence of a central dense overcast (CDO), measurements of central features and the (outer) banding features, etc. The EIR technique requires less subjective judgment than the visible technique, and the EIR imagery is available continuously—not just during daylight hours. However, the visual data is used to monitor situations where the EIR technique has weaknesses and may significantly misrepresent intensity. The Dvorak technique is designed for a typical daily rate of development, increasing by one T-number per day. However, depending upon environmental conditions, the rate may be rapid (~ 1.5 T-number per day) or slow (~ 0.5 T-number per day).

Table 3.3: Current Intensity (CI) Number. The relationship between the current intensity number (CI), the maximum wind speed (MWS) and the minimum sea level pressure (MSLP) in TCs (adapted from Dvorak 1984)

CI Number	MWS (Kt)	MSLP (NW PACIFIC)	TROPICAL CYCLONE CLASSIFICATION
1	25 kt		TD
1.5	25 kt		
2	30 kt	1000 mb	
2.5	35 kt	997 mb	TS
3	45 kt	991 mb	
3.5	55 kt	984 mb	
4	65 kt	976 mb	TY
4.5	77 kt	966 mb	
5	90 kt	954 mb	
5.5	102 kt	941 mb	
6	115 kt	927 mb	
6.5	127 kt	914 mb	ST
7	140 kt	898 mb	
7.5	155 kt	879 mb	
8	170 kt	858 mb	

Obviously, allowance must be made for long-lived TCs whose history extend beyond the typical development period of 4-6 days. While a complete description of the Dvorak Technique cannot be given in this handbook, interested forecasters are referred to Dvorak (1984). Below are two examples of Dvorak classifications included in TPPN bulletins:

T4.0/4.0/D1.0/24hrs

Decoded: T-number = 4.0, CI number = 4.0 (65 kt, typhoon, see Table 3.3)
Indication of ongoing change (BLANK), i.e., past trend continuing
D = Developing (Past change), 1.0 = Amount of past change, +1.0 T-number
24 hrs = hours since previous observation.

T5.0/6.0MINUS/W1.5/24hrs

Decoded: T-number = 5.0, CI number = 6.0 (115 kt, typhoon)
MINUS = Rapid weakening (Indication of ongoing change)
W = Weakening (Past change), 1.5 = Amount of past change, -1.5 T-number
24 hrs = hours since previous observation.

- The following are environmental conditions expected to increase the intensity of the maximum sustained winds of a tropical cyclone.
 1. Colder tops in the clouds surrounding the TC center and/or warmer eye temperatures (Dvorak 1984). These conditions indicate greater convection (upward vertical motion) in the towers surrounding the TC center and greater subsidence into the eye of the TC.
 2. Larger spiral arc distance of the curved band around the TC (Dvorak 1984).
 3. The TC enters a region of increased diffuence aloft. This is often indicated by the presence of multiple outflow channels, i.e., the greater outflow of mass aloft leads to a larger fall in the sea level pressure at the TC's surface center further leading to larger magnitude inflow (larger winds) at the surface. The multiple outflow channels are often directed toward cyclonic cells in nearby branches of a TUTT.
 4. The TC approaches a region of weaker vertical wind shear.
 5. The TCs exits a land area and begins a track over water with its associated smaller surface friction and added latent (and sensible) heat to fuel the tropical cyclone.
 6. The TC enters an oceanic area with a higher sea surface temperature (SST), thus experiencing additional availability of latent and sensible heat.

7. The TC departs a large-scale area of low-level stratus or stratocumulus clouds. This would generally indicate that the TC is leaving a region of lower SST and atmospheric subsidence—this situation is more common in the eastern North Pacific where colder SST is found.
- The following are environmental conditions expected to decrease the intensity of the maximum sustained winds of a tropical cyclone.
 1. Warmer tops in the clouds surrounding the TC center and/or colder eye temperatures (Dvorak 1984). These conditions indicate less convection (less upward vertical motion) in the towers surrounding the TC center and less subsidence into the eye of the TC.
 2. Smaller spiral arc distance of the curved band around the TC center (Dvorak 1984).
 3. The TC approaches a region of larger vertical wind shear. This may happen in the tropics, but is most common when the TC moves poleward and approaches the jet streams of the extratropics. It may also be manifested by southward-moving cirrus appearing less than 10° latitude to the north or west of the storm or a broadscale cyclonically curved cloud band within 25° latitude of a westward moving disturbance (or TC) (Dvorak 1984).
 4. The TC enters a region of decreased diffluence (or a region of increased confluence) aloft. This is often associated with the condition of larger vertical wind shear, i.e., the outflow reduces to one unidirection channel or the efficiency of outflow channels is decreased.
 5. The TC approaches land with its associated increase in surface friction and latent and sensible heat loss.
 6. The TC enters an oceanic area with a lower sea surface temperature (SST) thus experiencing a loss of latent heat.
 7. The TC enters an area of low-level stratus or stratocumulus clouds, which is often associated with colder SST and greater low-level stability.
 8. The TC begins to draw in cooler and dryer environmental air. However, as the colder air reaches the eyewall region, it can increase baroclinicity across the eyewall, causing a large but short-lived intensification (Guard 1992, personal communication).

3.4 Recent Tropical Cyclones Striking the Philippine Islands

3.4.1 Typhoons striking Luzon

Typhoon Yunya, 11–17 June 1991—including the Mount Pinatubo Eruption

The track of Typhoon Yunya, classified as a “Midget” typhoon, is shown in Fig. 3.1. As the legend indicates, Typhoon Yunya made landfall on Luzon, just south of Baler (see Fig. 1.2) at minimal typhoon strength (65 kt). Figure 3.2 indicates that after the two forecasts on 13 June, the official JTWC forecast accurately predicted the track of Yunya across central Luzon. The figure also shows that the recurvature was more rapid, than forecast, as the tropical cyclone departed Luzon heading toward the Luzon Strait. Additionally, note in Fig. 3.3, that the JTWC (see the track labeled JTWC) forecast accurately predicted the subsequent track over central Luzon as early as 0000Z on 14 June. The JTWC forecast followed the simpler guidance from the climatology aid (CLIM), the Colorado State regression equation model aid (CSUM) and the steering-type dynamical aid (FBAM) (see Table 3.2). It is evident that JTWC had to discount the track forecast from the large dynamic models (OTCM, NGPS (U. S. Navy’s FNOC NOGAPS Model), JTYM (Japanese Meterological Agency Typhoon Model) and EGRR (the United Kingdom Meterological Office Model)) all of which predicted premature recurvature. It appears that this problem is endemic to the current generation of vortex-tracking numerical models, i.e., these models have difficulty in describing the interaction between a small TC and its penetration of the subtropical ridge. Despite a slow speed bias of the JTWC forecasts (not shown), the forecasts that Yunya would cross central Luzon provided key warning support helping DoD officials to evacuate Clark Air Base.

This tropical cyclone formed as the surface winds in the South China Sea had changed to southwesterly—i.e., the southwest monsoon had just formed—, with the associated return flow aloft at 200 mb from the northeast. The timing of the arrival of Yunya was most unfortunate. If Yunya had not arrived on 15 June, much of the low-level ash from the Mount Pinatubo volcano would have been advected toward the north (away from U. S. Navy units in Subic Bay) and the upper-level flow would have carried the higher level ash toward the southwest (over the South China Sea and west of Subic Bay). Unfortunately the deep cyclonic circulation of Yunya swept much of the volcanic ash toward Subic Bay and Manila. The heavy rains and the weight of the ash led to the collapse of roofs and the subsequent loss of life (U. S. NOCC/JTWC 1992).

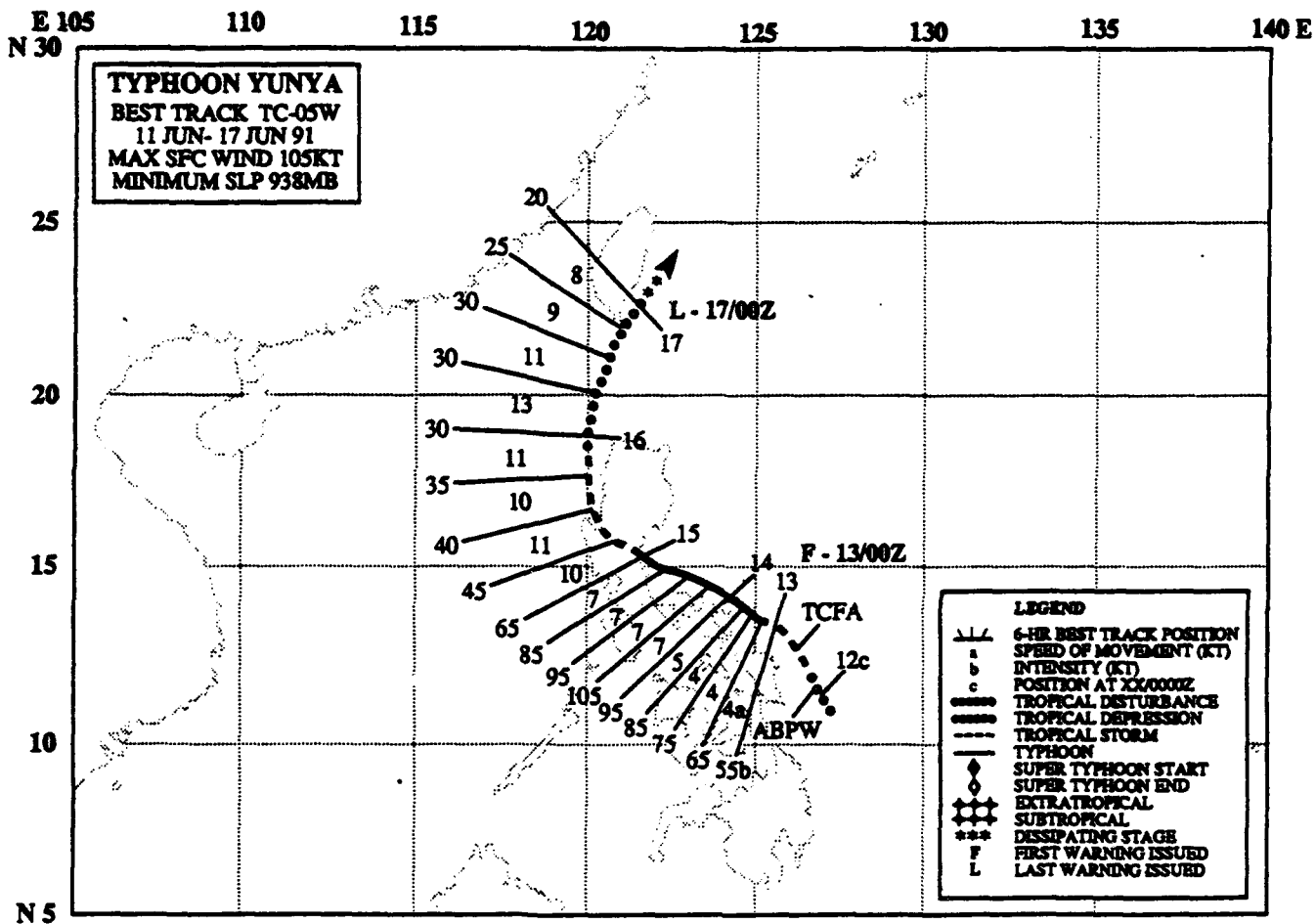


Figure 3.1: Official Best Track of Typhoon Yunya (adapted from U.S. NOCC/JTWC 1992)

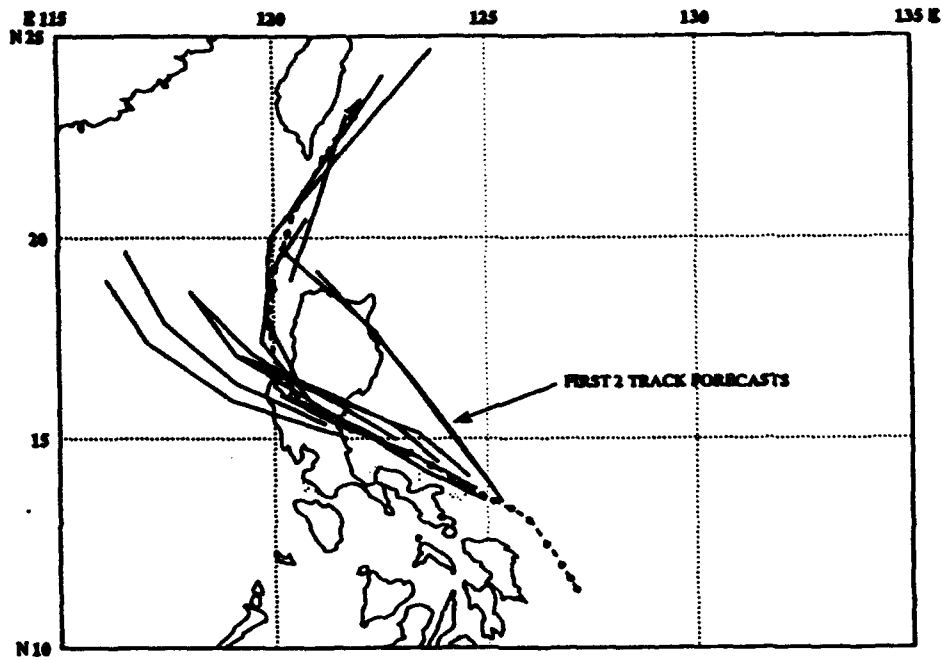


Figure 3.2: Graphics of all JTWC Official Forecasts (solid lines) issued for Yunya superimposed on the Final Best Track (dashed lines)(adapted from U. S. NOCC/JTWC 1992)

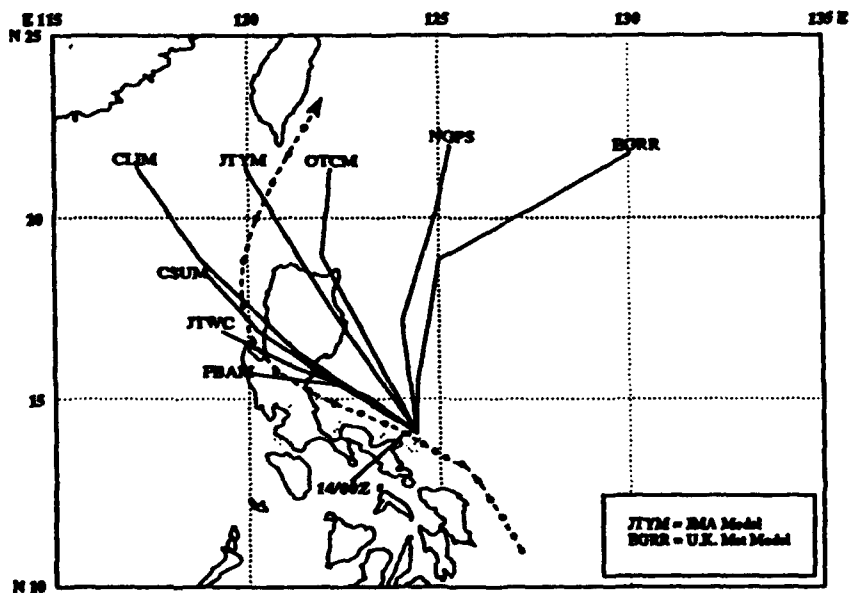


Figure 3.3: Graphics of JTWC Official Forecast and the Associated Objective Forecast Aids at 140000Z June 1991 (adapted from U. S. NOCC/JTWC 1992)

Figure 3.4 shows the eruption of the Mount Pinatubo at 0630 local time on 15 June 1991—although the commencement of this major eruption may have been as early as 0200 local time. Mount Pinatubo, located 40 nautical miles (nm) northwest of Manila, is under the small, dark circular ash cloud at the top of the figure, while much of the other cloudiness is from Typhoon Yunya, just making landfall on eastern Luzon. Note that the whiter upper-air clouds associated with approaching Typhoon Yunya do not have the characteristic circular configuration typical of a typhoon. The southwest-northeast orientation of the cloudiness is the result of strong northeasterly winds associated with the high pressure center aloft over China (and an associated 200-mb ridge extending east over Taiwan (not shown)). This strong shearing in the vertical, acting simultaneously with the frictional effects of land at low levels, quickly weakened the maximum sustained winds of small Typhoon Yunya to 45 kt at its first warning position over Luzon (see Fig. 3.1).

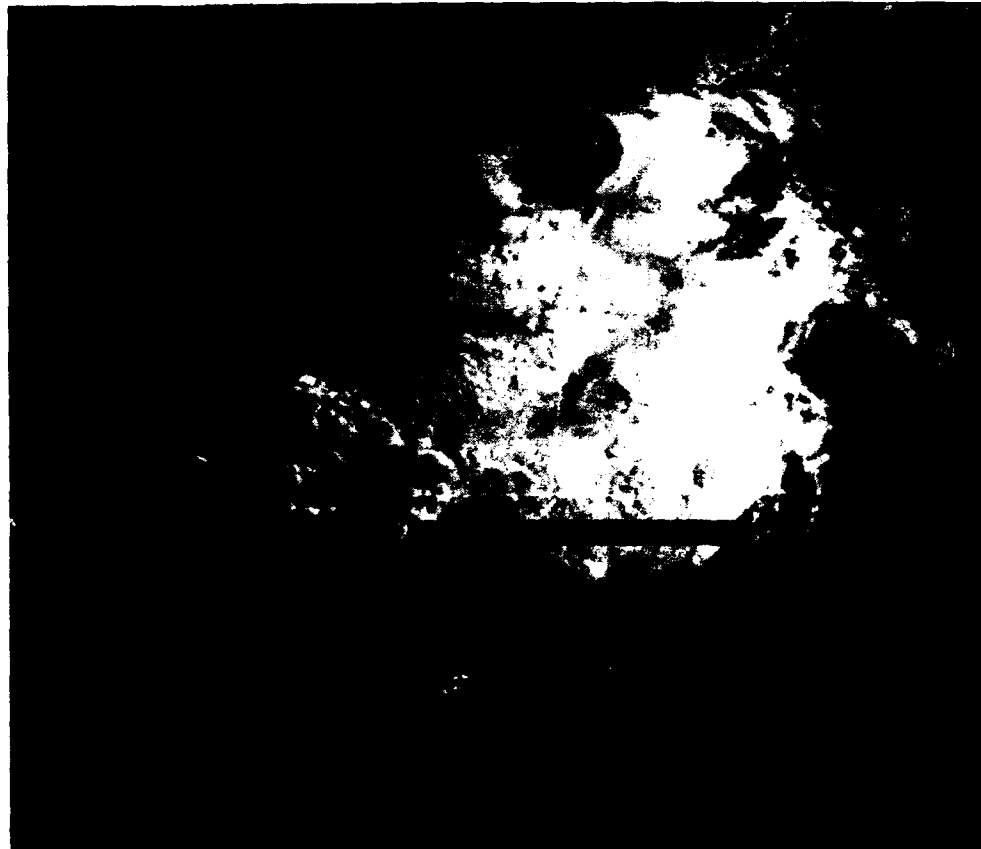


Figure 3.4: Visible Geostationary Satellite Imagery of the Mount Pinatubo Eruption - 0630 Local Time 15 June 1991 (courtesy of ENS Scott Oswalt, USN)

Climatologists were studying the continuing global and climatic effects of the volcanic debris still circling the earth in the stratosphere a year after the June 1991 eruptions. Figure 3.5 shows the ash cloud emanating from Mount Pinatubo 10 hours after Fig. 3.4. Note that the ash cloud already extends out radially more than 200 nm, as far south as Mindoro and north to the Luzon Strait. This image taken at 1630 local time depicts the great height of the ash cloud by the shadows cast to the northeast and east of the cloud.

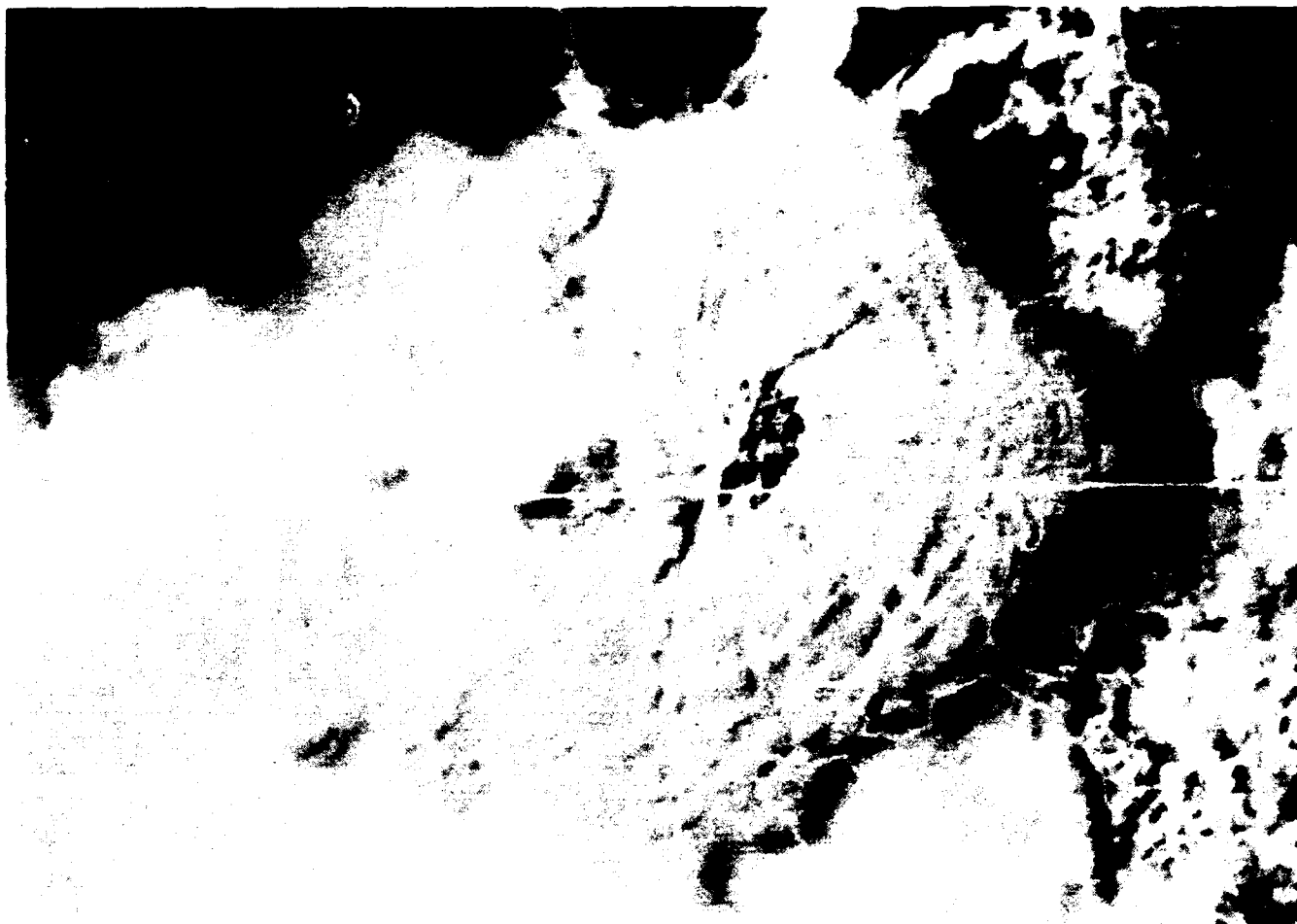


Figure 3.5: Visible Geostationary Satellite Imagery of the Mount Pinatubo Eruption - 1630 Local Time 15 June 1991 (courtesy of ENS Scott Oswalt, USN)




Further evidence of the destructive power of such a major eruption is given by the aerial view in Fig. 3.6. Note that the lush tropical growth on the surrounding mountains appears to be covered by many feet of deposited ash.



Figure 3.6: Aerial View of Mount Pinatubo after the Eruption (courtesy of ENS Scott Oswald, USN)

Typhoon Becky, 20-30 August 1990

The tropical disturbance that eventually became Typhoon Becky originated within the surface monsoon trough (not shown), when upper-level divergence (associated with a TUTT to its north) developed. As the final best track in Fig. 3.7 indicates, Typhoon Becky followed a near westward track during its lifetime, although the Philippine forecaster may have anticipated that the typhoon might recurve as it was upgraded to a tropical storm at 0000Z on 25 August (see Fig. 3.7). Sixty hours earlier, the deep layer mean circulation analysis (another product provided to JTWC by FNOC) displayed in Fig. 3.8 showed Becky approaching southerly steering flow over the Philippine Islands with a low center⁸ present over southeastern China, west of Taiwan. However, by 1200Z on 25 August (Fig. 3.9) the deep layer mean circulation analysis showed that the trough had moved eastward and filled (weakened), as it became the neutral point, just southwest of Japan. Thus Becky came under the influence of stronger westward steering and accelerated, making landfall on the northern Luzon coast while moving at 12 kt (see Fig. 3.7).

⁸Comparisons between pressure analyses and streamline analysis: (L)ow = (C)yclonic center; (H)igh = (A)nticyclonic center; Col = Neutral point .  = Tropical Storm symbol and  = Typhoon symbol.

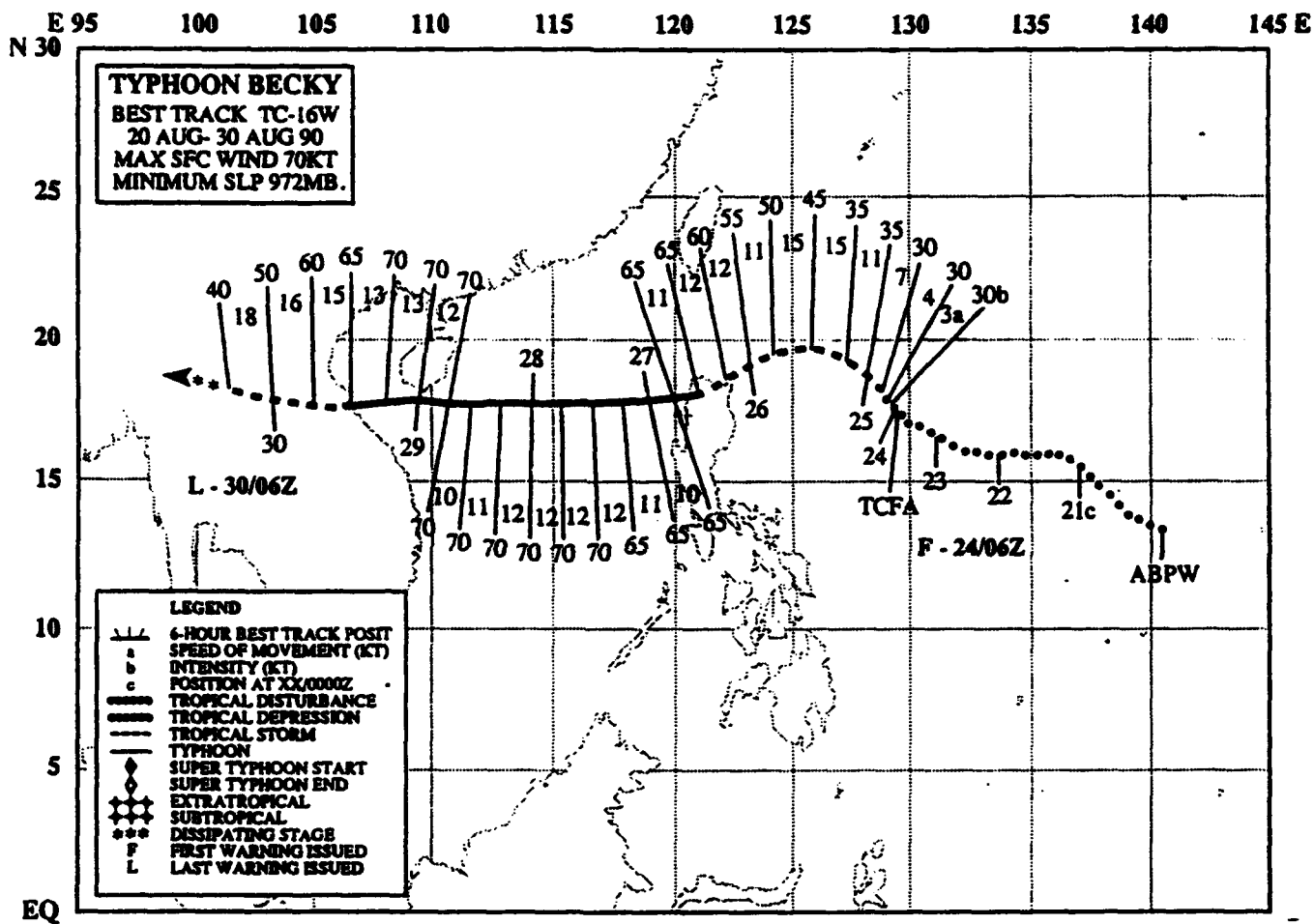


Figure 3.7: Official Best Track of Typhoon Becky (adapted from U.S. NOCC/JTWC 1991)

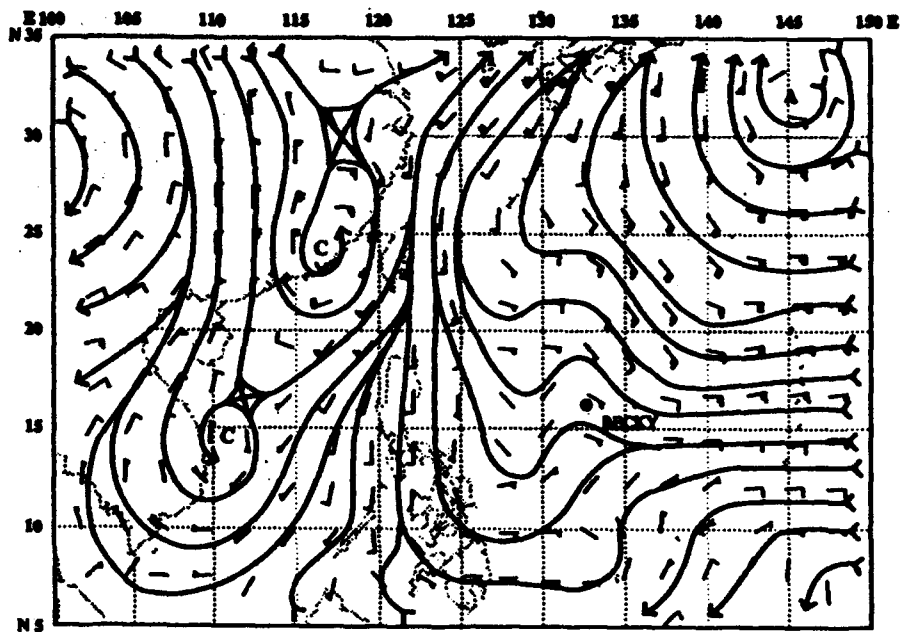


Figure 3.8: Deep Layer Mean Circulation Analysis for 221200Z August 1990 (adapted from U. S. NOCC/JTWC 1991)

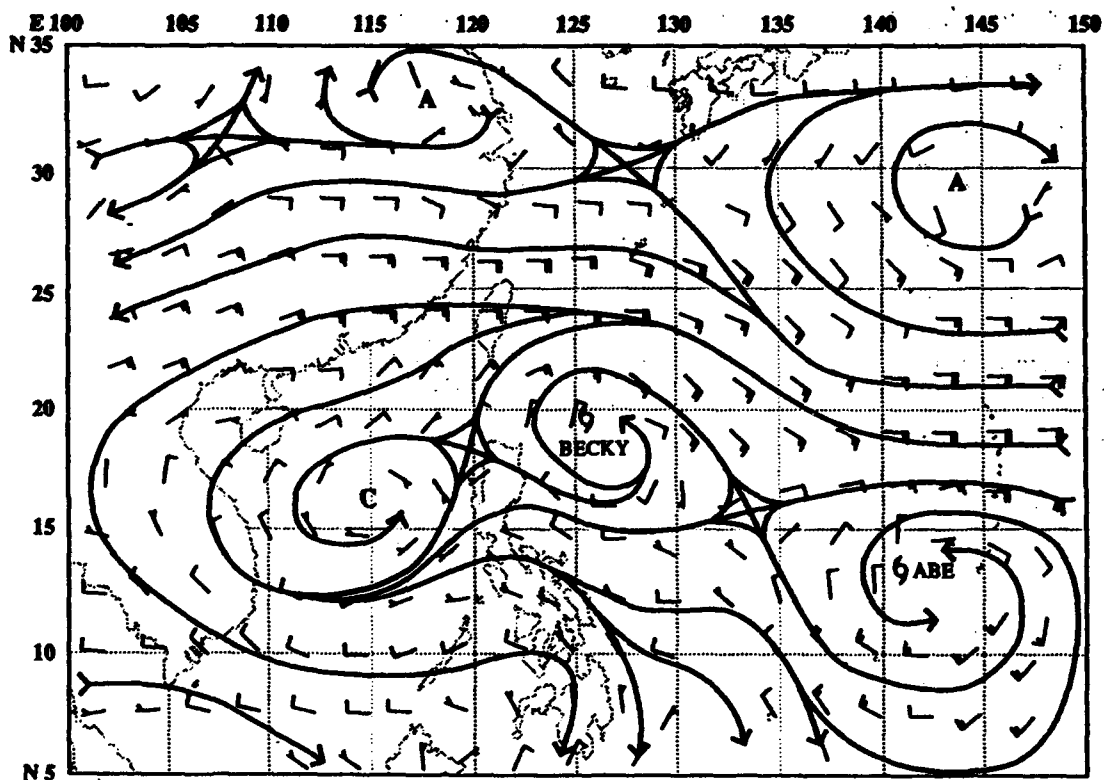


Figure 3.9: Deep Layer Mean Circulation Analysis for 251200Z August 1990 (adapted from U. S. NOCC/JTWC 1991)

A close examination of the best track (Fig. 3.7) reveals that Becky was upgraded to typhoon intensity at 261200Z while over land, based upon the appearance of a 10-nm eye (not shown) (U. S. NOCC/JTWC 1991). However, a contradiction appears to exist since JTWC also reports that Becky had reached minimum typhoon intensity in the Defense Meteorological Satellite Program (DMSP) visible image (Fig. 3.10) earlier at 260039Z. Consequently, there may have been other factors (synoptic reports, etc.) that dictated a delay in the formal upgrade. While this appears contradictory to the expected weakening due to friction at landfall, other environmental factors may have been dominant. Certainly in this case much of the spiral band of cloudiness associated with Typhoon Becky remained over water during its short six-hour track over northern Luzon.

Figure 3.11 displays the summary of all official JTWC warnings for Becky. The JTWC warning tracks were slow in predicting that Becky would track toward the southwest and strike northern Luzon. This failure was probably attributed to an underestimation of the strength of the ridge (which had followed the trough eastward across China, and intensified). Note that the TC performed characteristically as described in Appendix B (Shoemaker 1991), i.e., having approached the PI moving toward the southwest, the TC turned more westward after landfall. The typhoon also followed Shoemaker's rule that TCs moving 15 kt or slower experience little change in speed of motion. Note, however, that Typhoon Becky's time over land was only about six hours.

As a result of Typhoon Becky's passage, 32 people were reported killed, and thousands were forced to evacuate due to heavy flooding in northern Luzon (U. S. NOCC/JTWC 1991).

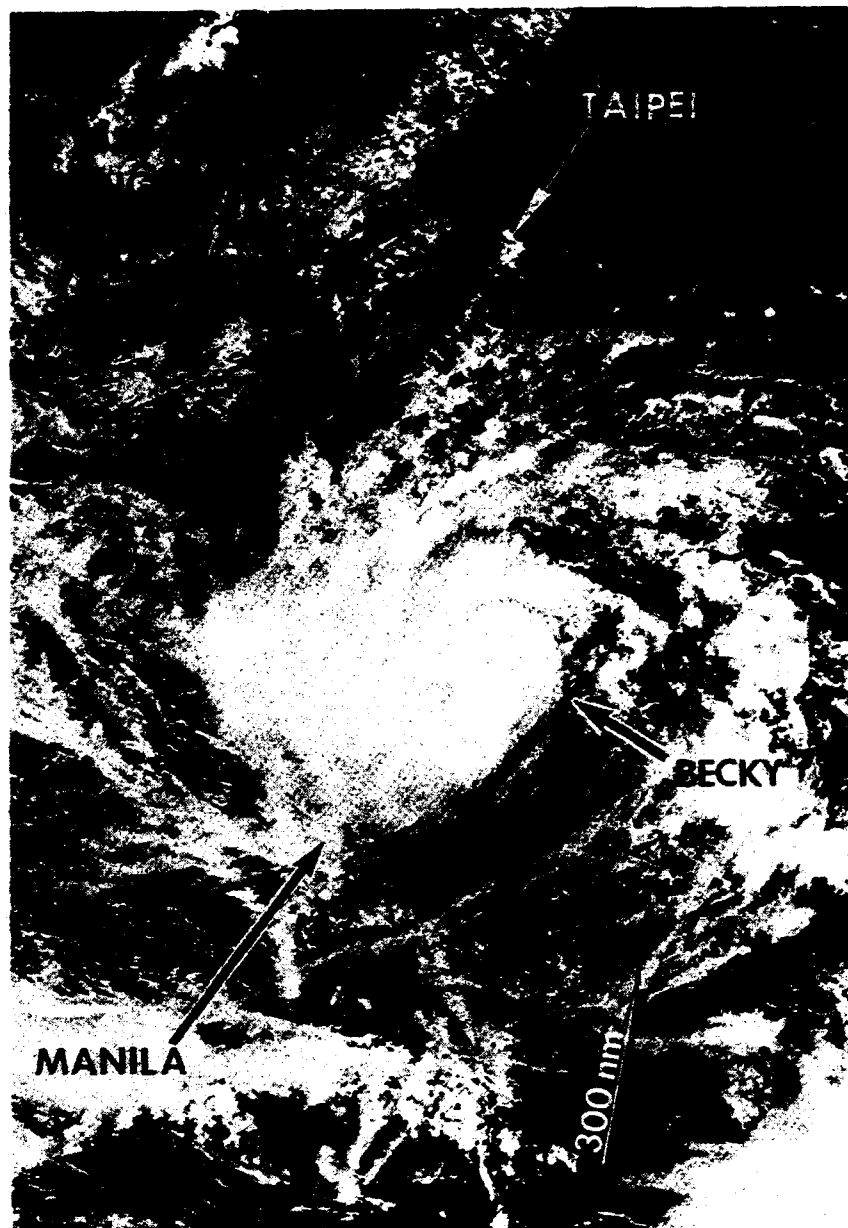


Figure 3.10: Typhoon Becky Reaches Minimum Typhoon Intensity just as it approaches northern Luzon (260039Z August DMSP visible imagery) (adapted from U. S. NOCC/JTWC 1991)

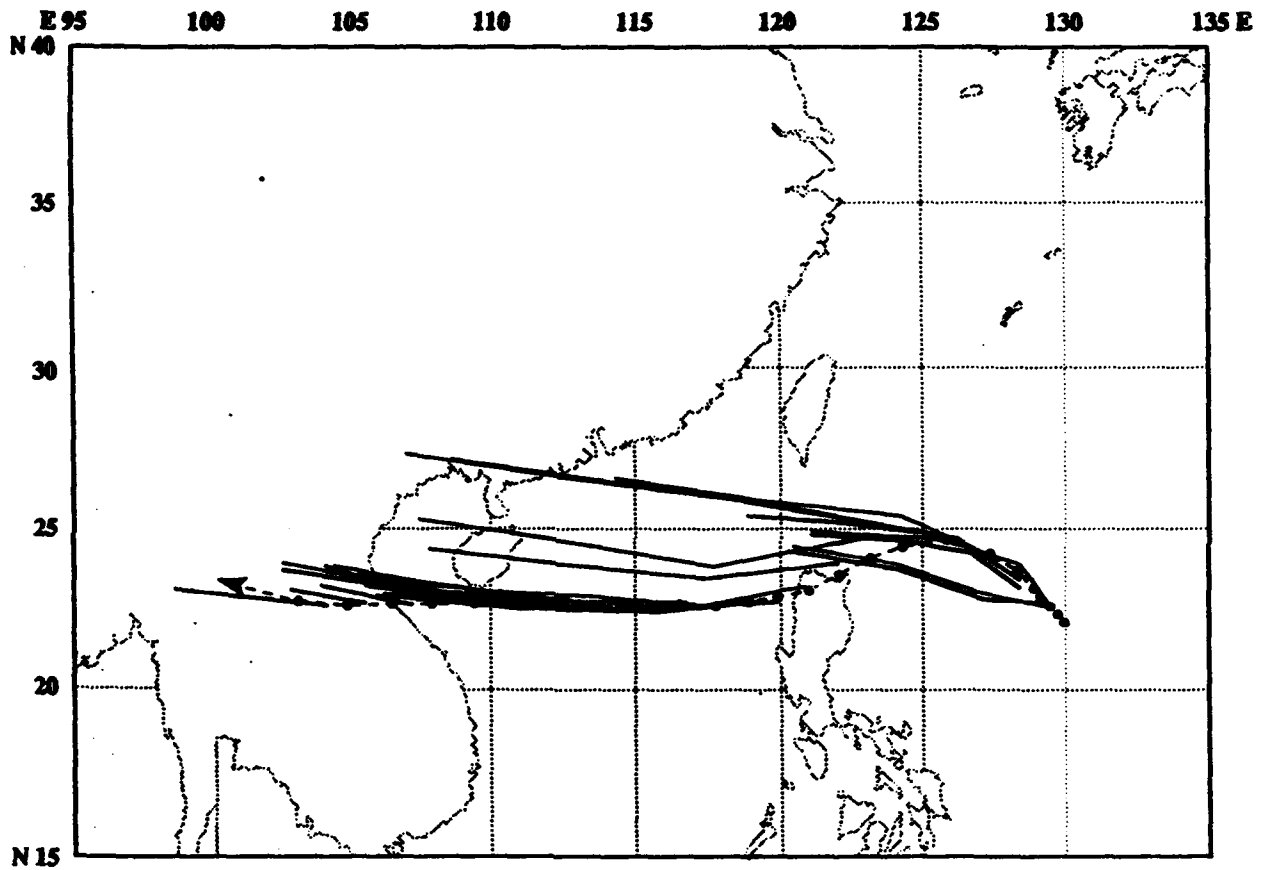


Figure 3.11: Summary of JTWC Forecasts (solid lines) for Becky superimposed on the Final Best Track (dashed lines) (adapted from U. S. NOCC/JTWC 1991)

3.4.2 Tropical Storm and Super Typhoon Striking The Visayas

Tropical Storm Thelma, 27 October–08 November 1991

TS Thelma is described to emphasize that tropical cyclones that do not attain typhoon intensity can still be deadly. Tropical Storm Thelma caused the worst loss of life due to natural disaster in the western North Pacific during 1991. An estimated 6000 people perished and 20,000 people were left homeless resulting from the passage of the tropical storm.

After persisting for four days as a tropical disturbance, Thelma was made the subject of a Tropical Cyclone Formation Alert (TCFA) at 311900Z October 1991 (see Fig. 3.12). Following a satellite-derived intensity report of 25 kt, Thelma became the 27th tropical cyclone of the western North Pacific for 1991, as a Tropical Depression Warning was issued at 1200Z on 1 November 1991. Approximately one week after being detected as a disturbance, Thelma was upgraded to a Tropical Storm (35 kt) at 031200Z. Simultaneously, the tropical cyclone commenced a track toward the west-southwest. Thelma made landfall on the island of Samar at approximately 041800Z, and continued on a course toward the southwest until 051200Z. As recalled by the author, the satellite imagery depicting Thelma was unimpressive, i.e., a forecaster might mistakenly expect no serious results from its passage. However, torrential rains dumped an estimated 6 inches of water in 24 hours, as the tropical storm passed over the island of Leyte. It is noted that the estimated winds had decreased to 40 kt over Leyte (see Fig. 3.12), just six hours after making landfall on Samar, and the maximum sustained winds remained at 35 kt as it finally departed the PI, moving westward from central Palawan.

The catastrophic events resulting from the passage of Tropical Storm Thelma—despite its never attaining typhoon strength—were attributed to widespread logging (stripping the hills bare of vegetation) in recent years above the port city of Ormoc on Leyte Island. Ormoc, lying approximately 25 nm southwest of Tacloban (see Fig. 1.1) experienced the effects of a dam failure, landslides and extensive flash flooding (U. S. NOCC/JTWC 1992)

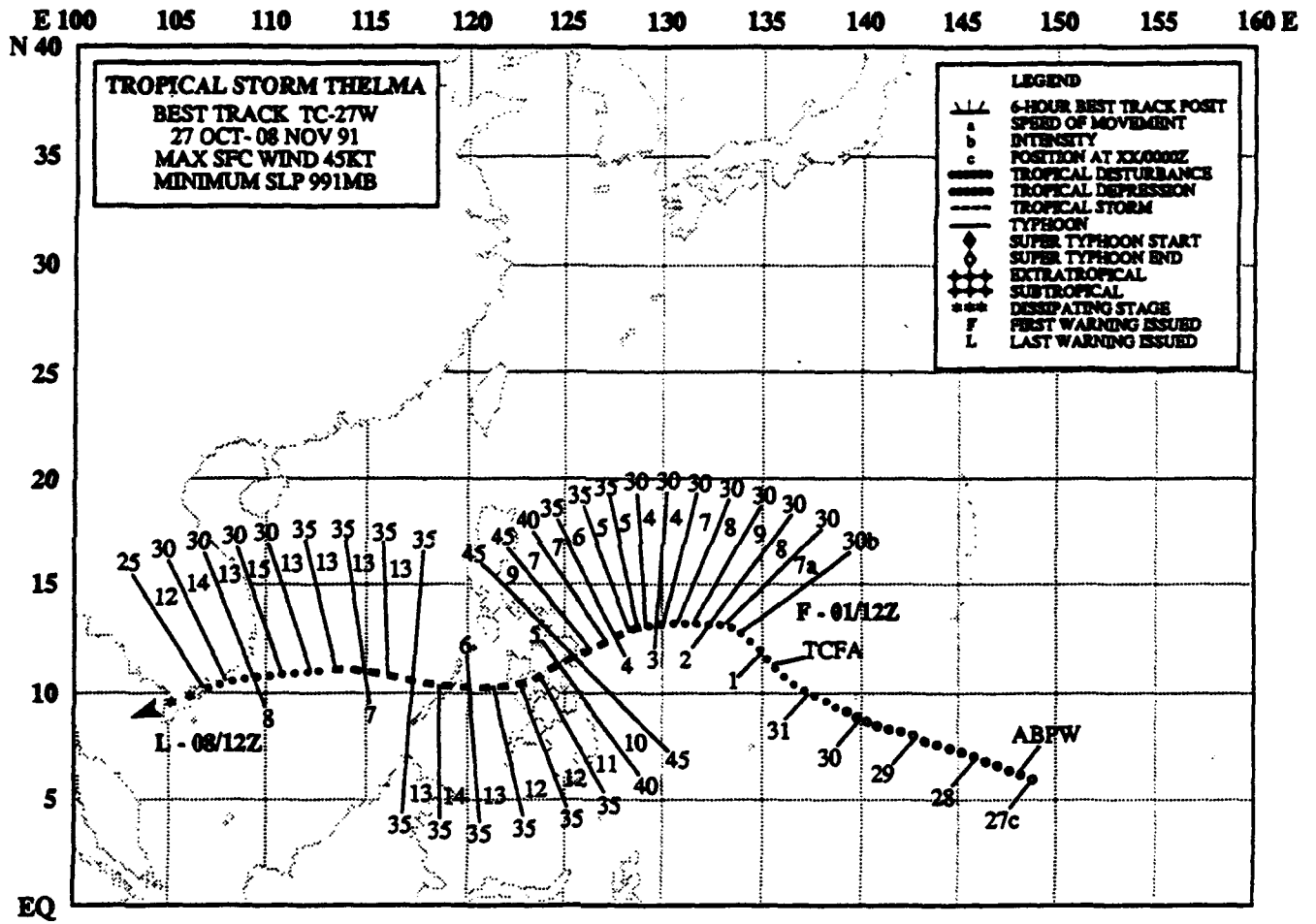


Figure 3.12: Official Best Track of Tropical Storm Thelma (adapted from U.S. NOCC/JTWC 1992)

As depicted in Fig. 3.13, the initial JTWC warnings on Thelma predicted recurvature. Objective aid guidance available to JTWC was split between recurvature and non-recurvature forecasts. A quick inspection of the figure also indicates the predominance of "persistence" forecasts, i.e., forecasting the continuation (or persistence) of the past motion vectors.

In retrospect, Beta advection models (such as FBAM) (not shown) exhibited some limited skill in providing early prognosis of the west-southwestward movement of Thelma that occurred for approximately 48 hours, after 031200Z (U. S. NOCC/JTWC 1992). Note, that Thelma followed the Thumb Rule (Section 2.3.2) that TCs approaching the PI, moving southwestward, tend to move more westward—at least Thelma moved westward, starting at 051200Z. However, Thelma's general west-southwestward track for 48 hours, between 031200Z and 051200Z, exceeded the 18–24 hours expected for a west-southwest track in the Thumb Rules.

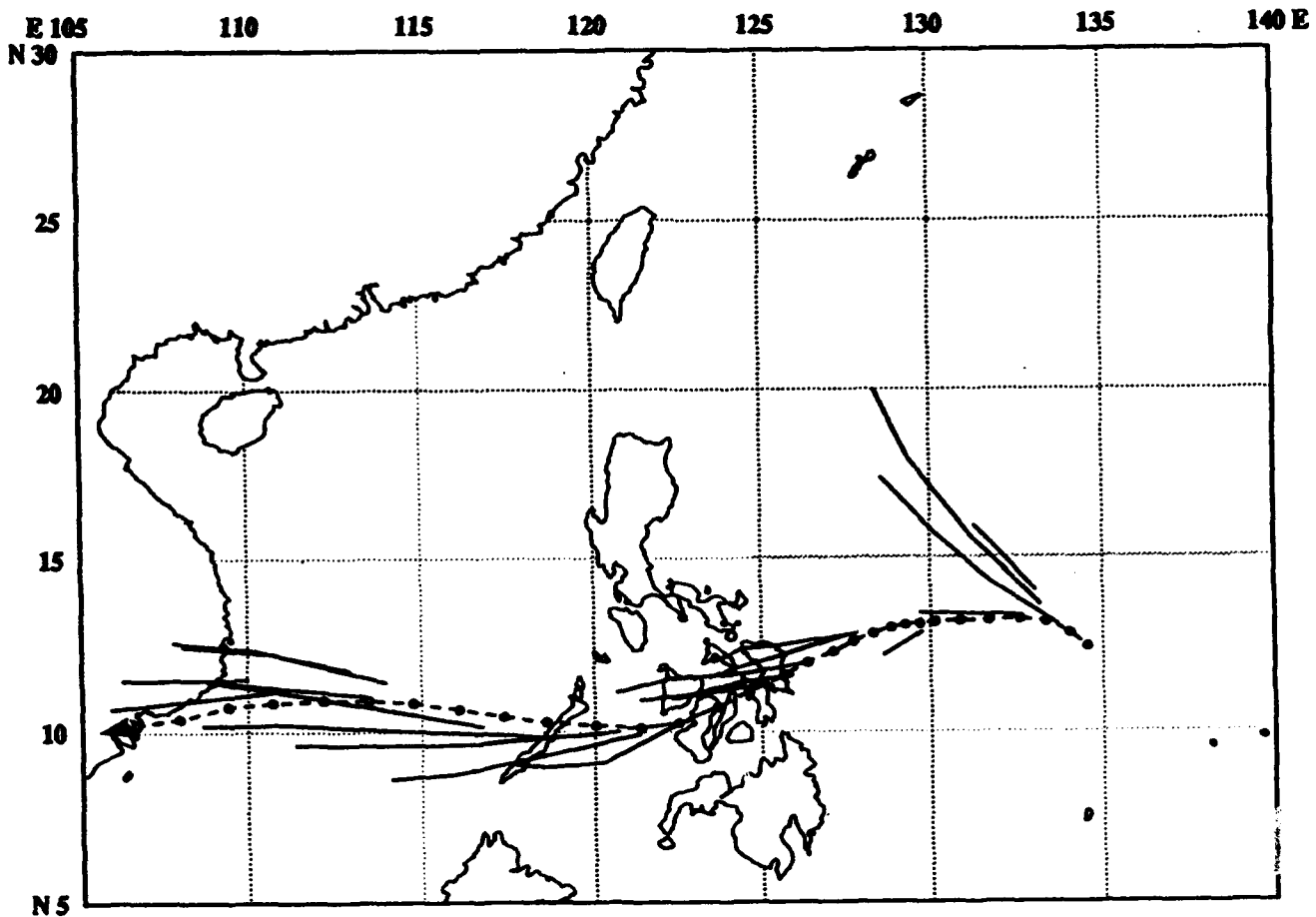


Figure 3.13: Comparison of the JTWC Official Forecasts (solid lines) issued for Thelma superimposed on the Final Best Track (dashed lines)(adapted from U. S. NOCC/JTWC 1992)

Super Typhoon Mike, 6–18 November 1990

The reader must keep in mind that the title of a tropical cyclone indicates the strongest intensity during its history. Thus a tropical cyclone could be *only* a typhoon, tropical storm or less while passing over the Philippine Islands, yet be a super typhoon before or after hitting the PI. As shown in Fig. 3.14 Super Typhoon Mike decreased from a super typhoon to a typhoon at 1200Z on 12 November 1990, just before making landfall in Leyte. Nevertheless, in this instance the commercial and transportation capital of the region, Cebu (see Fig. 1.1)—while appearing to be protected by its interior position—received severe damage.

Mike, which had tracked generally west-northwestward since its first warning at 071200Z, slowed to a speed of motion of only 5 kt, dipped to the southwest, developed a 15 nm eye and intensified rapidly to super typhoon strength at 101200Z. Providing divergence aloft were dual outflow channels carrying mass out of the center of the TC (not shown). One channel led to a 200-mb trough to the northeast, while the other crossed the Equator to the Southern Hemisphere. Resuming its track toward the northwest and passing only to within 45 nm of Koror a couple of hours later, the super typhoon caused extensive damage to this island east of Mindanao near 7.5°N, 134.5°E.

With the increased friction provided by the mountainous island chain in the path of the super typhoon, the weakening of Mike was revealed on satellite imagery by a ragged and cloud-filled eye. This change in the satellite imagery prompted the downgrading of Mike to a typhoon before the TC made landfall on Leyte, with maximum sustained winds of 120 kt winds, shortly before 121800Z. Mike then remained a typhoon while crossing the PI and the South China Sea (see Fig. 3.14).

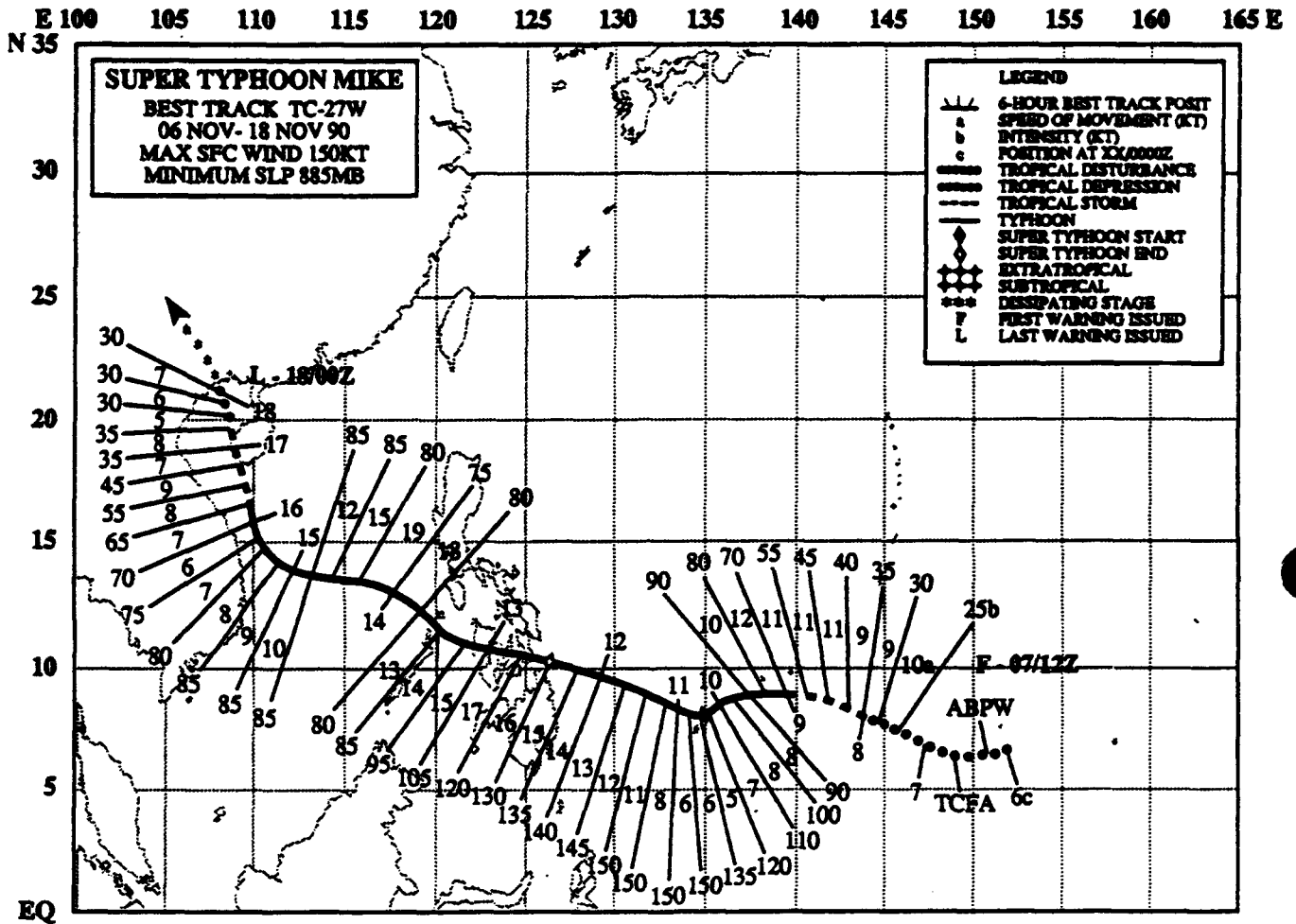


Figure 3.14: Official Best Track of Super Typhoon Mike (adapted from U.S. NOCC/JTWC 1991)

Figure 3.15 displays the JTWC official forecasts in comparison with the eventual best track of Mike. Earlier forecasts that the tropical cyclone would miss the PI, were prompted by objective aids guidance, including NOGAPS, that a weakness would develop in the ridge, just east of the Luzon, permitting a more northwesterly track. Fortunately, at 120000Z, the NOGAPS prognostics changed to predict a stronger subtropical ridge north of Mike. This supported JTWC's west-northwest forecast tracks across the central PI for about 18 hours preceding landfall.

Super Typhoon Mike was the most powerful typhoon to strike the Philippine Islands during 1990, and the most devastating since 1981. At least 250 people were dead or missing, mostly from landslides, while 2 million people were forced into temporary shelters. Over 37,000 houses were destroyed, and at least \$ 14 million damage recorded. More than 57 water craft, mostly in the port of Cebu, sank (U. S. NOCC/JTWC 1991).

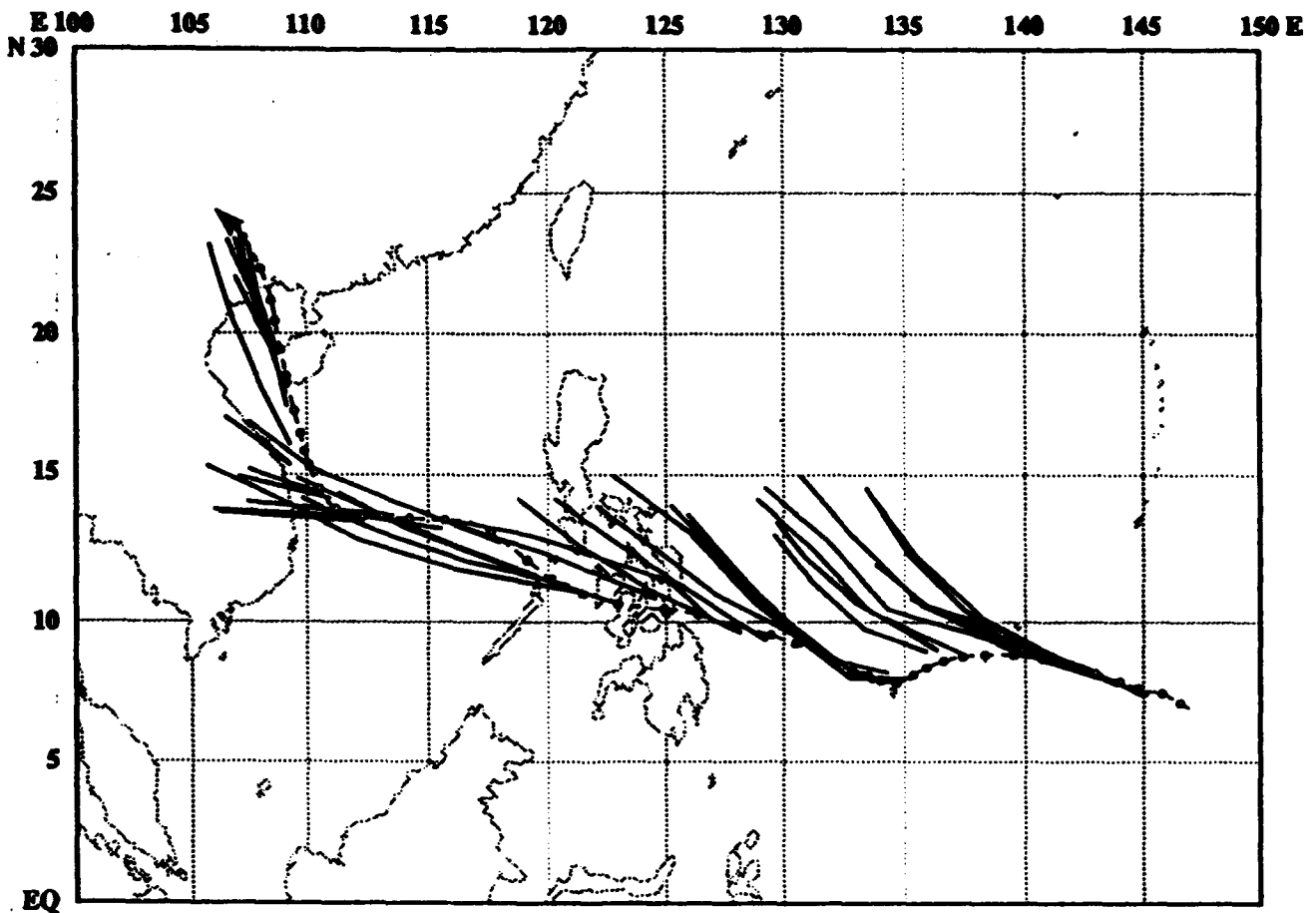


Figure 3.15: Comparison of the JTWC Official Forecasts (solid lines) issued for Mike superimposed on the Final Best Track (dashed lines)(adapted from U. S. NOCC/JTWC 1991)

To date, the forecasting of tropical cyclone intensity remains one of the most difficult tasks. Accordingly, it is encouraging to note that the rapid intensification of Mike—even to the super typhoon stage—was very ably performed by JTWC. Section 3.3.3 introduced the Dvorak technique of analyzing and forecasting TC intensity and discussed the Current Intensity Number (CI). Figure 3.16 shows impressive warning intensities compared to the final best track intensities during the greater than normal rate of intensification of Mike between 081200Z and 101800Z (U. S. NOCC/JTWC 1991).

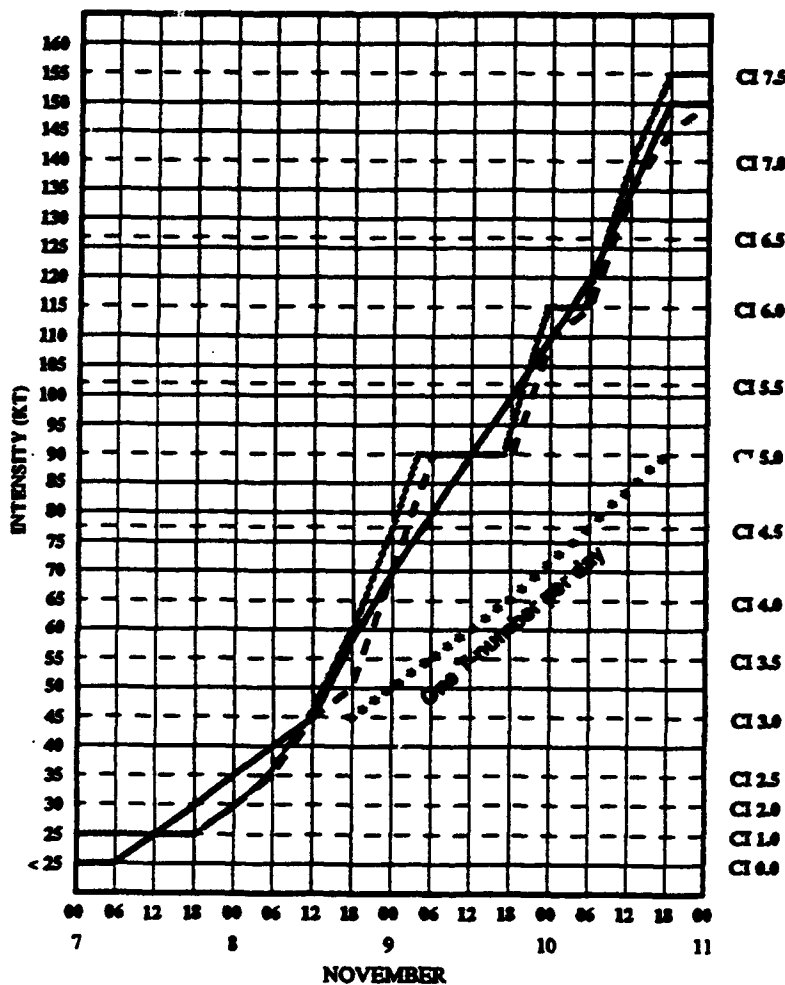


Figure 3.16: Plots of the Satellite Current Intensity Values (dotted line), Actual Warning Intensities (dashed line) and Final Best Track (solid line) on a Time-Intensity Comparison Chart for Mike. The normal development of one T-number per day (starred line) is included as a reference (U. S. NOCC/JTWC 1991).

3.4.3 Tropical Cyclones Striking Mindanao

While rare, Mindanao can get hit—typically by small, but intense typhoons. Typhoon Ike, with 115 kt winds in 1984, killed over 1000 people and caused considerable destruction near Suragao. During 1990 and 1991, only two tropical cyclones struck Mindanao, and with only very minimal impact. The nearness of Mindanao to the Equator (and the commensurate small value of f) reduces the likelihood of tropical cyclones affecting the island. Also, the monsoon trough moves poleward during the Northern Hemisphere summer, and thus removes this TC genesis region from the vicinity of Mindanao, until its return in late fall. The departure of the monsoon trough during the Northern Hemisphere summer, combined with the sparsity of TC passages, provides much of the island with less than 100 inches of rain per year (see Appendix C). There are exceptions such as at Hinatuan, located on the northeast coast (see Fig. 1.1), where the northeast trade wind enhances its average rainfall to about 175 inches. Nevertheless, the island, in its position so near to the Equator, was covered with cloudiness during a majority of the time during the past two years. Appendix C indicates that all the stations (except one) in Mindanao have an average cloud cover of 6 octas (6/8). Although they are not discussed in detail, the only two TCs to affect Mindanao during 1990 or 1991 are shown in Figs. 3.17(a)&(b).

Typhoon Marian, 9–20 May 1990

Marian was the only significant tropical cyclone to form in the western North Pacific Ocean during May 1990. After forming southeast of Koror, Marian moved toward 280° , passing over the southern tip of Mindanao four days later—still as a disturbance (see Fig. 3.17(a)). Its delay in development was attributed to restricted outflow aloft, and then to interaction with Mindanao to inhibit low-level development. From its inception, Marian traveled about 1200 nm before being designated a tropical depression when the first warning was issued at 150600Z May, as it passed by Palawan. Marian then tracked around the western end of the subtropical ridge (not shown) into the South China Sea, becoming a typhoon and later recurving to strike Taiwan as it was caught up in an approaching cold front and commenced extratropical transition.

Super Typhoon Owen, 14 November–5 December 1990

While Owen was both the longest lasting and one of the most interesting tropical cyclones (the 30th designated) of 1990, it reached Mindanao in its dying (or dissipating) stage (see Fig. 3.17(b)). As the figure shows, Owen actually developed as a convective cluster east of the dateline, 860 nm southwest of Hawaii on 14 November. Owen attained super typhoon status twice, once on 23 November when it slowed to a forward speed of only 4 kt (similar to Super Typhoon Mike described earlier, before it hit Visayas) and again on 27 November when it was moving faster at a speed of 10 kt. Owen caused extensive property and crop damage (plus 2 deaths) during its long track through islands and atolls, but no damage to Mindanao (U. S. NOCC/JTWC 1991).

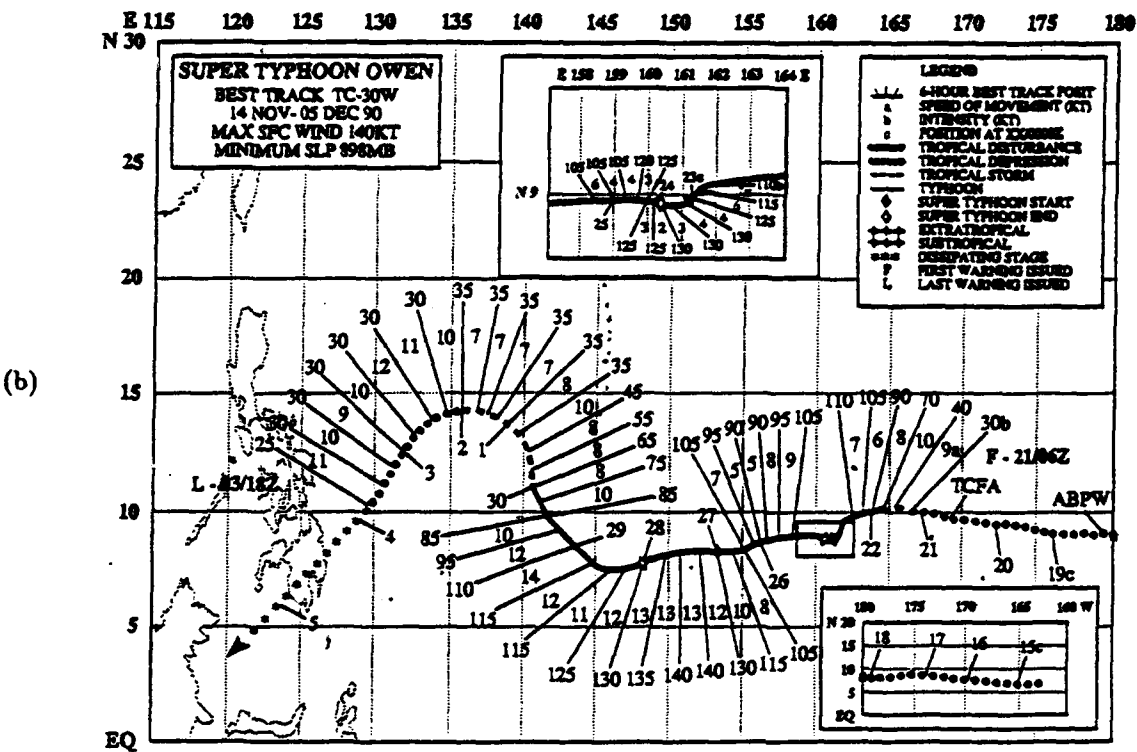
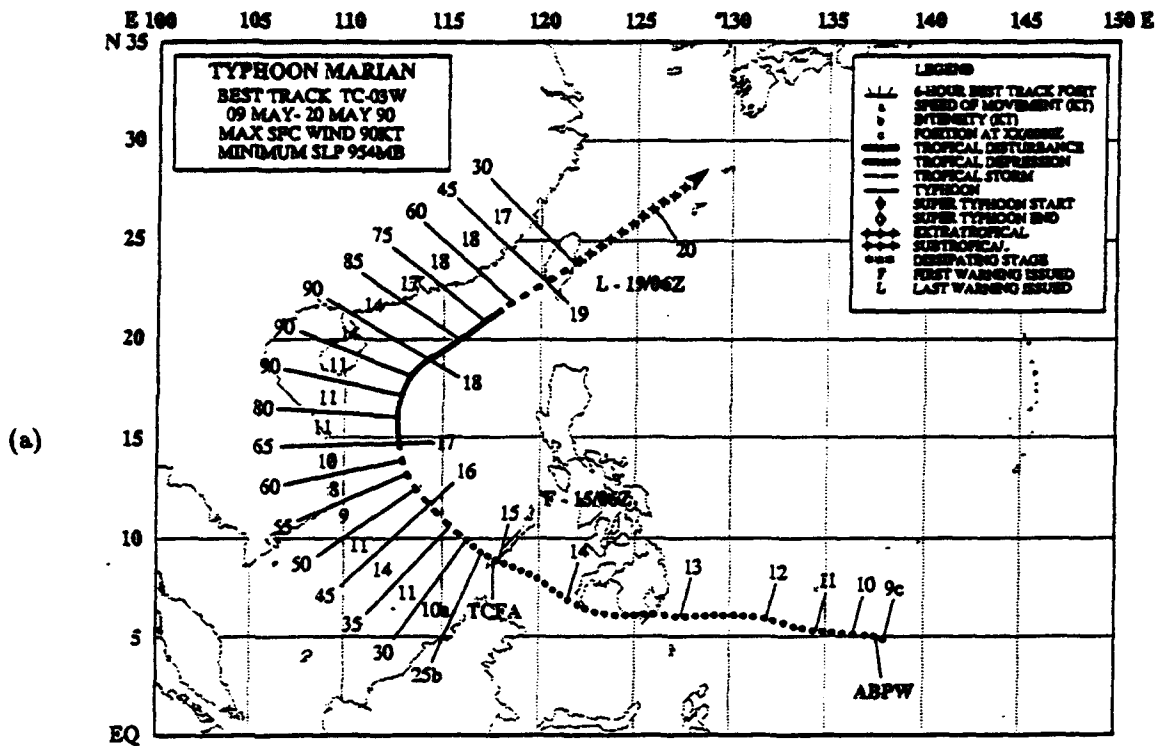


Figure 3.17: Official Best Track of Typhoon Marian (a) and Super Typhoon Owen (b) (adapted from U.S. NOCC/JTWC 1991)

3.5 Case Studies using NOGAPS

This section presents the products of the Navy Operational Global Atmospheric Prediction System's (NOGAPS) spectral forecast model⁹ produced by the Fleet Numerical Oceanography Center (FNOC). The primary purpose of this section is to evaluate analyses and prognoses produced by NOGAPS during typhoons, surges and shear line (frontal) events affecting the Philippine Islands. The case studies presented are from 1992, following the implementation of NOGAPS 3.3 in January 1992. Thus, the performance—specifically, the performance in the tropics—of the current NOGAPS model can be examined.

The bulk of the products presented during the following case studies were obtained in real time remotely via the Navy Oceanographic Data Distribution System (NODDS), also developed by the Fleet Numerical Oceanography Center (FNOC 1991). This system permits the user to effortlessly “down-load” meteorological, oceanographic and acoustical FNOC products, via a microcomputer (personal computer or “PC”)¹⁰ twice a day¹¹. Products, including analyses and prognoses to 72-h¹², are selected via “user-friendly” menus. Real time radiosonde soundings are available, and since early 1992, the latest delivery system (NODDS 3.0) has also provided Defense Meteorological Satellite Program (DMSP) visual and infrared (IR) imagery (Conlee 1991) for six northern hemisphere mercator projections, one of which is the western North Pacific Ocean region including the Philippine Islands.

While the NODDS products are enhanced when viewed on the VGA color monitor—on which as many as three analyses/prognoses can be superimposed in different colors, or a sequence of up to four images “looped” (animated)—, the following case studies contain only black and white (or grey shade¹³) copies, available via a laser printer. Unfortunately, the presented copies do not have the enhanced visual quality of the NODDS products viewed on the VGA color monitor by the operational user.

⁹The NOGAPS spectral model has a horizontal resolution of 79 wave triangular truncation (T79), corresponding to a 1.5° transform grid, and 18 levels in the vertical (Hogan and Rosmond 1991). The latest model, (NOGAPS 3.3), includes improvements in the moisture variables, radiation physics and diffusion. This version runs 10% faster and removes some of the major systematic errors present in earlier versions.

¹⁰The PC should be minimally an IBM AT class Intel 80286 based computer (or clone), having a 2400 baud communication modem, a math-coprocessor, a “mouse”, a VGA (Video Graphics Array) color monitor, and a dot-matrix or laser printer.

¹¹0000Z (or 0000 UTC) and 1200Z (or 1200 UTC) synoptic-time runs

¹²Sea-level pressure and 500-mb height prognoses are available to 120-h.

¹³Case studies of DMSP satellite images were prepared for the handbook using PIZAZZ software to produce black and white copies of the color monitor.

3.5.1 Typhoon Eli, 9-13 July 1992

Figure 3.18 shows the path^{14 15} taken by Typhoon Eli as it crossed Luzon on 11 July 1992.

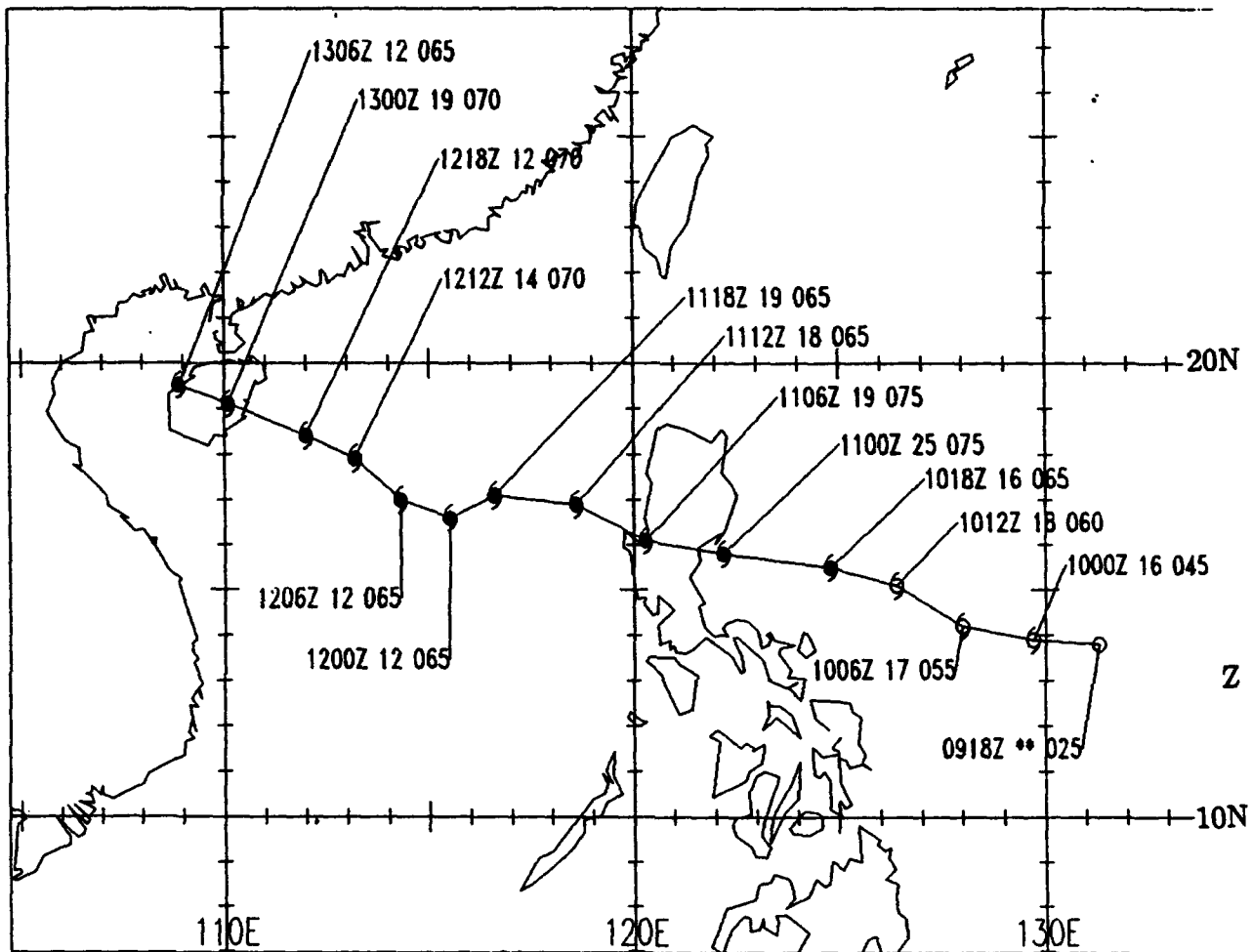


Figure 3.18: Working Best Track of Typhoon Eli. The position labels provide (1) time of warning position, (2) speed (kt) of movement during the previous 6 hours and (3) maximum sustained (one-minute average) wind.

¹⁴The track shown is the "working" best track. The positions along this track are those used to issue warnings by JTWC. The "final" best track will be determined when all relevant data are gathered after the typhoon season. This track was also obtained remotely in "real time" via an interactive computer program. The program, the Automated Tropical Cyclone Forecasting System (ATCF) was developed by the Naval Environmental Prediction Research Facility (now the Naval Research Laboratory, Monterey) under the guidance of Mr. Ron Miller, following a plan conceived by LT Brian Williams, USN. The capabilities of ATCF (see Miller et al. 1989) include (but are not limited to) computer-driven menus providing the Typhoon Duty Officer (TDO) with "mouse"-controlled graphics to (1) locate (or "fix") the position of the tropical cyclone, (2) plot objective aid forecasts (which the TDO uses as guidance for preparing the warning), (3) create the warning positions and wind radii, and (4) compose the tropical cyclone warning message.

¹⁵The track of Typhoon Eli is not shown after 0600Z on 13 July.

9 July 1992

A Tropical Cyclone Formation Alert (TCFA) was issued by JTWC at 1100Z on 9 July noting winds of 20 to 30 kt, with a circulation center, near 13.5°N, 134.8°E (point "Z" on Figs. 3.18, 3.19 and 3.20), moving westward at 17 kt. The TCFA commented on the presence of improved convective organization (Fig. 3.19), a low level circulation center (evident from the island station reports and the ship reports in the Philippine Sea in Fig. 3.20), and upper level anticyclonic cirrus outflow indicating that the system was located near a low (vertical) shear region—circulation features were available to forecasters at JTWC via animated visible and infrared geostationary satellite data. Sea surface temperatures were quite warm and further development likely.

Figures 3.21(a) and (b) are 1200Z radiosonde soundings¹⁶ (received via NODDS in real time) from the island stations of Yap (PTYA, WMO station 91413) and Koror (PTRO, WMO station 91408) east of Mindanao (see Fig. 3.20). The low-level southerly flow and the large moisture content in the vertical are supportive of the incipient tropical cyclone.

Four hours later at 1600Z¹⁷, Cubi Point NAS (RPMB, WMO station 98426) and Manila International Airport (RPMM, WMO station 98429) on Luzon were reporting temperatures/dewpoints¹⁸ of 27/20 and 28/25 respectively, with light winds from the east (land breeze) and scattered low clouds (not shown). Cubi Point NAS also had Thunderstorm Condition 2 set¹⁹. While Mactan International Airport on Cebu (RPMT, WMO station 98646) in Visayas reported temperatures of 27/20, a light northerly wind (land breeze) and broken multi-level clouds—note that this cloudiness over Visayas was evident 3 hours earlier on Fig. 3.19.

At 1800Z, eventual Typhoon Eli was designated the fifth tropical cyclone in the western North Pacific Ocean of the year (05W), and a Tropical Depression Warning was issued when the cyclone's sustained winds reached 25 kt. The warning announced that the TD was moving rapidly westward as it intensified, and that it would strike the east coast of Luzon with 60 kt winds in 36 hours (at 110600Z) near 15.4°N, 121.8°E. Note that this first warning was only about 30 nm to the south of the point of eventual landfall, although the actual landfall was about 4 hours earlier (see Fig. 3.18).

¹⁶Until the eruption of Mount Pinatubo in June 1991, 0000Z and 1200Z soundings were available from Clark AB. Soundings were then available from the Cubi Point Naval Air Station but ceased in early 1992, when preparations for its eventual closing commenced. (The soundings displayed on the VGA monitor are larger and in color.)

¹⁷The Philippine Islands are in the H Time Zone, i.e., 8 hours ahead of Zulu Time, thus 1600Z = 2400 Local (midnight).

¹⁸Temperatures are in degrees Celcius.

¹⁹Thunderstorm Condition 1 (T1) = Thunderstorms are within 5 miles of the station, possible at the station within one hour. Thunderstorm Condition 2 (T2) = Thunderstorms possible within 6 hours—commonly set during the southwest monsoon.

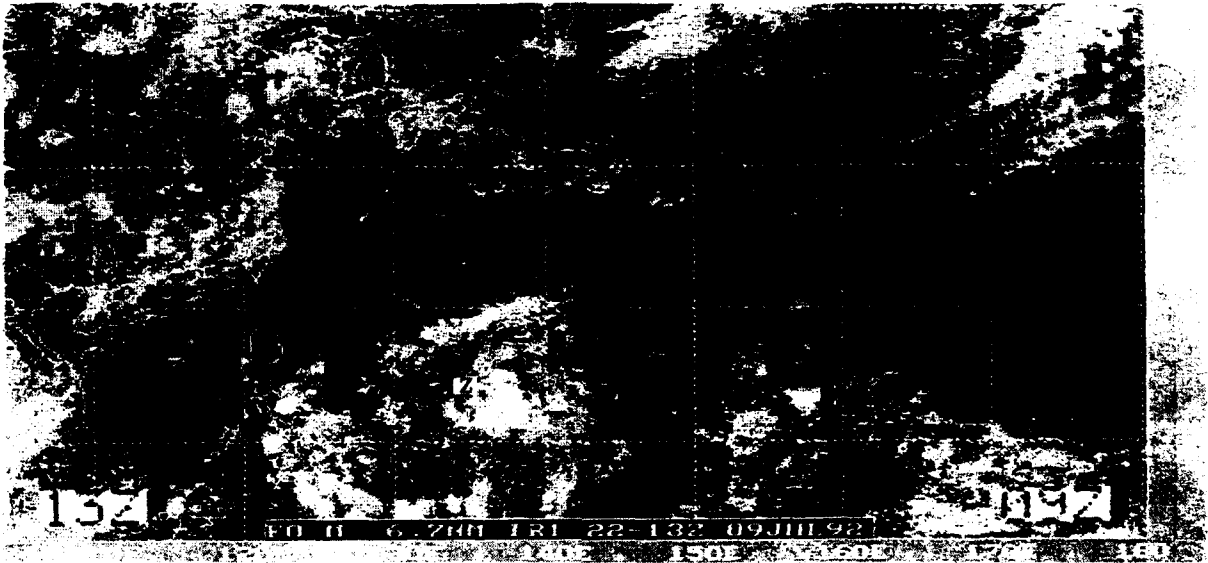


Figure 3.19: NODDS Mosaic of DMSP Infrared Satellite Imagery from 2200Z 8 July-1300Z 9 July 1992. (13Z in the lower left corner indicates that the swath nearest the PI occurred at 1300Z 9 July.)

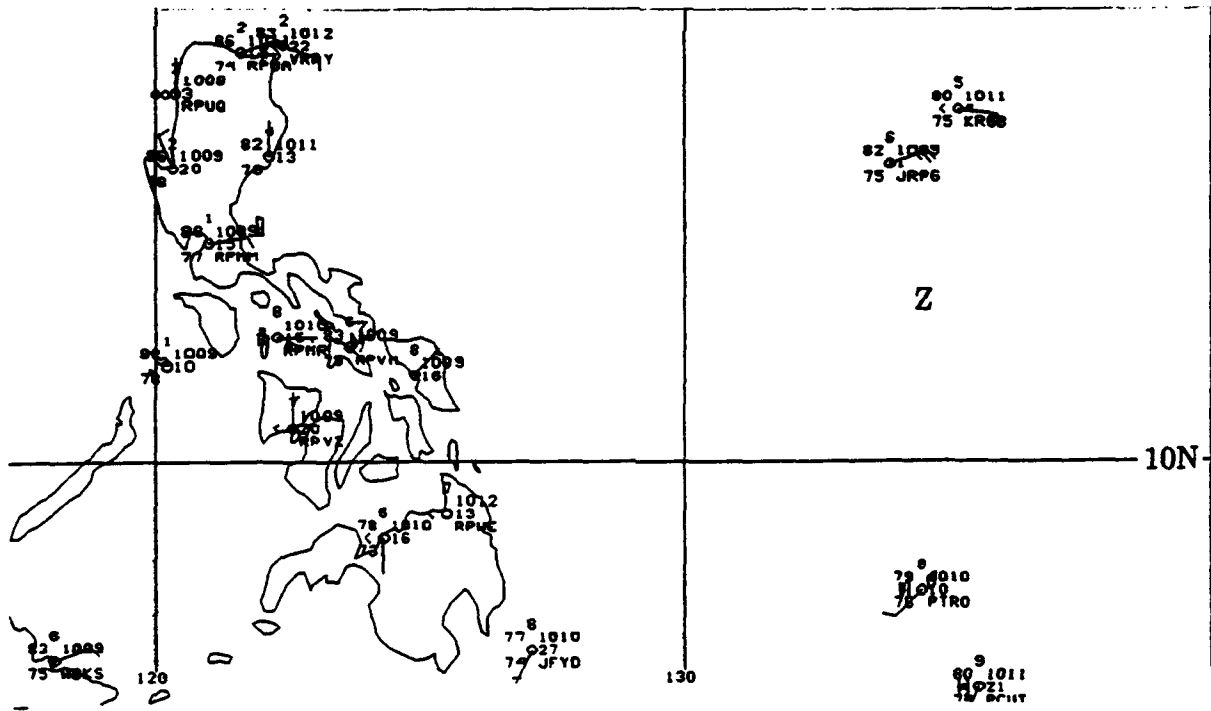
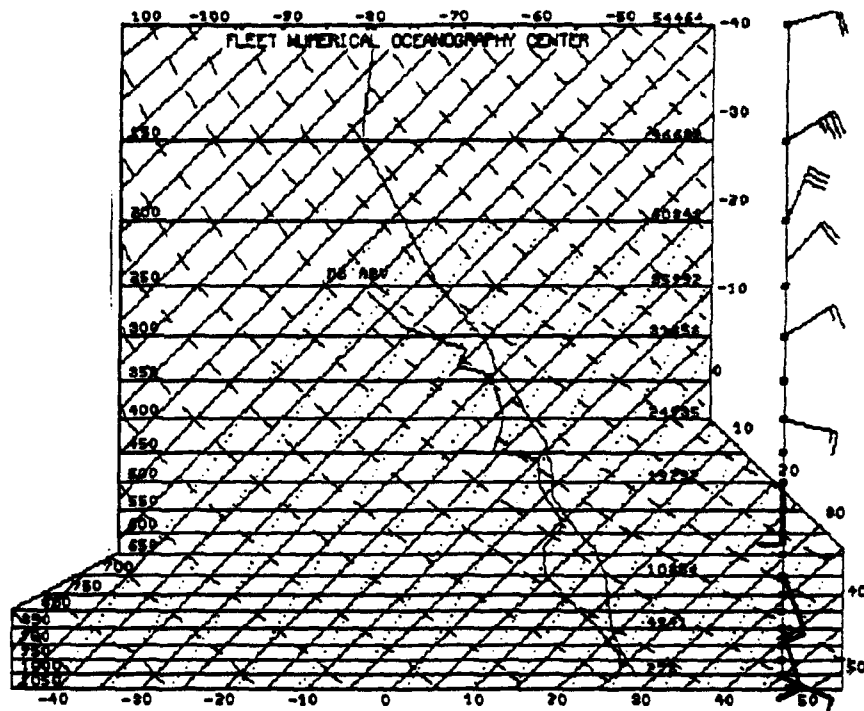
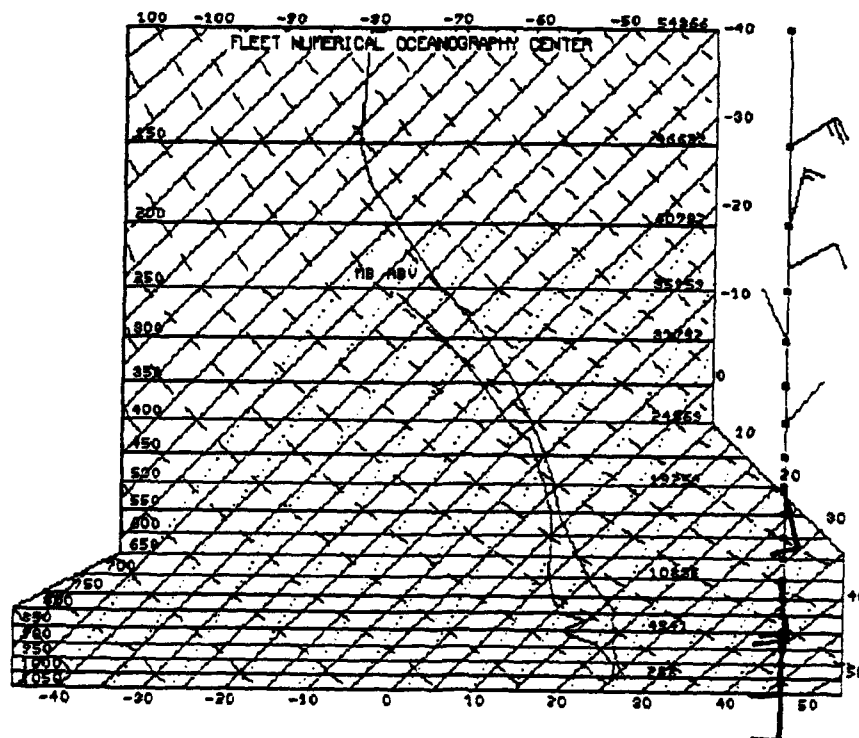


Figure 3.20: 1200Z 9 July 1992 Surface Reports (from the Naval Postgraduate School). The number above the station is the cloud cover code.



(a)



(b)

Figure 3.21: NODDS 1200Z 9 July Soundings at Yap, PTYA (a) and Koror, PTRO (b)

The JTWC Prognostic Reasoning Message (for Warning No. 1) further stated that the convective organization of 05W had improved significantly over the past 12 hours with low level cyclonic circulation, the presence of an anticyclone aloft, and convective bands tightly wrapped around a compact center—the tightly wrapped bands are visible in the satellite image below (7 hours later at 100100Z). The track was based on the latest NOGAPS and NMC (National Meteorological Center, WASHDC) upper air prognostic series. Both depicted the subtropical ridge extending further westward and intensifying. The TC was expected to be steered by deep easterly flow, south of the ridge. The dynamic aids were predicting a faster speed of movement than were the climatological or statistical aids. So, the TC was expected to track rapidly westward. The intensity (wind speed) forecast was based on a blend of climatology, analogs, and the interpretation of upper level winds from satellite and NOGAPS prognoses.

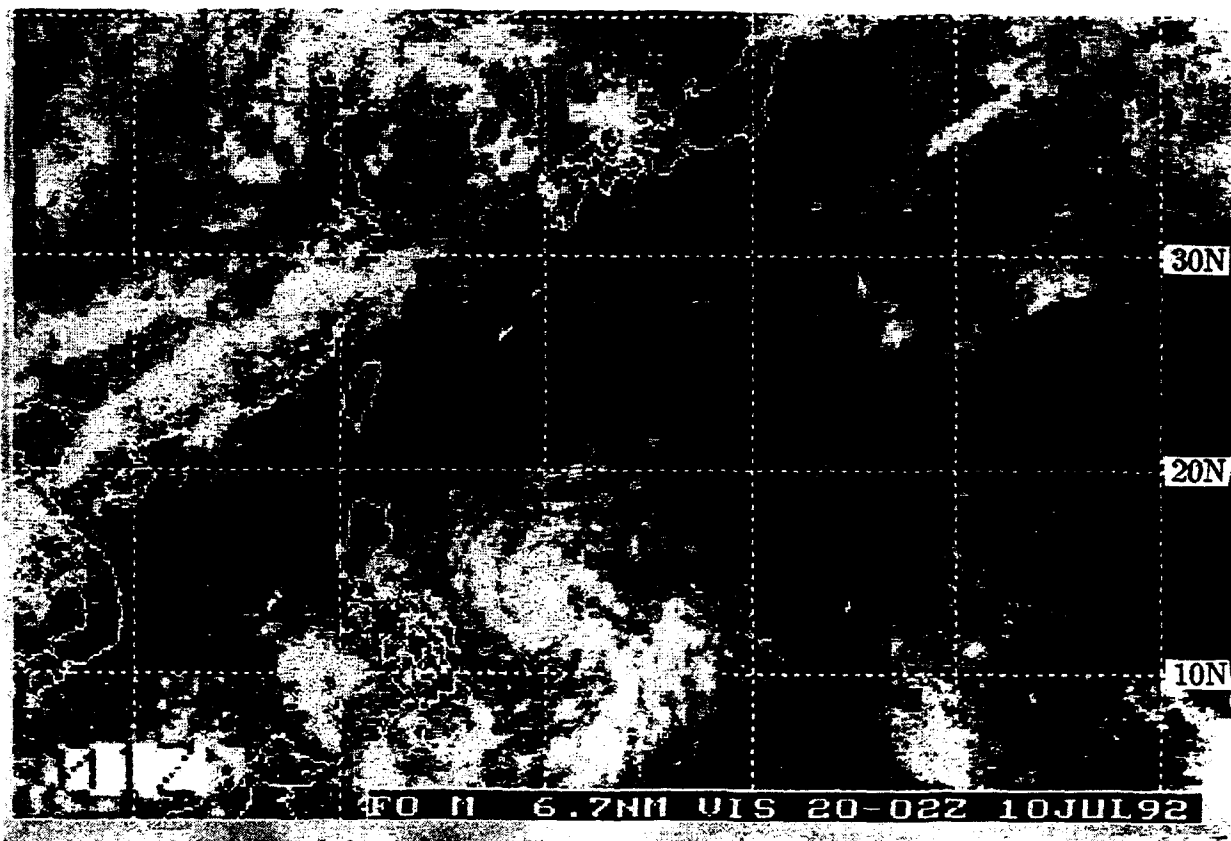


Figure 3.22: NODDS Mosaic of DMSP Visible Satellite Imagery from 2000Z 9 July–0200Z 10 July 1992. (01Z in the lower left corner indicates that the swath nearest the PI occurred at 0100Z 10 July.)

10 July 1992

At 100000Z, JTWC upgraded 05W to Tropical Storm Eli having 35 knots of wind based on a Dvorak T-number²⁰ of 2.5 (see Table 3.3 in Section 3.3.3). Eli was tracking westward in the Philippine Sea toward 275° at 16 kt. By 100600Z, its intensity increased to 55 kt—indicating the likelihood that the 100000Z intensity was too low, since this is too much intensification in 6 hours—and its speed of movement to 17 kt. JTWC reported that outflow (aloft) was good in all quadrants. The Prognostic Reasoning Message stated that the system was expected to slow²¹ due to land interaction and then accelerate after crossing into the South China Sea.

Figure 3.23 shows the ~1400Z²² NODDS DMSP IR image corresponding to the 1200Z Tropical Cyclone Warning for TS Eli. At 1200Z, Eli had maximum sustained winds of 60 kt, with gust to 75 kt, while moving toward 290° at 16 kt. The 101200Z warning position (15.1°N, 126.4°E) was a relocation to the north (see the 1012Z≡101200Z position on Fig. 3.18) based on well defined banding features into Eli's center. JTWC reported that despite the fact that animated satellite imagery did not show a strong subtropical ridge, the forecast track was toward the west-northwest (see Fig. 3.26) following dynamic²³ aids.

The NODDS surface pressure analysis, with station and ship synoptic reports, at 101200Z, is shown in Fig. 3.24. Figures 3.25(a) and (b) are "zoom" images available via NODDS²⁴. Figure 3.25(a) plots a ship report (JKRV) ~100 nm to the east of Eli reporting "3-dot" (continuous, moderate) rain with 35-kt wind from the southeast. An even greater NODDS zoom, Fig. 3.25(b), plots NAS Cubi Point (WMO 98426) with lightning visible, with a 5 kt wind from the north and Alabat (WMO 98435) with a thunderstorm and 5 kt wind from the north—the circulation of Eli had already reached the PI.

²⁰In a developing TC, Dvorak T-number = CI number.

²¹Note that the expected slowing after landfall agrees with climatology in Fig. B.12 of Appendix B. Figure B.14(b) indicates that 20 previous tropical storms decreased their average speed of movement for 12 hours, following landfall, and then held their speed; however, Fig. B.15(c) indicates that the speed of movement of 21 previous typhoons decreased their speed of movement for the first six hours after landfall, then increased their speed.

²²The direct readout of DMSP satellite imagery shown in Fig. 3.35 records the time of the same DMSP image as ~1230Z.

²³Dynamic aids are identified in Table 3.2 in Section 3.3.2.

²⁴Again, note that the VGA screen images (typically 14-inch diagonals), available to the operational user, are both larger and in color.

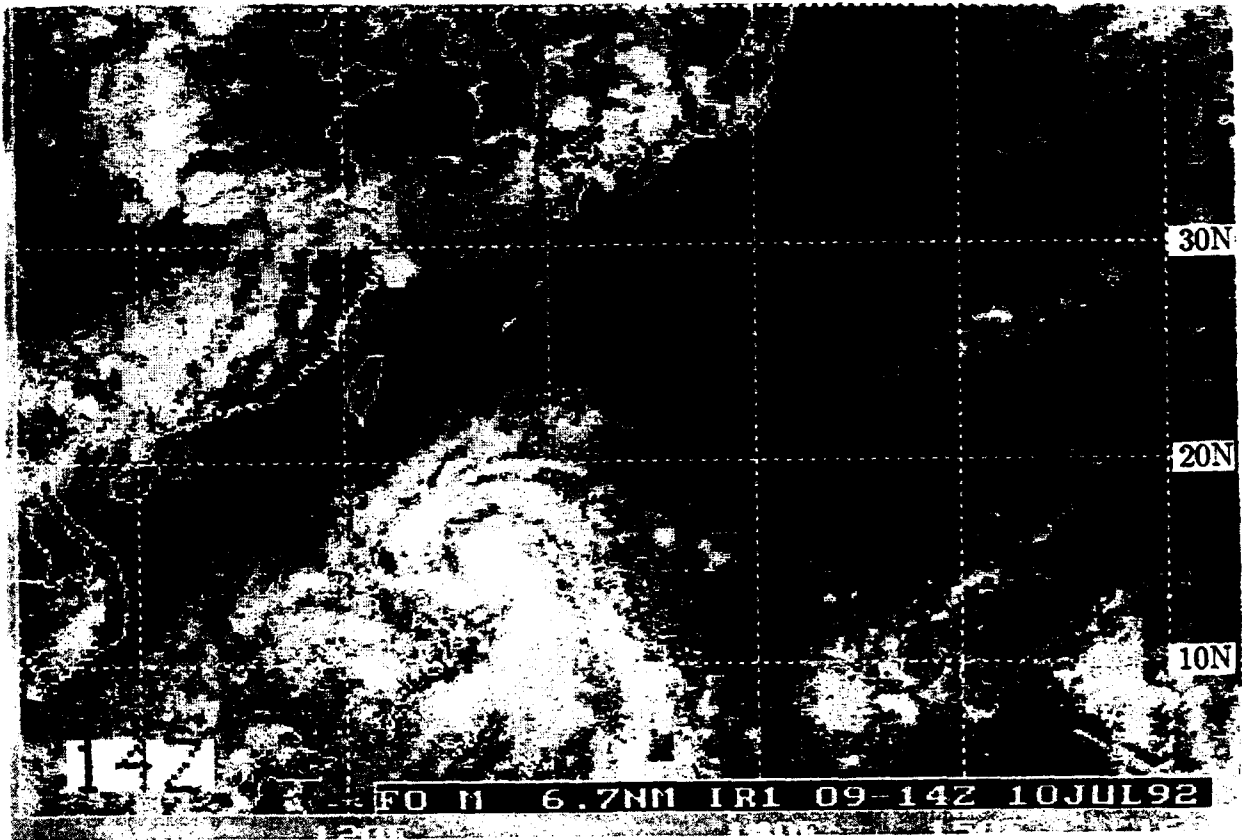


Figure 3.23: NODDS Mosaic of DMSP Infrared Satellite Imagery for 1400Z 10 July 1992.

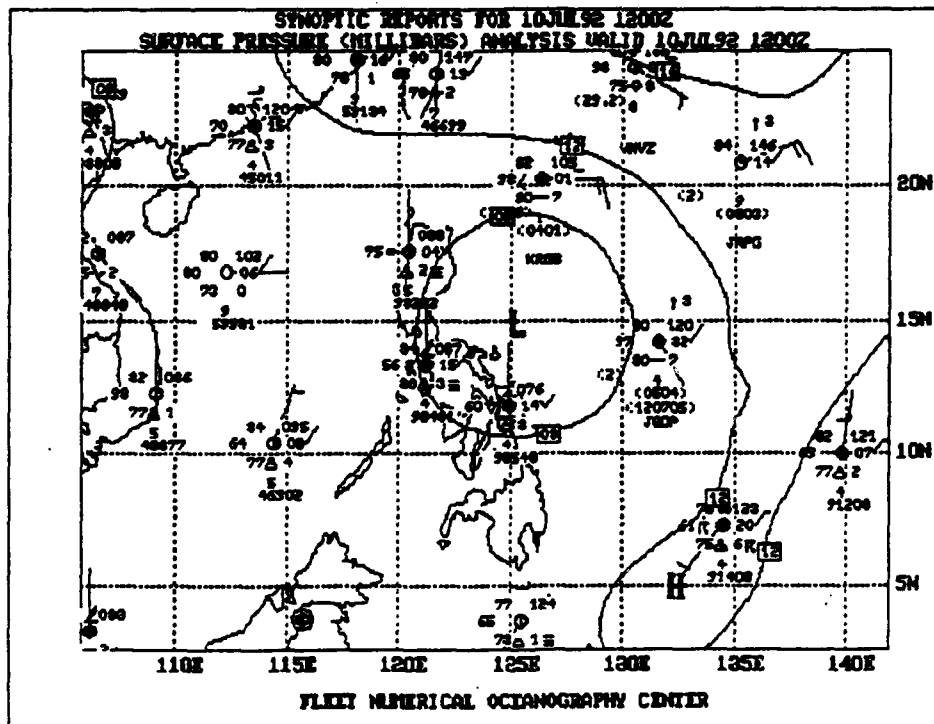
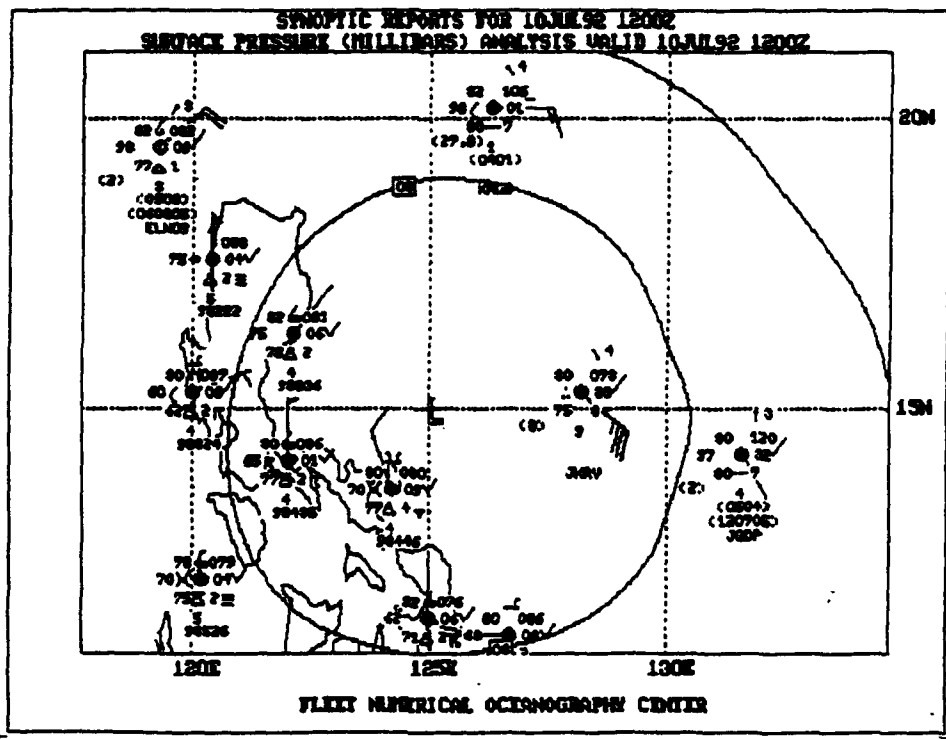
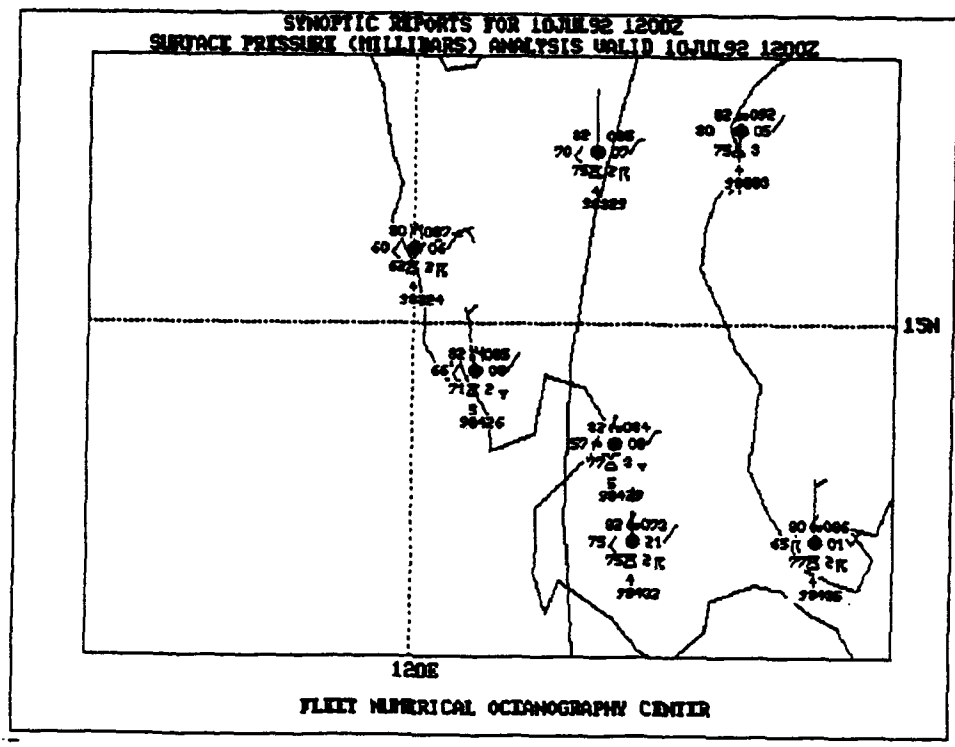


Figure 3.24: NODDS Synoptic Reports and Surface Pressure Analysis for 1200Z 10 July 1992.



(a)



(b)

Figure 3.25: NODDS Zoomed Synoptic Reports and Surface Pressure Analysis for 1200Z 10 July 1992.

Figure 3.26 is the NODDS graphical presentation²⁵ of the JTWC 101200Z warning message on Eli. The graphical warning (Fig. 3.26) does not plot the 12-hour JTWC warning which accurately forecast typhoon intensity (70 kt), compared to the actual warning intensity of 75 kt at 110000Z, before predicted landfall. (Indeed, as the working best track (Fig. 3.18) shows, Eli reached typhoon strength (65 kt), even earlier, at 101800Z.)

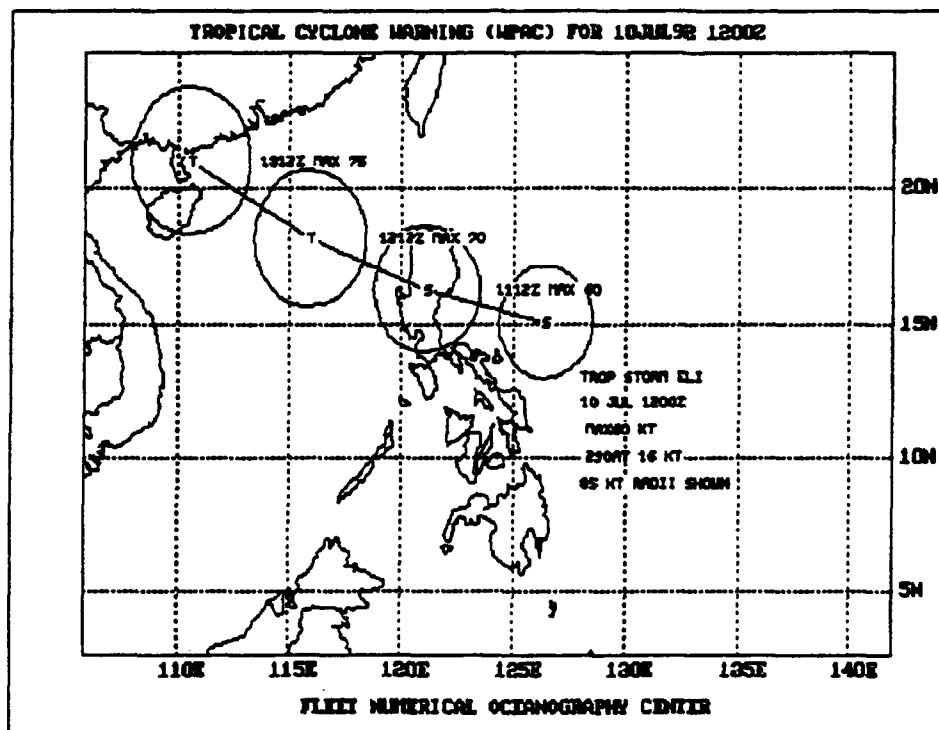


Figure 3.26: NODDS Tropical Cyclone Warning for TS Eli for 1200Z 10 July 1992 (Max winds 60 kt, moving 290° at 16 kt, 35 kt radii shown)

²⁵The reader is cautioned that the label of time and intensity is "offset" to the far right from the position of the tropical cyclone, where S = Tropical Storm and T = Typhoon.

Figure 3.27 shows the NOGAPS 101200Z surface pressure analysis (solid lines) and 24-h forecast (dashed lines). The analysis center's symbol L in Fig. 3.27 represents the position of Tropical Storm Eli²⁶. The forecast center of low pressure can be estimated by viewing the dashed isobars of Fig. 3.27, i.e., near Lingayen Gulf on the west coast of Luzon. This position represents the NOGAPS "objective aid" 24-h forecast position for TS Eli and is a direct result of NOGAPS prognostic model. While it represents a very good prognosis, forecasting for a "straight-runner", such as Eli, for only 24 hours, is not difficult—of course, a TC is identified as a "straight runner" only "after the fact."

Figure 3.28 shows the 500-mb trough and the center (L) associated with TS Eli. In the absence of nearby radiosonde stations, the analysis position of the low at 500 mb (solid contours), is also a direct result of the bogus soundings (surface to 400 mb) described in footnote 26. However, the 24-h forecast position (dashed contours) of the 500-mb low associated with Eli is a direct result of NOGAPS prognosis.

Similarly, Figs. 3.29(a) and (b) show the NOGAPS analysis and 24-h forecast of the streamlines²⁷ and winds in the region, on the 925-mb surface. This pressure surface was chosen because of its nearness to the "gradient" level, the level (~ 1 km) at which surface friction ceases to exist. Tropical analysts typically analyze low-level streamlines at the gradient level and upper-level streamlines at 200 mb—actually, JTWC does a surface-gradient composite and a 200 mb composite (300 mb–100 mb). Recognizing that no synoptic-scale analysis can depict the mesoscale features of a tropical cyclone (e.g., the maximum sustained winds at the radius of maximum winds (RMW)), both the analysis, Fig. 3.29(a), and the 24-h forecast, Fig. 3.29(b), appear to be excellent products for operational use.

²⁶In 1990, FNOG automated the insertion of "bogus" soundings (from the surface to 400 mb) based on the JTWC warning positions—thus forcing the NOGAPS analysis to accept the JTWC analysis position of the respective tropical cyclone. The scheme prescribes 5 bogus soundings for a tropical depression and 13 bogus soundings for TCs of tropical storm strength or greater: TD - one at the center and four at a radius of 2° in the direction of the cardinal points, north, east, south and west; TS or stronger - one at the center and four staggered at radii of 2° , 4° and 6° . Thus the forecaster should be aware that it is not unusual for the NOGAPS analysis to have a trough or low center at a considerable distance from the the position of an incipient tropical cyclone—i.e., no trough or low center where the TC forms, until its position is dictated by the "bogus" entries. Often this is caused by an absence of wind reports in the vicinity of the forming TC or by the coarse resolution of the NOGAPS model. However, it is also possible that the initial synoptic surface wind reports—from which an analyst would subjectively discern the position of the forming TC, especially in the presence of a satellite cloud cluster—are rejected by the NOGAPS Multivariate Optimum Interpolation (OI) Analysis scheme (Goerss and Phoebus, 1992).

²⁷Tropical meteorologists will recognize that these automated NOGAPS 925-mb analyses and forecasts are discontinuous streamlines which are very useful, but present no depiction of the flow pattern of neutral points, nor the labels of positive and negative points.

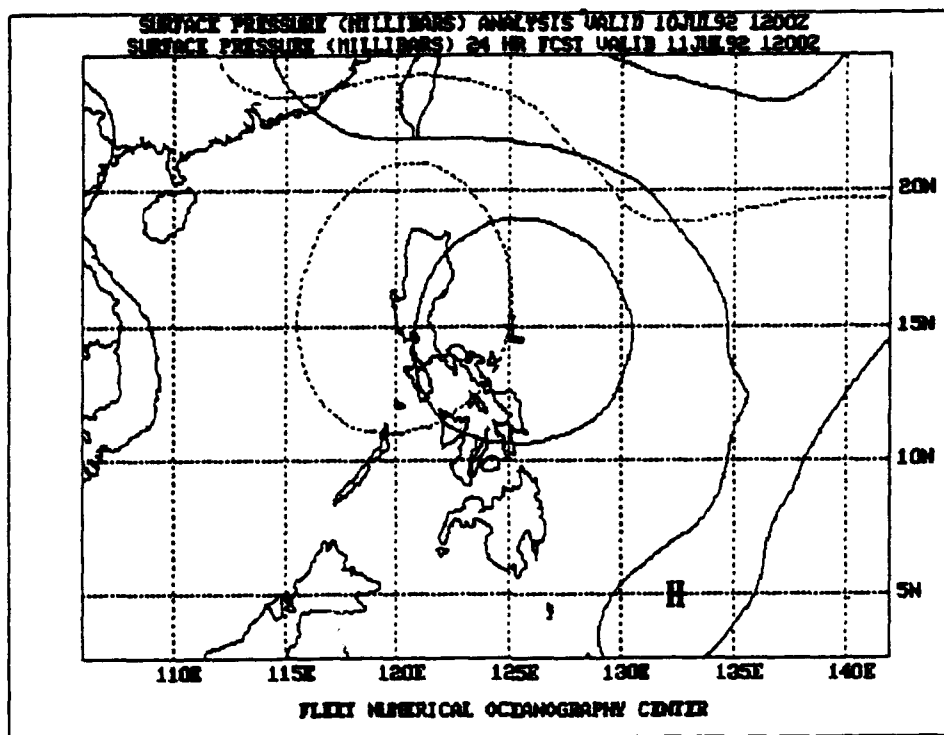


Figure 3.27: NODDS Surface Pressure Analysis and 24-h Forecast from 1200Z 10 July 1992.

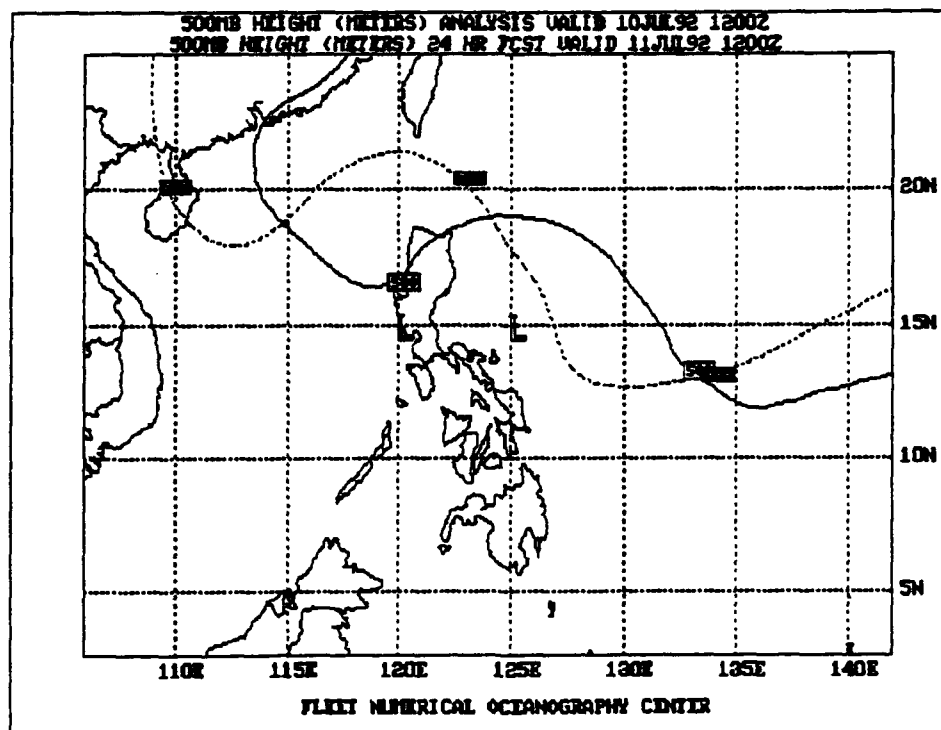
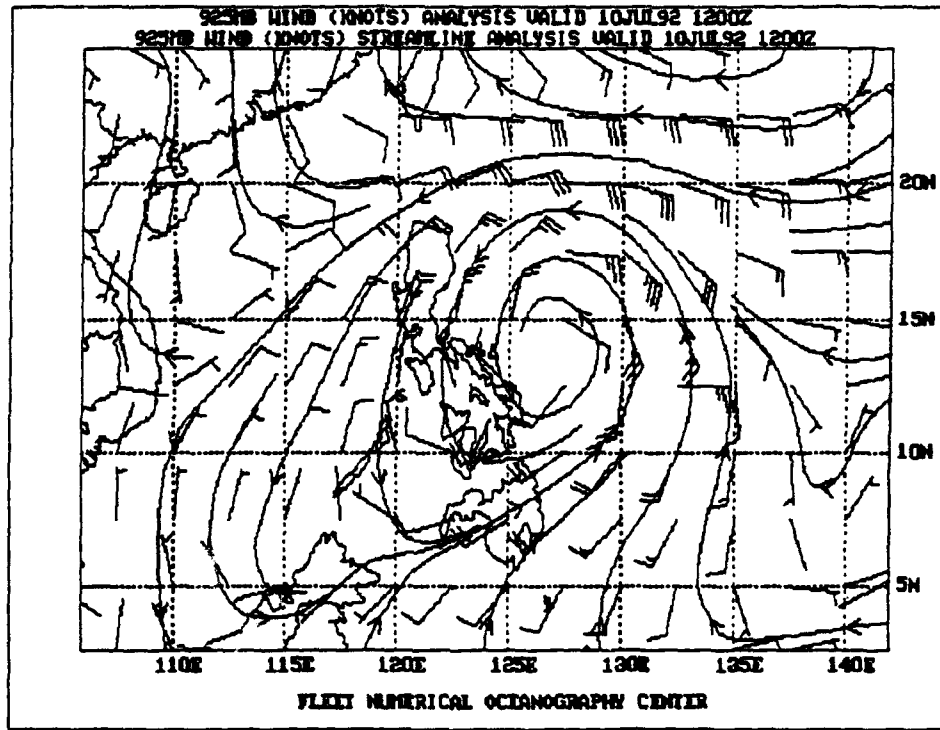
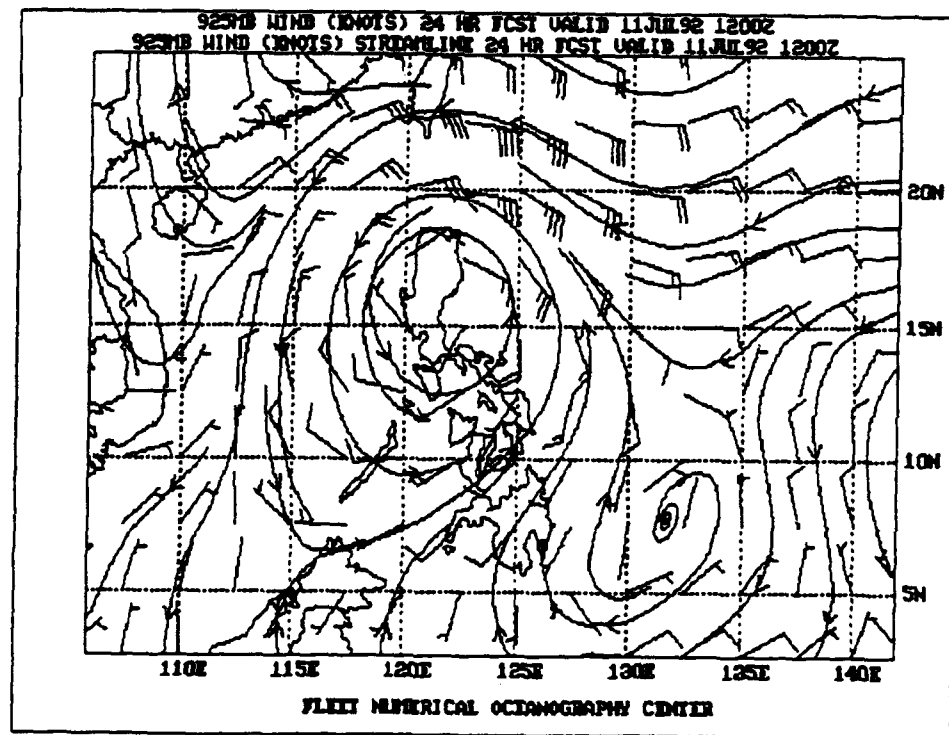


Figure 3.28: NODDS 500-mb Height Analysis and 24-h Forecast from 1200Z 10 July 1992.



(a)



(b)

Figure 3.29: NODDS 925-mb Winds and Streamline Analysis (a) and 24-h Forecast (b) from 1200Z 10 July 1992.

Figure 3.30 shows the FNOC produced significant wave height analysis and 24-h forecast. The NOGAPS surface winds generate wave heights >18 feet about 100 nm north of the center of Eli at 101200Z. The 24-h forecast (dashed) moves the maximum wave heights (still >18 feet) to the northeast coast of Luzon. The FNOC sea surface temperature (SST) (Fig. 3.31) shows the majority of the South China Sea and the Luzon Strait with SST above 28°C, with an area of SST >30°C in the Philippine Sea, east of the Visayas. This SST analysis compares well with the average August SST analysis (Appendix A, page A-8) which has an expanded area of SST >29°C in the northern Philippine Sea.

The NOGAPS 101200Z 200-mb streamline and wind analysis is shown in Fig. 3.32. While the analysis is acceptable over the South China Sea and over the Philippine Islands, the upper-level flow in the vicinity of the tropical storm is poor. Figure 3.32 does depict weak diffuence (lateral divergence) in the general easterly flow above the position of Eli at 200 mb. However, Fig. 3.33 is a copy of the operational 200-mb hand analysis produced by the duty TDO at JTWC depicting outflow in all quadrants at 200 mb. No doubt, the FNOC OI Analysis rejected the two satellite cloud-vector winds (northerly winds) at Point "Y", southeast of Eli.

The 200-mb wind observation over southeastern Luzon on Fig. 3.33 at Point "X", i.e., 090°/20 kt wind at Legaspi (see Table 1.1), was unexpected. (There are several meteorological upper air stations: Laoag (WMO 98223), Legaspi (WMO 98444), Cebu (WMO 98646) and Davao (WMO 98743); however, their operational status is unknown.) Legaspi was only ~190 nm southwest of Tropical Storm Eli at the time of launch, 101200Z. The sounding is shown on a NODDS "Skew T" plot in (Fig. 3.34). The reader quickly identifies the 20 kt easterly wind at 200 mb corresponding to the wind plotted at Point "X" on Fig. 3.33. An experienced analyst would suspect that the temperature inversion between 550 and 500 mb was caused by an erroneous temperature and dewpoint plotted at 550 mb. However, an inspection of the terrain around Legaspi revealed the presence of the Mayon Volcano (elevation 7946 feet) only 10 nm NNW of Legaspi. Thus, it is possible that the volcano had prevented the warmer, more moist air, from TS Eli, from moving over Legaspi at *lower* levels (from the northwest) at 101200Z. Note on the sounding (Fig. 3.34), that while the winds from 550 to 400 mb are 20–35 kt from the northeast—part of the circulation of TS Eli—the 1000 mb wind at Legaspi is 250°/5 kt and the 700 mb wind is 350°/10 kt.

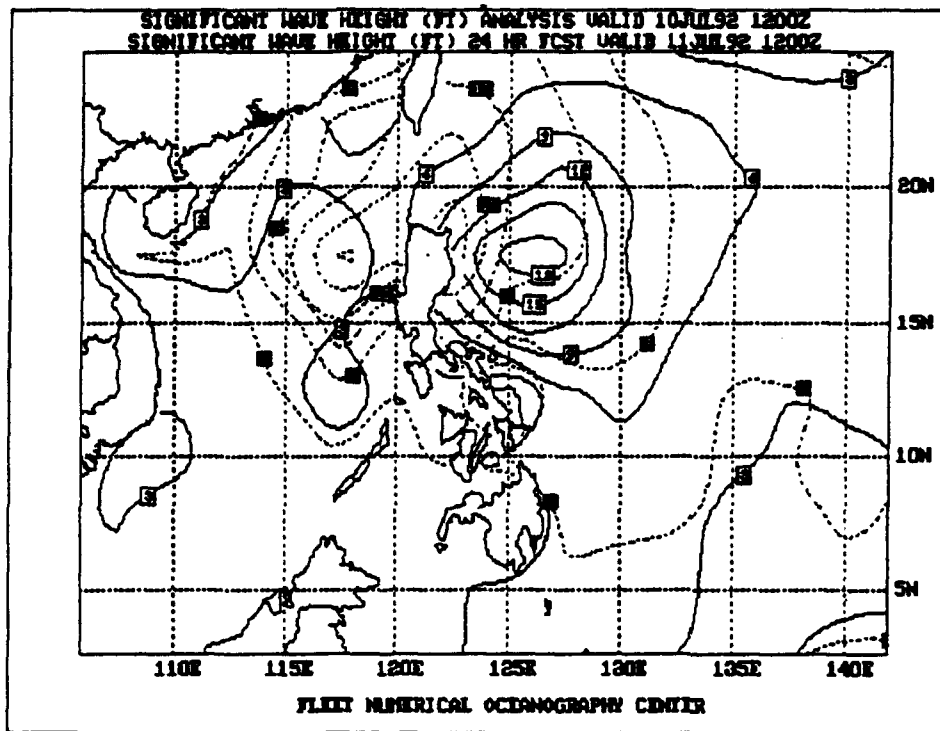


Figure 3.30: NODDS Significant Wave Height Analysis and 24-h Forecast from 1200Z 10 July 1992.

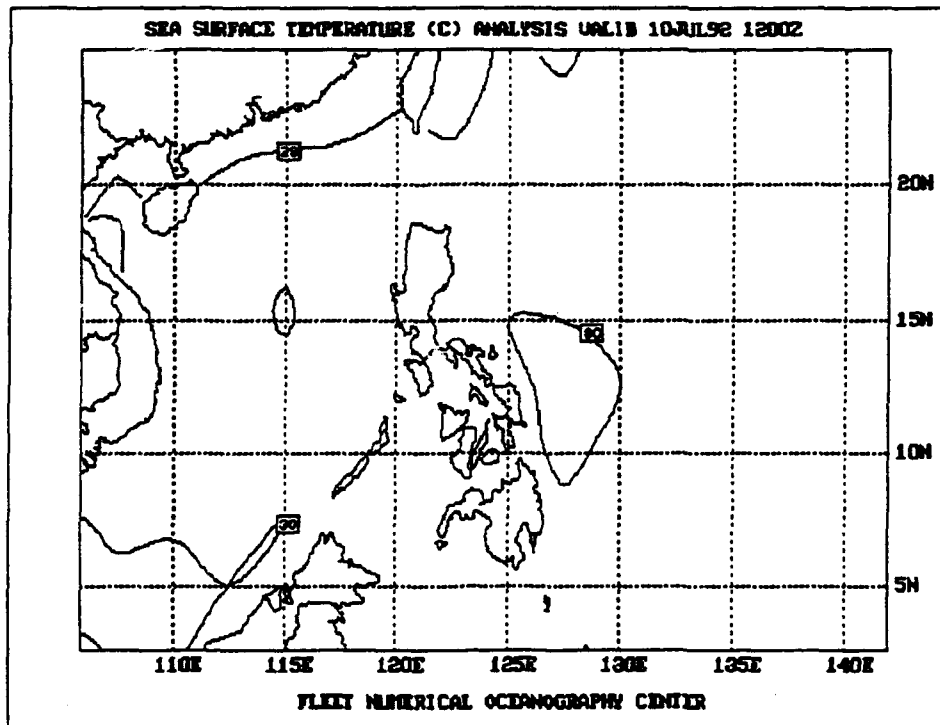


Figure 3.31: NODDS Sea Surface Temperature Analysis (°C) valid at 1200Z 10 July 1992.

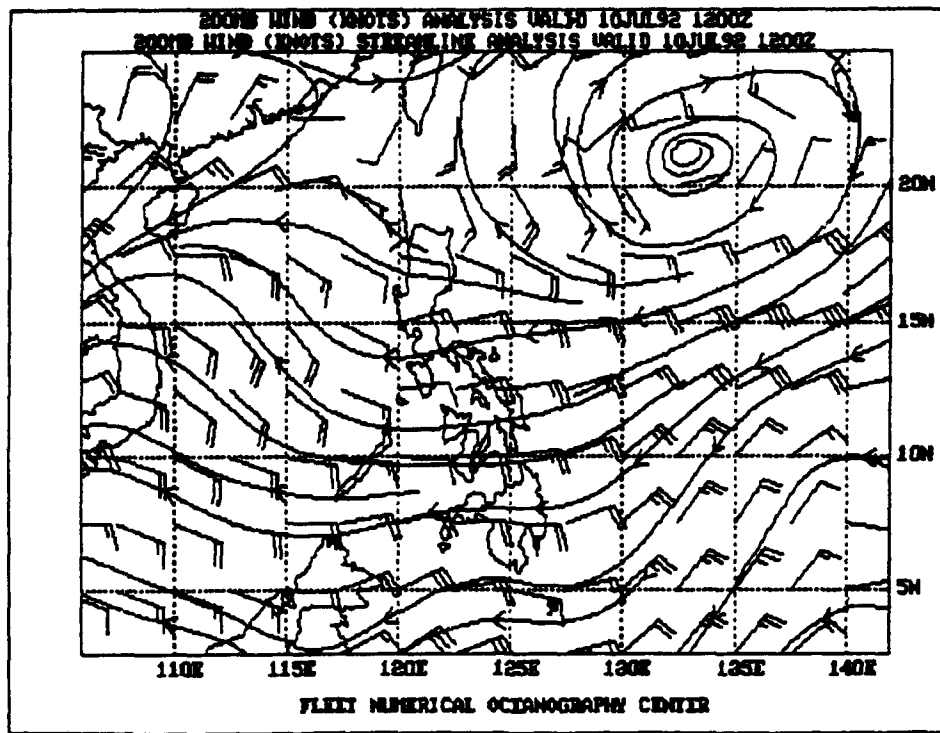


Figure 3.32: NODDS 200-mb Wind and Streamline Analysis valid at 1200Z 10 July 1992.

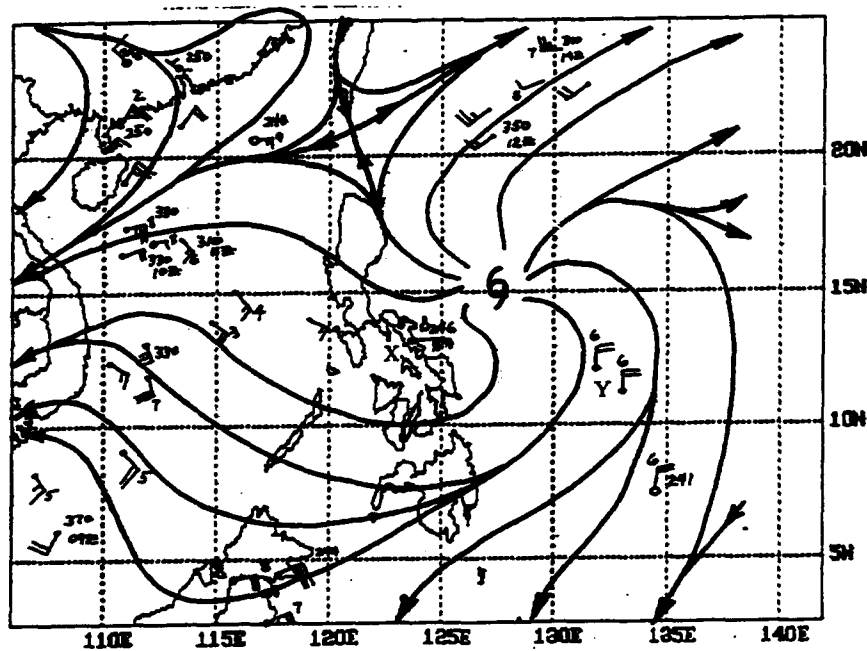


Figure 3.33: 200-mb Streamline Analysis valid at 1200Z 10 July 1992 (adapted from JTWC operational manual analysis)

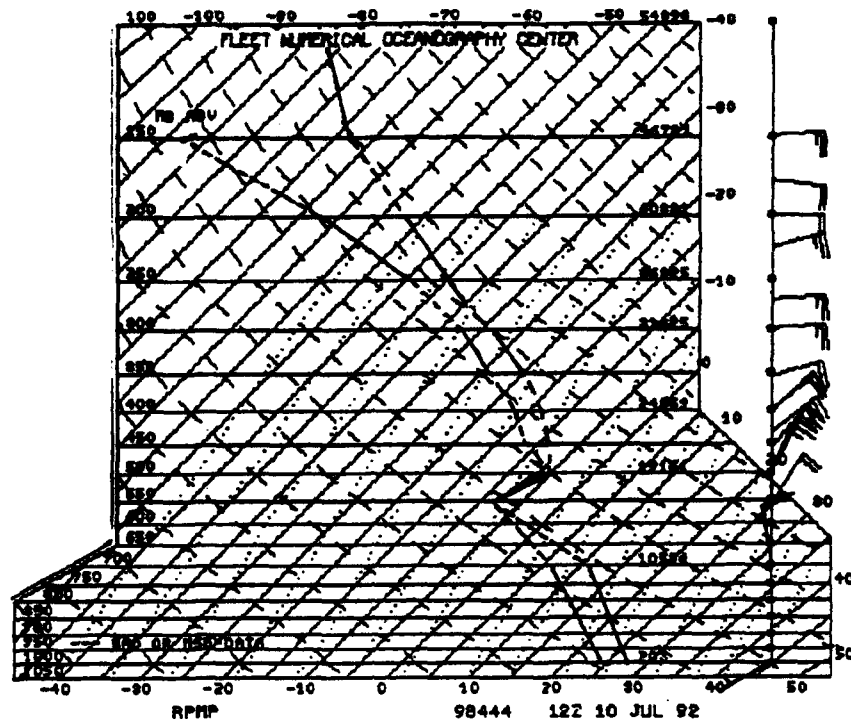


Figure 3.34: NODDS 1200Z 10 July Sounding at Legaspi, RPMP

Finally, Fig. 3.35 is presented to permit the forecaster to compare the resolution of the NODDS delivered DMSP satellite imagery with direct readout DMSP satellite imagery. This imagery was received at a ground station on Okinawa, and it displays the ~ 1.2 nm resolution IR imagery from which the NODDS satellite image (Fig. 3.23, with only 6.7 nm resolution) was prepared. While stations or ships receiving DMSP directly can readily identify individual thunderstorm cells in (Fig. 3.35), the NODDS imagery (Fig. 3.23), received effortlessly in about 1.5 minutes via a 2400 baud modem, will provide analysts and forecasters with excellent details on the location of heavy convection in rainbands, etc. In fact, a close comparison of the two images, permits the identification of cumulonimbus clusters, using only Fig. 3.23.

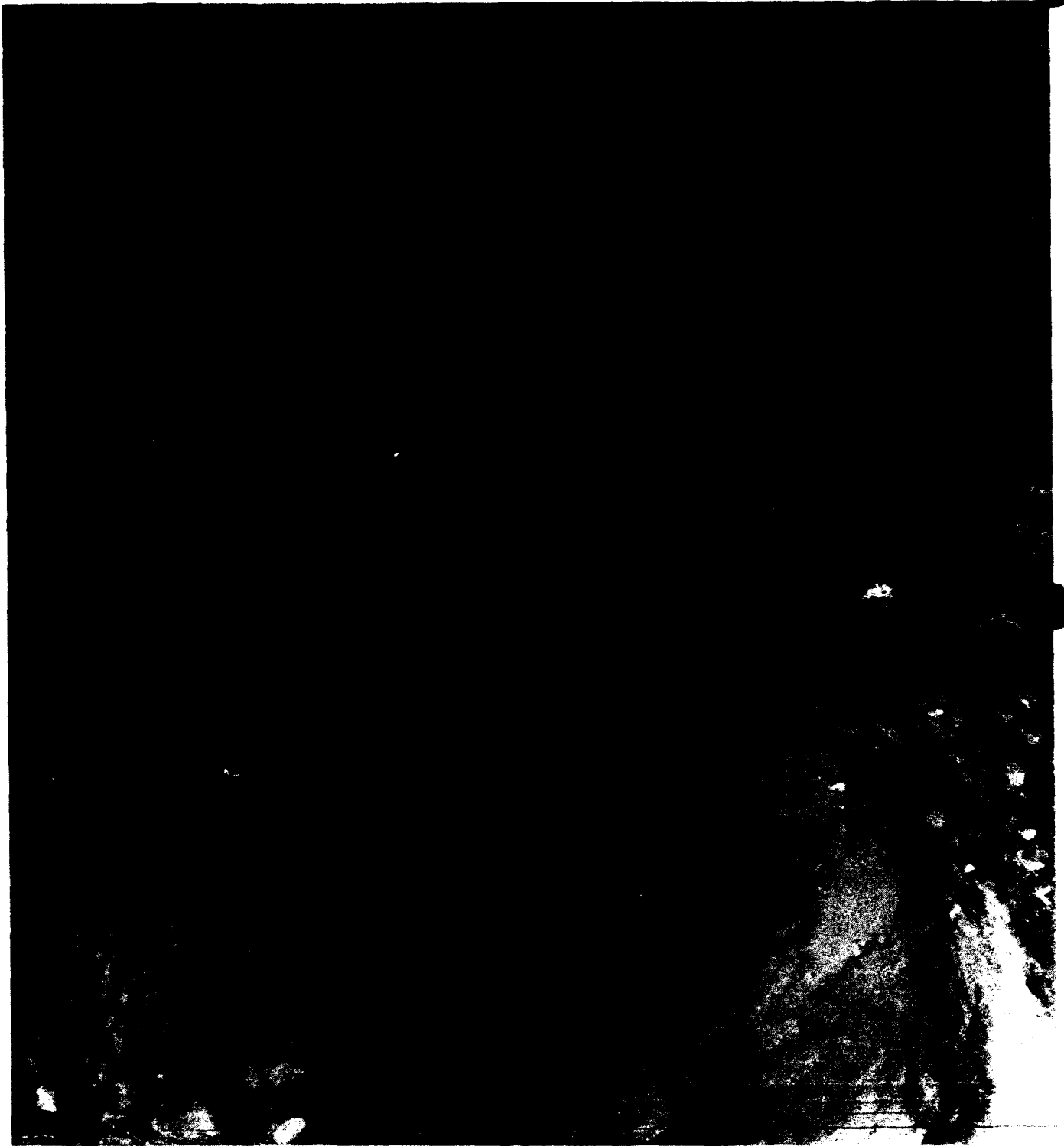


Figure 3.35: DMSP IR Satellite Swath for 1229Z 10 July 1992 (received at Kadena AB, Japan)

11 July 1992

Moving faster and intensifying faster than predicted, 05W became Typhoon Eli with maximum sustained winds of 75 kt located at 15.8°N, 122.2°E at 110000Z (110800Z Local Time), moving 275°/21 kt²⁸. As shown on the 110000Z surface pressure analysis, Fig. 3.37, NOGAPS locates the low pressure center (L) several degrees to the east of the warning position (see Fig. 3.18); however, the large-scale cyclonic circulation associated with Eli is well depicted by both ship and land station reports. The 110100Z DMSP visible satellite imagery, Fig. 3.36, shows the typhoon signature²⁹ with convective feeder bands from the south and east, one hour after the surface analysis of Fig. 3.37.

The first NODDS zoom, Fig 3.38(a), reveals a ship (7KFY), off the NW coast of Luzon, with 7.5-foot waves and 9-foot swell³⁰, reporting wind 050°/25 kt. A further zoom, Fig. 3.38(b), shows Gasiguran (WMO 98336) with 4-dot (continuous, heavy) rain, wind 045°/40 kt, with a 2.2 mb pressure fall³¹. Baler (WMO 98333) reports 2-dot (continuous, slight) rain with a larger pressure tendency of -3.4 mb—hinting at the eventual landfall of Eli near Baler, about 2 hours later (see Fig. 3.18). The direction of Baler's wind, 220°, is suspect—likely a transmission error changing its direction from 020° to 220°—; however, it may be the combination of a terrain-directed land and mountain breeze blowing “down” the valley in the early morning (0800 Local Time).

²⁸The 24-h terminal forecast made by Cubi Point NAS, RP (RPMB, WMO 98426) at 102200Z, available via transmission FAPN10 KAWN (not shown), forecast winds gradually becoming 340°/12 kt, with gusts to 22 kt in showers between 110500Z and 110700Z. Then, temporarily, the winds becoming variable 18 kt, with gusts to 28 kt, visibility 2 miles in thunderstorms between 110700Z and 112100Z.

²⁹As the geography of Luzon becomes covered by Eli's convection, the reader must visualize the position of Luzon directly south of Taiwan, which remains visible on Fig. 3.36.

³⁰Sea and swell are reported in units of 0.5 meter (~1.5 feet); therefore, (0805) = seas with a period of 08 seconds, height of 7.5 feet and (081006) = swell from 080°, with a period of 10 seconds and height of 9 feet.

³¹This barometer fall exists due to the approach of Typhoon Eli, despite the large (tropical) “atmospheric tide” increase experienced between 0400 and 1000 Local Time.

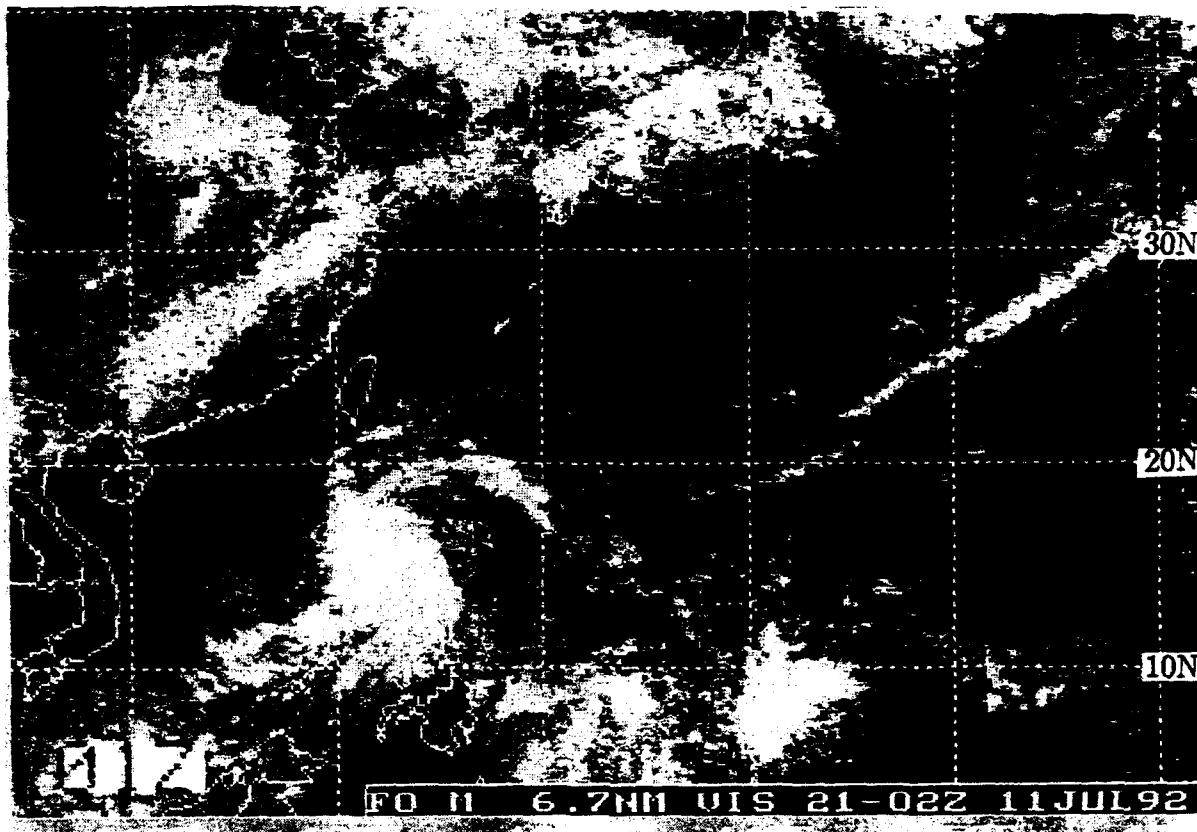


Figure 3.36: NODDS Mosaic of DMSP Visible Satellite Imagery for 0100Z 11 July 1992.

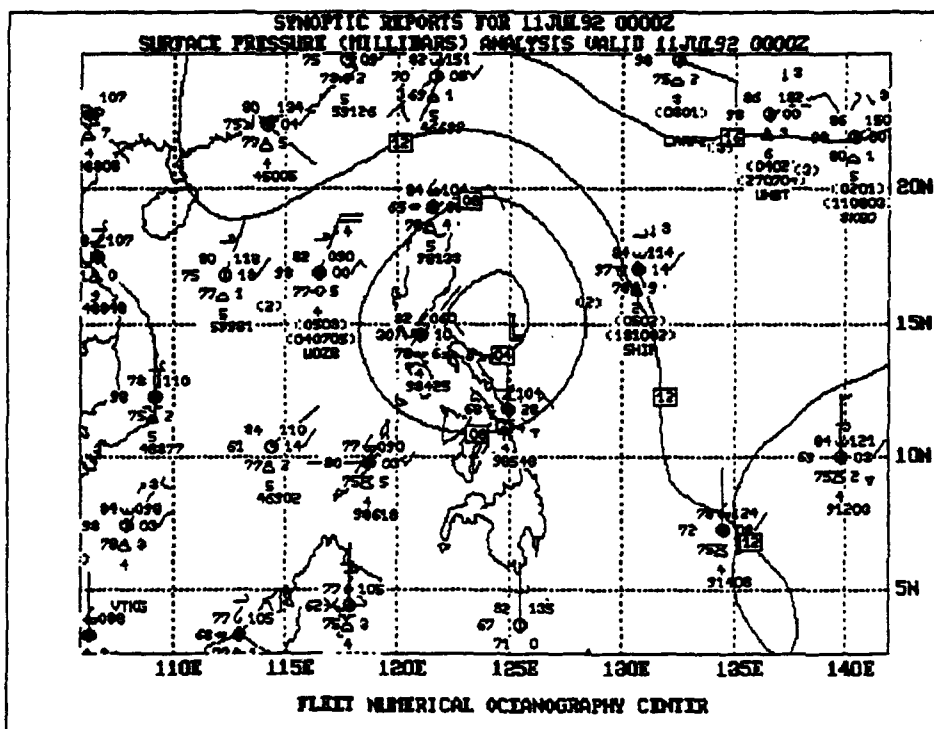


Figure 3.37: NODDS Synoptic Reports and Surface Pressure Analysis for 0000Z 11 July 1992.

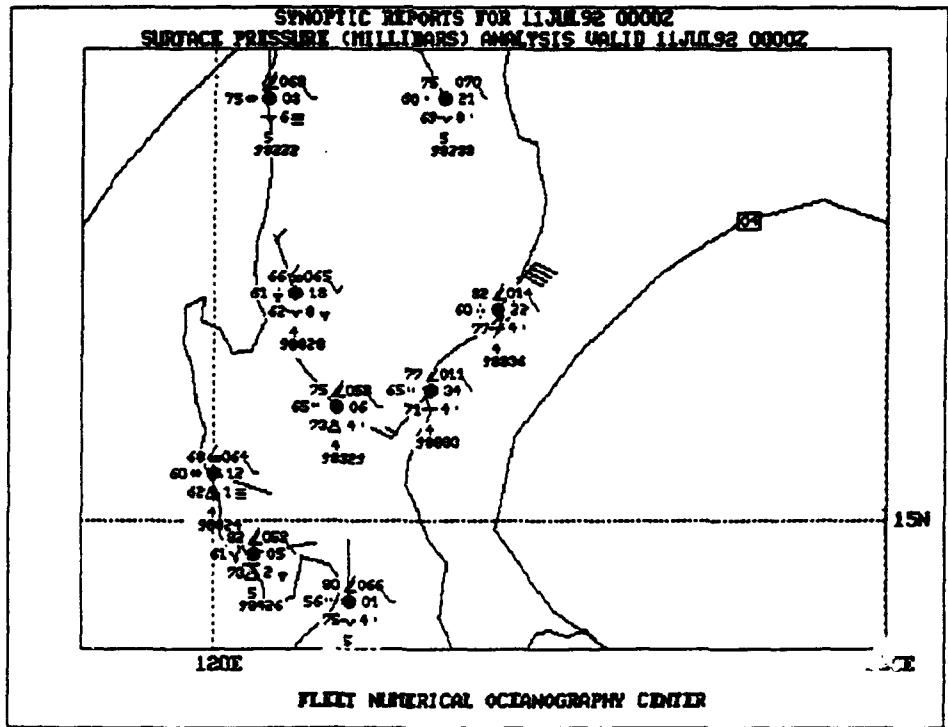
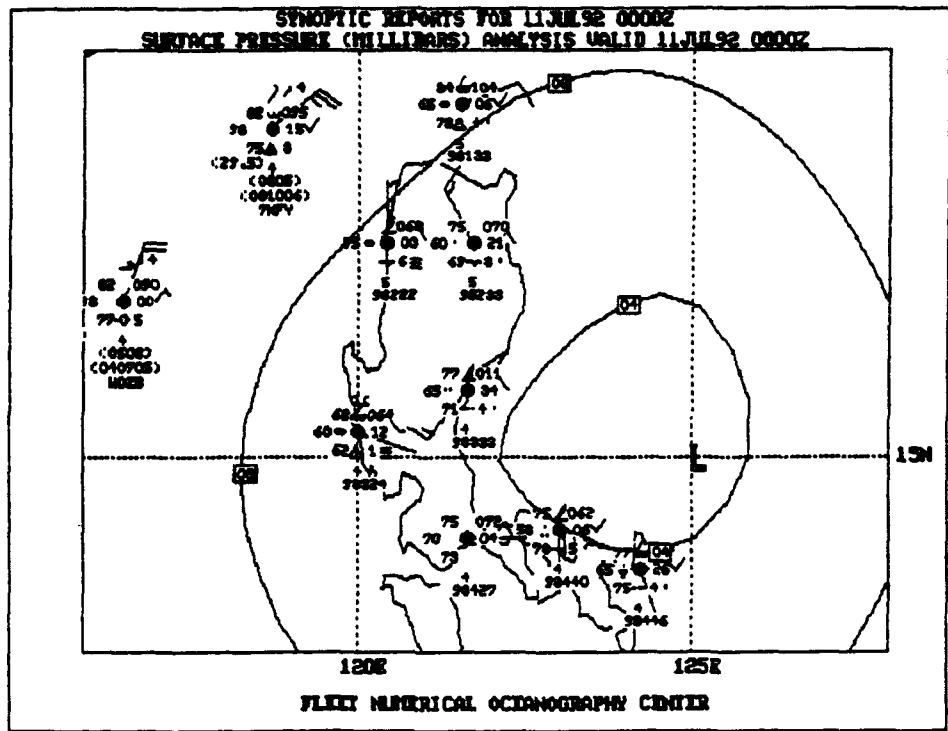


Figure 3.38: NODDS Zoomed Synoptic Reports and Surface Pressure Analysis for 1100Z 11 July 1992.

Figure 3.39 shows the graphic plot of JTWC 110000Z warning on Typhoon Eli. The JTWC Prognostic Reasoning Message reported more symmetrical convection, colder cloud tops and a weak 10 nm eye—not visible on the NODDS DMSP 6.7 nm visible image, Fig. 3.36. Eli was expected to cross Luzon in 6–8 hours, reaching mainland Asia within 72 hours (see Fig. 3.39). With winds expected to decrease after the 110000Z warning due to interaction with land, the 12-h warning position, not plotted on the NODDS graphics, was at 16.4°N, 118.6°E (west of Luzon), with 60 kt winds, followed by reintensification over the South China Sea.

Figure 3.40, shows the NOGAPS surface pressure analysis (solid isobars) and the NOGAPS 24-h prognosis (dashed isobars) valid at 120000Z, where the NOGAPS Eli forecast position is about 250 nm west of Luzon. The 24-h position is excellent, despite the “jog” toward the southwest, shown on the working best track, Fig. 3.18. Note that Fig. 3.40 also indicates that the NOGAPS model forecasts a higher-central pressure (filling) for Eli, i.e., the 24-h isobars (dashed) do not include a closed 04 isobar (1004 mb), as does the analysis (solid). The working best track (Fig. 3.18) indicates that the maximum sustained wind actually decreased to 65 kt at 120000Z.

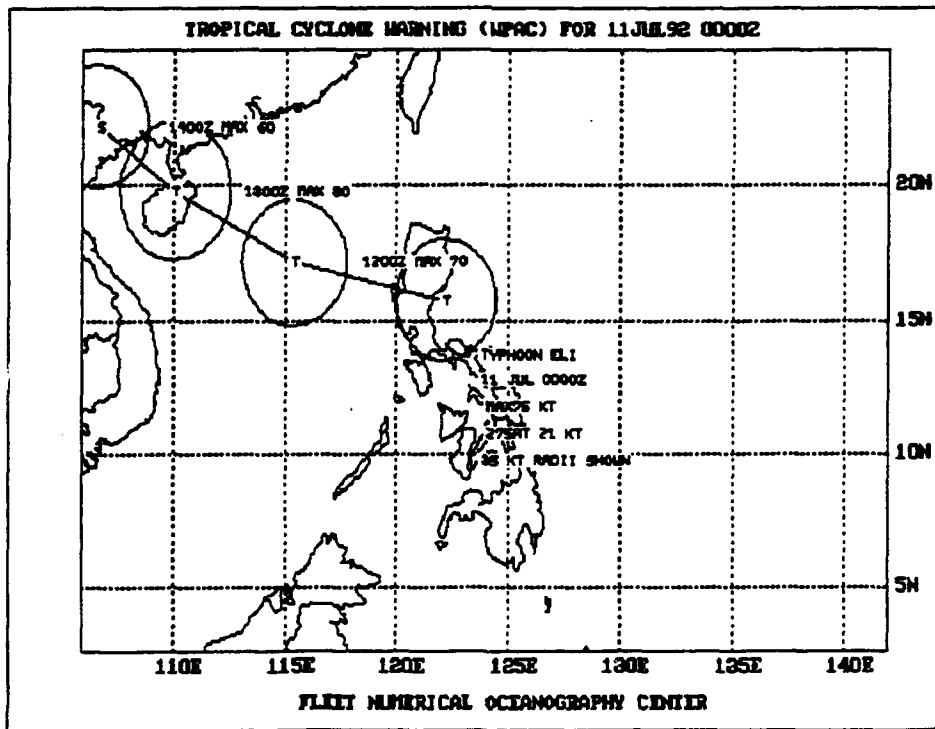


Figure 3.39: NODDS Tropical Cyclone Warning for Typhoon Eli for 0000Z 11 July 1992 (Max winds 75 kt, moving 275° at 21 kt, 35 kt radii shown)

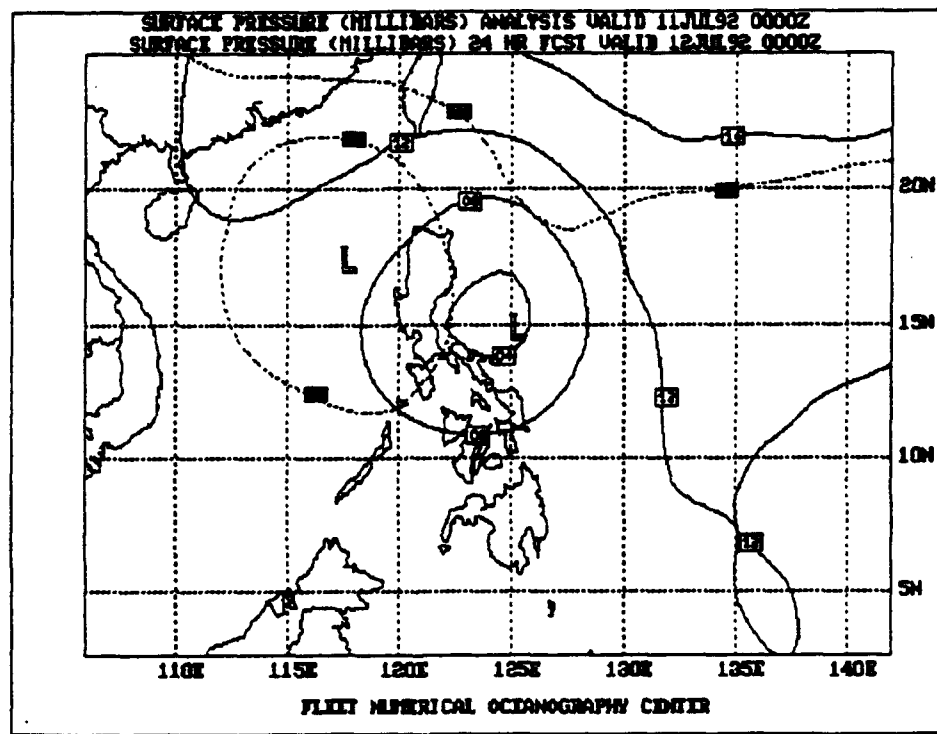


Figure 3.40: NODDS Surface Pressure Analysis and 24-h Forecast from 0000Z 11 July 1992.

In Fig. 3.41, the NOGAPS Significant Wave Height Analysis (solid isolines) shows 9 foot waves near Point "W" (18.5°N,118°E), the location of ship 7KFY in Fig. 3.38(a). The 24-h wave forecast (dashed isolines) moves the maximum wave heights (18 feet) far offshore, over halfway across the South China Sea. C. P. Guard (1992, personal communication) reports that a lee side low frequently sets up off NW PI as typhoons approach Luzon. Also whether or not a lee side low sets up, we frequently see higher seas just off NW Luzon than we would normal expect from NOGAPS prognoses.

The 925-mb streamline analysis and 24-h forecast are shown in Fig. 3.42, products of the NOGAPS spectral model run. As explained earlier, the bogus soundings, entered by FNOC, ensure that the position of the tropical cyclone on the NOGAPS analysis agrees with the JTWC warning position.

As at 101200Z, the 110000Z NOGAPS 200-mb analysis, Fig. 3.43, is compared with the JTWC manual 200-mb analysis, Fig. 3.44. Again, the NOGAPS 200-mb analysis differs substantially from the working hand analysis, where subjectivity permits placing cyclonic outflow aloft above the eye wall, becoming radially outward and then anticyclonic outflow (except to the northeast where a neutral point is drawn) farther from the typhoon.

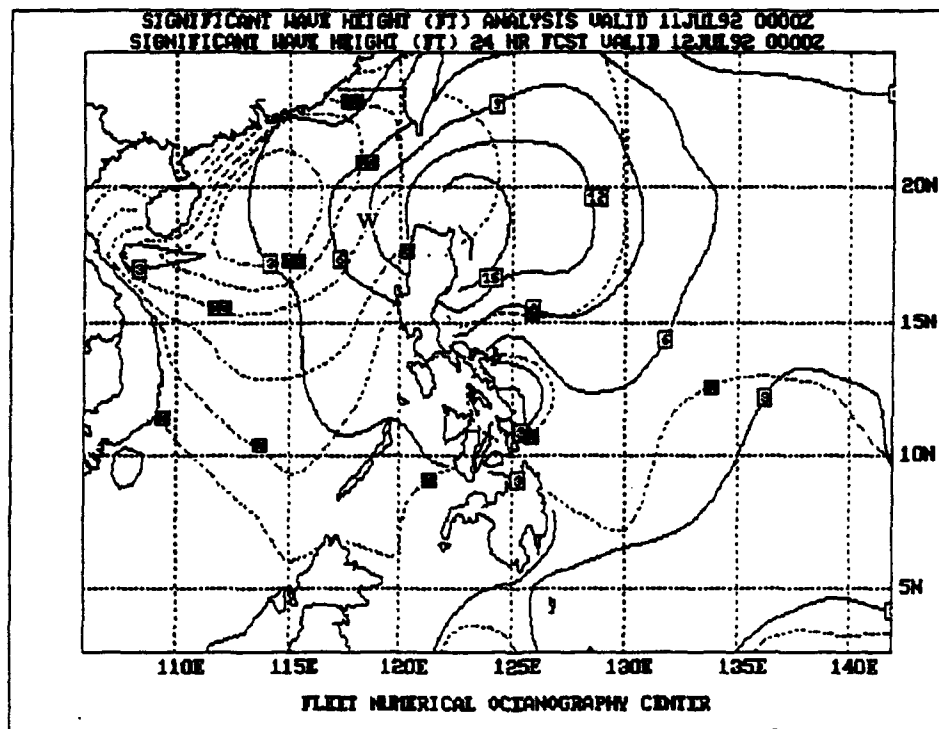
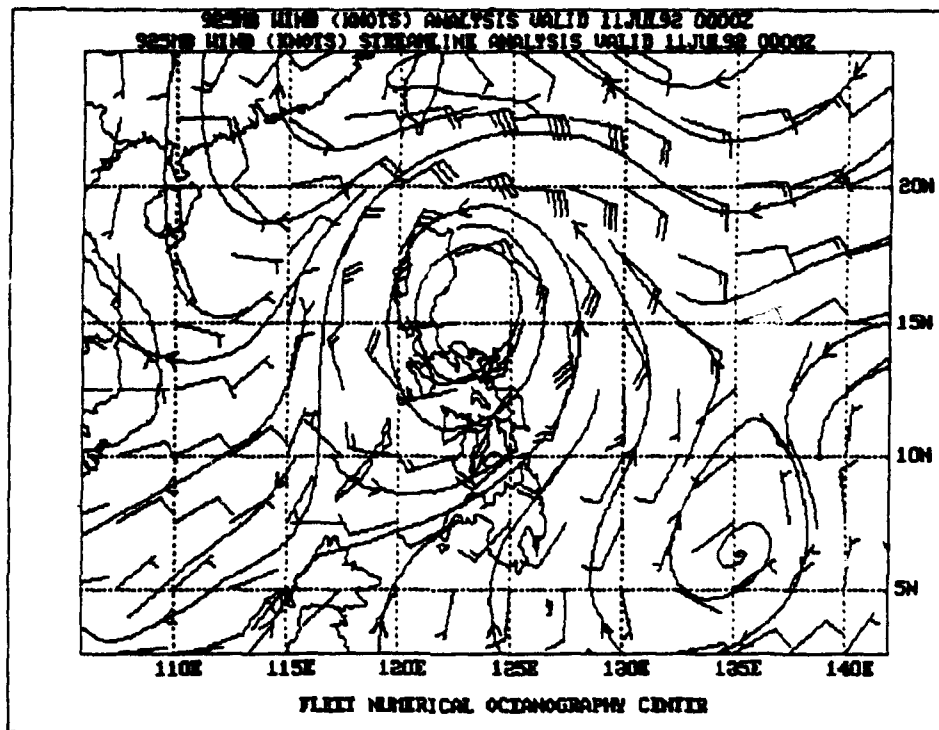
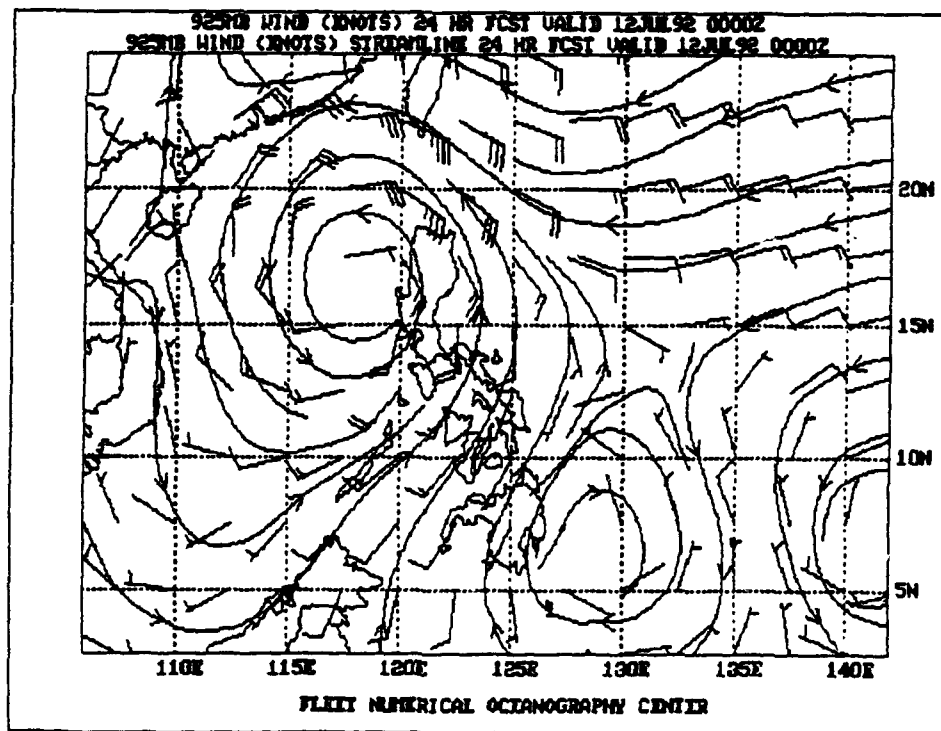


Figure 3.41: NODDS Significant Wave Height Analysis and 24-h Forecast from 0000Z 11 July 1992.



(a)



(b)

Figure 3.42: NODDS 925-mb Winds and Streamline Analysis (a) and 24-h Forecast (b) from 0000Z 11 July 1992.

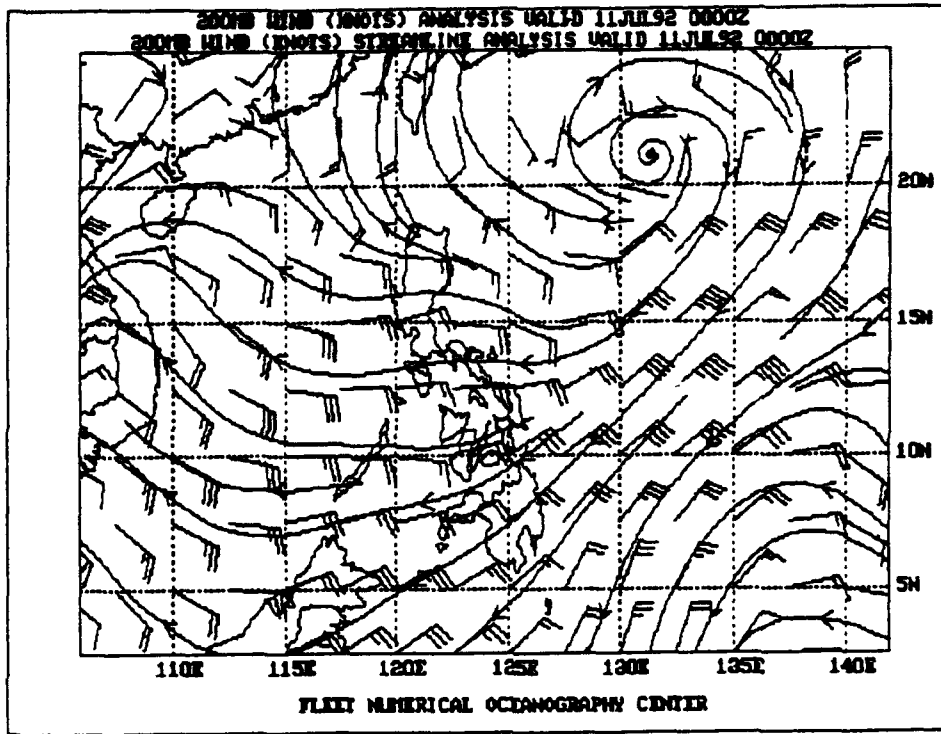


Figure 3.43: NODDS 200-mb Wind and Streamline Analysis valid at 0000Z 11 July 1992.

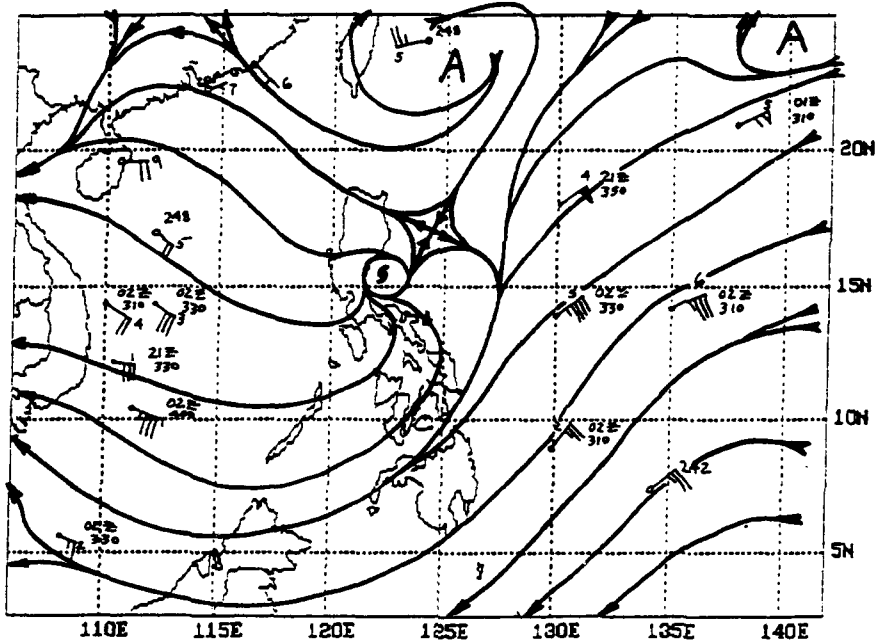


Figure 3.44: 200-mb Streamline Analysis valid at 0000Z 11 July 1992 (adapted from JTWC operational manual analysis)

Again, a direct readout DMSP satellite image, Fig. 3.45, is presented to permit comparison with the NODDS DMSP satellite image, Fig. 3.36. Note the characteristic signature of the north-south oriented sunglint, reflected from the ocean, north of Typhoon Eli in Fig. 3.45. This visible imagery, available to equipped stations, has a resolution of 0.3 nm.

Table 3.4 is a Tropical Cyclone "Satellite" Position Message (TPPN10 PGTW), prepared by JTWC. The text of the message (paragraph G) states that visible, infrared and enhanced infrared satellite imagery were used in locating Typhoon Eli at 16.2°N, 120.2°E (paragraphs C and D) (just off Dagupan (western Luzon) on Lingayen Gulf) at 0530Z (1330 Local Time). Paragraph E indicates that the position accuracy—Position Code Number (PCN)—of the TPPN message is a code "ONE", indicating that the determination of the position of Eli used the optimum combination of an "eye" and "geography"³².

Based on a combination of the satellite fix and synoptic data, the 110600Z warning placed Typhoon Eli at 16.1°N, 120.3°E, (in Lingayen Gulf) moving toward 280° at 20 kt with winds of 75 kt, gusting to 90 kt. (Note that despite the CI number of 5.0—corresponding to 90 kt in Table 3.3—in paragraph F of Table 3.4, the continued land interaction by the typhoon circulation prompted JTWC to reduce the 110600Z warning to 70 kt³³.)

Table 3.4: Tropical Cyclone Position Message (TPPN)

TPPN10 PGTW 110624Z July 1992

- A. TYPHOON ELI (05W)
- B. 110530Z
- C. 16.2N/9
- D. 120.2E/5
- E. ONE/SATELLITE
- F. T5.0/5.0/D1.5/24HRS (110530Z)
- G. VIS/IR/EIR LLCC

PBO 18NM RAGGED EYE. ORGANIZATION HAS REMAINED STEADY OVER THE PAST SIX HOURS WITH A SLIGHT DECREASE IN AMOUNT OF DEEP CONVECTION WHILE THE SYSTEM TRACKED OVER LAND. OUTFLOW IS GOOD ALQDS. CENTRAL EYE FEATURE HAS LOST SOME DEFINITION WITH WEAKENING OF SURROUNDING CONVECTION BUT REMAINS DISCERNABLE. DVORAK BASED ON DT AND PT.

The JTWC 110600Z Prognostic Reasoning Message then reported the 18 nm ragged eye and decreasing deep convection, as seen in paragraph G of the TPPN. The message continued that a slight slowing of movement was expected as Eli reorganized in the South China Sea—although slowing of Eli's movement did not occur until the 111800Z–120000Z period (see Fig. 3.18).

³²During the previous year (1991) 858 satellite position messages, with PCN of ONE & TWO, had a mean deviation from the JTWC Best Track Position of only 13.2 nm. The worse *mean* deviation, of positions using poorly defined circulations (PCN of FIVE & SIX), was 40.2 nm, but some individual cases may exceed 75 nm.

³³The Dvorak technique was developed for TCs over water, i.e., not located over land.

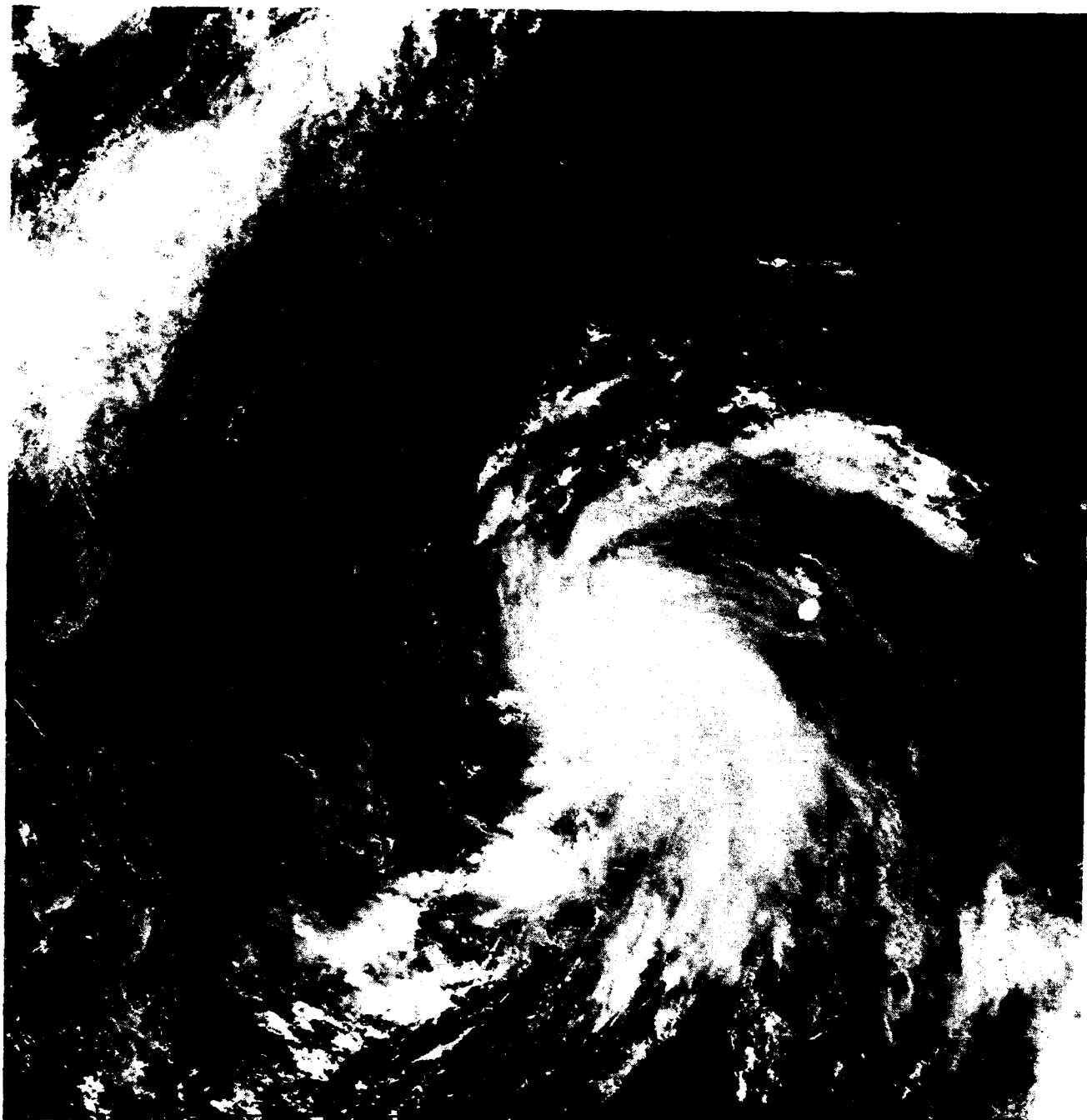


Figure 3.45: DMSP Visible Satellite Swath for 0103Z 11 July 1992 (received at Kadena AB, Japan)

At 110848Z, a TPPN message (not shown) from the USAF Global Weather Central (AFGWC) reported Eli near 17.1°N, 119.2°E. This TPPN assigned Eli a T-number of 4.0, but held the CI (Current Intensity) number at 4.5 in accordance with the Dvorak Technique for weakening systems (see Section 3.3.3). (Again, note that Table 3.3 equates a CI number of 4.5 with 77 kt winds; however, a portion of the typhoon was still over land.) Subsequently, this data (including wind radii information³⁴) was used in the 111200Z warning message.

Figure 3.46 is the NODDS DMSP IR image at 111300Z, one hour after the NODDS surface pressure analysis with synoptic reports at 111200Z, Fig. 3.47. While the NOGAPS "L" symbol, near 15°N, 120°E, is erroneously plotted, the 1008 mb isobar is well centered on the JTWC 111200Z Typhoon Eli warning position, 16.9N, 118.6E (Point "V" on Fig. 3.47). The warning reported maximum winds of 65 kt with gusts to 80 kt; the radius of 50 kt winds: 45 nm in the northeast semicircle and 25 nm elsewhere; and the radius of 35 kt winds³⁵: 100 nm in the northeast semicircle over water and 60 nm elsewhere.

The NODDS zoom Fig. 3.48(a) depicts wind of only 10 kt from the south at the coastal station of Vigan (WMO 98222); however, ships farther from the typhoon to the west (ELNA8) and to the north (9VNW) report winds of 20 and 25 kt, respectively. The greater zoom of Fig. 3.48(b) shows a shower at coastal city of Iba (WMO 98324) and continuous slight rain at Baquio (WMO 98328) in the mountains above 4000 feet in western Luzon.

³⁴AFGWC additionally supports JTWC by interpreting DMSP Special Sensor Microwave Imager (SSM/I) to provide the boundary (or radius) of gale force winds (34-kt) surrounding tropical cyclones. (SSM/I reports from AFGWC are 35-kt winds. Techniques used are the same as for 30-kt, but 17 m/s vice 15 m/s values are used.)

³⁵However, the NODDS graphical warning, Fig. 3.49, plots the 35 kt wind radius at 100 nm, entirely surrounding the warning position.

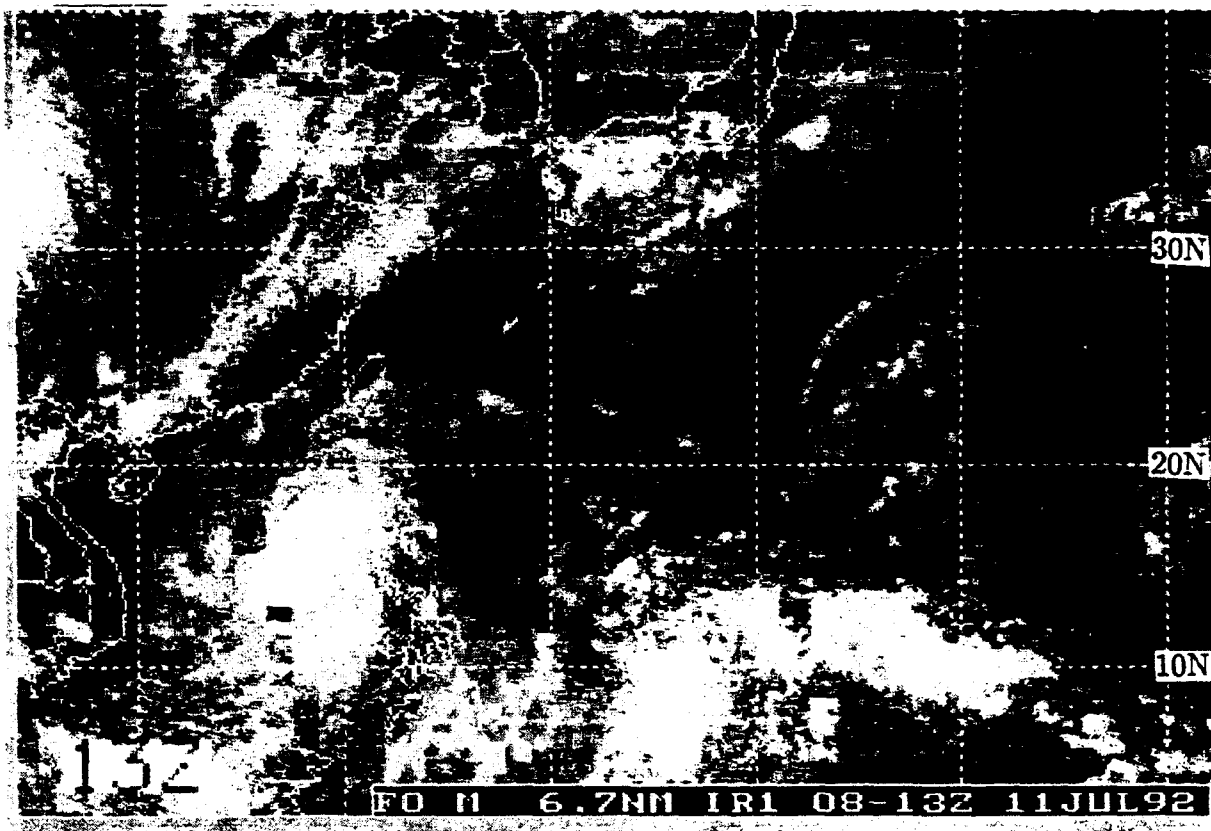


Figure 3.46: NODDS Mosaic of DMSP IR Satellite Imagery for 1300Z 11 July 1992.

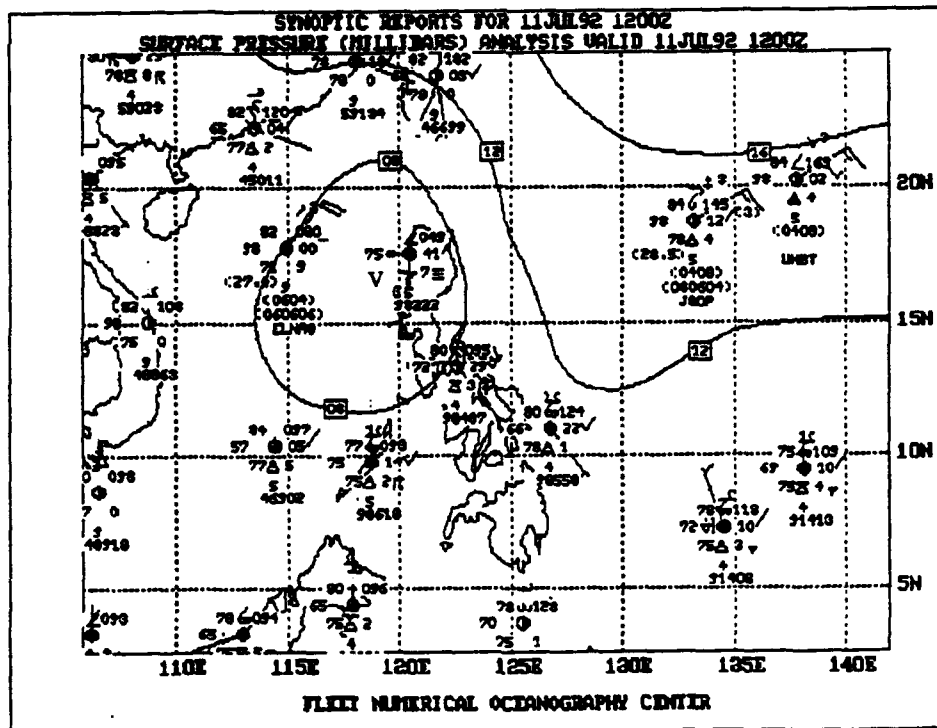
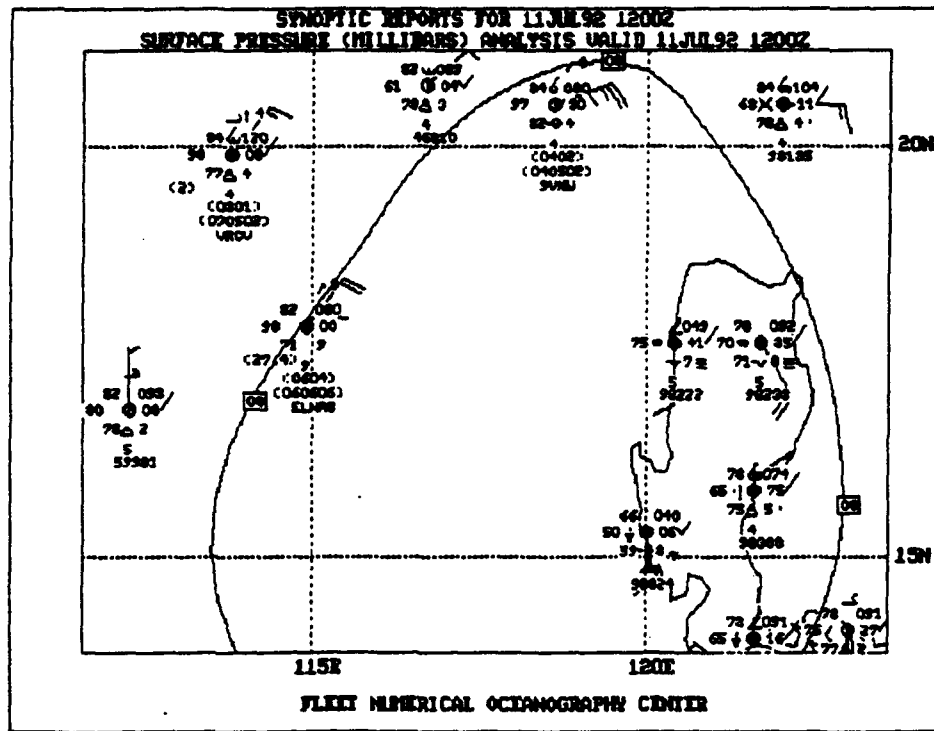
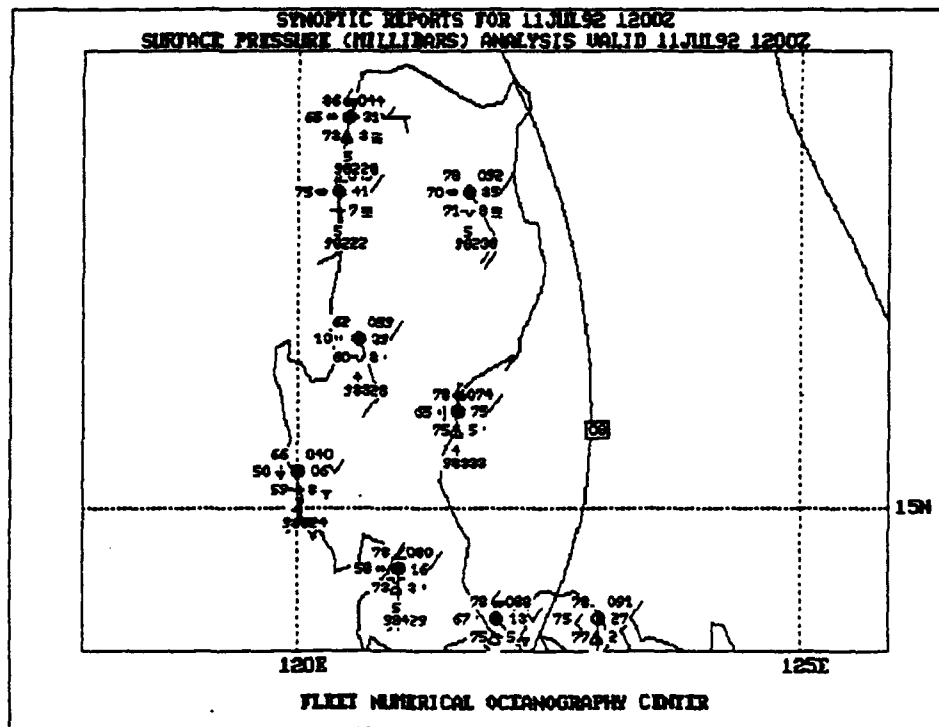


Figure 3.47: NODDS Synoptic Reports and Surface Pressure Analysis for 1200Z 11 July 1992.



(a)



(b)

Figure 3.48: NODDS Zoomed Synoptic Reports and Surface Pressure Analysis for 1200Z 11 July 1992.

Table 3.5 reveals a chronology of the sea-level pressure and wind at Cubi Point (WMO 98426), as Typhoon Eli passed about 100 nm, to the north. The table reveals that Cubi Point experienced a relatively low pressure of 1004.1 mb at 110400Z, likely at the time of the nearest point of approach of the typhoon³⁶. Then, after rising to 1004.4 mb, the pressure at Cubi Point resumed falling and reached its minimum of 1003.6 at 0700Z and 0800Z. Logic suggests that after moving over water (~0500Z), the central pressure of Typhoon Eli began falling again and/or the size of the low pressure area associated with the typhoon expanded. (Admittedly, surface pressure experiences a minimum at 1600 Local Time (0800Z) due to "Atmospheric Tides.") Regardless, the pressure gradient over Cubi Point increased, following passage of the typhoon. That is, while the wind was only 10 kt, gusting to 22 kt (0300Z-0400Z) when the typhoon was closest, the wind magnitude increased constantly until the 0800Z-0900Z period, when it peaked at 24 kt, gusting to 40 kt, coming from 190°, confirming that the typhoon was northwest of Cubi Point. The winds at the station dropped below 10 kt after 111200Z (not shown). Cubi Point reported 4.33 inches of rain associated with passage of the typhoon.

Next, the Cubi Point terminal forecast of winds during the typhoon passage, made at 102200Z (see footnote 28), is compared with the verifying observations in Table 3.5. Noting that Typhoon Eli had winds of only 65 kt at 101800Z—before the terminal forecast—, and that the typhoon intensified to 75 kt at the 110000Z warning—after the terminal forecast—, the wind forecasts³⁷ are quite good, despite being slightly under forecast. That is, wind forecasts for 0500Z-0700Z of 12 kt, gusts to 22 kt, were below the maximum of 16 kt, gusts to 28 kt, observed; and the forecast direction of 340° verified as 240° to 170°, due to the typhoon's moving so rapidly westward. Then, after 0700Z, the forecast of 18 kt, gusts to 28 kt (footnote 28), was below the maximum of 24 kt, gusts to 40 kt, observed during the 0800Z-0900Z period (Table 3.5).

Table 3.5: Cubi Point NAS (RPMB, WMO 98426) Surface Observations
AVERAGE WIND DURING PREVIOUS HOUR

TIME-July 1992	PRESSURE (mb)	Dir/Speed - Gust (kt)
110000Z	1005.9	VRB/01 - 04
110100Z	1005.6	CALM
110200Z	1004.9	200/04 - 07
110300Z	1004.7	200/09 - 14
110400Z	1004.1	330/10 - 22
110500Z	1004.4	240/12 - 34
110600Z	1003.8	180/14 - 27
110700Z	1003.6	170/16 - 28
110800Z	1003.6	180/20 - 35
110900Z	1004.0	190/24 - 40
111000Z	1005.1	180/14 - 31
111100Z	1005.5	170/13 - 37
111200Z	1006.3	190/13 - 20

³⁶The change of average wind direction to 330° between 110300Z and 110400Z was likely caused by nearby convection or a thunderstorm.

³⁷It is not known whether Cubi Point issued an amendment to the 102200Z forecast.

Figure 3.49, the NODDS graphics plot of the JTWC 111200Z Typhoon Eli warning, plots the warning position, with the radius of 35 kt winds reaching the northern portion of Lingayen Gulf. Now, refer to the original tropical cyclone warning, Fig. 3.26, made 24 hours earlier. While the predicted track direction is excellent, note that the original 24-h forecast position of Eli (for 111200Z) was over central Luzon—i.e., the forecast was slow. While the forecast speed of Eli crossing Luzon was 16 kt, Fig. 3.26, the working best track, Fig. 3.18, showed Eli moving at 16 kt for the first 6 hours, then at 25 kt, 19 kt and 18 kt, for the succeeding 6-hour periods. Also, while the 24-h maximum wind forecast at 111200Z was 60 kt, Fig. 3.26, and the verifying maximum wind was 65 kt, Fig. 3.49, note that Typhoon Eli had attained maximum winds of 75 kt earlier, while crossing the Philippine Islands.

Again, while Table 3.5 showed hourly observations at Cubi Point, this station, open on the southwest to the South China Sea, typically experiences much higher winds than the more protected Manila International Airport (WMO 98429). That is, Cubi Point had wind 190°/13 kt, gusts to 20 kt, during the 111100Z–111200Z period (Table 3.5), while Manila IAP had wind of only 180°/5 kt, at 111200Z (Fig. 3.48(b)).

Figure 3.50 is the 925-mb streamline analysis, “gradient level” analysis, in which the position of Typhoon Eli can be readily visualized west of Lingayen Gulf. Once again its position was forced to agree with the JTWC warning position, by the automated insertion of the 13 soundings in the near vicinity of the typhoon.

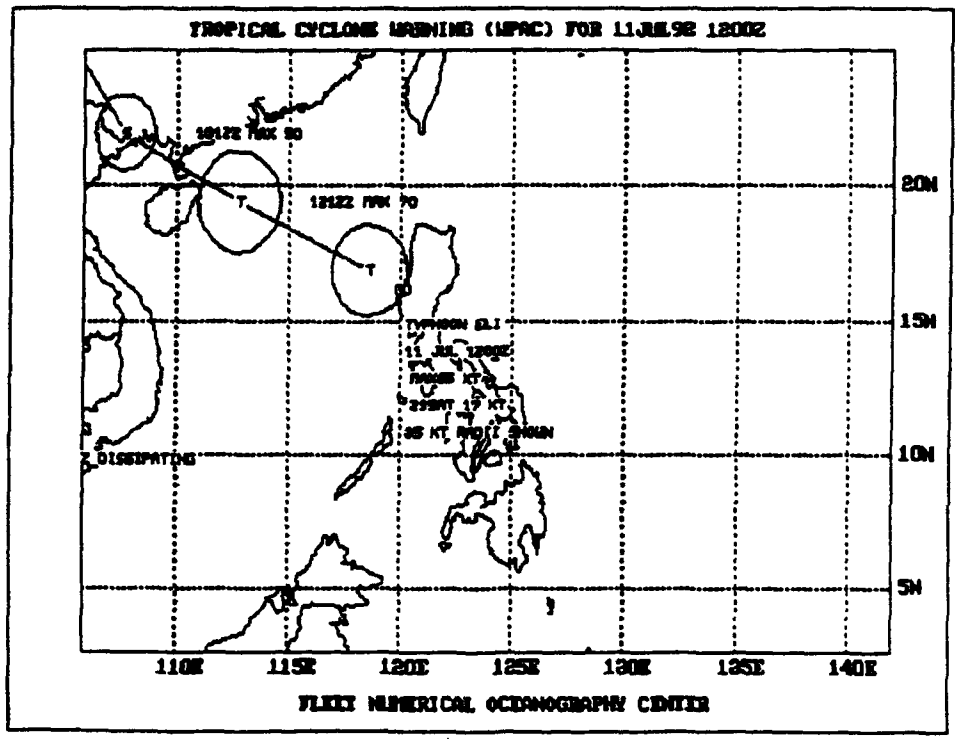


Figure 3.49: NODDS Tropical Cyclone Warning for Typhoon Eli for 1200Z 11 July 1992 (Max winds 65 kt, moving 295° at 17 kt, 35 kt radii shown)

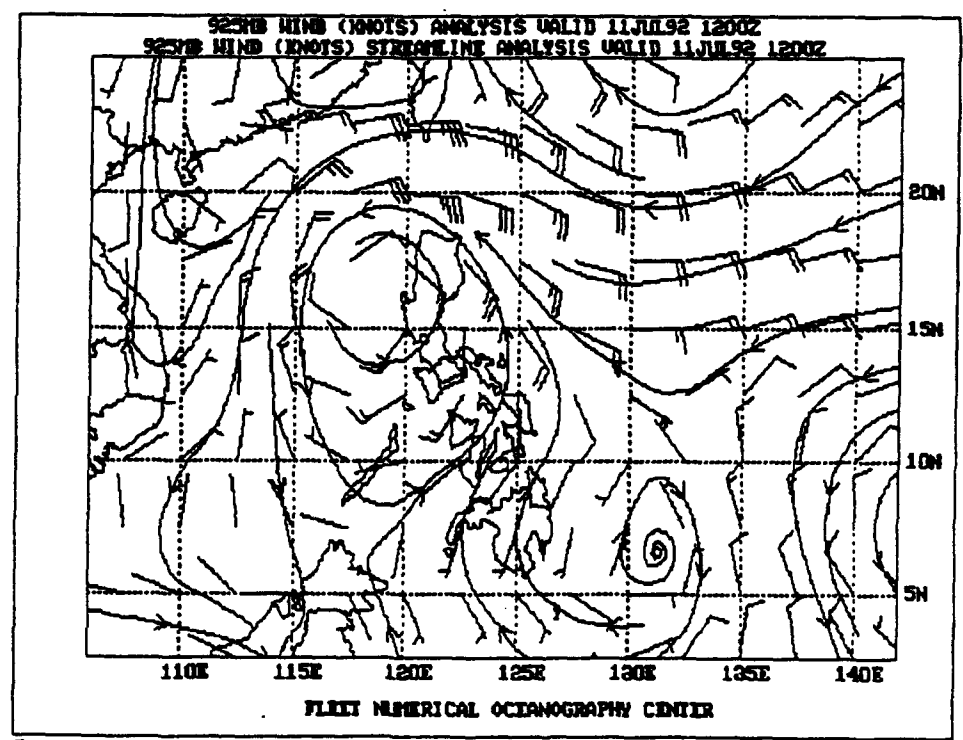


Figure 3.50: NODDS 925-mb Winds and Streamline Analysis for 111200Z 11 July 1992.

The solid isolines in Fig. 3.51, indicate the FNOC analyzed significant wave heights at 111200Z. Note that Fig. 3.51 places a maximum significant wave height of >18 feet centered near 17.5°N, 116.5°E, Point "U", just west of Typhoon Eli's position. A close examination of the 24-h significant wave height forecast, Fig. 3.30, reveals that while 18-foot waves were forecast near the northeast coast of Luzon—based on the earlier slower prognoses of Eli's speed of movement—, significant wave heights of ~15 feet were also forecast near Point "U".

However, a further examination of ship reports at 111200Z indicates that ship (ELNA8) at 17.5°N, 115°E on Fig. 3.48(a) is reporting waves of 6 feet and swells of 9 feet. Thus the FNOC significant wave height analysis of ~18 feet (Fig. 3.51) is much larger than the 6 foot wave height³⁸ reported by ship ELNA8. However, recall that the sea height observation at ship 7JFY in Fig. 3.38(a) at 110000Z verifies much better with the FNOC analysis. That is, 7JFY reports waves of 7.5 feet and swells of 9 feet compared with the FNOC significant wave height analysis of 9 feet at the position of ship 7KFY (Point "W") in Fig. 3.41. It should be noted that the FNOC seas (waves) are produced from the analysis and forecast of surface winds—i.e., the FNOC analysis of wave heights does not consider ship observations. Obviously, no conclusions can be made from such a small sample.

Finally Fig. 3.52 shows the FNOC SST analysis for 111200Z July 1992. The disappearance of the >30°C pool found earlier (101200Z) east of the Philippine Islands (see Fig. 3.31) follows the theory of Ekman transport. That is, the passage³⁹ of a tropical cyclone, produces Ekman transport of near-surface water outward. This horizontal divergence, near the surface, leads to upwelling of water from below. This, in combination with mixing caused by the strong winds of the tropical cyclone, plus cooling by evaporation, produces a cooler SST, in the wake of the tropical cyclone. The magnitude of the SST cooling caused by Eli was small, no doubt, since it moved so rapidly across the Philippine Sea.

12-13 July 1992

The rather straight track of Typhoon Eli as it left the Philippine Islands and rapidly crossed the South China Sea to make landfall in Vietnam (see Fig. 3.18) is not discussed. For its subsequent history, consult the forthcoming JTWC 1992 Annual Tropical Cyclone Report.

³⁸Even calculating the combined sea height—the square root of the sum of the squares of the wave height and swell height—places only ~11-foot combined seas at ship ELNA8.

³⁹It is recognized that the track of Typhoon Eli was along the northern periphery of the 30°C pool.

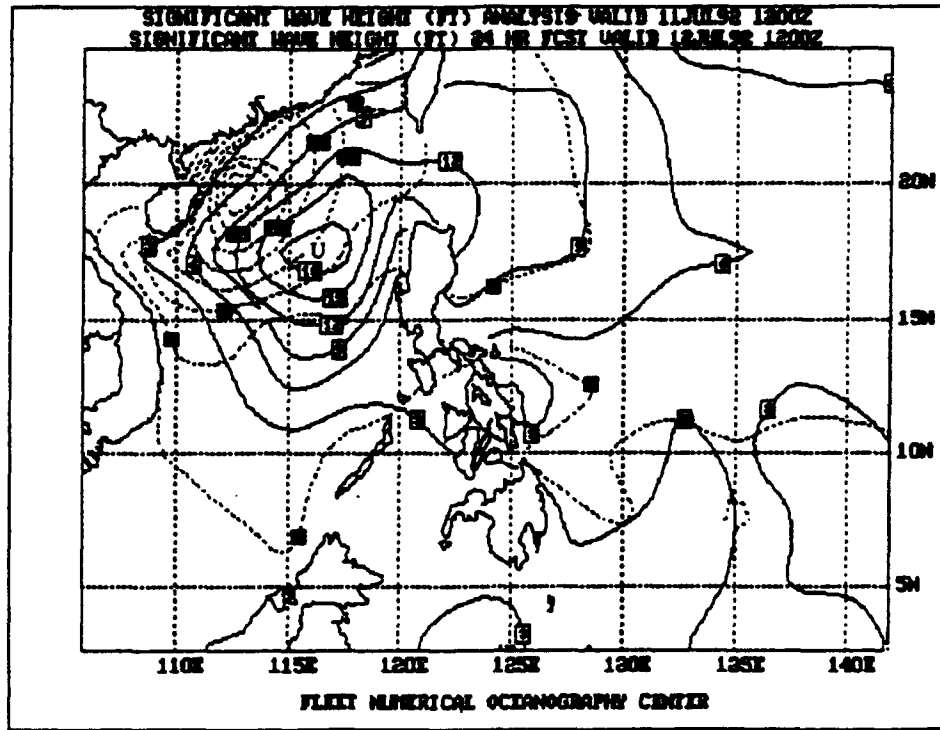


Figure 3.51: NODDS Significant Wave Height Analysis and 24-h Forecast from 1200Z 11 July 1992.

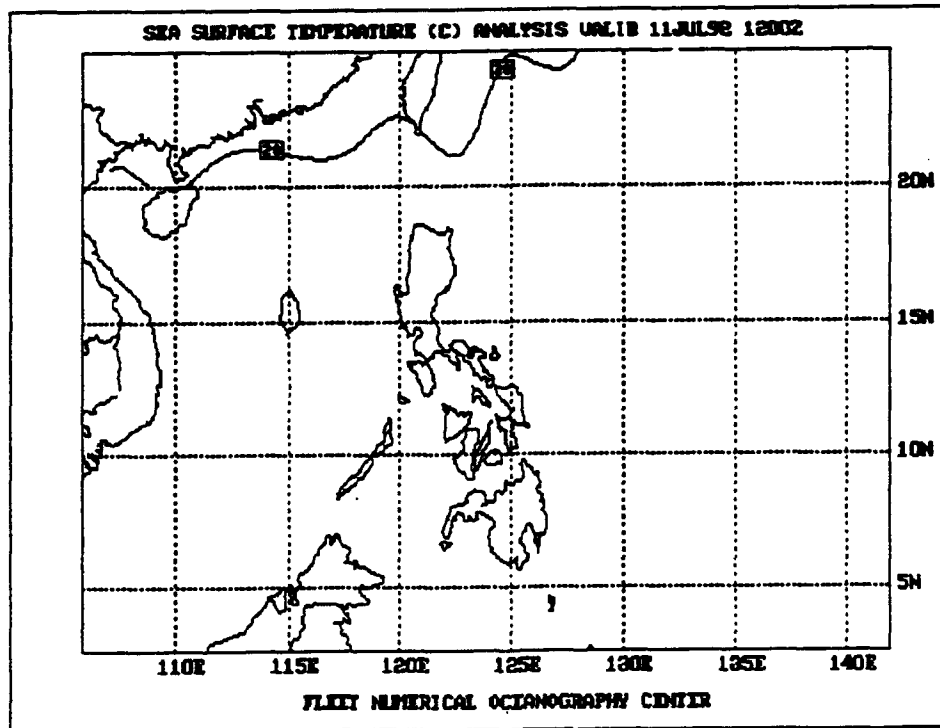


Figure 3.52: NODDS Sea Surface Temperature (°C) valid at 1200Z 11 July 1992.

3.5.2 Typhoon Bobbie, 23–27 June 1992 (A Quick Look)

For a comprehensive evaluation of the use of the NODDS distribution of NOGAPS analyses and prognoses of a typhoon see the first case study on Typhoon Eli. That case study presents examples of analyses and forecasts of many different parameters. This abbreviated case study of Typhoon Bobbie is presented to apprise the forecaster of (a) an example of the U. S. Navy's NOGAPS model forecasting the formation of a tropical disturbance that eventually becomes a typhoon and (b) an accurate JTWC forecast of a tropical cyclone that misses the Philippine Islands on a north-northwest track. Bobbie was destined eventually to become a "recurver", contrasted to the first case study of Typhoon Eli, a "straight-runner".

Following a very quite first half of 1992, Typhoon Bobbie was only the second tropical cyclone in the western North Pacific Ocean (02W) of the calendar year. The existence of fewer convective cells in the west, from which TCs could generate, may be tied to the warm episode in the eastern Pacific Ocean, the El Nino/Southern Oscillation (ENSO), as discussed in Section 2.3.1. However, it should be noted that the first five months of the year are typically inactive for the Philippine Islands. That is, Fig. 2.6 in Chapter 2 shows that during the 20 year period (1970–1989), a total of only 15 tropical cyclones hit the PI during the first five months of the year—contrasted to 11 TCs striking the PI during the month of June alone.

Figure 3.53 shows the path⁴⁰ ("working" best track) taken by Typhoon Bobbie as it moved north-northwestward across the Philippine Sea without making landfall on the PI.

23 June 1992

Figure 3.55⁴¹ is the NOGAPS 925 mb ("gradient level") streamline and wind analysis, at 230000Z June 1992. Southwesterly flow is evident over the South China Sea and the monsoon trough is present extending from northern Luzon toward the southeast. As shown by the NODDS DMSP IR image⁴², Fig. 3.54, most of the convection is south of the monsoon trough, with a strong convective cluster—cold cloud tops—centered near 8°N, 131°E (Point "T").

Note that the NOGAPS 24-h 925 mb streamline forecast ("prog"), Fig 3.56, made from the 230000Z analysis, predicts formation of a cyclonic vortex near 14°N, 131°E (Point "S"), at 240000Z. This is especially noteworthy, since the first "bogus" soundings were not inserted into the NOGAPS analysis until after JTWC issued the first warning on 02W, at 231200Z.

⁴⁰The track of Typhoon Bobbie is not shown after 1200Z on 27 June.

⁴¹Figures 3.55 and 3.56, 230000Z data, were obtained from the archives at the Naval Postgraduate School. When the first warning on Bobbie was issued 231200Z, only the 231200Z-run analyses and forecasts were available for real time recall ("down-loading" on a modem via NODDS) from FNOC.

⁴²Figure 3.54 additionally shows a cold front extending from east of Japan to a frontal wave (low) in the Sea of Japan, then extending along the coast of China to North Vietnam.

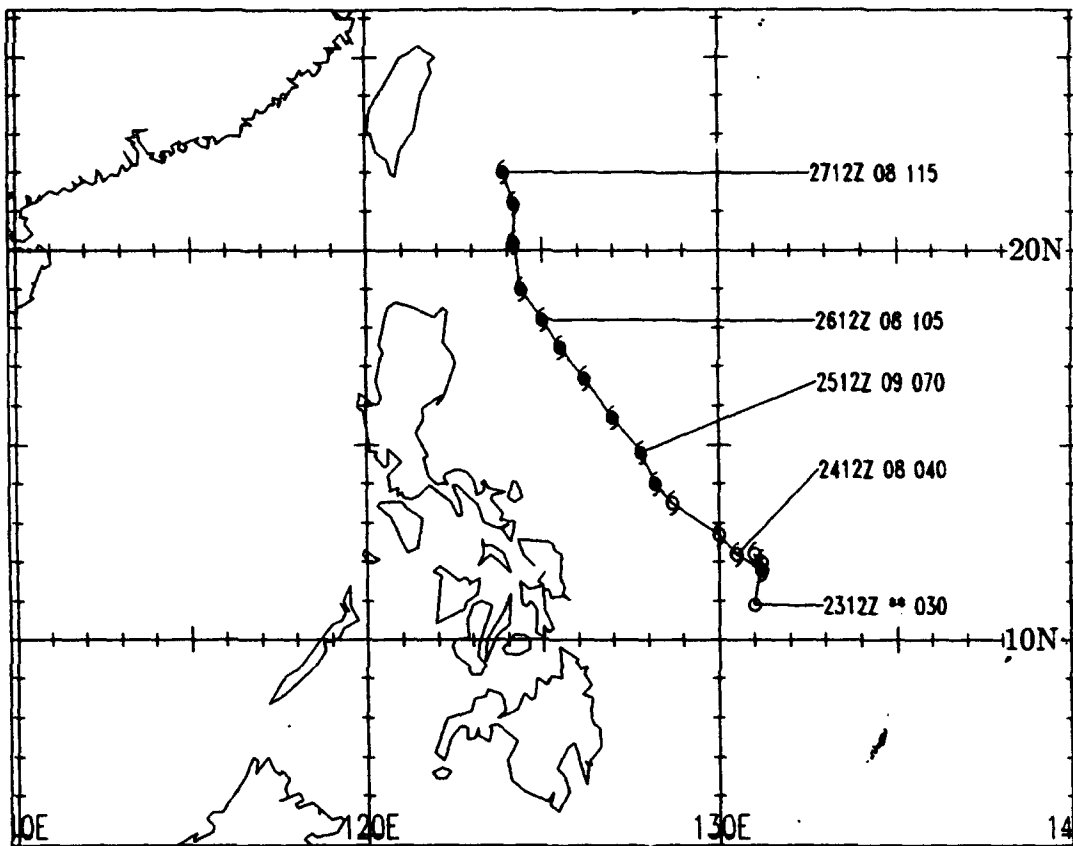


Figure 3.53: Working Best Track of Typhoon Bobbie in June 1992. (See Fig. 3.18 for label description.)

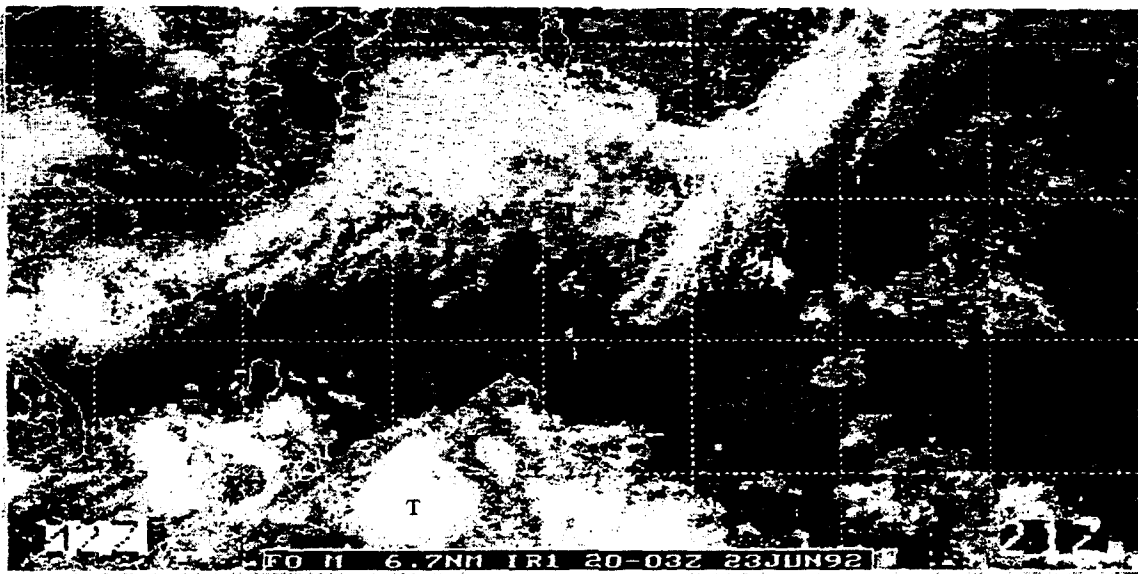


Figure 3.54: NODDS Mosaic of DMSP Infrared Satellite Imagery from 2000Z 22 June-0300Z 23 June 1992. (02Z in the lower left corner indicates that the swath nearest the PI occurred at 0200Z 23 June.)

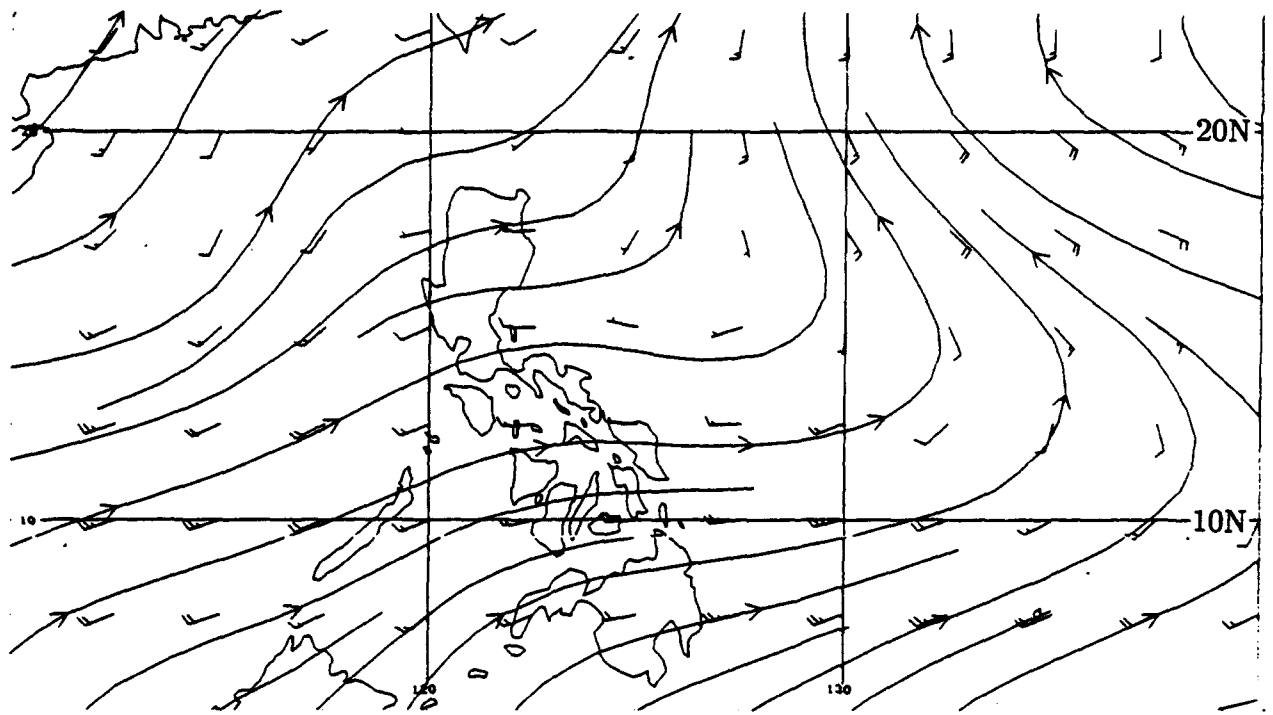


Figure 3.55: NOGAPS 925-mb Winds and Streamline Analysis at 230000Z June (from the Naval Postgraduate School)

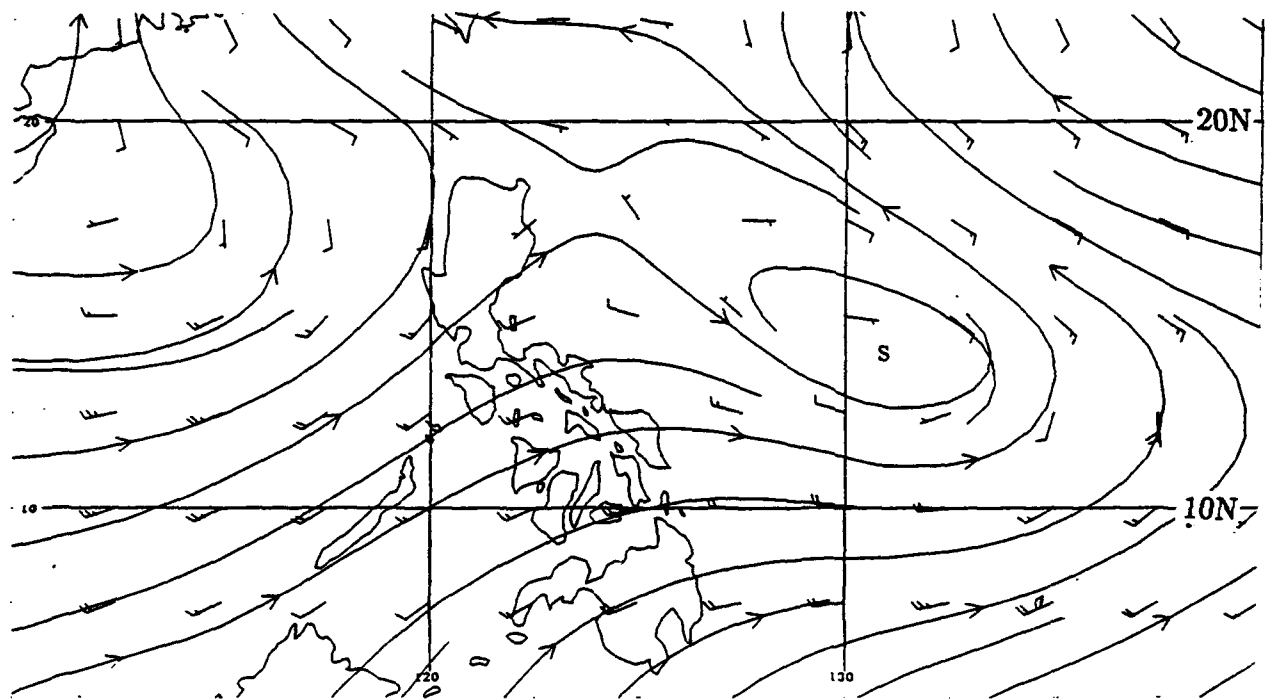


Figure 3.56: NOGAPS 925-mb Winds and Streamline 24-h Prognosis from 230000Z (from the Naval Postgraduate School)

24 June 1992

The track history of Bobbie, Fig. 3.53, shows that after the first position of 02W, the placement of the next several warning positions of the weak tropical cyclone was uncertain—or, at least, the tropical cyclone appeared to be quasi-stationary. However, by Warning No. 3 shown in Fig. 3.57, issued at 240000Z, 02W was located at 12.2°N, 131.0°E and designated Tropical Storm Bobbie, with maximum sustained winds of 35 kt and gusts to 45 kt. This position⁴³ is about 100 nm south of the vortex on the 24-h NOGAPS 925-mb prognosis verifying at 240000Z in Fig. 3.56—recalling, again, that there was no tropical cyclone on the 230000Z 925-mb streamline analysis, Fig. 3.55.

The JTWC Prognostic Reasoning Messages reported that Bobbie appeared to be embedded in the monsoon trough resulting in its slow motion. Movement to the north-northwest was still forecast by dynamic aids, with the NOGAPS deep layer mean circulation prognosis predicting little movement. As seen on Fig. 3.57, the 240000Z warning predicted Bobbie to move toward 330°, at 06 kt. More importantly, this early JTWC forecast, Fig. 3.57, from 240000Z, placed Bobbie, at typhoon strength, at 19.1°N, 123.8°E in 72 hours (270000Z), ~100 nm off the northeast top of Luzon—only about 50 nm⁴⁴ from the verifying position shown in Fig. 3.53.

Figure 3.58 shows the 240000Z NOGAPS Surface Pressure Analysis, with only weak cyclonic winds to support the JTWC warning position at Point “R”, while Fig. 3.59 is the NODDS DMSP image, one hour later.

More impressive is the 241400Z NODDS DMSP IR image, Fig. 3.60 showing a spiralling band, whose center position correlates well with the 241200Z warning position of TS Bobbie at 12.2°N, 130.5°E, with winds of 40 kt, gusts to 50 kt. JTWC’s Prognostic Reasoning Message reported that Bobbie was expected to track northwestward during the forecast period under the influence of the mid-level subtropical ridge, depicted by the latest NOGAPS 700-mb and 500-mb prognostic series (not shown). That is, no recurvature was anticipated within 72 hours.

Earlier, at 240430Z, a Tropical Cyclone Formation Alert (TCFA) was issued on the convection now located near Point “P” in the South China Sea, just west of the PI, Fig. 3.60. A Tropical Depression Warning was issued at 250000Z, and 03W went on to become Tropical Storm Chuck at 251200Z.

⁴³Since there had not been a WESTPAC tropical cyclone since January, the program that automatically inserts the bogus soundings into the FNOC analysis did not function for several synoptic runs, causing the low-level analyses to only show a trough at the location of Tropical Storm Bobbie. The insertion of the bogus soundings, to force the placement of a closed circulation at the location of Bobbie on the NOGAPS analysis, resumed proper operation at 251200Z.

⁴⁴JTWC official 72-h forecasts are not always so accurate; statistics published in the Annual Tropical Cyclone Report list the 1991 72-h average error as 287 nm.

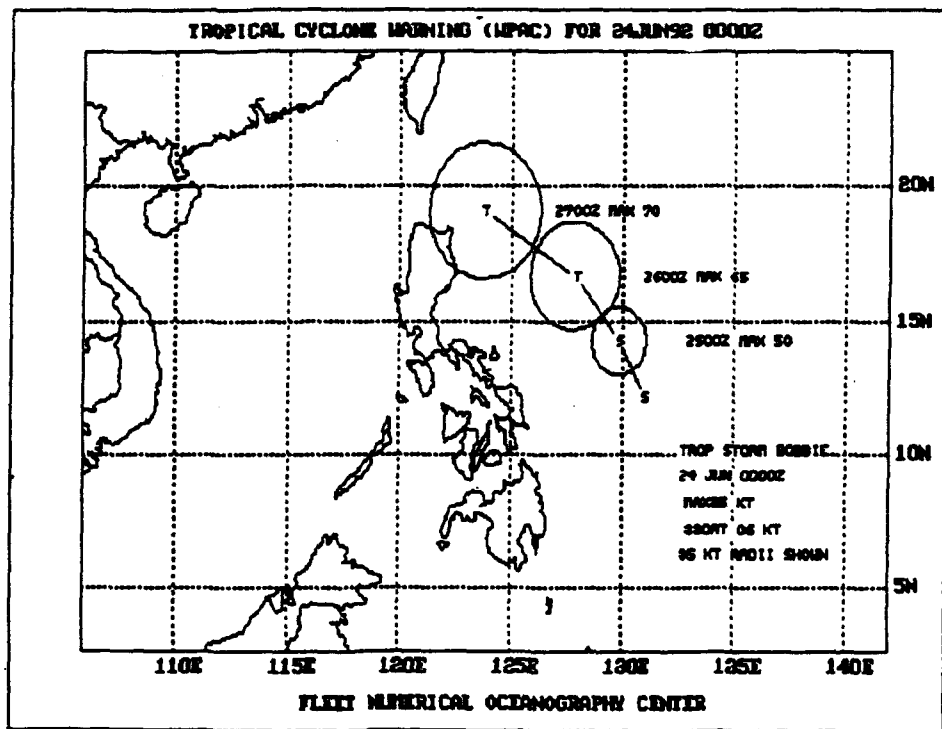


Figure 3.57: NODDS Tropical Cyclone Warning for TS Bobbie for 0000Z 24 June 1992 (Max winds 35 kt, moving 330° at 06 kt, 35 kt radii shown)

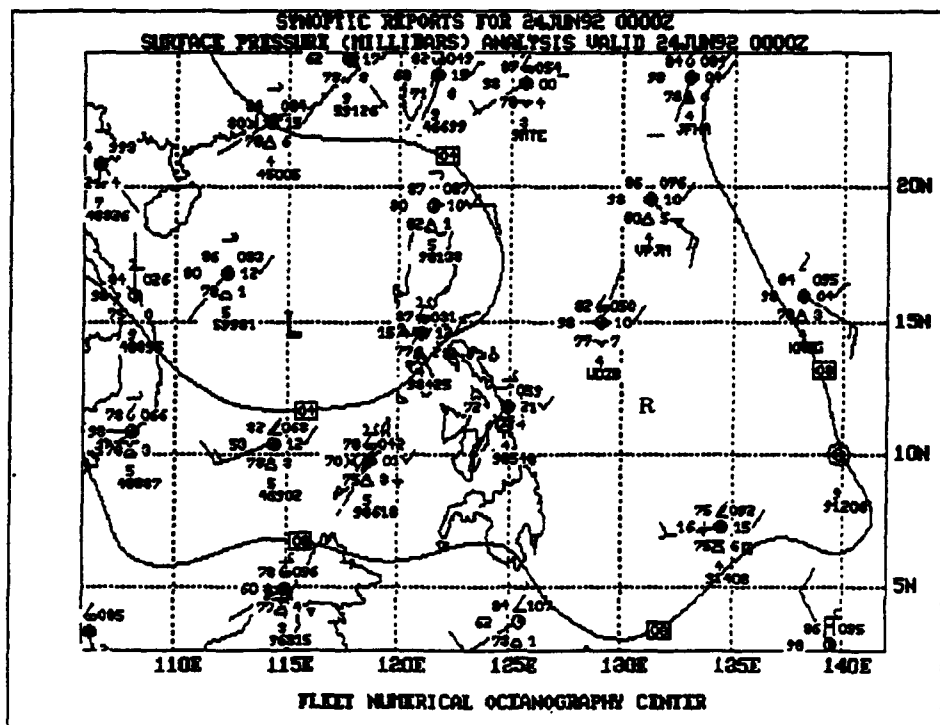


Figure 3.58: NODDS Synoptic Reports and Surface Pressure Analysis for 0000Z 24 June 1992.

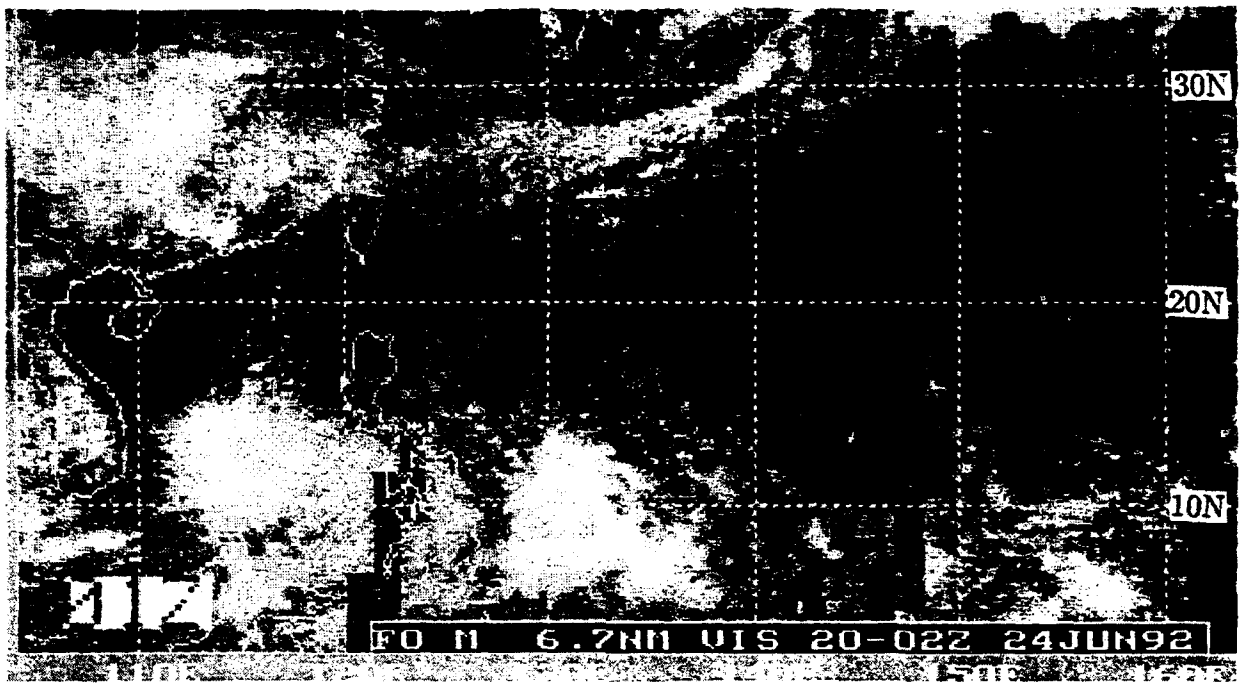


Figure 3.59: NODDS Mosaic of DMSP Visible Satellite Imagery from 0100Z 24 June 1992

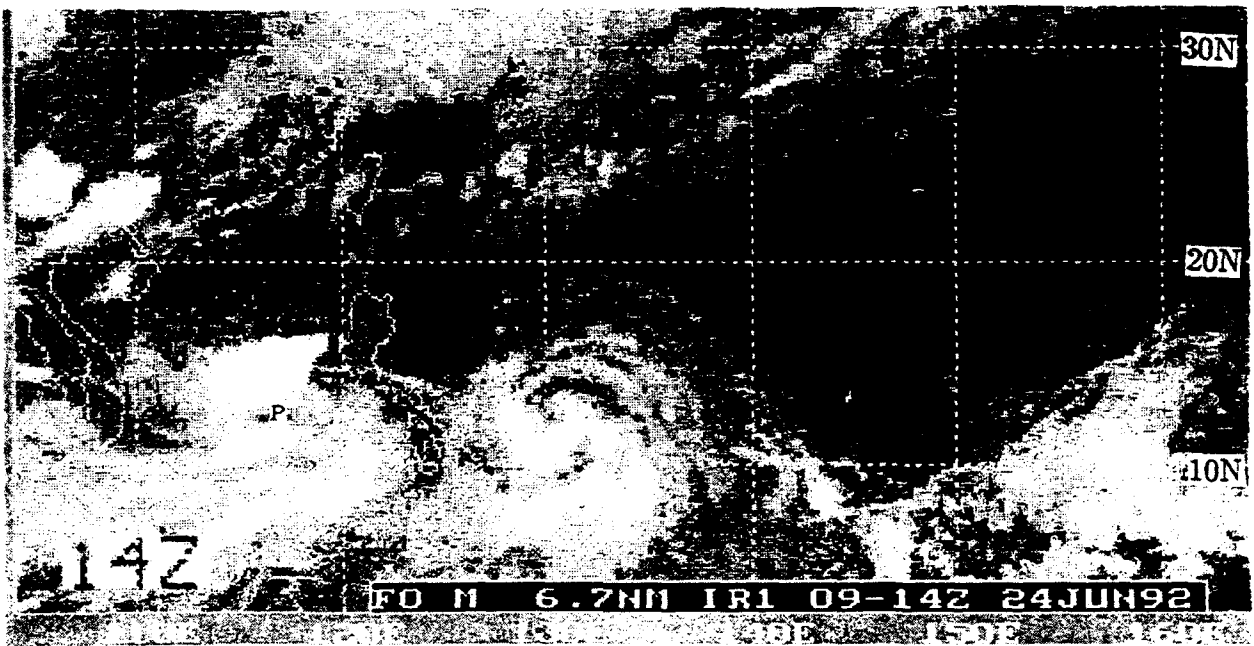


Figure 3.60: NODDS Mosaic of DMSP IR Satellite Imagery from 1400Z 24 June 1992

25 June 1992

Figure 3.61 shows the infrared signature of Typhoon Bobbie, east of the Visayas, and of the just designated Tropical Depression 03W (to become Chuck) in the western South China Sea at 250100Z. The NODDS graphical warnings of the two tropical cyclones at 251200Z⁴⁵ are then shown on Fig. 3.62. The 1200Z warning position for Bobbie, 14.8°N, 127.8°E is well located at the "L" symbol on both the NOGAPS surface analysis, Fig. 3.63, and zoomed surface analysis, Fig. 3.64. Note that this agreement between the FNOC typhoon position and the JTWC warning position is the result of the automated insertion by FNOC of 13 bogus soundings within 6° of the typhoon.

The 925-mb wind and streamline analysis and 24-h forecast are shown in Fig. 3.65(a) & (b). These gradient level streamlines are very useful; however, the maximum sustained winds will never be displayed on these synoptic scale charts. The forecast position of the vortex, Point "O", on Fig. 3.65 (b) represents the NOGAPS objective aid forecast for the 24-h movement of Typhoon Bobbie. Examination of the official JTWC warning 24-h position (labeled 2612Z Max 85) on Fig. 3.62 shows that the JTWC predicted movement was slower than the NOGAPS "objective aid" prognosis. Neither position is far from the verifying position on the "working" best track in Fig. 3.53.

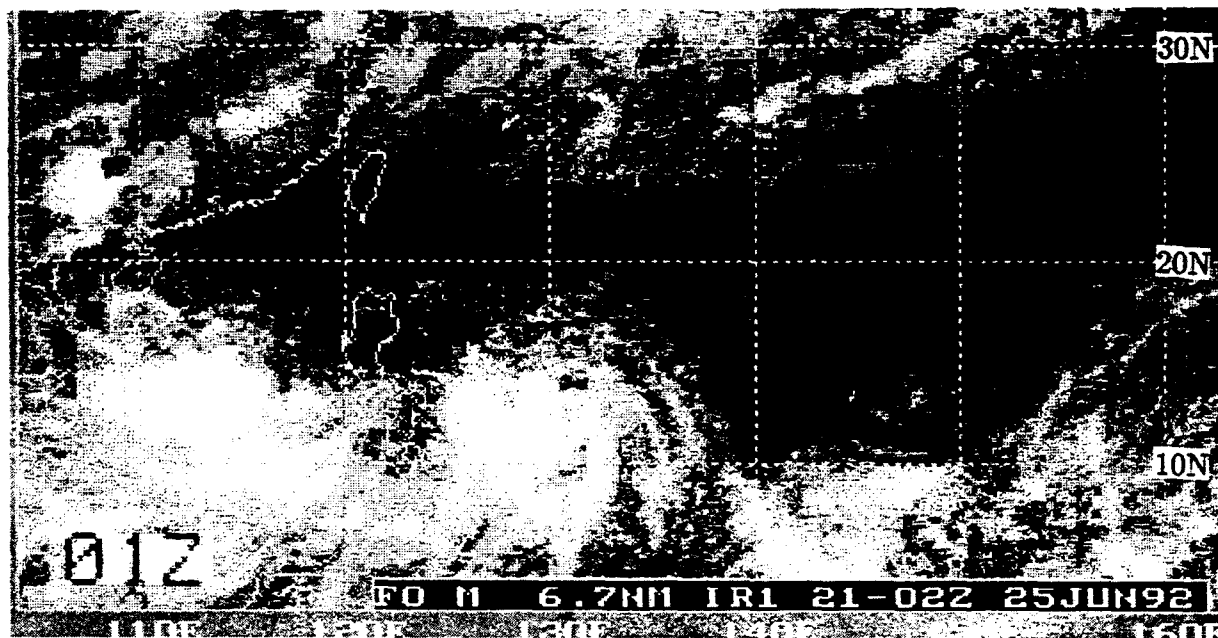


Figure 3.61: NODDS Mosaic of DMSP IR Satellite Imagery from 0100Z 25 June 1992

⁴⁵No 251200Z update of the NODDS DMSP satellite imagery was available—one of the few failures of the typically reliable NODDS operations during this typhoon season.

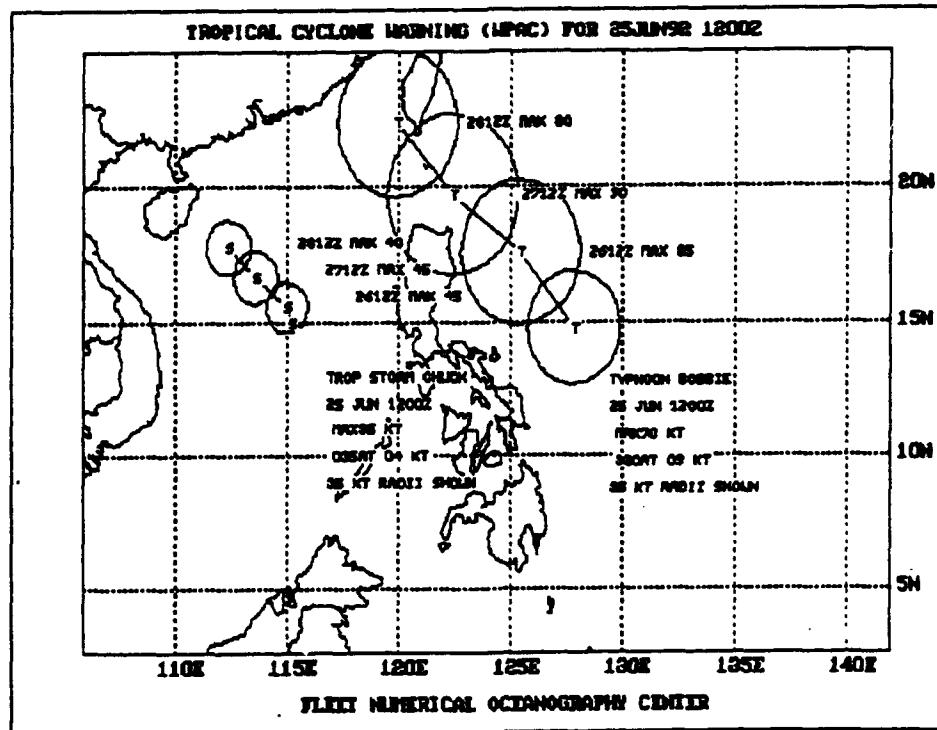


Figure 3.62: NODDS Tropical Cyclone Warning for Typhoon Bobbie for 1200Z 25 June 1992 (Max winds 70 kt, moving 330° at 09 kt, 35 kt radii shown) and for TS Chuck

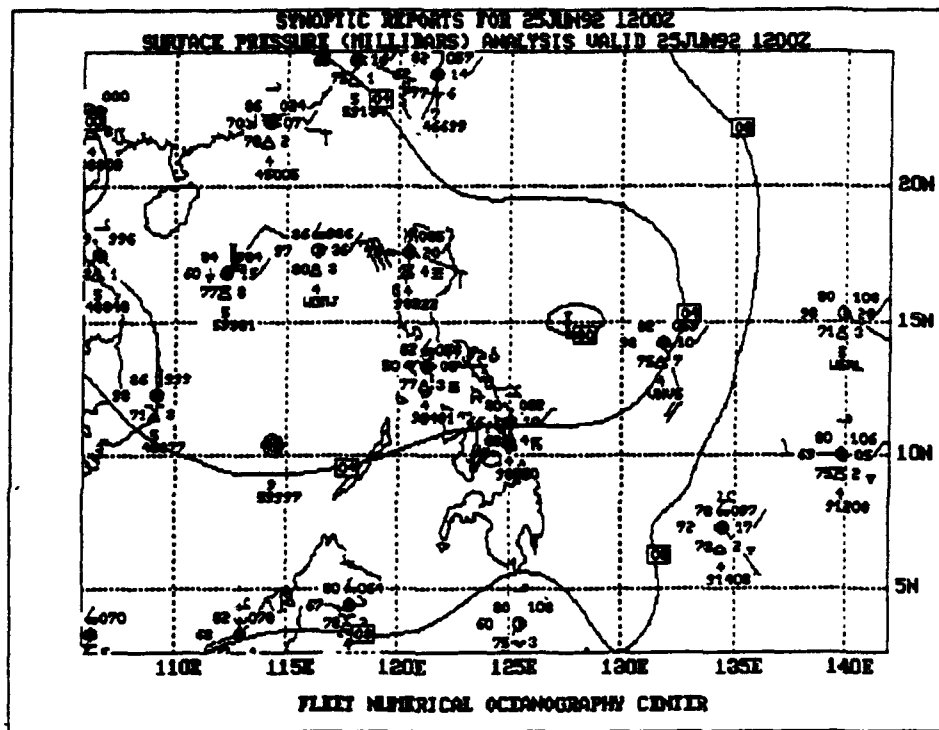


Figure 3.63: NODDS Synoptic Reports and Surface Pressure Analysis for 1200Z 25 June 1992.

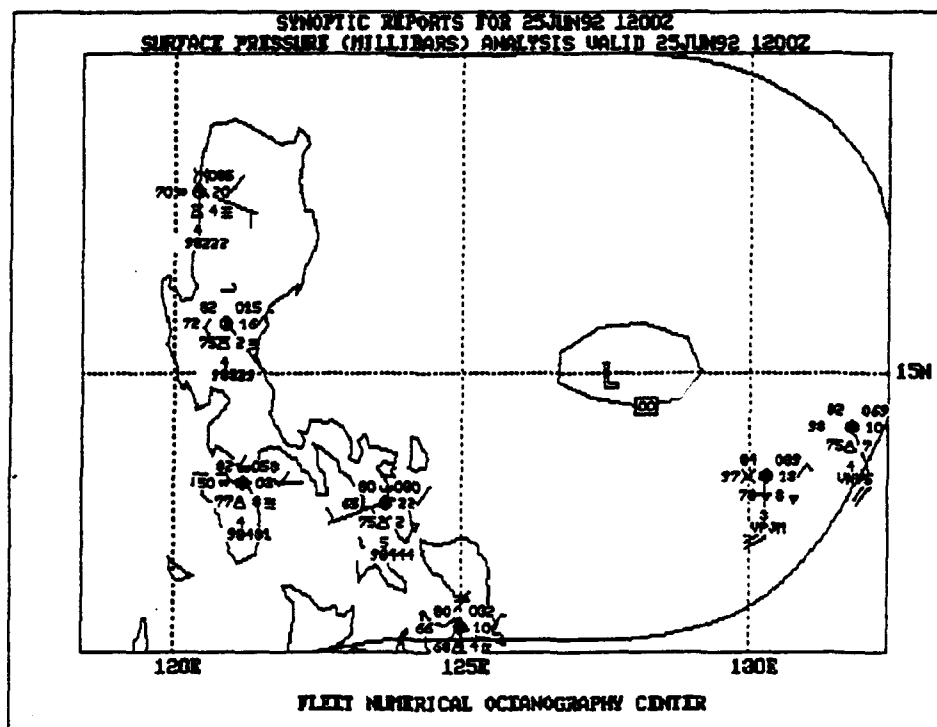
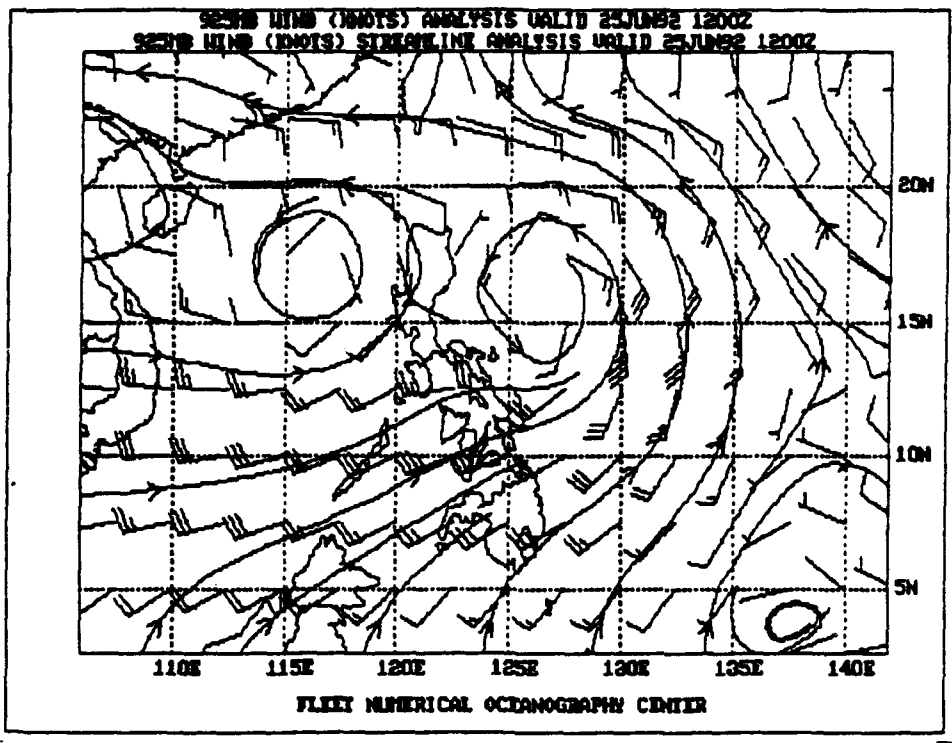


Figure 3.64: NODDS Zoomed Synoptic Reports and Surface Pressure Analysis for 1200Z 25 June 1992.

(a)



(b)

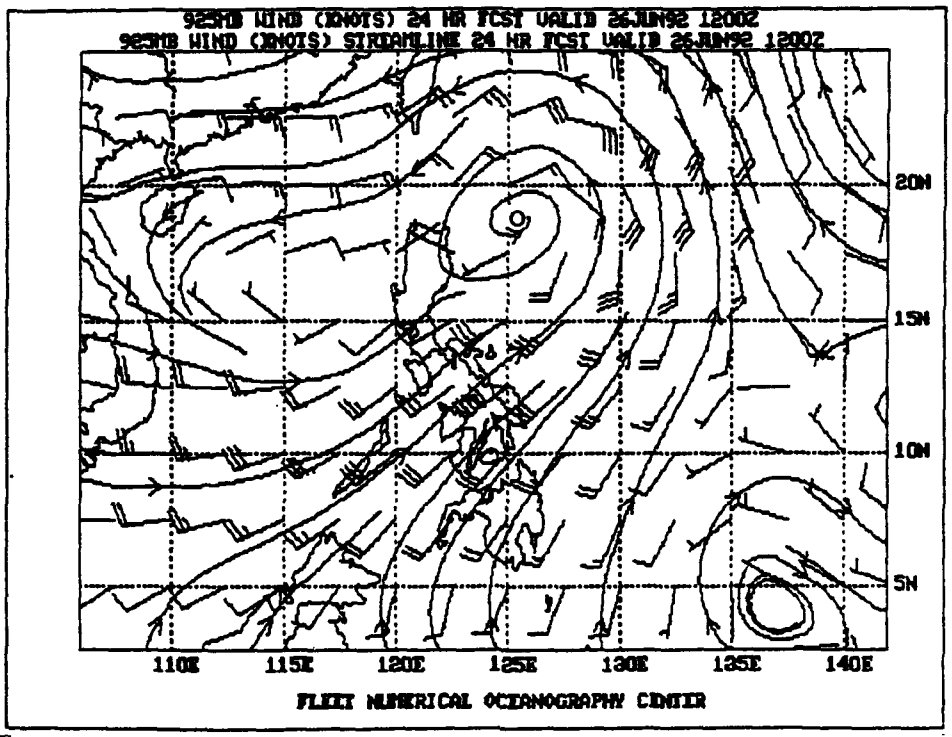


Figure 3.65: NODDS 925-mb Winds and Streamline Analysis (a) and 24-h Forecast (b) from 1200Z 25 June 1992.

26 June 1992

In this abbreviated case study, the last analyses to be examined are on 26 June. Figure 3.66 shows the graphical plots of three tropical cyclones in close proximity to the Philippines Islands. While TS Chuck is moving northwestward from the South China Sea toward Hainan Island and Tropical Depression 04 is entering the southern Philippine Sea, Typhoon Bobbie⁴⁶ is about 150 nm east of the northeast tip of Luzon, intensifying and moving northwestward at 10 kt. All three tropical cyclones are easily identifiable on the NODDS DMSP IR satellite imagery in Fig. 3.67, although the IR cold-cloud-top cluster representing Bobbie may be from the 0900Z DMSP swath. That is, the center of the "Bobbie" cluster in Fig. 3.67 appears south of the latitude, 18.2°N, the 1200Z warning position of Typhoon Bobbie in Fig. 3.66.

The JTWC Prognostic Reasoning Message stated that the track forecast philosophy on Typhoon Bobbie remained unchanged. It was expected that the mid-level ridge, located near 23°N (not shown), would weaken and allow Bobbie to take a northward track. The JTWC forecast track was a blend of dynamic, statistical and climatological forecast guidance.

Figures 3.68 and 3.69 show the NODDS 261200Z synoptic reports⁴⁷ and surface pressure analysis. While the NOGAPS surface analysis in Fig. 3.68 incorrectly labels the center of Bobbie with the computer symbol "L" at 20°N, the NOGAPS 925-mb wind and streamline analysis in Fig. 3.70 places the vortex (Bobbie) south of 20°N—more in agreement with the JTWC warning position in Fig. 3.66.

As discussed in detail in the preceding case study of Typhoon Eli, the NOGAPS 200-mb analysis over a typhoon is normally unsatisfactory to the tropical analyst. Therefore, despite the maximum sustained surface wind (105 kt) in Bobbie at 261200Z, the NOGAPS 200-mb winds and streamline analysis in Fig. 3.71 shows no anticyclonic outflow. It does appear that the FNOC-inserted bogus soundings (to 400 mb) are reflected by cyclonic streamlines on the 200-mb analysis in Fig. 3.71. It is possible that the anticyclonic outflow occurs at higher elevations⁴⁸, e.g., 100 mb. However, during two years of nearly constant monitoring of western Pacific typhoons by the author, no anticyclonic flow was observed on a NOGAPS 200-mb analysis above a typhoon. While few 200-mb winds, other than satellite wind vectors—such as those used by JTWC analysts to draw anticyclonic flow at 200 mb—, are received in the near vicinity of typhoons, it is possible that the Optimum Interpolation (OI) analysis scheme rejects these satellite wind vectors.

⁴⁶The NODDS "download" of Tropical Warnings in the northwest Pacific Ocean includes the latest warnings available. In Fig. 3.66, the TS Chuck and TD 04 warnings are for 1800Z, while the Typhoon Bobbie warning is for 1200Z.

⁴⁷Note that the Bobbie case study synoptic reports, in contrast to those of the Eli case study, do not include wave heights for the surface ships. Bobbie was the first Typhoon to affect the PI during 1992, and wave periods and heights were not included in the NODDS station model menu.

⁴⁸Flow was found to be cyclonic above Super Typhoon Flo at 200 mb in September 1990. However, the upward flux of cyclonic vorticity is, naturally, expected to extend much higher for super typhoons with surface winds >130 kt.

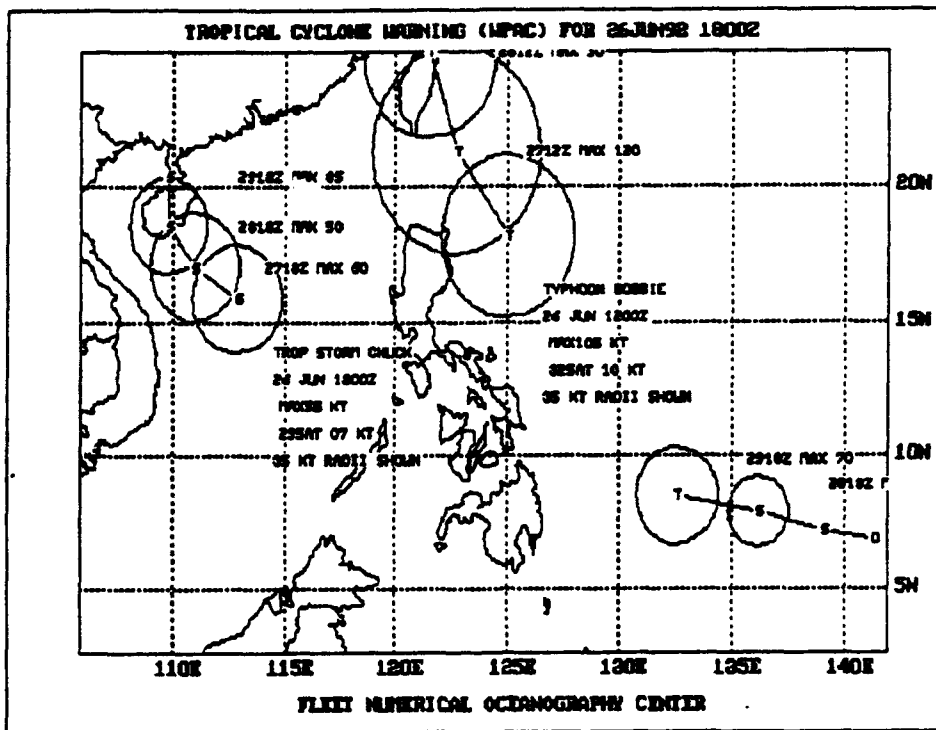


Figure 3.66: NODDS Tropical Cyclone Warning for Typhoon Bobbie for 1200Z 26 June 1992 (Max winds 105 kt, moving 325° at 10 kt, 35 kt radii shown), plus Tropical Storm Chuck and TD 04W for 1800Z

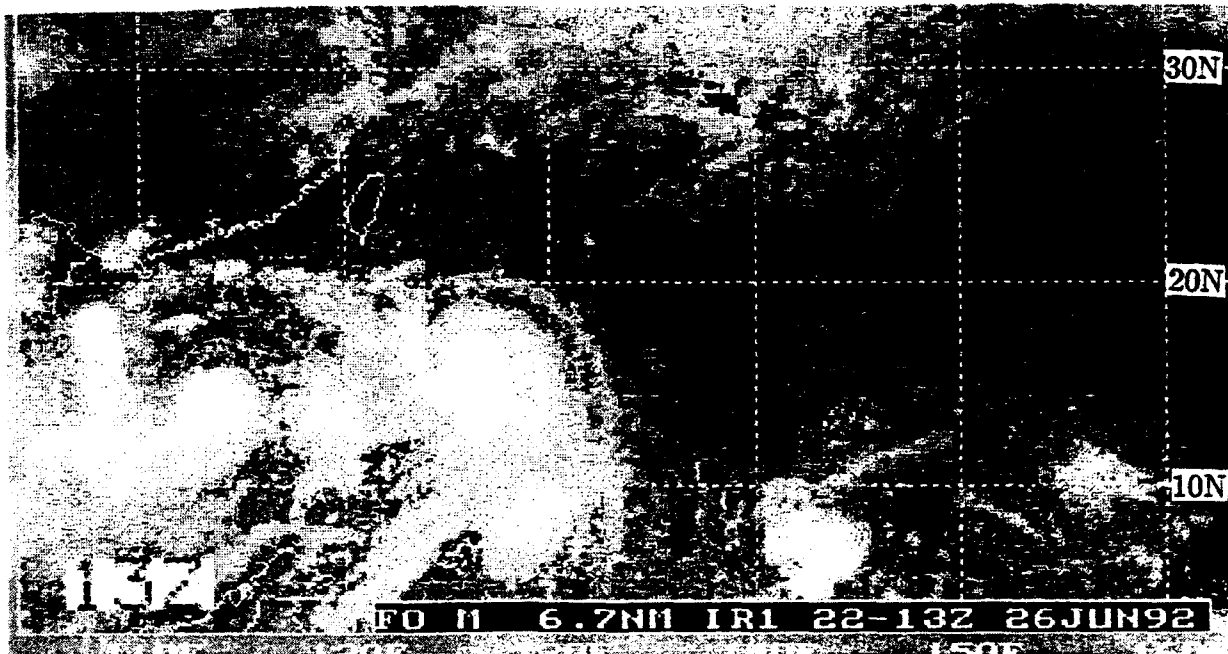


Figure 3.67: NODDS Mosaic of DMSP Infrared Satellite Imagery for 1300Z 26 June 1992.

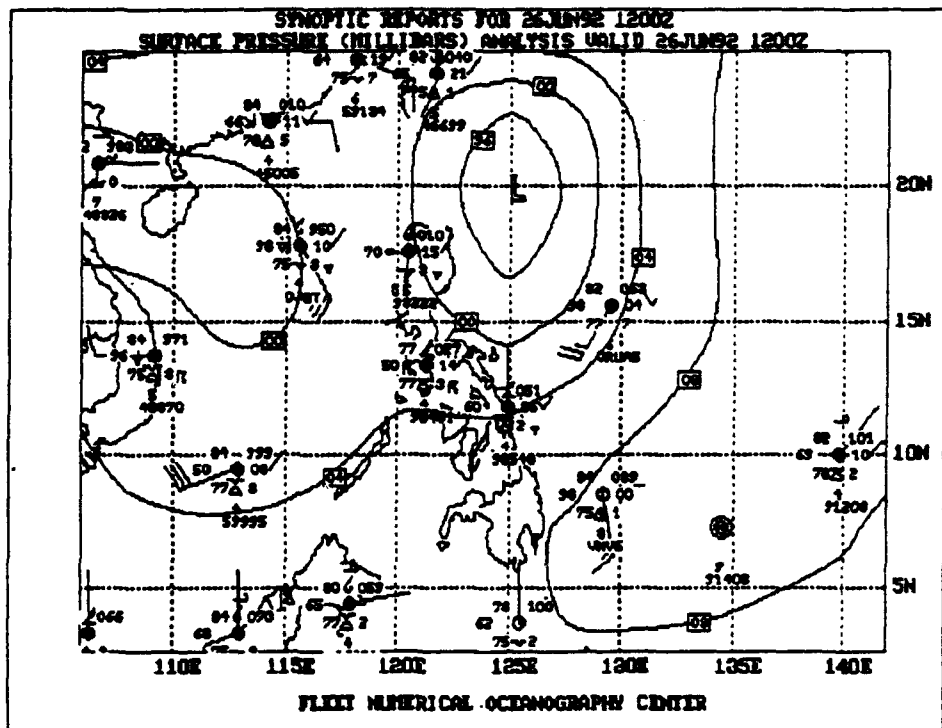


Figure 3.68: NODDS Synoptic Reports and Surface Pressure Analysis for 1200Z 26 June 1992.

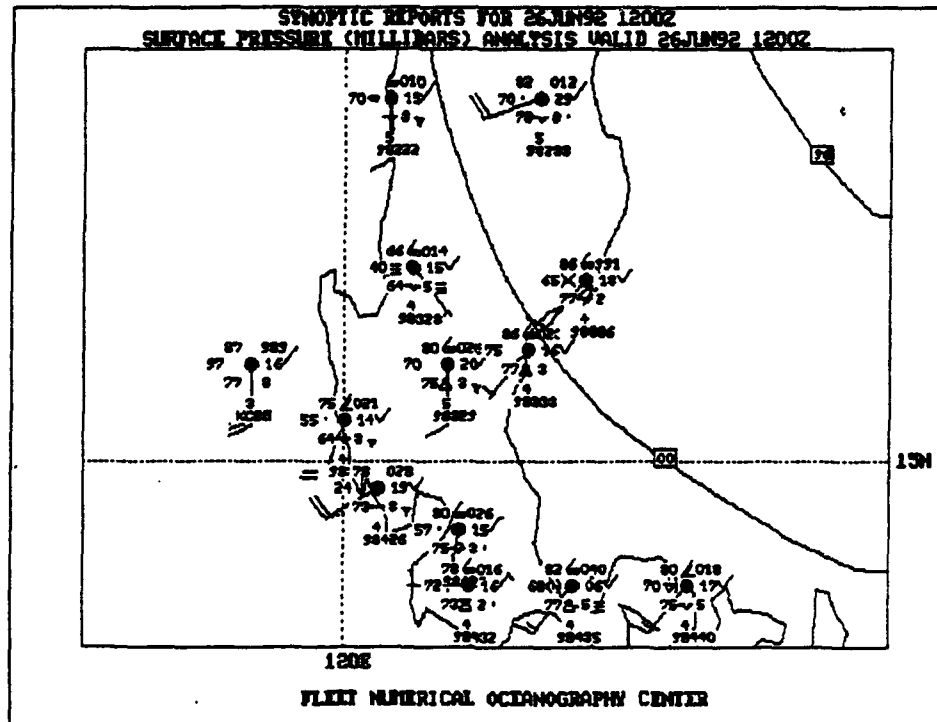


Figure 3.69: NODDS Zoomed Synoptic Reports and Surface Pressure Analysis for 1200Z 26 June 1992.

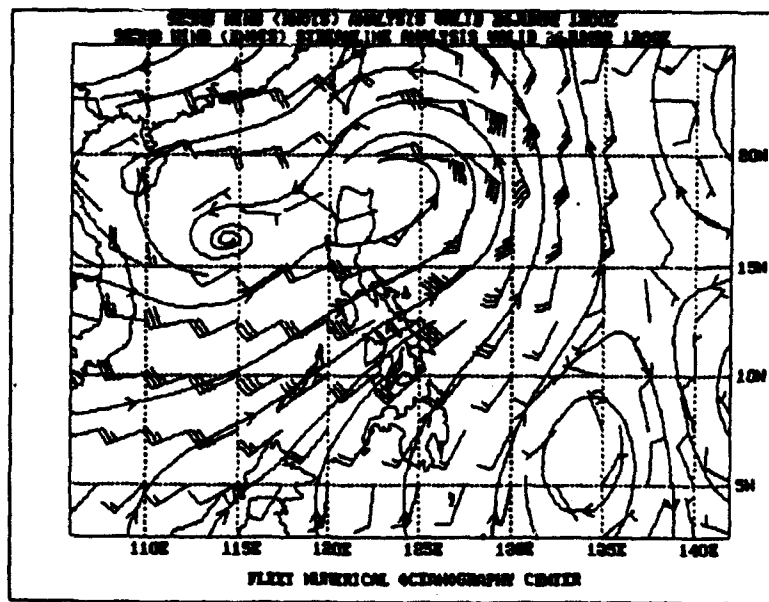


Figure 3.70: NODDS 925-mb Winds and Streamline Analysis for 1200Z 26 June 1992.

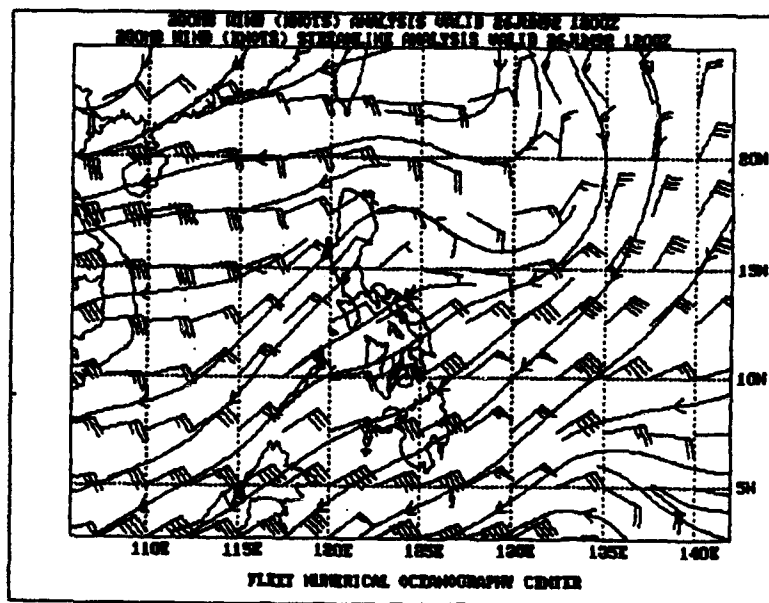


Figure 3.71: NODDS 200-mb Winds and Streamline Analysis for 1200Z 26 June 1992.

27 June 1992

Figure 3.53 shows the working best track of Bobbie only to 271200Z. After the storm passed to the east of Taiwan, its course changed toward the northeast (not shown). Thus the typhoon case studies display examples of a "straight-runner" (Eli) and a "recurver" (Bobbie).

3.5.3 An Atypical Southwest Monsoon Surge, 08–18 August 1992

While typhoons and tropical storms bring heavy, but generally localized, rainfall to the Philippine Islands, surges in the southwest monsoon bring heavy precipitation over much larger areas for much longer periods of time. As described by Guard (1985), these episodes are frequently caused by tropical cyclones located northeast of the PI which enhance low-level southerly and southwesterly winds (with the attendant returning upper-level northeasterly flow). A recent surge occurred over the PI in 1990 when Typhoon Yancy passed—no closer than 200 nm to the northeast tip of Luzon—on a northwest track, eventually striking Taiwan. The enhancement of the southwesterly winds over the PI can be readily visualized, as the winds spiral cyclonically over the PI into the tropical cyclone near Taiwan. Yancy resulted in heavy rains and flooding, leaving at least six people dead and more than 60,000 people fleeing to evacuation centers in Luzon (JTWC 1991). A brief examination of a weakening Super Typhoon Omar striking Taiwan in early September 1992—with its induced surge in the southwest monsoon over the PI—is presented in Section 3.5.4.

Figure 3.72 depicts the three types of monsoon surges: weak, moderate and strong, in accordance to the depth and intensity of the low-level southwesterly flow (Guard 1985). While Guard earlier attributed the associated cloudiness and weather with the depth of the low-level southwesterly winds—rather than the strength of the low-level wind—, he later states in Guard (1986) that the associated weather is contingent on the strength and distribution of upper-level divergence. Obviously the depth of the low-level winds is linked to the upper-level divergence. The characteristics of the three types follow (Guard 1986):

1. **Weak Monsoon Surge:** Southwesterly winds up to 15 kt extending to 5,000 feet; northeasterlies dominate above 15,000 feet. Weather is characterized by isolated cumulonimbus and dense cirrostratus. Weather is generally fine—showers regime (Ramage 1971).
2. **Moderate Monsoon Surge:** Southwesterly winds up to 25 kt extend to about 15,000 feet; northeasterlies dominate above 20,000 feet. Weather is characterized by nimbostratus (most tops to 15,000 feet) with imbedded cumulonimbus. Light rain is interspersed with moderate and occasionally heavy, but patchy rainfall and broken to overcast ceilings—rains regime (Ramage 1971).
3. **Strong (Deep) Monsoon Surge:** Southwesterly winds up to 50 kt extend above 25,000–30,000 feet; strong northeasterlies dominate above 35,000 feet. Weather is characterized by dense nimbostratus (tops to ~25,000 feet) with embedded cumulonimbus. Precipitation is light to moderate with frequent episodes of heavy rainfall and dense overcast (rains regime). Fog frequently forms when rains become light or intermittent.

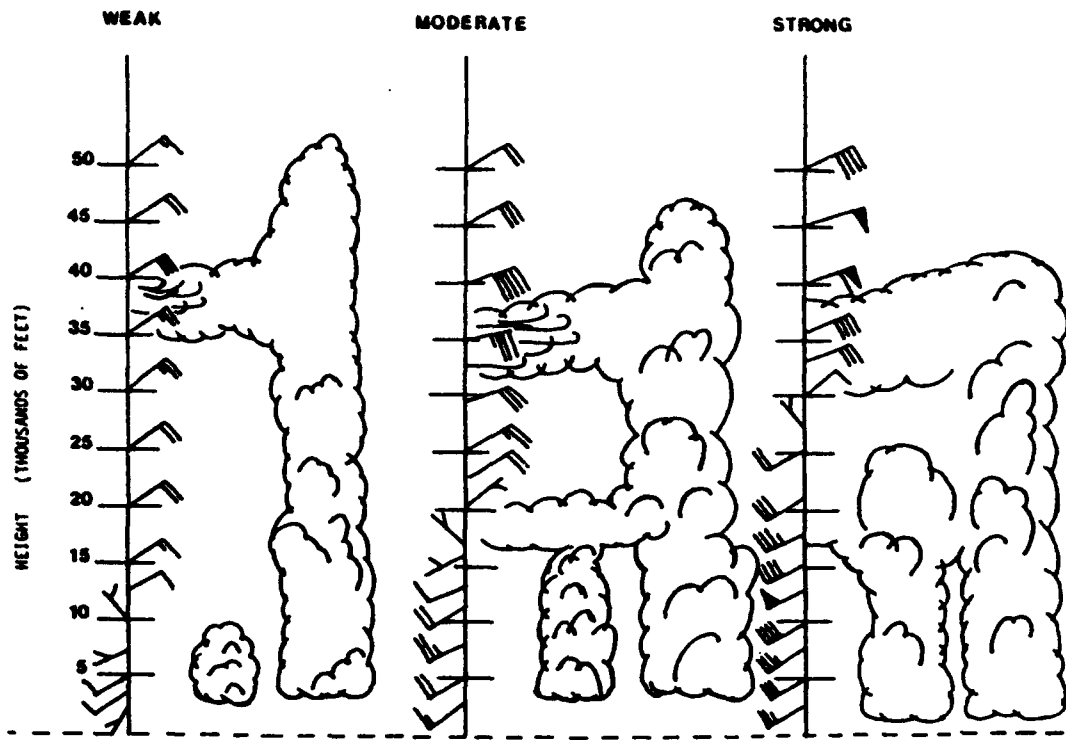


Figure 3.72: Vertical Cross Sections depicting the Wind Profile associated with the Weak, Moderate and Strong Monsoon Surges. Winds are in knots: pennants equal 50 kt, full barbs equal 10 kt, and half barbs equal 5 kt (from Guard 1986).

08-13 August 1992

Although the gradient level flow over the Philippine Islands first became southwesterly in June, 1992, the staff of the Naval Oceanography Command Facility (NOCF) Cubi Point reported that the “real” southwest monsoon appeared to commence on 9 August. That is, a “rains regime” commenced. Table 3.6 lists the 24-h precipitation⁴⁹ recorded at Cubi Point during the period 9-18 August 1992.

Table 3.6: NOCF Cubi Point 24-h Rainfall during August 1992 (inches)

Date	09	10	11	12	13	14	15	16	17	18
Precip. (inches)	1.66	1.29	0.13	0.20	0.25	2.11	3.15	6.45	3.01	3.92

FNOC products (not shown) revealed that while the 080000Z August 925-mb flow was westerly, crossing the South China Sea and flowing over Luzon, the NOGAPS 24-h forecast 925-mb wind for 090000Z was southwesterly, coming from Palawan and Mindoro toward

⁴⁹NOCF Cubi Point 24-h rainfall is recorded for the time period 0000-2400 Local Time, i.e., 0800Z-0800Z.

Manila. The NOGAPS 24-h southwesterly wind direction verified⁵⁰ and thus correlates well with the statement of the NOCF staff that their southwest monsoon actually began on 9 August.

14 August 1992

Examination of the wind at the grid point nearest to Cubi Point (NOGAPS grid point (15°N, 120°E)) reveals the following:

1. From a 700-mb wind analysis of 225°/15 kt at the grid point at 140000Z, NOGAPS made an excellent increasing wind forecast of 225°/20 kt for 150000Z. The verifying wind, at 150000Z was 225/25 kt—the first 700 mb wind above 20 kt, at the grid point, during the case study. (Note that the rainfall increased significantly to 2.11 inches on the 14th (see Table 3.6)).
2. The 700-mb (~10,000-foot) wind remained at 25–30 kt magnitude at the grid point for the remainder of the case study—however, it was noted that the 24-h prognosis of the 700-mb wind, at the grid point (not shown), was normally the same strength as that of the starting analysis. Nevertheless, this southwest wind with a magnitude of >20 kt near 10,000 feet, meets the requirements for the southwesterly 10,000 foot wind for the moderate surge in Fig. 3.72.
3. The 925-mb wind (again, not shown) at the grid point increased from 180°/5 kt (at 130000Z) to 225°/15 kt (at 140000Z or 140800 Local). This near-surface wind magnitude also meets the requirements for the moderate surge in Fig. 3.72. The 925-mb wind further increased, at the grid point, to 25–30 kt for the remainder of the case study, 15–18 August, as 3–6 inches of rain fell, each day (see Table 3.6). (While this increased near-surface wind magnitude meets the requirement for a strong surge, the 700-mb (~10,000-foot) wind magnitude was never over 30 kt (below the 40–50 kt required), and the 200-mb (35,000–40,000-foot) wind magnitudes ranged between 10–25 kt, (far below the 40–60 kt required for a strong surge.)
4. While the 200-mb wind record was incomplete, it was found to be easterly, 10 kt on 16 August, 25 kt on 17 August, and then finally decreasing to 20 kt at 180000Z and 10 kt at 181200Z. This magnitude for the 200 mb (35,000 to 40,000-foot) wind is marginally acceptable for even a weak surge, and it is not from the northeast as specified in Fig. 3.72.

⁵⁰While NOGAPS tropical analysis has made substantial improvements in the recent past, the author—pleased when even the numerical tropical analysis is satisfactory and still a skeptic of tropical numerical prognosis—chose to examine wind prognoses only to 24-hours. Also, the analyst is often suspicious even when a 24-h prognosis verifies, since the OI analysis may have very few observations to change the the first guess (“background”) or the OI analysis may reject wind observations that differ substantially from the first-guess.

Recognizing the large magnitudes of the rainfall from 14–18 August and accepting the possibility that the divergent upper-level outflow may have been stronger at a level other than 200-mb, it is possible to marginally classify the episode as a moderate surge. The 200-mb wind direction of easterly, vice northeasterly, as required by Fig. 3.72 and the eventual development of a tropical cyclone in the South China Sea prompts the classification of the episode as “atypical.”

Figure 3.74 shows the NOGAPS surface pressure analysis with scattered synoptic station reports at 141200Z. The tight pressure gradient at the upper righthand corner of the chart indicates the presence of Typhoon Kent, just off the chart. Figure 3.73 is the DMSP IR imagery showing Typhoon Kent, max. winds of 85 kt, at Point “N” at $\sim 27^{\circ}\text{N}$, 143°E , plus heavy cloudiness in the South China Sea, including a cold-cloud-top cluster, “Point M”, which eventually becomes Tropical Storm Mark. The pressure pattern in Fig. 3.74 while not that of the classic southwest monsoon surge does show the alignment of the 1008 mb isobar from the west of Palawan, across the Visayas, toward the southern periphery of Typhoon Kent.

With cloudiness covering much of Luzon, the following observation was received from Cubi Point seven hours after the satellite image (142100Z or 150500 Local): rain shower, wind $220^{\circ}/14$ kt, gusts to 36 kt (or 22014/36) overcast with a ceiling of 4000 ft and temperature/dewpoint of $25^{\circ}\text{C}/20^{\circ}\text{C}$ (or $T/T_d=25/20$). Approximately 50 nm away in its more protected harbor location, Manila IAP reported haze, wind 24006, broken clouds, with $T/T_d=25/22$. Meanwhile in the Visayas, on the east side of Cebu Island, the Mactan International Airport (RPMT, WMO 98646) was reporting no weather, wind 27004, multilayer clouds with 6/8 cirrus high cloud, and $T/T_d=25/24$. The 6/8 coverage of cirrus over Cebu correlates well with the slight break in the clouds near the eastern Visayas in Fig. 3.73.

Figure 3.75 is a combination plot of the FNOC significant wave height and sea surface temperature (SST) analyses at 141200Z. Note the wave heights >6 feet—under the influence of the surge in the southwest monsoon—throughout much of the South China Sea and the 15 foot waves near Typhoon Kent. SST maxima ($>30^{\circ}\text{C}$) were analyzed both near Hainan Island and between Luzon and Kent to the northeast.

As mentioned earlier the author planned to examine tropical prognoses only to 24 hours; however, Fig. 3.76 is a “one-time” view of the NOGAPS 72-h 925-mb wind and streamline prognosis. While the general pattern is representative, the vortex forecast to be west of Luzon in the South China Sea, in 72 hours, will be found to be almost 400 nm farther north near the southern tip of Taiwan.

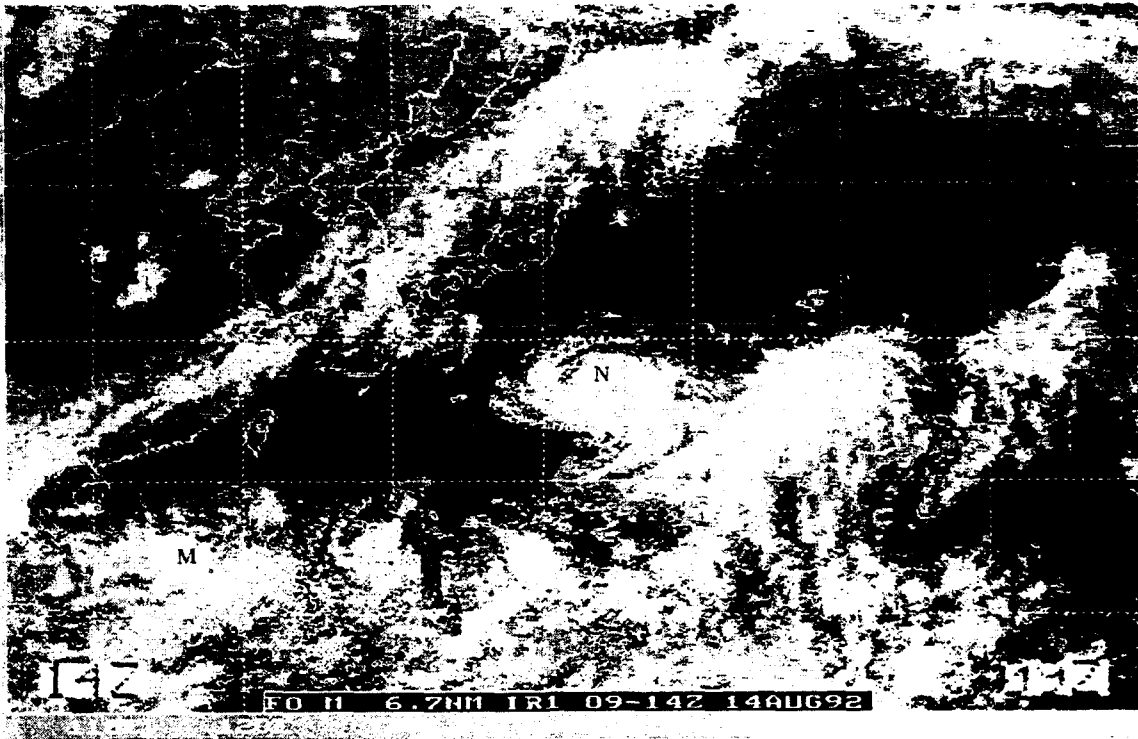


Figure 3.73: NODDS Mosaic of DMSP IR Satellite Imagery for 1400Z (western swath) and 0900Z (eastern swath) for 14 August 1992

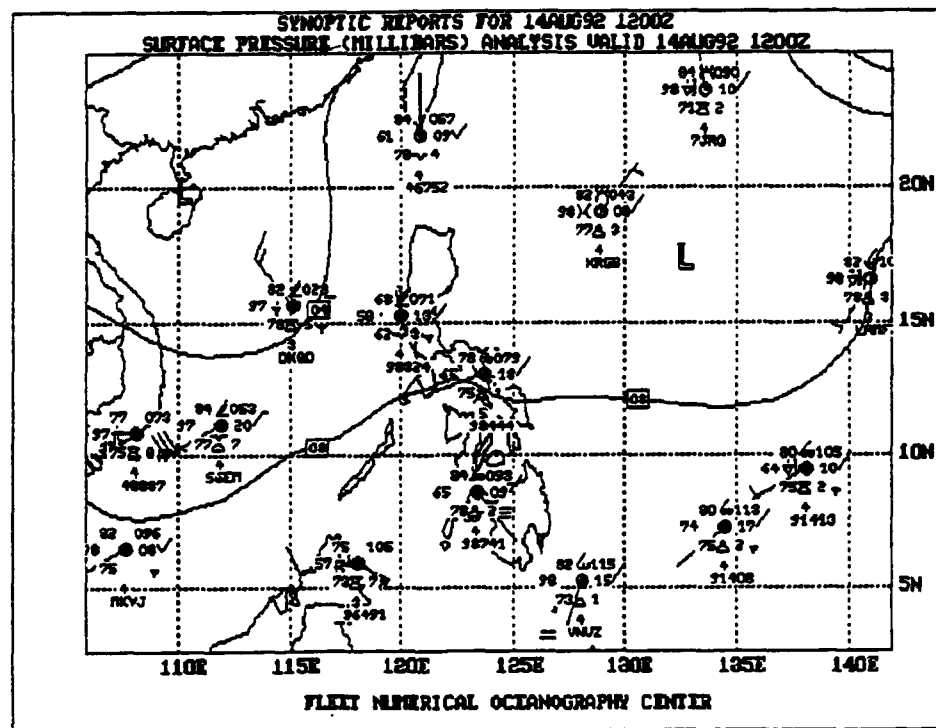


Figure 3.74: NODDS Synoptic Reports and Surface Pressure Analysis for 1200Z 14 August 1992.

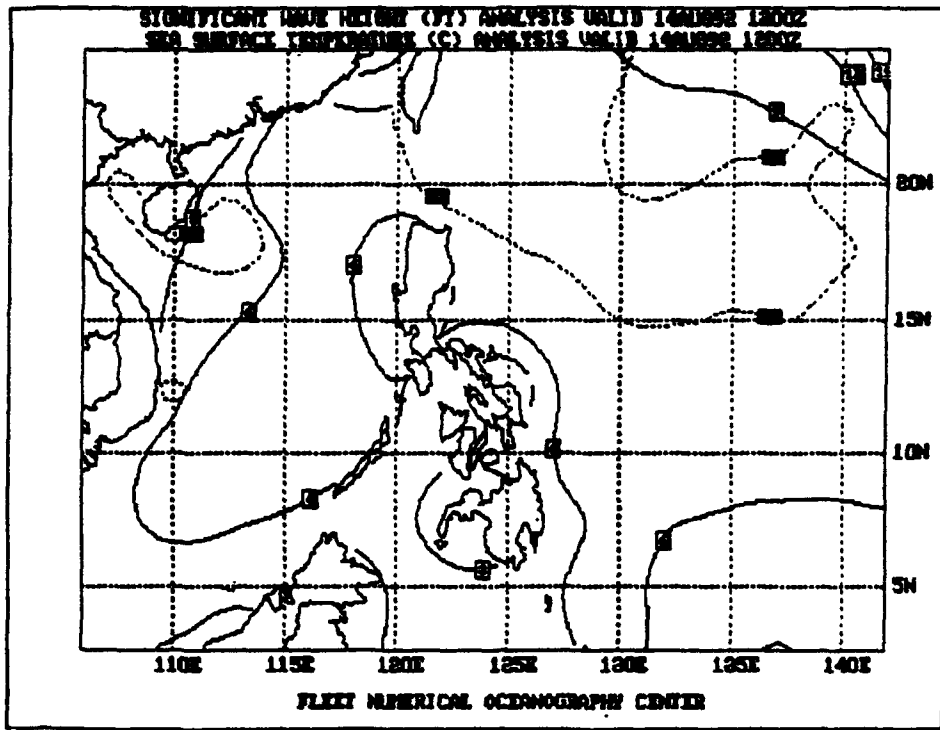


Figure 3.75: NODDS Significant Wave Height, Feet, (solid) and Sea Surface Temperature, °C, (dashed) Analyses for 1200Z 14 August 1992

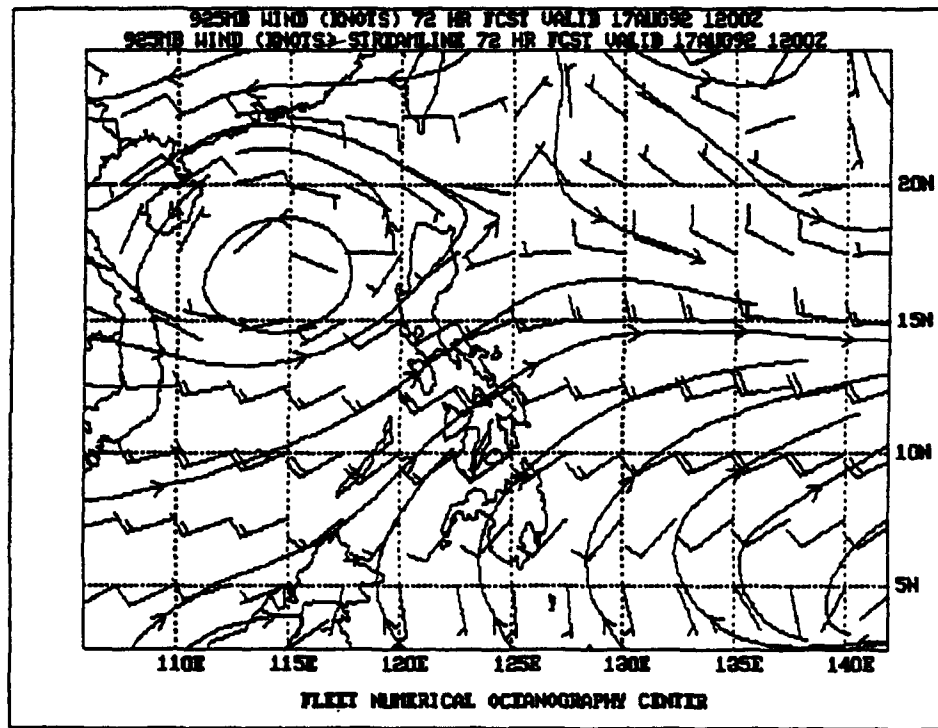


Figure 3.76: NODDS 925-mb Winds and Streamline 72-h Prognosis from 1200Z 14 August

15 August 1992

At 151200Z, Fig. 3.77 shows the NOGAPS surface analysis with very little change in the pressure pattern during the last 24 hours (see Fig. 3.74). The zoomed analysis in Fig. 3.78 shows rain over much of Luzon, e.g., continuous slight (2-dot) rain at both Vigan (98222) and Manila IAP (98429) (the station number has been plotted over by an adjacent report) and rain within the last hour at Cubi Point (98426). Here in Fig. 3.78, the present weather symbol is much more difficult to see than on the larger color VGA monitor.

The 925-mb winds and streamline analysis shown in Fig. 3.79(a) strongly supports the surge in the southwest monsoon, in particular with the 225°/30 kt wind at the grid point near Cubi Point (15°N, 120°E)—the NOGAPS surface wind (not shown) at the grid point was 225°/25 kt. However, the position of the vortex (Point "L"), near 18°N, 117°E, is ~200 nm from the JTWC Tropical Depression 13W Warning position near 20°N, 119°E (see Fig. 3.81). Also the position of Tropical Depression 12W, 17°N, 129°E, in its early formation, on Fig. 3.81 appears on the western perimeter of a neutral point on the NOGAPS 925-mb streamlines in Fig. 3.79(a). (While bogus soundings have not been entered here, TDs are *now* operationally bogussed by FNOC). The 24-h streamline prognosis in Fig. 3.79(b) shows little forecast change for 161200Z.

While the significant wave height analysis and prognosis in Fig. 3.80 depicts >6-foot waves over much of the South China Sea, the FNOC 24-h wave height prognosis "shrinks" the size of the area of maximum wave heights.

Four hours later at 151600Z (160000 Local), the following observations were made at Cubi Point (RPMB, 98426), Manila IAP (RPMM, 98429) and Mactan IAP (RPMT, 98646):

Cubi Point ...19011/18kt 6000 63RA 3CU015 8NS025 26/23 2972INS...VIS W3200...

Manila IAP ...19004kt 5000M 3CUSC022 8ACAS090 25/22 1007 CONTUS LGT RA...

Mactan IAP ...24003 9999 2CU020 4AC100 5CI300 27/24 1009...

(NOTE: The above reports are in the METAR Code used by most overseas stations, e.g., Manila IAP observation decoded is: wind from 190° 4 kt, visibility 5000 meters, 3/8 coverage of cumulus/stratocumulus with bases at 2200 feet, 8/8 coverage of altocumulus/altostratus bases at 9000 feet, T/T_d=25°C/22°C, sea-level pressure 1007 mb. While Cubi Point reports moderate rain in the 63RA group, Manila omits the group and reports precipitation in plain language at the end; also Cubi Point reports an altimeter setting of 29.72 inches, vice sea-level pressure in millibars.)

Again, as on the previous day, the windward stations on Luzon are receiving rain while Mactan IAP on the lee side of Cebu in the Visayas has ≥10 km visibility (code 9999) with only broken clouds.

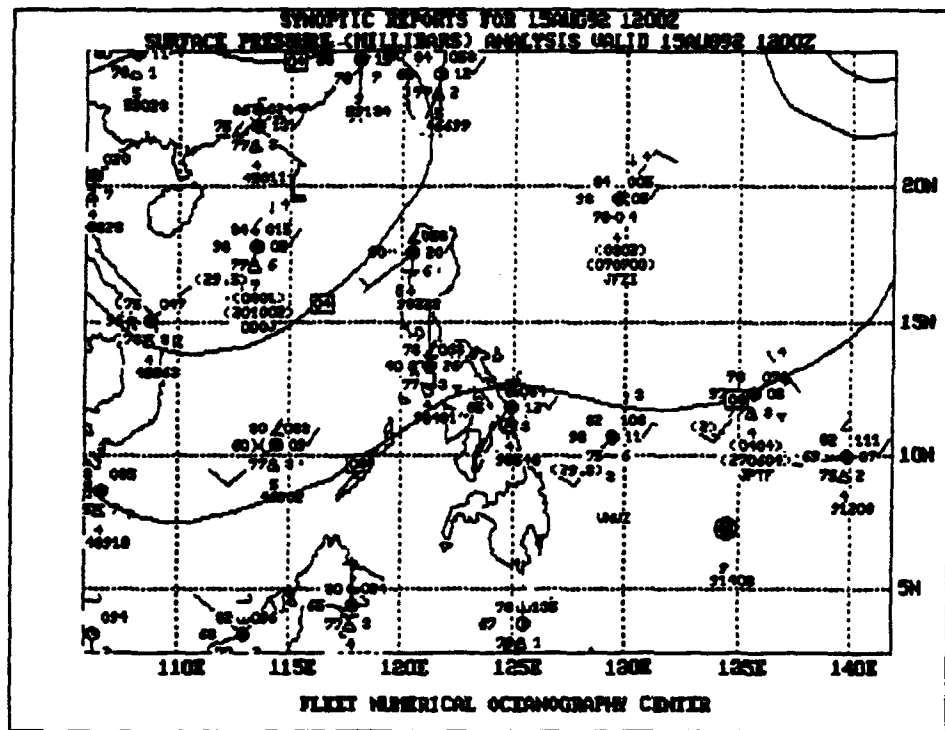


Figure 3.77: NODDS Synoptic Reports and Surface Pressure Analysis for 1200Z 15 August 1992.

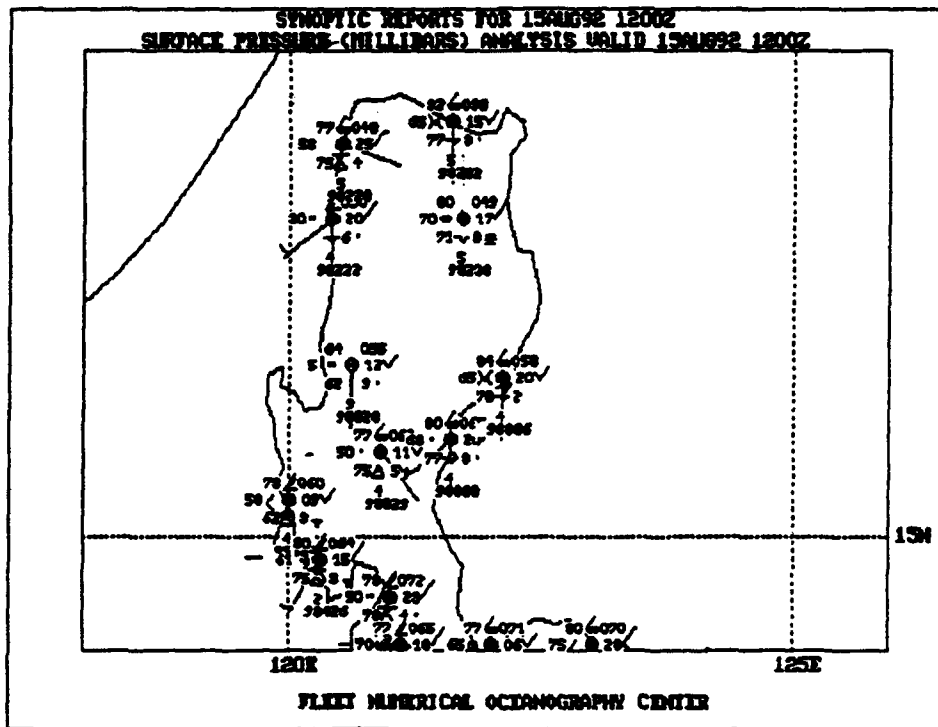
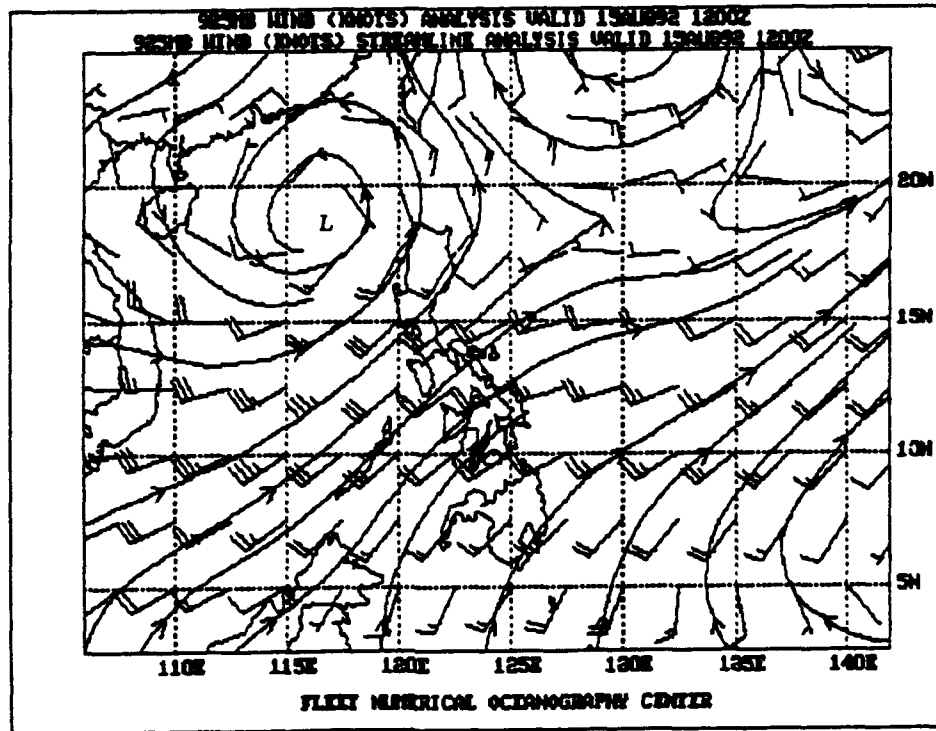
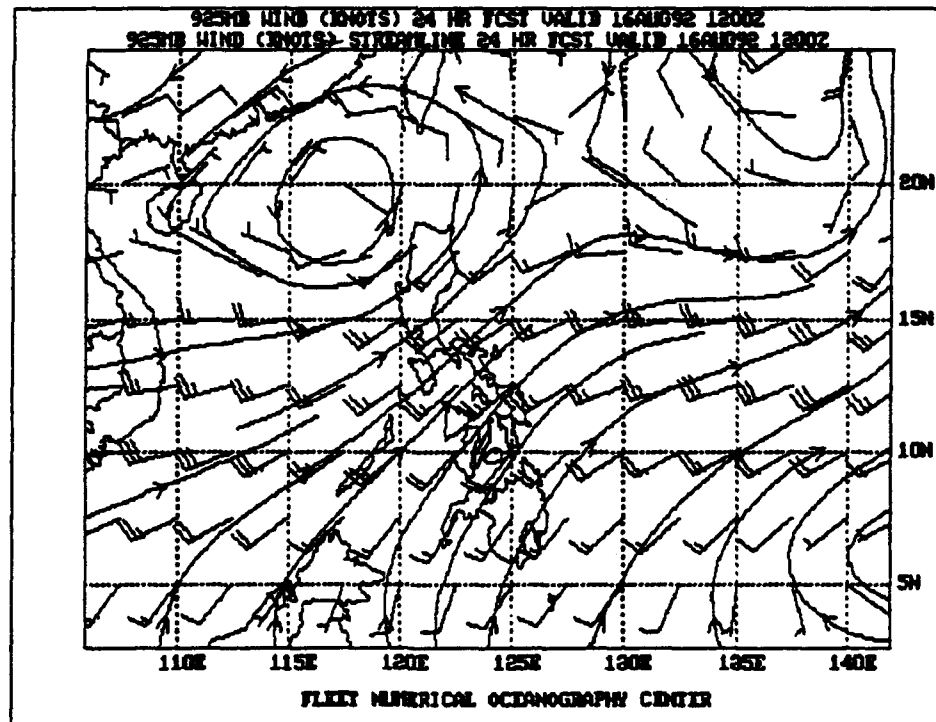


Figure 3.78: NODDS Zoomed Synoptic Reports and Surface Pressure Analysis for 1200Z 15 August 1992.



(a)



(b)

Figure 3.79: NODDS 925-mb Winds and Streamline Analysis (a) and 24-h Forecast (b) from 1200Z 15 August 1992.

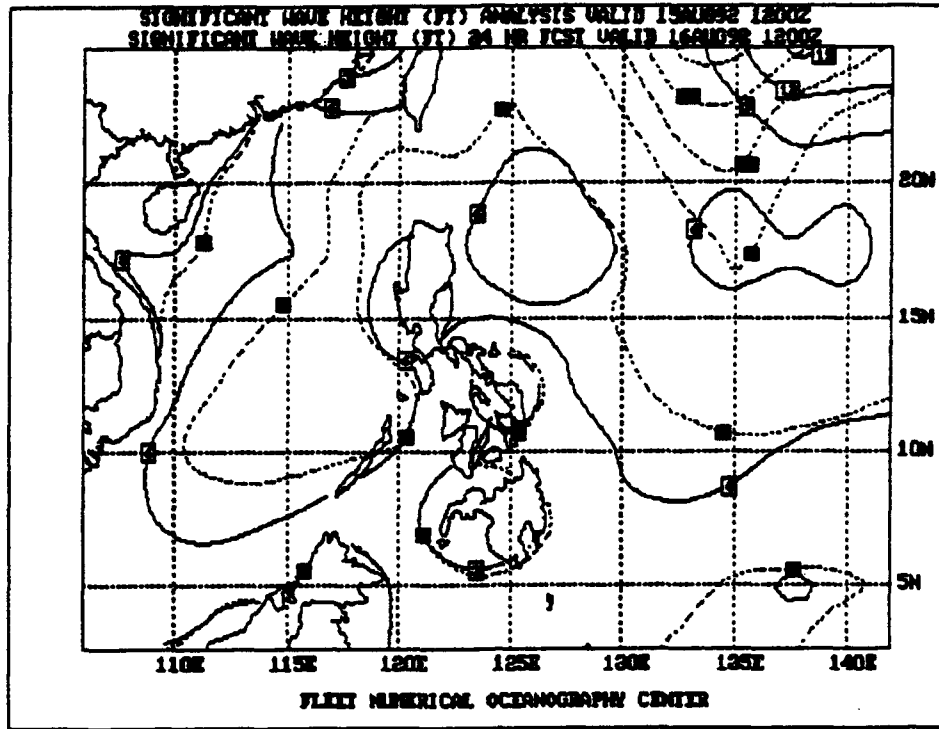


Figure 3.80: NODDS Significant Wave Height Analysis (solid) and 24-h Forecast (dashed) from 1200Z 15 August 1992.

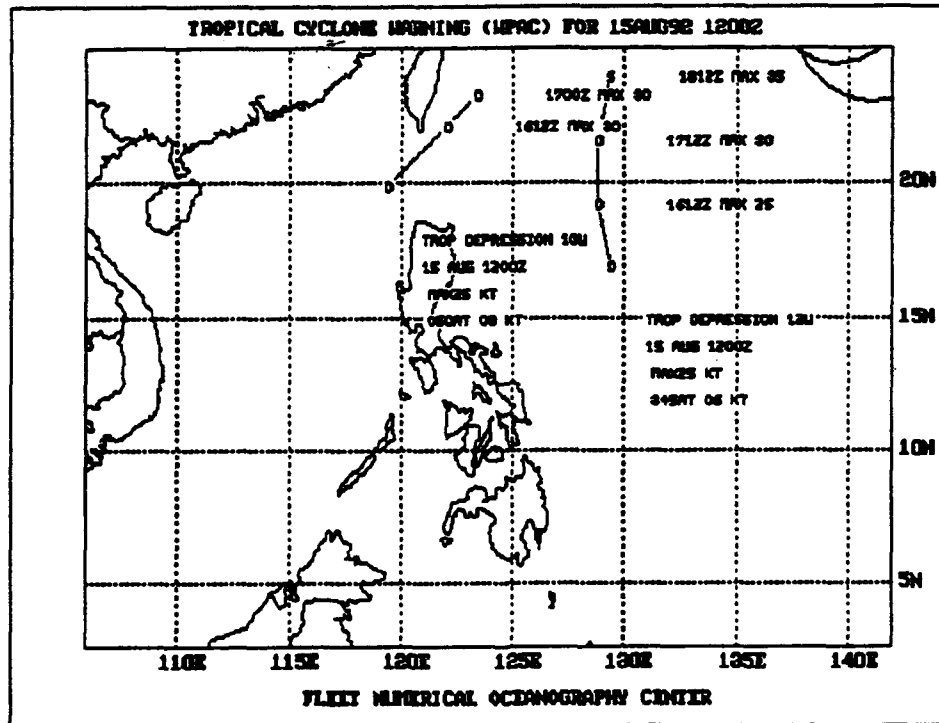


Figure 3.81: NODDS Tropical Depressions 12W and 13W Warnings for 1200Z 15 August 1992

16 August 1992

Figures 3.82(a) and (b) permit comparison of DMSPP visible and IR imagery as received via NODDS. With Typhoon Kent far to the northeast approaching Japan, an impressive cluster on the 160200Z satellite imagery depicts 12W, now Tropical Storm Lois (Point "K") near 17.5°N, 131°E, and a weaker cluster depicts Tropical Depression 13W (Point "J") near 21°N, 118°E. Recalling the reported cirrus clouds eight hours earlier (151600Z) at Mactan IAP, the NODDS DMSPP imagery adequately displays dark grey on the visible and light grey on the IR over the eastern Visayas—indicating a cold, thin cirrus deck, thin enough to permit "contamination" by radiation penetrating through from warmer cloud tops or sea level below.

In particular note the satellite signature of deep convective clouds emanating from the west coasts of the Philippine Islands and being blown southwestward (at least from the Visayas and Mindanao) over the South China Sea by the winds aloft. This imagery is associated with the heavy convection occurring along the western (windward) coasts of the PI, as verified by the 6.45 inches of rain received at Cubi Point on 16 August (see Table 3.6). The NOGAPS 200-mb streamlines in Fig. 3.86 show diffluent flow from the PI westward, but streamlines are aligned toward the southwest, only south of Palawan. Thus, it is possible that insufficient observations are available or accepted on the NOGAPS 200-mb surface analysis or the general upper-level flow toward the southwest over the South China Sea is on a pressure surface (or pressure surfaces) other than 200-mb, e.g., 100-mb.

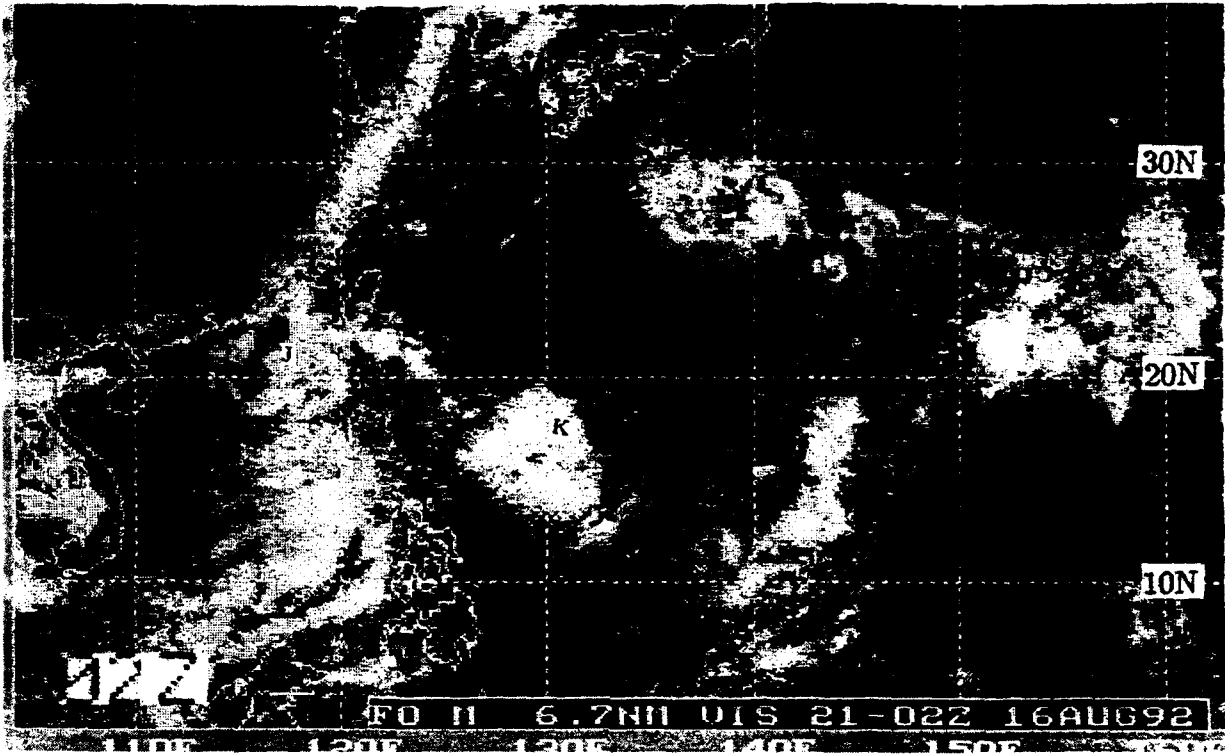
Note on Fig. 3.83 that continuous moderate (3-dot) rain is occurring at Manila, while ship DDOJ to the west in the South China Sea is reporting distant rain, a weak 5 kt wind from the west, plus 3-foot waves and 4.5-foot swells. The zoomed surface chart, Fig. 3.84 shows rain intensity increasing from north to south on Luzon, e.g., haze (no rain) at Vigan (98222) and Laoag (98223), one-dot rain at Baguio (98328), two-dot rain at Munoz (98329) and the coastal station of Iba (98324) (illegible due to the "over plot" of an adjacent station), and 3-dot rain at Cubi Point (98426)⁵¹.

The 925-mb NOGAPS wind and streamline analysis at 160000Z, Fig. 3.85(a) still shows strong gradient level winds (225°/25 kt) at the grid point nearest to Cubi Point. The wind magnitude on the NOGAPS surface analysis, at the grid point, was 20 kt (not shown). On this 925-mb analysis, the vortex position is in good agreement with the JTWC warning position of TD 13W on Fig. 3.87; however, surprisingly, the 925-mb streamlines depict only a sharp trough near the warning position of Tropical Storm Lois, despite its stronger intensity. The 24-h 925-mb streamline prognosis, Fig. 3.85(b) is very similar to the analysis except for westerly winds along 20°N (north of the current position of Tropical Storm Lois), possibly associated with the forecast position of TS Lois, to the north.

Later at 161200Z, the NODDS surface analysis in Fig. 3.88 presents reporting stations throughout the entire length of the PI. While precipitation reports appear less dominant than in the recent past, a zoom analysis (not shown) showed 2-dot rain at Baguio and a shower at Cubi Point.

⁵¹Again, the present weather symbol is much more legible on the color VGA monitor.

(a)



(b)

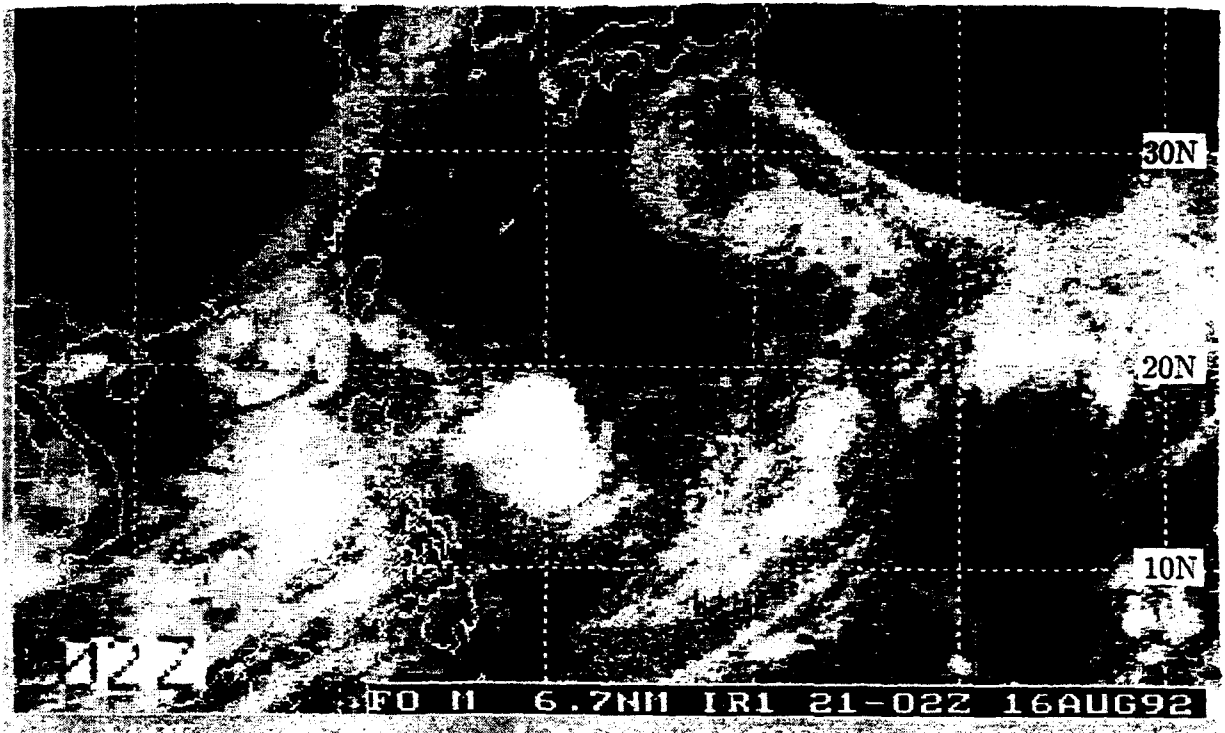


Figure 3.82: NODDS Mosaic of DMSP Satellite Imagery, Visible (a) and IR (b) for 0200Z on 16 August 1992

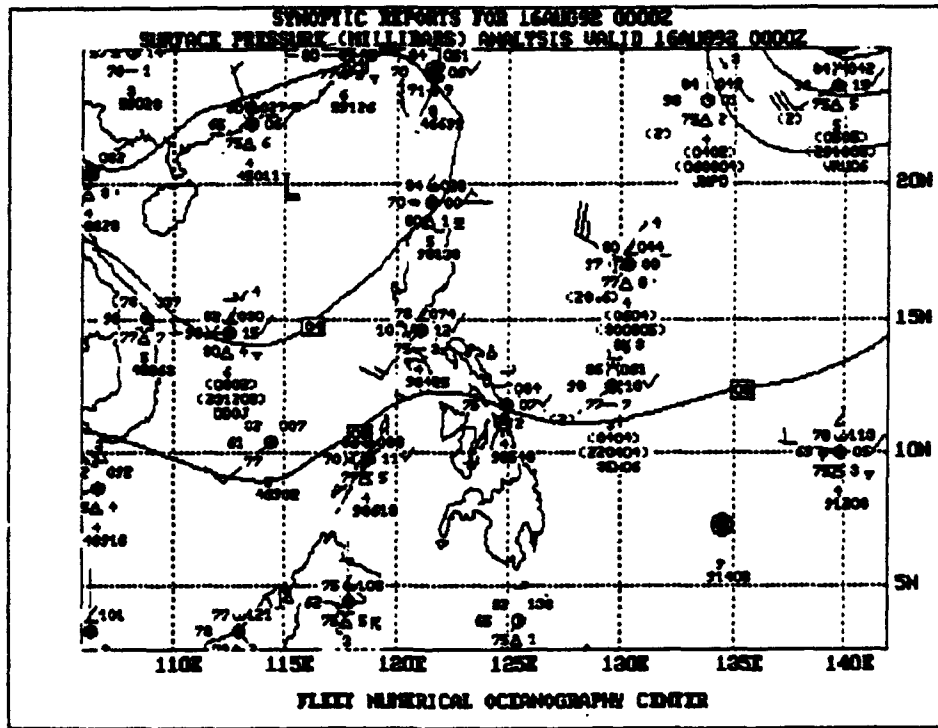


Figure 3.83: NODDS Synoptic Reports and Surface Pressure Analysis for 0000Z 16 August 1992.

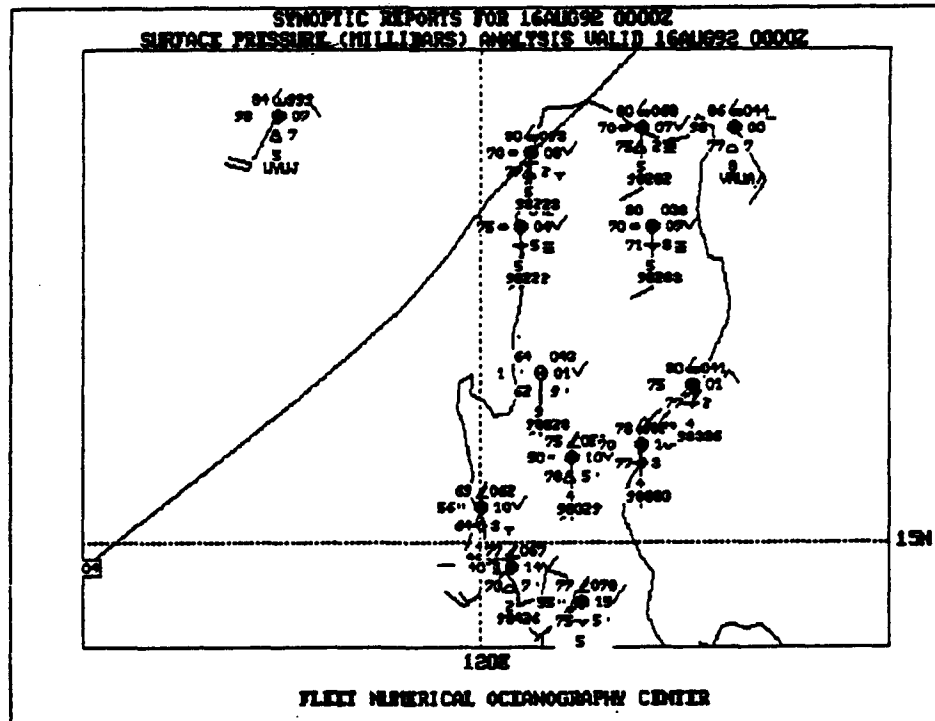
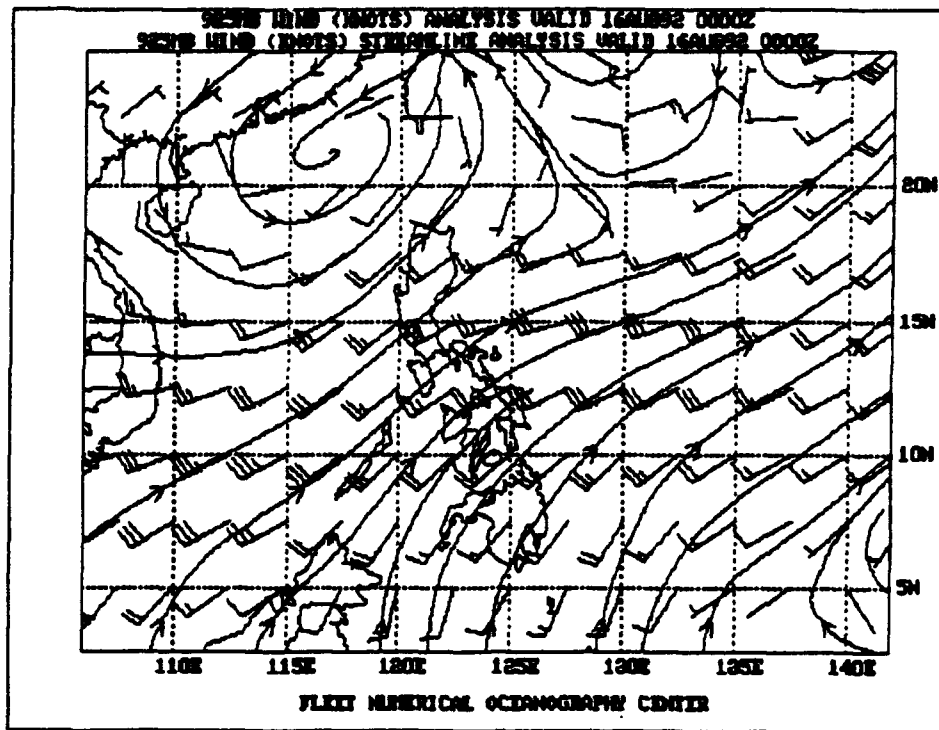


Figure 3.84: NODDS Zoomed Synoptic Reports and Surface Pressure Analysis for 0000Z 16 August 1992.

(a)



(b)

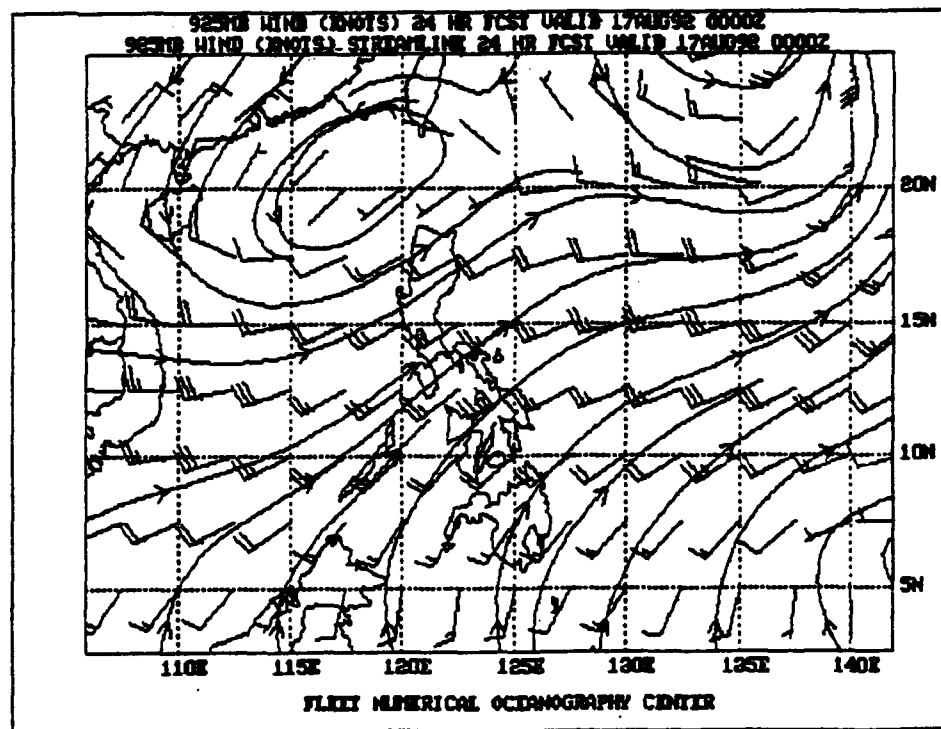


Figure 3.85: NODDS 925-mb Winds and Streamline Analysis (a) and 24-h Forecast (b) from 0000Z 16 August 1992.

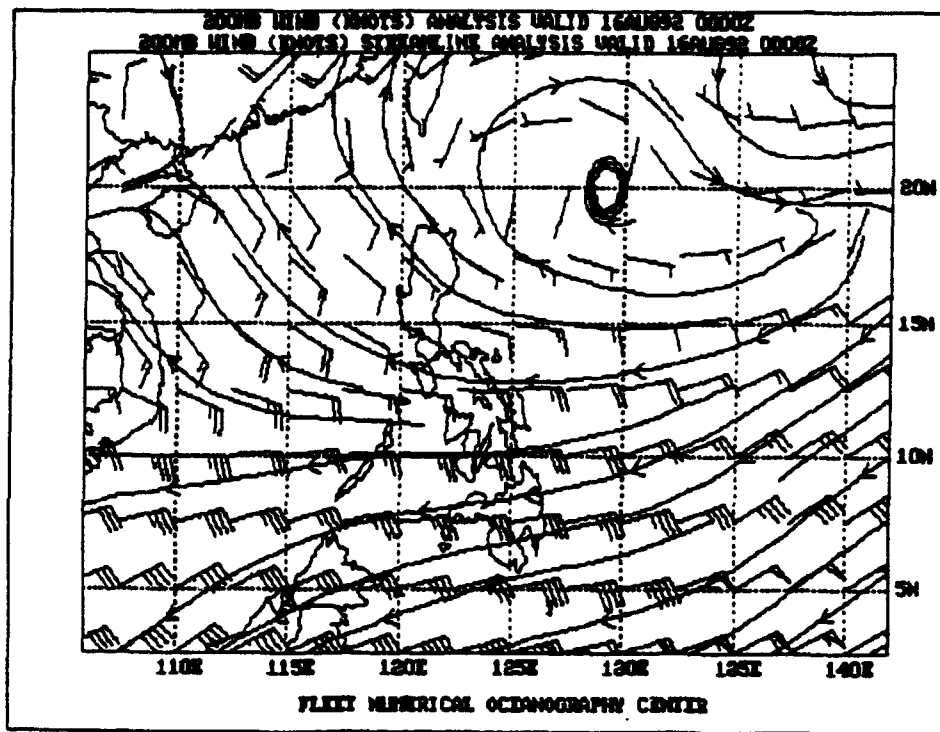


Figure 3.86: NODDS 200-mb Winds and Streamline Analysis for 0000Z 16 August 1992.

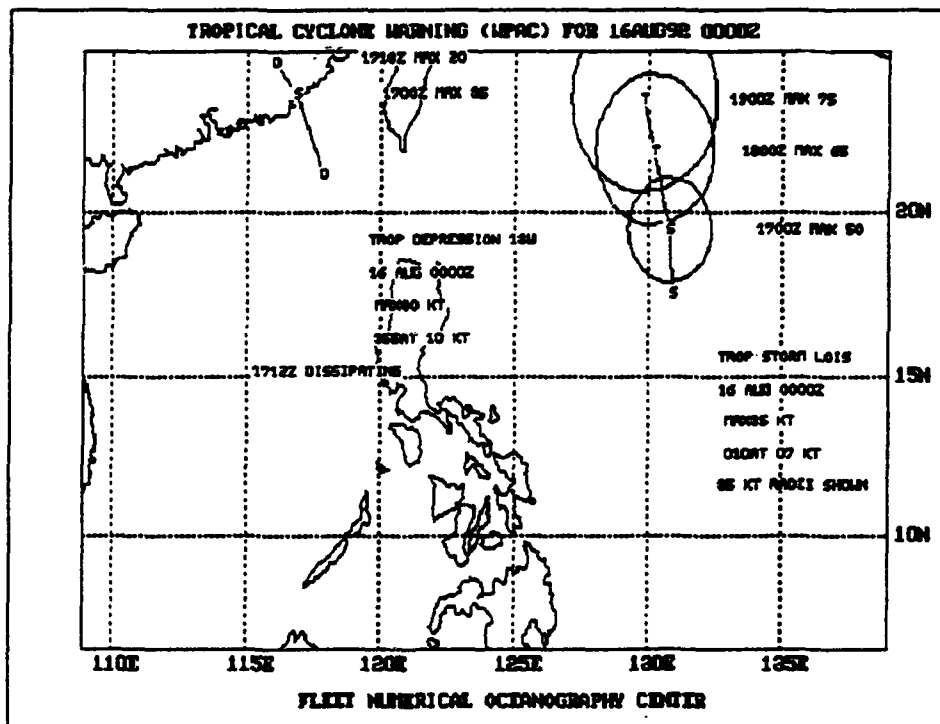


Figure 3.87: NODDS Tropical Storm Lois and Tropical Depression 13W Warnings for 0000Z 16 August 1992

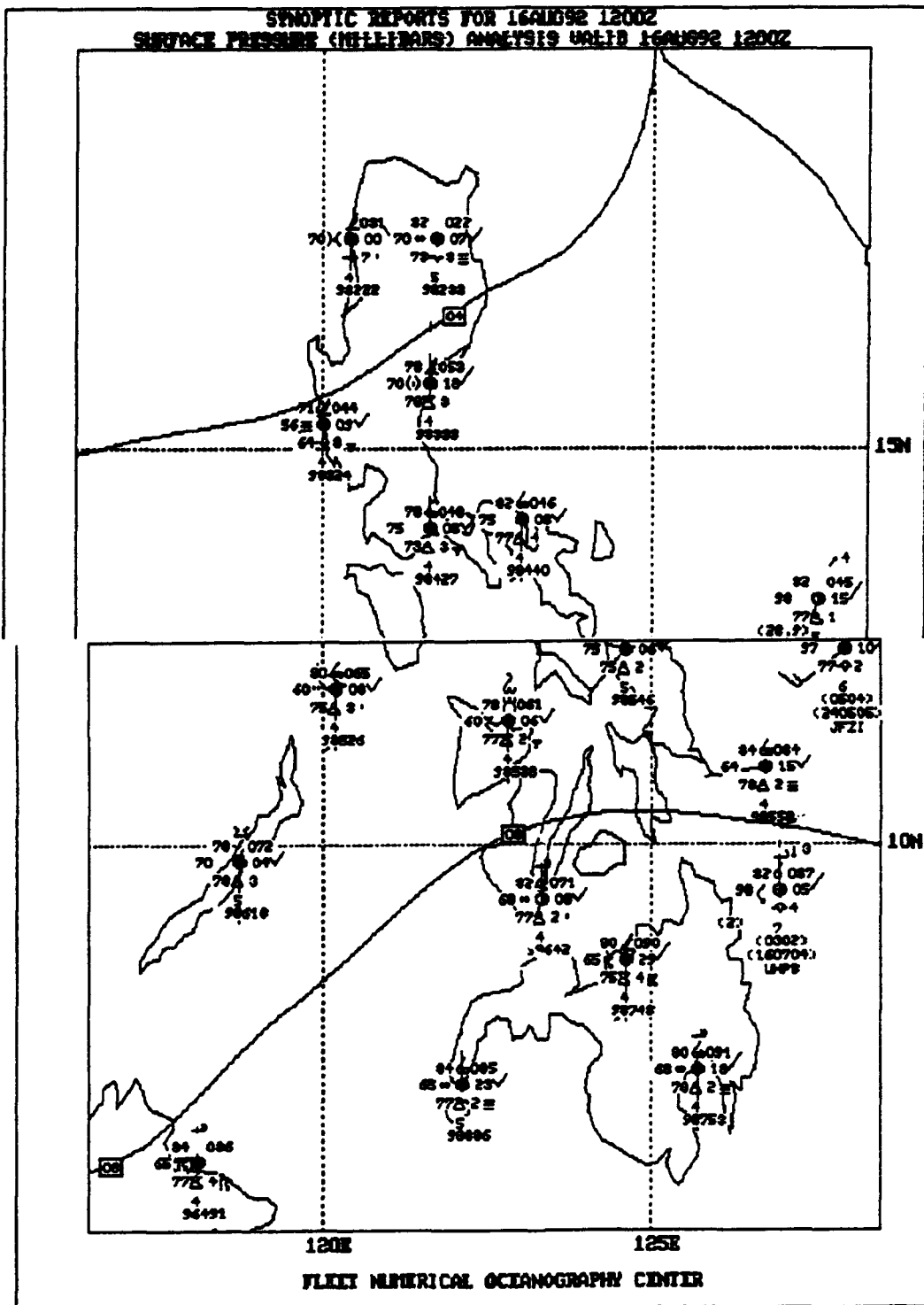


Figure 3.88: NODDS Synoptic Reports and Surface Pressure Analysis for 1200Z 16 August 1992.

At first look, the 161200Z 925-mb streamline analysis in Fig. 3.89(a) appears to indicate a satisfactory verification of the 24-h prognosis, Fig. 3.79(b). True, the forecast position of 13W (now TS Mark with winds of 35 kt) was only ~100 nm south of its verifying position southwest of Taiwan. However, the vortex representing TS Lois (winds of 35 kt), relocated to the east by JTWC at Point "I" (18°N, 133°E) on Fig. 3.89(a), is obviously still not properly depicted.

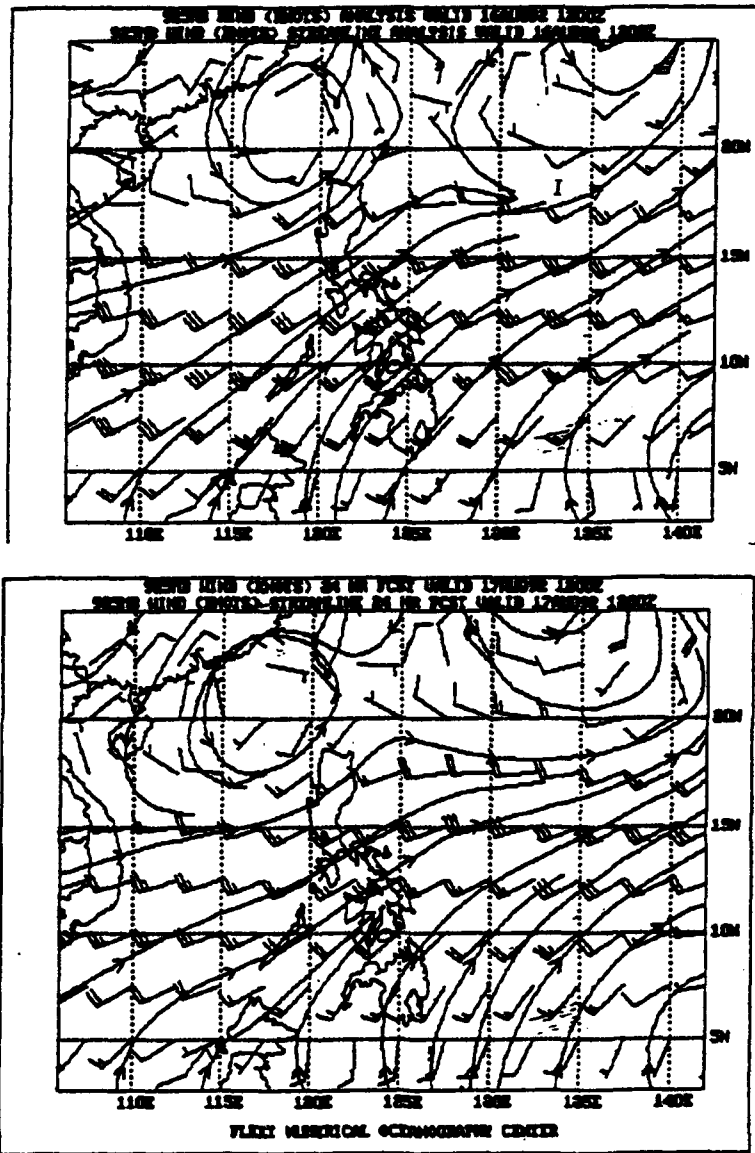


Figure 3.89: NODDS 925-mb Winds and Streamline Analysis (a) and 24-h Forecast (b) from 1200Z 16 August 1992.

17 August 1992

Again Figs. 3.90(a) & (b) permit an examination of the NODDS transmitted satellite mosaic of the DMSP visible and IR swaths at 170100Z. Figure 3.90(b) clearly shows the IR clusters associated with Kent (just south of Japan), Lois (east of Luzon), Mark⁵² (west of Taiwan) and the elongated cold-cloud-tops emanating from near Manila. The continuing satellite signature over the South China Sea is indicative of the convection along the west coast of the PI, caused by the low-level southwest monsoon surge. Its persistence is confirmed by the recorded precipitation at Cubi Point during the period 14–18 August 1992, as shown in Table 3.6.

Figure 3.91 shows the pressure trough existing between Tropical Storm Mark and Tropical Storm Lois at 170000Z. The concurrent JTWC warning positions of the two tropical cyclones are found on Fig. 3.92. The Prognostic Reasoning Message for TS Lois attributed the forecast northeastward track of Lois to interaction with TS Mark—i.e., Mark was now stronger (45 kt) than Lois (35 kt).

Again, a chart displaying the synoptic reports and surface pressure analysis (170000Z), throughout the entire length of the Philippine Islands, is shown on Fig. 3.93. Precipitation is occurring from central Luzon⁵³ into the Visayas.

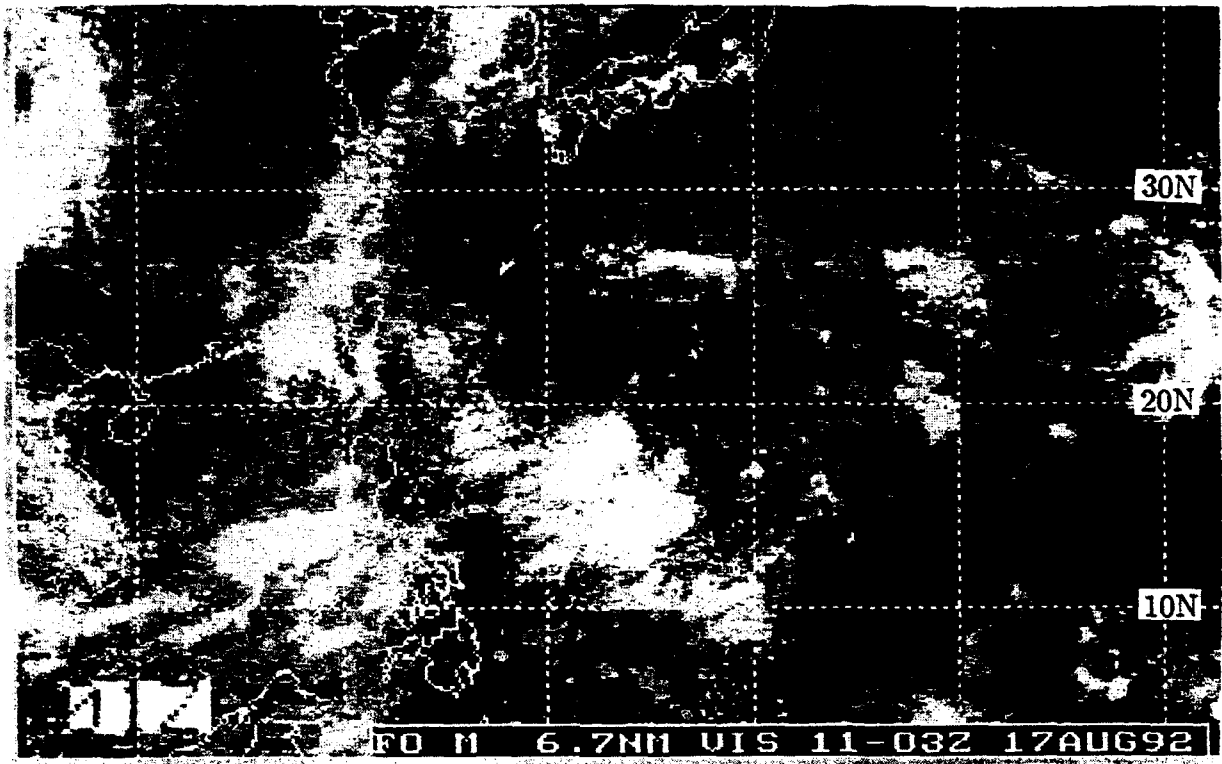
In Fig. 3.94, the NOGAPS 170000Z 925-mb streamline analysis includes a vortex in the Taiwan Strait near the JTWC warning position of TS Mark on Fig. 3.92; unfortunately, as before, the tropical analyst is disappointed to find only a trough at the warning position (19°N, 134.5°E) of TS Lois.

However, the analyst is encouraged by Fig. 3.95 showing both wave height and sea surface temperature (SST) analyses. Note that the ship JFIW reporting 4.5 foot waves and 7.5 foot swell, in Fig. 3.93, correlates well with the FNOC wave heights, >6 feet, at Point "H" (17°N, 117°E) on Fig. 3.95. The >9 foot waves analyzed at Point "G" (17.5°N, 135°E), in the vicinity of Tropical Storm Lois, is realistic; however, the collocation of SST >30°C would be expected to disappear with the subsequent⁵⁴ upwelling and mixing of the tropical cyclone.

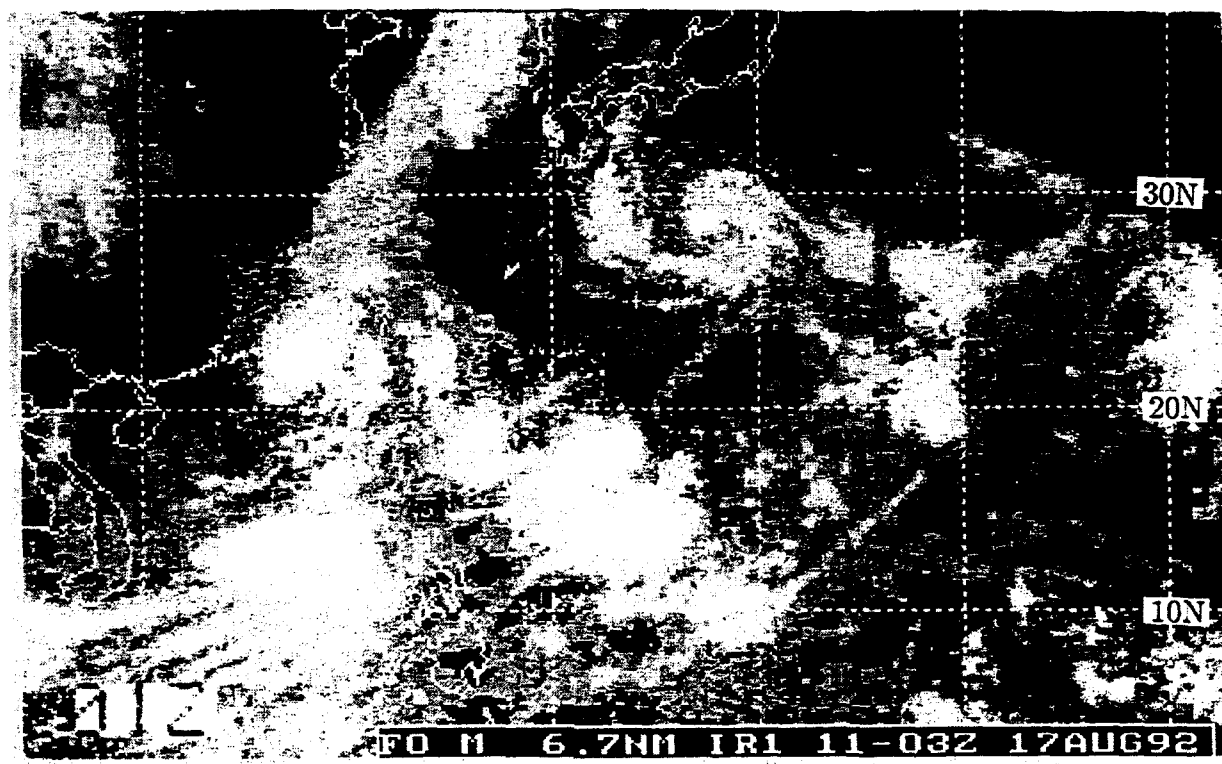
⁵²The presence of the cloud line extending NNE from TS Mark is associated with upper-level outflow from Mark and southerly flow ahead of a mid-latitude trough approaching from the west.

⁵³A shower was reported at Cubi Point on the NODDS zoom analysis (not shown).

⁵⁴The FNOC SST analysis 12 hours later at 171200Z (see Fig. 3.100) has a slightly smaller >30°C pool.



(a)



(b)

Figure 3.90: NODDS Mosaic of DMSP Satellite Imagery, Visible (a) and IR (b) for 0100Z on 17 August 1992

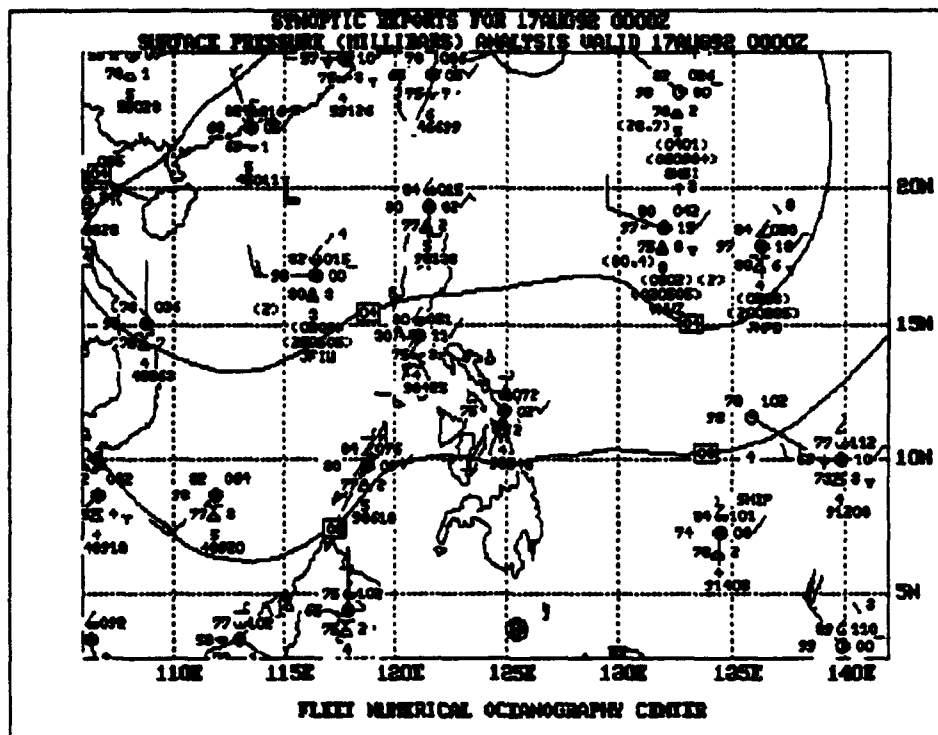


Figure 3.91: NODDS Synoptic Reports and Surface Pressure Analysis for 0000Z 17 August 1992.

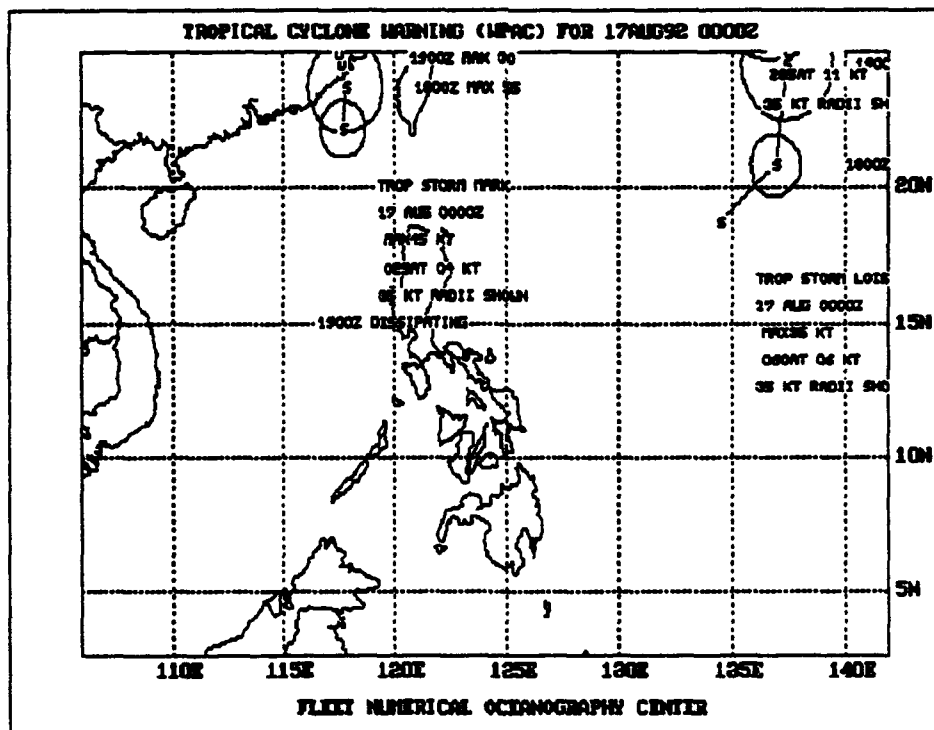


Figure 3.92: NODDS TS Lois and TS Mark Warnings for 0000Z 17 August 1992

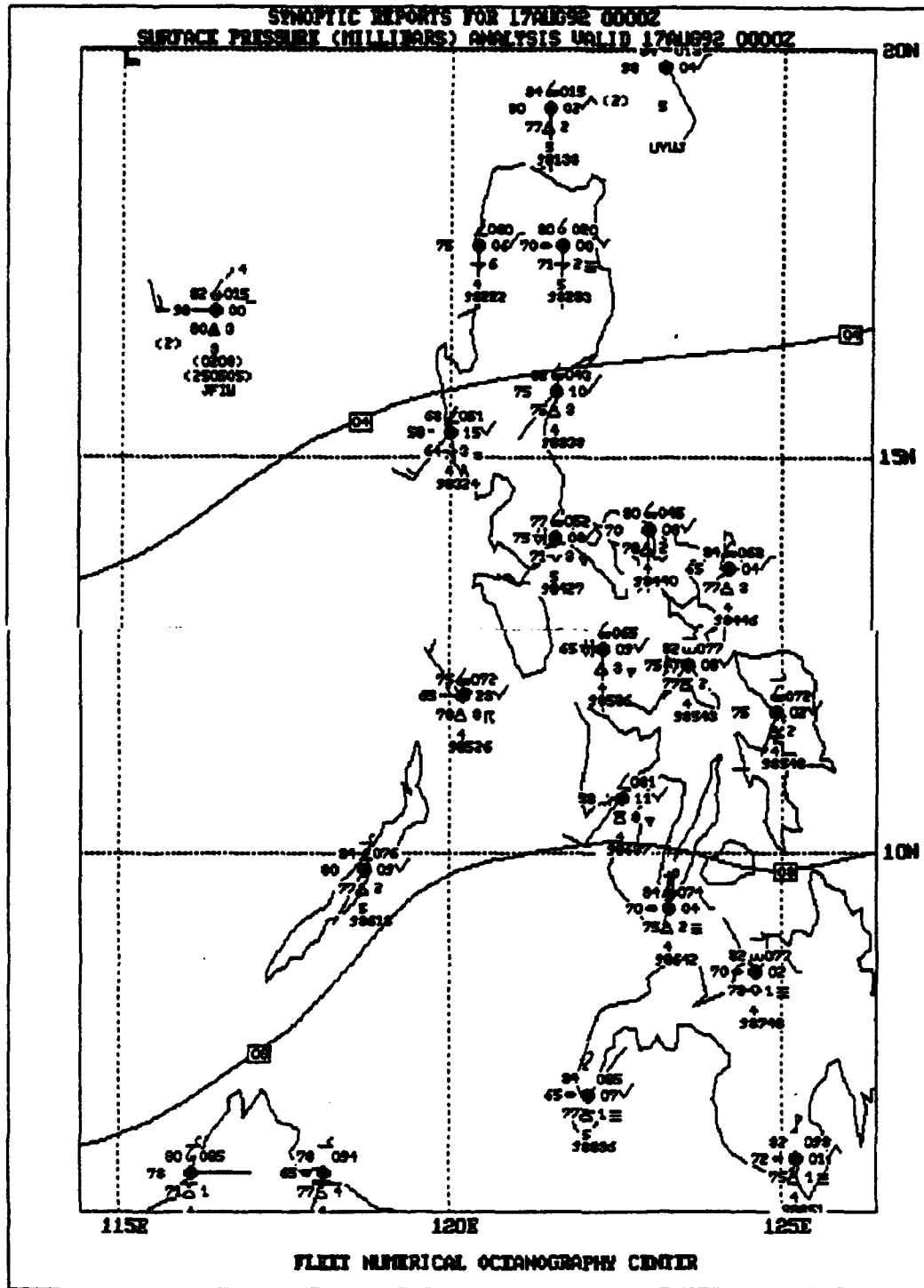


Figure 3.93: NODDS Synoptic Reports and Surface Pressure Analysis for 0000Z 17 August 1992.

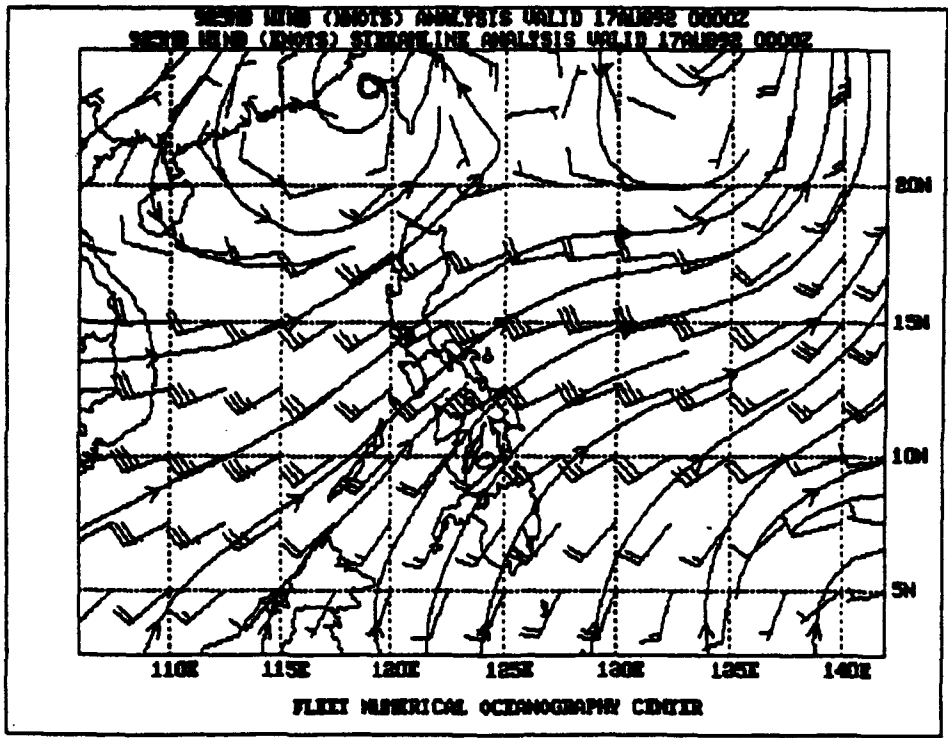


Figure 3.94: NODDS 925-mb Winds and Streamline Analysis for 0000Z 17 August 1992.

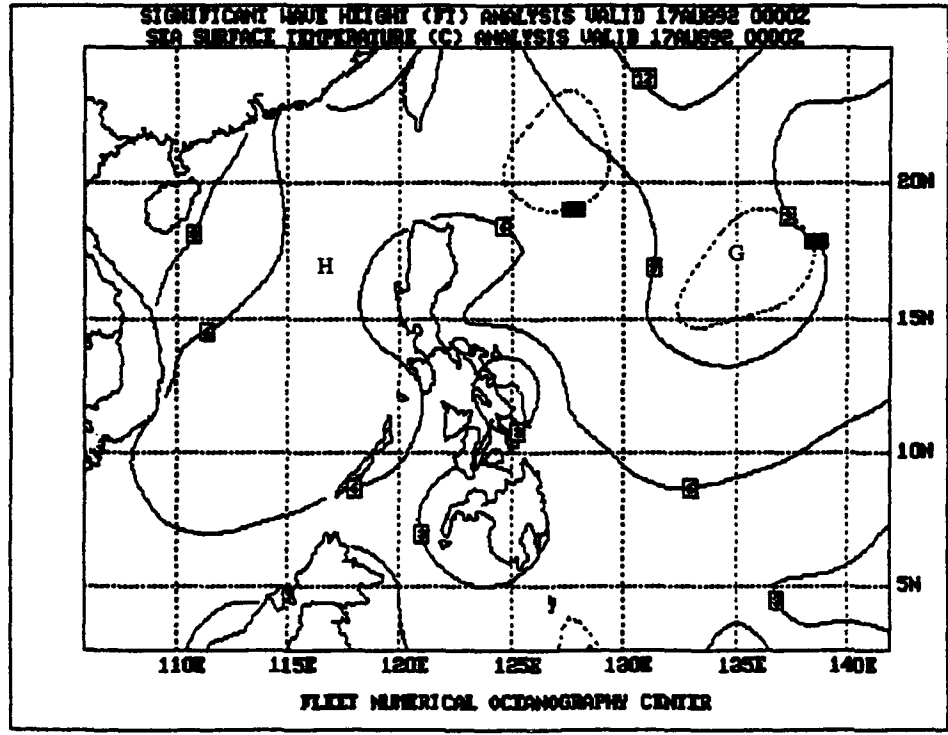


Figure 3.95: NODDS Significant Wave Height Analysis (solid) and Sea Surface Temperature (dashed) for 0000Z 17 August 1992.

Twelve hours later, Figs 3.96 and 3.97 show good correlation between the NOGAPS surface pressure analysis and the JTWC warning positions⁵⁵ of Tropical Storms Lois and Mark. Even at this synoptic scale, the NODDS screen clearly shows distant rain reported at Vigan (98222) on the northwest coast of Luzon, and a shower symbol at Calapan (98431) on the northern coast of Mindoro—more visible on Fig. 3.98.

The NODDS zoom surface analysis at 171200Z on Fig. 3.98 shows the Vigan and Calapan reports plus showers at Baler (98333) on the east coast of Luzon and at Coron (98526), south of Mindoro. Several stations are reporting rain in the distance, but the only thunderstorm on this zoom chart is at Catarman (98526) on northern Samar. The zoom also reveals a ship, ELJF, in the Luzon Strait reporting 20 kt of wind, 7.5-foot waves and 9-foot swell, correlating well with the ~9 foot FNOC significant wave height analysis at Point "F" (20°N, 119°E) on Fig. 3.100.

Checking the 171200Z 925-mb streamline analysis, Fig. 3.99, against the 24-h prognosis in Fig. 3.89 reveals that while the forecast decrease to 25 kt of the wind at the grid point nearest Cubi Point (15°N, 120°E) did not materialize, the forecast was not much in error, since the wind remained at 30 kt⁵⁶. Again the streamline analysis does *not* put a vortex at the position of Tropical Storm Lois.

Figures 3.101 and 3.102 permit comparison of the NOGAPS 200-mb streamline analysis with a tropical 200-mb streamline hand analysis⁵⁷. As in the case study of Typhoon Eli, the hand analysis identifies outflow at upper levels above strong tropical cyclones—classical anticyclonic outflow above the stronger TS Mark. These features of the hand analyses were identified by satellite cloud-vector winds from the geostationary satellite and by winds reported in AIREPS (aircraft reports) received from military and commercial aircraft.

⁵⁵When "down-loading" NODDS data, for the 0000Z or 1200Z run, the graphics of the latest JTWC warnings were included. Unfortunately, Fig. 3.97 includes the 171800Z warnings which had just replaced the 171200Z warnings in the FNOC data base.

⁵⁶The surface wind at the grid point was analyzed by NOGAPS at 25 kt (not shown).

⁵⁷While the hand analysis contains no small contribution of subjectivity, the support of satellite cloud-vector winds and AIREPS for several days (not shown) before Fig. 3.102, lends credibility to the analysis.

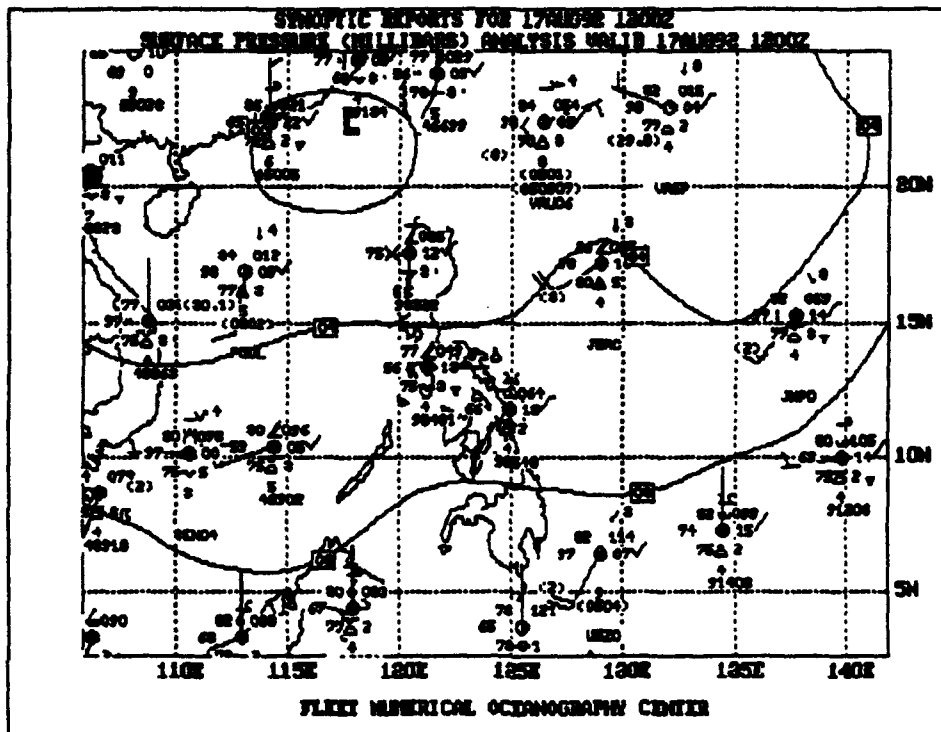


Figure 3.96: NODDS Synoptic Reports and Surface Pressure Analysis for 1200Z 17 August 1992.

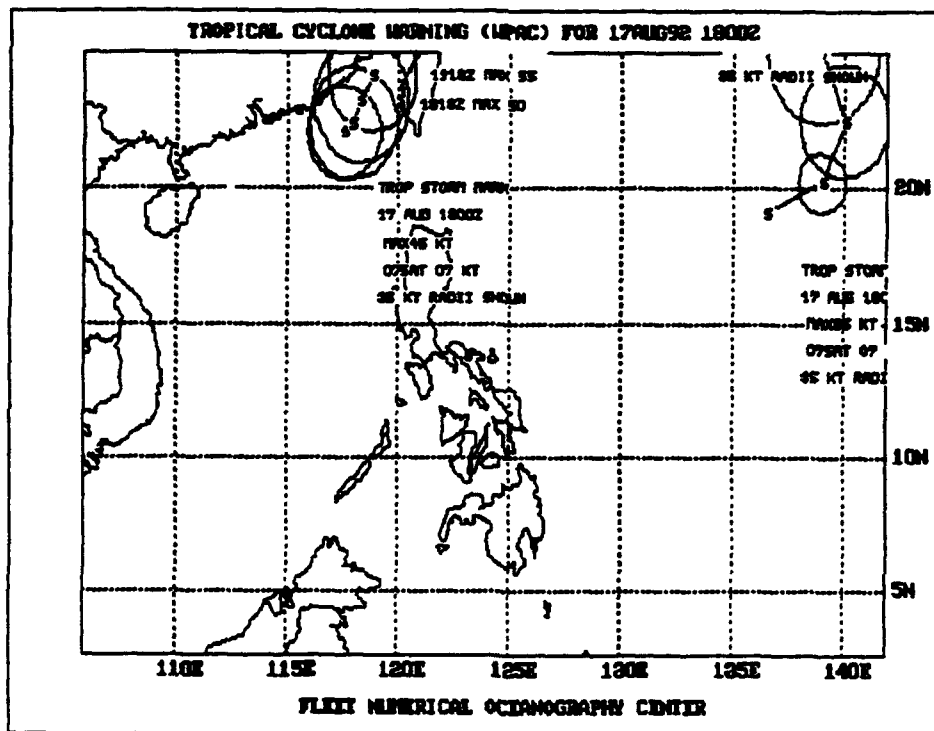


Figure 3.97: NODDS TS Lois and TS Mark Warnings for 1800Z 17 August 1992

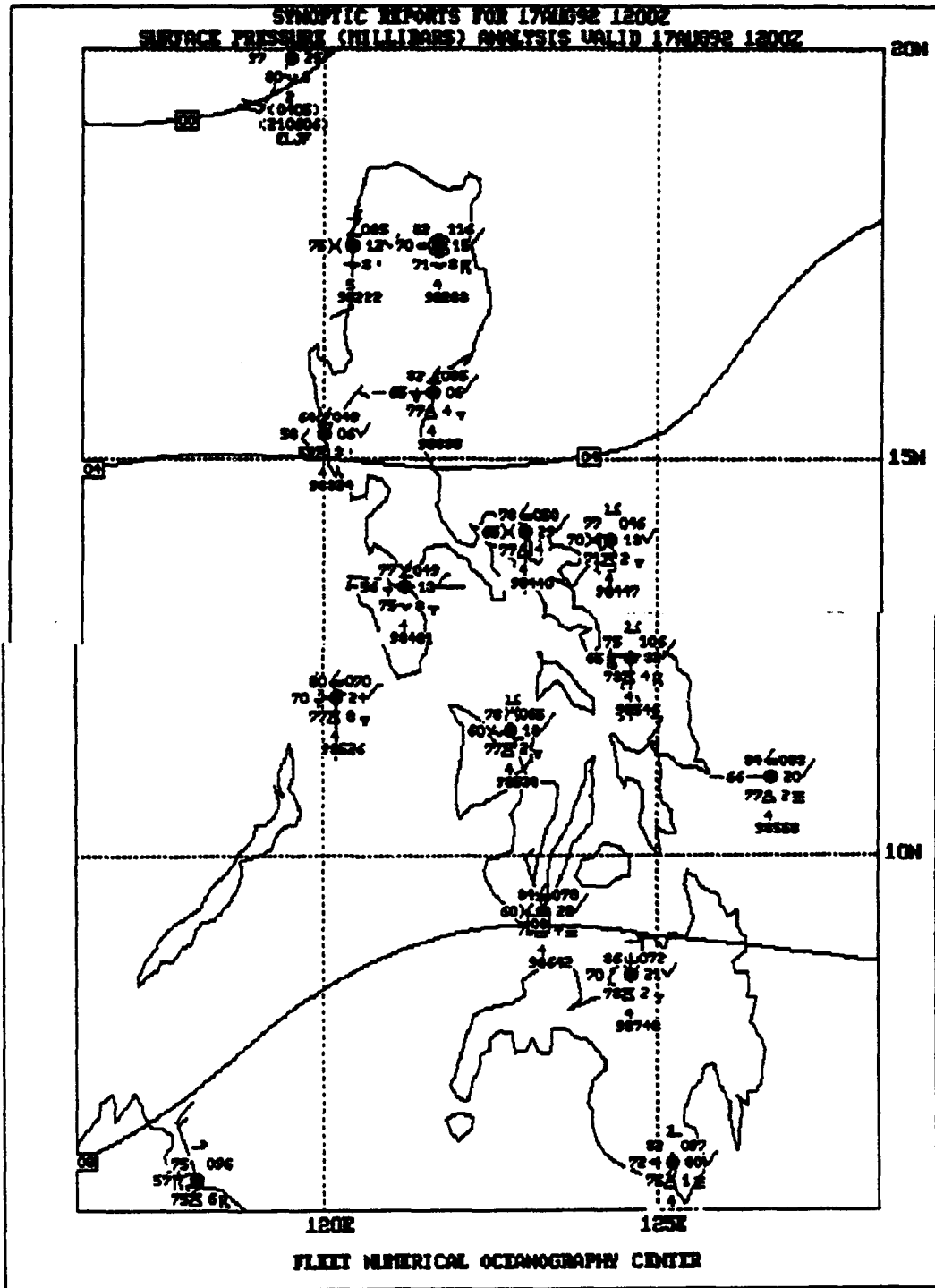


Figure 3.98: NODDS Synoptic Reports and Surface Pressure Analysis for 1200Z 17 August 1992.

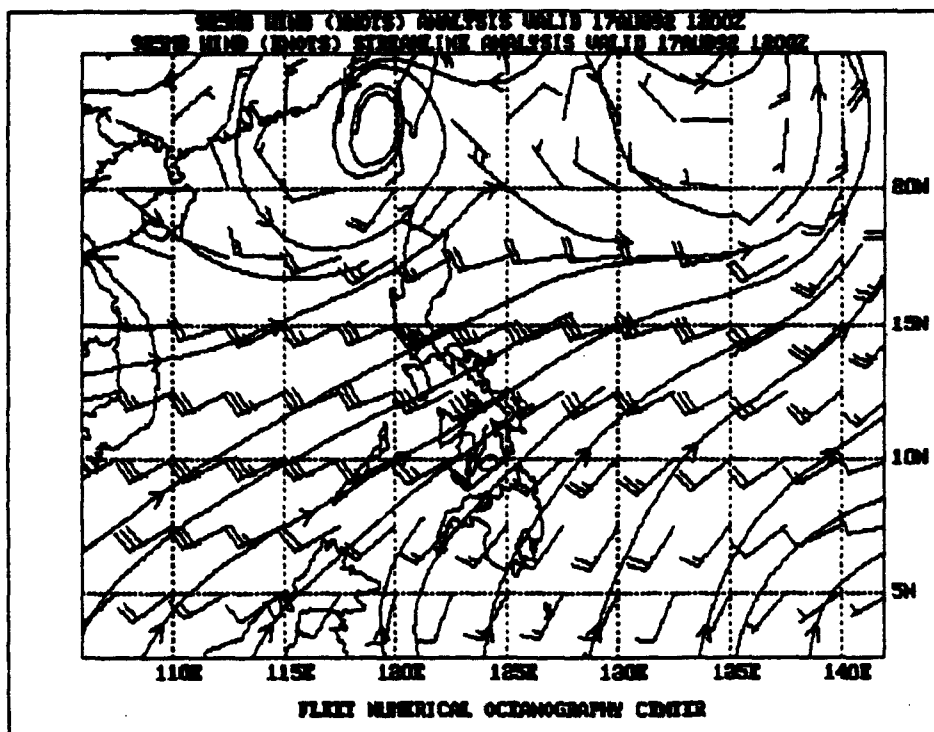


Figure 3.99: NODDS 925-mb Winds and Streamline Analysis for 1200Z 17 August 1992.

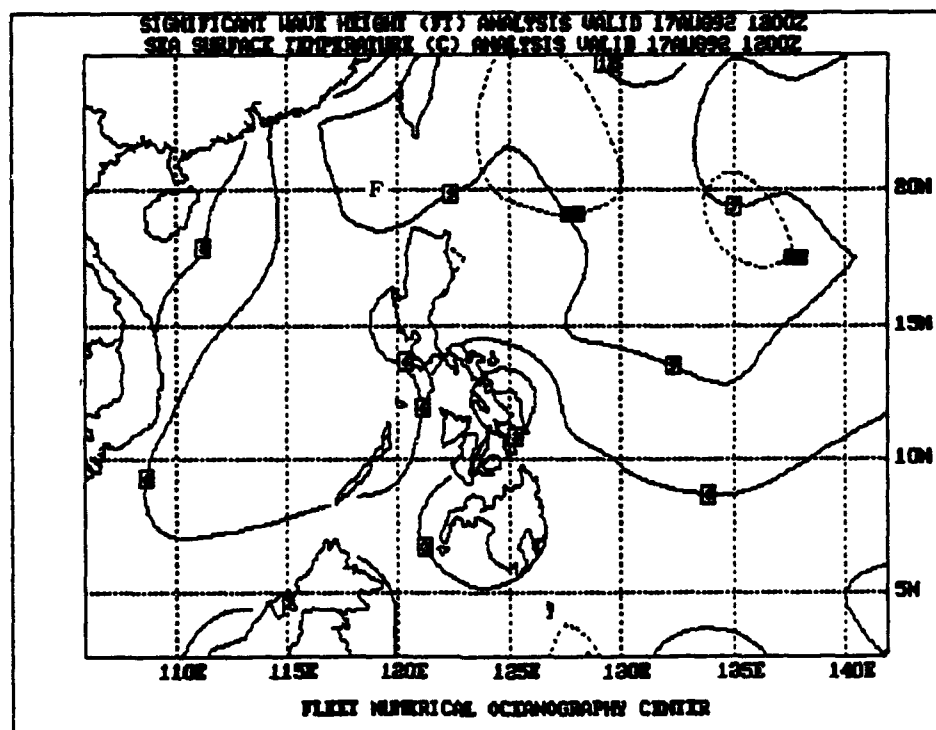


Figure 3.100: NODDS Significant Wave Height Analysis (solid) and Sea Surface Temperature (dashed) for 1200Z 17 August 1992.

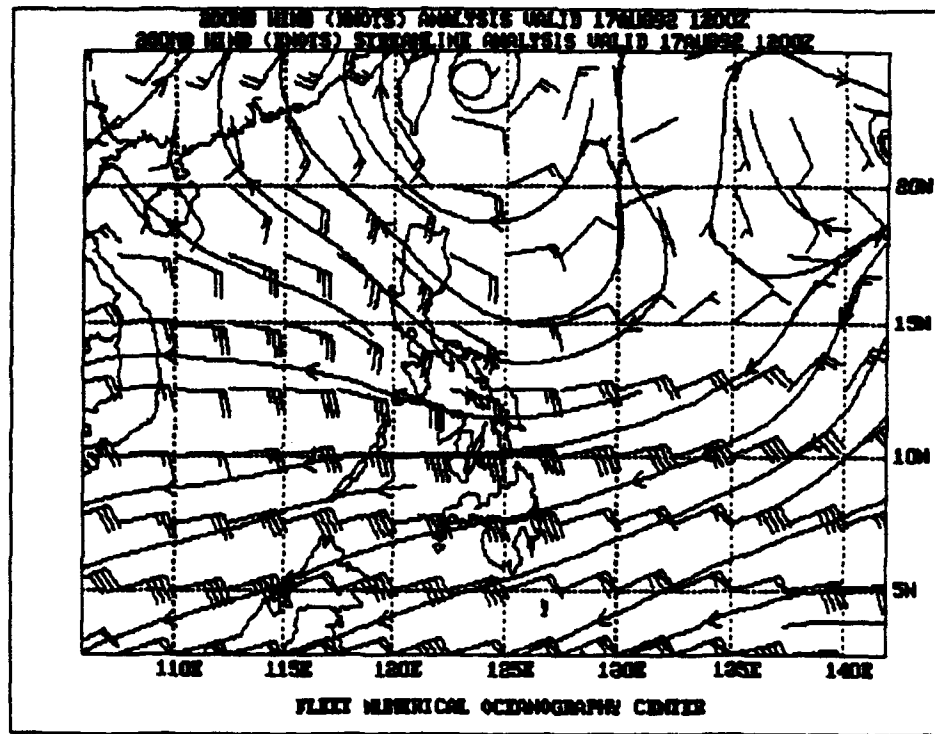


Figure 3.101: NODDS 200-mb Winds and Streamline Analysis for 1200Z 17 August 1992.

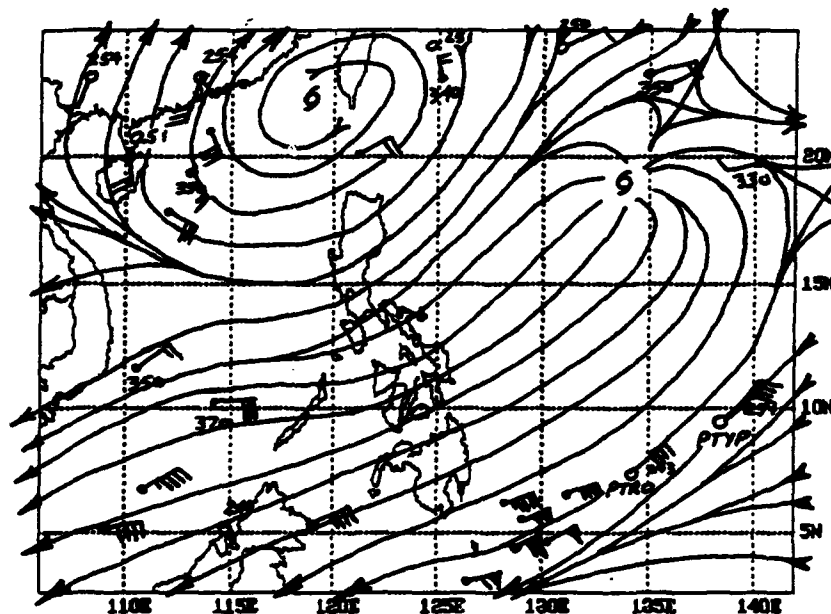


Figure 3.102: NODDS 200-mb Manual Streamline Analysis for 1200Z 17 August 1992 (adapted from NPS hand streamline analysis)

18 August 1992

At 172100Z (180500 Local), four hours before the 180100Z NODDS DMSP visible image shown below in Fig. 3.103, the following observations were made at Cubi Point, Manila IAP and Mactan IAP:

Cubi Point ...23014kt 9999 61RA 1ST010 3CU020 6SC030 27/23 2965INS...

Manila ...25006kt 5000M 61RA 3SC020 8AS090 25/23 1003 CONTUS LGT RA...

Mactan ...22004 9999 2CU020 4AC100 5CI300 27/23 1007...

While the 61RA group in the Cubi Point observation indicates only light rain, the satellite image shows the familiar patterns of convection associated with Tropical Storms Lois and Mark, and with the surge cloudiness across the South China Sea.

Figure 3.104 shows Vigan (98222) and Iba (98324) reporting rain, a rain shower at Romblon (98536) and a thunderstorm at Iloilo (98637) on the Panay Gulf.

Finally, the Cubi Point sounding in Fig. 3.105 may represent one of the last radiosondes launched before the scheduled closure of the NOCF. The surge intensity is likely between weak and moderate, i.e., the 25 kt wind at 700 mb supports moderate, but the 15 kt wind at 200 mb supports weak (see Fig. 3.72). The 15 kt wind at 200 mb suggests less upper level divergence and thus less upward vertical motion than in a moderate surge. Also, there may be stronger winds above 200 mb.

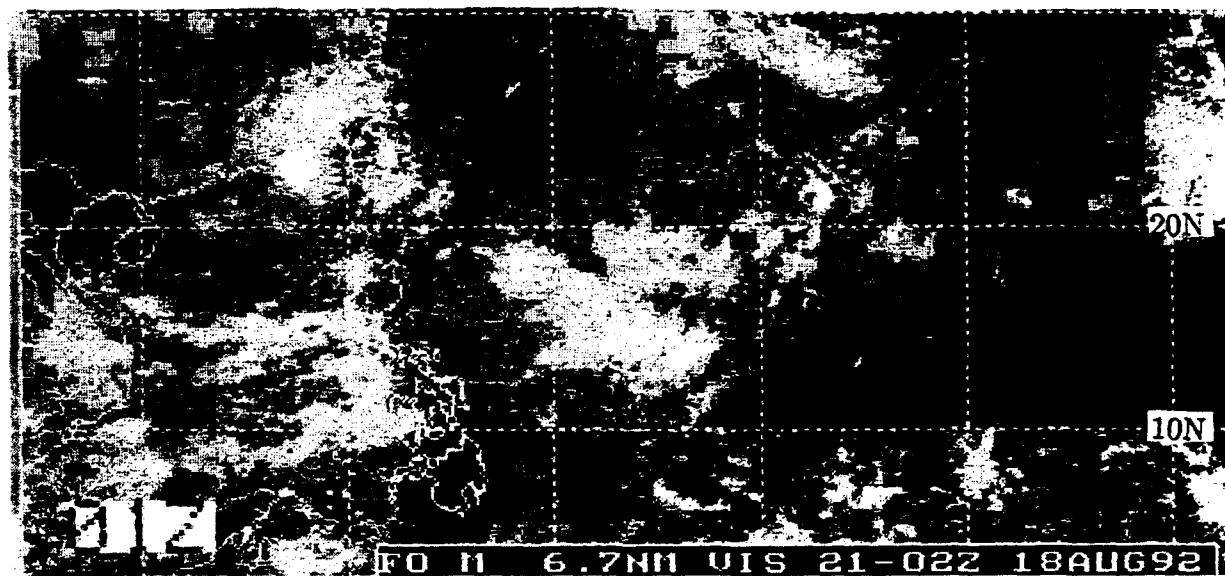


Figure 3.103: NODDS Mosaic of DMSP Visible Imagery for 0100Z on 18 August 1992

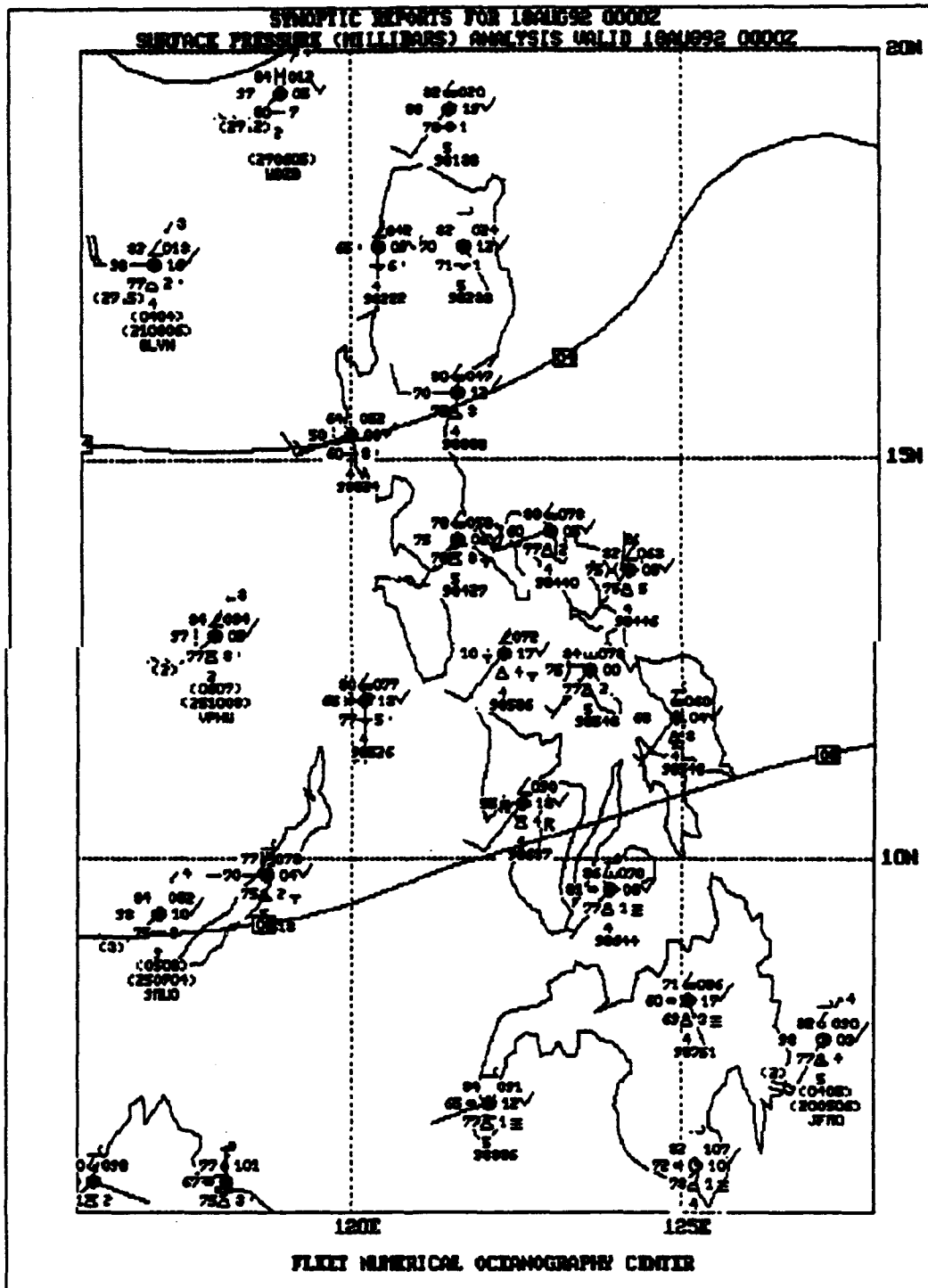


Figure 3.104: NODDS Synoptic Reports and Surface Pressure Analysis for 0000Z 18 August 1992.

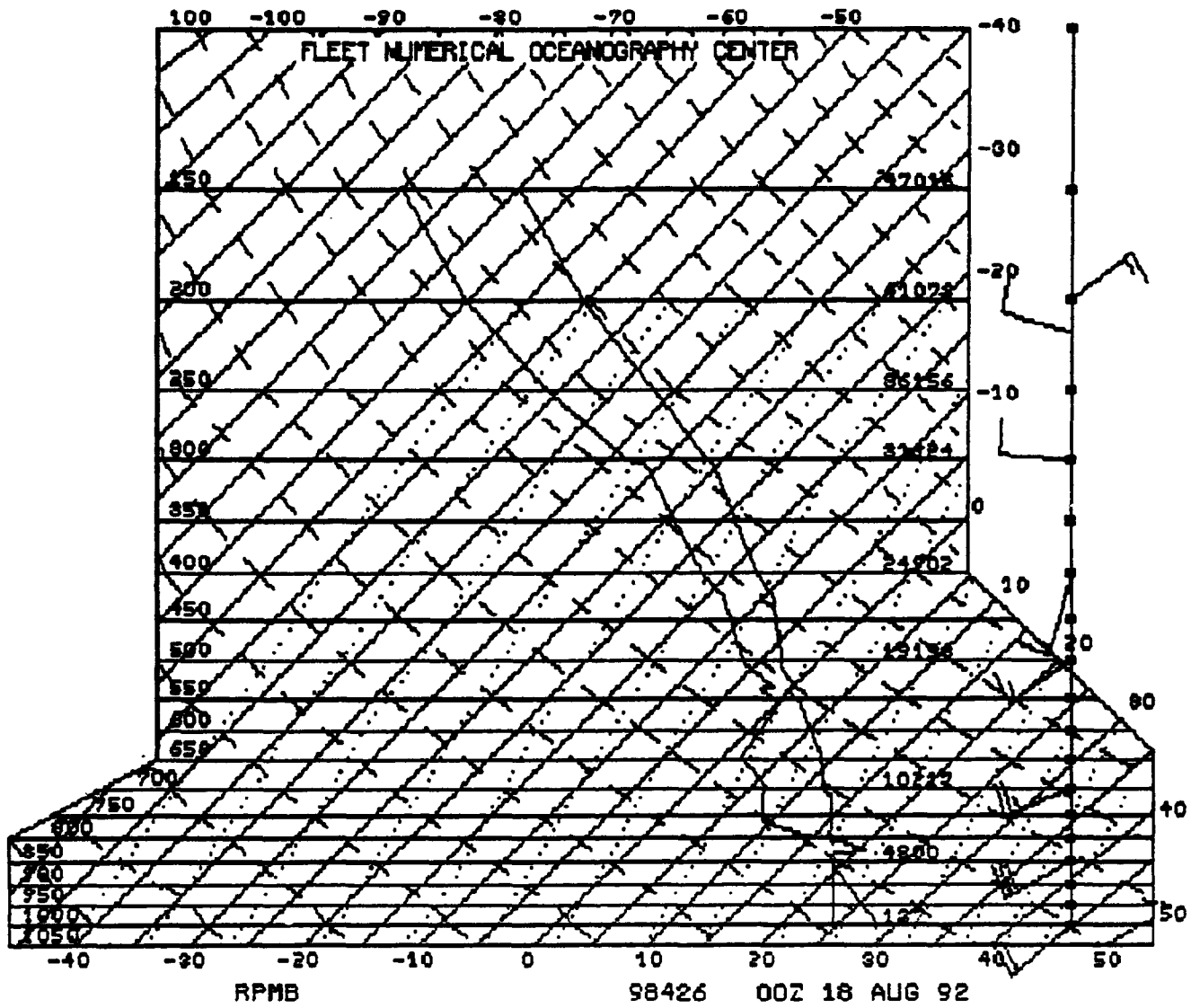


Figure 3.105: NODDS Skew T, Log P Sounding from NOCF Cubi Point (RPMB) at 0000Z 18 August 1992

3.5.4 Southwest Monsoon Surge "Snapshot", 4 September 1992

While this abbreviated look at conditions over the western North Pacific Ocean on one day, 4 September 1992, falls short of a case study, per se, the conditions are typical of a surge in the southwest monsoon. Typical, in that Tropical Storm Omar is located to the north-northeast of Luzon near 23°N, 123°E at 040200Z (Point "E" on Fig. 3.106(b)), see Fig. 3.107 on which a portion of the working best track of Omar⁵⁸ is plotted. Note that the convective cloudiness, associated with Omar, extends far south of Omar's center position, and covers much of Luzon. Thus the surge is manifested by an enhancement of the southwesterly flow spiralling from the equator toward the tropical cyclone.

Figure 3.106(b) further labels the position of the more classical TC image of typhoon Ryan, near 19.6°N, 146.5°E, (Point "D") north of Guam. Guard (1985) also discusses how "cells" within the TUTT may extend downward in the troposphere leading to areas of low pressure which appear to trigger surges in the southwest monsoon. However, these phenomena produce surges generally distant to the east of the Philippine Islands.

The working best track of Omar at 041200Z, Figure 3.107, was obtained real time from FNOC's data base using the Automated Tropical Cyclone Forecasting (ATCF) system, while Fig. 3.108 is the graphical NODDS product of JTWC's warning on TS Omar. Figures 3.109 and 3.110 then show the NODDS surface pressure analysis and synoptic observations over the Philippine Islands. Figure 3.110 records the cloudy conditions still observed over Luzon, with thunderstorms reported from the west coast of Luzon, at Vigan (98222) and Iba (98324), at 041200Z.

Figures 3.111, 3.112⁵⁹ and 3.113 are the NOGAPS 041200Z wind and streamline analyses at the 925-, 700- and 200-mb pressure surfaces, respectively. Note that the following winds along the west coast of Luzon exceed the requirements for a moderate surge (see Fig. 3.72): 925-mb winds⁶⁰ are 25–30 kt (Fig. 3.111) and 700-mb (or ~10,000-foot) winds are 30–35 kt (Fig. 5.112). However the 200-mb (or 35,000–40,000-foot) winds are only 15–20 kt, i.e., below the expected 200-mb strength of even the weak surge (see Fig. 3.72). Of course, the larger required upper-level divergence may take place on a surface other than 200-mb.

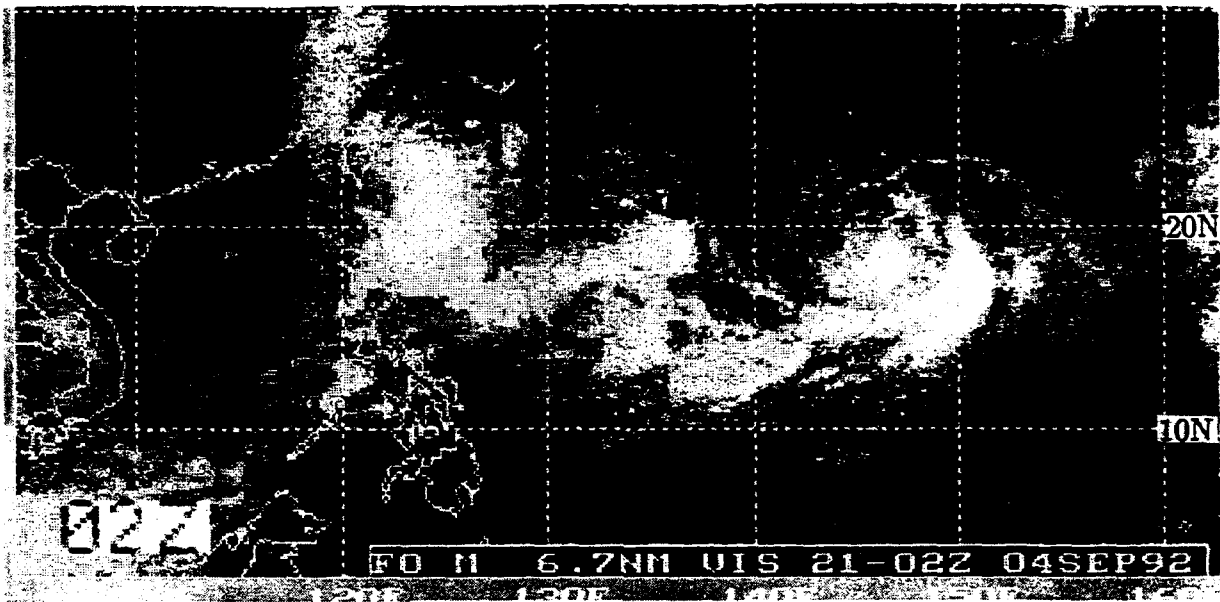
On Figure 3.114 significant wave heights >6 feet, associated with the surge, are analyzed in South China Sea, with an 18-foot contour, associated with Omar, off the northeast coast of Taiwan. The SST analysis shows a small warm pool (>30°C) south of Hainan Island and cooler water (<28°C) near the west coast of Luzon, surrounding Taiwan, and near 15°N, 140°E.

⁵⁸On 28 August (one week earlier), Omar had struck Guam with winds of 105 kt with gusts to 130 kt causing extensive damage (\$457 million) to the island.

⁵⁹When products from the current 00Z or 12Z run are not available, NODDS transmits the 12-h forecast of the respective product. On this particular "down-load" for 041200Z, NODDS transmitted 12-h forecasts (from the 040000Z run) for the 925-mb and 700-mb streamline analyses. Thus the 925-mb and 700-mb streamlines analyses are those received by delayed transmission to the Naval Postgraduate School.

⁶⁰The NOGAPS surface winds are 20–25 kt (not shown).

(a)



(b)

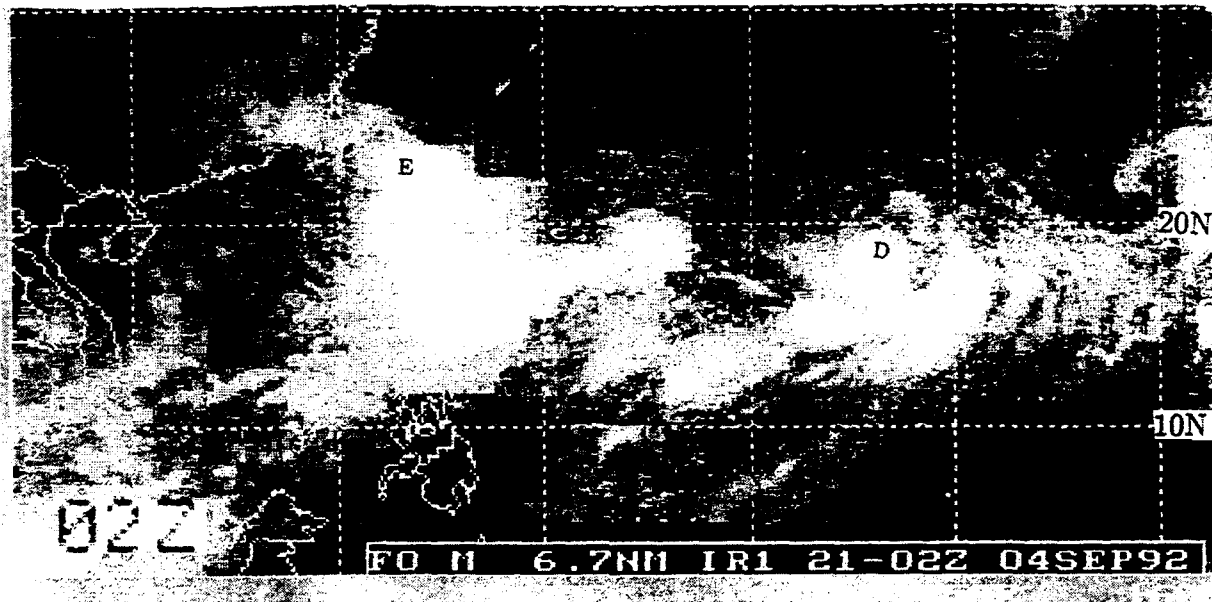


Figure 3.106: NODDS Mosaic of DMSP Satellite Imagery, Visible (a) and IR (b) for 0200Z on 4 September 1992

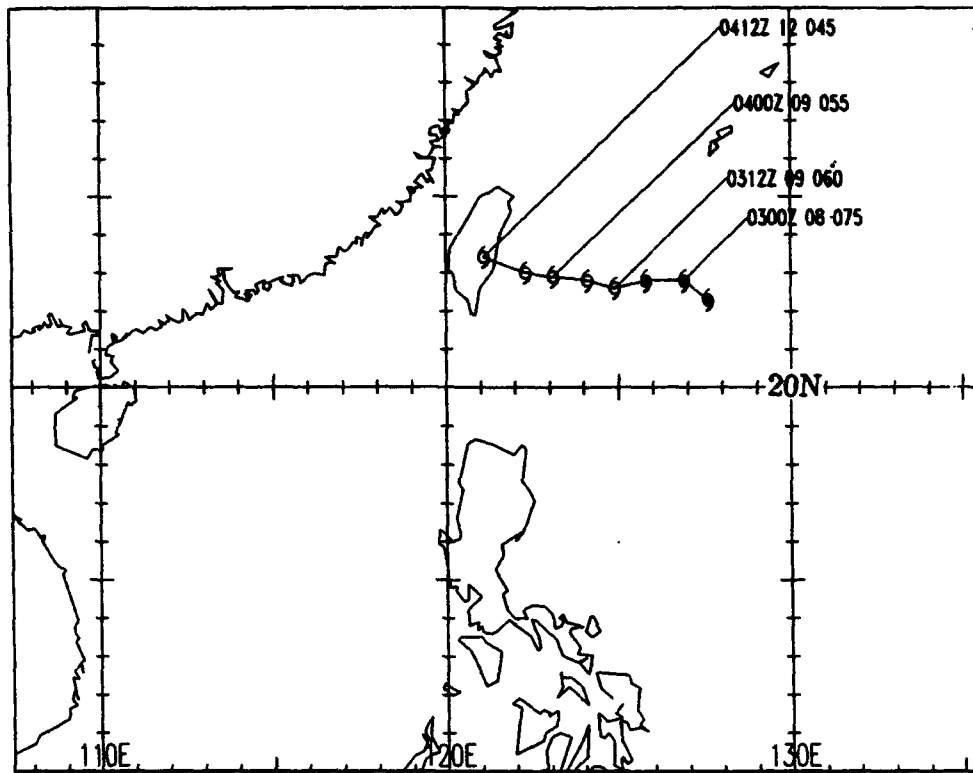


Figure 3.107: Working Best Track of Typhoon Omar. The position labels provide (1) time of warning position, (2) speed (kt) of movement during the previous 6 hours and (3) maximum sustained (one-minute average) wind.

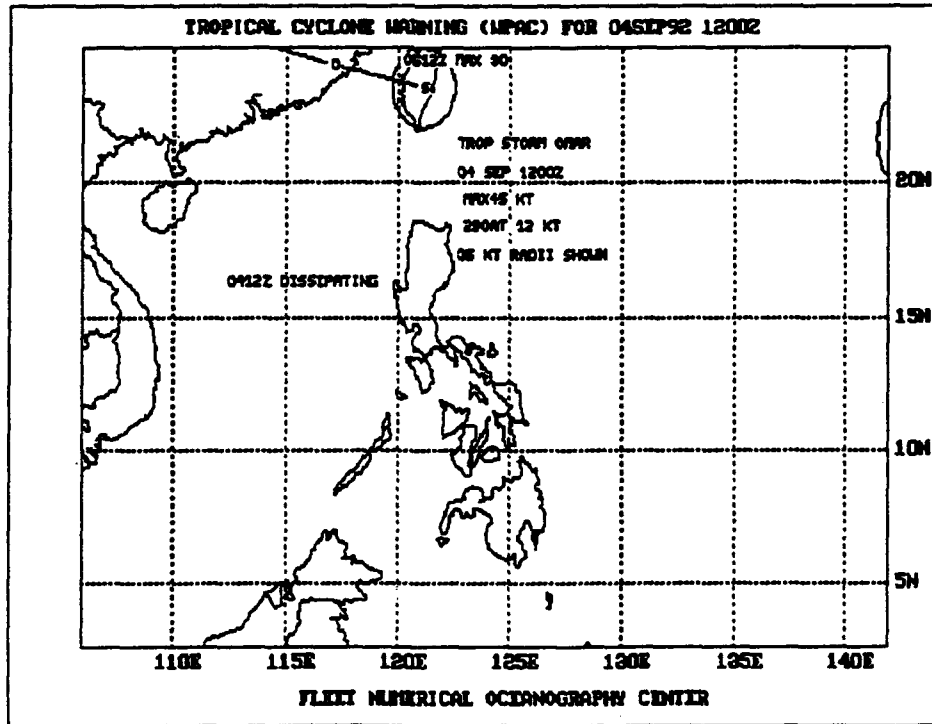


Figure 3.108: NODDS TS Omar Warning for 1200Z 4 September 1992

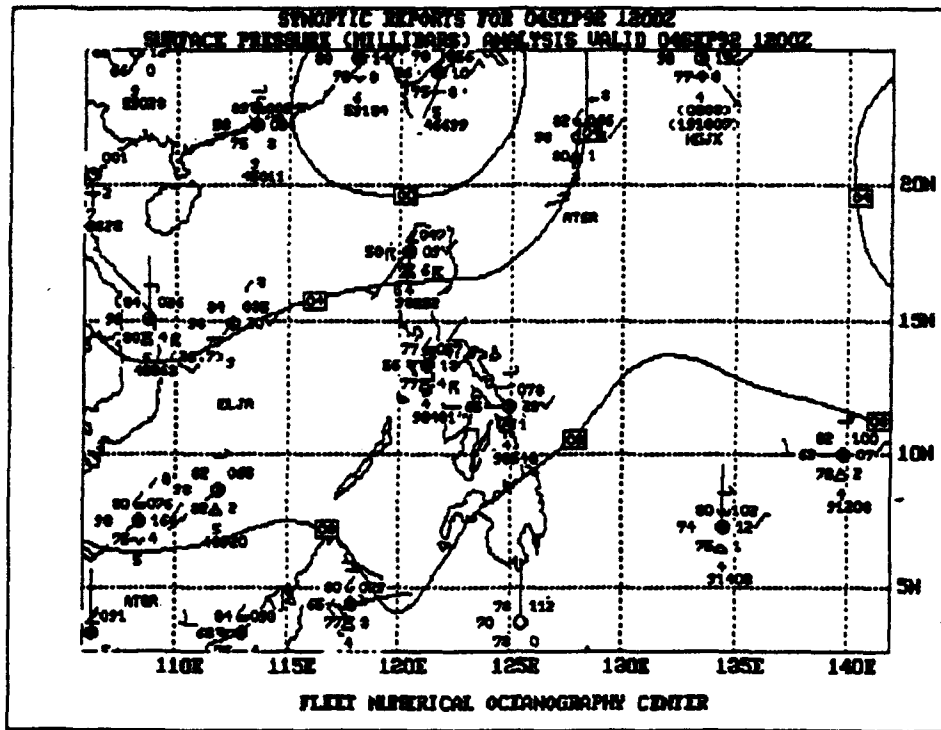


Figure 3.109: NODDS Synoptic Reports and Surface Pressure Analysis for 1200Z 4 September 1992

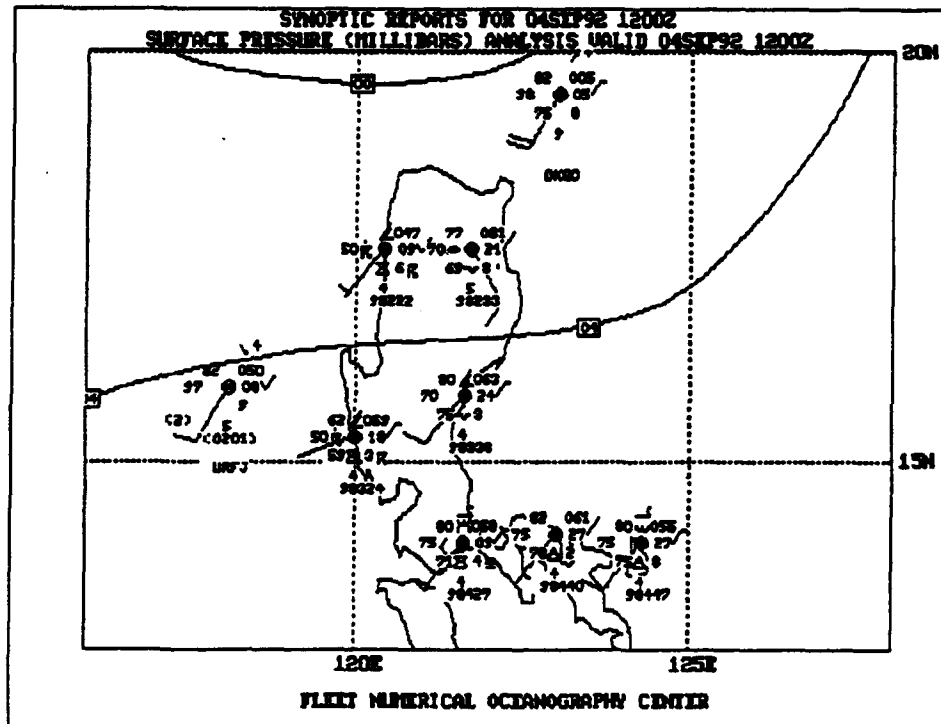


Figure 3.110: NODDS Zoomed Synoptic Reports and Surface Pressure Analysis for 1200Z 4 September 1992.

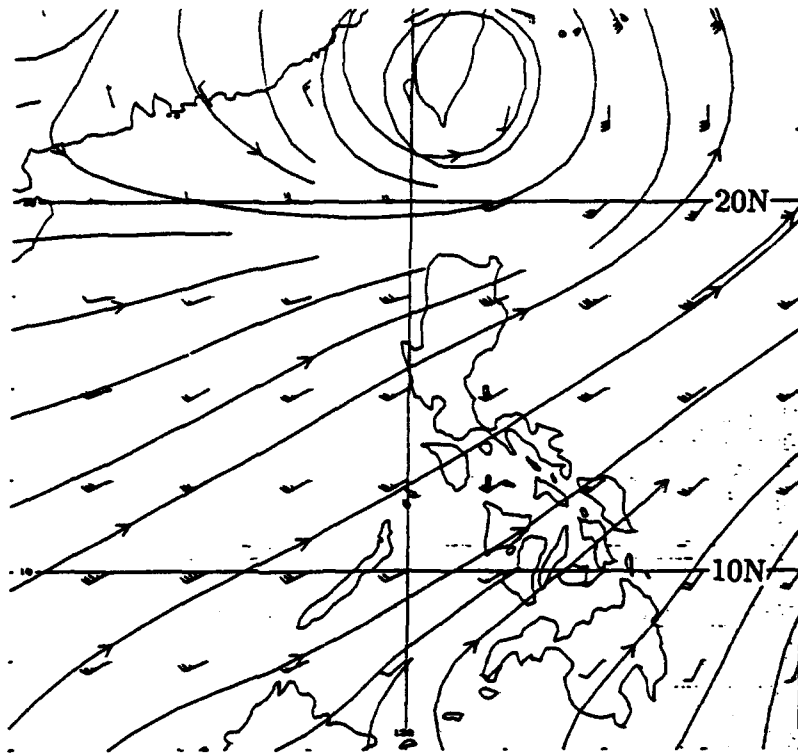


Figure 3.111: NOGAPS 925-mb Winds and Streamline Analysis for 1200Z 4 September 1992 (from the Naval Postgraduate School)

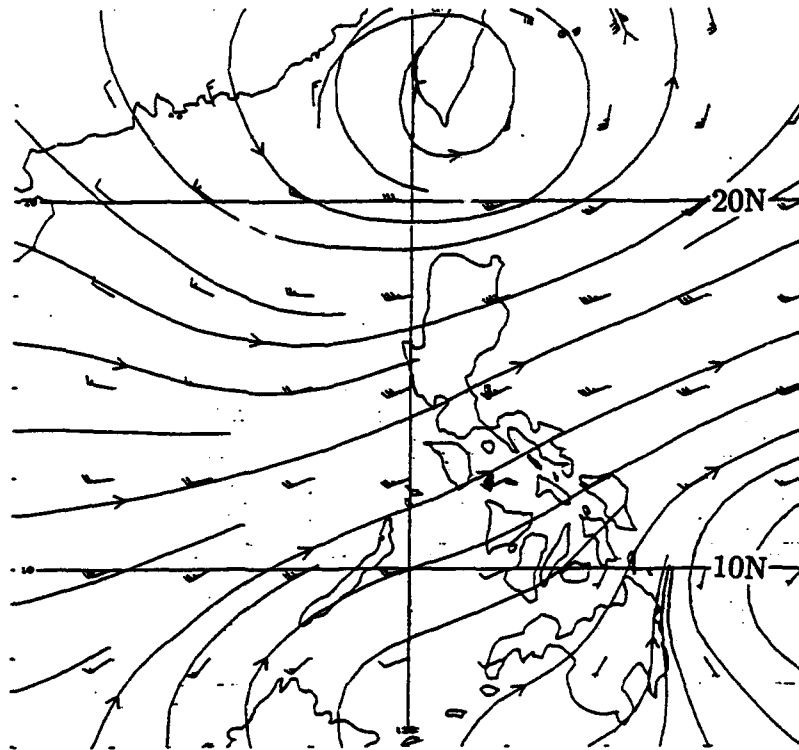


Figure 3.112: NOGAPS 700-mb Winds and Streamline Analysis for 1200Z 4 September 1992 (from the Naval Postgraduate School)

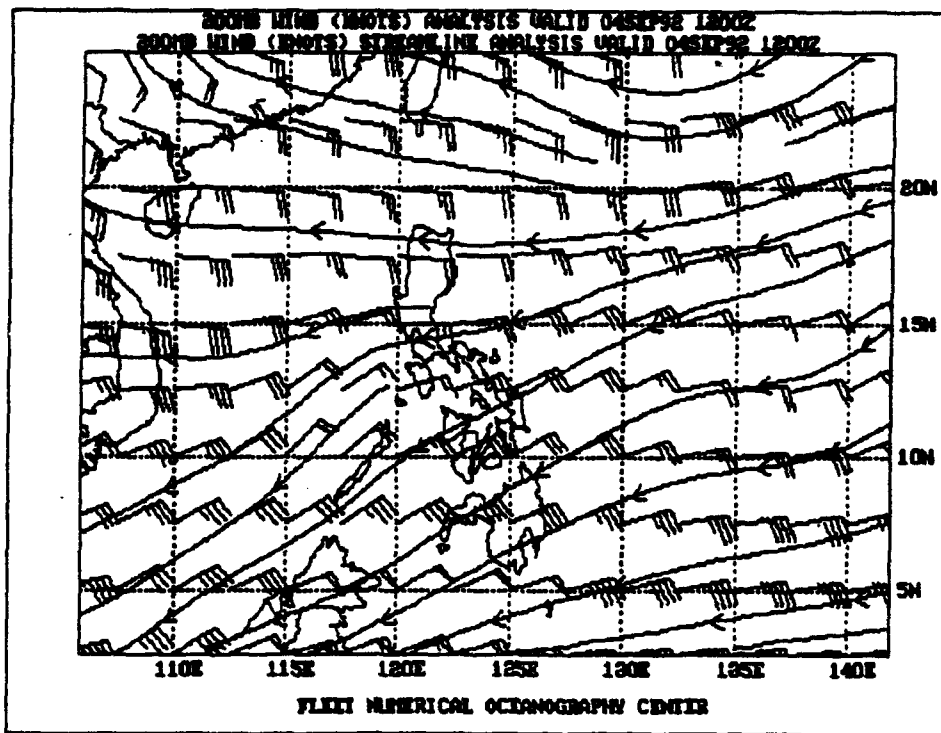


Figure 3.113: NODDS 200-mb Winds and Streamline Analysis for 1200Z 4 September 1992.

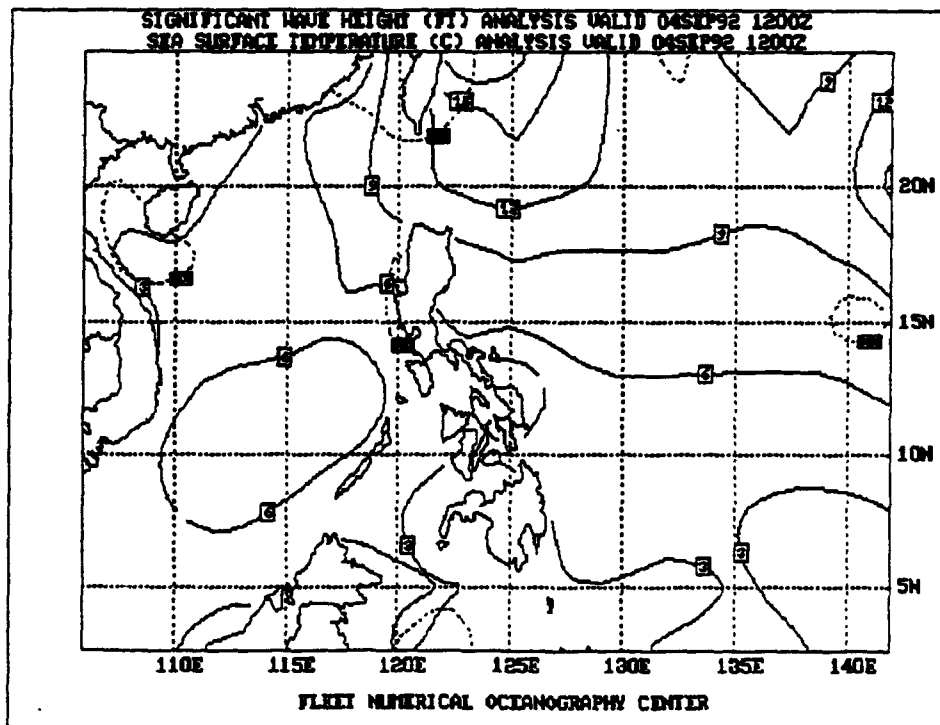


Figure 3.114: NODDS Significant Wave Height Analysis (solid) and Sea Surface Temperature (dashed) for 1200Z 4 September 1992.

AT 041600Z (050000 Local), four hours after the previous analyses, the following observations were made at Cubi Point, Manila IAP and Mactan IAP:

Cubi Point ...21014/20KT 9999 25RESH 1CB015 3CU020 3SC030 8AC080 28/24
2969INS/CIG030 OCNL LTGIC CB N STNR CB SE DSIPTD...

Manila ...22004KT 6000 3CU020 8AC090 26/23 1005 INTMT LGT RA...

Mactan ...24002 9999 2CU020 28/24 1008...

i.e., rain showers and wind 14 kt gusting to 20 kt at Cubi Point; light rain at Manila IAP; but only scattered clouds at Mactan IAP in the Visayas.

The 24-h terminal forecast for Cubi Point for the period 041500Z-051500Z called for wind 21010/16kt, overcast, ceilings 2000-3000 feet, with thunderstorms and rain showers in the vicinity; temporary periods of thunderstorms and moderate or heavy rainshowers, wind 21016/25kt, visibility 4000 meters, ceiling lowering to 1000 feet; and then gradually, between 050300Z-050500Z, ceilings and visibility improving, except for temporary light rain or thunderstorms.

To support this episode as a bonafide surge, the following is quoted from an Associated Press news release on 6 September 1992.

... Avalanches of volcanic debris caused by heavy rains roared down the slopes of Mount Pinatubo yesterday, causing thousands to abandon their villages. Monsoon rains have inundated a wide area around Pinatubo, 60 miles northwest of Manila, and more than 50 people have died during the past few weeks. The flooded area includes Clark Air Base, abandoned by the U. S. Air Force when the volcano erupted in June 1991. The rains have caused debris from that eruption to plunge down Pinatubo's slopes and swell rivers...at least three rivers are filled with up to 20 feet of volcanic muck...Scientists say heavy rains could trigger massive avalanches, called lahars, for years around Pinatubo...Pinatubo came to life again in July (1992), when lava began oozing from the crater created by the 1991 eruption. Scientists say the renewed activity indicates another violent eruption may be near.

As noted above, avalanches must have occurred "during the past few weeks." Since the surge case, in Section 3.5.3, ended on 18 August, much of the surge precipitation was caused by Tropical Storm Polly that moved on a track to the northeast of Luzon (not shown) during the last week of August.

3.5.5 Northeast Monsoon Cold Surge 6–8 February 1992

During the 1990–1992 time period, the most significant rainfall events occurred during the southwest monsoon. However, the forecaster must be aware of the strong winds often associated with cold surges and shear lines occurring during the northeast monsoon. While northeasterly surges and shear lines may reach Luzon and Visayas near the end of their life span—often manifested by only a dissipating, unimpressive cloud line over Luzon—, these phenomena are responsible for strong winds primarily in the northern South China Sea, the Luzon Strait and the northern Philippine Sea.

Many studies define differently the East Asian cold surges by observations (on and adjacent to the coast of China) of: surface pressure gradients, drops in surface temperature, increases in the northerly wind component, etc. However, Boyle and Chen (1987) examine the evolution of contour patterns⁶¹ on constant pressure surfaces over Asia to identify precursors of the cold surge event. They examined the strongest surge⁶² in terms of cooling rate and minimum temperature, to affect Hong Kong during the winter of 1978–1979. Similarities of this case study of a cold surge to that of Boyle and Chen will be identified.

6 February 1992

The 060200Z February 1992 infrared imagery of Fig. 3.115 shows the typical warm and dry conditions so often prevalent over the Philippine Islands during the northeast monsoon. Note, in particular, the clear conditions over the northern South China Sea and the Luzon Strait. Of course, imagery of such gross resolution, 6.7 nm will not identify many of the smaller mesoscale features.

Following the example of Boyle and Chen (1987), the 061200Z 300 mb contour analysis is examined in Fig. 3.116. With the trough existing over Mongolia and extending through Point “B”, it is easy to visualize the ridge existing just north of the figure, i.e., to the northwest of Lake Baikal (spelled Baykal, on some atlases), which is seen on the northern edge of the figure at Point “Z”. The development of this ridge—attributed in the Boyle and Chen (1987) study, to warm advection to the west—is a key event of the sequence for the surges. The developing ridge initiates a northwesterly flow over Lake Baikal (see the 300-mb contour 24-h forecast in Fig. 3.117). Figure 3.117 also shows the upper-level trough having moved eastward, and now extending through Point “Y” north of Korea. It is this feature, the trough, that will be the key force in initiating the surge—however, it is noted that this trough does not have so great an amplitude (is not as deep) as the one in the Boyle and Chen study. Forecasters at the Royal Observatory of Hong Kong use northwesterly flow in the region of Lake Baikal at 500 mb as one indication that a surge is imminent. By 48 hours, the 300-mb forecast in Fig 3.118 predicts the trough to have moved over the Sea of Japan, extending through Point “X”.

⁶¹Boyle and Chen (1987) also examine thickness layers and thermal advection in their discussion.

⁶²Their study was of the second (8–11 December 1978) of 11 surges occurring in that season.

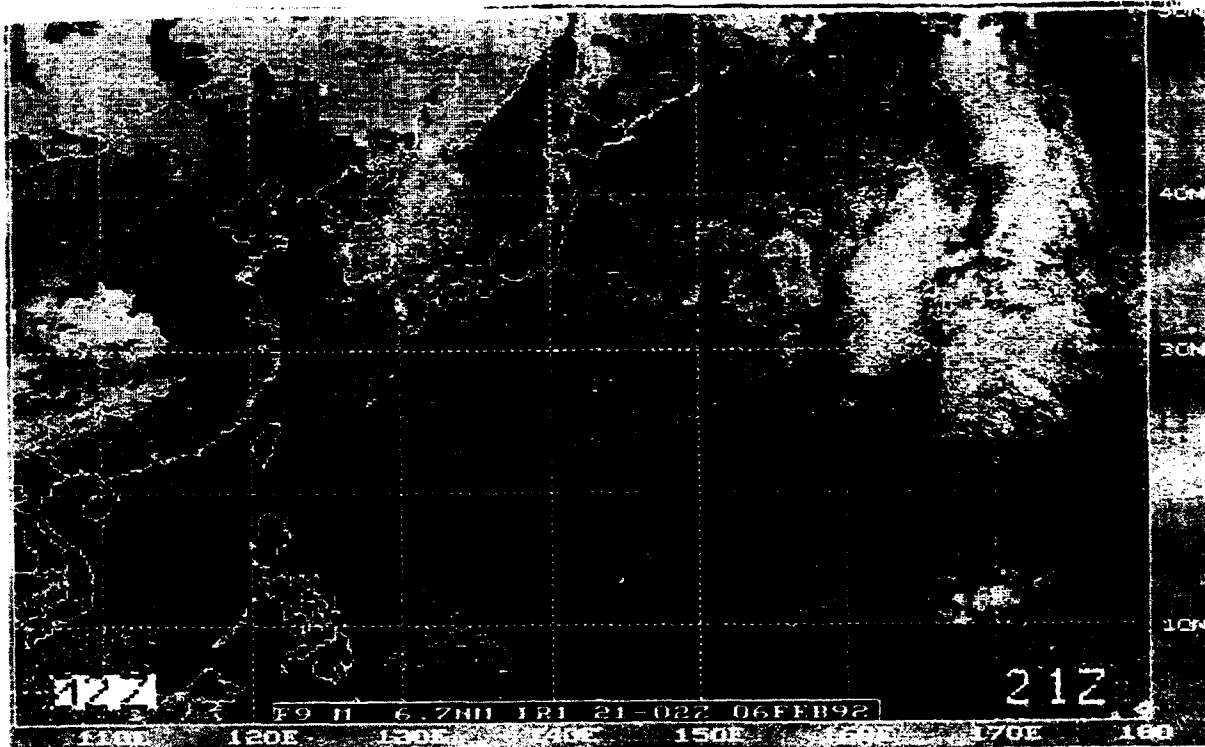


Figure 3.115: NODDS Mosaic of DMSP IR Imagery for 0200Z on 6 February 1992

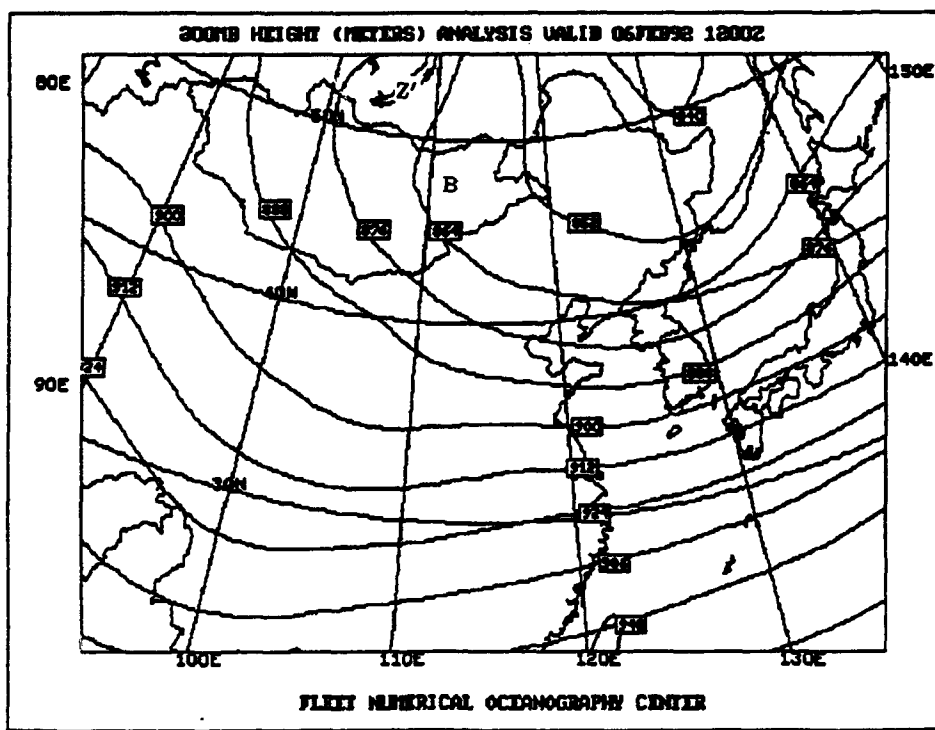


Figure 3.116: NODDS 300-mb Height (meters) Analysis for 1200Z 6 February 1992

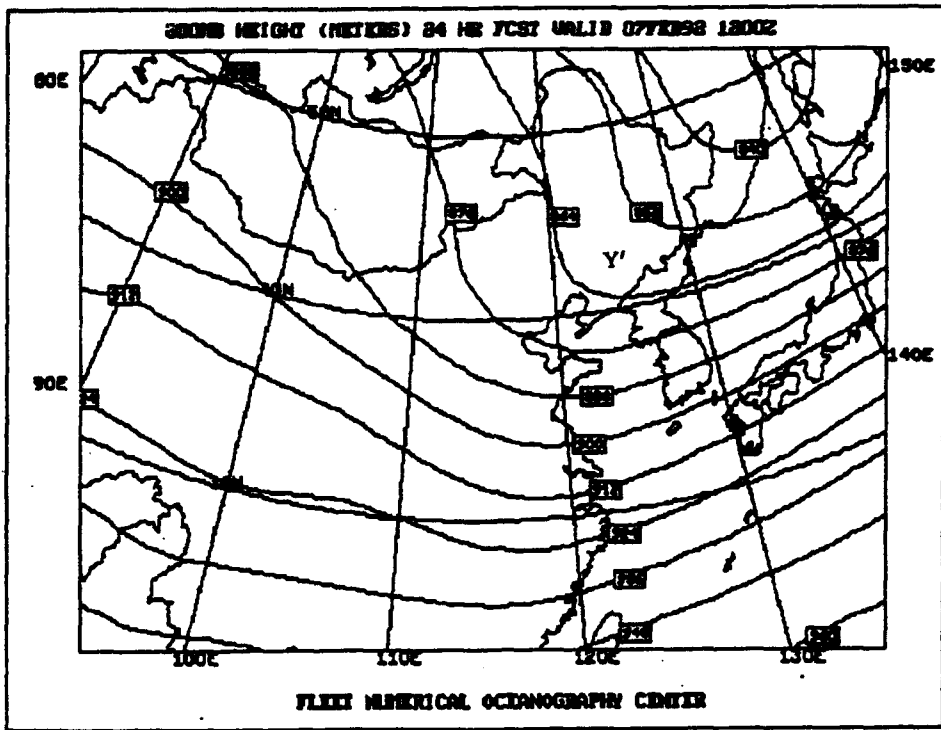


Figure 3.117: NODDS 300-mb Height (meters) 24-h Forecast from 1200 6 February 1992

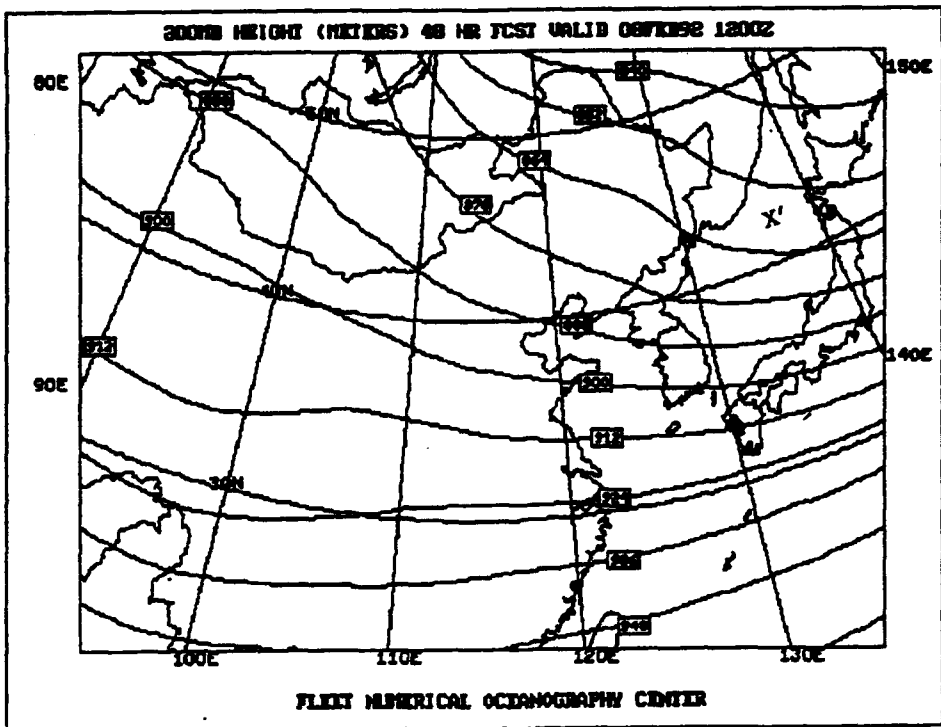


Figure 3.118: NODDS 300-mb Height (meters) 48-h Forecast from 1200 6 February 1992

On Fig. 3.119, the 061200Z 1000-mb height analysis, coincident with 300-mb analysis in Fig. 3.116, shows a high center just west of Lake Baikal. On the 24-h forecast, Fig. 3.120, the high has moved southeastward to the China-Mongolian border, near 42°N, 106°E. with height (pressure) increases evident over eastern China, and, in particular, a stronger height (pressure) gradient east of Taiwan (Point "W").

Figure 3.121 then shows the surface pressure and synoptic reports⁶³ near the Philippine Islands at 061200Z (062000 Local), with the zoomed analysis in Fig. 3.122.

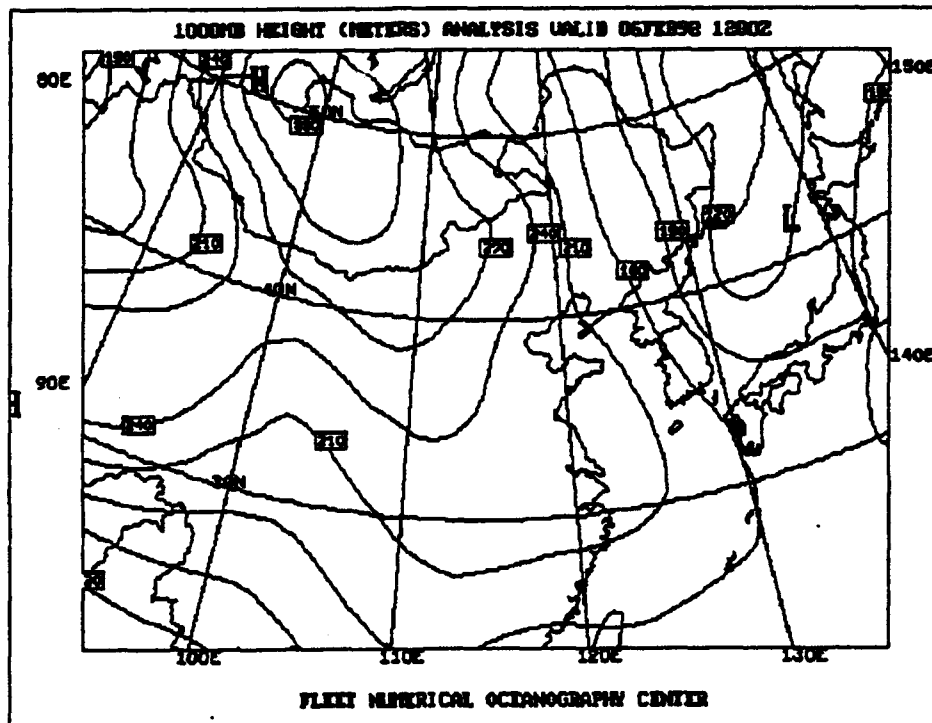


Figure 3.119: NODDS 1000-mb Height (meters) Analysis for 1200 6 February 1992

⁶³These data are some of the first NOGAPS 3.3 runs "downloaded" via NODDS in real time in February 1992. However, the setting on the NODDS menu requiring the plotting of wave and swell data was omitted.

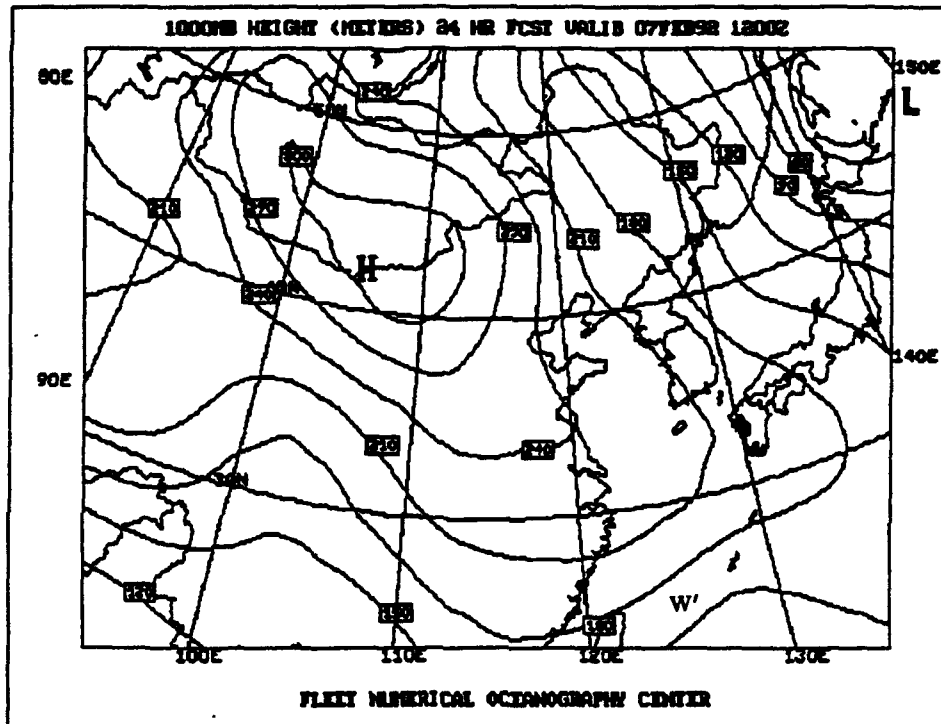


Figure 3.120: NODDS 1000-mb Height (meters) 24-h Forecast from 1200 6 February 1992

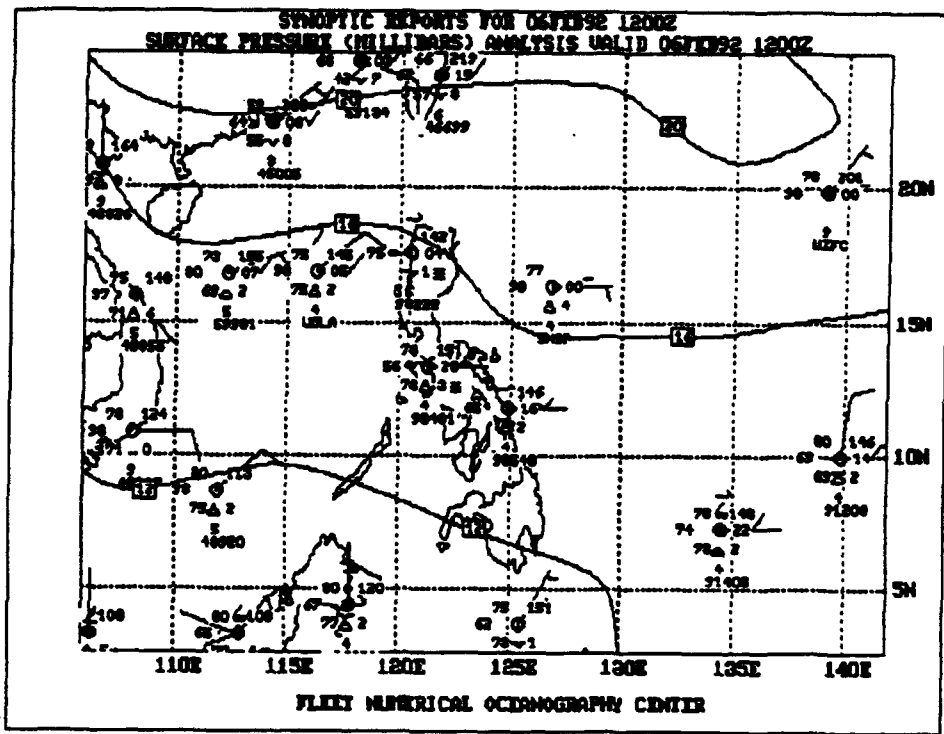


Figure 3.121: NODDS Synoptic Reports and Surface Pressure Analysis for 1200Z 6 February 1992

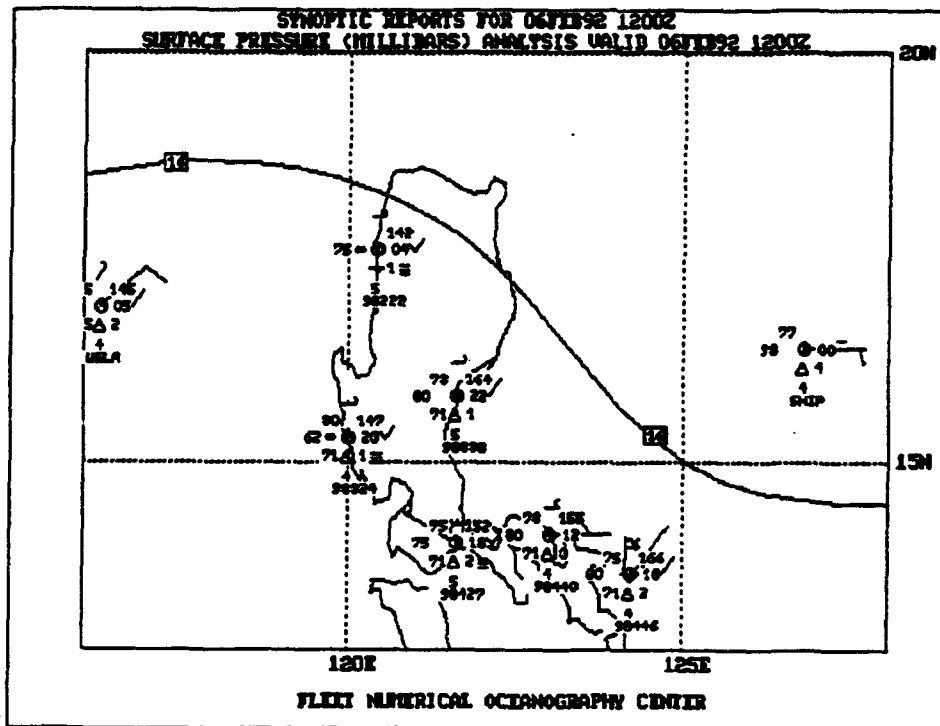


Figure 3.122: NODDS Zoomed Synoptic Reports and Surface Pressure Analysis for 1200Z 6 February 1992

Next, Fig. 3.123 shows the 925-mb (near the gradient level used by tropical analysts) wind and streamline analysis at 061200Z. Note the small magnitude winds (~ 10 kt) from east of Taiwan over the northern Philippine Sea to northeastern Luzon. The forecasts depict a shear line, running from east of Taiwan to northern Luzon at 071200Z, Fig. 3.124, followed by stronger northeasterly winds (15–20 kt) over the Luzon Strait at 081200Z, as the shear line is “progged” to reach the southeastern portion of Luzon, Fig. 3.125.

In Fig. 3.126, the polar front jet is manifested by the 95 kt winds on the 200-mb surface near Hong Kong at 061200Z. In particular note that the wind at the grid point near Cubi Point, 15°N , 120°E , is forecast to increase to 35 kt in 24 hours on Fig. 3.127, indicating the closer approach of the polar front jet.

Figure 3.128 shows >6 -foot waves in the Luzon Strait and lower seas on the lee side (west) of northern Luzon, at 061200. The SST analysis, Fig. 3.129, shows $>26^{\circ}\text{C}$ water near the Visayas and Mindanao, 20°C water in the Taiwan Strait, and a SST gradient in the Luzon Strait.

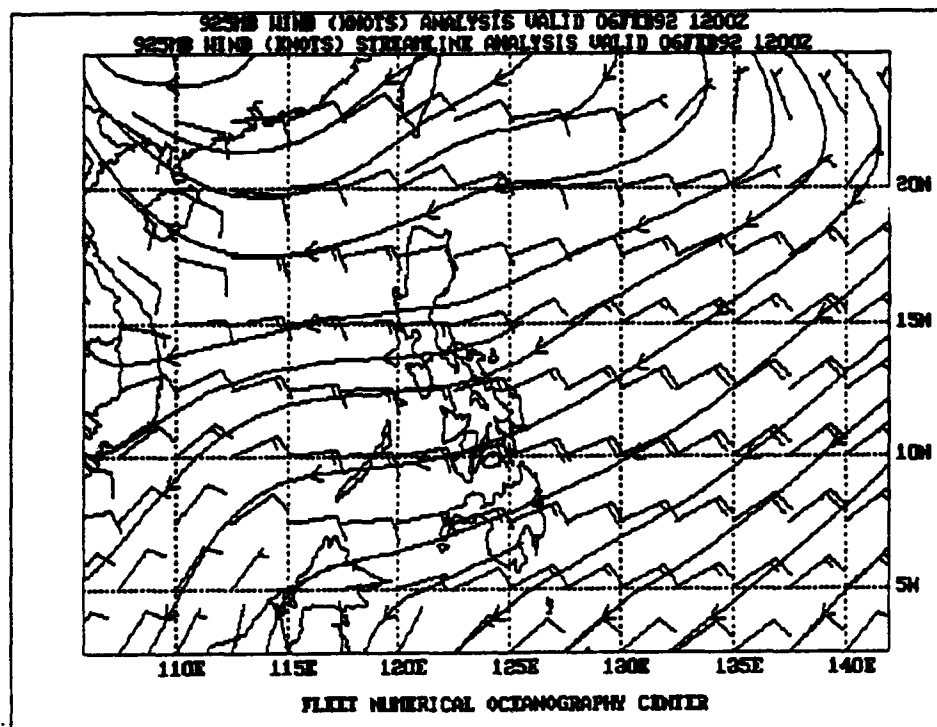


Figure 3.123: NODDS 925-mb Winds and Streamline Analysis for 1200Z 6 February 1992

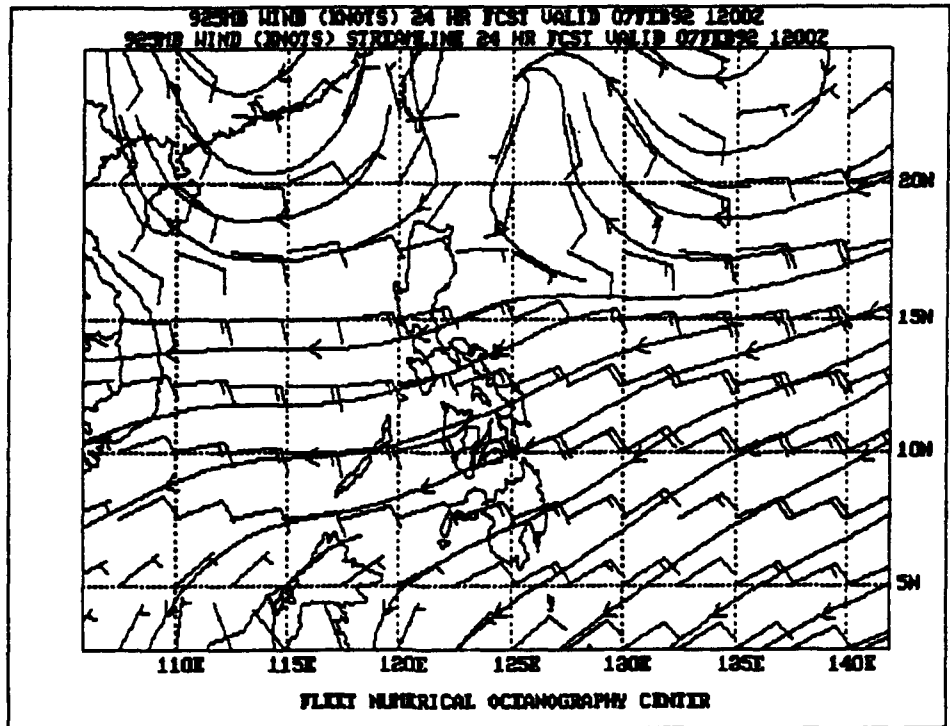


Figure 3.124: NODDS 925-mb Winds and Streamline 24-h Forecast from 1200Z 6 February 1992

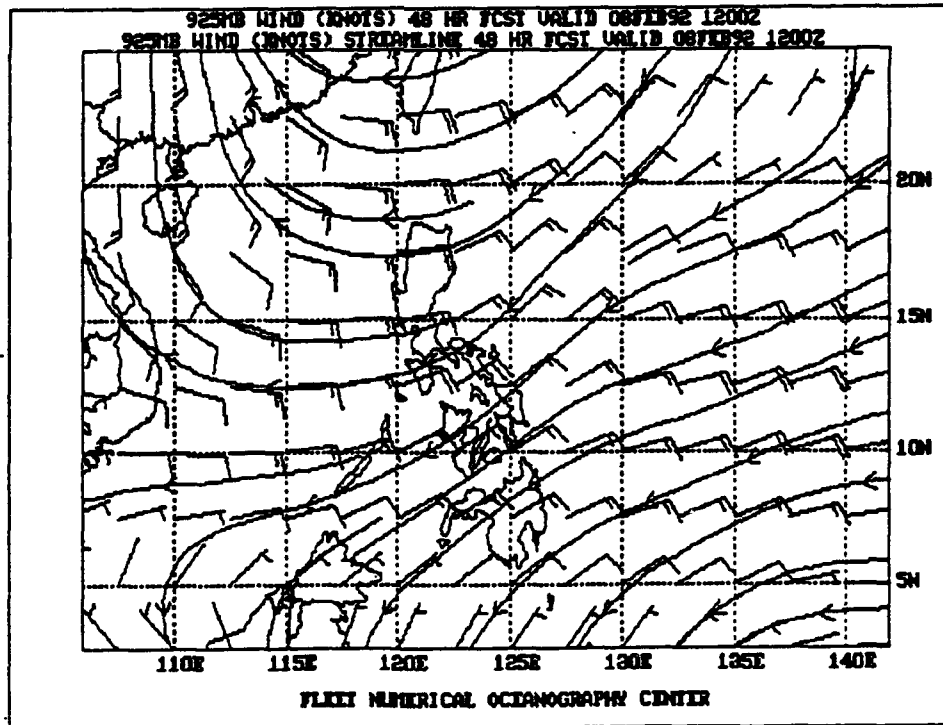


Figure 3.125: NODDS 925-mb Winds and Streamline 48-h Forecast from 1200Z 6 February 1992

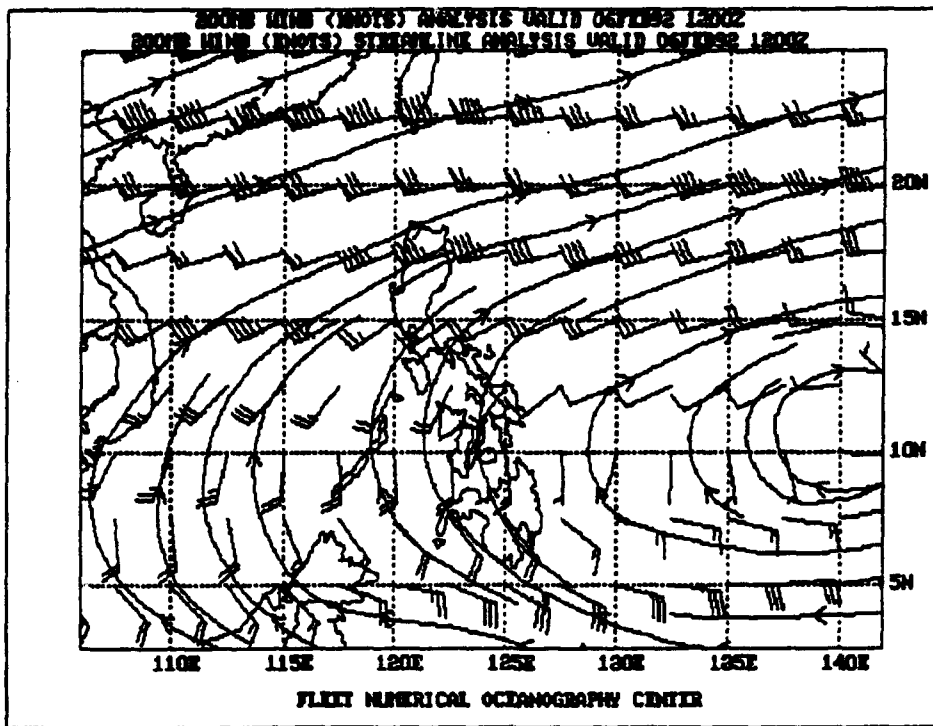


Figure 3.126: NODDS 200-mb Winds and Streamline Analysis for 1200Z 6 February 1992

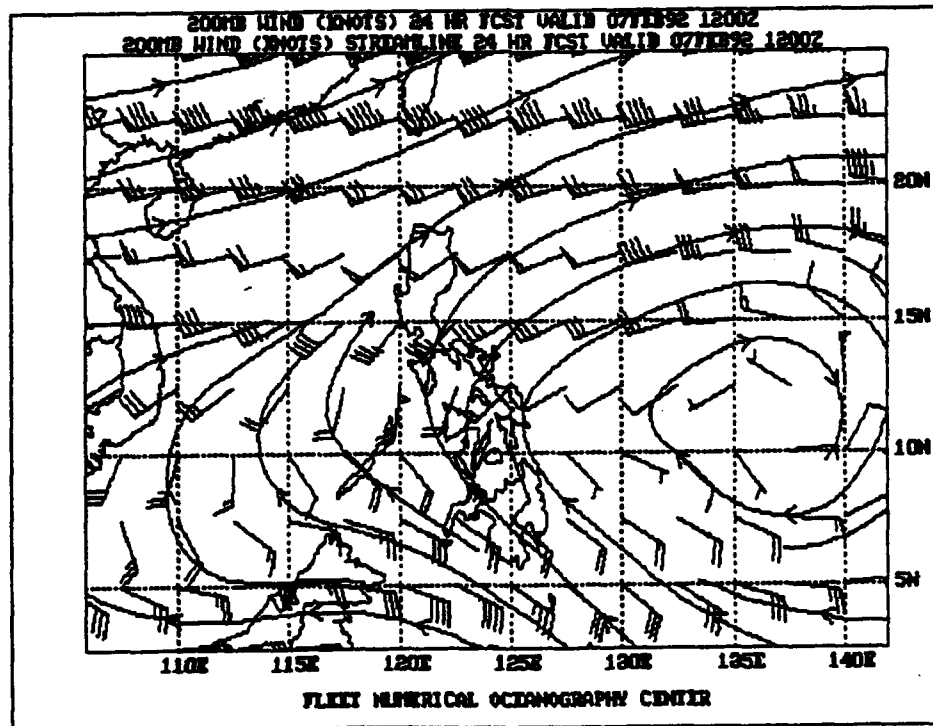


Figure 3.127: NODDS 200-mb Winds and Streamline 24-h Forecast from 1200Z 6 February 1992

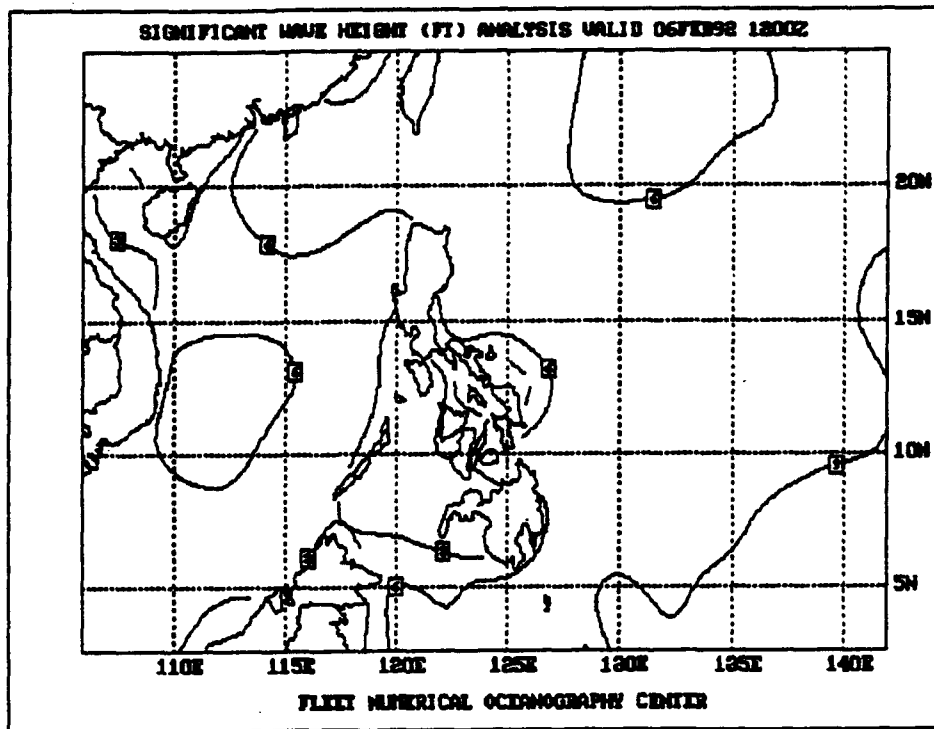


Figure 3.128: NODDS Significant Wave Height Analysis for 1200Z 6 February 1992

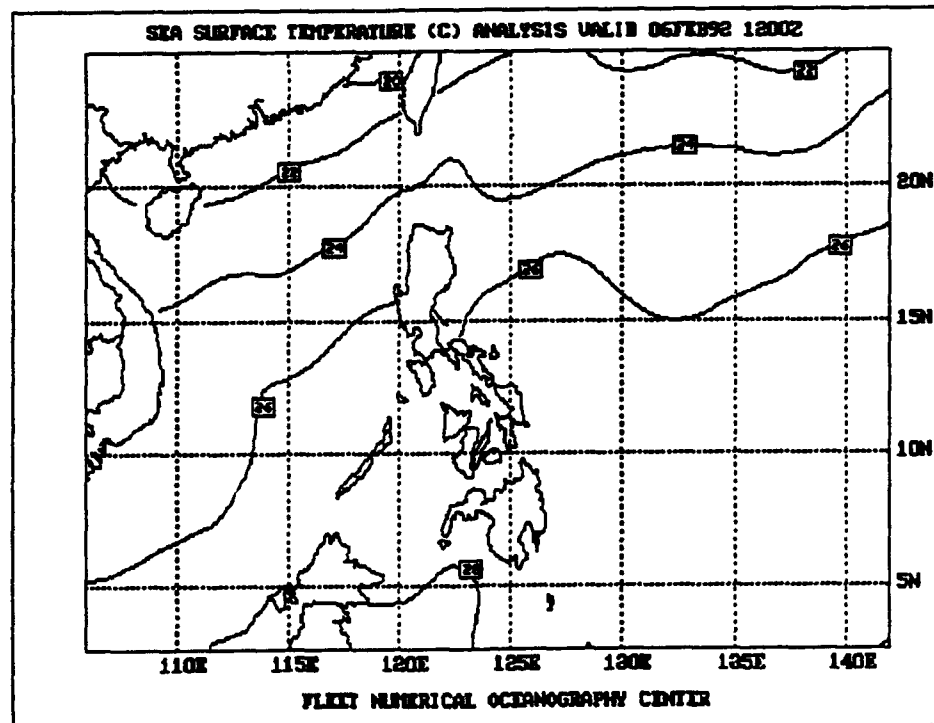


Figure 3.129: NODDS Sea Surface Temperature for 1200Z 6 February 1992

7 February 1992

Figure 3.130, the 071200Z 1000 mb contour analysis, shows that the 24-h NOGAPS forecast, Fig. 3.120, verifies well as the high center moves near the China-Mongolian border and the pressure gradient increases east of Taiwan at Point "V". This stronger pressure gradient near Taiwan is further shown on Fig. 3.131, where "2-dot" rain is occurring at station 46699.

On the 925-mb 071200Z streamline analysis, Fig. 3.133, the NOGAPS analysis shows a shear line extending from the east coast of Taiwan across the Luzon Strait through Point "U", an acceptable verification to the 24-h forecast, Fig. 3.24. The NOGAPS 24-h 925-mb forecast, Fig. 3.134, moves the shear line eastward to near 21°N, 137°E. In particular this 24-h forecast predicts stronger northeasterly winds behind the advancing shear line, 20 kt over the Luzon Strait and 15 kt over southeastern Luzon—and this 24-h forecast compares well with the earlier 48-h forecast verifying at the same time (see Fig. 3.125).

Figure 3.135 is the NOGAPS 071200Z 200-mb wind and streamline analysis, showing verification⁶⁴ of the stronger winds at the grid point near Cubi Point, 15°N, 120°E, representing the closer approach of the polar front jet. Figure 3.136 is a sounding from Cubi Point for 071200Z, although it extends only to 300 mb.

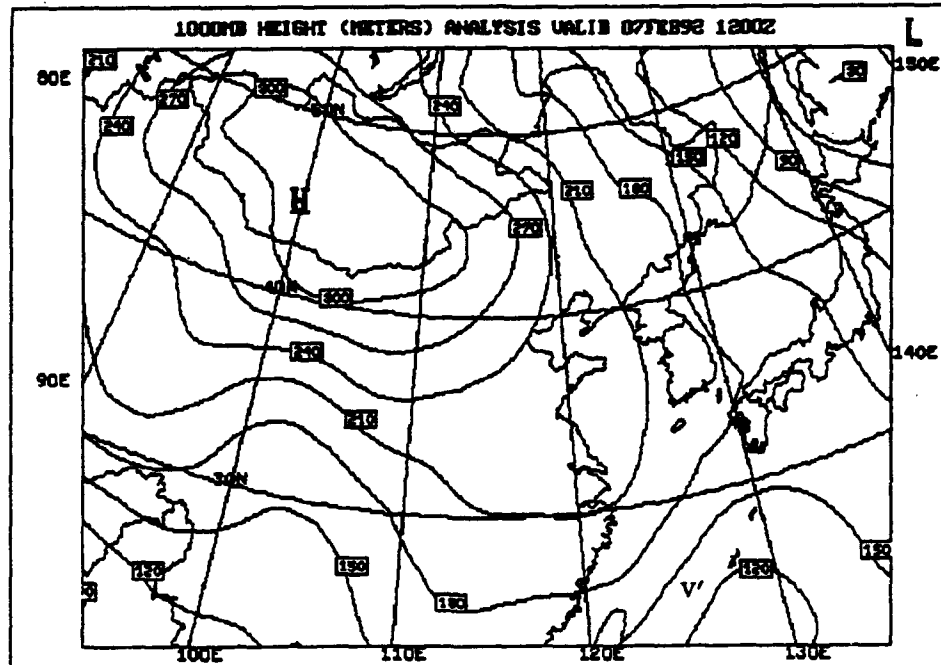


Figure 3.130: NODDS 1000-mb Height (meters) Analysis for 1200Z 7 February 1992

⁶⁴The analyst must keep in mind that the analysis will look much like the prognosis if observations are not present, or accepted.

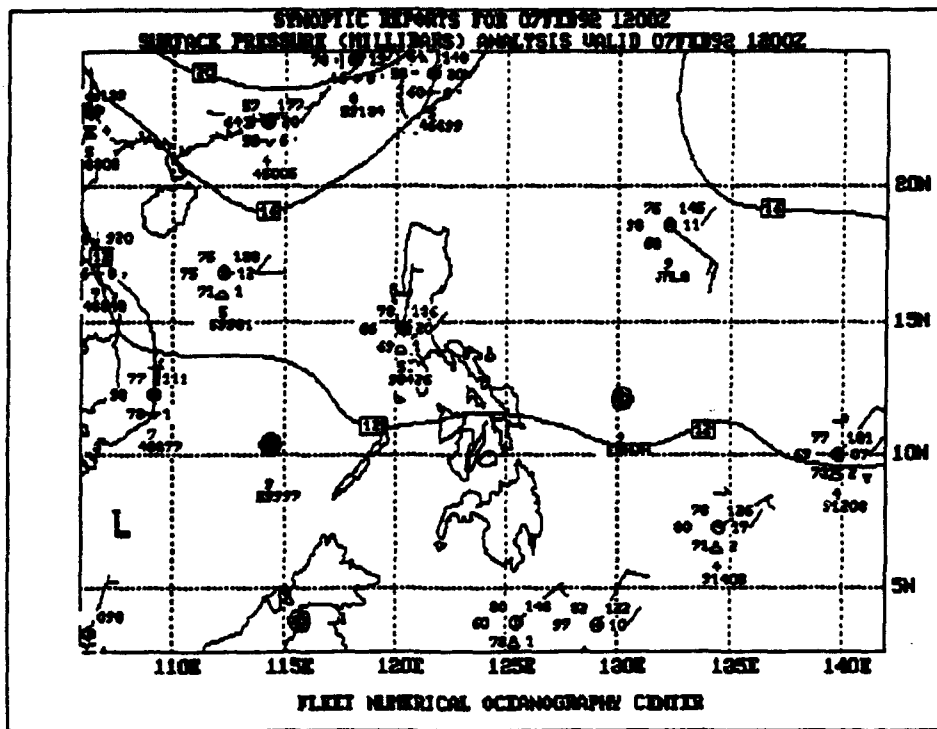


Figure 3.131: NODDS Synoptic Reports and Surface Pressure Analysis for 1200Z 7 February 1992

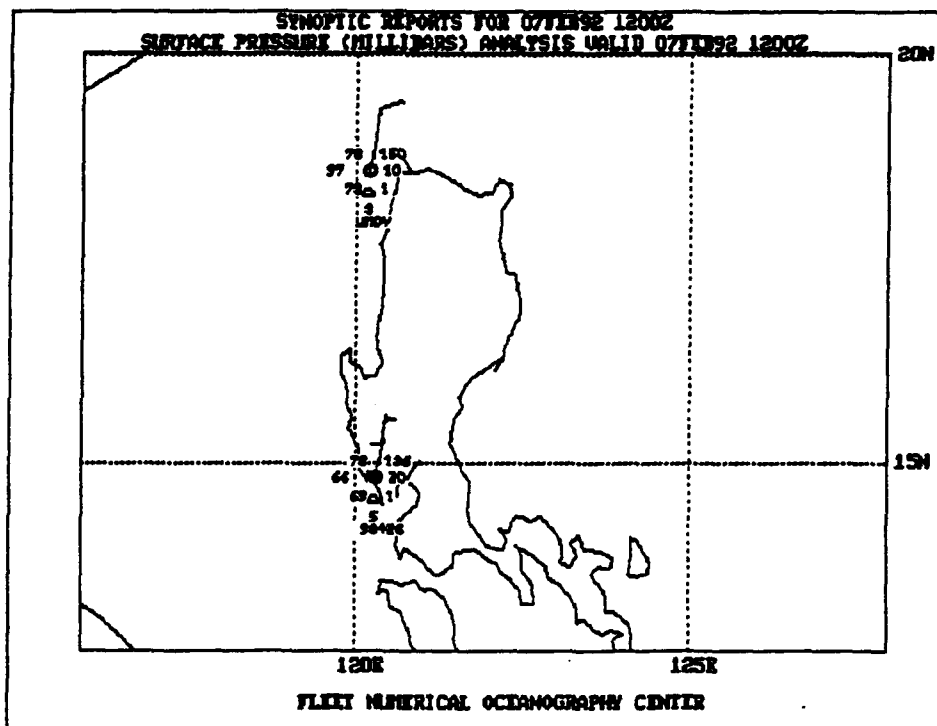


Figure 3.132: NODDS Zoomed Synoptic Reports and Surface Pressure Analysis for 1200Z 7 February 1992

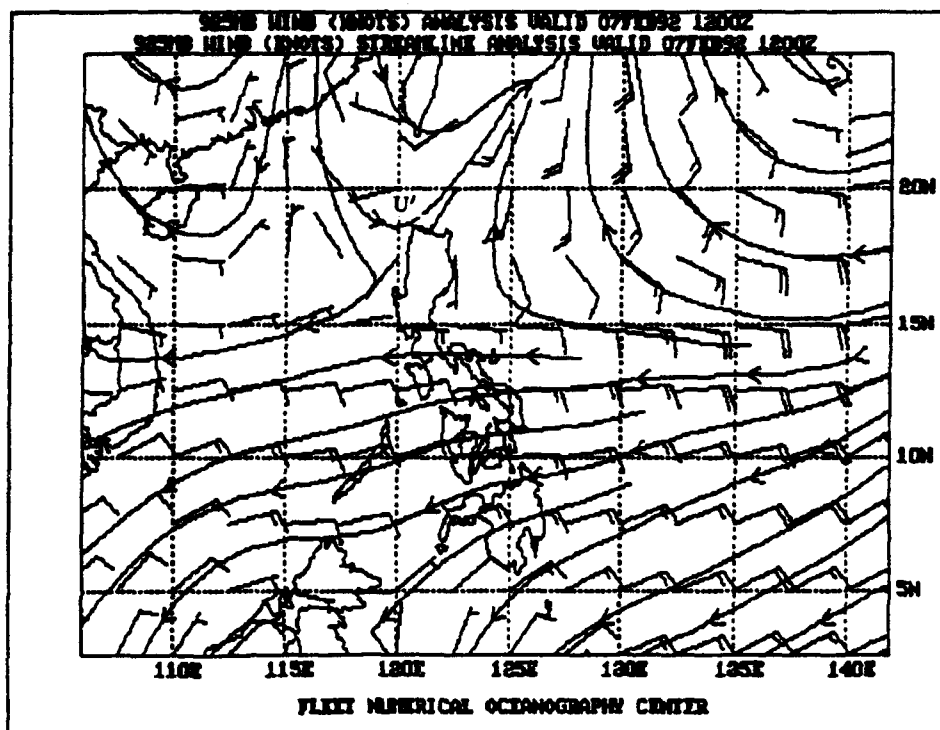


Figure 3.133: NODDS 925-mb Winds and Streamline Analysis for 1200Z 7 February 1992

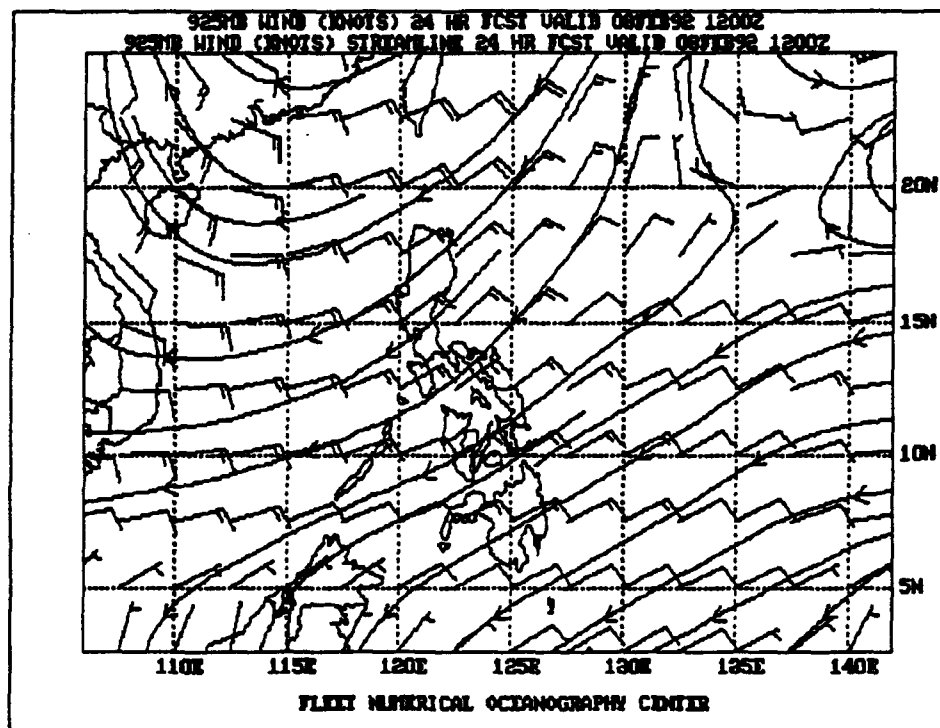


Figure 3.134: NODDS 925-mb Winds and Streamline 24-h Forecast from 1200Z 7 February 1992

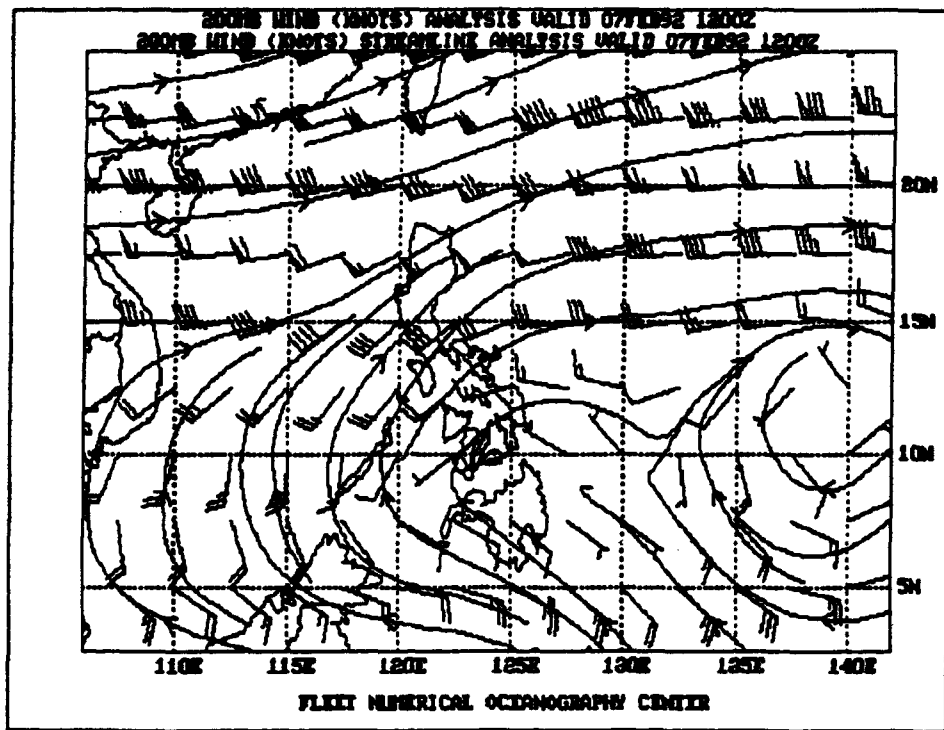


Figure 3.135: NODDS 200-mb Winds and Streamline Analysis for 1200Z 7 February 1992

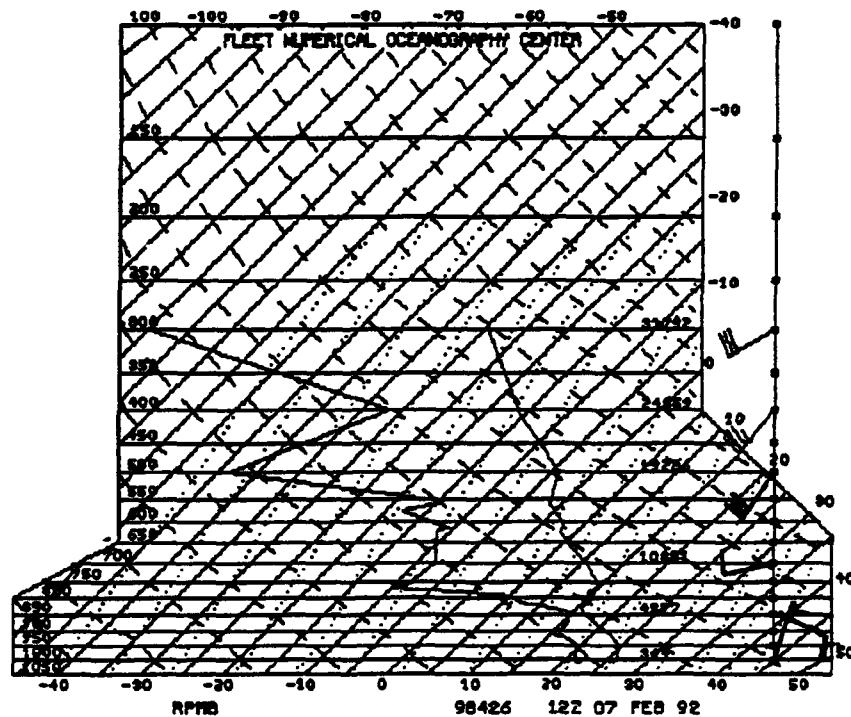


Figure 3.136: NODDS Skew T, Log P Sounding from NOCF Cubi Point (RPMB) at 1200Z 7 February 1992

Figure 3.137 shows the 071400Z NODDS DMSP IR imagery. Compare the cloud tops now covering Taiwan with those in Fig. 3.115. That is, the current IR imagery over Taiwan (Fig. 3.137) is much lighter, indicating colder, higher cloud tops than on 6 February. The imagery therefore supports the premise that Taiwan lies on the cold side of the shear line (front), and this is supported with the rain reported over eastern Taiwan on the surface chart in Fig. 3.131. The 071200Z sounding⁶⁵ from Taipei (RCTP, 58968), Fig. 3.138, gives further support showing the classic saturated stable frontal inversion from 850–700 mb.

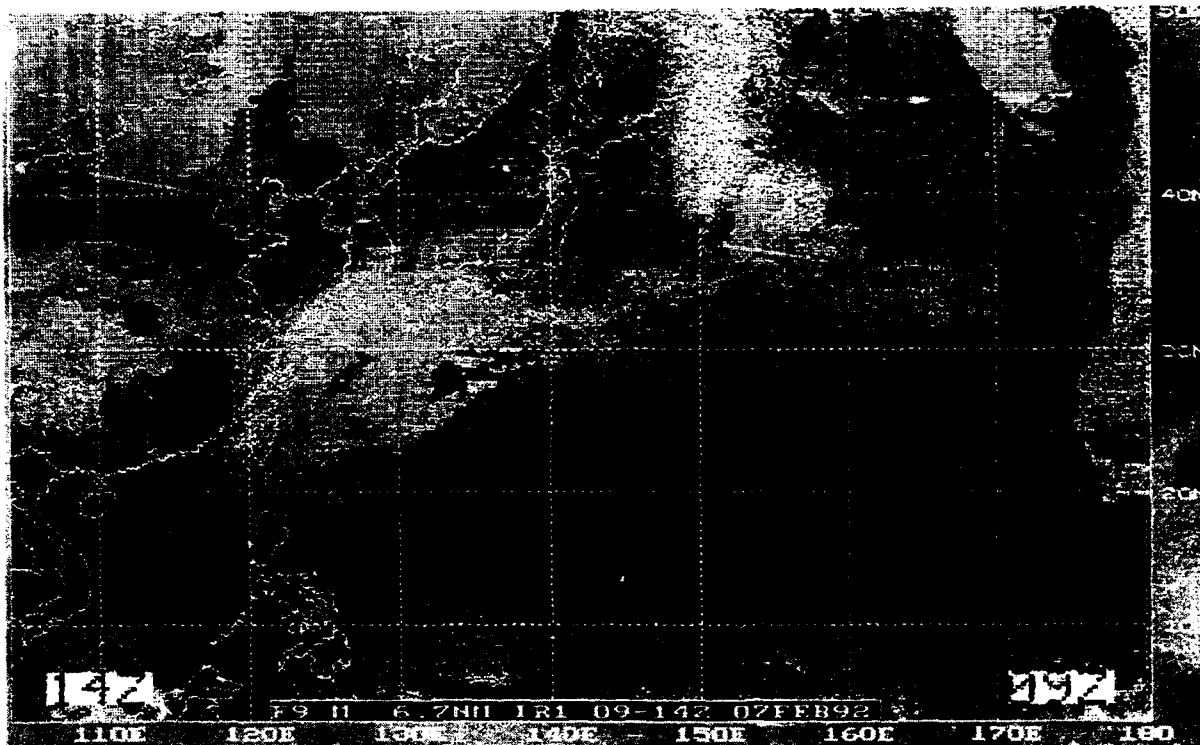


Figure 3.137: NODDS Mosaic of DMSP IR Imagery for 1400Z on 7 February 1992

⁶⁵It appears that data only for the mandatory levels was received on the Taipei sounding.

920207/1200 58968

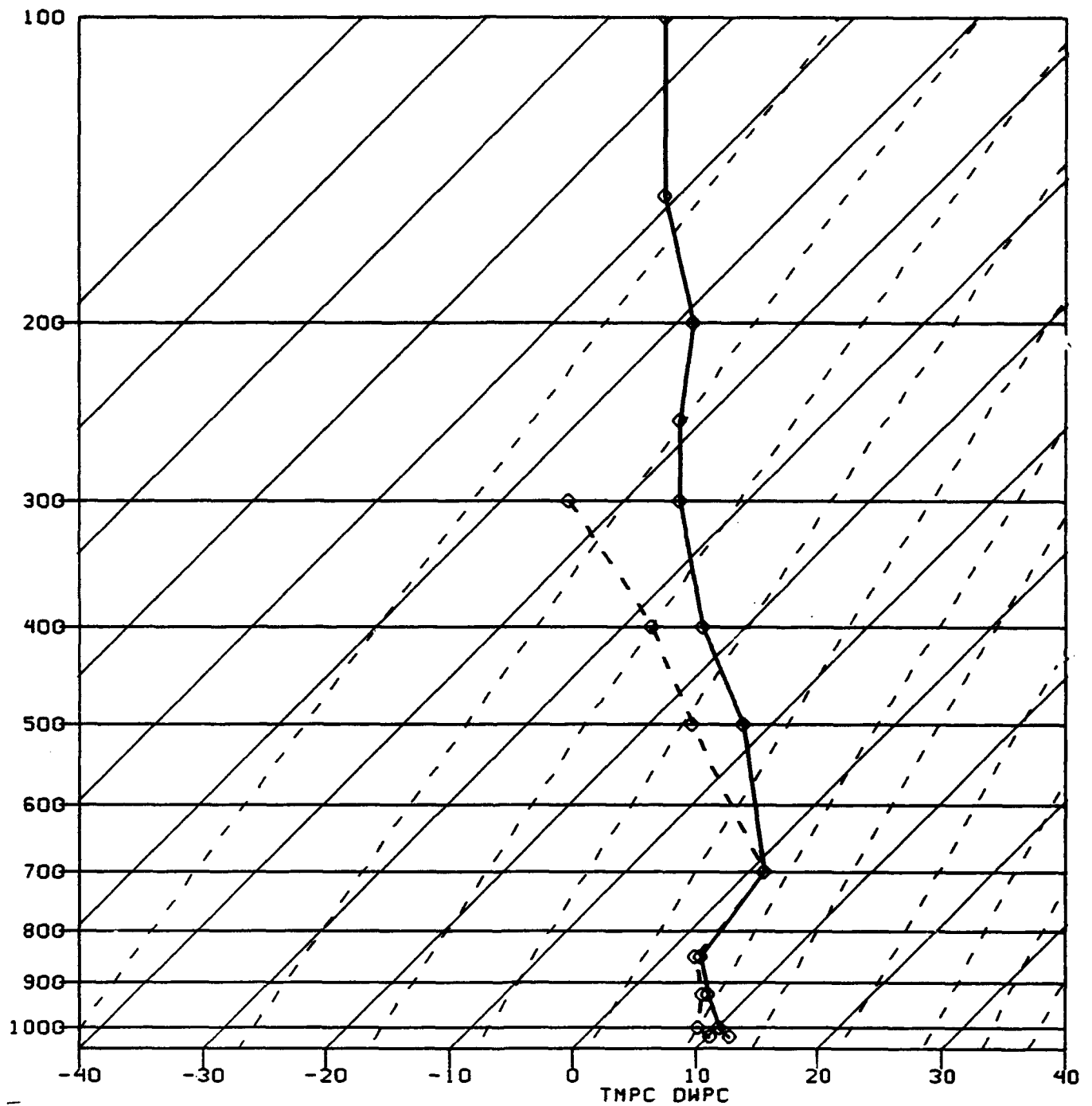


Figure 3.138: Skew T, Log P Sounding from Taipei (RCTP, 58968) at 1200Z 7 February 1992 (from the Naval Postgraduate School)

8 February 1992

On the last day of the case study, Fig. 3.139 shows that the NOGAPS 48-h 300-mb contour forecast, Fig. 3.118, was quite good, i.e., the trough position over the Sea of Japan verified very nicely. Furthermore, the satellite imagery, Fig. 3.145, reveals heavy convection and a comma-shaped cloud configuration just east of Japan. The 1000-mb contour analysis Fig. 3.140 shows a stronger gradient over southern Japan behind the surface frontal position (off the figure to the east), while ships are reporting strong northeasterly winds on the NODDS surface analyses, ship "JFZI" with 30 kt near 23°N, 131°E on Fig. 3.141 and ship "DIDT" with 25 kt in the Luzon Strait on Fig. 3.142.

The NOGAPS 081200Z 925-mb wind and streamline analysis, Fig. 3.143, shows the stronger northeasterly winds over the Luzon Strait, as forecast by NOGAPS; however, the two ships, noted above, reported higher winds. Nevertheless, the NOGAPS forecast trend of increasing lower-level wind strength was correct. Furthermore, Fig. 3.144, the FNOC significant wave height analysis at 071200Z shows higher seas, >9 feet in the Luzon Strait and >12 feet just east of Taiwan.

The 080100Z NODDS mosaic of DMSP infrared satellite imagery, with its resolution of 6.7 nm, Fig. 3.145, shows a broken cloud line striking the northeast coast of Luzon. However, examination of the geostationary satellite imagery (not shown) confirmed that the front extended southwestward as a shear line through Point "T" striking eastern Luzon near Baler (98333).

Finally, while it is not a part of this last case study, Fig. 3.146, a NODDS DMSP IR image, is presented to demonstrate that NODDS satellite imagery can show convection over northern Luzon associated with a shear line or front. This image was received during the transition season in May of 1992. Figure 3.147 is the zoomed NODDS synoptic reports chart showing thunderstorms occurring along the northwest coast of Luzon at the time of the satellite image in Fig. 3.146.

During the transition season of 1992, the author observed quasi-stationary fronts bringing copious amounts of rain to Hong Kong, but the front seldom penetrated south into Luzon. Most often it remained in an east-west orientation over the Luzon Strait.

While this last case study (6-8 February 1992) witnessed a cold surge moving rapidly and primarily eastward toward Japan, an informal conversation with Johnny Chan (1992, personal communication) indicated that this type of surge is more common during the early and late winter season. During the mid-season, e.g., in February, anticyclones frequently become quasi-stationary over mainland China, and cold surges propagate southward toward Luzon.

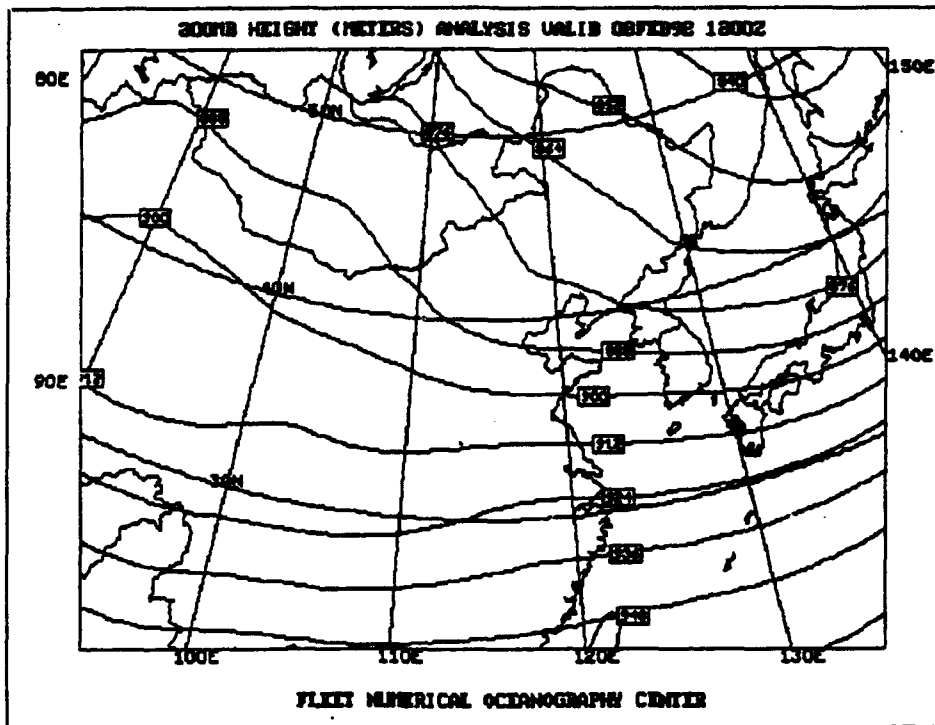


Figure 3.139: NODDS 300-mb Height (meters) Analysis for 1200Z 8 February 1992

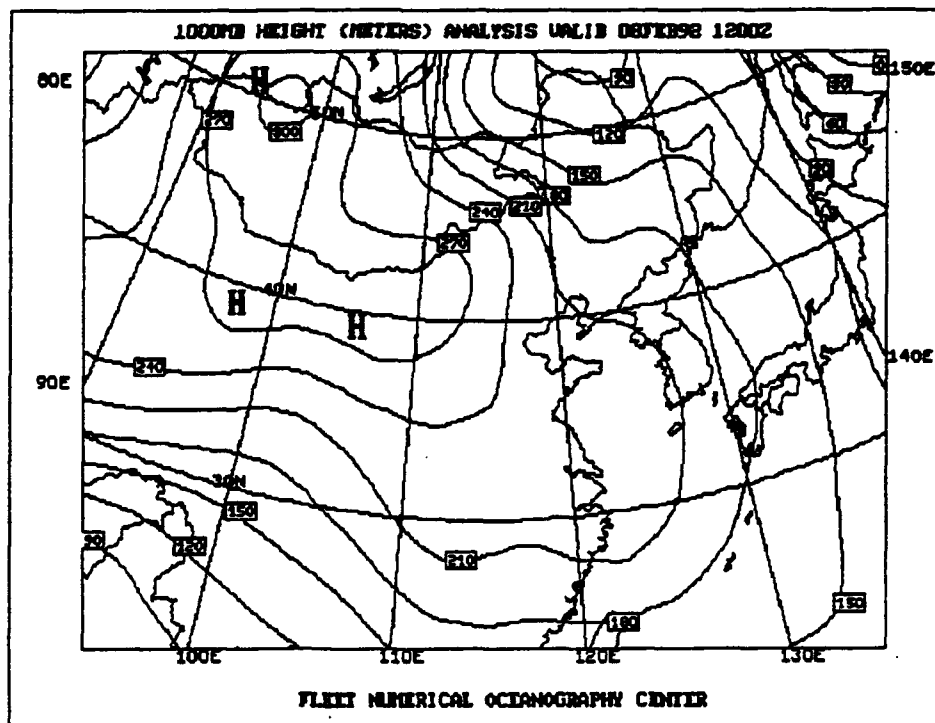


Figure 3.140: NODDS 1000-mb Height (meters) Analysis for 1200Z 8 February 1992

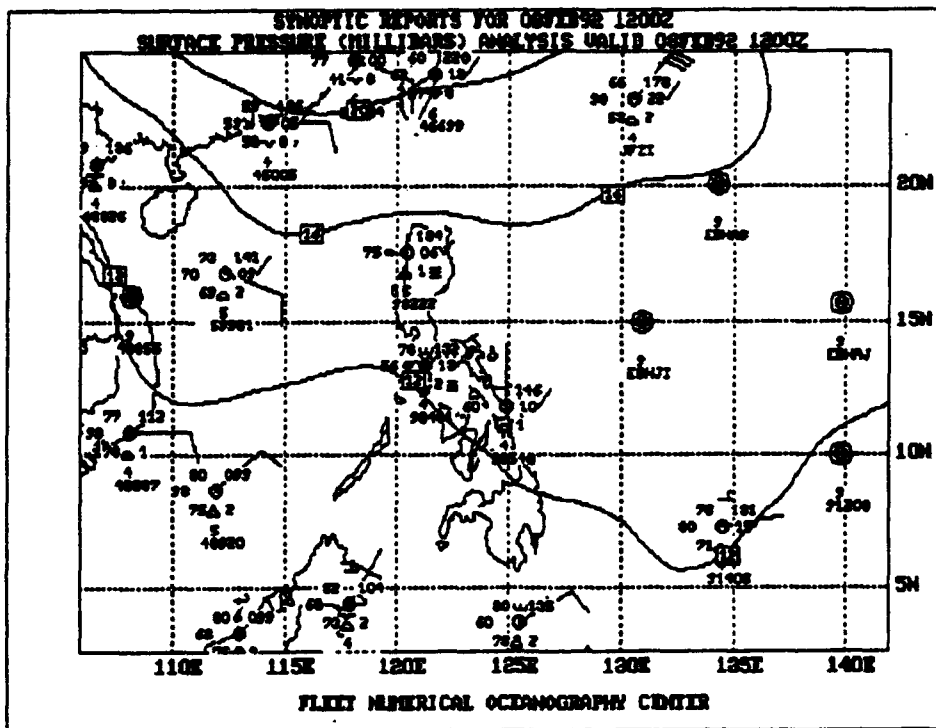


Figure 3.141: NODDS Synoptic Reports and Surface Pressure Analysis for 1200Z 8 February 1992

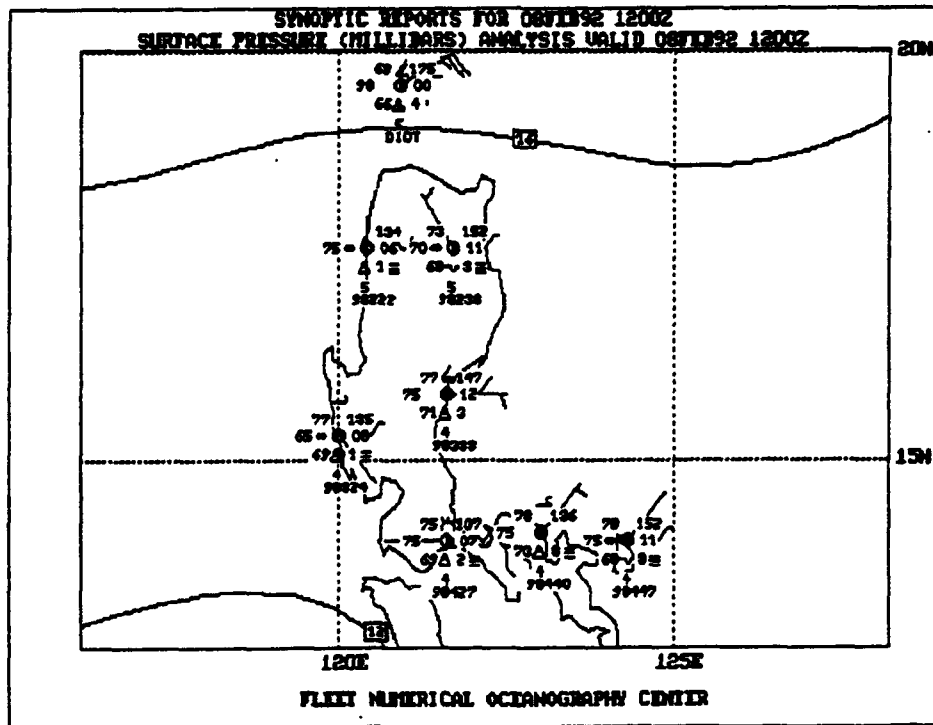


Figure 3.142: NODDS Zoomed Synoptic Reports and Surface Pressure Analysis for 1200Z 8 February 1992

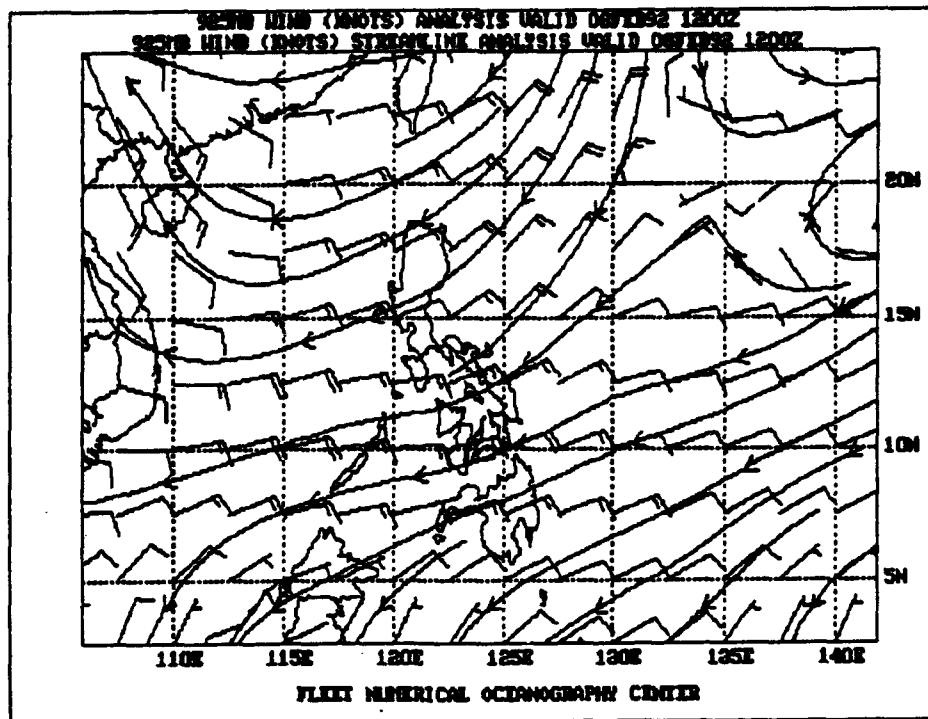


Figure 3.143: NODDS 925-mb Winds and Streamline Analysis for 1200Z 8 February 1992

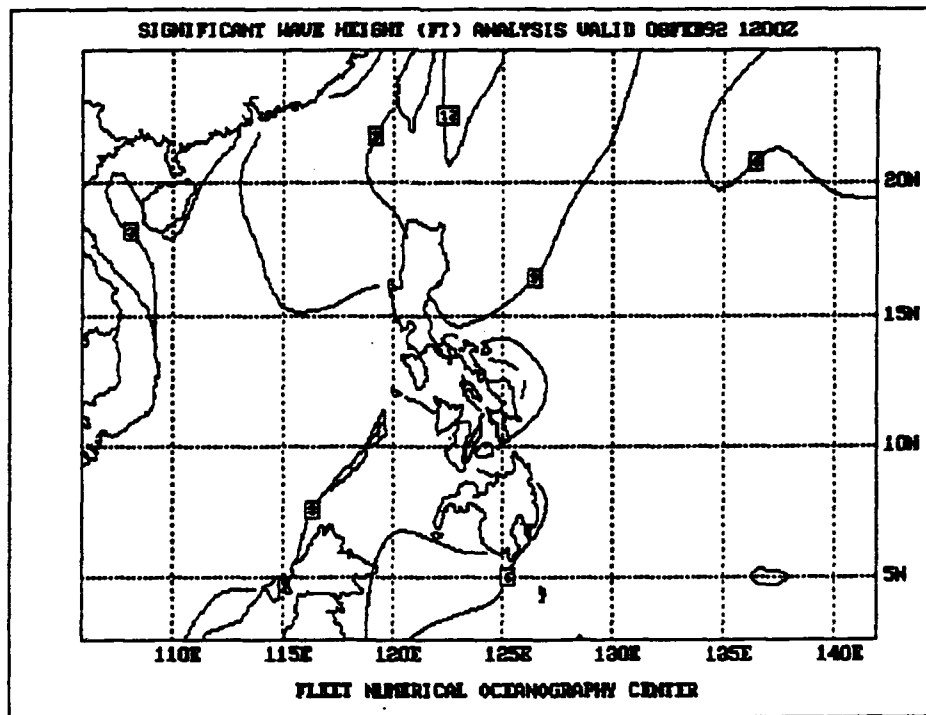


Figure 3.144: NODDS Significant Wave Height Analysis for 1200Z 8 February 1992

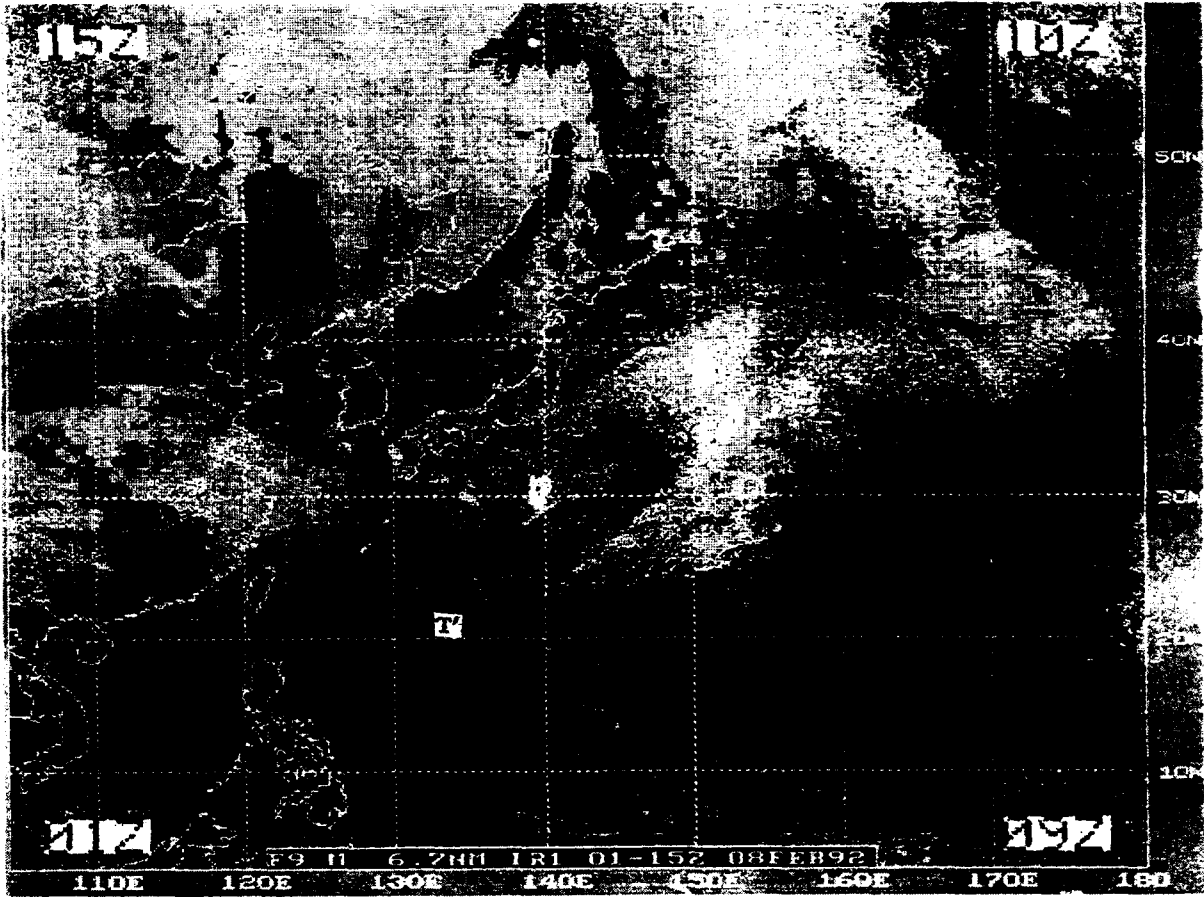


Figure 3.145: NODDS Mosaic of DMSP IR Imagery for 0100Z on 8 February 1992

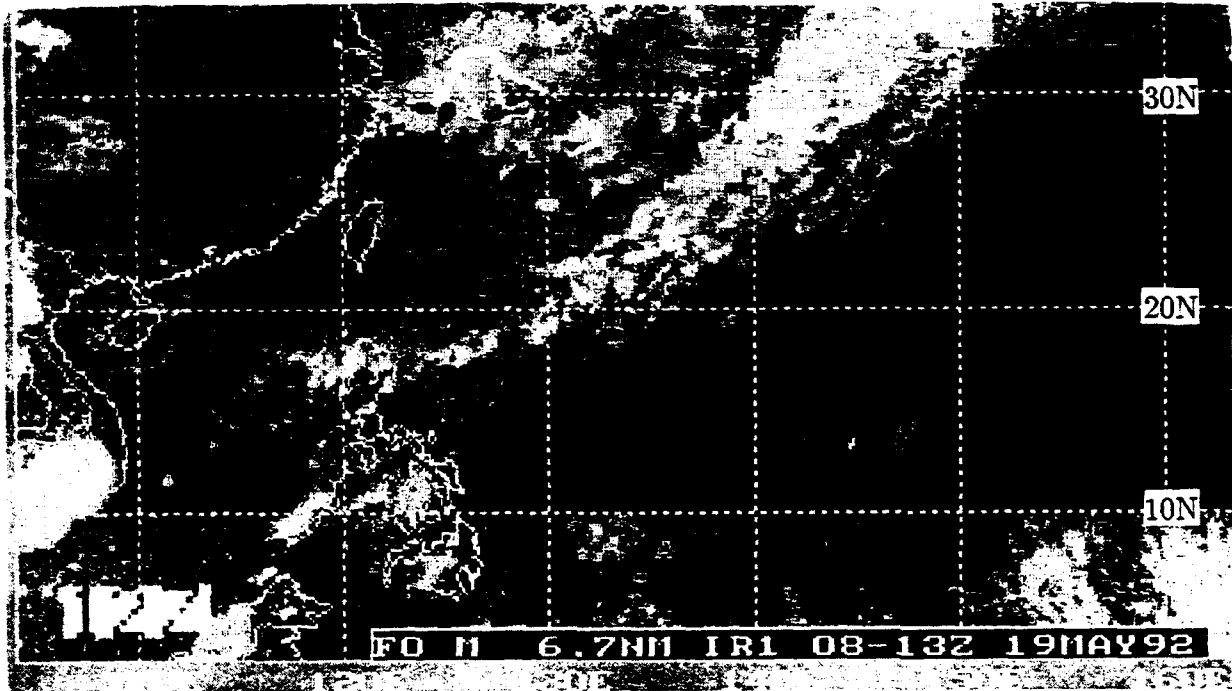


Figure 3.146: NODDS Mosaic of DMSP IR Imagery for 1200Z on 19 May 1992

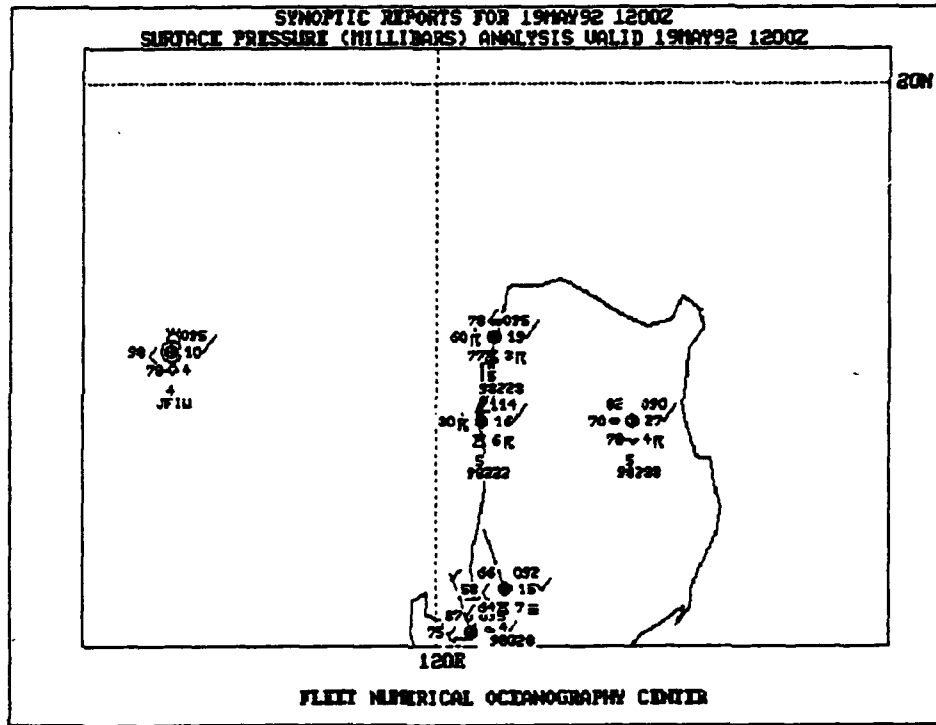


Figure 3.147: NODDS Zoomed Synoptic Reports and Surface Pressure Analysis for 1200Z 19 May 1992

3.5.6 Lessons Learned while preparing Case Studies

The following impressions were noted by the author during 2 years of nearly continuous monitoring of the tropical analyses and prognoses in the vicinity of the Philippine Islands by FNOC's NOGAPS model. Comments are also made concerning the use of NODDS as a means of receiving the products of the Navy's NOGAPS 3.3 model.

- The Navy's atmospheric analysis and prediction model in the tropics (FNOC's NOGAPS 3.3 operational since January 1992) has continued to improve, since the introduction of the first NOGAPS model in 1982, and its "upgrading" to a spectral model in 1988.
- The NODDS delivery system offers a wide variety of atmospheric, oceanographic, and acoustic products, including the transmission of mosaic DMSP visible and IR imagery since activation of NODDS 3.0 in October 1991.
- Of particular interest to tropical analysts:
 1. The surface pressure analysis and synoptic reports, with the zoom capability, provide excellent graphics for apprising synoptic-scale tropical sea-level pressure in the vicinity of the Philippine Islands.
 2. The 925-mb wind barb and streamline analyses and prognoses provide acceptable gradient level coverage. (The NOGAPS model is not expected to adequately describe mesoscale features such as the wind magnitudes at the radius of maximum winds—accomplished by no operational model as yet, to the knowledge of the author.)
 3. While the automated insertion of bogus soundings (from sea level to 400 mb) in the vicinity of tropical cyclones generally locates the 925-mb vortex center at the JTWC warning position, there are instances when only a trough—vice a low center—is analyzed by NOGAPS, at the position of the TC warning. Obviously, in these instances, the bogus soundings did not "get into" the analyses.
 4. Unlike the 925-mb streamlines, the NOGAPS 200-mb analysis in the vicinity of tropical cyclones and typhoons is unsatisfactory to the tropical analysis—necessitating that hand analysis be accomplished, such as that performed twice daily at JTWC. That is, upper-level (200-mb) anticyclonic outflow above a typhoon was never observed by the author during the two-year study. Even assuming that an intense typhoon might dictate cyclonic rotation still existing at 200 mb, that circulation was missing. Additionally, cells in the TUTT were often missing. The NOGAPS analysis typically placed only one large (low-height) cell within the TUTT, while hand analysis, using the geostationary cloud-vector winds and AIREPS, often identified multiple low cells in the same TUTT.
 5. While one case study confirmed the ability of the NOGAPS model to forecast the formation of a tropical cyclone circulation—where only a trough existed

at the time of the analysis—, there are instances when the initial (or early) NOGAPS forecast of movement of a tropical cyclone is very erratic. There are also many cases in which NOGAPS predicts the development of tropical cyclones that in fact do not develop.

6. The case studies of Typhoons Eli and Bobbie demonstrated the capability of JTWC to accurately forecast tropical cyclone movement, for both a “straight-mover” and a “recurver.” However, as presented in the most current Annual Tropical Cyclone Report, and should be known by tropical forecasters, the unpredictable movement of “loopers”, etc. produced the following mean tropical cyclone forecast errors in the Northwest Pacific during 1991: 96 nm (24-h), 185 nm (48-h), and 287 nm (72-h) (JTWC 1992).
 7. Forecasters should anticipate erratic movement of tropical cyclones toward the northeast when (1) the monsoon trough becomes oriented on a NE-SW anomalous axis (Lander 1990, personal communication) or (2) when mid-tropospheric steering is dominated by a surge in the southwest monsoon (Guard 1985).
- In the last presented case study, the NOGAPS model was shown to have the capability of forecasting a northeastern monsoon cold surge. That is, the NOGAPS model forecasted a surge emanating from near Lake Baikal in the Russian Republic, resulting in shear lines with stronger northeasterly surface winds over the Luzon Strait and the island of Luzon, 48 hours later. However, a more complete study of a large sample should be performed.
 - Regarding the use of NODDS 3.0:
 1. NODDS users must take care to specify wave and swell heights in the NODDS station model menu. Otherwise, the observations of sea height, sea surface temperature, etc., although received in the “down-loaded” message, will not be plotted.
 2. Until subsequent NODDS upgrades are activated, users can only down-load the current 0000Z or 1200Z run, i.e., the NODDS delivery system is designed to provide operational analysis and prognosis to DoD users. It is not designed as an archival source, unless the user is prepared to down-load runs during the night—such as performed by the author.
 3. The NODDS graphics of the JTWC tropical cyclone warnings were both informative for real time use and provided excellent “no effort” plots for use in the typhoon case studies.
 4. While the NODDS DMSP visible and IR imagery is available—although delayed and in a resolution of only 6.7 nm—, the study showed that NODDS satellite imagery was useful in depicting areas of convection associated with tropical cyclones and shear lines near the Philippine Islands.

4. GEOLOGICAL STRUCTURE & PHYSICAL OCEANOGRAPHY

4.1 Geological Structure

Introduction. The Philippine Islands are situated along the western margin of the tropical North Pacific Ocean, between 6° and 18° North Latitude (see Fig. 4.1). This island chain is one of several island arcs within the western North Pacific Ocean and around its perimeter.

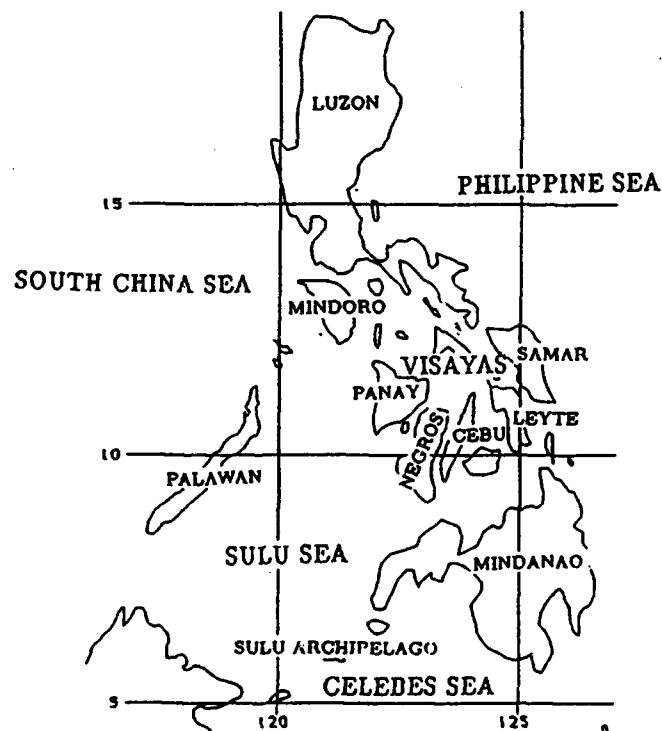


Figure 4.1: Map of the Philippines.

Typically, these island arcs are associated with significant volcanic activity in the mountains along the arc as well as under the sea itself, and with deep ocean trenches along the adjacent ocean (see Fig. 4.2). The Philippine arc displays these typical characteristics. In addition, there are marginal seas that separate the Philippine arc from the Asian continent to the west (see Fig. 4.3).

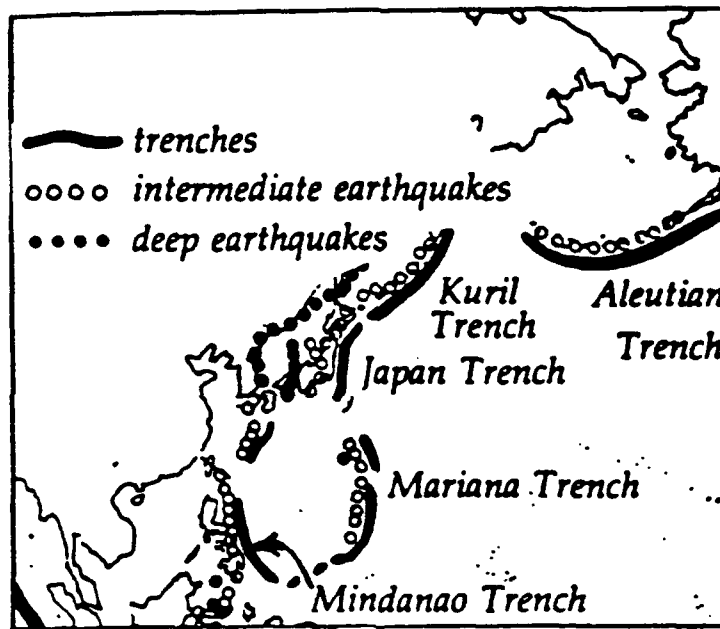


Figure 4.2: Island Arcs showing Earthquake Foci (adapted from Ingmanson and Wallace (1973)).

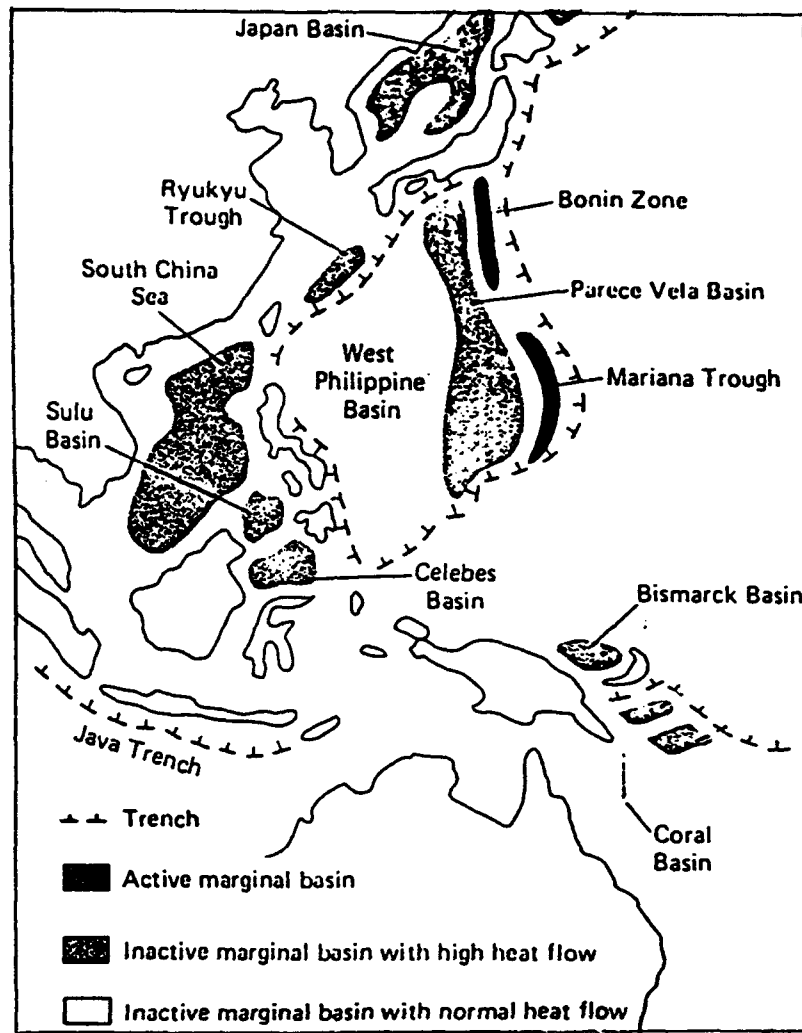


Figure 4.3: Distribution of Marginal Basins in the Western Pacific (adapted from Eicher and McAlester (1980)).

This arc/trench/marginal sea structure has developed in response to geological forces operating within the earth's crust and upper mantle underneath this region; those forces appear to have influenced this region throughout its geological history, continuing into the present. Geologists believe this region has been subject to an unusually large number of such forces.

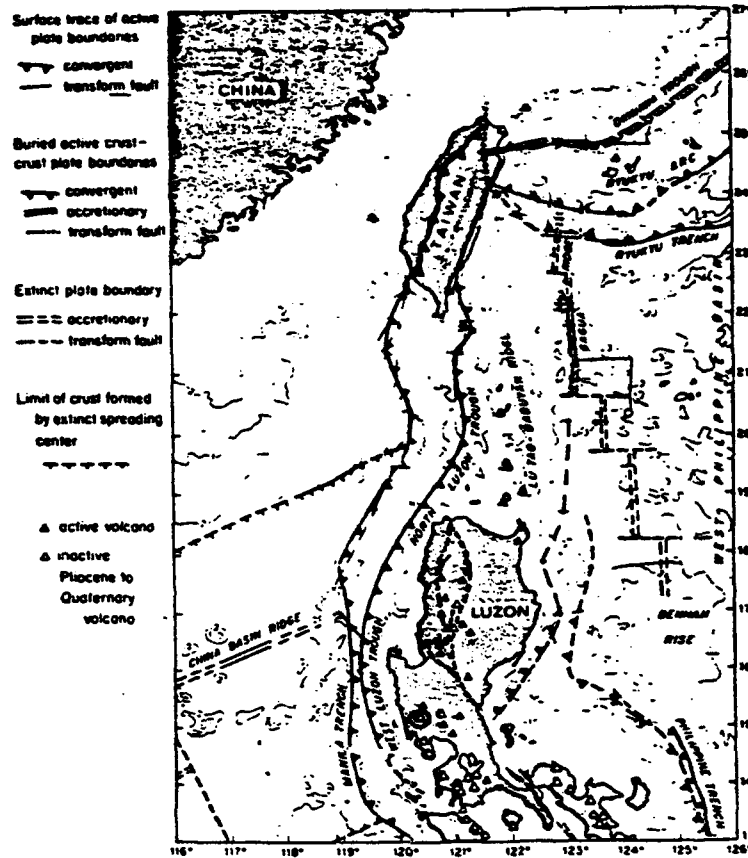


Figure 4.4: Active and Extinct Plate Boundaries in the Taiwan-Luzon Region. The Mount Pinatubo Volcano which became active in June 1991 is circled (adapted from Bowin et al. (1978)).

The earth's crust appears to be made up of numerous large plates on which the present continents and oceans lie (see Dewey 1972, pp 34-35). These plates move in response to forces within the earth's mantle, which lies beneath the earth's outer crustal layer; this motion is often described as "Continental Drift".

Mid-ocean ridges or rises are the surface (or subsurface) features above the upward part of the convective current; subduction zones mark the descending portion of the convection current at the plate boundary. The marginal seas west of the Philippines are on continental crustal plates (see Dewey 1972, p. 40). Subduction zones are associated with volcanoes, deep ocean trenches and earthquakes. The volcanoes observed in the Philippine Islands originate from the subduction zone activity (see Dewey 1972, p.40). The large numbers of active volcanoes on Luzon, as well as inactive volcanic mountains, is shown in Fig. 4.4. The relationship between the convergent plate boundaries, and the Philippine and Manila Trenches is illustrated here as well.

Earthquake activity located off the coasts of northern Luzon and extending across Luzon Strait to Taiwan, for the years 1904-1974, is shown in Fig. 4.5.

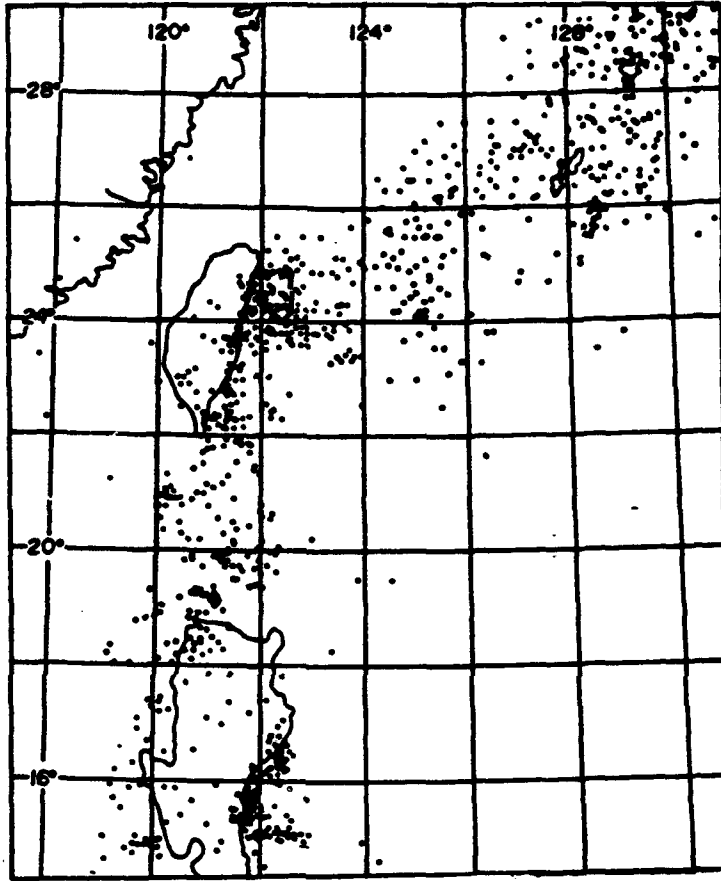


Figure 4.5: Map showing the Epicenters of the Earthquakes occurring between 1904 and 1974 in the Taiwan Region including Parts of the Ryukyus and the Philippines (adapted from Chingchang et al. (1985)).

Shallow-focal depth earthquakes dominate in the region seaward from the Philippine fault zone; this zone is shown as the solid line along the eastern portion of the major Philippine Islands in Fig. 4.6. On the marginal-sea side of the fault zone, deep-focus earthquakes appear; some shallow-focus earthquakes have occurred in this region also.

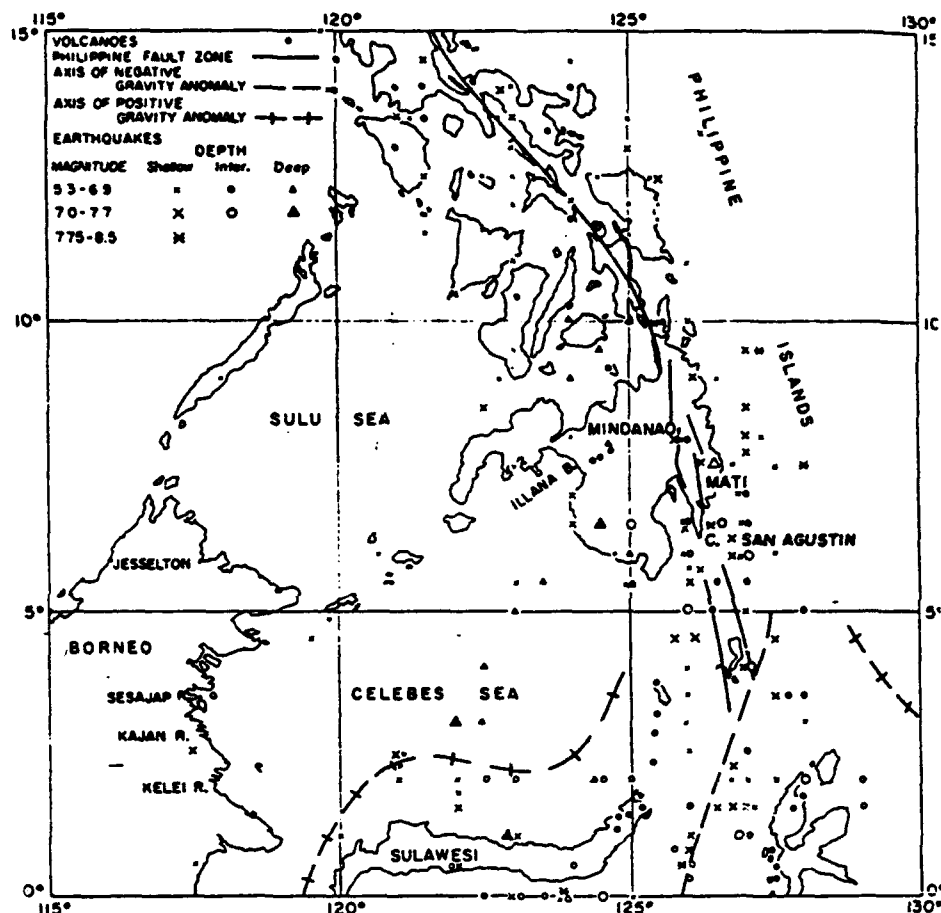


Figure 4.6: Location of Earthquakes, Volcanoes, Gravity Anomalies and Philippine Fault Zone (adapted from Krause (1966)).

All of these influences have given the Philippine Islands region a complex configuration of ocean and marginal sea basins, interspersed with many island chains; see the bathymetric chart of this region (Fig. 4.7).

The complexity of this bathymetry and the many island chain configurations influence the physical ocean characteristics within the marginal seas and the adjacent ocean regions.

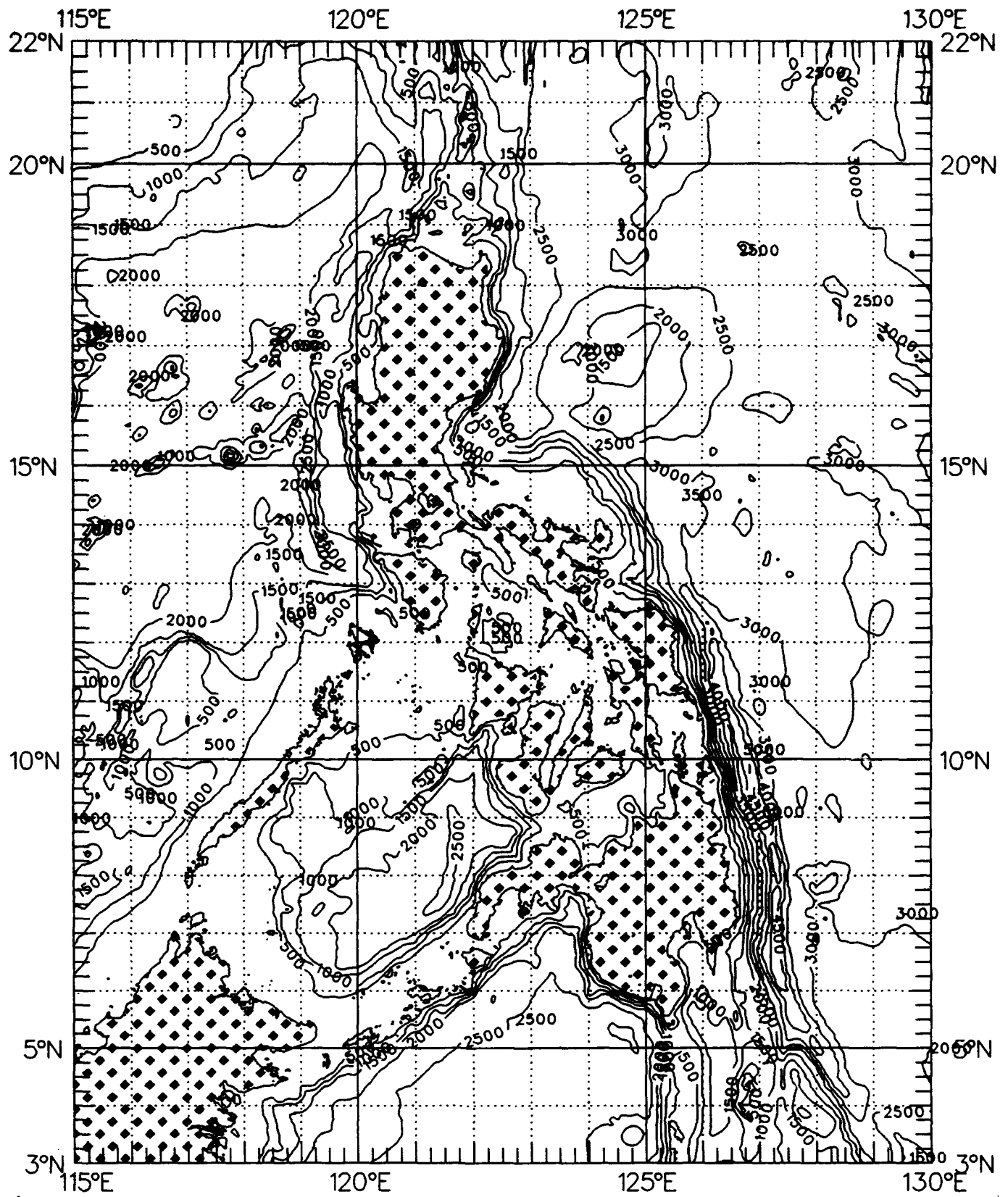


Figure 4.7: Bathymetry surrounding the Philippine Islands with depths in fathoms (The Naval Oceanographic Office).

Tides and ocean currents are constrained by narrow island passages and by the island chains that surround the various marginal seas. Restrictions to water exchange between the open ocean and the marginal seas greatly influence the temperatures and salinities observed along the Philippine Islands coastlines. These restrictions affect the ocean response to influences such as long- and short-wave radiation reaching the water surface, or the advection by ocean currents of temperature and salinity differences into a marginal sea.

Thus the oceanography along the Philippine Islands coastlines and within adjacent marginal seas is quite complicated. It is helpful to focus this discussion on several different regions in turn, to better describe the resulting oceanography.

The following regions will be treated: (1) the western portion of the Philippine Sea (the open ocean region to the east of the Philippine Islands); (2) the northern portion of the South China Sea (west of the major Philippine Islands, separating them from the Vietnam and China coasts of the Asian mainland); (3) the Sulu Sea (which separates the southern Philippine Islands from Palawan Island and the South China Sea; and (4) one of the two major straits which are to the north and south of the Philippines chain, separating the Philippine Sea from the marginal seas, and through which much of the water exchange occurs: Luzon Strait and Bashi Channel (on the north between Luzon and Taiwan); Balabac and Sibutu Straits (on the south, separating Palawan and the Sulu Archipelago from North Borneo) are regions with few, if any, published oceanography studies.

4.2 Ocean Parameters

4.2.1 Introduction

The following is a description of ocean factors which can affect weather occurring in the Philippines and the adjacent ocean areas.

1. Some ocean factors directly affect the overlying atmosphere:
 - (a) Sea surface temperature provides a modifying influence on the atmosphere above, so that air temperatures that differ initially from those on the ocean surface beneath are quickly modified, through radiative and sensible heat exchange across the air/sea boundary, toward the more slowly-changing temperatures of the ocean water surface. In the tropical latitudes of the Philippines, the sea surface remains warm, varying relatively little throughout the year.
 - (b) Moisture is also provided to the air by the sea surface, so the warm air can become saturated with substantial amounts of water vapor in layers adjacent to the surface.
2. Ocean factors that contribute indirectly to the atmospheric weather above include:
 - (a) Ocean Currents which act to advect ocean water into a region; this advected water tends to retain the temperature and salinity of the source region, although these may be modified somewhat as the water moves along into another region.
 - (b) The Vertical Distribution of Temperature and Salinity in the near-surface ocean layers affect the exchange of heat across the ocean surface; that heat exchange, in turn, helps determine the convective character and vertical stability of the overlying atmosphere.
3. Several ocean factors may influence naval operations in an area:
 - (a) Nearshore Bathymetry affects tides, tidal currents, acoustic propagation (reflection, absorption and scattering of underwater sound), and determines shoreline accessibility.
 - (b) Coastal Type and Configuration can also limit access for particular types of naval vessels and operations.
 - (c) Waves.
 - (d) Tides.
 - (e) Internal Waves may affect both surface and subsurface operations.
 - (f) Bottom Sediment Type and Character influence the performance of submarine detection systems.
 - (g) Underwater Visibility affects nearshore diving and photography operations.

4.2.2 Ocean Parameters by Region

A. Western Philippine Sea (open ocean to the east of the Philippine Islands)

This region is more subject to influences from remote ocean areas than the other regions to be discussed later.

1. Ocean Circulation Patterns here are determined by forces acting on the broad North Pacific Ocean. As the North Pacific Equatorial Current moves westward, it encounters the land barrier of the Philippine Islands. Part of the water carried by this current is directed southward past Mindanao Island to make up the Mindanao Current; this Current carries a significant portion of the North Pacific Equatorial Current water along the Philippine Islands between 10° and 5° North Latitude before it turns eastward; there, it merges with other water to form the narrow North Equatorial Counter-Current that returns eastward, centered at about 5°N (see Fig. 4.8; & Fig. 4.9).

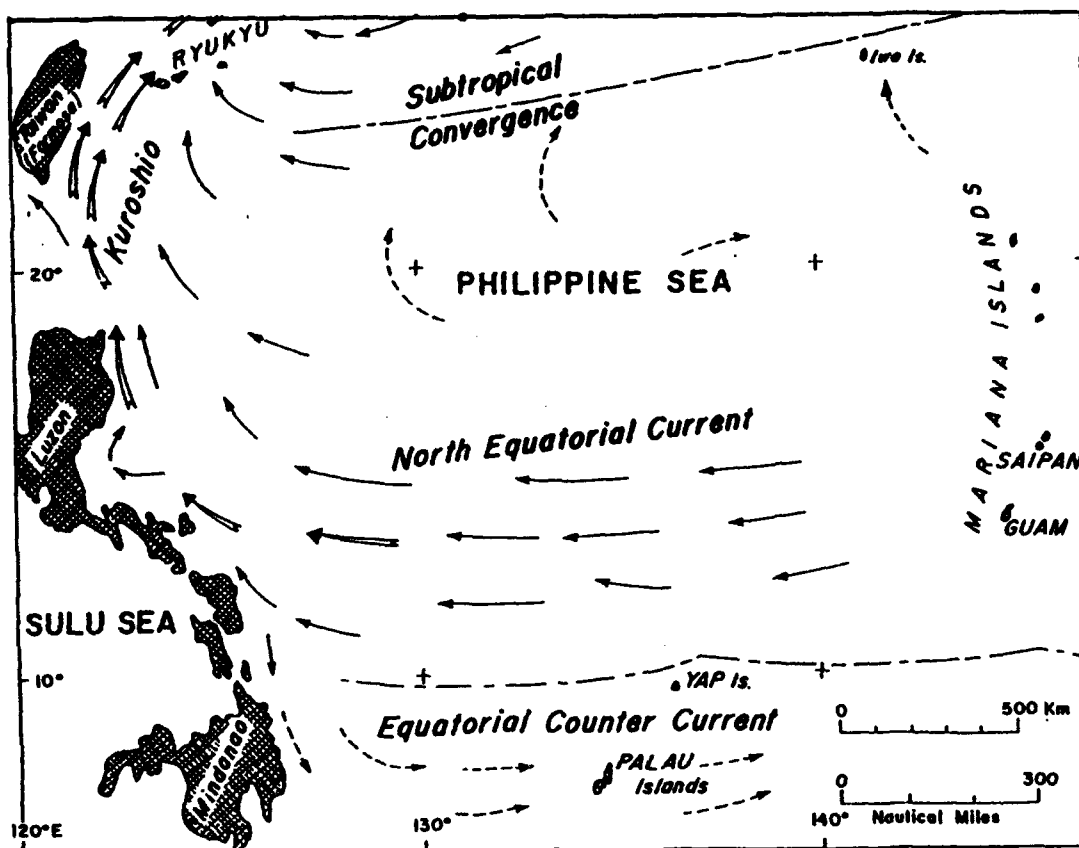


Figure 4.8: Major Currents in the Philippine Sea and Waters South of Japan (adapted from Uda (1966)).

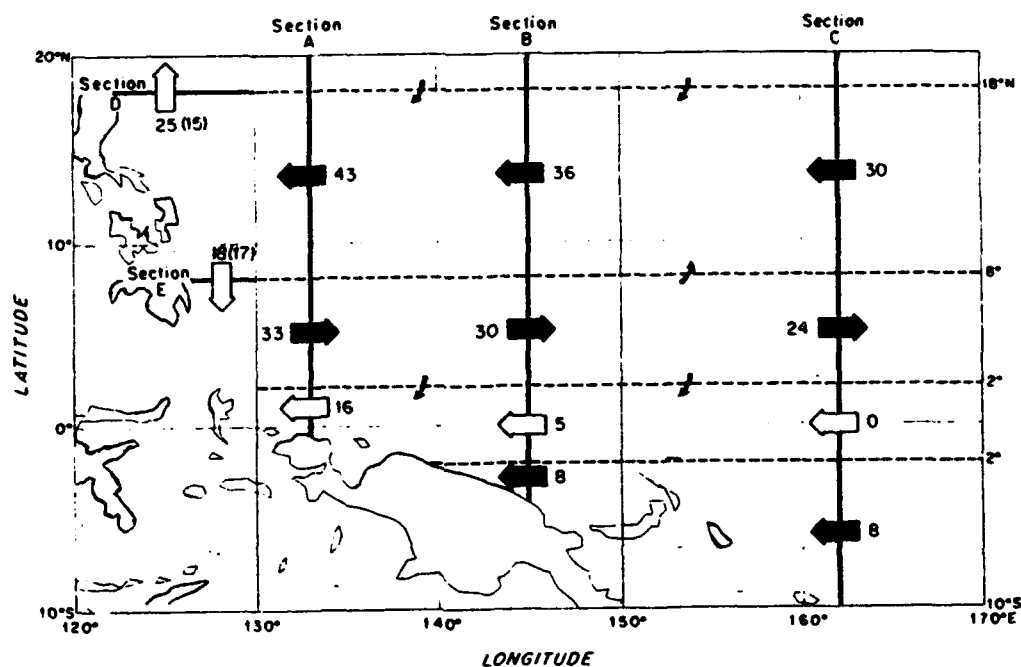


Figure 4.9: A Circulation Diagram for the Water Warmer than 12°C deduced from Annual Mean Hydrographic Sections and Water Budgets (transports in Sv, $10^6 \text{m}^3 \text{sec}^{-1}$). Bold typeface arrows represent directly calculated transports. Open-faced arrows are transport values inferred from water mass budgets. Shown in parentheses are the transports computed directly for these sections with the available data (adapted from Toole et al. (1988)).

A somewhat larger amount of the North Pacific Equatorial Current water is directed northward past Luzon, when it reaches the Philippine Islands, to make up part of the Kuroshio Current, the major western boundary current of the North Pacific Ocean. The Kuroshio becomes fully developed further to the north, along the Japanese Islands.

There are seasonal variations in the location and strength of the different currents, especially in the boundary between the opposing North Pacific Equatorial Current and Counter-currents. See the variation between summer and winter current patterns from 7° to 10°N to the east of Mindanao (see Figs. 4.10a & 4.10b). The boundary becomes confused and widens during summer; also, the Counter-current receives a large volume of water from the southern hemisphere as it dominates the weaker Mindanao Current outflow.

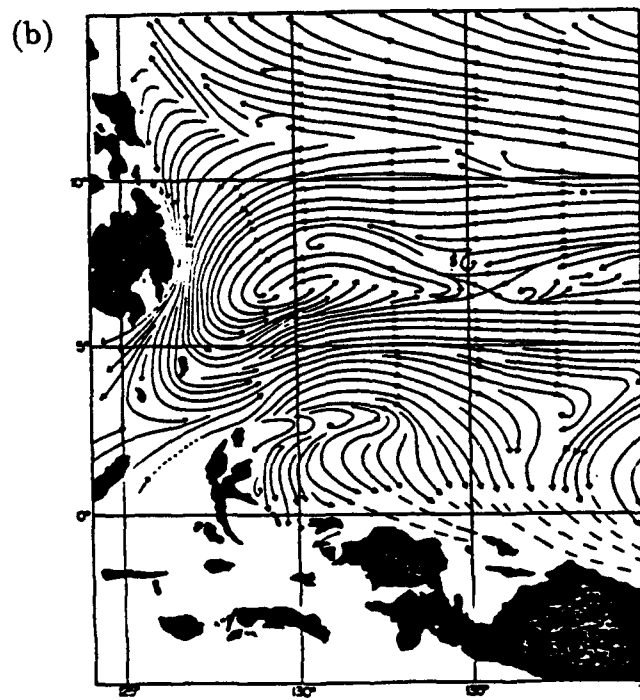
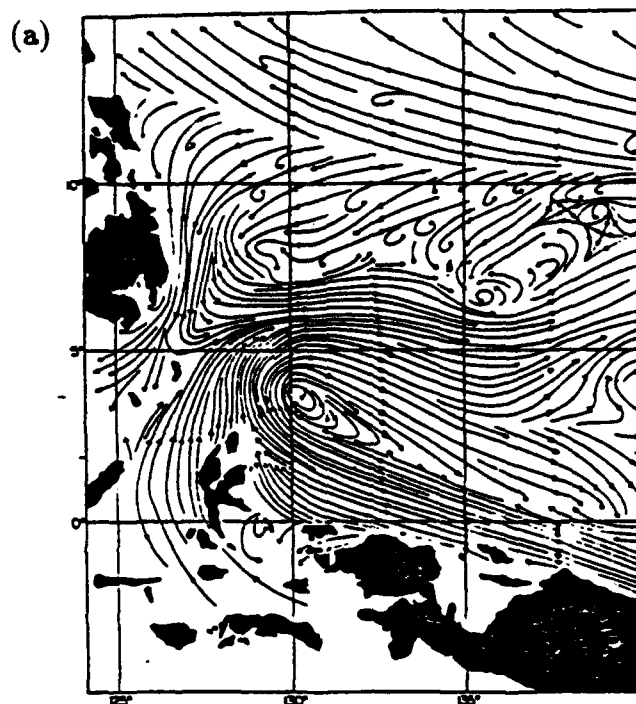


Figure 4.10: The Equatorial Currents of the Western Pacific Ocean in the Northern Hemisphere during (a) Summer and (b) Winter (adapted from Kendall (1969)).

In July, three Lagrangian drifters were launched in the Mindanao Current; the launch point and date, the length of record and failure mode for Buoys 52, 53 and 55 are indicated in Table 4.1 below, taken from Carpenter (1989).

Table 4.1:

BUOY	Date of launch	Location of launch	Record length	Failure Mode
Buoy 52	16 July 88	6.944°N 126.619°E	53 days	Lost drogue
Buoy 53	22 July 88	7.983°N 127.958°E	220 days	Grounded
Buoy 55	16 July 88	6.861°N 126.861°E	63 days	Grounded

Trajectories of these buoys are plotted in three figures (see Carpenter (1989), Figs. 4.11(a), 4.11(b) & 4.12); squares are placed as markers for buoy locations at 12Z each second day, and the beginning and ending Julian dates are indicated on each trajectory. Although Buoys 52 and 55 were launched on the same date (16 July 88, Julian day 198), and very close together, the paths traced after the third square (sixth day) are entirely different. Buoy 52 is caught in the North Pacific Equatorial Counter-current and is carried rapidly eastward; it describes one counter-clockwise loop in a 2-week period during its trajectory. Buoy 55 moves to the southwest, describes a counter-clockwise loop of almost 3 weeks duration, and continues northwestward through the Celoes (Sulawesi) Sea toward Borneo; there the coastline directed the buoy trajectory southward into the Southern Hemisphere.

Buoy 53 was launched 6 days later and at about one degree further to the north and to the east from the launch point for Buoys 52 and 55. After a very slow start for the first 53 days, Buoy 53 moved eastward in the Equatorial counter-current; it then describes half a loop (counter-clockwise) northward, where it was caught in the westward and relatively slow drift of the North Pacific Equatorial Current. It finally grounded along the southeast coast of Luzon.

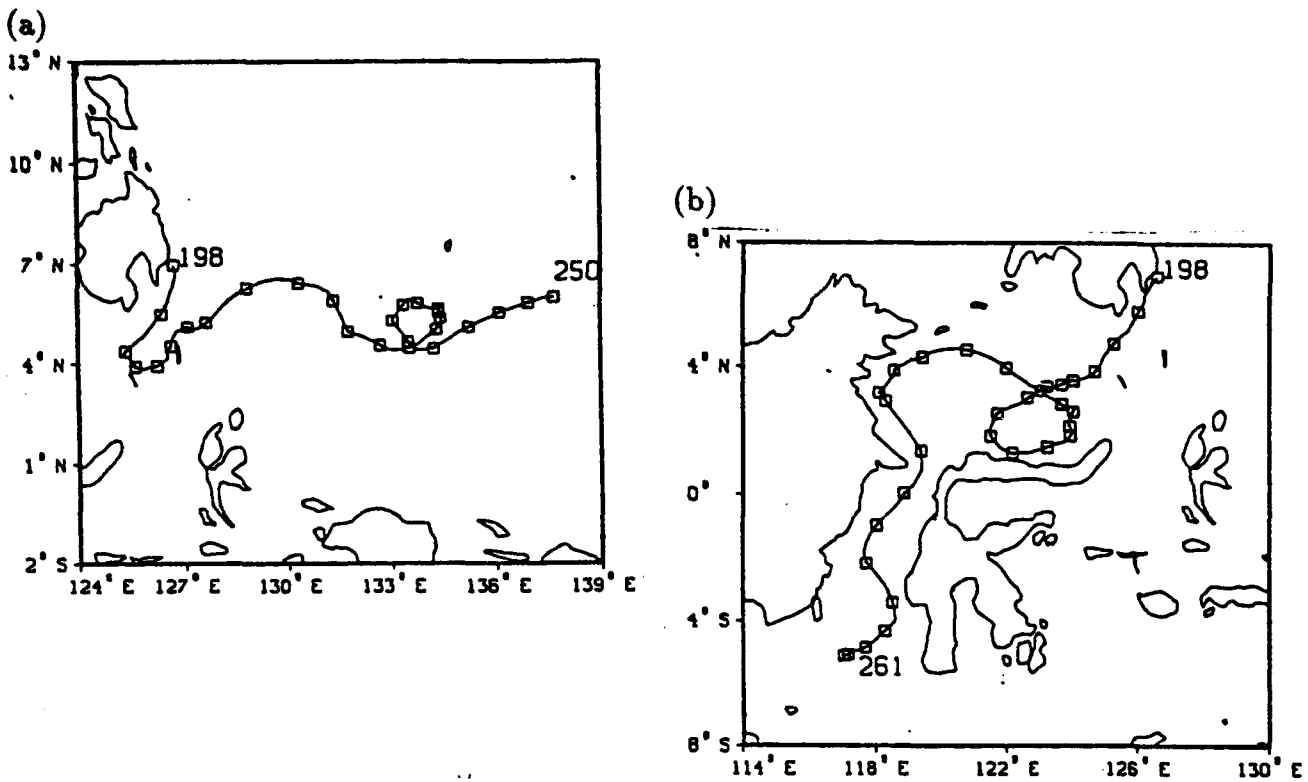


Figure 4.11: Lagrangian Trajectories of (a) Buoy 52 and (b) Buoy 55. Julian dates mark the beginning and end of each record and a square is placed as a marker for 12Z every second day (adapted from Carpenter (1989)).

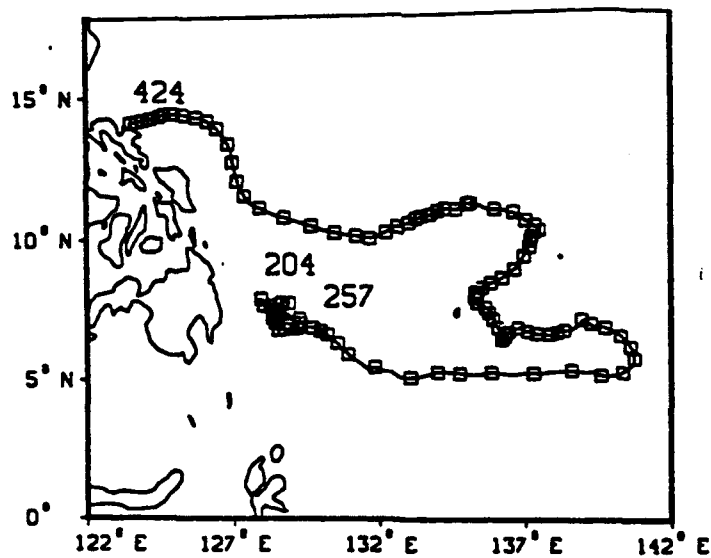


Figure 4.12: Lagrangian Trajectory of Buoy 53. Julian dates mark the beginning and end of each record and a square is placed as a marker for 12Z every second day (adapted from Carpenter (1989)).

Current speeds calculated in the Mindanao Current during winter are shown in Fig. 4.13. These vary from 0.6 to 2.0 knots in the strongest part of the current.

The vertical variation in speed is shown in Fig. 4.14 for three stations in the Mindanao Current during winter 1968 along 7°30' N (see Fig. 4.15 for station locations). Stations RY 3234 and RY 3235 show a pronounced maximum speed at about 50 meters depth (1.25 to 1.60 $\text{m}\cdot\text{s}^{-1}$); a minimum speed occurs at about 10 meters depth (about 0.9 and 1.05 $\text{m}\cdot\text{s}^{-1}$). Below the maximum, an almost-steady decline in speed with depth occurs, approaching zero at about 380 and 510 meters depth.

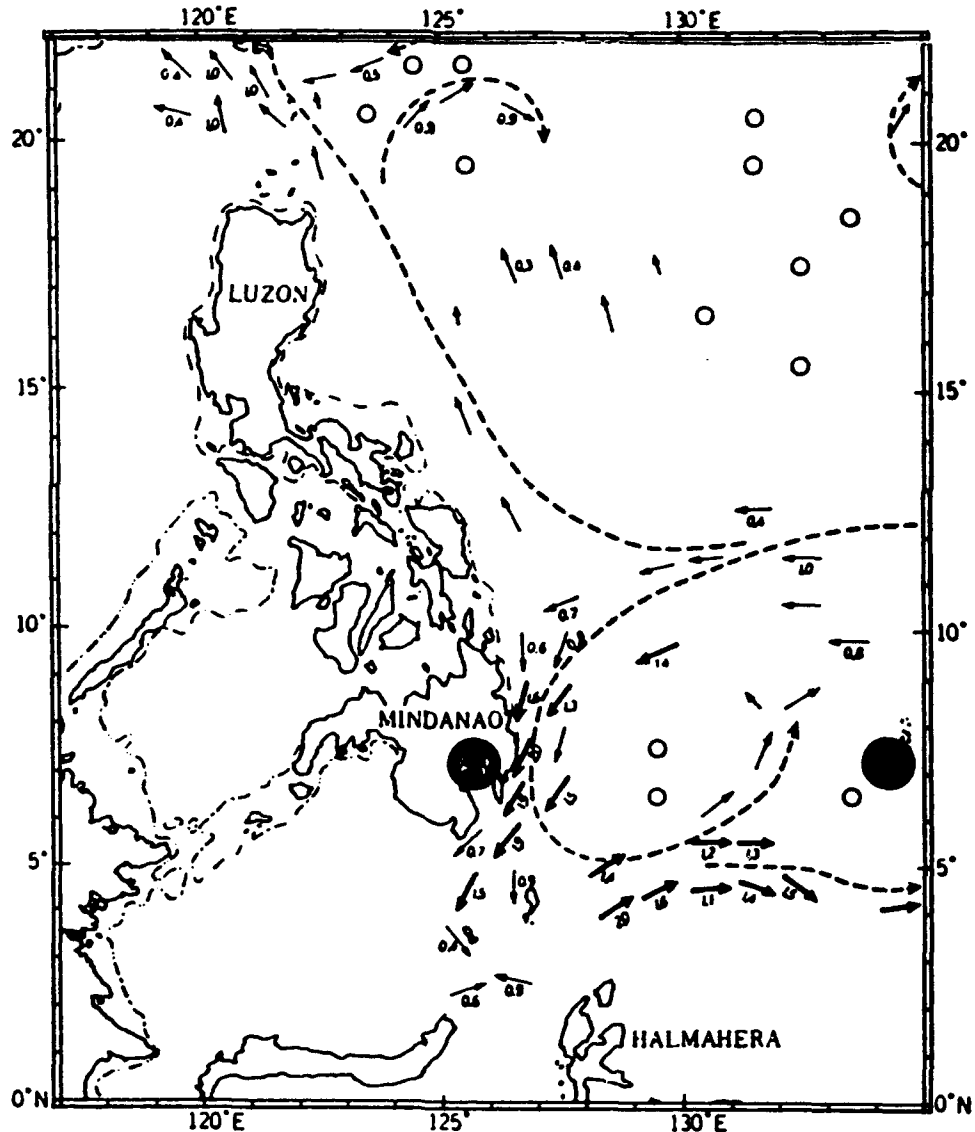


Figure 4.13: Currents (in knots; 1 knot equals 0.51 m s^{-1}) for Northern Hemisphere Winter. Solid circles are locations of two tide gauge stations (adapted from Lukas (1988)).

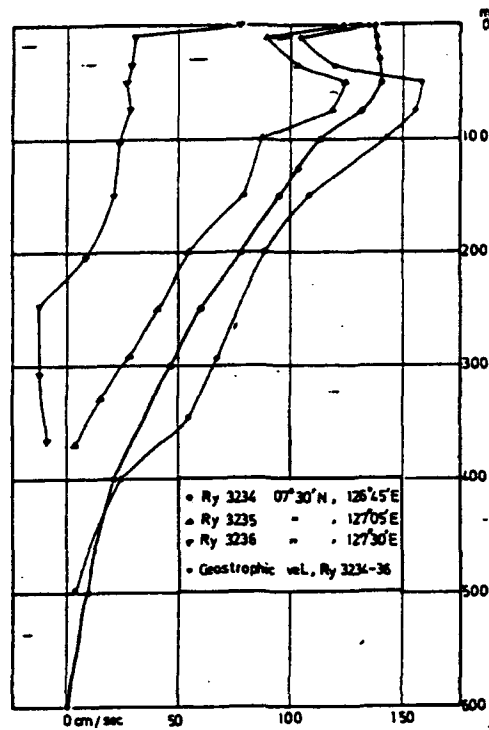


Figure 4.14: Vertical Distributions of the Measured and Computed Speed Relative to 600 db in the Mindanao Current at 7°30'N (adapted from Matsuzawa (1968)).

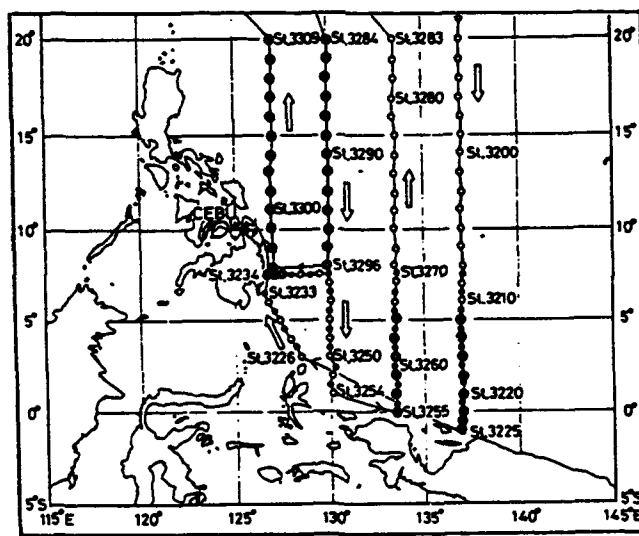


Figure 4.15: Track Chart of the Second Cruise for the Cooperative Study of the Kuroshio made by the *Ryofu Maru* of the JMA in January to March 1968. The open circle, double circle and dot indicate the deep station, current measurement station and shallow station (adapted from Matsuzawa (1968)).

2. Sea Surface Temperature. During August, the western North Pacific Ocean shows maximum values between about 5°S and 30°N along its western boundaries. The Philippine coastlines experience these high temperatures, with a value of 29°C along the western coast of Luzon; Fig. 4.16(a). By February, the region of temperature maximum has moved into the southern hemisphere, from the equator to about 20°S; see Fig. 4.16(b). Then there is a weak temperature gradient along both east and west coasts of the Philippines; the temperature ranges from 27°C off Mindanao to 25°C in Luzon Strait.

Monthly charts prepared from Comprehensive Ocean-Atmosphere Data Set (Sadler et al. 1987) are included as part of Appendix A. These charts represent averages of 80 years of data for 2-degree latitude/longitude areas from 5° to 26°N and from 110° to 140°E; the Philippine Islands are centered in this region. Charts for August, November, February and May are reproduced here in Figs. 4.17 & 4.18. Details of the seasonal changes in temperature are provided in Figs. 4.17 & 4.18 as they change between the extreme values shown earlier. Sea surface temperatures reach maximum value (>29°C) in the South China Sea in May, while coldest temperatures in the area (<15°C) occur adjacent to China in Taiwan Strait in February. Thus the marginal seas experience a greater annual range in surface temperature than do regions in the open ocean to the east of the Philippine Islands.

Somewhat north of the Philippines, off Taiwan, sea surface temperatures measured in winter (December '62 - January '63) and summer (June '63) are shown in Figs. 4.19(a) & 4.19(b). About 4°C seasonal variation occurs nearshore and in Luzon Strait, but it lessens to 2.5 to 3°C further offshore, south of 22°N in the Philippine Sea. Figure 4.19(a) shows the location of two coastal stations on the eastern coast of Taiwan from which vertical sections are made of temperature that are shown later: Ho Peng (Ho stations) and Shi Ti (ST stations); those sections of temperature versus depth extend offshore from these locations about 4 and 5 km.

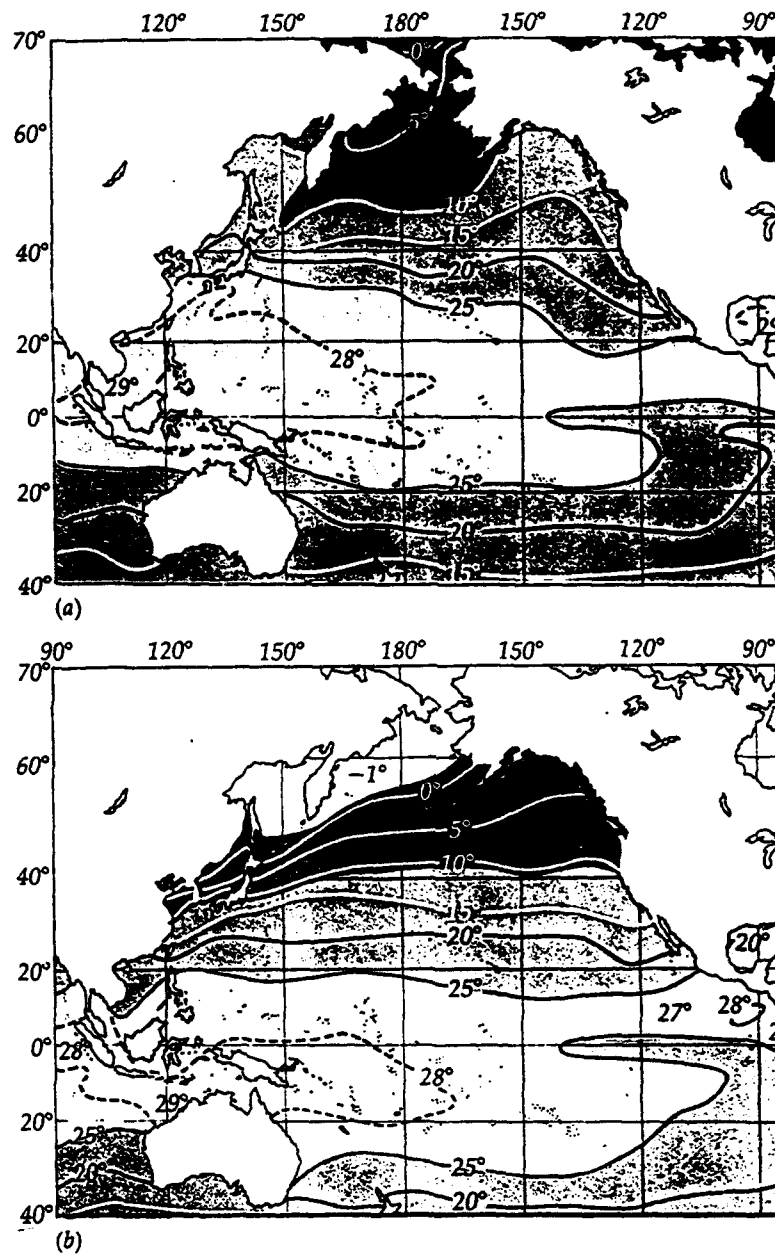


Figure 4.16: Surface Temperature of the Oceans (a) in August and (b) in February (adapted from Ingmanson and Wallace (1973)).

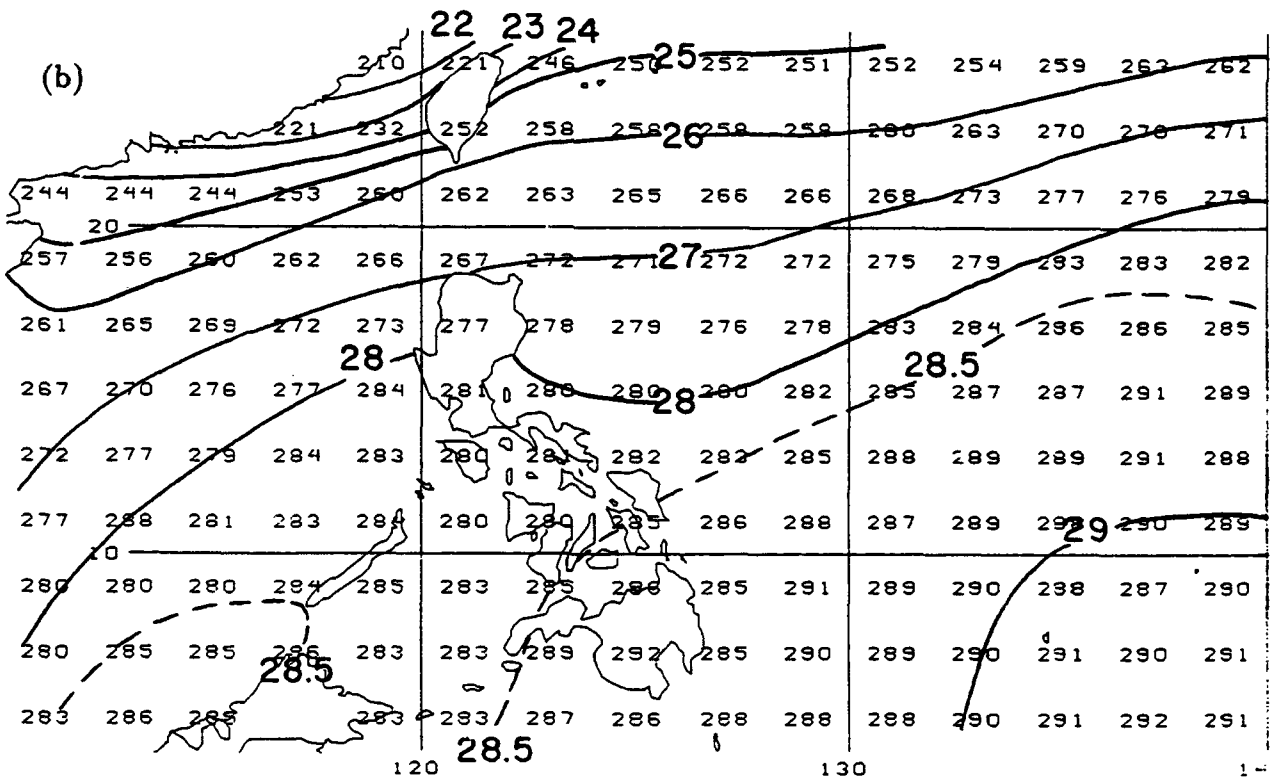
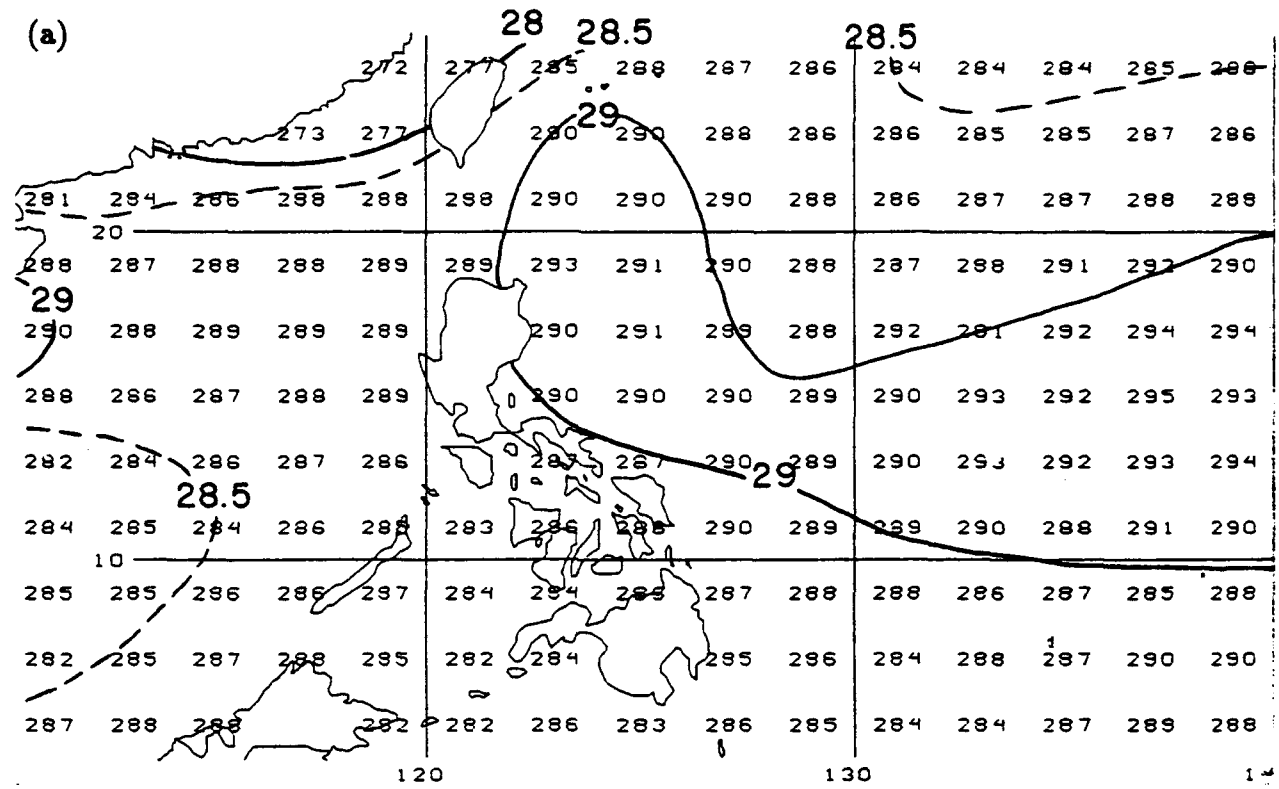


Figure 4.17: Monthly Sea-Surface Temperature; August (a), November (b). (Adapted from Sadler et al. (1987). See Appendix A for details.)

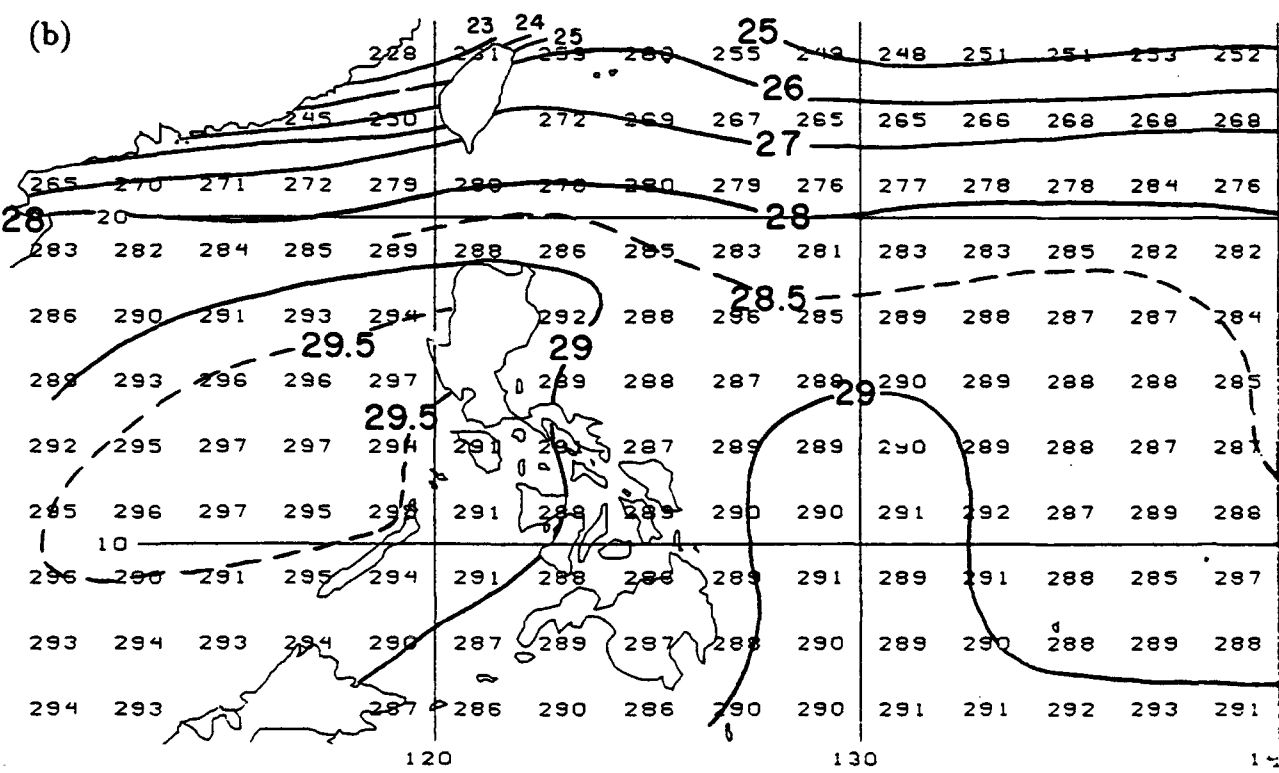
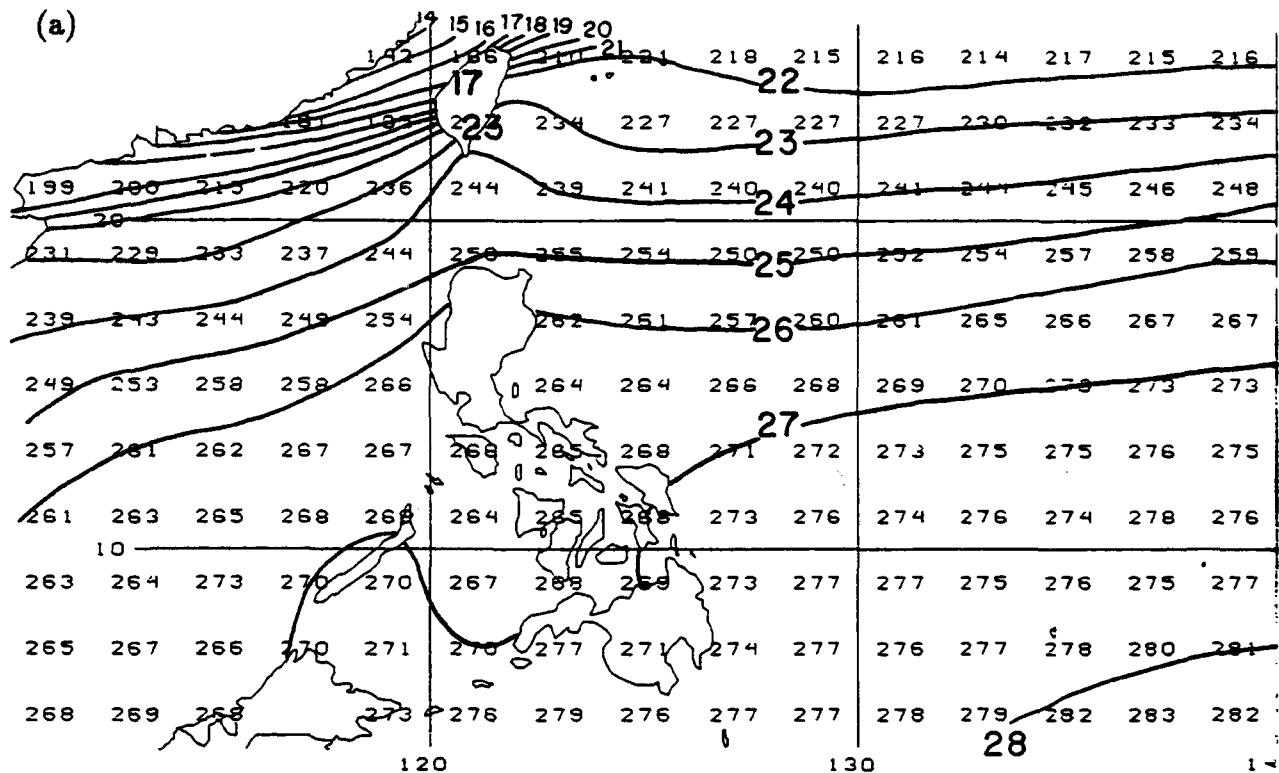


Figure 4.18: Monthly Sea-Surface Temperature; February (a), May (b). (Adapted from Sadler et al. (1987). See Appendix A for details.)

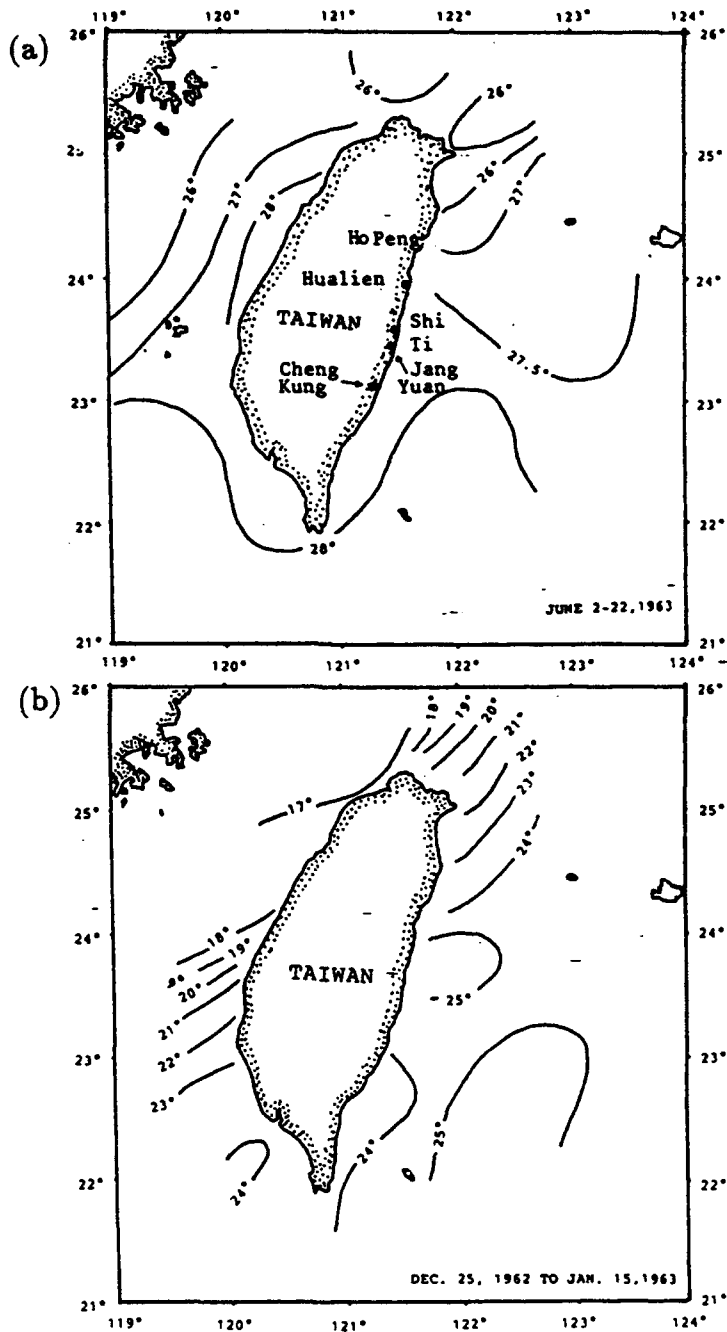


Figure 4.19: Sea Surface Temperature ($^{\circ}\text{C}$) around Taiwan in Summer (a) and Winter (b) (adapted from Yin (1988)).

3. Vertical Variation of Temperature. At the nearshore locations off Taiwan (H_o stations are at $24^{\circ}20'$ N; ST stations are at $23^{\circ}30'$ N), the cross-sections for winter and summer are shown in Figs. 4.20(a), 4.20(b), 4.21(a) & 4.21(b). Pronounced mixed layers of uniform temperature adjacent to the surface extend to about 100 m depth in winter, with a thermocline that shows a pronounced gradient immediately below the mixed layer. Winter surface temperatures of 23 to 25°C are replaced in summer by temperatures of 26 to 29°C. In summer, the strong thermocline begins at the sea surface, and becomes less strong below 100 to 150 meters in depth.

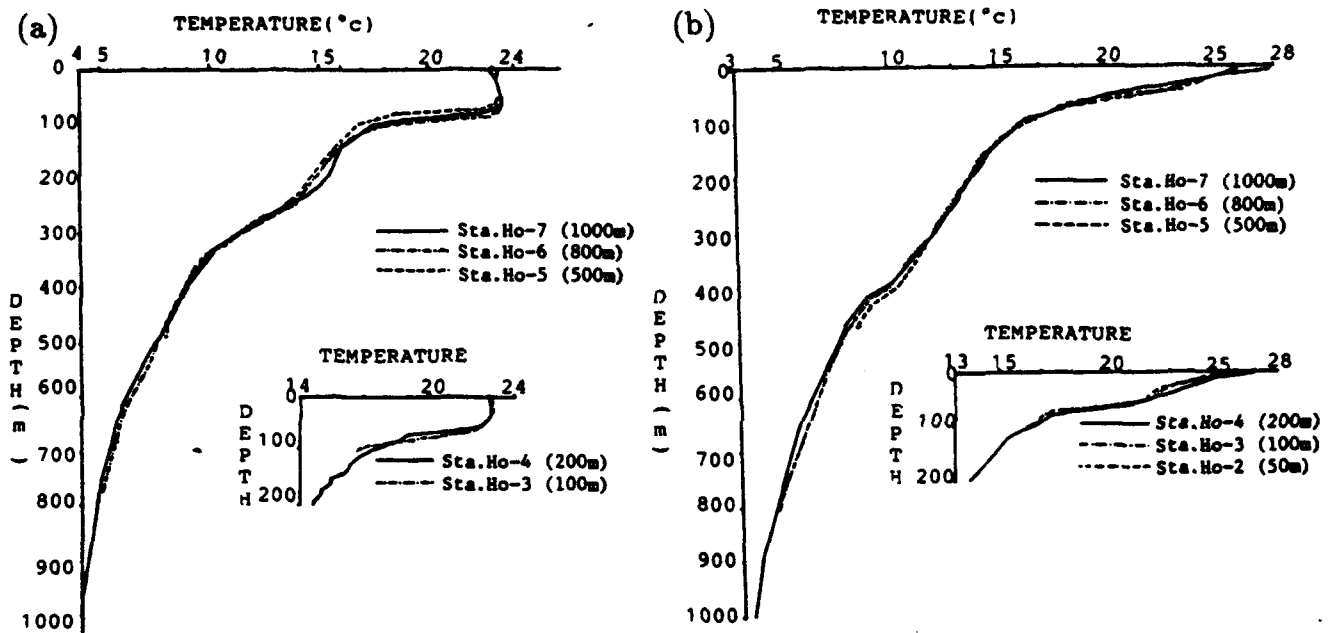


Figure 4.20: Temperature Distribution at Stations Ho-1 to 7 in (a) December 1984 and (b) May 1985 (adapted from Yin (1988)). Lowermost thermometer depth in parentheses.

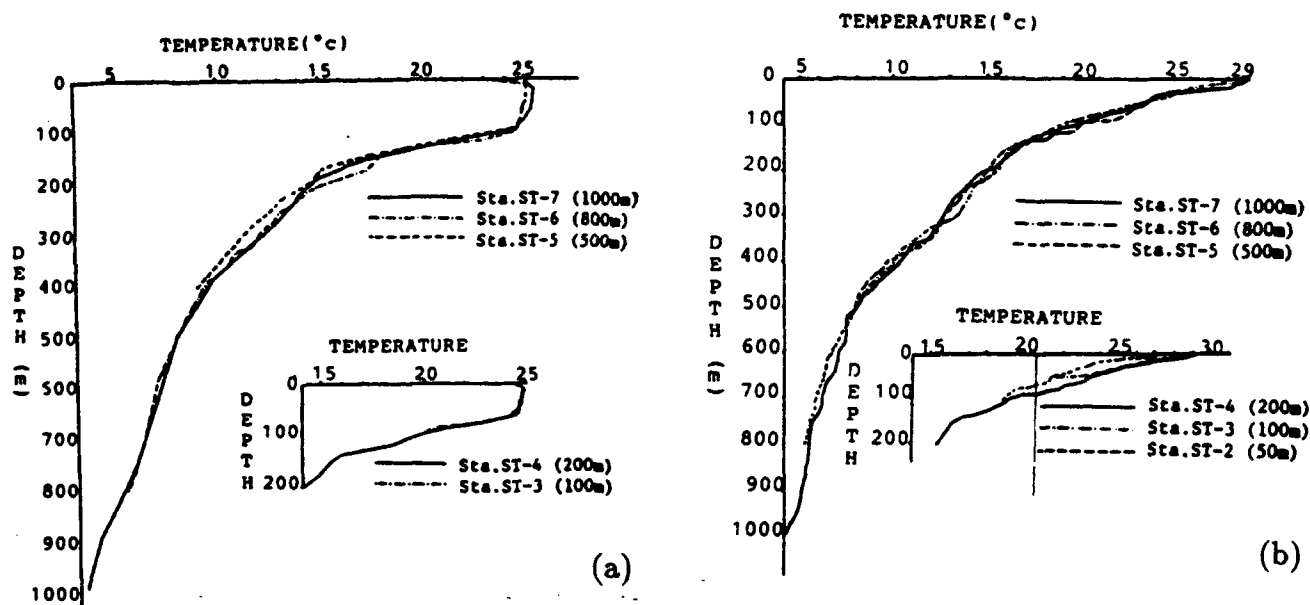
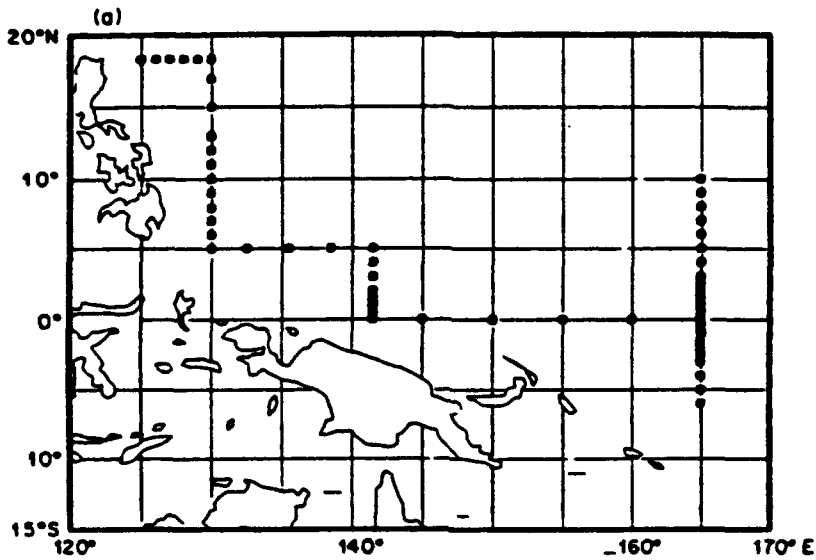


Figure 4.21: Temperature Distribution at Stations ST-1 to 7 in (a) November 1984 and (b) July 1984 (adapted from Yin (1984)). Lowermost thermometer depth in parentheses.

Further south, at the latitudes of the Philippines and along 130°E. Longitude, vertical sections are shown drawn from stations observed on two cruises of the US/PRC (People's Republic of China) cooperative program of 1987; the first cruise occurred in January-February 1987; the second cruise was in November-December 1987. Both cruises thus represent winter conditions (station locations are shown in Fig. 4.22 along 130°E. Longitude). Figure 4.23(a) of Toole et al. (1988) shows the temperature section from the surface to 1000 meters depth for the first cruise; Fig. 4.23(b) shows similar results for the second cruise. In both sections, a strong thermocline is present in the region from 50 to 150 meters, extending from low latitudes northward to about 10°N. Further north, the thermocline gradient weakens somewhat, deepening and extending much deeper; the gradient occurs between 100 and 400 meters depth at 18°N.

CTD STATION POSITIONS
TOGA PRC-1 LEG 3



CTD STATION POSITIONS
PRC-2 LEG 1 & LEG 2

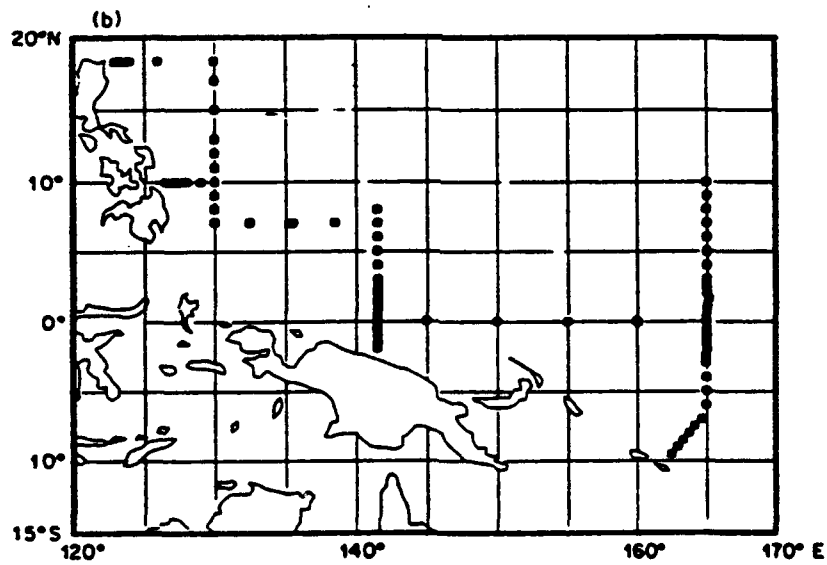


Figure 4.22: Section Maps for the CTD Observations obtained during the First Two Cruises of the US/PRC Cooperative Program. (a) The first cruise observations: 30 January to 18 February 1987. (b) The second cruise observations: 18 November to 16 December 1987 (after Toole et al. (1988)).

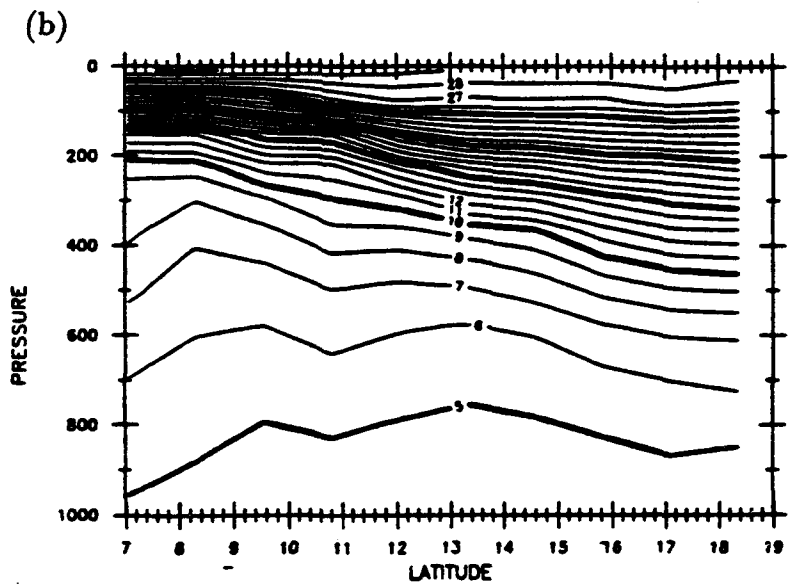
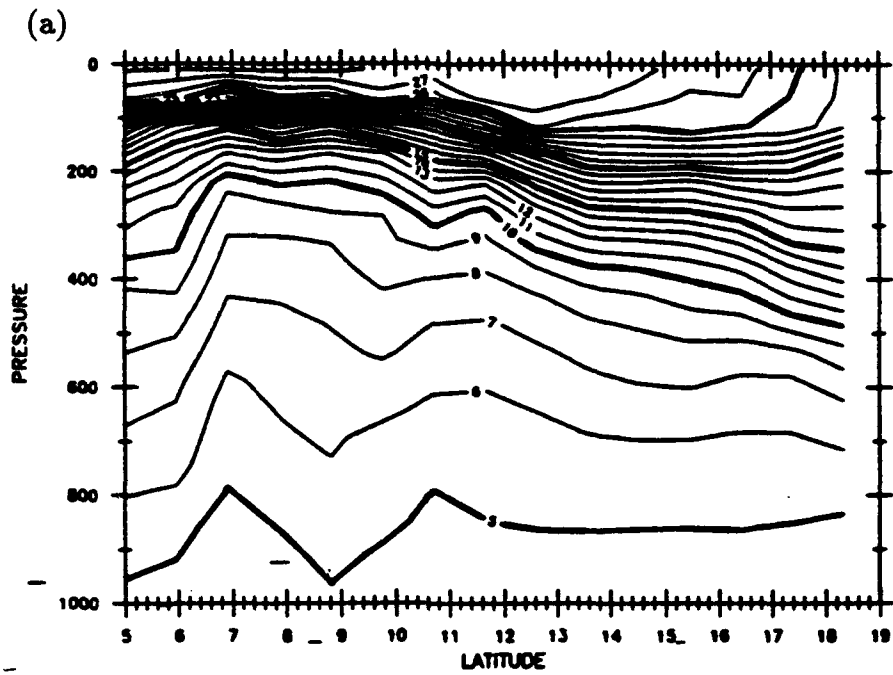


Figure 4.23: Sections of Temperature in °C, constructed along 130°E during the (a) first cruise and (b) second cruise of the US/PRC cooperative program (adapted from Toole et al. (1988)).

Along 129°E. Longitude, and further south (from 1.5° to 5.5°N) in the Philippine Sea, a cross-section of temperature to 300 db (read "300 meters") depth during July 1988 is provided in Fig. 4.24, a study of the Mindanao Eddy (Carpenter 1989). This section was produced from airborne expendable bathythermograph (AXBT) observations. Two of the observations are shown in Fig. 4.25(a) (at about 1°15'N) and in Fig. 4.25(b) (at about 7°24'N), both near 129°E. Longitude; note the change in thermocline character between these two latitudes. Further north, the thermocline gradient becomes steeper and less irregular.

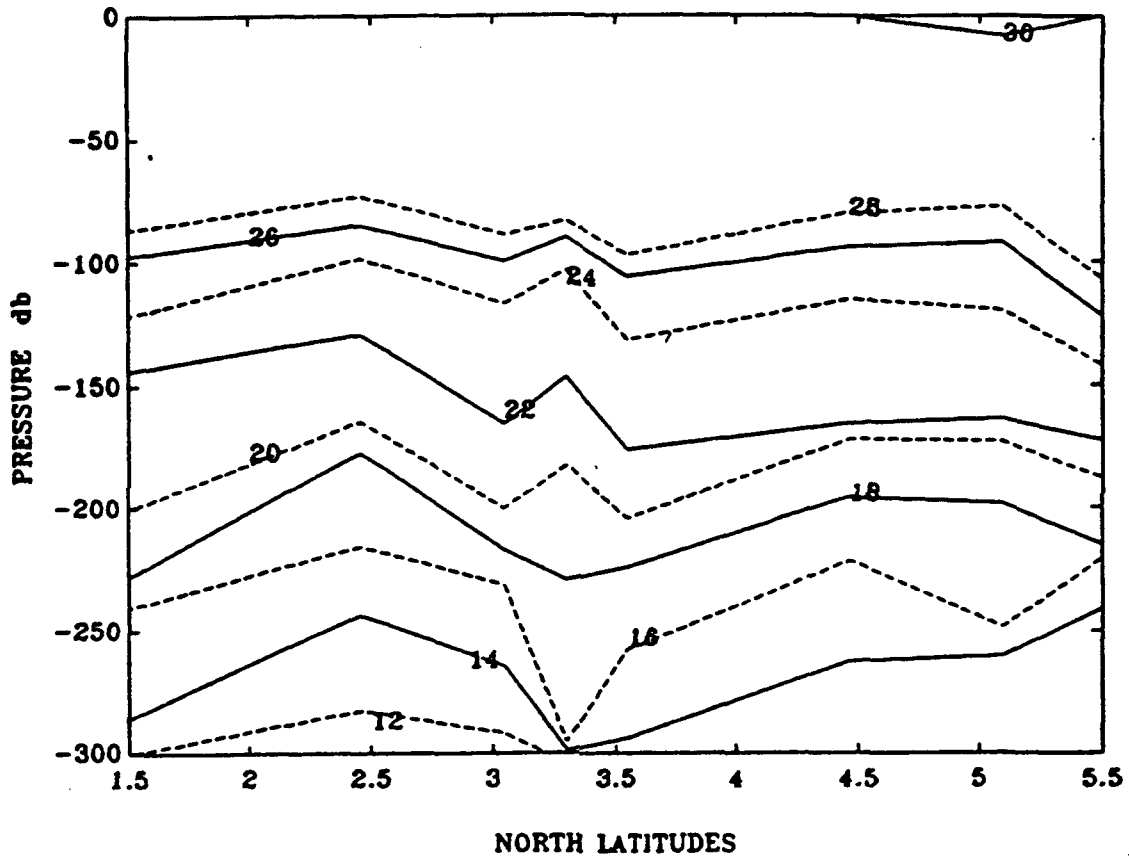
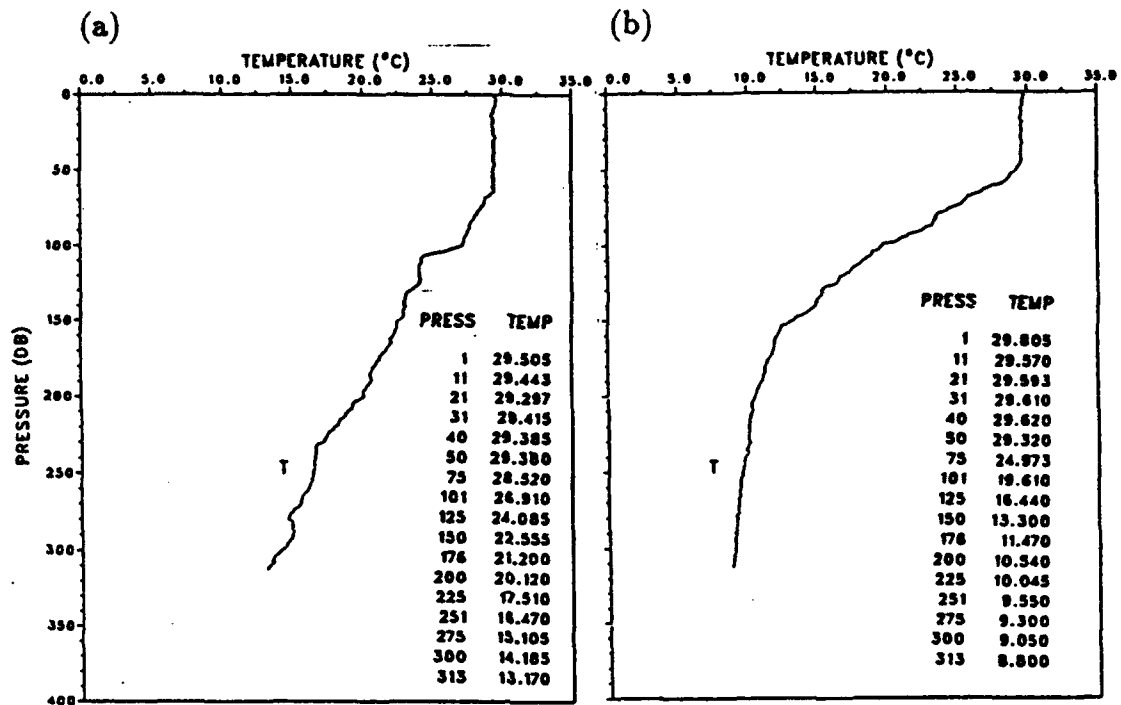


Figure 4.24: Vertical Temperature Cross-section B: Located along 129°E (adapted from Carpenter (1989)).



STATION: 102 LAT: 1 14.8 N LON: 129 2.5
 DATE: 7/11/88 TIME: 1023Z

STATION: 4 LAT: 7 23.6 N LON: 128 9.7
 DATE: 7/12/88 TIME: 1106Z

Figure 4.25: Vertical Temperature Distribution at two locations in the Mindanao Current region, measured by Airborne Expendable Bathythermograph (AXBT) Observations in July 1988 (adapted from Carpenter (1989)).

A conductivity-temperature-depth (CTD) measurement for a nearby location (6.95°N; 126.71°E) shows characteristics intermediate between these AXBT observations. There is a definite mixed layer in all three examples, extending from the surface to 40-60 meters depth. This mixed layer probably is maintained by the North Pacific Equatorial Counter-current flowing in this region.

A study (Schramm 1979) describes temperature changes in the ocean caused by Typhoon Phyllis as it passed across the Philippine Sea during August 14–17, 1975 (see Fig. 4.26). The measurements were made by calibrated AXBT's dropped from Navy P-3 aircraft during three flights across the area: 14 hours ahead of the storm passage, 10 hours after storm passage; and two days later. The region studied was 20° to 26°N; 133° to 140°E within dashed lines on Fig. 4.26. During this interval, Typhoon Phyllis moved northward along 137°E. Vertical sections of temperature are shown later below the line A–B along 24°N; point A is at 24°N, 133°E, while point B is at 24°N, 140°E. Sea surface temperature prior to the Typhoon passage ranges from 27.7° to 29°C, with a very weak horizontal gradient (see Fig. 4.27(a)).

After the Typhoon passage on the 15th (see Fig. 4.27(b)) pronounced cooling has occurred, especially adjacent and to the right of the storm track along 137°E.

The vertical distribution of sea temperatures along line A–B is shown for 14 August (see Fig. 4.28); for 15 August (see Fig. 4.29); and for 17 August (see Fig. 4.30) between the surface and about 350 meters depth. The initial mixed layer at about 35 meters on the 14th is interrupted extensively adjacent to the storm path; it is destroyed immediately to the right, with deep, colder water brought to the surface; and it is deepened considerably to the left of the storm path, to about 50 meters. Temperatures are affected to depths greater than 300 meters; these effects persist for at least two additional days (see Fig. 4.30). Temperature change at various depths on the section are shown in Fig. 4.31; they exceed 5°C decrease just to the right of the storm path at about 45 meters depth; about 2°C change occurs at points about 2 degrees of longitude to the left (negative) and to the right (positive) at about 50 meters depth. The negative temperature changes represent upwelling of deeper water into a region (see Figs. 4.32 and 4.33).

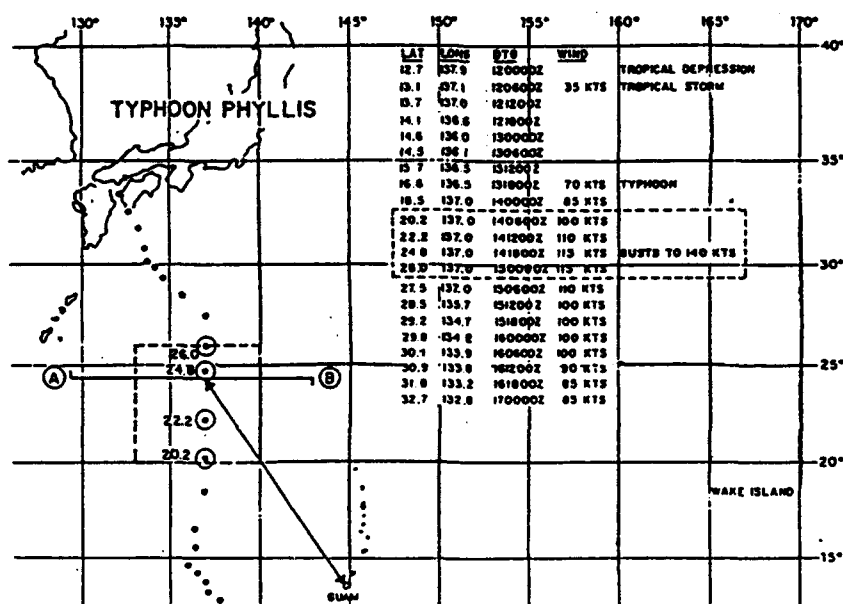


Figure 4.26: Track of Typhoon Phyllis (adapted from Schramm (1979)).

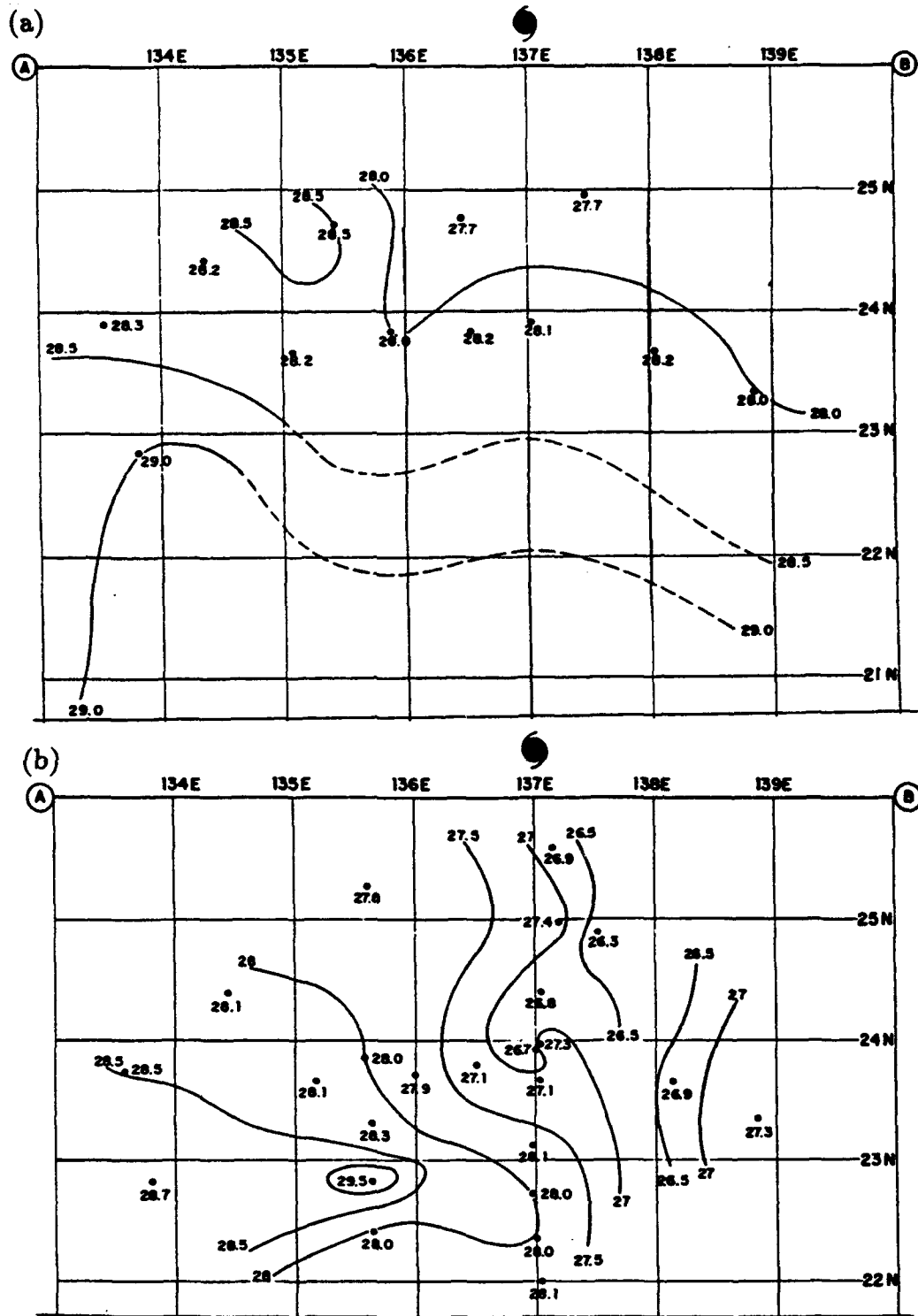


Figure 4.27: Sea Surface Temperature on (a) 14th and (b) 15th (adapted from Schramm (1979)). Isotherms in degrees C.

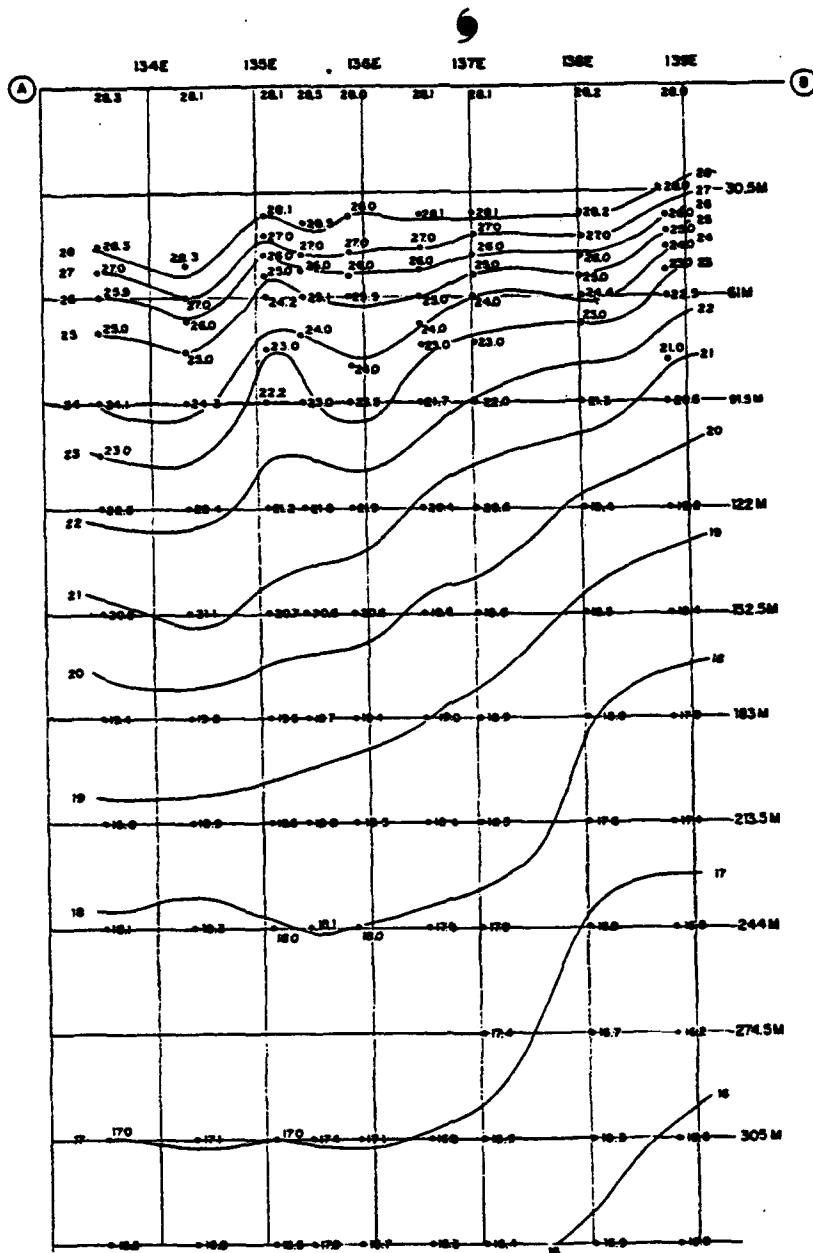


Figure 4.28: West to East Vertical Cross-section, along 24°N, perpendicular to Track of Typhoon Phyllis, on 14 August (adapted from Schramm (1979)). Isotherms in degrees C.

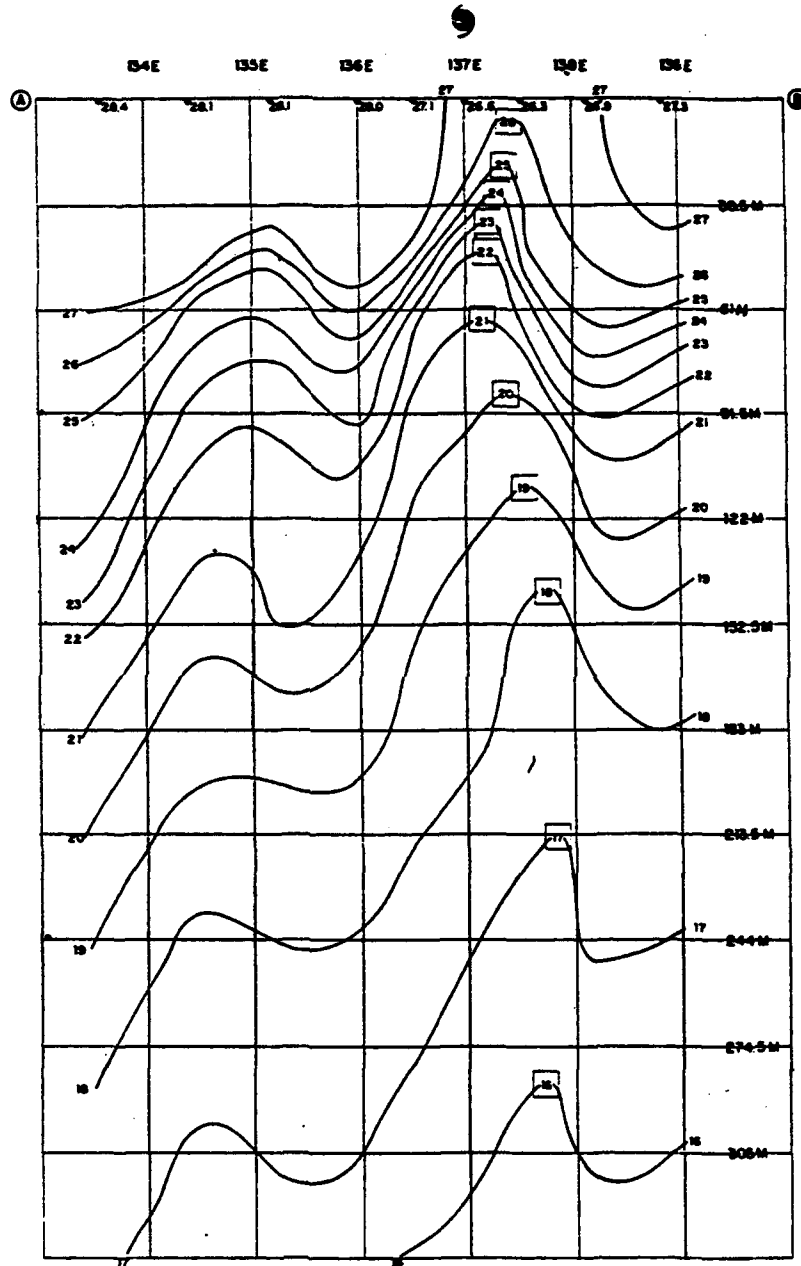


Figure 4.29: West to East Vertical Cross-section, along 24°N, perpendicular to Track of Typhoon Phyllis, on 15 August (adapted from Schramm (1979)). Isotherms in degrees C.

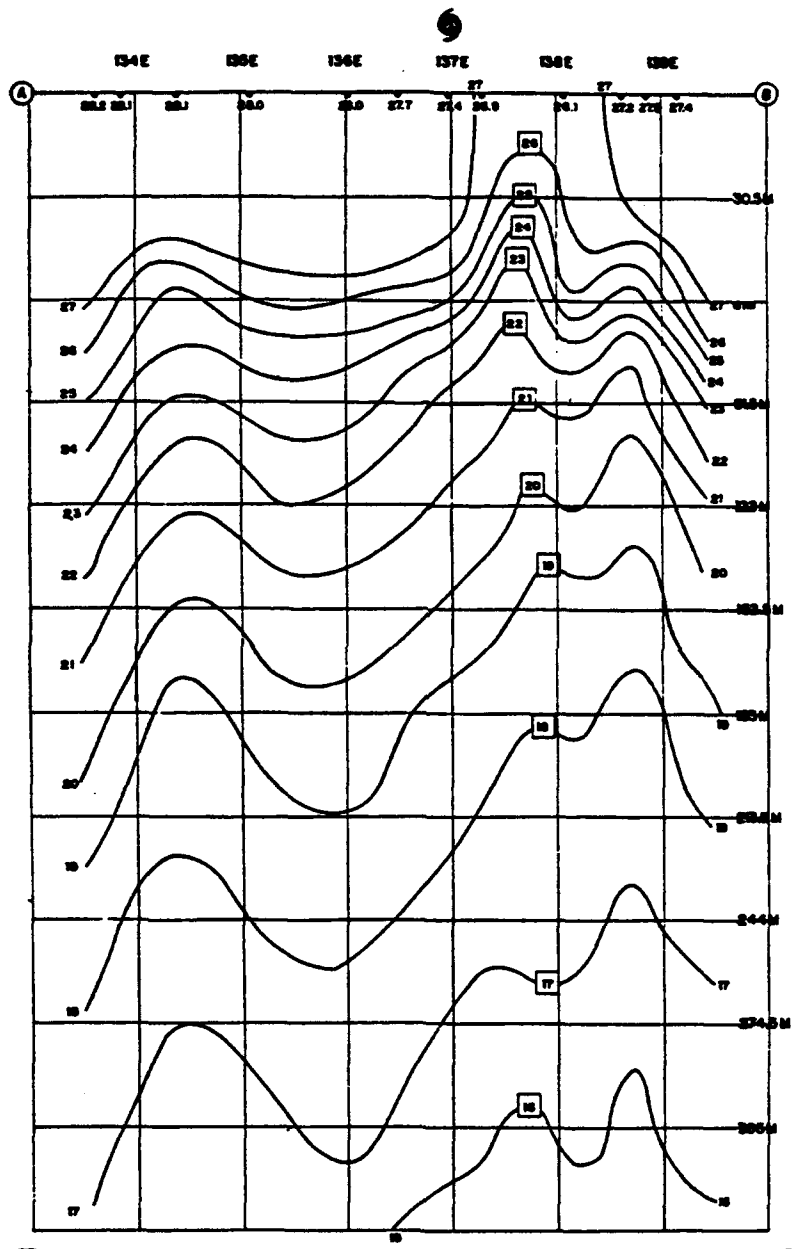


Figure 4.30: West to East Vertical Cross-section along 24°N, perpendicular to Track of Typhoon Phyllis, on 17 August (adapted from Schramm (1979)). Isotherms in degrees C.

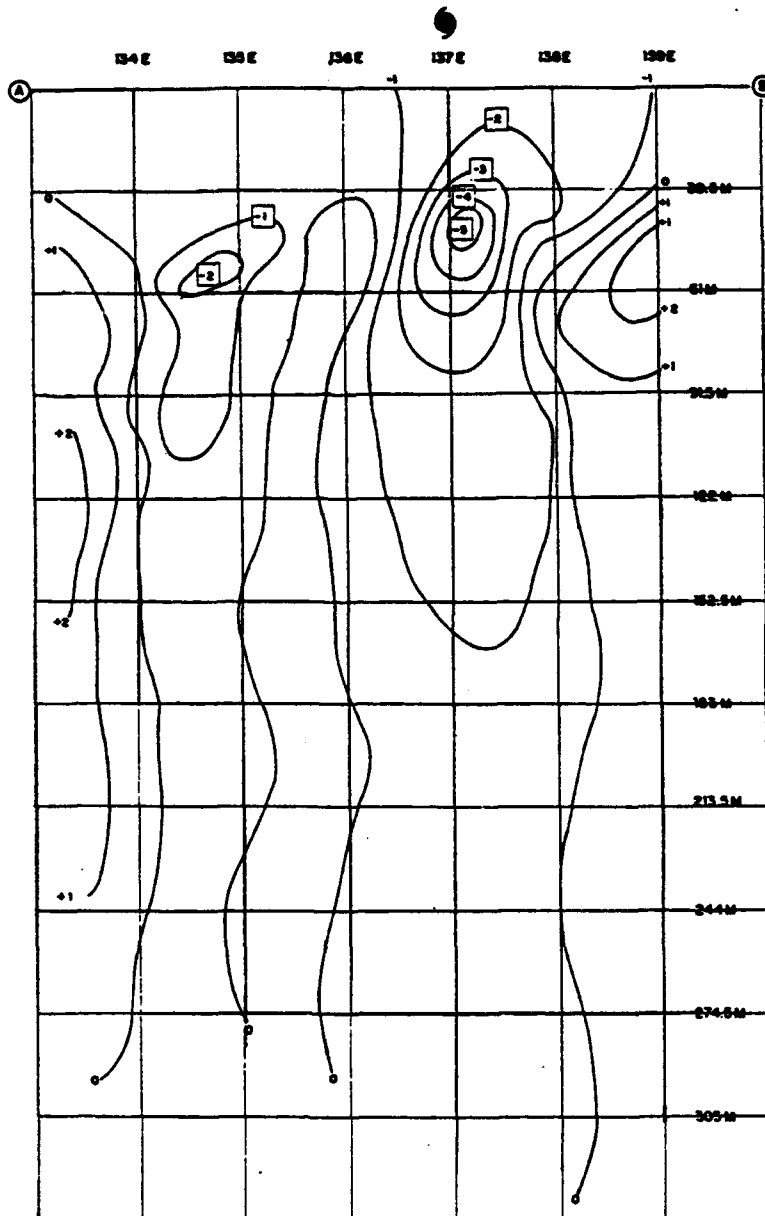


Figure 4.31: Vertical Cross-section depicting Changes in Temperature from the 14th to the 15th (adapted from Schramm (1979)).

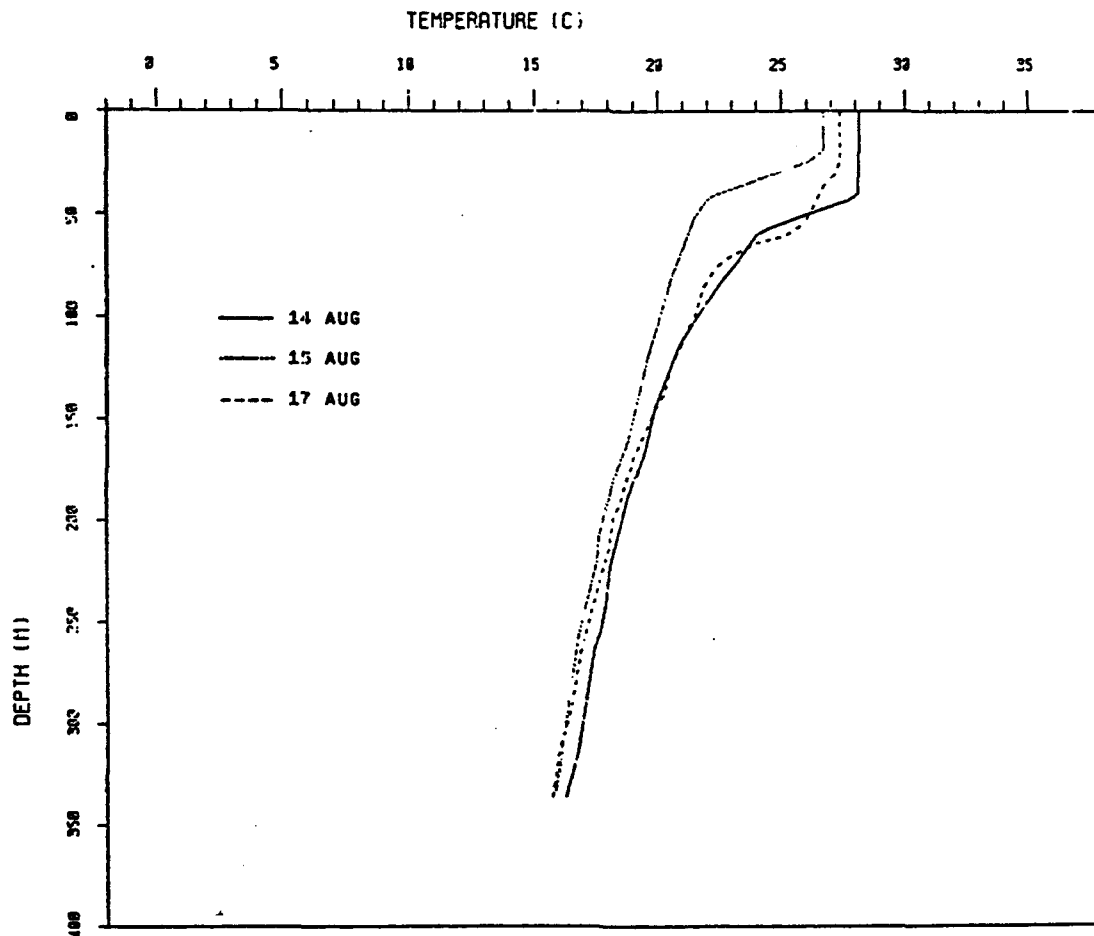


Figure 4.32: Under Eye of Track of Typhoon Phyllis: Profiles 3 (14th), 35 (15th) and 51 (17th) (adapted from Schramm (1979)).

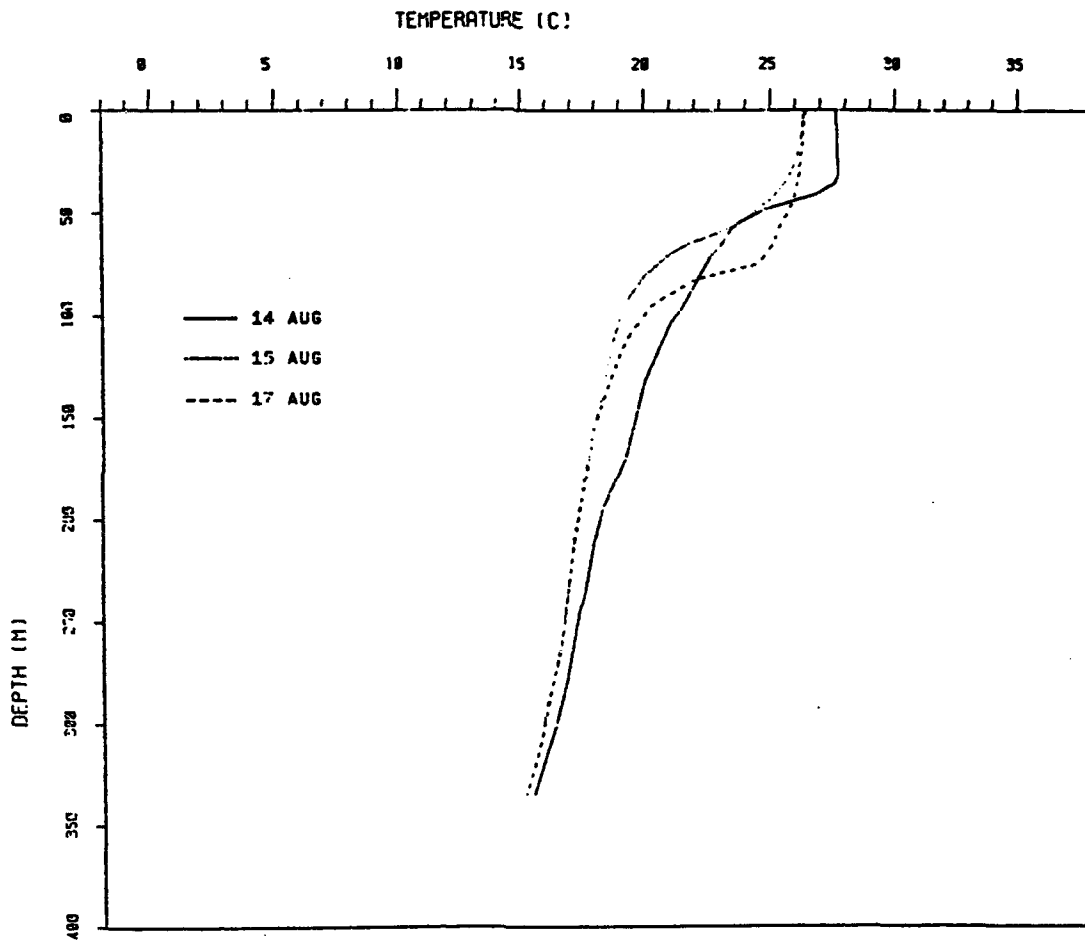


Figure 4.33: 30 n mi to Right of Track of Typhoon Phyllis: Profiles 22 (14th), 32 (15th) and 53 (17th) (adapted from Schramm (1979)).

4. **Salinity.** The mean annual salinity at the sea surface for the western North Pacific Ocean and the region surrounding the Philippine Islands is shown in Fig. 4.34. More detailed seasonal charts of surface salinity for February and August are shown by Figs. 4.35(a) & (b) for the regions immediately adjacent to the Philippines.

To the east of the Philippines, salinities occur that are higher than 34.0 ppm (parts per thousand). Salinity values higher than this extend through the Bashi Channel to the north of Luzon into the South China Sea, and bring 34.4 ppm values close to the shore north of 12°N during February. In August 34.4 ppm values are pushed offshore and are replaced by lower salinity values adjacent to the Philippines. Then, the 34.0 ppm value stretches from Luzon to Taiwan, in the north; and 34.0 ppm value is in the Basilan Strait southward from Mindanao. In the Celebes (Sulawesi) Sea southwest of Mindanao, salinity values are from 34.0 to 33.0 ppm in February; in August, values there are greater than 34.0 ppm.

In the Bashi Channel north of Luzon, the Northeast Monsoon in February brings higher salinity values westward into the extreme northern part of the South China Sea.

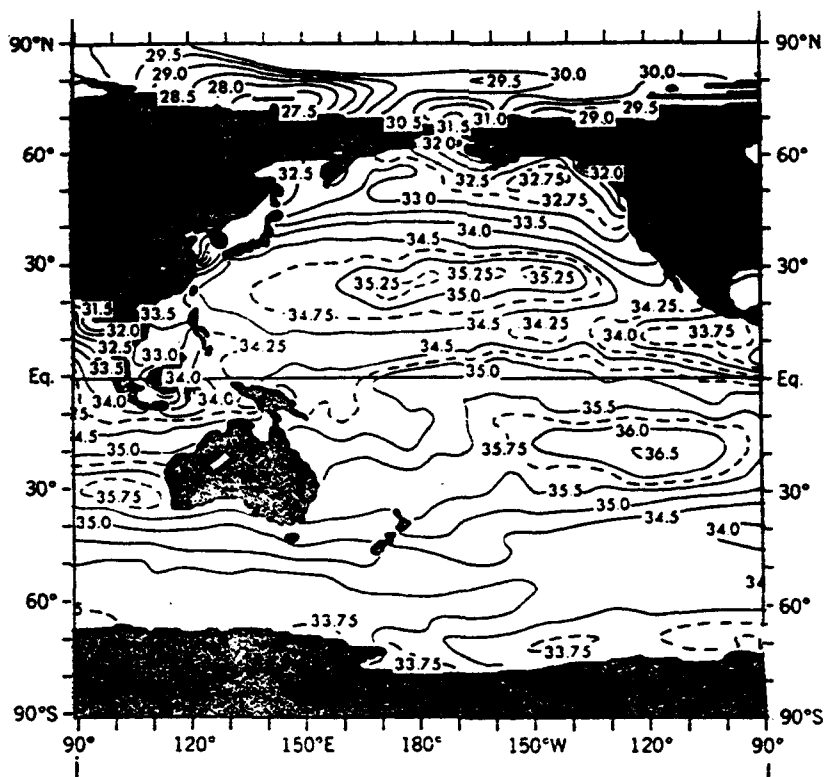


Figure 4.34: Annual Mean Salinity (ppm) at the Sea Surface (adapted from Levitus (1982)).

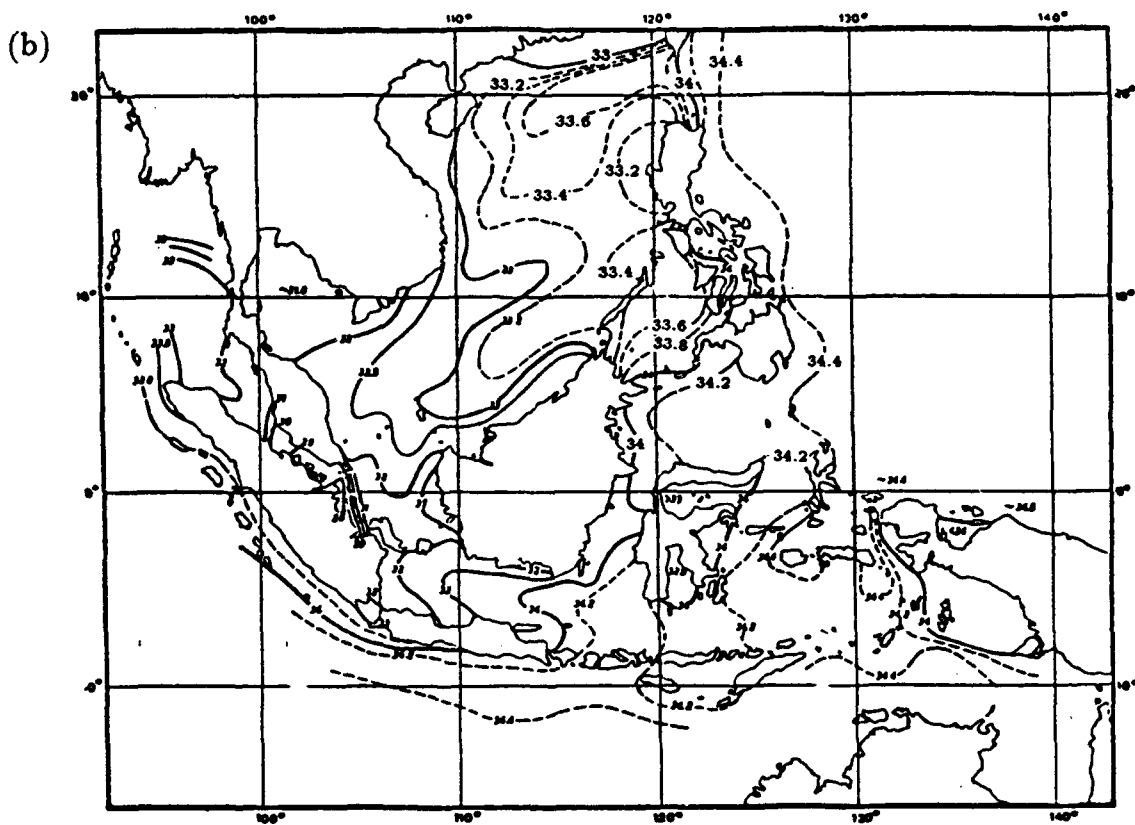
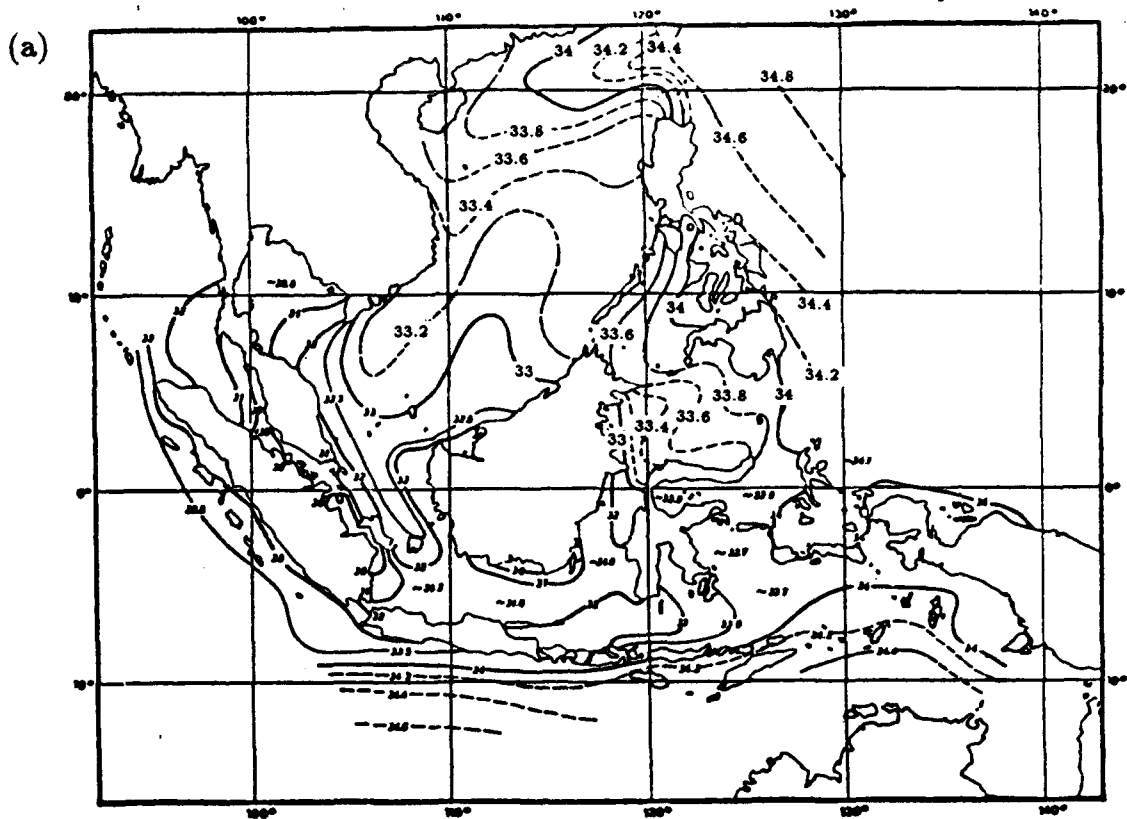


Figure 4.35: Average Surface Salinity (ppm) in Southeast Asian Waters in (a) February and (b) August (adapted from LaFond (1966)).

5. Salinity Variation with Depth. A schematic cross-section in the Philippine Sea from the equator to Taiwan (Formosa) shows the different salinity features in the upper 1200 meters of ocean (see Fig. 4.36). The uppermost layer features a salinity maximum that varies from 80 to 200 meters depth. Sections prepared from observations show the complexity of salinity distribution in these upper layers; the vertical section across the Mindanao Current at 7°30'N (eastward from Station 3234 through Station 3240, as shown by Fig. 4.37(a)) shows this maximum (>34.8 ppm) occurring at about 100 meters depth. Further south, in a section extending to the northwest from Halmahera toward Mindanao (stations 3226 through 3233 in Fig. 4.37(b)), this maximum appears also at about 100 meters. In both cases, there is a pronounced salinity gradient, with values increasing with depth, northward from 5°N; this gradient region starts at about 50 meters, associated with the strong thermocline also present. This maximum salinity feature also is displayed along 130°E taken by US/PRC Cruises 1 and 2 (see Fig. 4.22 for station locations and time).

A salinity minimum occurs below the maximum region; it is centered at about 400 meters depth at 5°N, and then deepens toward the north to 650 meters at 20°N (see Fig. 4.36). This feature is especially pronounced in the US/PRC sections along 130°E, reaching values at the core below 34.3 ppm north of about 15°N (see Figs. 4.38(a) and 4.38(b)).

These salinity features are illustrated also on a section made across the northern Philippine Sea region by Cruise CHIPS-1 of the Institute of Oceanography, National Taiwan University in May-June 1985, eastward from Taiwan along about 21°45'N (Fig. 4.39). The large section extends from the surface to 5000 db (read "5000 meters depth"); the upper 1000 db (1000 meters) is shown with an enlarged vertical scale in the upper part of the figure. A salinity maximum of about 34.9 ppm occurs centered at about 200 meters, while the salinity minimum, at or below 34.3 ppm, appears at 600-700 meters.

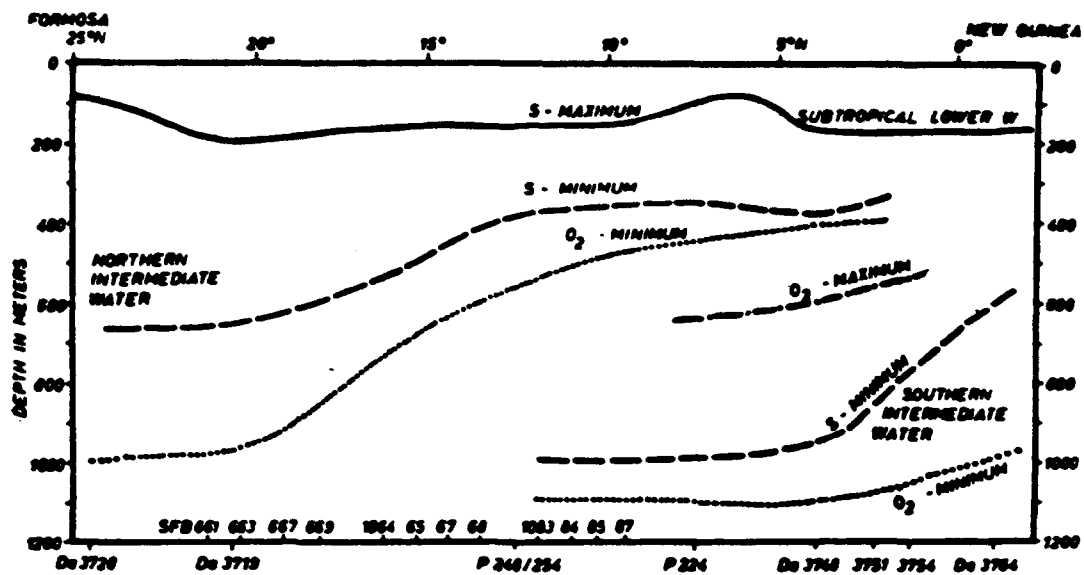


Figure 4.36: Schematic Representation of the Position of the Core Layers of the Different Water Masses in the Philippine Sea in a Section from Taiwan (Formosa) to New Guinea (adapted from Uda (1966)).

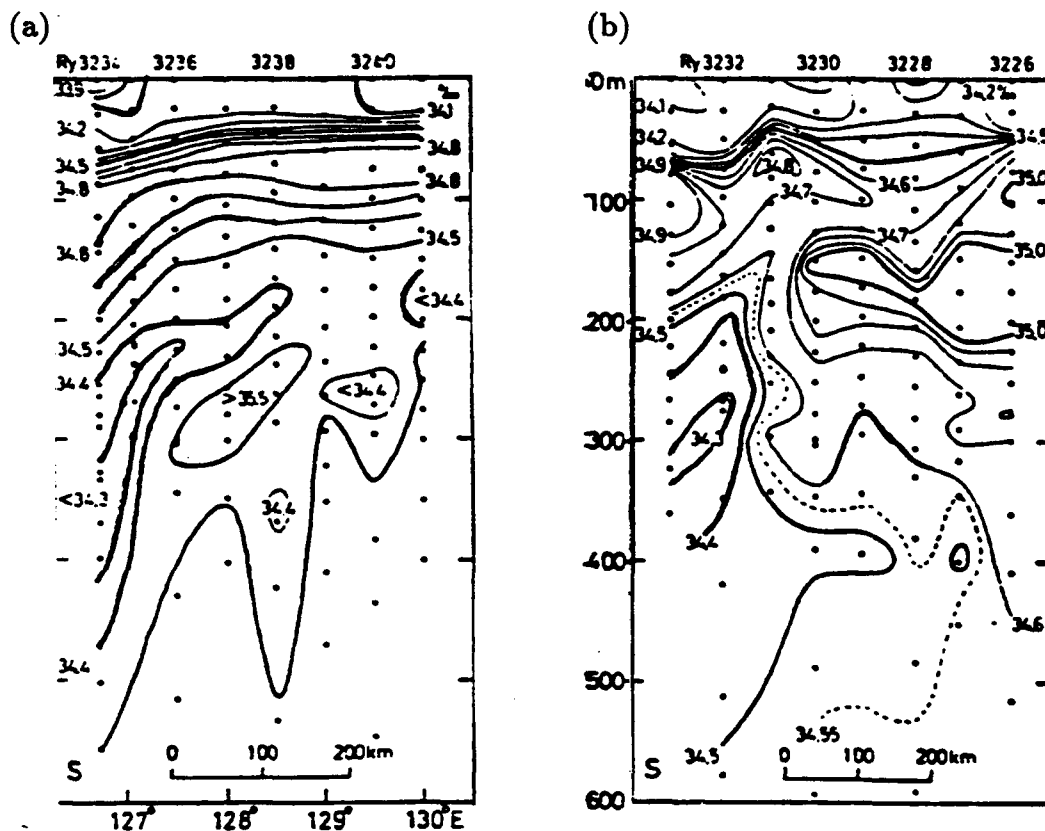


Figure 4.37: Vertical Section of Salinity (a) across the Mindanao Current at 7°30'N and (b) between Mindanao and Halmahera (adapted from Matsuzawa (1968)).

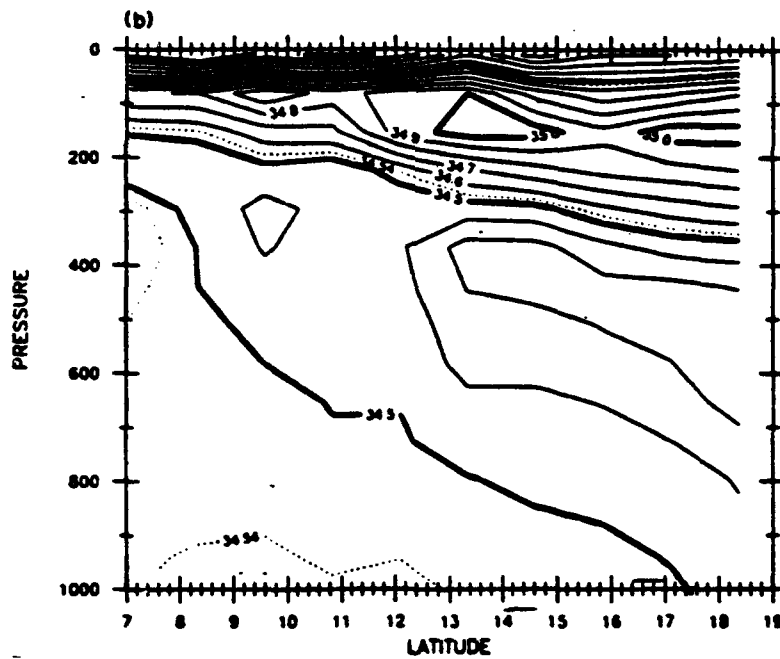
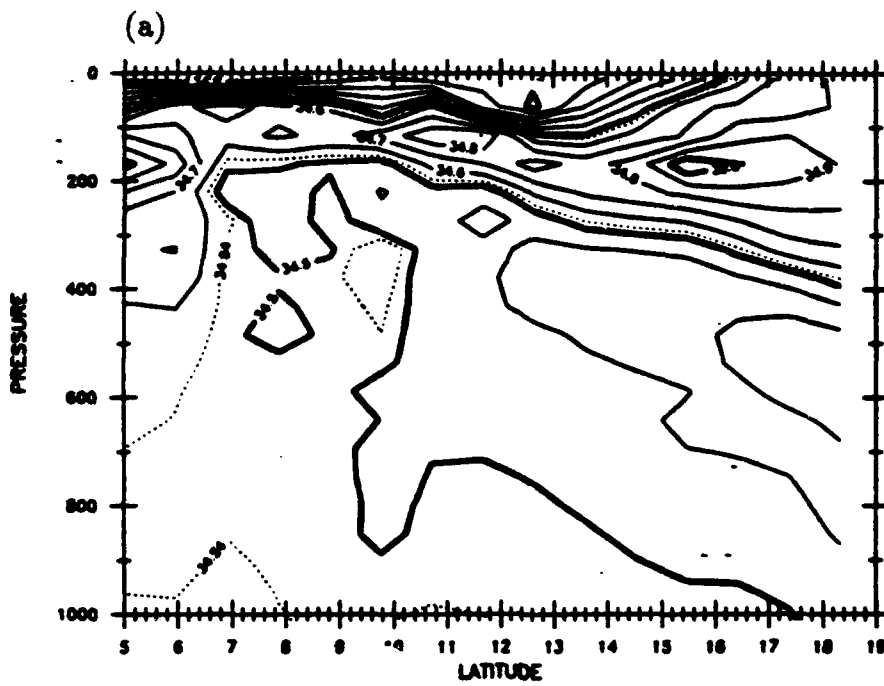
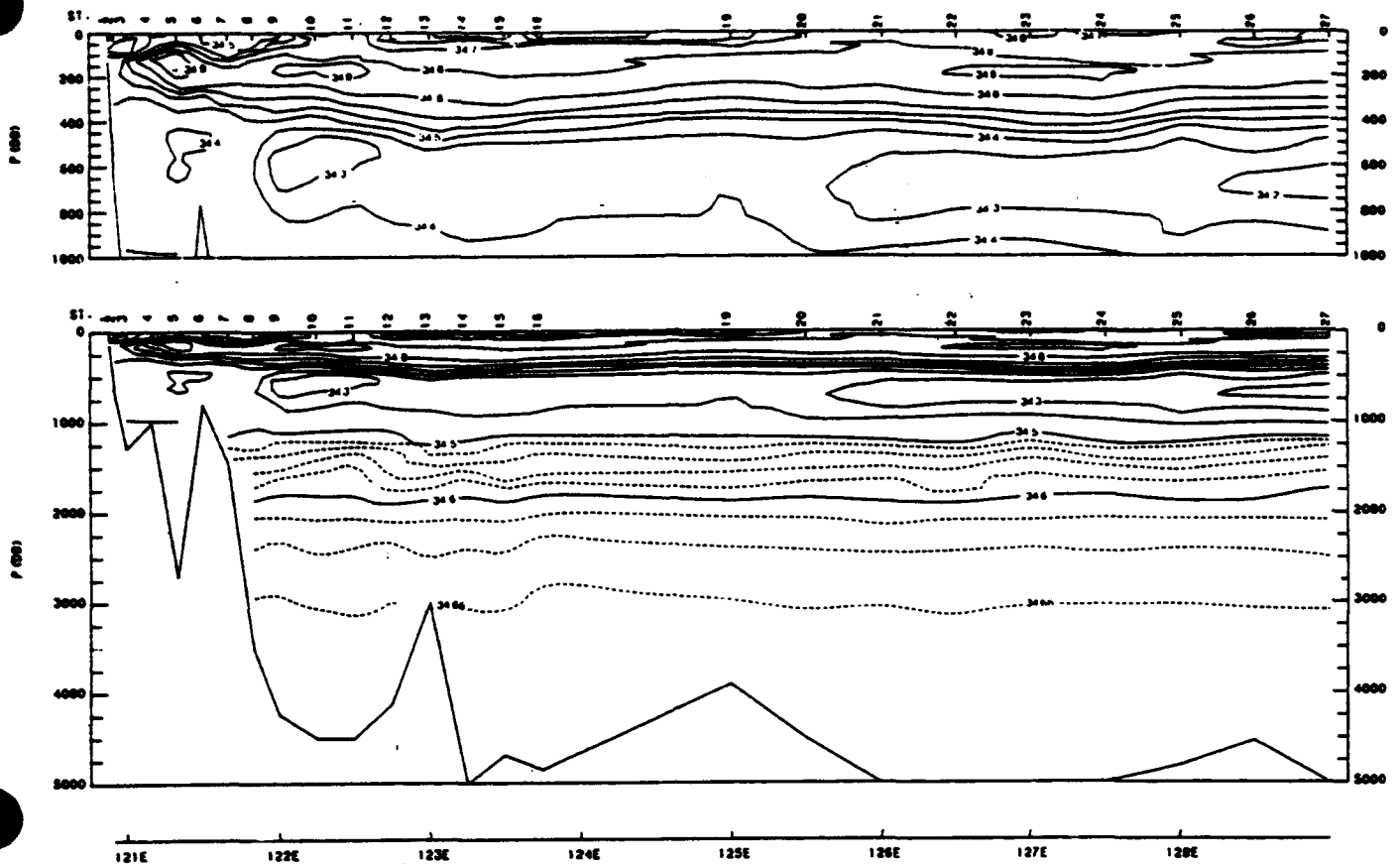


Figure 4.38: Sections of Salinity in psu (read ppm) Constructed from data obtained along 130°E during the (a) First and (b) Second Cruises of the US/PRC Cooperative Program; Station Locations are shown in Fig. 4.22 (adapted from Toole et al. (1988)).

SALINITY



OCEAN RESEARCHER I CRUISE: CHIPS-1

Figure 4.39: Section Plot of Salinity (adapted from Liu et al. (1986)).

6. Temperature versus Salinity. A plot of these variables is used to identify water masses in the oceans. Along the CHIPS-1 section (see Salinity-Depth discussion above) observations of potential temperature (θ) were plotted against salinity (S) for the water flowing northward across the section, and for the water flowing southward (see Figs. 4.40(a) and 4.40(b)). The envelopes of values that identify the open ocean watermasses are shown for the western North Pacific Ocean on those diagrams for Western North Pacific Water (WNPW) and for Equatorial Pacific Water (EPW). WNPW originates in the subtropics while EPW originates along the equator. When observed θ -S (or T-S) curves fall within the envelope which defines a watermass, it indicates no modifying influences (such as mixing with other waters having different characteristics) have been experienced as the water is carried away from its source region by ocean circulation. The results along 21°45'N CHIPS-1 section in the western Philippine Sea indicate some slight modification has occurred from WNPW toward EPW as the water has been carried along the western boundary of the North Pacific Ocean. There appears to be little or no difference between the northward and southward flowing water.

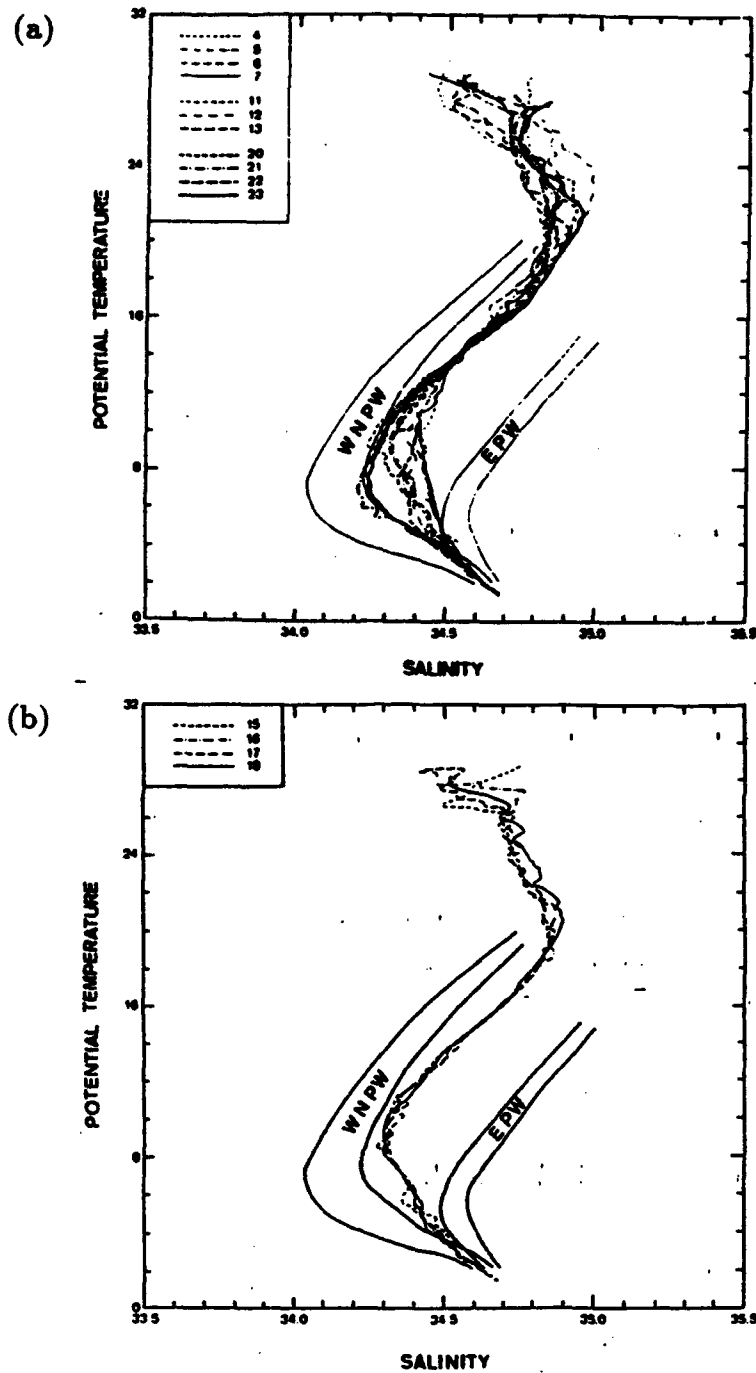


Figure 4.40: (a) θ -S Diagram for Stations that have Northward-flowing Water along 21.75°N. WNPW means the western North Pacific water type and EPW means the equatorial Pacific water type. Station numbers are indicated in the upper left corner, extending eastward from Taiwan from 121°E to 129°E. Longitude. (b) θ -S Diagram for ST. 15-18 for Southward-flowing Water (adapted from Liu et al. (1986)).

7. Mixed Layer Depth versus Wave Height. For the region just offshore from Taiwan, as described above in the temperature-depth section, Yin (1988) plotted the value of the highest 1/10 of the observed waves ($H_{1/10}$) against mixed layer depth (MLD) for the stations along the Ho and ST sections and obtained a linear best-fit correlation curve. The monthly variation of MLD at Station Ho-1 is shown in Fig. 4.41. The effects of the strong Northeast Monsoon winds are clear from November–January.

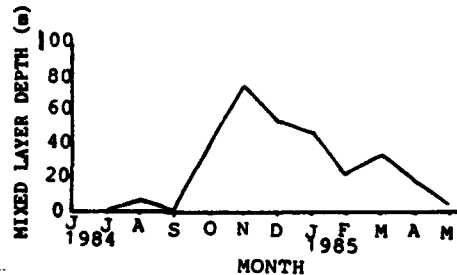


Figure 4.41: Variation of the Mixed Layer Thickness at Station Ho-1 (adapted from Yin (1988)).

8. Wave Height. Detailed statistics of wave heights have been analyzed over this region from ship data compiled between 1854–1987, with most observations taken from 1948–1987. Charts from the Naval Oceanography Command Detachment, Asheville (1989) are included in Appendix D. Wave heights are influenced strongly by surface winds; thus the greatest percentage of high waves occur during the wintertime periods of strong winds. In other seasons, approaching typhoons provide high waves in the region, especially on the right-hand side of the typhoon forward-motion vector. These storm waves are forecasted routinely along with the path of the typhoon and expected windspeed, as described in the case studies included in the handbook.

9. Visibility. The visibility underwater has been measured traditionally by observing the depth at which a white disc of standard size can no longer be seen from the sea surface: the Secchi Depth¹. A chart of this value, in meters, is shown for the Philippine Sea in Fig. 4.42. The values vary considerably, but generally occur in the range of 20 to 40 meters. Items which might reduce this value are plankton blooms or suspended sediment in nearshore regions.

¹Modern instruments and definitions for visibility have serious questions regarding the Secchi Depth observation technique. However, the mass of measurements by this technique still provide a means of comparison for this elusive underwater parameter that may be significant for the Navy diver or photographic operations.

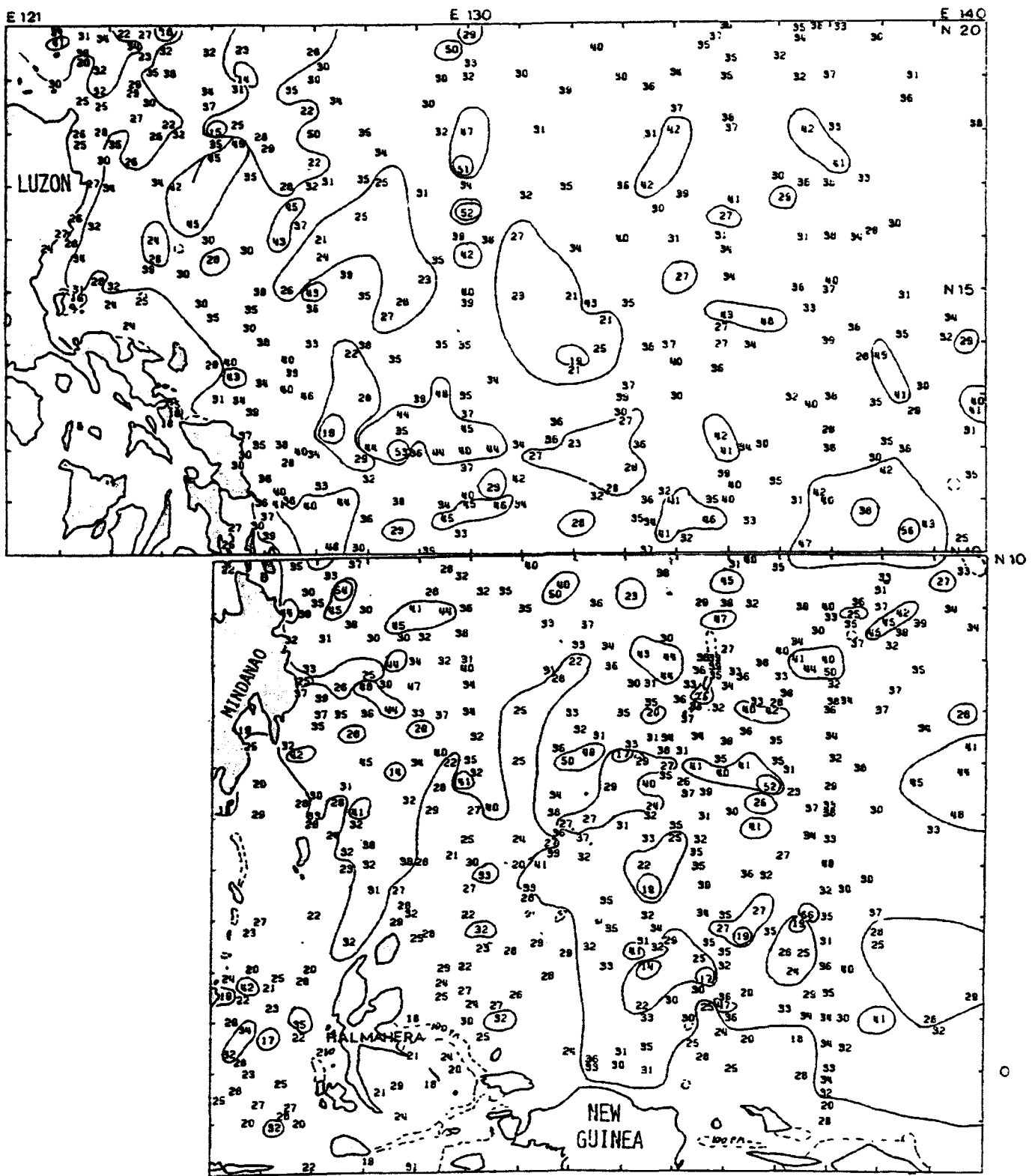


Figure 4.42: Entire Year, Secchi Depths, Philippine Sea and Pacific Ocean (2°S-20°N) (adapted from Murdock (1980)).

10. **Sediments.** Sediment covering the sea floor can affect several types of naval operations in an ocean region. The Philippine Sea adjacent to the Philippines is covered with lithogenous sediment (see Fig. 4.43). A preponderance of terrigenous and pelagic clay nearshore occurs there (Fig. 4.44(a)); some calcareous ooze occurs in Luzon Strait and off the southeastern coast of Luzon. Further seaward, south of 20°N, are regions of biosilicious ooze and mud; while north of 20°N, calcareous ooze and marl occur. A substantial area of pelagic "red" clay is shown near the Philippines in fig. 4.44(b), which further distinguishes the various sediment categories.

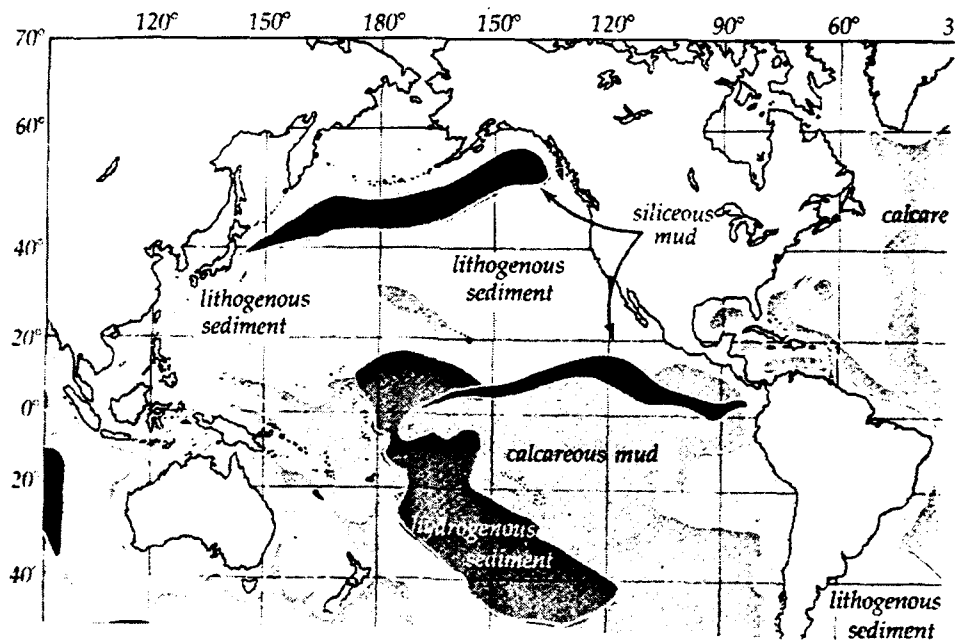


Figure 4.43: Distribution of Ocean Bottom Sediments (adapted from Ingmanson and Wallace (1973)).

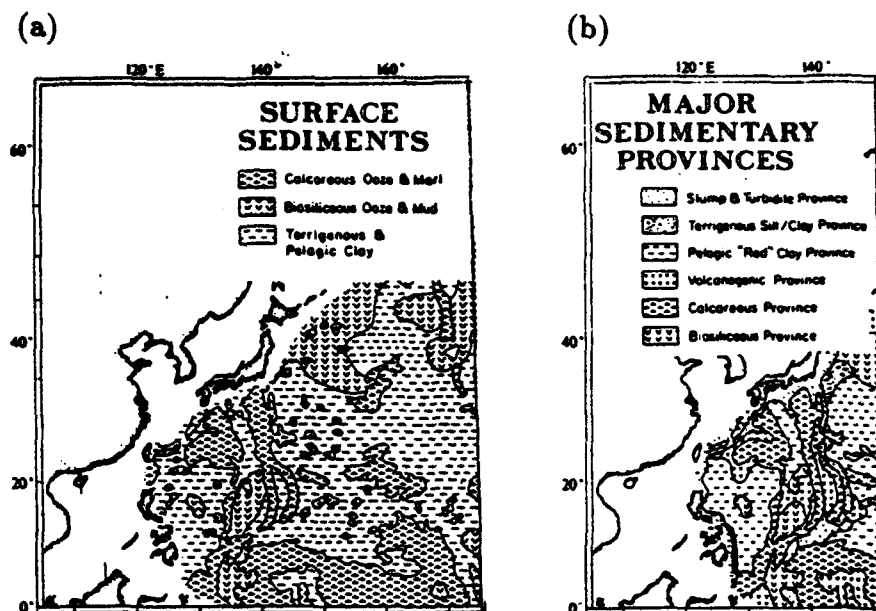


Figure 4.44: (a) Distribution of Surficial Sediments on the Seafloor of the North Pacific Ocean in Terms of the Three Major Types of Pelagic Sediments: Terrigenous and Pelagic Clays, Calcareous Oozes and Marls, and Biosiliceous Oozes and Muds. (b) Pelagic Sedimentary Provinces of the North Pacific Ocean (adapted from McCoy and Sancetta (1985)).

11. Sound Backscattering. A Russian study (Shevtosov et al. 1985) has presented results of backscattering of sound measurements for the western tropical Pacific Ocean (see Figs. 4.45(a) & (b) and 4.46). In Fig. 4.45(b) averages for night conditions are shown for 30 kHz sound (line 1); for 12-kHz sound (line 2), and the sound velocity profile (line 3). At night, the backscattering signal level for both frequencies is low at the sea surface, but increases through the mixed layer and thermocline layer (at 100–150 meters depth). The 30-kHz scattering decreases abruptly below that depth, while the 12-kHz scattering decreases erratically and much more gradually. The 12-kHz values are considerably larger at and below the maximum value, through all depths to 750 meters.

The maximum backscattering values for daytime conditions in Fig. 4.45(a) are much smaller than for night, never approaching the minimum values shown for night. The daytime values are much more consistent with depth, but indicate some layering which is not at the same depth for both frequencies.

In Fig. 4.46, the indicated migrating sound scattering layer (1) in the upper levels is consistent with the contrasting scattering levels between day and night shown in Table 4.2 and in Fig. 4.46. The deeper layering "of a physical nature" also shows that consistency.

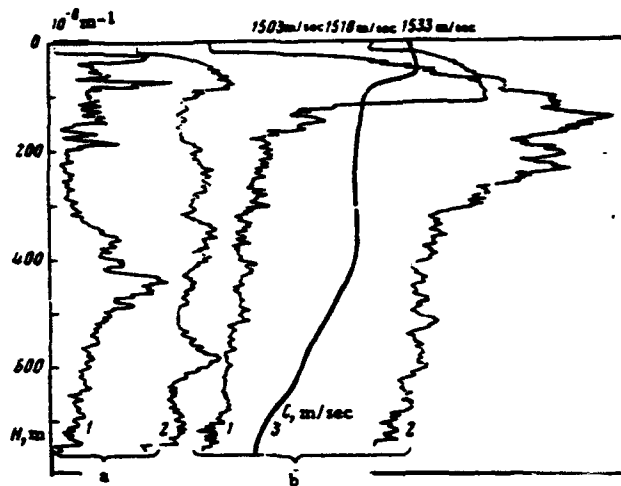


Figure 4.45: Profiles of the Backscattering Signal Level, averaged over 100 Pulses at 2.5-sec Intervals, for 12- and 30-kHz Frequency Sound, obtained during the Day (a) and Night (b) in the Tropical Zone of the Pacific Ocean: 1) 30-kHz frequency; 2) 12-kHz frequency; and 3) Vertical Profile of the Sound Velocity (adapted from Shevtosov et al. (1985)).

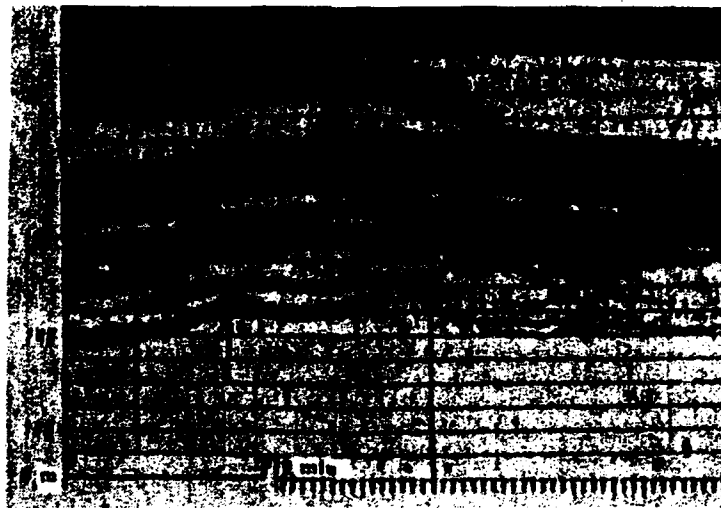


Figure 4.46: Comparative Trace of Acoustic Inhomogeneities of a Physical Nature and a Migrating Sound-scattering layer (SSL): 1) Migrating SSL; 2) Acoustic Inhomogeneities of a Physical Nature (adapted from Shevtosov et al. (1985)).

Table 4.2: Layer-Averaged Values of the Backscattering Intensity for 30-kHz Frequency Sound from the Results of Measurements at Stations Typical of the Southern and Northern Regions of the Northwest Pacific Ocean (Shevtosov et al. 1985)

Depth, m	Backscattering intensity dB per 1 m^{-1}				Noise
	Northern region		Southern region		
	Day	Night	Day	Night	
20-75	-90	-85	-76	-70	-125
75-150	-100	-90	-70	-62	-118
150-225	-95	-95	-73	-65	-113
225-300	-96	-97	-74	-74	-109
300-450	-	-	-65	-70	-103
450-600	-	-	-68	-76	-98
600-750	-	-	-70	-72	-93

12. **Tides.** Tide reference stations in the Philippine Islands are located at Cebu, on Cebu Island; at Davao, on Davao Gulf on Mindanao; at Jolo, on Jolo Island in the Sulu Archipelago; at Legaspi Port on Albay Gulf, southeastern Luzon; at Manila on Manila Bay, Luzon; and at San Fernando Harbor on Lingayen Gulf, Luzon (see Tide Tables for 1990, U. S. Dept. of Commerce National Ocean Service, 1989). The time and height of high and low waters is given daily through the year for these reference stations. Current year tide tables may be purchased from National Oceanic and Atmospheric Administration (NOAA) Distribution Branch, 6501 Lafayette Ave., Riverdale, MD 20737, telephone (301) 436-6990.

B. South China Sea (northern portion)

The major northern islands of the Philippines (especially Luzon and Mindoro) and Palawan are bounded to the west by the northern portion of the South China Sea (see Fig. 4.47). This Sea fills a broad, deep central basin of >4000 meters depth that extends eastward into the Manila Trench (>4000 meters) and into the Palawan Trough (>3000 meters) as shown in Fig. 4.47. To the northwest there are very broad and shallow shelf regions, less than 200 meters in depth, along the Vietnamese and Chinese coasts and extending into the Formosa (Taiwan) Strait.

1. Current Circulation Patterns. Since the South China Sea is a marginal basin along the Asian continent, it is influenced greatly by the monsoon circulations in the atmosphere there, which reverse direction between winter and summer.

The strong Northeast Monsoon in February is shown by the inset diagram (upper right) in Fig. 4.48(a). The resultant ocean currents have a counter-clockwise circulation. Much of the South China Sea is occupied by currents directed generally toward the west or southwest; a narrow strong current flows to the south along the western boundary (Asian coastline); eventually this water flows toward the southeast between Borneo and Sumatra into the Southern Hemisphere.

By August, the Southwest Monsoon is blowing strongly (see inset diagram on Figure 4.48(b)) over this region. The resulting currents have also reversed direction, moving toward the northeast over most of the South China Sea. Water enters the Sea from the Southern Hemisphere between Sumatra and Borneo and it exits through both Formosa and Luzon Straits at the northern end.

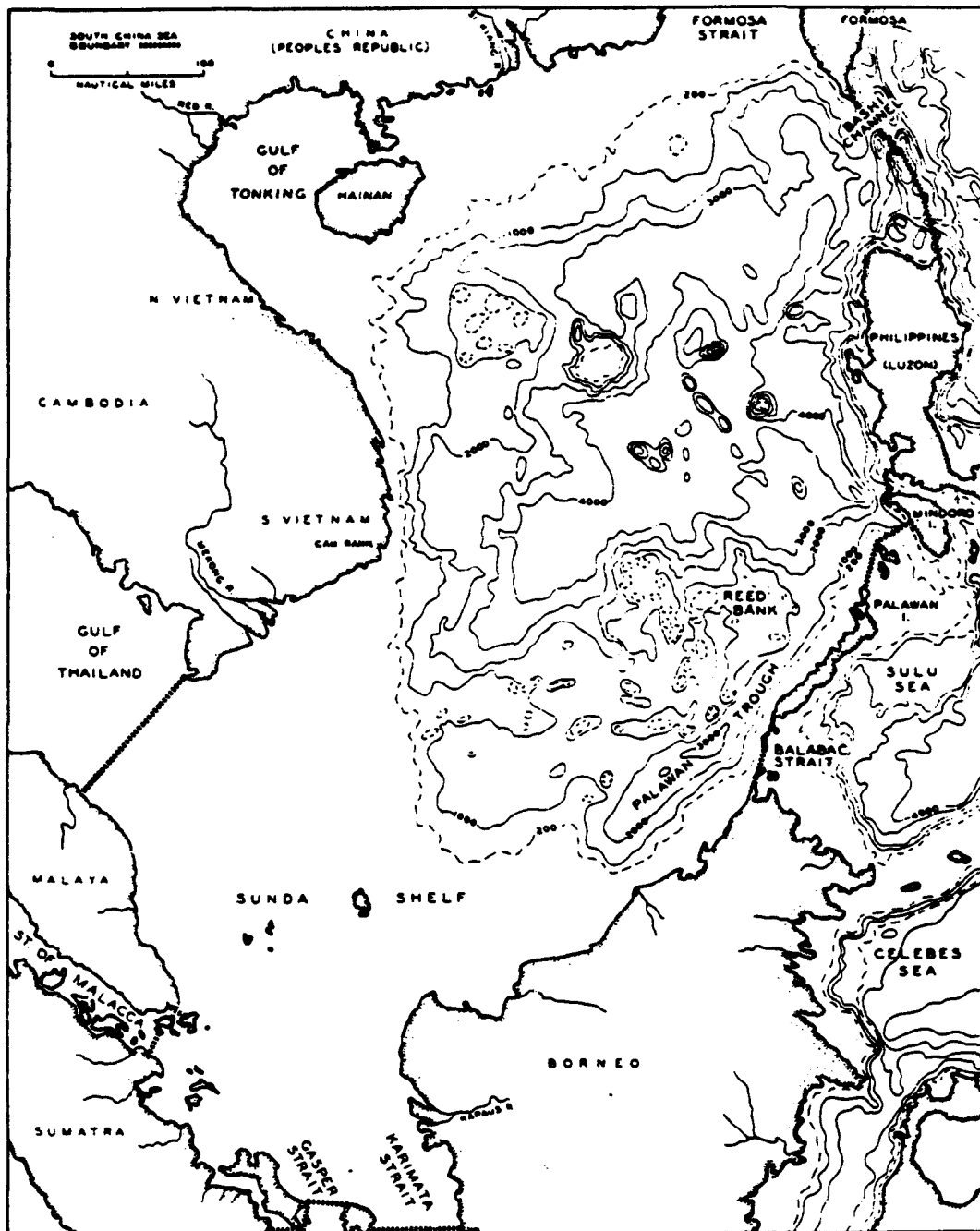


Figure 4.47: General Topography and Boundary Features of South China Sea (contours in meters) (adapted from LaFond (1966)).

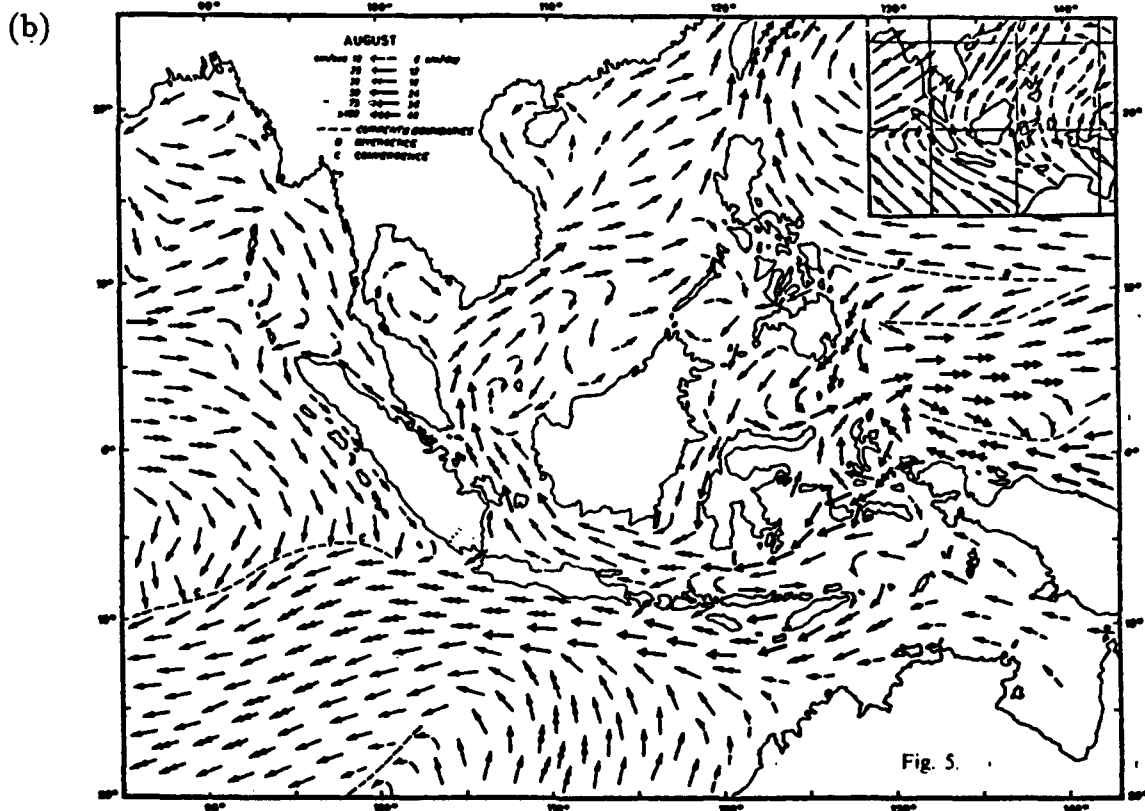
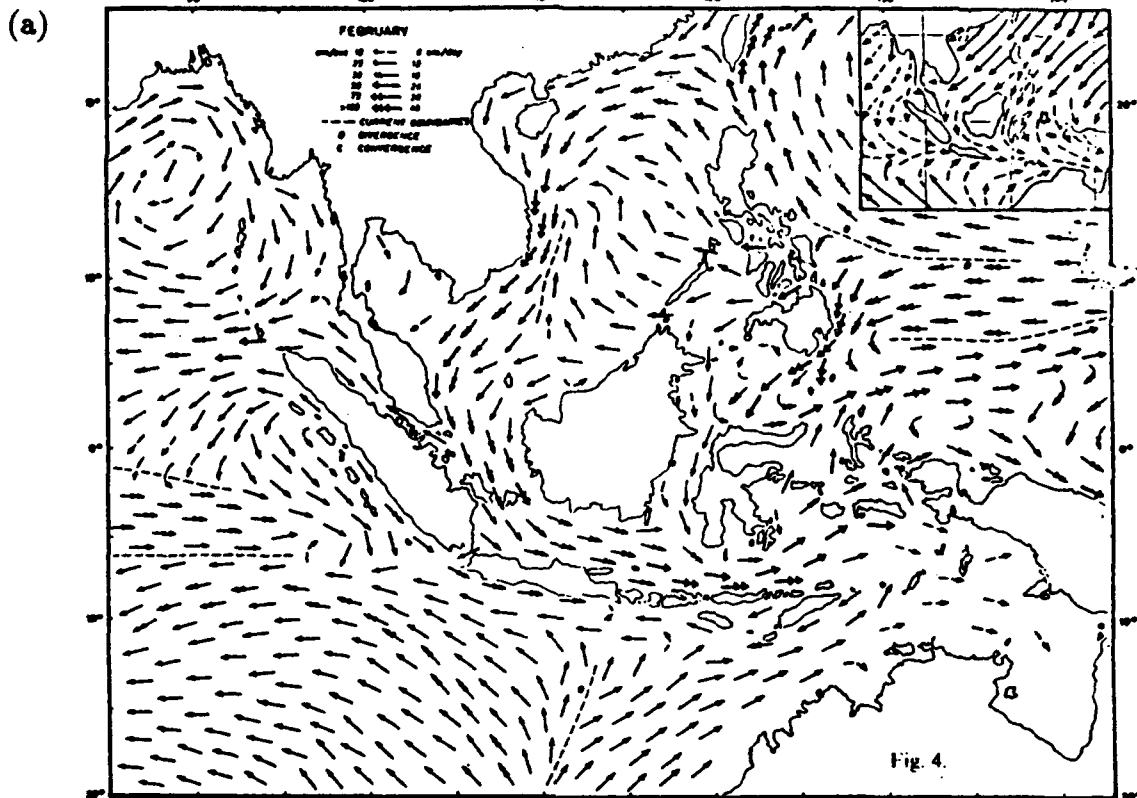


Figure 4.48: Sea Surface Current Distribution for South China Sea: (a) February and (b) August. Inset diagrams show surface winds that reverse seasonally (Monsoon Winds) (adapted from LaFond (1966)).

In a study in 1985–1986, a number of stations were sampled off the southwestern coast of Taiwan, in the northernmost part of the south China Sea (see Fig. 4.49(a)). The bottom topography is shown in Fig. 4.49(b); the depths vary considerably in this slope region, from less than 100 meters in Taiwan Strait to over 2000 meters further south. Figure 4.50 illustrates the current pattern reversal between July (Southwest Monsoon) and October (Northeast Monsoon).

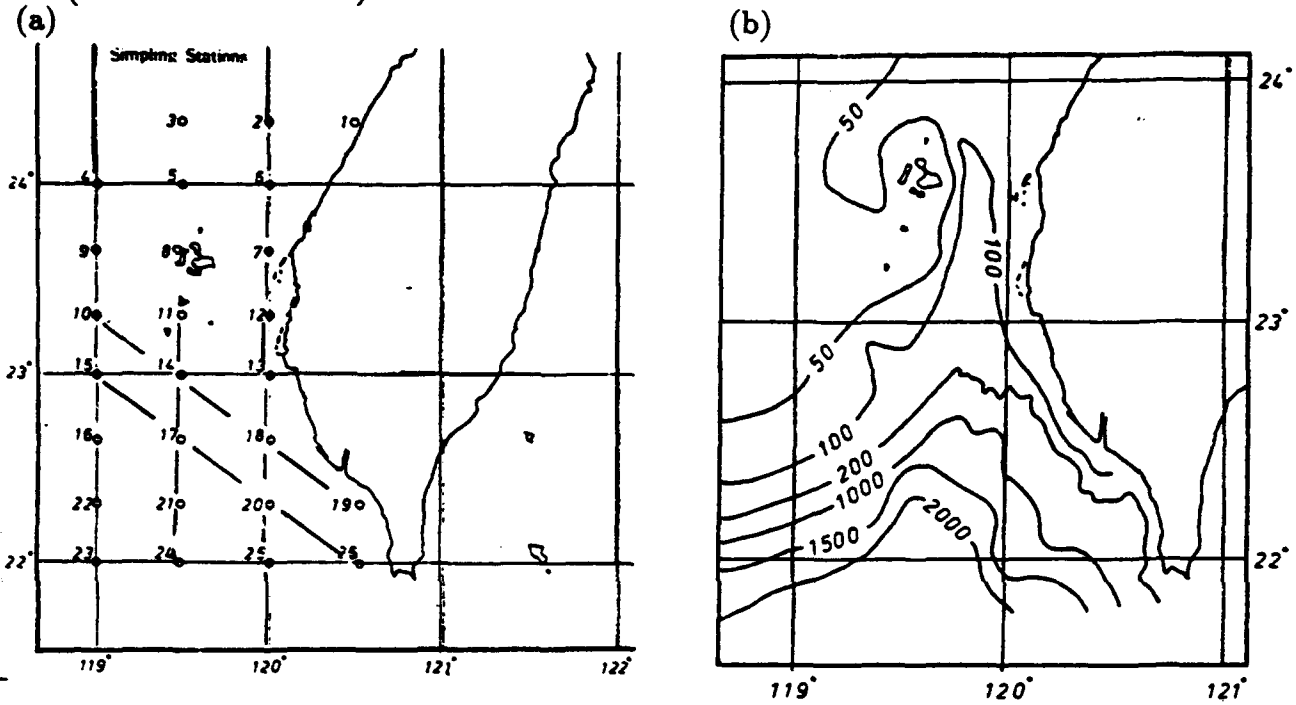


Figure 4.49: (a) Sampling Locations along the Southwestern Coast of Taiwan. (b) Bottom Topography of Southwestern Coast of Taiwan (adapted from Hung et al. (1986)).

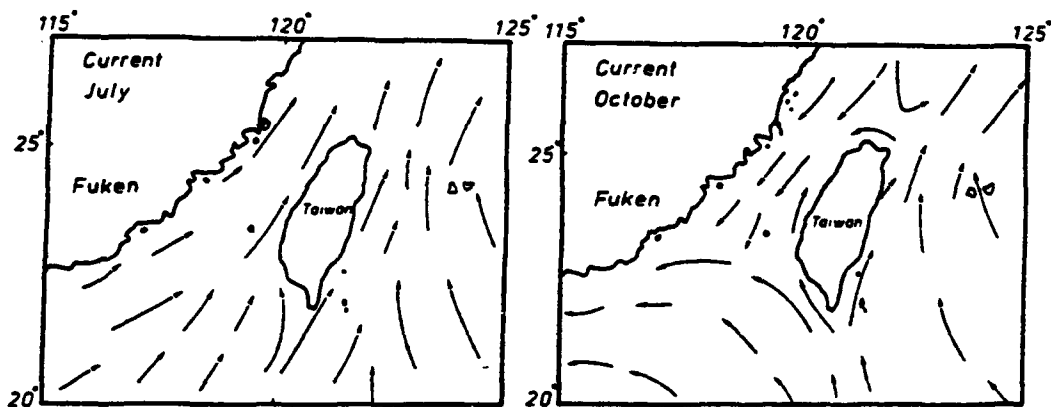


Figure 4.50: Currents Patterns surrounding Taiwan (adapted from Hung et al. (1968)).

2. Sea Surface Temperature. The charts shown in Figs. 4.17 and 4.18 indicate the seasonal changes that occur, while sea surface temperatures for each month are included in Appendix A. In February there is a broad region of the Philippines which show temperatures of 26° to 27°C. Extending to the southwest of northern Luzon, the 26° isotherm marks the southeastern limit of a sea surface temperature gradient that occupies the region to the northwest. The 22° isotherm that extends west-southwestward from Taiwan marks the southern boundary of a very strong temperature gradient that occupies the Taiwan Strait region and the China coastal area. The temperature drops to 14°C in Taiwan Strait.

By May, effects of the spring warming have developed temperatures over 29°C (the seasonal maximum value for this region) over a broad area of the eastern South China Sea. Toward the north, a weak temperature gradient occurs, with temperatures below 23°C in Taiwan Strait.

In August, temperatures lie between 27 and 29°C over the region, with most areas showing 28.5 to 29°C. By November, cooling has established temperatures as low as 21°C in Taiwan Strait, and temperature gradients are increasing over the region; most areas show temperatures from 28.5 to 26°C.

3. Temperature Variation with Depth. Observations were made in a series of studies to the southwest of Taiwan at locations shown in Fig. 4.49(a). These stations were sampled 9 August and 11 October 1985; and on 2 March and 25 May 1986 (see Fig. 4.51). Sections of temperature from the sea surface to the bottom, or to a maximum depth of 200 meters, are shown along the lines of stations drawn in this figure: line 10-19; line 15-26; line 11-24; and line 12-25. The first two lines are oriented NW-SE at two different distances offshore. The other two lines are oriented N-S, also at two different distances offshore. The four sections are arranged in the figure so the seasonal variation can be traced easily from left to right (Summer, Fall, Winter (lower right) and Spring (upper right)); the sections are arranged vertically with those oriented NW-SE above the N-S sections. The temperature distributions display the usual seasonal variation; the seasonal thermocline reaches the sea surface in summer, and then descends below a cooler mixed layer that forms during the fall and winter (especially evident in water over the greater depths. The thermocline gradient increases as the seasonal cooling and deepening proceeds.

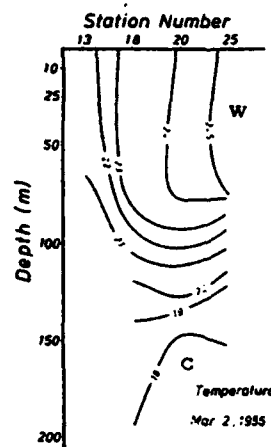
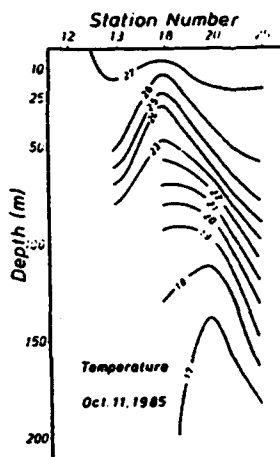
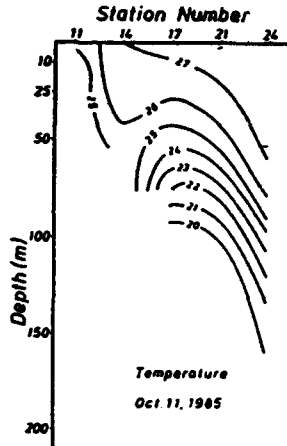
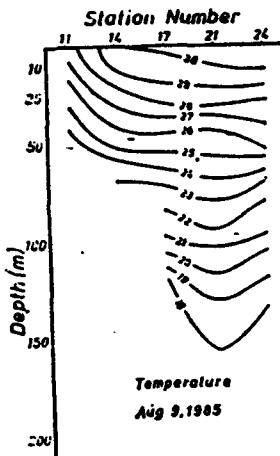
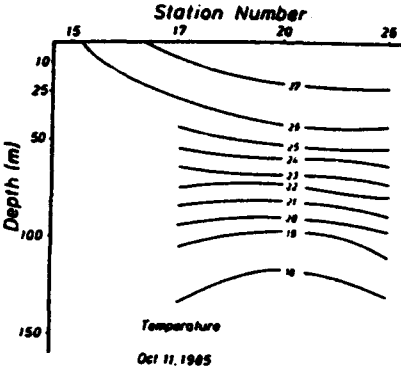
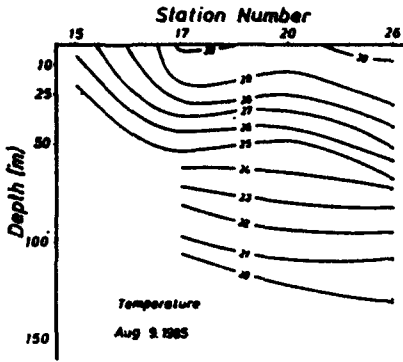
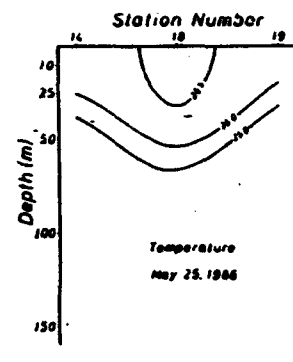
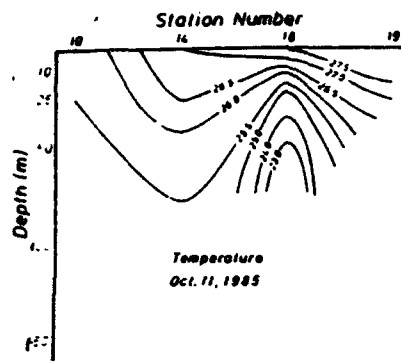
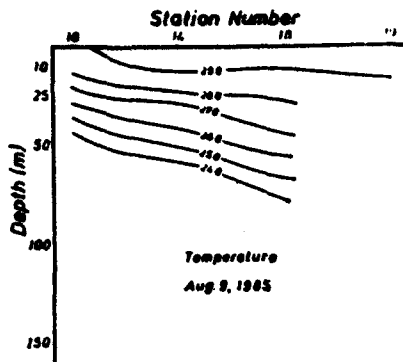


Figure 4.51: Temperature ($^{\circ}\text{C}$) versus Depth (meters) along the Various Sampling Lines in Fig. 4.49(a) (adapted from Hung et al. (1986)).

4. Salinity. The winter (February) salinity distribution at the sea surface shows effects of the counterclockwise circulation during the Northeast Monsoon (see Fig. 4.35(a)). Water with salinity values in excess of 34.0 ppm enters through the Luzon Strait from the Philippine Sea, and gradually becomes modified to lower values (to 33.3 ppm) as it is carried to the southwest along the Chinese and Vietnamese coasts. Water with lower salinity (33.0 ppm) moves to the north along the eastern half of the South China Sea; it gradually is increased during its movement northward. Salinity values along Palawan and the west coasts of the northern Philippines range from 33.2 to 34.0 ppm. The summer (August) salinity distribution shows the influence of the southwest Monsoon (see Fig. 4.35(b)). The strong currents from the southwest along the western boundary carry water with lower salinity (33.0 ppm) into the western South China Sea. This forces the tongue of higher salinity water offshore into the middle of the Sea. The lower salinity tongue cuts across from SW-NE from Vietnam to northern Luzon and forces the higher salinities to the region northward from about 15°N.

5. Salinity Variation with Depth. The sections with the observations taken to the southwest of Taiwan are shown in Fig. 4.52, similar to those shown earlier for temperature. These seasonal salinity changes closely follow those of temperature. In August, the salinity values increase from the low values (33.0 to 33.7 ppm) at the surface toward a layer of maximum salinity (34.5 to 34.7 ppm) that occurs at about 100 meters depth. The salinity gradient is strongest at the top of the (temperature) thermocline region, weakening somewhat at greater depths.

In October, surface salinity values are higher (33.8 to 33.9 ppm), and the gradient increases with depth through the observed water column to values of 34.7 or 34.8 ppm at the greatest depths observed (no evidence of the salinity maximum layer shows at these depths). Strong salinity gradients occur associated with the deeper thermocline.

In March, the one section observed shows no evidence of strong salinity gradients anywhere in the 150-meter layer adjacent to the surface. The salinity values there are as high (34.65 to 34.8 ppm) as the maximum values observed at any depth in other seasons.

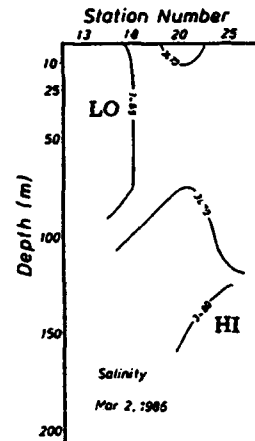
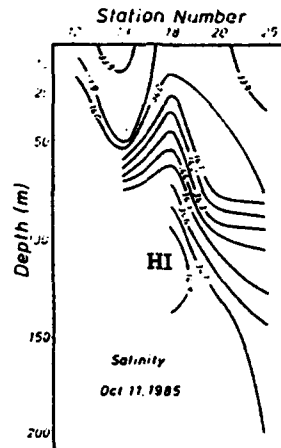
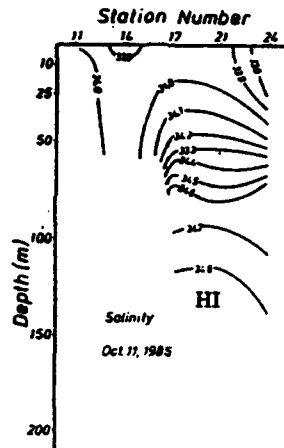
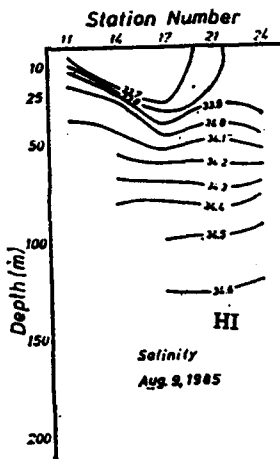
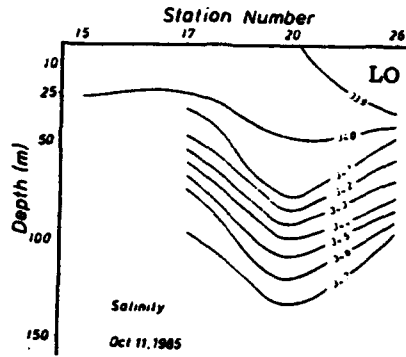
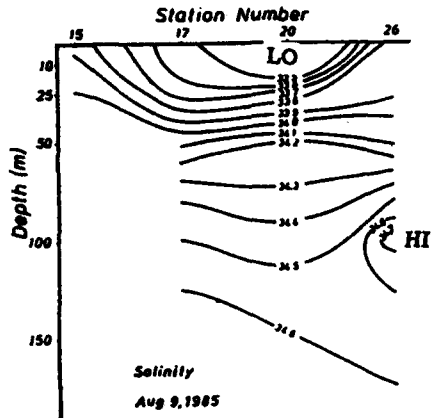
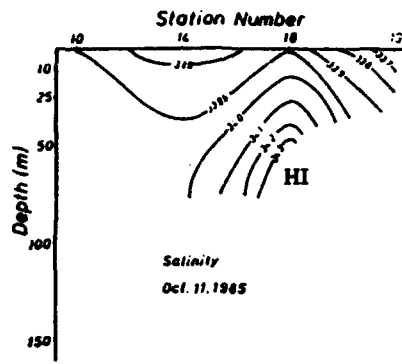
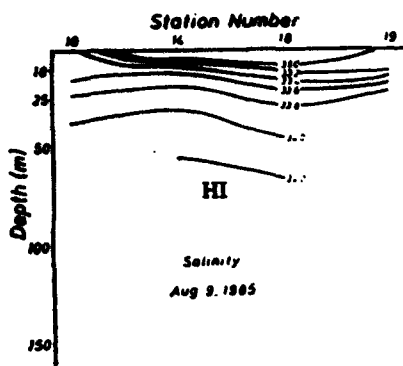


Figure 4.52: Salinity in ppm versus Depth (meters) along the Various Sampling Lines in Fig. 4.49(a) (adapted from Hung et al. (1986)).

6. Temperature versus Salinity Relation. Summer cruise observations (August–September 1970) are plotted from locations shown by Fig. 4.53(a) in the northern South China Sea and are shown in Fig. 4.53(b). Most of the values are in the upper 150 meters. The low surface salinities increase abruptly at the top of the thermocline and then generally increase gradually as temperatures decrease down to near 150 meters depth.

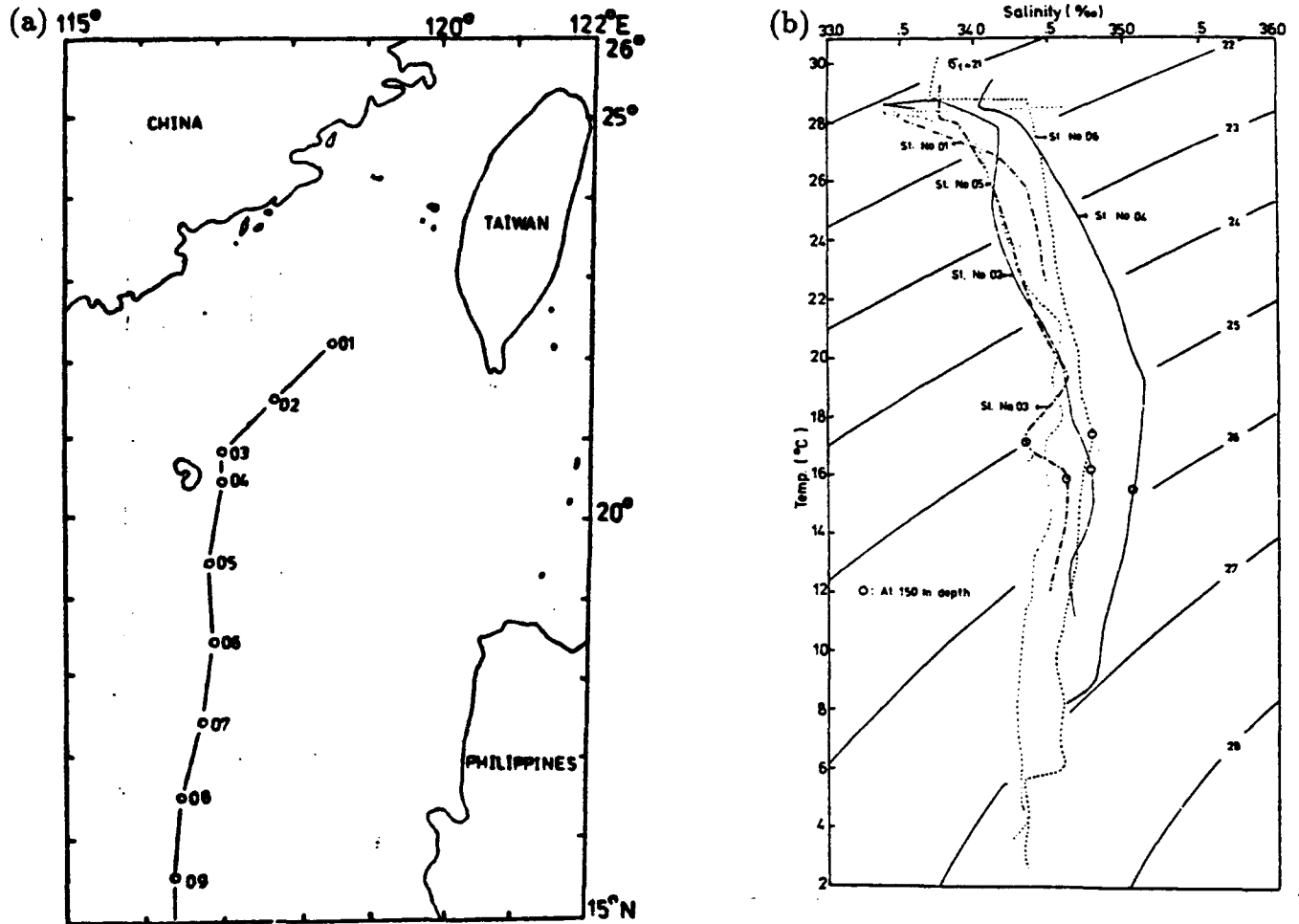


Figure 4.53: (a) Some of the Stations in the South China Sea Cruise in 1970. (b) TS-diagrams for the Six Selected Stations from South China Sea Cruise in August-September 1970 (adapted from Fan and Yu (1981)).

7. Upwelling. Seasonal upwelling is supported by the study from which the salinity and temperature observations with depth were reported above (see Fig. 4.51); other nutrient and chemical observations were made which support seasonal upwelling at some stations in the region off southwestern Taiwan, during August and October, 1985; the upwelling appeared to shift to other stations during the Northeast Monsoon (December and March), and then return to the original stations with the onset of the Southwest Monsoon in May. Currents from the South China Sea, northern China coast and the Kuroshio Current appear to influence this upwelling, in addition to effects from bottom topography and the monsoon winds. An extension of this study into an adjacent region (to the north) was reported in Hung et al. (1987), with observations made in September & December, 1986; and in February & May, 1987.

8. Transparency. Values of Secchi Depth are reported for the northern South China Sea for the winter (December–March) and for other seasons (April–November); see Murdock (1980), Figs. 4.54(a) & (b). Values less than 20 meters occur in Taiwan Strait and along the China coastline in both charts; the low values extend further offshore from China during the winter, and a tongue of low value extends southwest from Taiwan and Bashi Strait. Few locations show values greater than 30 meters.

The remainder of the year, however, shows more regions with greater depths; the small values (20 meters or less) occur generally very close to adjacent coastlines.

Figure 4.55 shows the annual values for the central region of the South China Sea. Features here resemble those for the northern section in April–November (see Fig. 4.54(b)).

9. Typhoon Surge Model. A study (Li and Su 1987) has reported the development of a model that calculates sea level changes that combine effects of typhoons approaching Taiwan and the astronomical tide. Typhoon surges during periods of spring tides (during full or new moon phases) have caused coastal lowland flooding. Air pressure gradient and windstress are considered the driving forces for the typhoon surge. The model was tested by use with conditions during Typhoon Wayne, which struck western coastal Taiwan with great resulting damage. The observed sea surface height agrees well with the model computations.

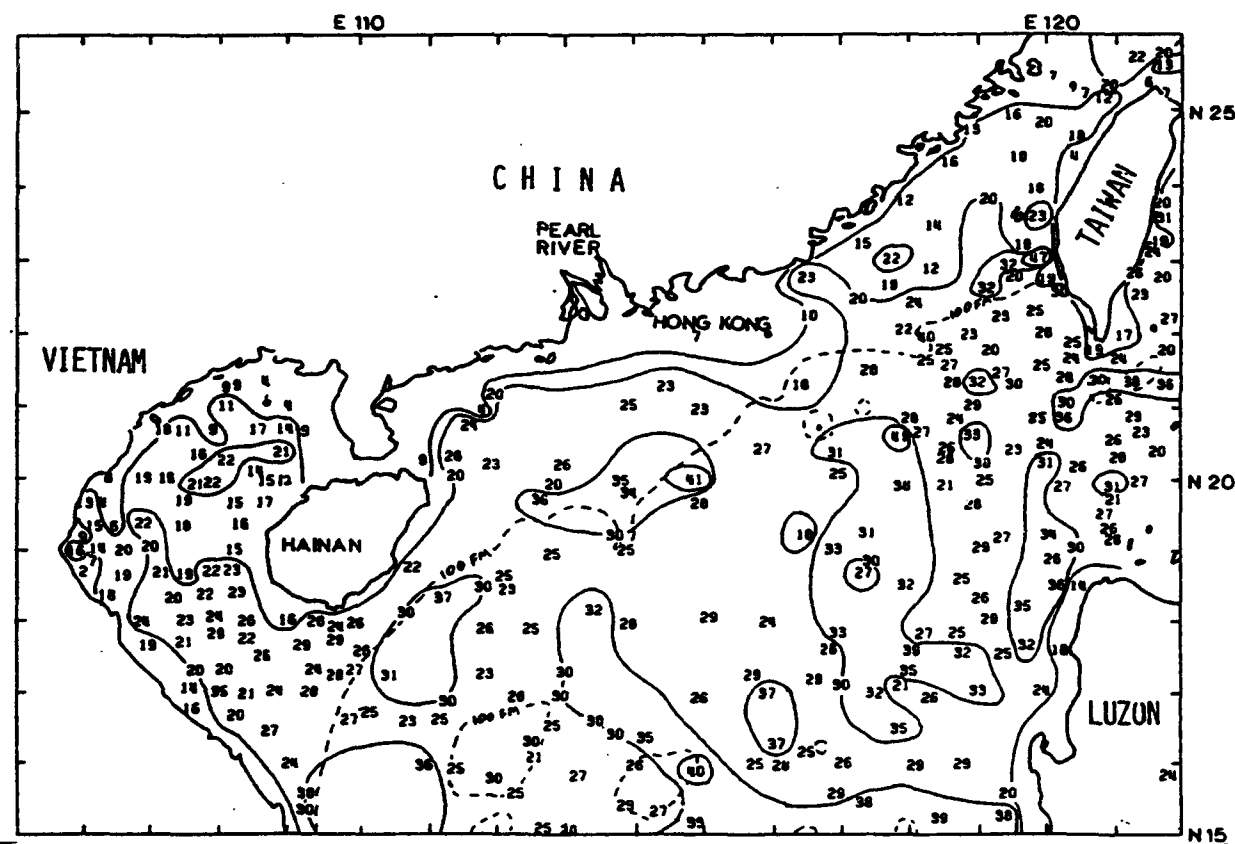
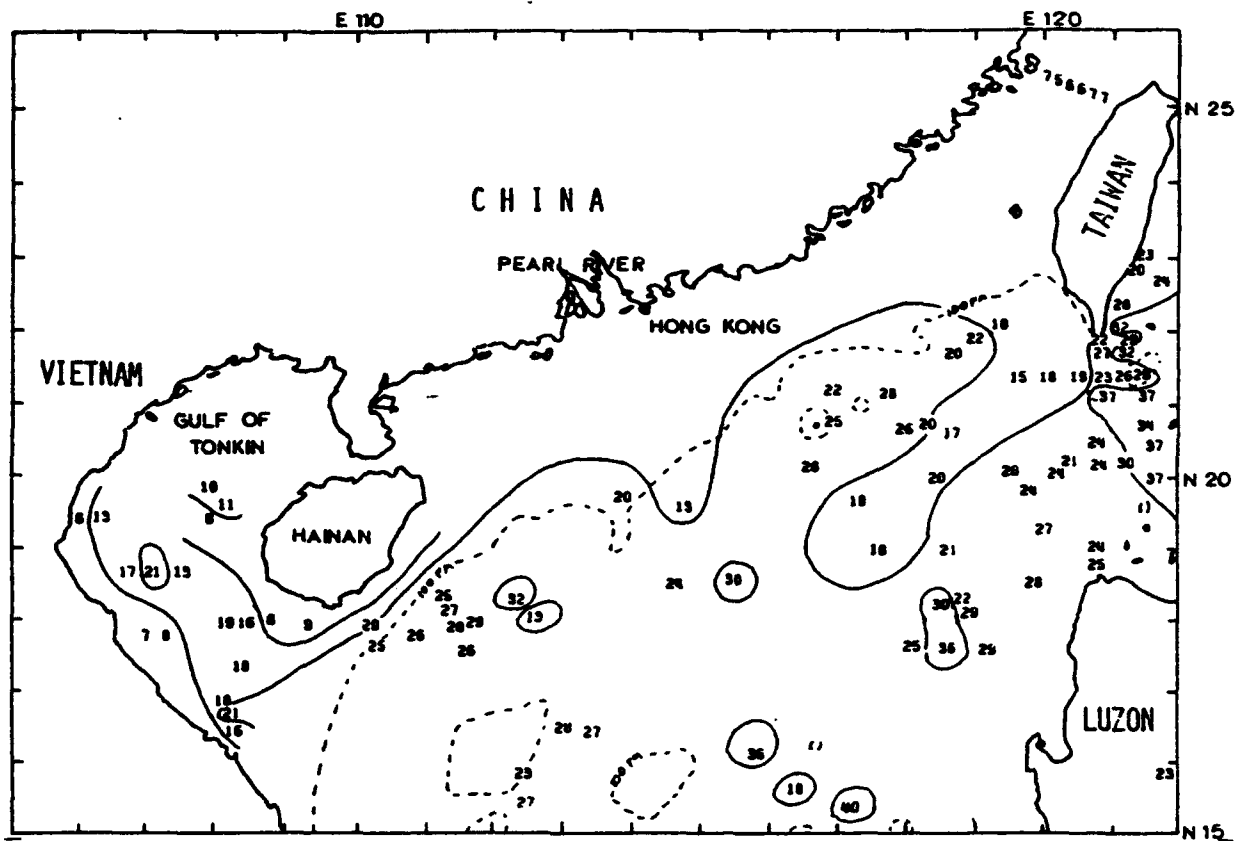


Figure 4.54: Secchi Depths, South China Sea (Northern Section), (a) DEC-MAR & (b) APR-NOV (adapted from Murdock (1980)).

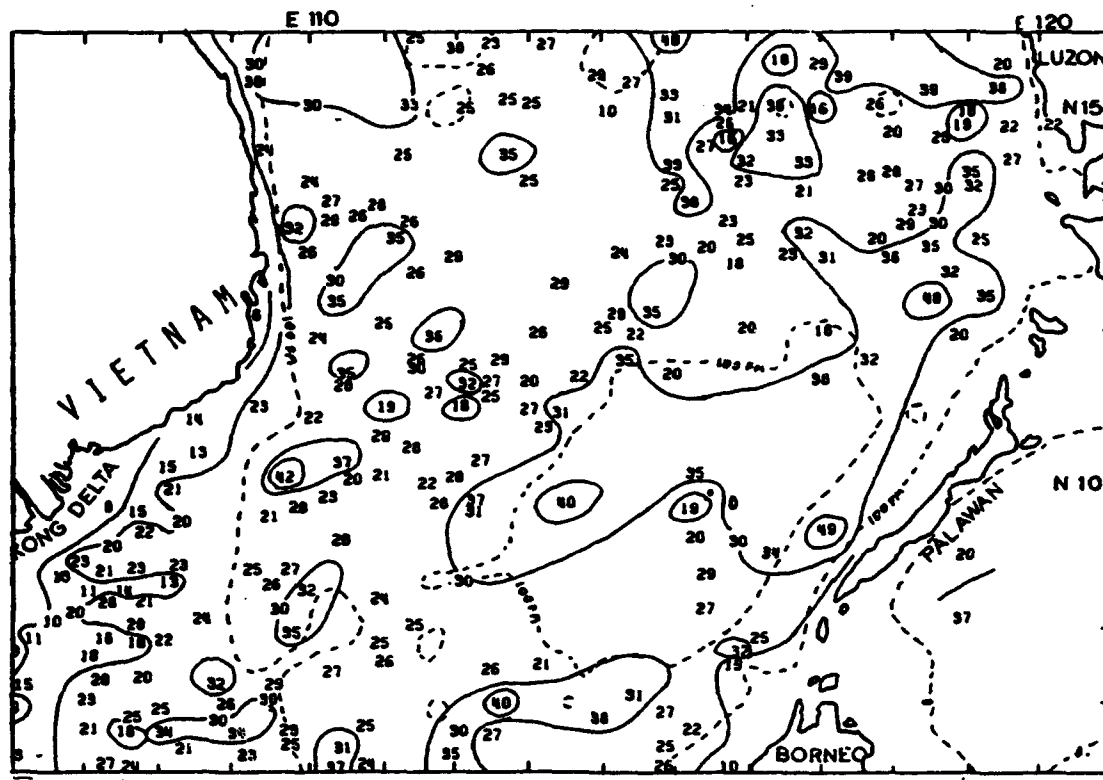


Figure 4.55: Secchi Depths, South China Sea (Central Section), Entire Year (adapted from Murdock (1980)).

10. Turbidity Currents. Current meter records have been made of turbidity currents that flowed in Abra Canyon off the Abra Delta along the northwest coastline of Luzon, during flood conditions (Shepard et al. 1977). Figures 4.56, 4.57, & 4.58 illustrate flow characteristics of such currents along a canyon floor: Fig. 4.56 shows one instance of up-canyon flow, followed by strong down-canyon flow for many minutes before a lull interval. Figure 4.57 indicates this type of alternating flow occurred many times in Abra Canyon (at a depth of 622 meters). The turbidity current extends at least 30 meters above the canyon floor. Figure 4.58 illustrates the assymetry of the current with time; a rapid build-up occurs to the peak speed, followed by a slow decay, down to zero current.

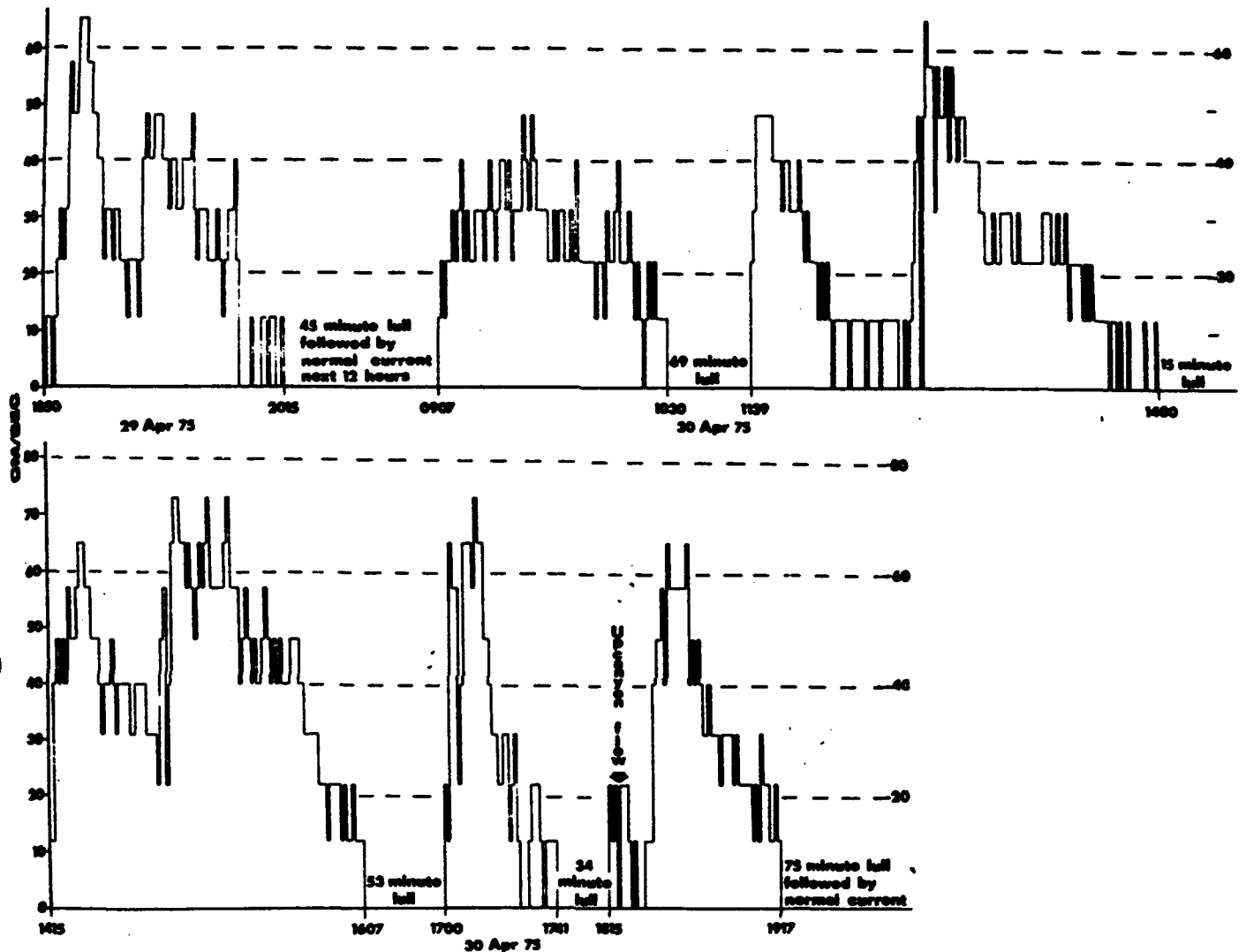


Figure 4.56: One-minute Current Averages during the Strong Downcanyon Surges in Rio Balsas Canyon (depth = 285 m). Note length of time with no measureable current following the flows. Also note that only one period of upcanyon flow was observed (at time = 18:15). The steplike changes are due to nature of recording for 1-min averaging, each step representing one additional mark on the tape during the 1-min period (adapted from Shepard et al. (1977)).

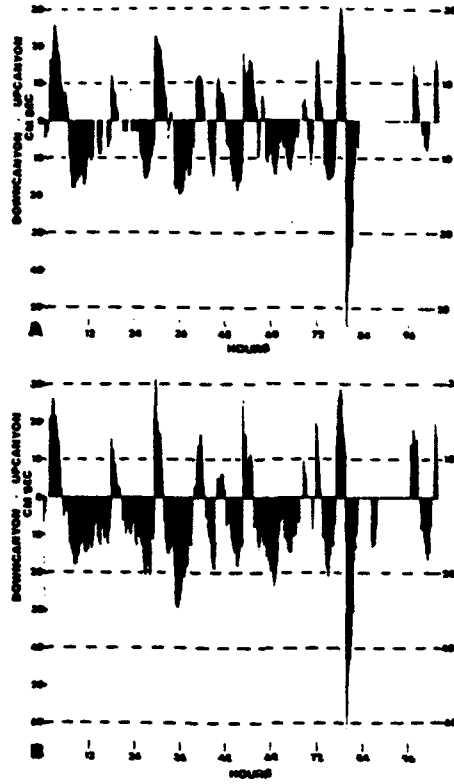


Figure 4.57: Turbidity Current in Abra Canyon off Northwest Luzon (depth = 622 m). The velocity profile shows (A) 5-min averages at 3 m above the bottom and (B) 7.5-min averages for 30 m above the bottom (1 min for peak flow) (adapted from Shepard et al. (1977)).

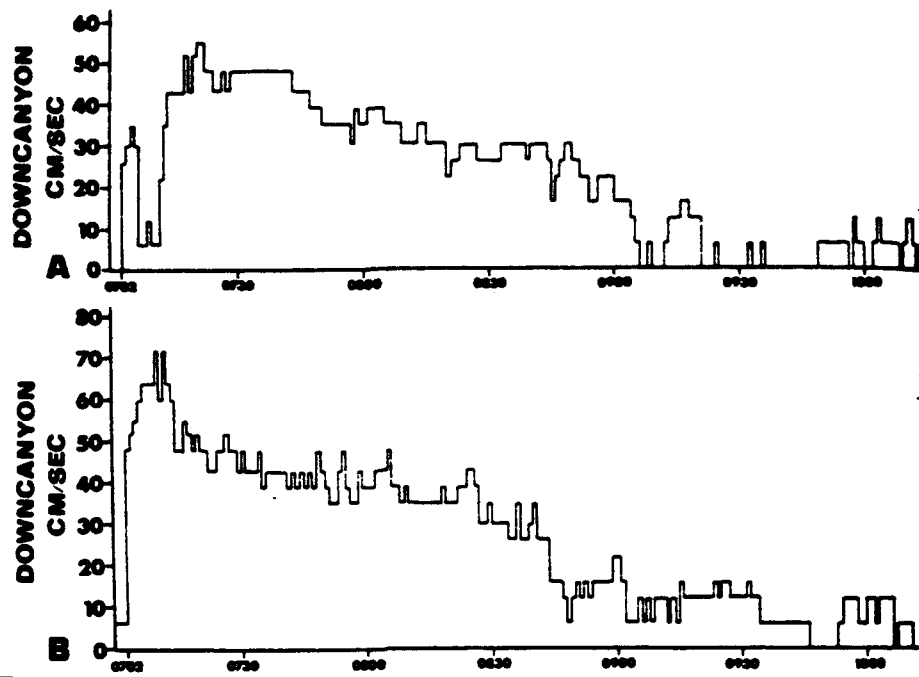


Figure 4.58: One-minute Averages for Current Velocities during the Abra Canyon Turbidity Current (depth = 622 m). Note rapid build-up to the peak and the slow decay to the period of no measurable velocity. A. 30 m above the bottom; downcanyon flow followed by an amazingly long period (14.5 h, not shown in the figure) of no velocity. B. 3 m above the bottom; downcanyon flow followed by 3.5-h lull (not shown in the figure) (adapted from Shepard et al. (1977)).

C. Sulu Sea

This is a basin that lies to the west of Mindanao; it is bounded on the northwest by Palawan and to the northeast by the Philippine Islands Mindoro, Panay, and Negros (see Fig. 4.1). The Sulu Archipelago and northeastern Borneo provide the southeastern and southwestern boundaries (see Fig. 4.59; and Fig. 4.60). Broad coastal shelves appear along those southern coastlines, as well as to the northeast of Palawan. A few locations reach depths greater than 5000 meters along the eastern perimeter off Mindanao and Negros. Note Basilan Island just south of Mindanao. Between Basilan and Mindanao lies Basilan Strait, which separates the major Philippine Islands from the Sulu Archipelago.



Figure 4.59: Sulu Sea and northern Sulawesi (Celebes) Sea shows bathymetry (depths greater than 5000 m are shaded); flow of bottom water (arrows); and bottom sediments: T = terrigenous mud; G = globigerina ooze; C = coralline mud and sand; VT = volcanic and terrigenous mud; V = volcanic mud (adapted from Tjia (1966)).

1. Current Circulation Pattern. The surface current pattern undergoes a seasonal change in direction; currents are from the east and northeast in February (see Fig. 4.48(a)), but they adopt a clockwise circulation pattern in August (Fig. 4.48(b)), when inflow from the west occurs north of Palawan to replace the outflow to the west found there in February.

2. Sea Surface Temperature. Figures 4.16 (a) and(b), 4.17, 4.18 and Appendix A all display the seasonal and monthly variation in sea surface temperature in areas adjacent to the Philippine Islands. Discussion of these figures is given on Page 4-20, to which the reader is referred. In the Sulu Sea the sea surface temperature in May varies from 29.0° to 29.5°C; it becomes one degree lower in August and November. The horizontal gradient is extremely small in all seasons.

3. Temperature Distribution with Depth. At locations SS2 and SS3 shown in Fig. 4.61, average T-Z soundings (Fig. 4.62) are shown (Apel et al. 1985); data from two additional stations are given (Fig. 4.63). In each case, no mixed layer is evident, and a pronounced thermocline extends from the surface (temperature at about 29°C) to about 200 meters depth. The temperature continues to decrease slowly to 500-600 meters depth and then appears uniform below, at about 10°C.

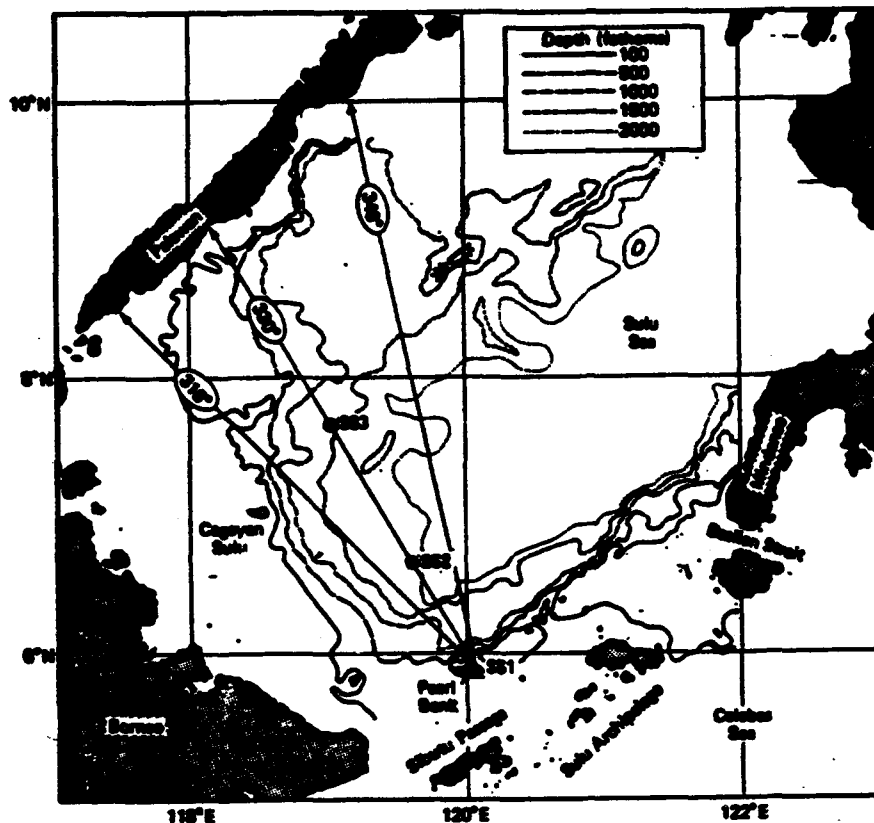


Figure 4.61: Bathymetry of Sulu Sea, showing Locations of Current Meter Moorings SS1, SS2 and SS3 and Radius from Soliton Source near Pearl Bank along 316, 330 and 348° (adapted from Apel et al. (1985)).

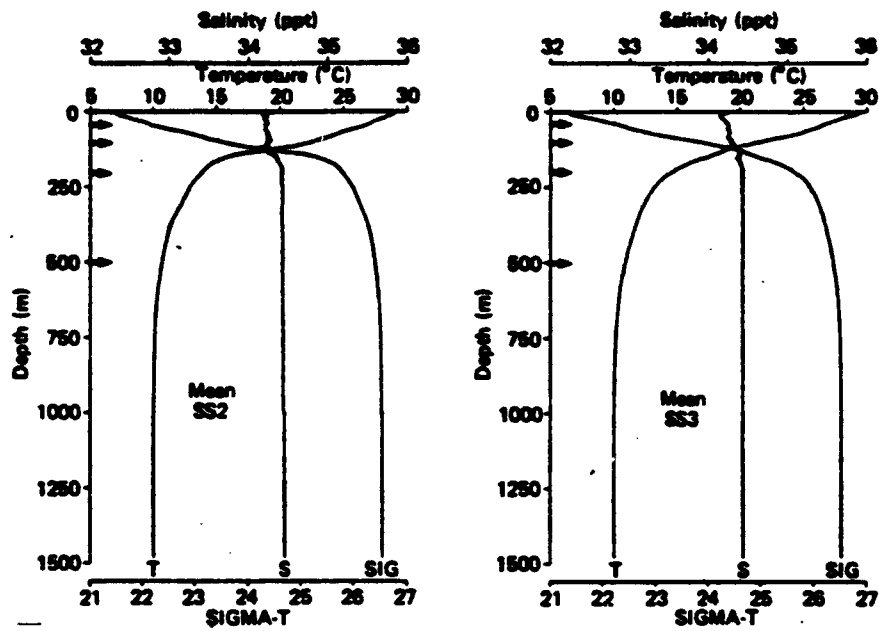


Figure 4.62: Averaged Background Profiles near SS2 and SS3 Moorings. No mixed layer of consequence existed during this period, and density is essentially temperature-controlled (adapted from Apel et al. (1985)).

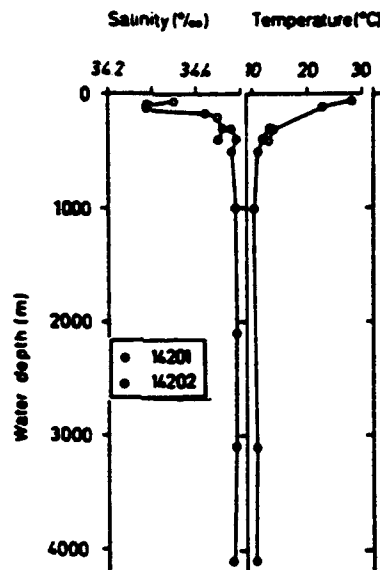


Figure 4.63: "Valdivia" Hydrographic Profiles. Data from stations 14201 ($7^{\circ}38.8'N$, $118^{\circ}27.9'E$) and 14202 ($7^{\circ}32.8'N$, $121^{\circ}30.4'E$) combined (adapted from Exon et al. (1981)).

4. Salinity. In February, salinity at the surface varies from >34.0 ppm along the Philippines to about 33.5 ppm along Palawan (see Fig. 4.35(a)). By August, salinity values have decreased generally and are all between 33.4 and 34.0 ppm (see Fig. 4.35(b)). The general gradient direction has shifted from westward in February to northwestward in August.

5. Salinity Variation with Depth. For the same locations noted above for Temperature/Depth profiles, salinity variation with depth is shown (see Fig. 4.62 & Fig. 4.63). In the Fig. 4.62 profiles, the salinity value at the surface (>34.0 ppm) increases irregularly with depth and becomes slightly larger near the bottom of the strong tropical thermocline (at about 200 meters); it retains that value (about 34.4 ppm) into the deep basin. The other profiles (see Fig. 4.63) experience a minimum value (about 34.3 ppm) at about 100 meters, then increase to values near 34.5 ppm at about 300 meters and deeper to the basin floor. At the south entrance to the Sulu Sea from the Celebes (Sulawesi) Sea through Sibutu Strait (see Fig. 4.60), a vertical section of salinity is given by Fig. 4.64. A salinity maximum value (>34.8 ppm) occurs at about 1200 meters depth outside the Strait, but it becomes modified and weakened as it enters the Sulu Sea, showing a very small increase with depth below 1100 meters.

6. Sediments and Turbidity Currents. The broad shelves adjacent to Palawan, Borneo and the Sulu Archipelago are covered with calcareous sand, gravel and rocks (see Fig. 4.65). Calcareous ooze and silt covers the northwestern two-thirds of the deep basin; it is assumed that turbidity currents moving along the indicated paths have carried the materials from the broad shelves into deep basins as calcareous turbidites. The shelf off Panay, Negros and Mindanao is covered with sediment (silt) that is muddy and poorly sorted; turbidity currents carried this into the adjacent deep basin region as mostly non-calcareous turbidites.

7. Seiches, Internal Waves. The Sulu Sea has had evidence of long-wave seiches traveling from SE-NW in the form of lines of surface roughness that have been photographed by satellites (Landsat-1 and Nimbus 7), by radar backscattering, by expendable bathythermographs and by echo sounder records underwater. The seiches appear to be surface evidence of large internal waves that extend from the surface to as deep as 500 meters below the surface. These features show wave lengths of 7 to 16 km, and the "crests" extend horizontally for more than 350 km. The "crests" are about 2 km wide; and they travel in packets that are about 80 km apart (see Fig. 4.66; and Figs. 4.67, 4.68, 4.69, 4.70 & 4.71).

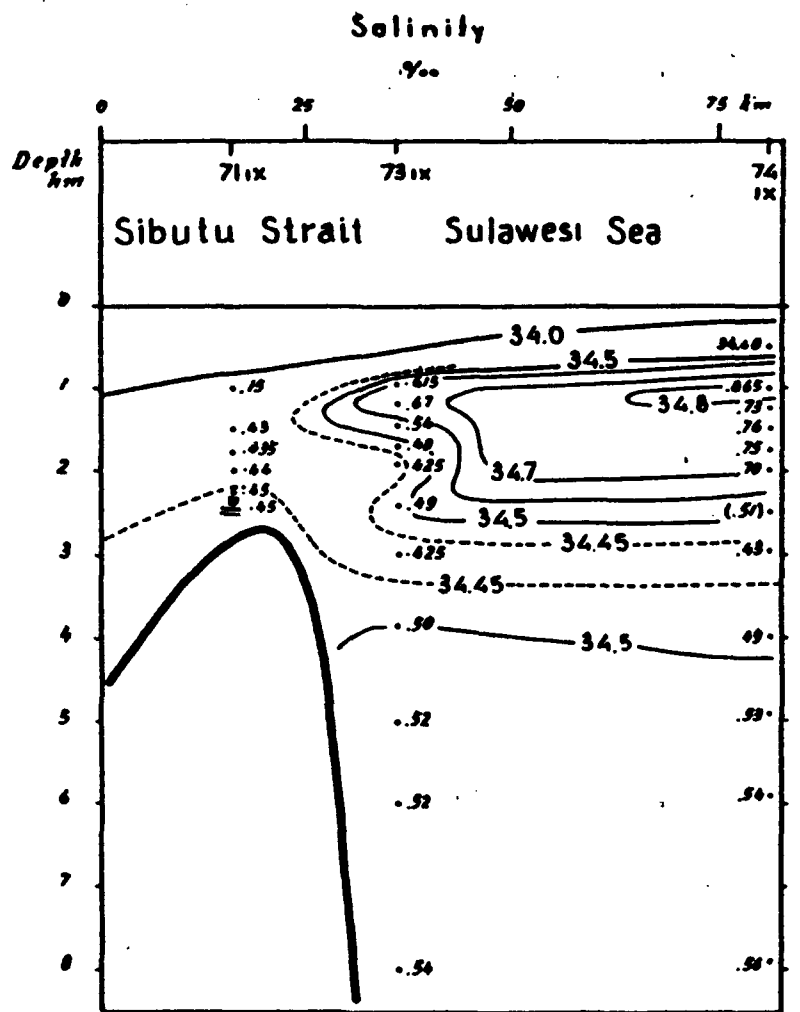


Figure 4.64: Salinity Distribution at the Entrance of the Deepest Passage Leading from Sulawesi (Celebes) Sea to Sulu Sea; depths in m x 100 (adapted from Tjia (1966)).

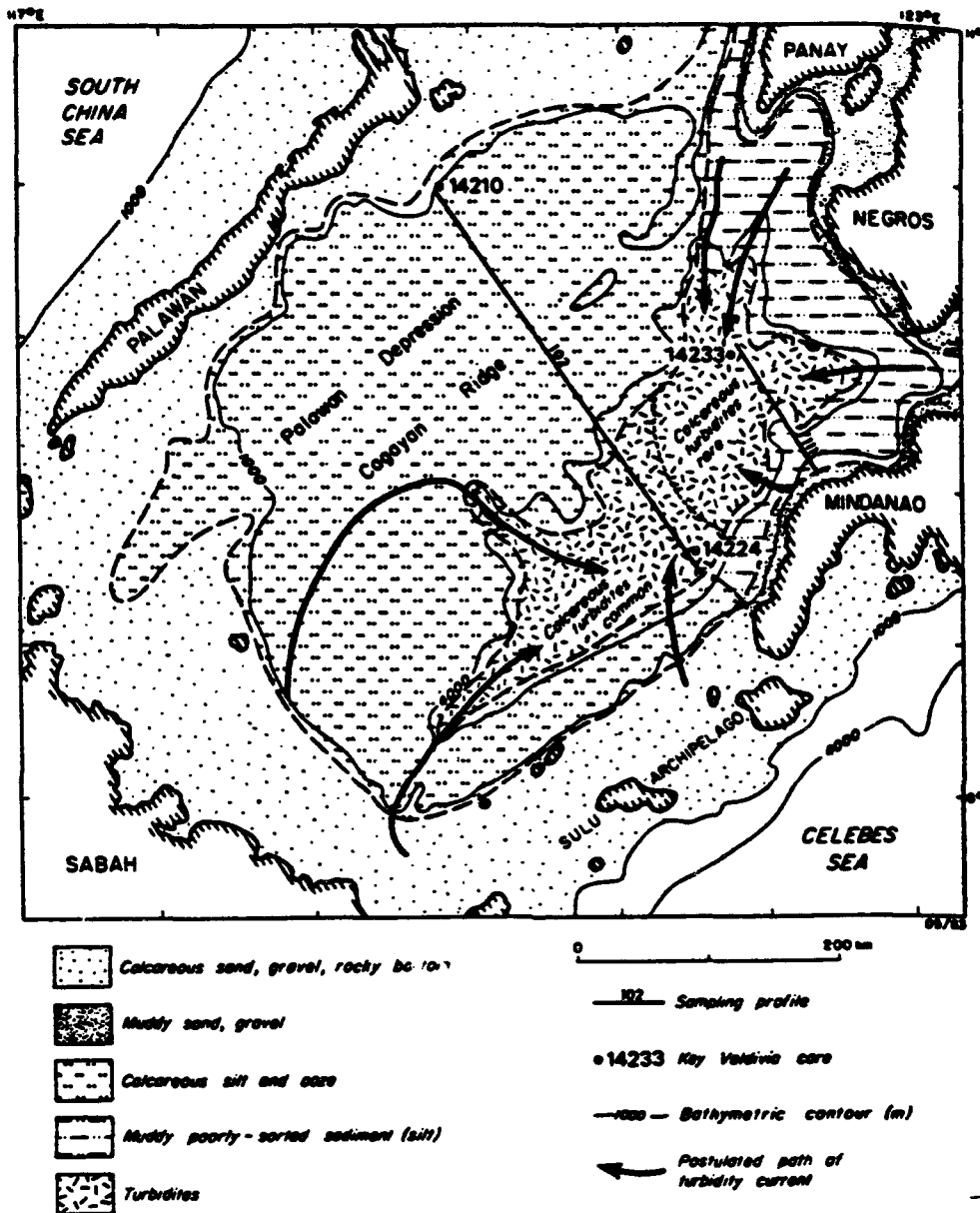


Figure 4.65: Sketch Map showing Distribution of Surface Sediment in the Sulu Sea, and Postulated Paths of Turbidity Currents in the Sulu Sea Deep (adapted from Exon et al. (1981)).

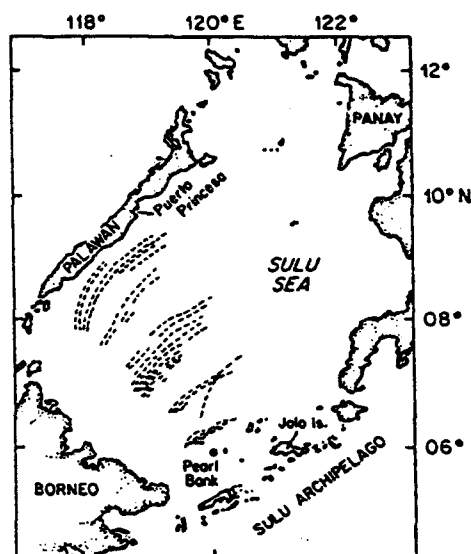


Figure 4.66: Map of the Sulu Sea showing Patterns produced by Surface Manifestations of Internal Solitary Wave Packets (adapted from Geise and Hollander (1987)).

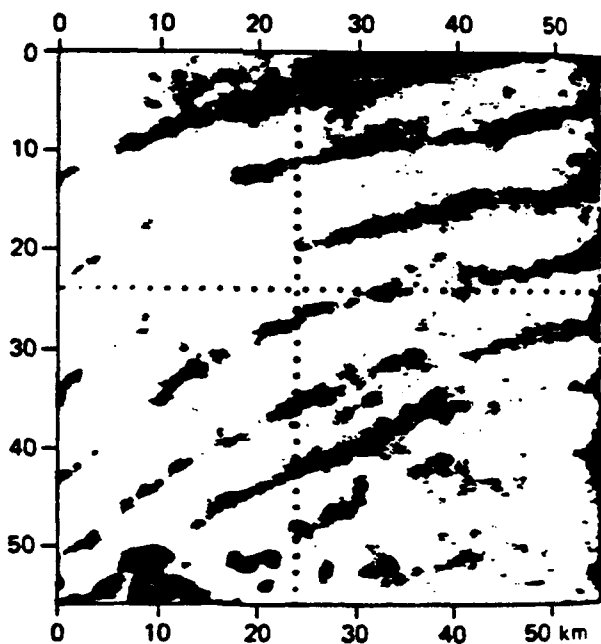


Figure 4.67: Nimbus-7 Image of Internal Solitons in Sulu Sea made during Sulu Sea Cruise on 5 May 1980. Contrast image is 55.55 km on a side; resolution is 868 m (adapted from Apel et al. (1985)).



Figure 4.68: Enlarged View of DMSP VHR (Low Enhancement) Satellite Photograph which shows Internal Waves in the Sulu Sea within the Sunglint Pattern at 0419 GMT 2 April 1973. Five packets of internal waves are marked; in packet 3 the longest wave length is about 7 km, and wavelength decreases from the front to the rear of the packet (adapted from Fett et al. (1977)).

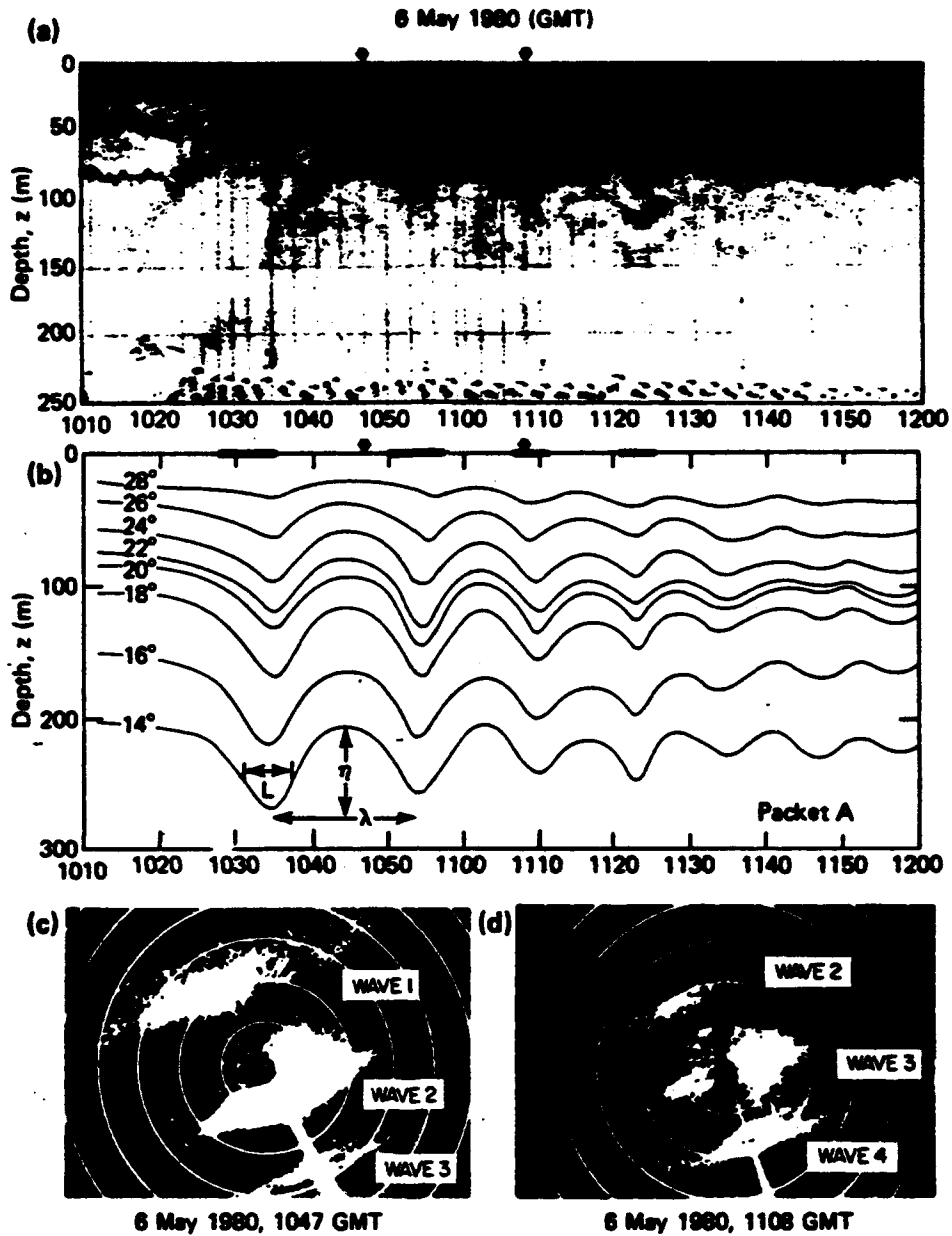


Figure 4.69: Upper: Echo-sounder Record for Packet A at a point well out in the Sulu Sea. The deep scattering layer has obscured the lead soliton. Center: Isotherm Displacements of Packet A constructed out of Repeated XBT Casts made at the Locations shown on the Upper Record. An amplitude of about 60 m was obtained at this time. Lower: Backscatter from Ship's X-band Radar PPI showing Packet A. Range rings at 1.0 n mi intervals. Surface roughness was concentrated in the darkened regions shown at $z = 0$ in the center plot (adapted from Apel et al. (1985)).

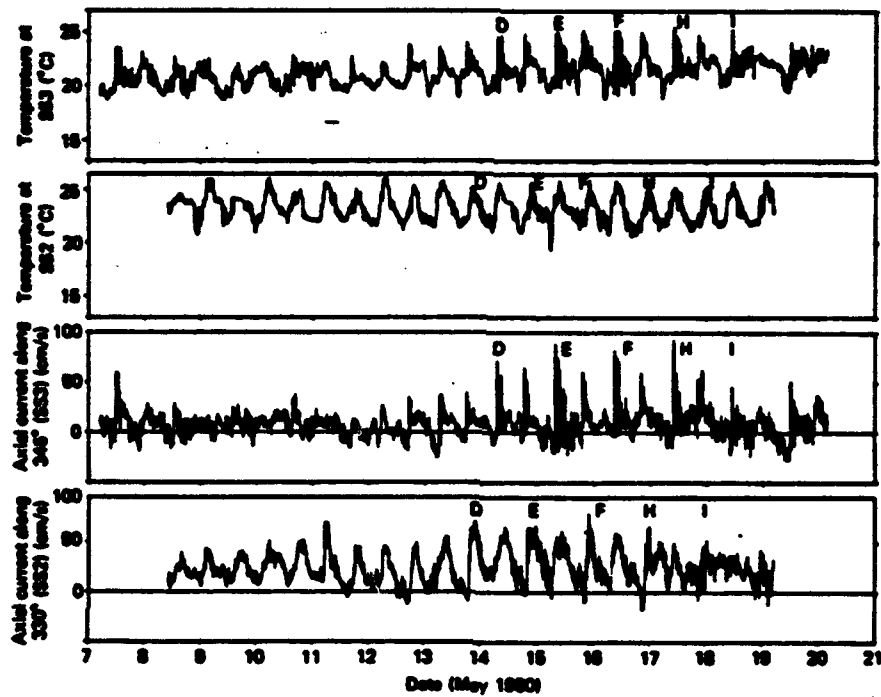


Figure 4.70: Time Series of Temperature and Axial Currents at 100 m Depths at SS3 and SS2. More energetic soliton packets are labeled (D, E, F, H and I). Note the evolution between SS2 and SS3 (adapted from Apel et al. (1985)).

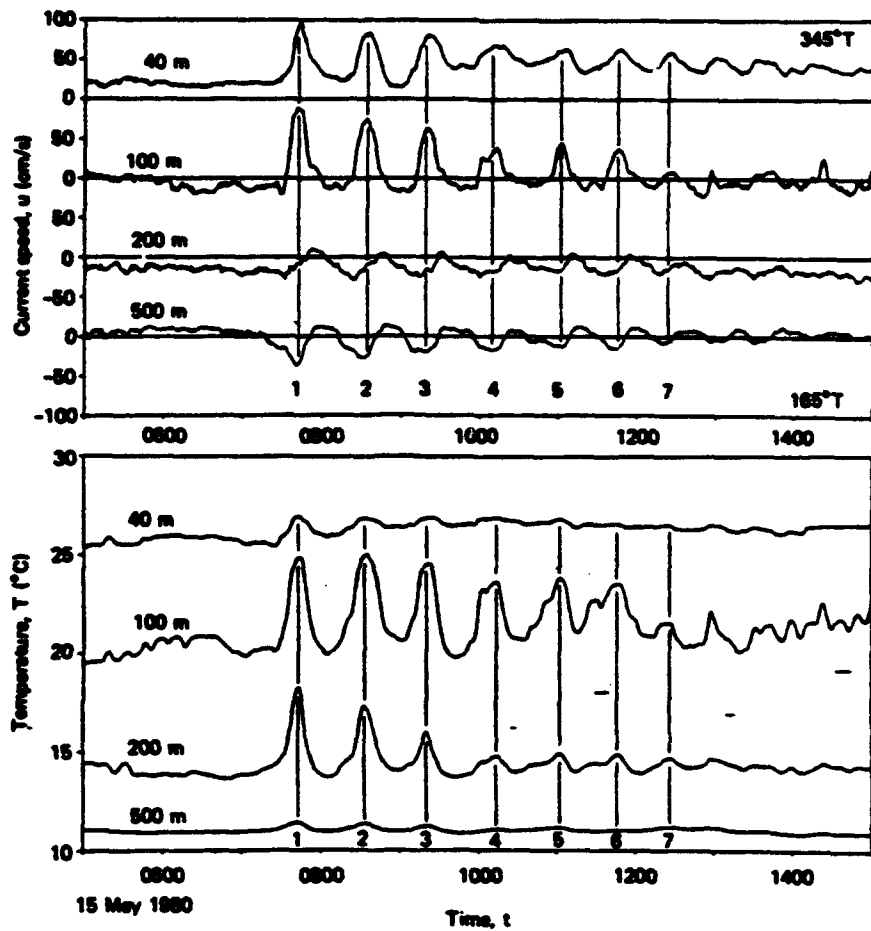


Figure 4.71: Time Series of Currents and Temperature of Packet E at SS3, at four depths. The 180° phase change in current with depth indicates the cellular nature of the streamlines (adapted from Apel et al. (1985)).

D. Luzon Strait (Bashi Channel)

This is the opening between Luzon and Taiwan at the north of the Philippine Island arc. This relatively deep connection between the Philippine and South China Seas has bathymetry as shown in Chuang (1986), Fig. 4.72.

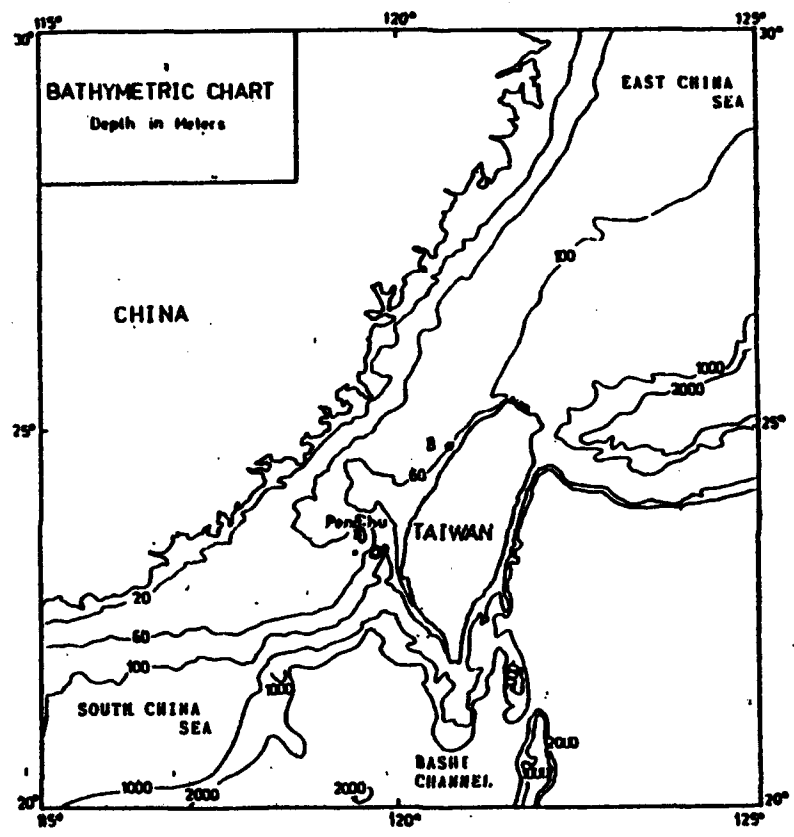


Figure 4.72: Bathymetric Chart of Taiwan Strait and Vicinity. Note Station B and Station C Location (adapted from Chuang (1986)).

1. Current Circulation Patterns. The surface currents are dominated by the presence of the strong Kuroshio Current (see Fig. 4.73; and Fig. 4.74) in both summer and winter. During summer, there appears to be some outflow from the South China Sea through Bashi Channel (or Strait) into the Philippine Sea; in winter, that is reversed. Plots of the current components along Bashi Channel appear directly related to windstress, and inversely related to sea level (see Figs. 4.75 and 4.76).

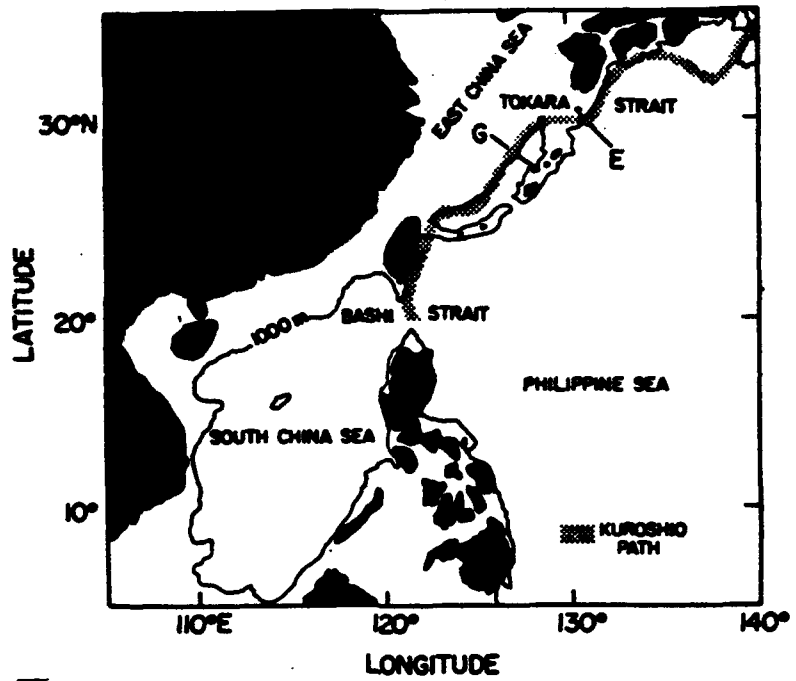


Figure 4.73: The Main Path of the Kuroshio Front and the 1000 m Bottom Bathymetry (adapted from He and White (1987)).

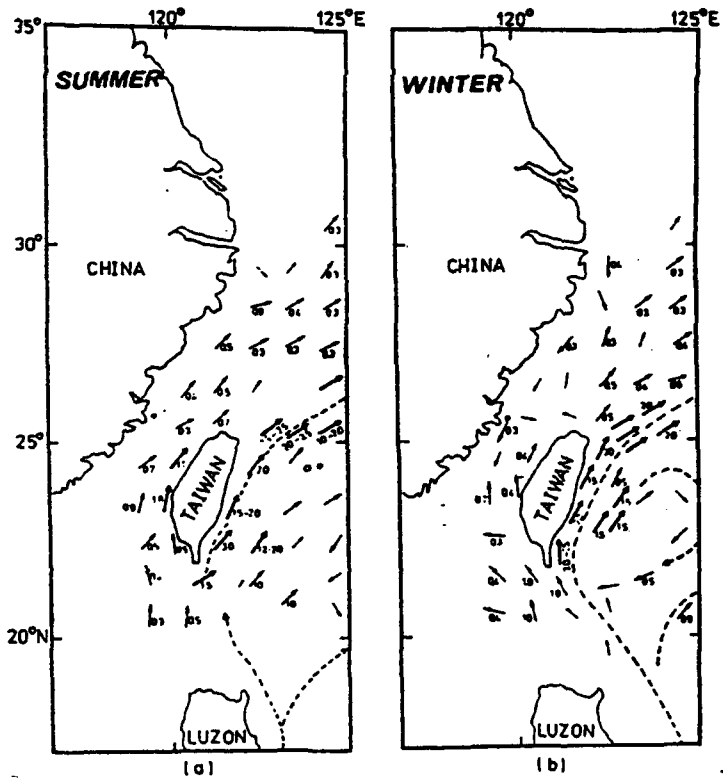


Figure 4.74: Current Chart in Knots: (a) Summer, and (b) Winter adapted from Chuang (1986)).

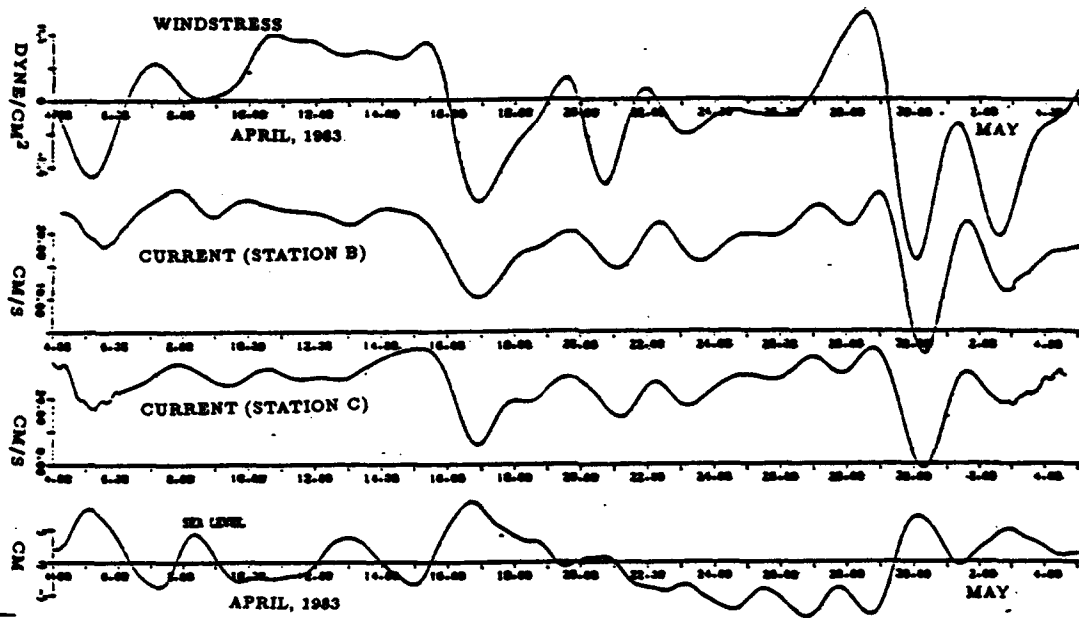


Figure 4.75: Time Series of the Filtered Along-strait Components of Windstress, Current, and Sea Level. See Fig. 4.72 for locations of Stations (adapted from Chuang (1985)).

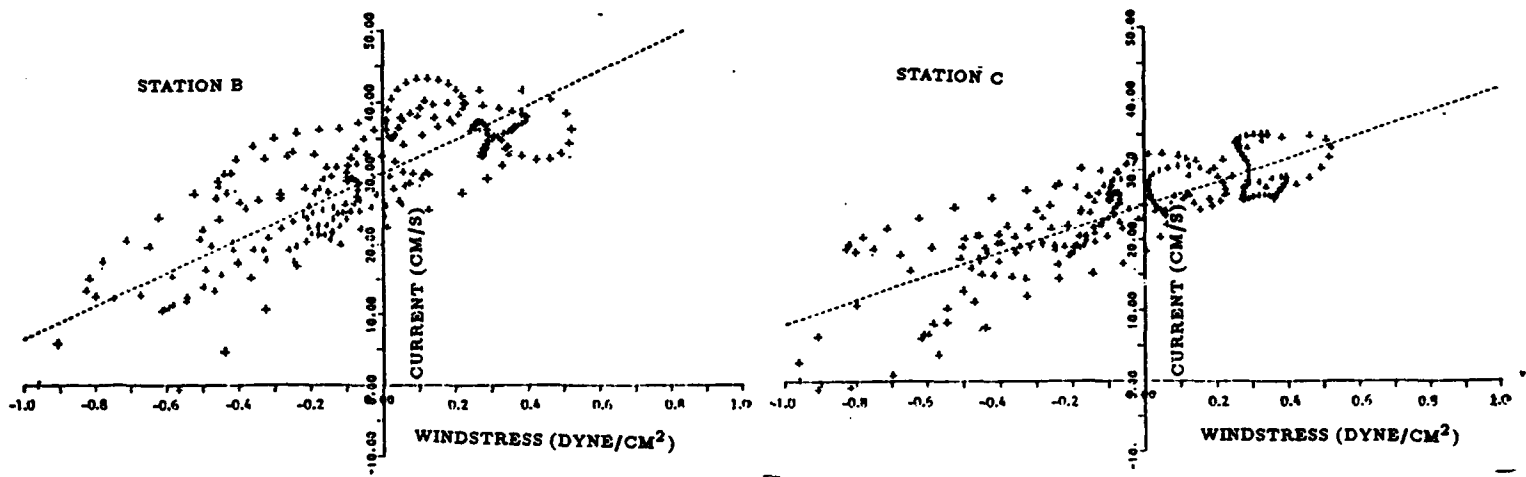


Figure 4.76: Scatter Diagrams of Windstress Versus Current Velocity (at 3-h Sampling Interval), with the Fitted Line resulting from Linear Regression Analysis plotted (adapted from Chuang (1985)).

Scatter diagrams of windstress against current velocity shows reasonable correlation. Currents calculated using zero-lagged and 4-hour lagged windstress data are shown plotted against measured currents with good results at the sampled stations B & C (Figs. 4.77 and 4.78).

Cotidal lines for diurnal and semidiurnal tide components are shown for highwater times across Bashi Strait in Fig. 4.79.

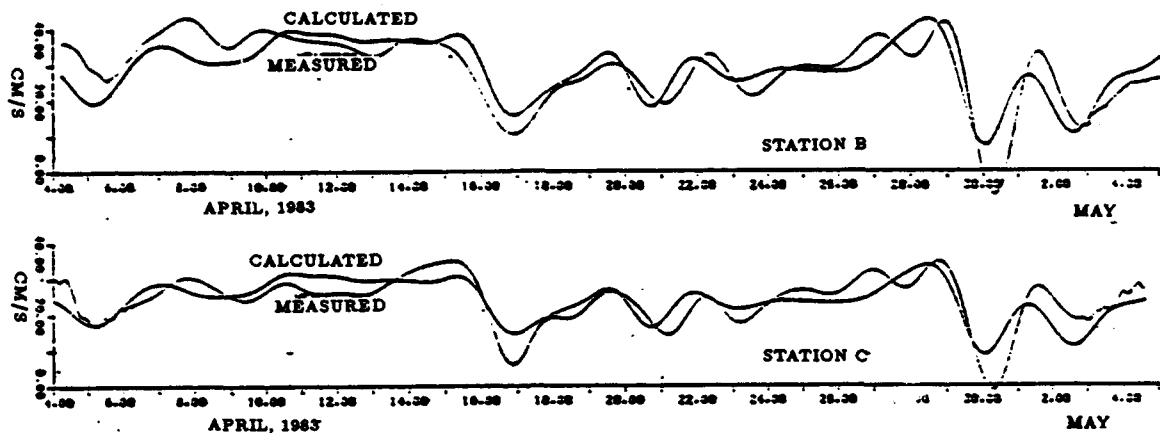


Figure 4.77: Measured Current and Calculated Current using Zero-lagged Windstress Data (adapted from Chuang (1985)).

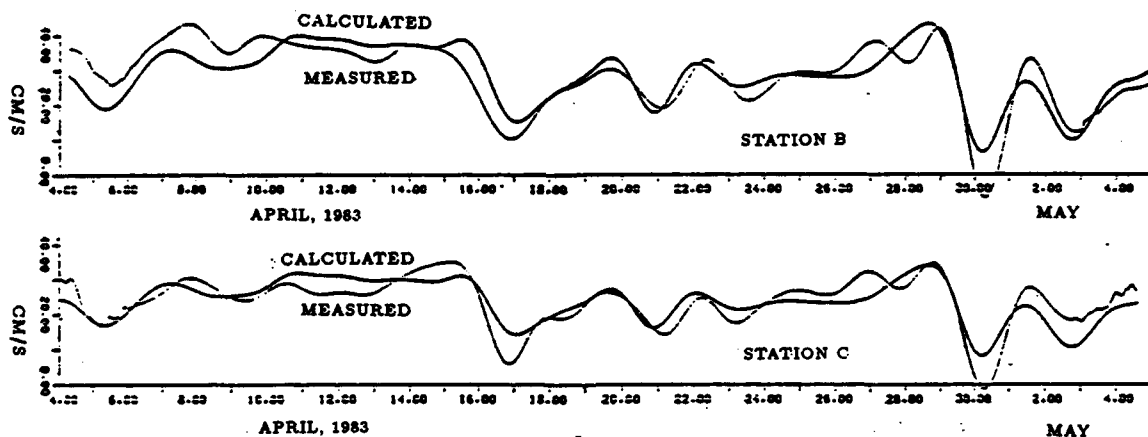


Figure 4.78: Measured Current and Calculated Current using 4-hour lagged Windstress Data (adapted from Chuang (1985)).

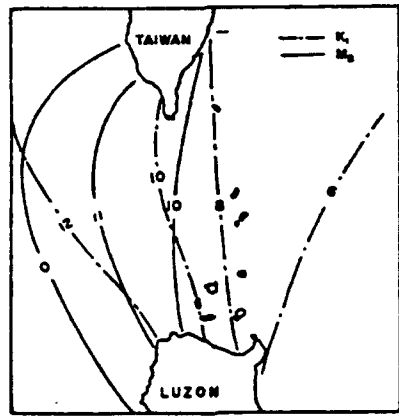


Figure 4.79: Cotidal Lines of the Diurnal Tide K_1 and the Semidiurnal Tide M_2 (adapted from Kanari and Teramoto (1981)).

2. Sea Surface Temperature. Average temperature charts (Figs. 4.17 and 4.18) show some seasonal variation in Bashi Channel. In August the temperature is essentially uniform in the Channel and very warm: almost 29°C . By November it has dropped by 2 to 2.5°C , with a gradient that shows temperature decreasing northward. In February, another decrease (by almost 2°C) has occurred, with a stronger N-S gradient present, showing the coldest temperatures of the year (about 24 to 25°C). In May, the N-S temperature gradient remains strong with values from 27 to 29°C . (Sea surface temperature for all 12 months are available in Appendix A.)

3. Temperature Variation with Depth. An E-W section of temperature in Bashi Channel is presented in Fig. 4.80 for 17–20 May 1985. Below 1000 meters, the resulting distribution reflects the lack of free exchange across the Channel.

Long-term bimonthly averages of temperature that are values averaged over the upper 200-meters of water are shown by Fig. 4.82. One feature in Bashi Channel is the strong gradient present between the warm conservative values to the east and more variable values to the west of the Channel. Annual mean values are shown in Fig. 4.81, and the strong gradient across the Bashi Channel is very much in evidence, as expected.

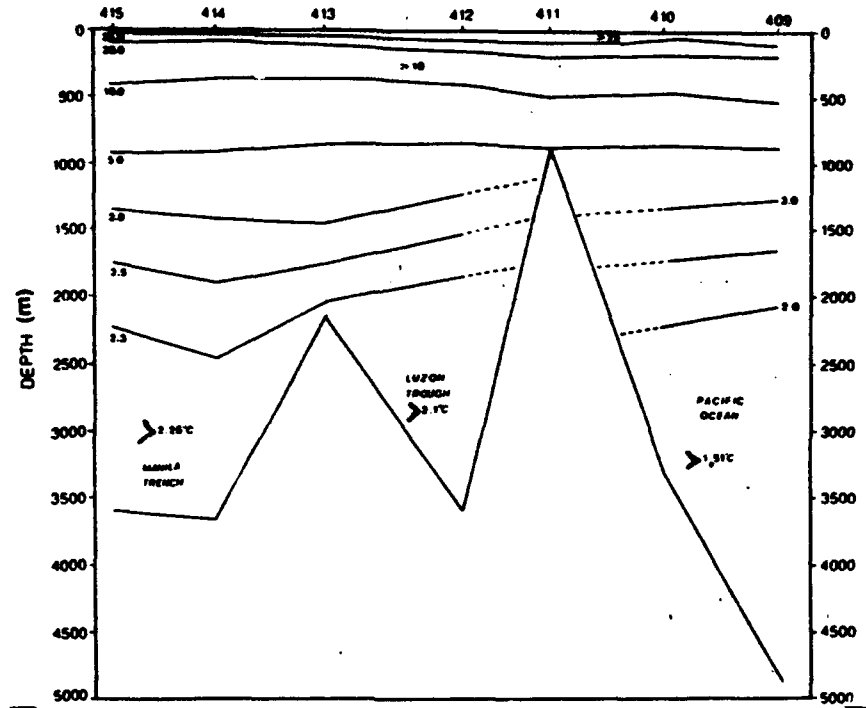


Figure 4.80: A Vertical Section of the Water Temperature ($^{\circ}\text{C}$) in the Bashi Channel, 5/17-5/20, 1985 (adapted from Wang (1986)).

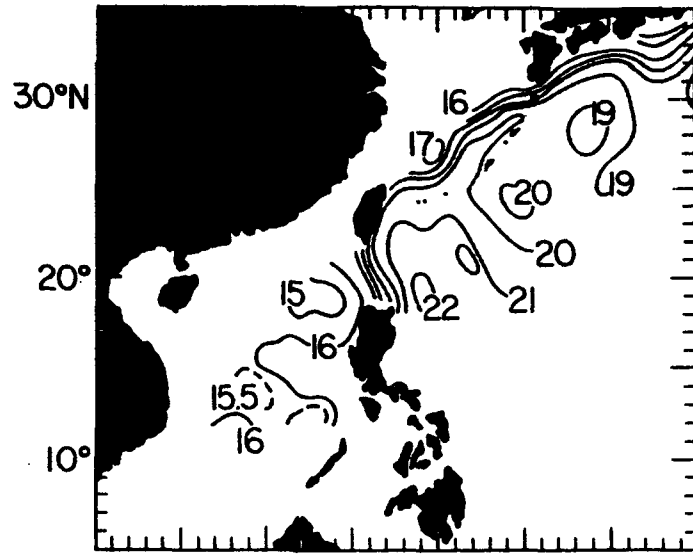


Figure 4.81: Long-term Annual Mean (1979-1982) (adapted from He and White (1987)). The contour interval is 1°C .

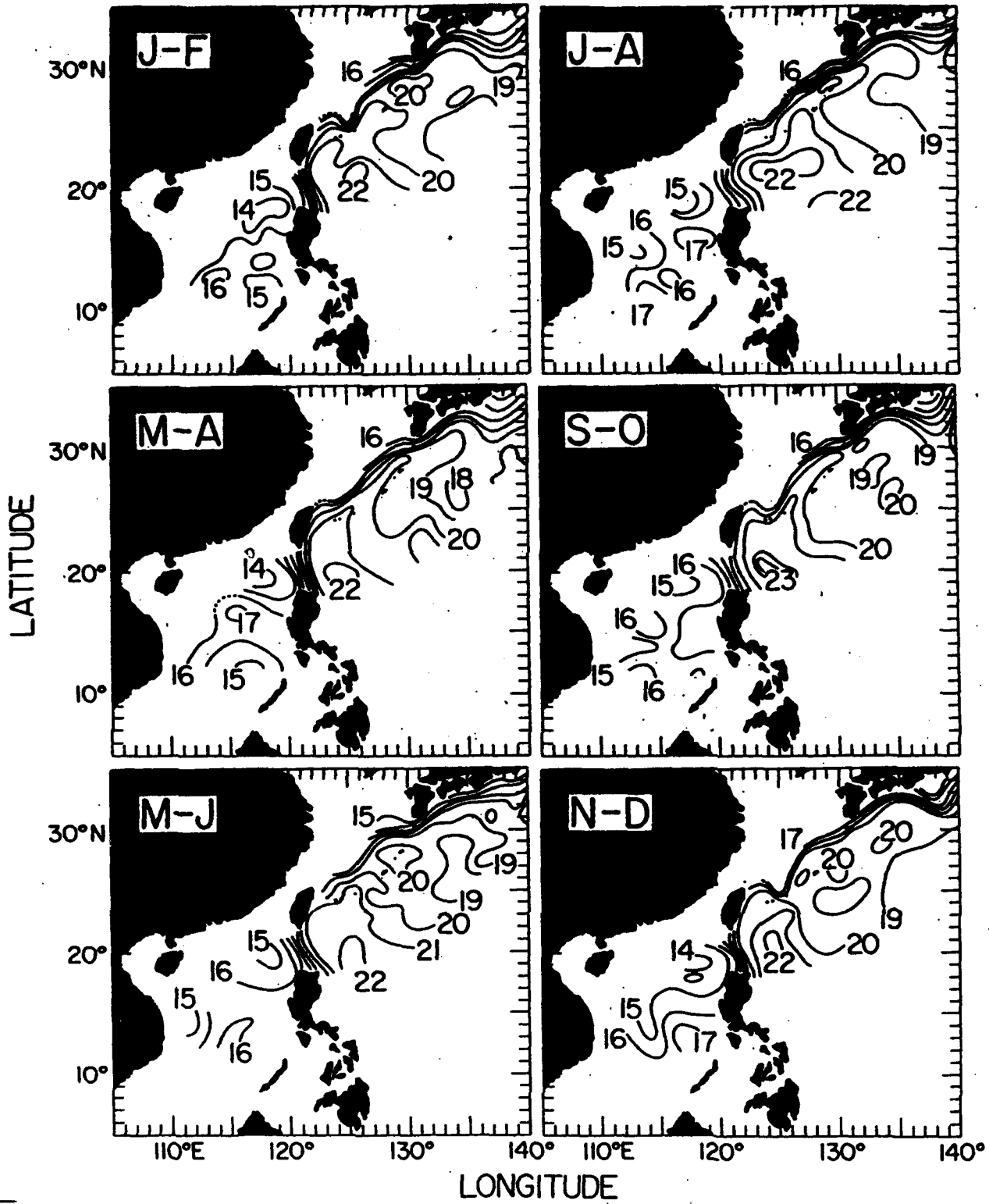


Figure 4.82: Long-term bimonthly Mean Maps of Vertically Averaged Temperature (adapted from He and White (1987)). The contour interval is 1°C.

Contours of temperatures measured at depths of 2000 db (read "meters") and at 2500 db (meters) in the Bashi Channel vicinity show some horizontal temperature variation (0.03 to 0.05°C) occurring in Figs. 4.83(a) & (b).

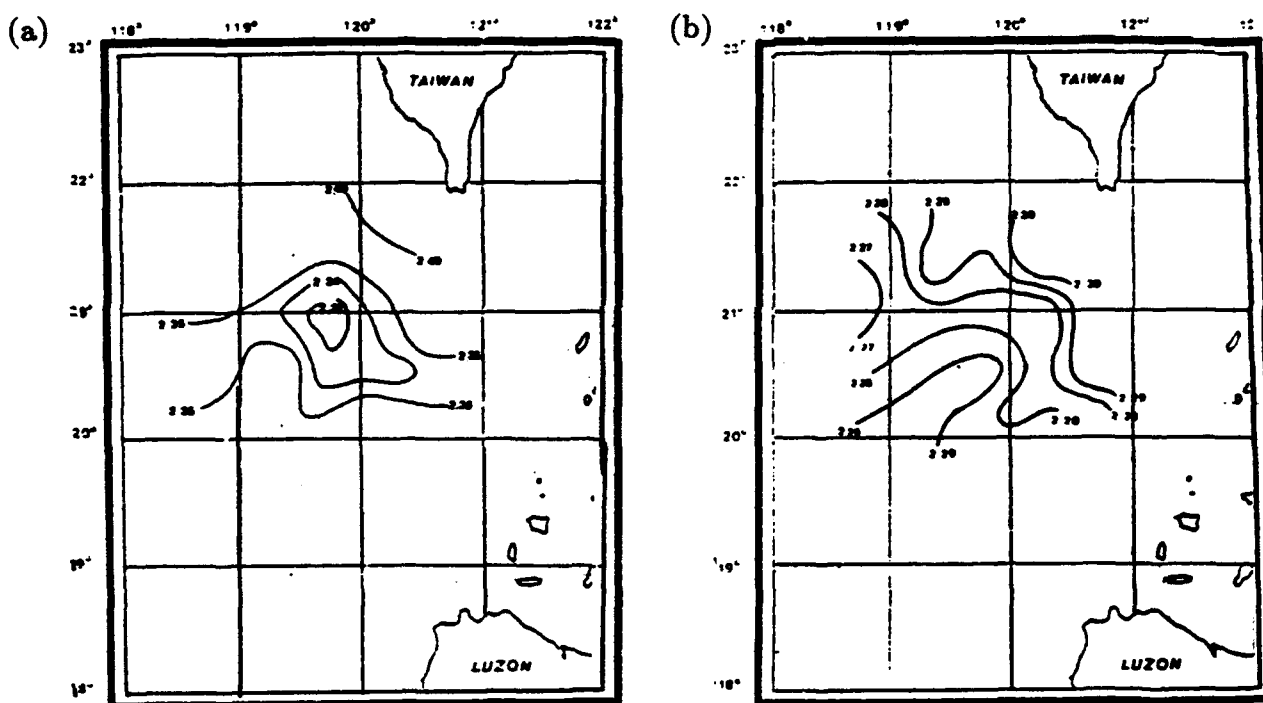


Figure 4.83: The Horizontal Distribution of Water Temperature (°C) (8/1-8/6, 1985) at (a) 2000 dB and (b) 2500 dB (adapted from Wang (1986)).

4. **Salinity Variation with Depth.** An E-W section across Bashi Channel from data observed during May 1985 shows sharp increases in value from the surface to the depth of the salinity maximum, at about 150 meters. Below this, values decrease to the minimum salinity core at about 500 meters depth. Below this minimum, salinity values increase slightly toward the bottom (see Fig. 4.84).

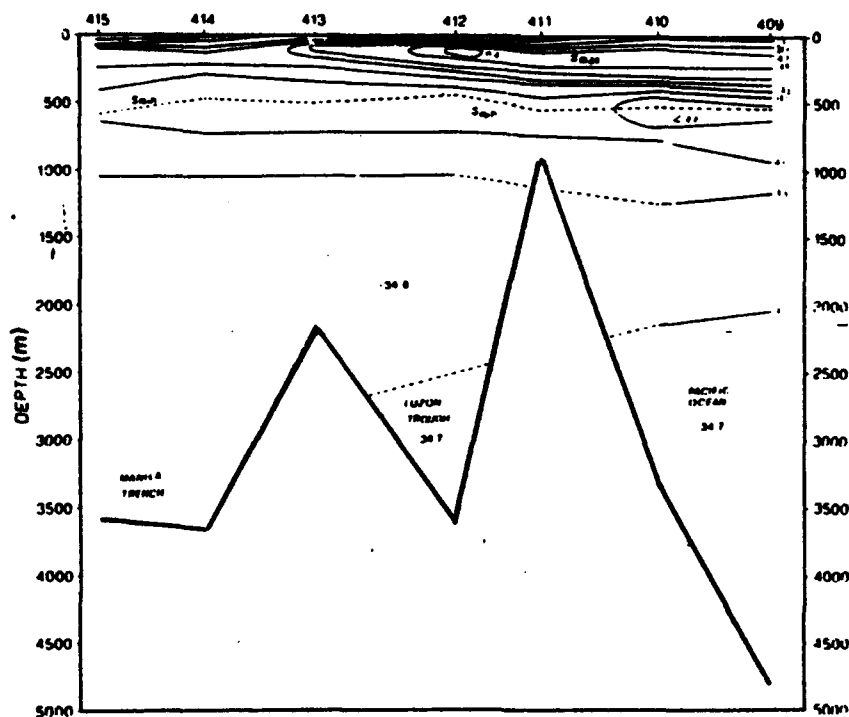


Figure 4.84: A Vertical Section of the Salinity (ppm) in the Bashi Channel, 5/17-5/20, 1985 (adapted from Wang (1986)).

Near southern Taiwan, a study reported in Fan and Yu (1981) shows sections prepared from data observed at stations whose locations are shown in Fig. 4.85. The salinity distributions along a vertical section in the Bashi Channel are shown for three seasons (August, December and April) in Fig. 4.86. The stations locations are along an east-west line (see Fig. 4.85) near southern Taiwan; the sections extend from the sea surface to 700 meters depth. A salinity maximum extends from the Pacific ocean (to the right) into Bashi Channel, centered at about 150 meters depth. In August and April, a marked salinity gradient extends from lower values at the surface down to this maximum; in December the deep mixed layer extends from the surface to about 100 meters depth in the Channel and the Pacific Ocean, and the lower values of salinity near the sea surface are not observed then; however, this does not apply to the northern South China Sea in December. There, also, the August salinity values are lower than in other parts of the section; this applies as well to the salinity maximum values observed between 100-200 meters depth.

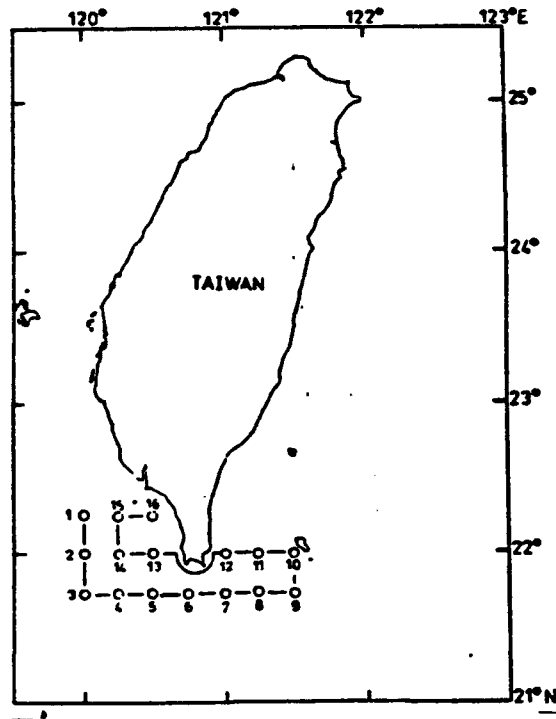


Figure 4.85: Map of Station Locations (adapted from Fan and Yu (1981)).

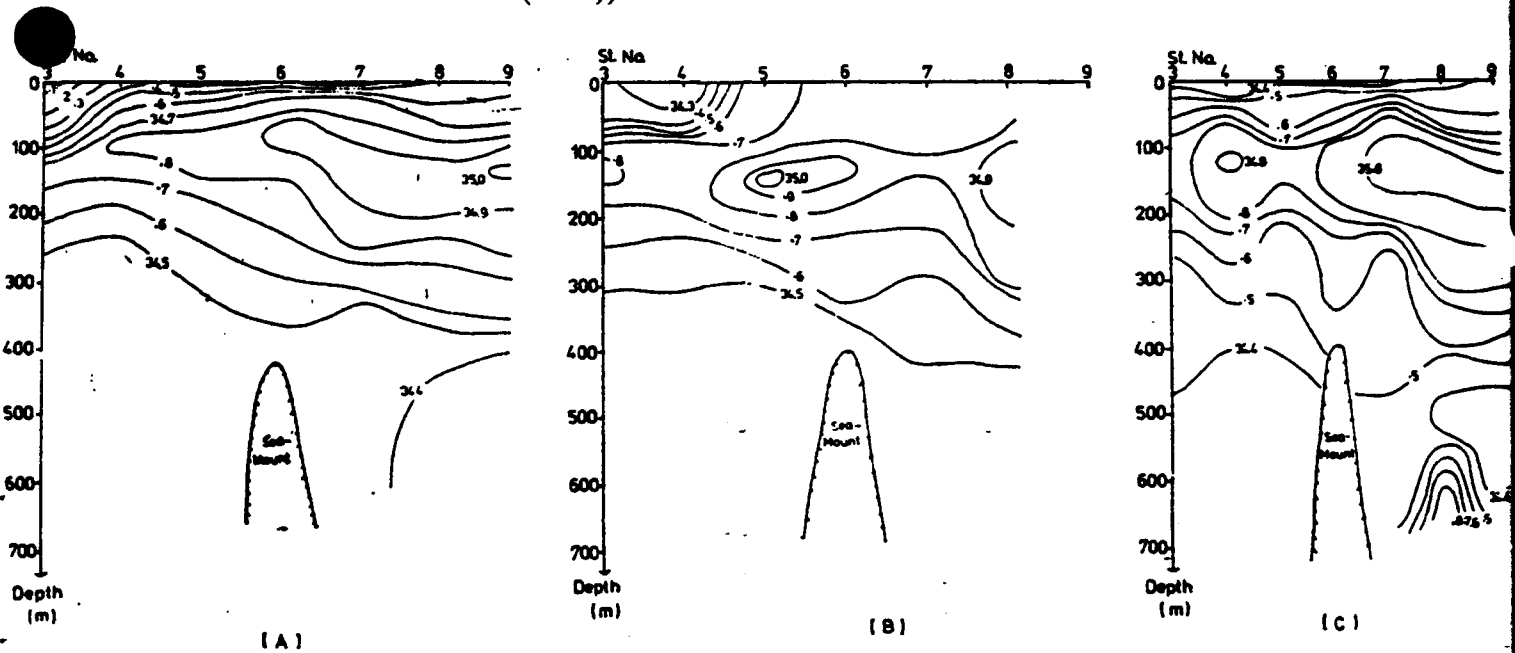


Figure 4.86: Vertical Salinity (ppm) Distribution in (A) late August; (B) middle December and (C) middle April in Bashi Channel (adapted from Fan and Yu (1981)).

5. Temperature versus Salinity. The Temperature-Salinity (T-S) diagrams for the three seasons studied in Bashi Channel by Fan and Yu (1981) are shown in Figs. 4.87-4.89; the stations locations (shown in Fig. 4.85) are nearer southern Taiwan than those in Fig. 4.86. The T-S values at 150 meters depth (near the maximum salinity value) are shown as open circles on each T-S plot. Stations 2, 13 and 14 are in the South China Sea; these show values that depart most widely from the other station plots above 150 meters depth, especially in August. Below 150 meters the station plots vary little from one another in all three seasons. This indicates a consistent watermass occurs below 150 meters, which is relatively unaffected by the seasonal influences above that depth. At great depths just west of Bashi Channel, the T-S relation for abyssal waters is clearly linear, with salinity increasing with decreasing temperature (see Fig. 4.90).

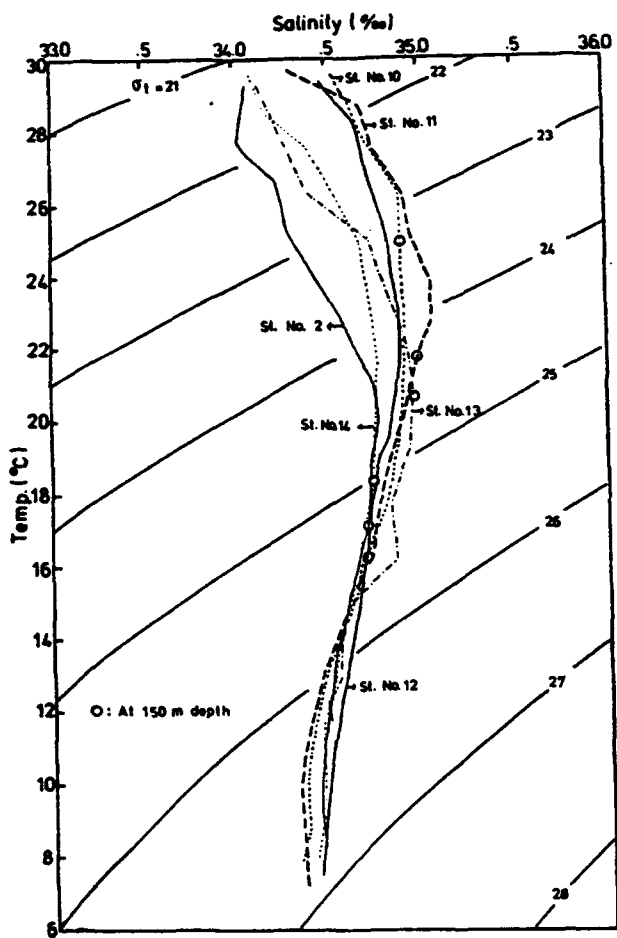


Figure 4.87: TS-diagrams for six stations in late August 1980 (adapted from Fan and Yu (1981)).

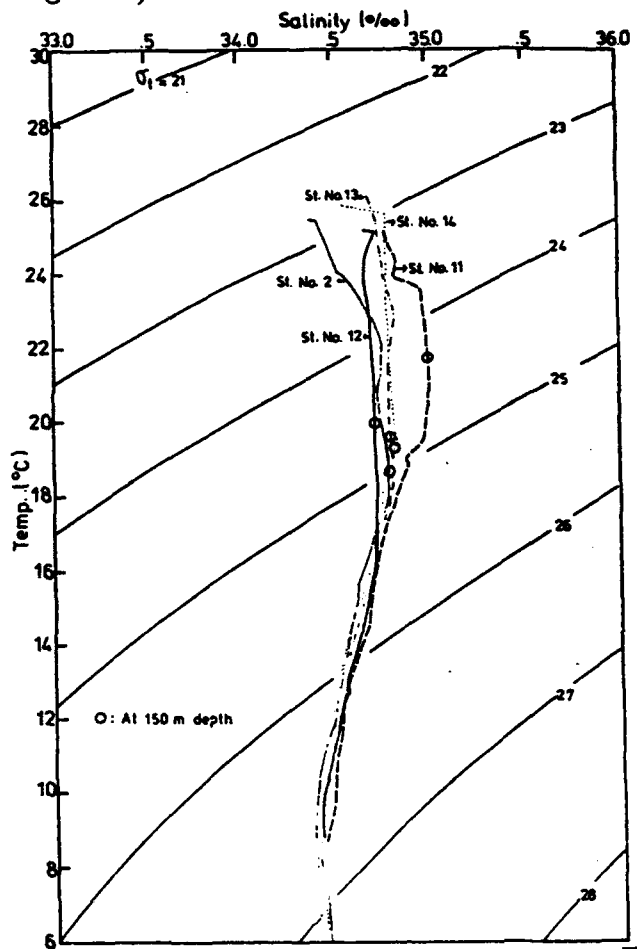


Figure 4.88: TS-diagrams for six stations in middle December 1980 (adapted from Fan and Yu (1981)).

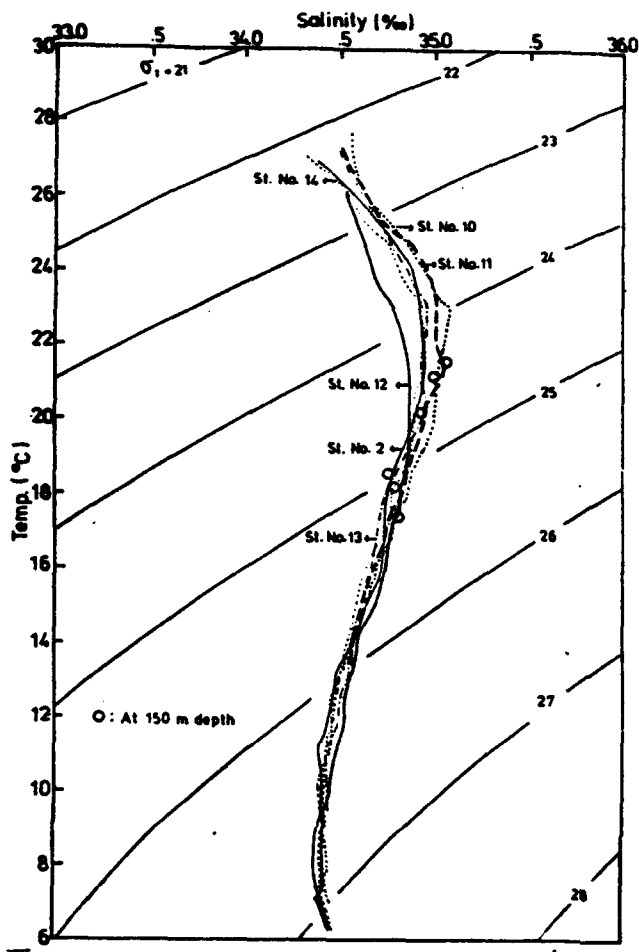


Figure 4.89: TS-diagrams for six stations in middle April 1981 (adapted from Fan and Yu (1981)).

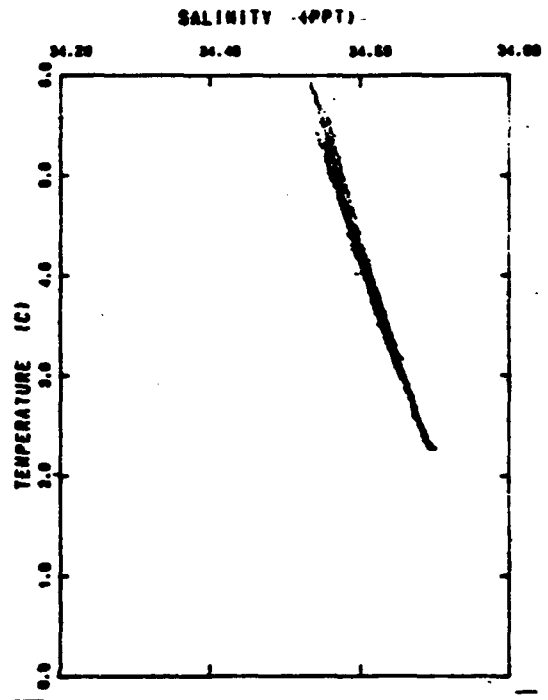


Figure 4.90: The T-S relation of the abyssal waters of the Northern South China Sea below 800 dB (adapted from Wang (1986)).

E. Shallow Seas (between islands)

The seas between the central Philippine Island group, the Visayas, are areas of coral growth. Regions of the Visayas (including Panay, Negros, Cebu, Bohol, Samar and others) where studies of coral have been made are shown on Fig. 4.91. Percentages of coral in various categories for the different types of locale in these shallow seas are shown (see Fig. 4.92). The presence of corals in a region will greatly affect the feasibility of naval operations in the area.

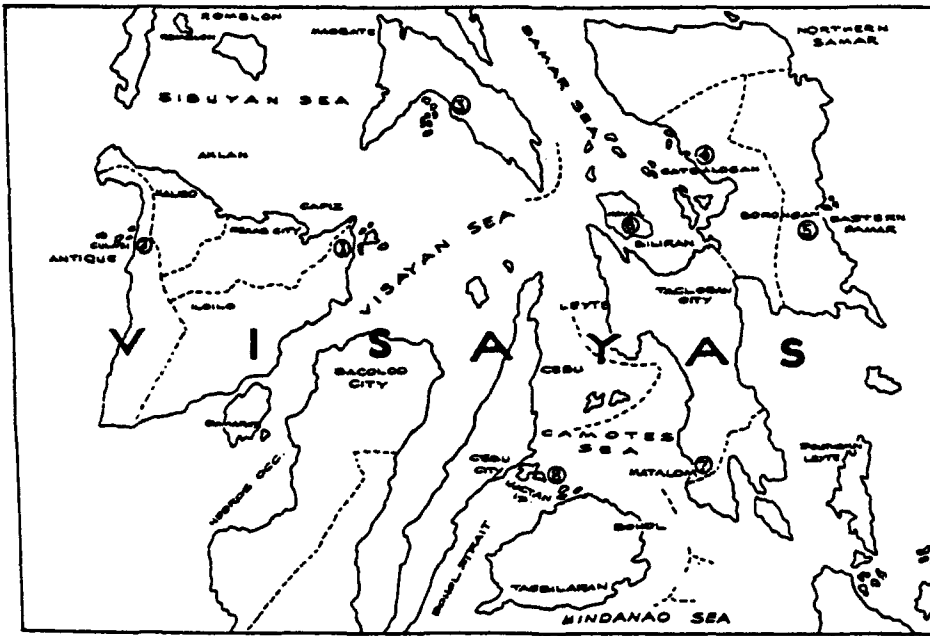


Figure 4.91: Central Philippines (adapted from Cordero (1981)).

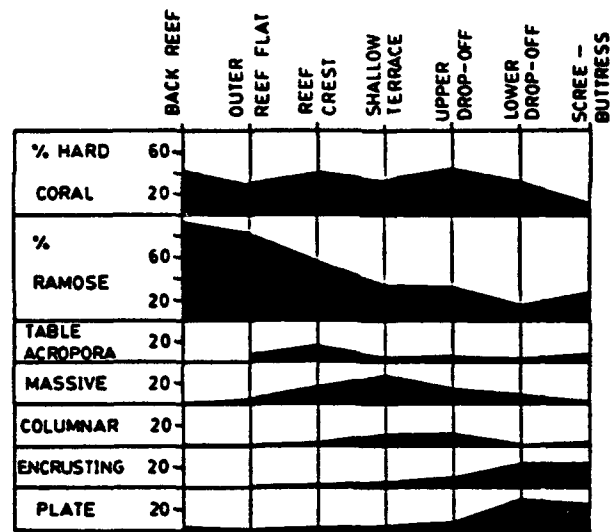


Figure 4.92: Percent Coral Cover per Biotope, and the Percent of the Cover contributed by Each of the Major Growth Forms (adapted from Ross and Hodgson (1981)). Note the clear progression from ramose to plate forms with increasing depth.

CONCLUSION. It is important to consider these ocean parameters when preparing for particular Naval operations within the Philippine Islands region. Relative significance of the ocean factors depend on the nature of the Naval operation considered—whether it is an amphibious landing, navy resupply, hurricane evacuation, weather forecasting for air operations or any of the other many possibilities.

5. OCEANIC ASPECTS OF OPERATIONAL WEATHER FORECASTING

5.1 Introduction

The temporal and spatial variations of oceanic, atmospheric and terrain features result in tactical challenges for use of operational systems in the sub-surface, surface and marine planetary boundary layer (MPBL) regimes. To optimize forecast skill and subsequent conversion to tactical advantage requires development of a comprehensive understanding not only of the relationships between large scale climatological, regional and local forcing but also the intricacies of the interactions between the different time and space scale features. Understanding the translation of dominance between the different scale of forcing in the time and space of concern requires yet a higher level of understanding. It is the ability to recognize the changing forcing patterns that provides forecasters with the tools to address with some degree of confidence and skill, the over the horizon, around the corner and/or vertical structure changes in environmental conditions. Application of insights is applicable to both in-situ evaluations as well as interpretation of numerical guidance products.

Several factors compound the problems of forecasting in the geographical region of the Philippines. While the large scale forcing and general conditions under northeast and southwest monsoon regimes are relatively straightforward, the oscillating nature of the advance and retreat of the coming season's flow regime makes for difficult near term (days to weeks) forecasts. Tracking of the transition zone between the onset and retreating patterns requires access to and close analysis of observations, including satellite imagery, that reflect local conditions. Even under established large scale monsoon flows, local forcing and features over open ocean areas (showers, shear lines, terrain influences, ocean currents, etc.) tend to create short term (hours to days) variability and forecast problems. Terrain influences and diurnal variations add further complications especially for coastal area forecasting. Local forcing, as is typical of most warm weather climates or seasons, is a dominant factor in coastal forecasting. While persistence is a characteristic of sub-tropical regime weather, the ability to properly forecast non-routine or changing events is the real challenge for forecasters.

Many factors of changing conditions can result in alteration of dominant forcing and subsequent further changes in conditions. While full understanding of the climatology of the regime is essential, development of forecasting skill requires the understanding of the variability of environmental parameters and the ability to anticipate short term and near term trends and changes.

The material in the remainder of this section is provided as an aid in developing an appreciation for the oceanic and atmospheric patterns and interactions for the region surrounding the Philippine Islands. Some discussions on applications of environmental information to tactical situations and forecast aids are also provided. The emphasis here is on surface and MPBL aspects, the strata within which most of the navy operations occur. General atmospheric aspects are addressed in the first three sections of this handbook and oceanographic aspects in Section 4. For a review of ocean thermal and acoustic properties and resulting sound propagation readers are referred to general publications such as Aerographer's Mate Training manuals and area specific information in Special Publications 3160-NP7. Additional data and application programs can be obtained from the Tactical Environmental Support System (TESS).

5.1 Seasonal and Regional Variations

The atmospheric seasonal variability (climatology) is presented in Section 2. Oceanic regional variability is presented in Section 4. This section will combine aspects of both seasonal and regional variations that can be used as forecast aids.

The largest temporal and spatial scale variability reflects the differences between the warm season southwest monsoon and cold season northeast monsoon, and the transition periods from one to the other. Forecast reasoning for this subtropical region must be adjusted for differing seasonal conditions just as must be done in midlatitudes. Oceanic structure and conditions also have pronounced seasonal variability.

The next largest spatial variability of atmospheric conditions reflect the interactions of synoptic circulation features including the subtropical high, Intertropical Convergence Zone, trade wind regime, alternating Asian continent warm season low and cold season high pressure systems, and the monsoon trough. Comprehending the various roles of these features during the opposing monsoons and transitions can be viewed as a basic requirement for developing forecasting reasoning specific to this region. Generally only the northern most part of Luzon and waters to the north are influenced by midlatitude type migratory synoptic systems, and only during the winter period. Translation of the variations of atmospheric flow conditions to the forcing of the MPBL and upper layer of the ocean is the next step. Modifications of the synoptic scale atmospheric forcing and conditions due to local terrain and sea surface conditions is yet another level of complexity in forecast reasoning.

The geography and topography (Section 1.2) of the Philippines is very complex. Even under relatively uniform open ocean flow patterns such as those typical of the periods of fully developed monsoons, terrain features induce a multitude of local effects including channeling

corner effects, lee/wind-ward side subsidence/convergence, barrier effects, etc. Routine study of satellite imagery is the best way of rapidly acquiring expertise on local wind, weather, cloudiness and humidity patterns.

Oceanic features, in addition to the forcing by atmospheric conditions, are strongly influenced by bathymetric and internal circulations (Section 4). In contrast with the atmosphere the variation of oceanic subsurface features are tied more to spatial than to temporal constraints. The oceanic transition from open basin to marginal sea occurs in the vicinity of the Philippines and has significant impact on surface conditions and air/sea interactions as well as on subsurface conditions. Details on spatial variations are presented in Section 4.2.2.

5.3 Ocean Currents and Associated Fronts

The area east of the Philippines is dominated by the broad North Equatorial Current which flows westward between 9° and 19° N, with speeds as high as 2.0 kt but generally at about .5 kt. The current splits off southern Luzon and Lamar with the northern branch flowing through the Luzon Strait and then curving northeastward near 25° N as the Kuroshio Current. The southern branch becomes the south-flowing Mindanao Current, with mean speeds of 1.5 to 2.0 kt, which enters the Celebes Sea southeast of Mindanao. An eastward extension of the Mindanao Current merges with other waters to form the east-flowing North Equatorial Countercurrent with an axis generally located between 3° and 6° N. A large cold eddy about 300 nm in diameter and centered near 7° N, 134° E, produced by upwelling, exists between the North Equatorial Current and the North Equatorial Countercurrent.

The strongest ocean front in the western North Pacific region is associated with the Kuroshio Current. The current and front increase in intensity as the current flows northward east of Taiwan and then northeastward west of the Ryukyu Islands. However, the Kuroshio shows little, if any, sea-surface-temperature signatures through the Luzon Strait area. The location of the 16° C isotherm at a depth of 200 m is an indicator of the western boundary of the Kuroshio at the surface and the 18° C isotherm at 200 m is representative of the location of the maximum velocity core at a depth near 100 m. When crossing the Kuroshio the following acoustic changes can be expected:

- o Sound speed change of as much as 100 ft per sec.
- o Sonic layer depth changes of as much as 330 m.
- o In and below layer gradient changes.
- o Deep-sound channel axis changes of up to 800 m.
- o Sea-state changes and related ambient noise where SST gradients exist.
- o Refraction of sound rays with oblique crossing of the front.

The Mindanao Current results in acoustic changes similar to those of the Kuroshio.

Steep bathymetry gradients in coastal areas, along deep trenches, and regions of transition from deep basins to marginal seas can result in rapidly changing acoustic conditions. The Luzon Strait area has been noted for troublesome acoustic condition changes due to the combination of bottom slope and ocean current/front conditions. An unclassified section of SHAREM Report 35 of March 1980 addresses one such specific site located southeast of Okinawa. In general the numerical guidance provided by grid point or single point ASW data does not account for the loss of bottom bounce or redirection of bottom bounce in areas of steeply sloped bottoms.

Areas of opposing ocean currents and winds are known to result in waves that are higher, steeper, and of shorter wavelength. Additionally, it has been shown that areas of warm SST decrease the stability of the lower atmosphere and allow for more efficient transfer of energy from the wind to the sea surface. These elements are brought into focus in the area north of the Philippines when northwesterly winds behind frontal systems or migratory low pressure systems flow over the oceanic frontal zones. The most extreme conditions of this nature for the western North Pacific region occurs off southeastern Japan when northeasterly winds, associated with migratory highs moving off Asia or lows passing south and east of Japan, oppose the warm northeastward setting Kuroshio Current.

Some general purpose forecast aids for oceanographic conditions include:

1. There is little seasonal change of the near-surface sound speeds, except for the area north of the subtropical convergence zone (15° to 17° N).
2. The majority of the oceanic area is shallower than the critical depth; about 70% of the area does not have enough depth excess to allow reliable convergence zones.
3. The cold eddy associated with upwelling of deep water, located in the vicinity of 7° N between Palau and Mindanao, results in a pronounced thermocline, and hence a stronger negative sound speed gradient below the mixed layer.
4. Over the northern oceanic areas, the mixed layer depth generally increases in response to the strong northeast monsoon winds during winter with a steep thermocline gradient below. During summer there is generally no mixed layer.
5. Over the near equatorial region the seasonal pattern of the mixed layer and thermocline tend to be reversed from the subtropical region.
6. The seasonal changes will be extreme over the shallow marginal sea areas; see Figures 4.19a and b for seasonal variation examples.
7. The seasonal patterns follow the seasonal migrations of the sun.

5.4 Marine Planetary Boundary Layer

The marine atmosphere can be divided into two layers: the marine planetary boundary layer (MPBL), and the free atmosphere. The MPBL is typically on the order of 1 km thick, well mixed, and topped by a stable marine inversion. The free atmosphere is controlled by the circulation of large-scale highs and lows. The surface effects exert little influence on the free atmosphere. In contrast, the MPBL is influenced by both local and large scale patterns and is strongly influenced by surface effects. The primary surface effects are heating or cooling and friction. Surface effects cause the MPBL to be highly turbulent. Electro-optical (E-O) and Electromagnetic (EM) systems performance are strongly influenced by the variability of atmospheric conditions that characterize the MPBL.

5.5 Introduction to Electro-Optical and Electromagnetic Conditions

Electro-Optical (E-O) and Electromagnetic (EM) systems are playing an increasing role in U.S. Navy operational activities. Fleet environmentalists have a growing requirement to support these systems and therefore a need for understanding the interactions between the marine environment and E-O/EM conditions. This introduction section provides some basic background material on electromagnetic (EM) radiation, its interaction with atmospheric constituents, and general types of E-O systems of concern to fleet environmentalists. The primary sources of the information provided here are: Electro-Optical Handbook Volume I, ASW/TR-79-002, Cottrell et al, 1979, and Proceedings of Workshop to Standardize Atmospheric Measurements in Support of Electro-Optical Systems, UDR-TR-83-71, Huffman et al, 1983.

5.5.1 E-O/EM and the Atmosphere as a Medium

E-O and EM systems respond to electro-magnetic radiation as a sensed stimulus. The atmosphere interferes to various degrees with these systems because it interacts with both the source and propagation of radiation. The interaction depends on the atmospheric constituents and the radiation wavelength. In this section the portions of the magnetic spectrum from visible through microwave wavelengths (0.4 micrometers through 10.0 centimeters) are addressed. Table 5-1 provides categories of sensor wavelengths, general types of systems, and significance of adverse weather elements.

There are four atmospheric physical processes which affect electromagnetic (EM) radiation: reflection, scattering, absorption, and emission. The type and size of the atmospheric constituents, gaseous molecules and particulates (dust, haze, smokes, fogs, other aerosols, cloud droplets, and precipitation) affect the propagation of radiation. The influence on various wavelengths is determined by the relationship between the size of the atmospheric constituents and the wavelength of the radiation. This relationship, referred to as the size parameter, is stated as:

$$\text{size parameter} = \frac{2\pi r}{\text{radiation wavelength}}$$

where r is the particle radius.

Table 5-1. Electro-Optical and Electromagnetic Systems and Significance of Adverse Weather Elements as a Function of Sensor Wavelength Categories (after Cottrell et al, 1979).

	MICROWAVE		FLIR				VIDICON T.V.
SYSTEMS	COMMUNICATIONS	RADAR	LASER				EYE T.V. CAMERA
WAVELENGTH CATEGORIES	MICROWAVE	MILLIMETER	INFRARED				VISIBLE
			FAR FAR	FAR	MIDDLE	NEAR	
WAVELENGTH/ FREQUENCIES	10ca-1ca 36Hz-306Hz	1ca-0.1mm	0.1mm-15μ	15μ-6μ	6μ-2μ	2μ-0.74μ	0.74μ-0.4μ
WEATHER SENSITIVITY	GENERALLY INCREASES WITH DECREASING WAVELENGTH (TO THE RIGHT IN THIS TABLE)						
CLOUDS/FOG	SIGNIFICANT			EXTREMELY SIGNIFICANT			
DRY AEROSOLS	INSIGNIFICANT			SIGNIFICANT		EXTREMELY SIGNIFICANT	
PRECIPITA- TION	SIGNIFICANT		EXTREMELY SIGNIFICANT				
ABSORPTION	SIGNIFICANT		CAN BE EXTREMELY SIGNIFICANT			EXTREMELY SIGNIFICANT	
SCATTERING	SIGNIFICANT			EXTREMELY SIGNIFICANT			

Reflection takes place when the size parameter is greater than approximately 10, that is, when the wavelength is much smaller than the particle radius. Scattering causes such phenomenon as the blue sky on clear days and the milky sky on hazy days. The blue sky results from preferential scattering of the short visual wavelengths (blue) of sunlight by molecules in the atmosphere, known as Rayleigh scattering. Larger particles such as cloud droplets, dust, haze, and smoke particles, which have a size parameter near one with respect to visible light, scatter all the visible wavelengths and cause the sky to appear white or milky. This non-preferential scattering of the sunlight is called mie scattering. Absorption takes place on the molecular scale and occurs selectively with respect to wavelengths. Each absorbing constituent of the atmosphere (mainly water vapor, carbon dioxide, ozone, and oxygen) absorbs in specific wavelength intervals, which are referred to as absorption bands. Radiatio

at other wavelengths is not significantly affected by that constituent. Emission is the emitting of electromagnetic radiation (for example, a flashlight beam or the heat from a household radiator). The process operates on the molecular scale, and every constituent of the atmosphere or earth emits radiation. However, emission occurs selectively with respect to wavelength, therefore the amount of energy emitted at a given wavelength may not be significant.

The bulk or fundamental atmospheric parameters of concern in E-O/EM forecasting are temperature, pressure, humidity, and wind. These elements determine the refractive index, absorption in the infrared, and the size and contribution to refractive index of atmospheric aerosols. Low-level profiles determine the atmospheric stability, which influences turbulence. Weather elements such as drizzle, rain, and snow can severely limit the performance of all of the E-O/EM systems.

Optical turbulence, which degrades laser imaging systems, results from small-scale temperature and humidity fluctuations associated with atmospheric turbulence or mixing of air of different temperature and humidity. This turbulence causes fluctuations in the optical refractive index in the atmosphere. The turbulence parameter that is related to laser system performance is known as the refractive index structure parameter, labeled C^2N , which is a function of temperature and humidity structure parameters. The turbulence or eddies that are of concern to lasers are very small, on the order of 10 to 20 cm. Surface effects of heating, cooling and friction cause the MPBL to be highly turbulent, and therefore large values of C^2N are encountered. The larger the C^2N value the greater the degradation of laser systems.

E-O systems in the visual through infrared wavelengths can be classified as either broadband or laser (narrow line) types. Broadband means to extend over a range of wavelengths, such as visual or infrared systems. A weapons system may combine both broadband and laser components e.g., a T.V. or forward looking infrared (FLIR) system used to locate a target that is then designated (illuminated and tracked) with a laser. Environmental support of combined systems would require consideration of the atmospheric parameters affecting the wavelengths of each of the systems.

5.5.2 Comments on E-O/EM Systems and Atmospheric Interactions

This section addresses some general E-O/EM systems and atmospheric interactions of concern to the fleet environmentalist.

Visual Systems: (E-O) Cameras and human eyeballs are visual systems that require cloud-free line-of-sight between the sensor and target. Furthermore, reduced visibility due to scattering and absorption by haze, fog, and precipitation limit the capabilities of visual systems. Also, each visible system requires a minimum level of illumination.

Infrared Systems: (E-O) Lasers and Forward Looking Infrared Radar (FLIR) are active and passive systems, respectively, that operate in the infrared wavelength and require cloud-free line-of-sight to the target. Some lasers can penetrate thin cloudiness, and passive infrared systems may detect hot targets through thin clouds. Haze, fog, and precipitation degrade the transmission of energy at near infrared wavelengths. Systems operating at longer infrared wavelengths are degraded by absorption of energy by atmospheric water vapor.

Millimeter/Microwave Systems: (EM) Radar and microwave system performance is degraded by two main atmospheric factors: Heavy cloudiness (thick cloudiness with large droplet distributions of near-precipitation-sized particles), and precipitation.

5.5.3 High Energy Laser

Atmospheric conditions degrade High Energy Laser (HEL) system performance by reducing fluence (energy density per unit time deposited on the target) on the target in a variety of ways: aerosols and water vapor absorb energy, atmospheric turbulence spreads the beam fluence, and atmospheric turbulence also causes the beam to wander off its intended target (Burk et al, 1979).

Environmental conditions such as heavy rainfall and fog-induced low visibility can reduce the effectiveness of HEL systems to a point that precludes operation of such systems. Goroch and Brown (1980) produced a climatology of the frequency of occurrence of adverse weather conditions which would preclude operations of the HEL system.

In general the highest rain rates occur in the tropical zones (short periods of intense rain under convection cells), while higher latitudes tend to experience longer periods of relatively light rain. Local conditions related to upwelling and SST gradients, as well as large-scale warm surface air flow over cold water patterns, result in relatively high fog frequencies. Degraded HEL performance potential can be related to the climatology patterns of heavy rainfall and dense fog. Day-to-day performance will be influenced by these same conditions.

5.5.4 Forward Looking Infrared

The Forward Looking Infrared (FLIR) information presented in this handbook was taken from the Naval Environmental Prediction Research Facility (NEPRF) technical report 81-06, Climatology of Infrared Ranges in Pacific Ocean Regions of the Northern Hemisphere (Goroch and Brown, 1981). This climatology was computed for a nominal FLIR sensor attempting to detect a broadside cruiser target. Expected range and standard deviations by month are available in this referenced report.

The basic concept of thermal sensing, such as FLIR, is the detection of a target by a thermal detector which senses or perceives a temperature difference (contrast) between the target and its background. The temperature differences result from solar heating (insolation) or cooling by the ambient wind. The sensed or perceived contrast by the detector is diminished by the atmosphere between the source (target and its background) and the receiver.

(the infrared detector). The loss of contrast is termed the attenuation. The strongest reduction in contrast occurs during fog or precipitation. When visibility is less than 1 km, FLIR ranges can be considered the same as the visibility.

These absorption characteristics give the FLIR ranges a close relationship to the general atmospheric circulation patterns. In general there is a latitude-FLIR range correlation (increasing range with increasing latitude) reflecting a change from the warm moist stable equatorial area, to the cooler drier but variable mid-latitudes, and finally the cold dry polar regions. Effects such as continental outbreaks, stratus and fog regimes, upwelling, and oceanic currents and associated areas of cyclogenesis result in extreme variability of FLIR ranges over near coastal waters.

In the infrared wavelengths (3.4 to 5 micrometers and 8-12 micrometers) the absorption by water vapor is generally the primary effect. Absorption by aerosol particles is normally of secondary importance. However, under conditions of atmospheric low water vapor content (low temperature and/or relative humidity) the aerosol absorption becomes dominant. The open ocean north Pacific climatology of FLIR has the following general characteristics:

1. Increases from equator northward through mid-latitudes.

Winter:	Equator	10-15 km
	40-50°N	30-35 km
Summer:	Equator	10-15 km
	near 60°N	30 km

2. Summer equatorial type ranges extend into mid-latitudes in central and western Pacific. Reflects the northward advection of warm/moist equatorial air on the western side of northern hemisphere oceanic highs.

3. The variability of ranges increases with latitude and near coastlines. Reflects the variation of the general weather patterns and specifically the associated variations in temperature, relative humidity, and pressure.

FLIR climatology for the area of the Philippine Island and surrounding seas is influenced by coastal, as well as seasonal and latitudinal changes. FLIR ranges and variations over the area south of about 40°N correlate highly with the monsoon patterns. Equatorial values, near 15 km with about 2 km variations, occur during July and August under the fully developed Southwest Monsoon. Mid-latitude ranges of 25 to 30 km with variations of 10 to 20 km are found during December through March reflecting the Northeast Monsoon and migratory systems.

5.5.5 Radar and Microwave

The refractive index "n" is defined as the ratio of the speed of propagation of an electromagnetic (EM) wave in a vacuum to that in the actual atmosphere. Since EM waves travel slightly slower in air than in a vacuum, the index is slightly greater than unity. In order to have numbers that are easy to handle, refractive index is expressed as $(n-1) \times 10^6$ or simply N, which at the earth's surface has a numerical range between 250 and 400. This corresponds to an n range of 1.000250 to 1.000400. Refraction is the bending of waves due to a change in density of the medium (atmosphere) through which they are passing. Under standard, or "normal", conditions the density of the atmosphere decreases at a gradual but continuous rate with altitude. This density change is a function of decreasing temperature, humidity, and pressure and results in a rate-of-change of N of 12 units/1000 ft. When non-standard temperature and humidity vertical distributions occur the rate-of-change of N becomes non-standard too unless the changes cancel each other out.

The speed of propagation of an EM wave in a vacuum is greater than in air. Therefore, under normal conditions with decreasing density with height, EM waves travel faster at higher levels in the atmosphere than at lower. The result is that as a wave front, with some vertical extent, moves through the atmosphere the upper portion moves fastest and results in a downward bending or refraction of the wave front. The standard refraction rate however, is less than the curvature rate of the earth's surface. The end result is that under standard atmospheric conditions the wave front gradually moves away from (to higher altitude) the earth's surface but at a lesser rate than a line tangent to the earth's surface.

5.5.6 Elevated and/or Surface Based Ducts

In the real world the atmosphere is seldom, if ever, standard. The actual refractive gradient is typically slightly greater (super refraction) or less (subrefraction) than standard. Certain conditions occur which disrupt the standard temperature and humidity distributions to the extent that a significant degree of EM wave bending occurs and the wave becomes trapped within a layer of the atmosphere. This occurs under conditions of increasing temperature or sharply decreasing humidity with increasing altitude (as with an inversion). Anomalous propagation (AP) of the radar or microwave energy will then take place. The energy trapped within the layer will provide extended ranges in the layer or duct, but reduced ranges will result in the region which the waves were refracted away from.

There are three general types of ducts: 1) elevated ducts, 2) surface-based ducts that extend down from elevated trapping layers, and 3) evaporation ducts.

Elevated ducts primarily affect airborne operations. They are the result of moisture layers and/or elevated temperature inversions. They may be found anywhere from the surface to 20,000 ft or more, but are most common below 10,000 ft.

Surface-based ducts can result in extended detection, intercept, and communication ranges for all frequencies above 100 MHz (Petit and Hamilton, 1984). These extended rang

presuppose that both the transmitter and receiver are in or near the duct. Surface-based ducts are typically associated with subsidence under high pressure systems or other areas highly stable atmospheric condition. In reference to high pressure cells they form most frequently under the southeast quadrant (northern Hemisphere), northeast quadrant (southern hemisphere) and near the center of the systems.

Evaporation ducts are created by strong negative vertical water vapor gradients (i.e., water vapor rapidly decreases with height). Normally they occur within 100 ft of the surface and tend to extend ranges for surface-to-surface systems operating above 3 GHz.

Meteorological factors affecting evaporation duct height climatology for 10 Atlantic ocean weather stations were studied by Sweet (1980). Some general observations from this study that are considered applicable to the general problem include:

1. Evaporation duct heights are normally within 100 ft of the sea surface.
2. Evaporation duct heights increase as latitude decreases. Median annual duct heights (the height exceeded half the time during the year) ranged from about 50 ft at 35°N to about 20 ft at 55°N and remained nearly constant to 62°N, the northernmost station in the study.
3. Increased air and sea surface temperatures result in higher duct heights.
4. Stronger winds result in higher duct heights.
5. Sea surface temperatures greater than air temperatures result in higher duct heights.

Helvey and Rosenthal (1983) conducted a study to define ways of inferring refraction conditions from synoptic parameters. Considerable scatter or variation in duct conditions was found when attempting to correlate synoptic conditions with refractive conditions, resulting in an acknowledgement in the report that the procedures developed should be considered tentative interim guidance.

Ducting in the open ocean areas surrounding the Philippines is representative of the general latitudinal (subtropical) and atmospheric circulation (subtropical high and monsoonal conditions) conditions. The largest variations will be found in those regions that experience the greatest amount of synoptic pattern variability. In general the area to the north and west of the Philippines, which experiences both of the monsoon patterns plus northeast trades under the westward extension of the oceanic subtropical high as well as cold season passage of shear lines and midlatitude frontal systems, will experience the greatest variability in ducting conditions and heights. The complex terrain of the Philippine Islands will result in large localized variations in EM and E-O conditions. Satellite imagery and local knowledge of terrain/wind flow interactions are important in recognizing existing or potential conditions of leeside drying, funneling of low level flow, areas of convergence, land/sea breeze regimes and other locally forced conditions.

General forecast aids based on region-specific conditions include:

1. Evaporation ducts tend to be slightly higher (4-8 m) east relative to west of the Philippines.
2. During the winter the area to the east tends to have a greater frequency of enhanced surface-to-surface range conditions.
3. The conditions throughout the region are more homogenous in space and time during summer than during winter.
4. Spatial variations are greater from east to west over the northern oceanic areas relative to the more equatorial latitudes.
5. In the region north and west of the Philippines surface ducts are most common during summer, while elevated ducts are more common during winter.
6. The region north and west of the Philippines experiences significant seasonal atmospheric circulation change (NE and SW monsoons) and therefore is the area of largest seasonal variations in E-O/EM conditions.
7. Over the cold eddy, centered near 7°N 134E, there is a winter seasonal maximum of elevated ducts, but a summer maximum of surface ducting.
8. Over the northern oceanic areas evaporation ducts with heights exceeding 40 m (132 ft) are more frequent during day than night, while evaporation ducts of 20 m (66 ft or less) are more common at night.
9. In general elevated ducts are most common in the 5 to 10,000 ft range, with lower heights (<3,000 ft) occurring over the southern oceanic areas during summer and fall.

5.5.7 Forecast Aids for Elevated and/or Surface Based Ducts

The following synoptic features and inferred elevated trapping layer (ETL) indicators are provided for assistance in forecasting existing ETL conditions. When coupled with forecasting of synoptic or climatological patterns, these inferences can also be helpful in forecasting future ETL conditions.

1. The strongest and most persistent inversions and associated refractive layers occur in the equatorward half of subtropical oceanic highs, particularly the southeast quadrant in the northern hemisphere and northeast quadrant in the southern hemisphere.
2. Tracking westward under the equatorward half of the subtropical highs, convection related to warmer SST results in a progressively higher and weaker inversion (and refractive layer) with a correspondingly deeper marine planetary boundary layer (MPBL).

3. Changes from fog through low stratus areas to higher stratocumulus and cumulus areas infer a higher and weaker inversion.

4. Ocean currents influence the thickness of the MPBL. Warm currents, such as the Kuroshio of the western North Pacific weaken and increase the thickness of the MPBL while cold currents intensify and reduce the thickness of the MPBL.

5. Because inversions and ducting are associated with subsidence and stable layers, therefore highs rather than lows, the frequency of ducting shows a strong correlation with SLP. When the SLP is below 1000 mb, the probability of ducting is very low (<10%) while with SLP >1020 the probability approaches 50%.

6. Duct frequency versus surface wind direction is at a minimum for S through WNW winds and a maximum for NNW through SE winds.

7. Duct frequency increases as the temperature difference between the surface and 700 mb decreases. Small differences indicate a stable atmosphere (high frequency of inversion and ducts) and large differences indicate an unstable atmosphere and convective activity (low frequency of inversion and ducts).

Forecast Aids for Prediction of Standard Refractive Conditions

1. Area of concern is located within the northwest quadrant of subtropical highs.
2. Under or immediately following an active front.
3. Area of cyclonically curved isobars.
4. Close to a low pressure center.
5. Surface pressure less than 1000 mb.
6. Cold air aloft, 700 mb temperature less than -10C.
7. Presence of cumulus and deep convective clouds.
8. Unstable, windy conditions.
9. Open celled clouds behind frontal systems.

Forecast Aids for Duct Height

1. The maximum frequency of oceanic ducts occurs in the 4,000 to 6,000 ft layer.
2. A secondary frequency maximum occurs between the surface and 2000 ft when the SLP is >1018 mb and surface winds are <6 kt (near centers of highs).

3. When a migratory upper-level trough replaces a anticyclone, strong low-level ducts are likely to become weak ducts near 10,000 ft within a 48-hour period.

4. Within oceanic anticyclones, duct heights vary by about 3000 ft from the lowest level in the SE quadrant to the highest in the NW quadrant.

5. In addition to synoptic variations there are general latitude variations. On the average ducts are higher in lower latitude (over warmer water) and lower towards the poles (over colder water).

6. There is a tendency for the mean elevated duct heights to increase with increasing SST. Table 5-2 provides approximate mean duct heights for areas within 300 n mi of the center of highs for SST intervals.

Table 5-2. Approximate Mean Elevated Duct Heights (ZD) for areas within 300 n mi of highs for Specified Sea Surface Temperature Intervals (Helvey and Rosenthal, 1983).

Sea Surface Temperature (SST)		Height MSL (ZD)	
(C)	(F)	(m)	(ft)
5-7	41-45	1000	3300
8-10	46-50	1200	3900
11-12	51-55	1300	4300
13-15	56-60	1400	4600
16-18	61-65	1500	4900
19-21	66-70	1600	5200
22-24	71-75	1700	5600
25-27	76-80	1800	6200
>27	>80	2000	6600

7. A best fit linear regression for optimum coupling height (OCHT), where OCHT is defined as the altitude at which electromagnetic energy is most effectively "coupled" into the duct, is:

$$\text{OCHT (m)} = 42 (\text{SST in } ^\circ\text{C}) + 743$$

Example: SST = 20°C then OCHT = 1583 m

Based on 5 year study by Ortenburger, L.N. et al. (1978) of GTE, Sylvania, Electronic Systems Group, Western Division, Mountain View, California.

Forecast Aids Based on Satellite Interpretation

1. In regions of offshore flow where clear conditions extend seaward and change to lighter gray shade areas and then smooth stratus type clouds, surface-based ducts are likely. These areas are under the influence of high pressure and subsidence.
2. In regions of offshore flow where distinct cloudlines are seen forming, near-standard propagation conditions are probable. The areas generally have well mixed and unstable atmospheric conditions.
3. Improved visibility, EM ranges, and weakened low level inversions are typically found in the lee of mountainous islands. In visual imagery these areas will appear darker than surrounding areas, unless they are in a sunglint area in which case very bright return will be seen if surface winds are light.
4. Cornering effects result in increased winds, convergence, cloud development, and typically degraded visibility and EM conditions. Cornering effects occur where moderate or stronger winds blow around islands or points of land.
5. Increasingly lighter gray shades over water areas imply increased atmospheric humidity and/or aerosols and reduced visibility and EM ranges.
6. When smoke plumes from coastal facilities can be seen extending for some distance in satellite imagery or by eye, a temperature inversion is likely near the top of the smoke plume level.
7. The SST pattern in shallow coastal water areas will exhibit a strong seasonal reversal relative to the deep water SST. Coastal waters tend to be hot in summer and cold in winter and will modify the atmosphere above it and the EM conditions. Summer heating provides well mixed and near normal conditions. Winter cooling will stabilize the lower levels resulting in low level inversions and generally reduced EM ranges.
8. Areas of smooth low-level stratus are likely to be topped by a low-level inversion, and ducting is likely (may be surface-based).
9. The appearance of ship condensation trails indicates a strong shallow marine layer and probable surface-based ducts.
10. Frontal bands imply strong winds, well mixed atmosphere, and near-standard propagation conditions.
11. The areas of open cells, to the rear of fronts, indicate unstable conditions and therefore are likely to have near-standard propagation conditions.
12. Areas of closed cells indicate stable conditions, and inversions and ducting are probable.

13. Over the region where the closed cells become smaller and change to smooth continuous structures the inversions and duct heights will be lowering.

5.6 REGIONAL ATMOSPHERIC CIRCULATION PATTERNS

The following paragraphs cover circulation patterns over and to the west of the Philippine Islands. Forecast aids for the oceanic area east of the Islands are contained in Section 5.7.

5.6.1 Northeast Monsoon

During the Northeast Monsoon, a Siberian high cell commencing to move southeasterly will cause the gradient to strengthen across southern China and the northern South China Sea. Usually a surface wind maximum will move south from the Yellow and East China Seas. The wind maximum may not be gale force, but when it reaches the Taiwan Strait it will increase by 10 to 15 kt. If a wind maximum with speeds of 20 kt or greater is approaching Taiwan, the forecaster should expect gale force winds in the channel. If the wind maximum was already gale force, then a storm warning should be considered. Similar conditions occur with an approaching tropical cyclone (FWC/JTWC, 1978).

When the 1017 mb isobar reaches the south coast of China and the pressure at Hong Kong (45005) is higher than the pressure at the southern tip of Taiwan, gale force winds will occur in the Taiwan Strait with speeds up to 40 kt (NOCF, Cubi Point, 1984).

Within 6 to 12 hours after a cold frontal passage at station 46734, gale force winds will prevail in the Taiwan Strait and spread into the South China Sea (NOCF Cubi Point, 1984).

The following has been extracted from NOCF, Cubi Point, 1984):

1. During the Northeast Monsoon, when strong winds are being funneled through the pass to the northeast of Cubi Point, moderate turbulence may be expected for all aircraft departing on runway 07 on climb through 5,000 feet.
2. During the Northeast Monsoon, light to moderate turbulence up to 10,000 feet may be forecast on the lee side of mountains in northern Luzon. Lenticular clouds are common with mid-level inversion.
3. Indications that a northeast surge is invading the Cubi Point area are: Gusty winds starting about 0200L, sea level pressure above normal between 0200L and 0400L, and temperatures slightly cooler than normal.

4. During the Northeast Monsoon, when the 3,000 to 5,000 ft winds are 10 to 15 kt and the inversion on the 1200 GMT Clark AB sounding is¹ fairly deep, small craft conditions may be forecast for the following day.

5. The oceanic region around and north of Luzon experiences the highest wind speeds during autumn as the northeast monsoon builds up. Over the rest of the area, wind speeds reach a maximum in winter at the height of the combined northeast monsoon and trade winds regimes.

5.6.2 Shear Lines

1. If the outbreak of polar air is weak, there will be increased mid-level cloudiness but no precipitation with the passage of a shear line at Cubi Point. If the shear line is particularly intense and well defined, rainfall will be heavier but will last for only a few hours and be followed by clearing weather.

2. With an isotach maximum of 30 kt or more over the South China Sea and moving westward, a shear line may form over Luzon.

3. When the sea level pressure difference between Cubi Point and Okinawa is 10 mb or more, light rain or drizzle will be experienced with passage of a shear line. If the pressure difference is less than 10 mb, only increased cloudiness will occur.

4. When the continental high pressure cell is moderate to strong and ridging east-southeastward behind a moderate cold front, the following guidelines apply.

a. If the low associated with the front moves north of Japan, expect shear line passage at Cubi Point when the low moves east of 115°E.

b. When the Shanghai low forms and moves along the southern coast of Japan, expect passage of the shear line at Cubi Point when the low passes 140°E.

5.6.3 Easterly Waves

Because of the lack of a good network of reporting stations east of the Philippines, it is difficult to forecast or detect passage of easterly waves at Cubi Point. At no time are they a typical occurrence and only in the spring when the easterly flow is best established is there much likelihood of their passage over the Cubi Point area.

¹Not available since 1991.

The following guidelines have been taken from the 1984 edition of the Forecaster's Handbook, NAS Cubi Point, R.P., published by the NOCF, Cubi Point, R.P.

1. Unless it is possible to analyze and follow the progress of an easterly wave from the time it passes Belau (91408), the first indication of entry into the Philippines may be its passage across eastern Mindanao.
2. Easterly wave passage at Cubi Point may be anticipated roughly 24 hours after the first indications of its approach are observed along the east coast of the Philippines.
3. Weather conditions during passage of an easterly wave consist of drizzle or showers, scattered to broken low clouds, broken middle clouds, and a high overcast.
4. If an easterly wave passes during the period of maximum heating of the day, it may set off a wide area of thunderstorm activity.
5. The most adverse weather conditions at Cubi Point during the winter months usually occur when an easterly wave passes over the Philippines at the same time that a shear line is approaching from the north.
6. Easterly waves move at an average speed of 10 to 15 kt and reach their maximum intensity in the layer from 700 to 500 mb, sloping eastward with height.
7. When the wave moves slower than the basic current in the low levels and faster than the basic current in the upper levels, the area west of the wave is characterized by subsidence and fair weather while areas of convergence and disturbed weather occur east of the trough.
8. The best aid in looking for easterly waves is by use of consecutive satellite pictures. By looking for the inverted "V" cloud pattern, which is often diffused, and by keeping a daily track on these cloud patterns, the forecaster can determine its movement.
9. Easterly wave generally stagnate over the Philippines or intensify the "lee side" trough to the west.
10. Any time a station in the tropics is observed reporting haze, with the exception of industrialized Manila, it should be immediately suspected as being below the subsidence inversion in advance of an easterly wave.

5.6.4 Southwest Monsoon

1. A shift from southwesterly to easterly flow during the Southwest Monsoon will bring a period of fair weather to Cubi Point for the duration of the easterly flow.

2. With moderate southwesterly flow, weather over Cubi Point will be low overcast with reduced visibility and intermittent light to moderate rain and thunderstorms. This condition can be expected to last for at least a 24-hour period.

3. Tropical cyclones crossing the Philippines or moving through the Bashi Channel enhance the southwest flow once they reach the South China Sea.

4. During the Southwest Monsoon, expect the most frequent rainshower or thunderstorm activity between 0600L and 1000L with a break between 1100L and 1300L with rainshower activity commencing again at 1300L until 1700L. If the showers do not let up between 1100L and 1300L, but persist until about 1400L, there will be no further afternoon showers.

5. During the Southwest Monsoon, if the winds are southwesterly greater than 15 kt between the surface and 300 mb, continuous rain may be forecast.

5.6.5 Cloudiness

1. When surface winds are from the south-southwest through west-southwest (190° - 240°), coming right up the mouth of the bay, conditions within the bay will be solid overcast. With surface winds from the west-southwest through west (240° - 270°), coming over the mountains to the west of Cubi Point, broken conditions or breaks in the overcast may be forecast.

2. During the Northeast Monsoon, when the 1200Z Clark sounding² shows a strong inversion and surface winds are forecast in the 6-10 kt range, broken stratocumulus may be forecast over the field from just before sunrise to two hours after sunrise. When the 1200Z sounding shows a mid-level inversion and the 850 mb winds are 10-20 kt, a middle cloud layer may be forecast over the field during the same time period.

5.6.6 Visibility

When showers are coming in from the east, visibility may be forecast as low as 3 to 5 miles; if approaching from the southwest through west, it is possible for visibility to go below minimums.

5.6.7 Thunderstorms

1. When the southwesterly flow is comparatively deep in the spring transition months or during the Southwest Monsoon, afternoon thunderstorms may be expected at Cubi Point.

²Not available since 1991.

2. The frequency of occurrence of elevated ducts or superrefraction layers over the Philippine Sea is at a maximum during winter (30-70%) and in general increases in frequency and height under the portion of the subtropical flow where subsidence/trade wind capped inversions is developed. Frequencies of occurrence decrease to the south due to surface heating and to the west due to atmospheric mixing and synoptic scale circulation.

3. During the Southwest Monsoon when a land breeze, however light, exists, expect a line of thunderstorms and associated rainshowers to form off the coast between 0500L and 0700L.

4. There is a good chance of thunderstorms if 850 mb winds are southwesterly 25 kt or greater.

5. Well developed cumulus buildups often result in a weak counter-clockwise micro-circulation that may extend 3 to 5 miles out from the cell and result in 5 to 10 kt of extra wind speed.

5.6.8 Turbulence

1. During a strong surge in the southwesterly flow, the easterly jet stream is directly over Luzon and creates moderate turbulence between 10,000 and 25,000 feet.

2. During the Northeast Monsoon, when strong winds are being funneled through the pass to the northeast of Cubi Point, moderate turbulence may be expected for all aircraft departing on runway 07 on climb through 5,000 feet.

3. During the Northeast Monsoon, light to moderate turbulence up to 10,000 feet may be forecast on the lee side of the mountains in northern Luzon. Lenticular clouds are common with a mid-level inversion.

4. During a strong surge in the southwesterly flow, the easterly jet stream is directly over Luzon and creates moderate turbulence between 10,000 and 25,000 feet.

5.7 FORECAST AIDS FOR OCEANIC AREAS EAST OF THE PHILIPPINES

The following guidelines have been taken from the 1969 edition of NWSED, Agana, Guam's Local Area Forecaster's Handbook and generalized for forecasting shear line passage over the oceanic area east of the Philippine Islands.

5.7.1 Forecasting the Movement of Shear lines

The forecasting of the movement of shear lines has been a difficult experience for many meteorologists due to their unique nature and the paucity of reference material.

1. A weak frontal inversion will be associated with the shear line.
2. As the shear line approaches within about 200 n mi the trade inversion will strengthen.
3. As the shear line passes, winds will back from easterly and increase in speed. There will be a marked decrease in convective type clouds. An increase in the temperature-dew point spread will occur following passage of the shear line.

5.7.2 Intertropical Convergence Zone (ITCZ)

Pilot reports and satellite data, along with oceanic island reports, are essential for locating and determining movement of the ITCZ³. An increase in middle clouds and above normal convective activity can be expected as the ITCZ approaches from the south. When the ITCZ moves to within about 100 n mi to the south of a location a marked increase in shower activity can be expected. Weather will improve rapidly when the ITCZ moves to the north and dissipates. The situation will be of short duration, however, as a new ITCZ will form within 12 to 24 hours near the mean seasonal position.

5.7.3 Easterly Waves

Troughs in the easterlies are sometimes difficult to locate. Often the best indication of a wave approaching the area will be from a pilot debrief or satellite imagery. Sharp questioning by the forecaster concerning winds and weather enroute will often provide the clues needed to ascertain the location of a wave. Factors to determine include: The location and extent of any significant weather, significant wind shifts, and the position of the shift in relation to the weather. The line of weather should be oriented north-south, and the wind shift from easterly to southeasterly, thence northeasterly, when proceeding westbound. A good rule of thumb is to advance the wave westward at an average speed of 10 kt when actual data are not available.

³If the winds to the south of the convergence zone cloudiness have a westerly component, the phenomena is the Monsoon Trough, not the ITCZ.

References

- Apel, J. R., J. R. Holbrook, A. K. Liu, and J. J. Tsai, 1985: The Sulu Sea Internal Soliton Experiment. *Journal of Physical Oceanography*, 15, 1625-1651.
- Atkinson, G., 1971: Forecasters' Guide to Tropical Meteorology. Air Weather Service Technical Report 240, 300 pp.
- Bowin, C., R. S. Lu, C.-S. Lee, and H. Schouten, 1978: Plate Convergence and Accretion in the Taiwan-Luzon Region. *Bull. Am. Assoc. Pet. Geol.*, 62 (9), 1645-1672.
- Boyle J. S. and T.-J. Chen, 1987: Synoptic Aspects of the Wintertime East Asian Monsoon. *Monsoon Meteorology*. Eds. C.-P Chang and T. N. Krishnamurti. Oxford Monographs on Geology and Geophysics No. 7. Oxford University Press, New York.
- Brand, S. and J. Blueloch, 19-12: Changes in the Characteristics of Typhoons Crossing the Philippines. ENVPREDRSCHFAC Technical Paper No. 6-72, Naval Research Laboratory, Monterey, CA 93943-5502, 31 pp.
- Burk, S. D., A. K. Goroch, A. I. Weinstein, and H. A. Panofsky, 1979: Modeling the Refractive Index Structure Parameter in the Marine Planetary Boundary Layer. NEPRF 79-03, Naval Research Laboratory, Monterey, CA 93943-5502.
- Carpenter, G. H., 1989: Surface Circulation Associated with the Mindanao and Halmahera Eddies. Master's Thesis, Naval Postgraduate School, Monterey, CA, 122 pp.
- Chingchang, B., C. T. Shyu, J. C. Chen, and S. Boggs, Jr., 1985: Taiwan: Geology, Geophysics & Marine Sediments. Chapter 11, pp. 520, 522, 536. *The Ocean Basins and Margins*, Vol 7A, The Pacific Ocean, A. E. M. Nairn, F. G. Stehli, and S. Uyeda, Eds. Plenum Press, New York & London.
- Chuang, W.-S., 1985: Dynamics of Subtidal Flow in the Taiwan Strait. *Journal, Oceanographical Society of Japan*, 41, 65-79
- Chuang, W.-S., 1986: A Note on the Driving Mechanisms of Current in the Taiwan Strait. *Journal, Oceanographical Society of Japan*, 42, 355-361.
- Commander Naval Oceanography Command (CNOG), 1989: U. S. Navy Regional Climatic Study of the Central East Asian Coast and Associated Waters. NAVAIR 50-IC-556. NAVOCEANCOMDET Asheville NC, 313 pp.

- Commander Naval Oceanography Command (CNOC), 1990: Naval Oceanography Command Facility, Cubi Point Forecaster's Handbook. NAVOCEANCOMFAC USNAS Cubi Point, Republic of the Philippines, 127 pp.
- Conlee, D. T., 1991: Satellite Image Display and Processing with Microcomputers: A Proof-of-concept for the Navy Oceanographic Data Distribution System. MS thesis. Naval Postgraduate School. Monterey, CA 93943-5000, 56 pp.
- Cordero, P. A., Jr., 1981: Eco-morphological Observation of the Genus SARGASSUM in Central Philippines, including Notes on their Biomass and Bed Determination. *THE REEF AND MAN*, Vol. 2 (Gomez, E. L. et al., Editors). University of the Philippines, Quezon City, Philippines, p. 401.
- Cottrell, K.G., P.D. Try, D.B. Hodges, and R.F. Wachtmann, 1979: Electro-Optical Handbook, Volume 1, Weather Support for Precision Guided Munitions Air Weather Service. AWS/TR-79/002, 97 pp.
- Dewey, J. F., 1972: Plate Tectonics. *Continents Adrift and Continents Aground*. W. H. Freeman & Co., San Francisco, 34-35, 40.
- Dvorak, V. F., 1984: Tropical cyclone intensity analysis using satellite data. NOAA Tech. Report NESDIS 11, Washington D.C., 47 pp.
- Eicher, D. L., and A. L. McAlester, 1980: *History of the Earth*. Prentice-Hall, Inc., Englewood Cliffs, NJ, p. 291.
- Elsberry, R. L., W. M. Frank, G. J. Holland, J. D. Jarrell and R. L. Southern, 1987: *A Global View of Tropical Cyclones*. Marine Meteorology Program, Office of Naval Research, Washington, DC, 185 pp.
- Exon, N. F., F.-W. Haake, M. Hartmann, F.-C Kogler, P. J. Muller, and M. J. Whitiker, 1981: Morphology, Water Characteristics and Sedimentation in the silled Sulu Sea, southeast Asia. *Marine Geology*, 39(3/4), 165-195.
- Fan, K.-L., and C.-Y. Yu, 1981: A Study of Water Masses in the Seas of Southernmost Taiwan. *Acta Oceanog. Taiw.*, 12, 94-111.
- Fan, K.-L., 1982: A Study of Water Masses in Taiwan Strait. *Acta Oceanog. Taiw.*, 13, 140-153.
- Fengqi L, S. Yusong, and F. Liqun, 1988: Application of Method of Fuzzy Sets to the Analysis of Water Masses in the northern South China Sea. *Acta Oceanologica Sinica*, 7(2), 170-185.

- Fett, R. W., P. E. La Violette, M. Nestor, J. W. Nickerson, and K. Rabe, 1977: Navy Tactical Applications Guide. Vol. II. Naval Research Laboratory, Monterey, CA 93943-5502, p. 3D-5.
- First Weather Wing, U. S. Air Force, 1987: Terminal Forecast Reference Notebook. Detachment 5, 20th Weather Squadron, Clark Air Base, Republic of the Philippines, 73 pp.
- Fleet Weather Central/Joint Typhoon Warning Center (FWC/JTWC), Guam, 1978: Area of Responsibility Forecaster's Handbook. U.S. Naval Weather Service Command, NSTL Station, Bay St. Louis, MS 39529.
- Flores, J. F., and V. F. Balagot, 1969: Climate of the Philippines. *World Survey of Climatology* (H. Arakawa, Ed.), Vol. 8, Elsevier Scientific Publishing Company, Amsterdam, The Netherlands, 159-213.
- FNOC, 1991: Navy Oceanographic Data Distribution System (NODDS 3.0) Users' Manual. Fleet Numerical Oceanography Center, Monterey CA 93943-5005, 76 pp.
- Fu, R., A. D. Del Genio and W. B. Rosso, 1990: Behavior of Deep Convective Clouds in the Tropical Pacific Deduced from ISCCP Radiances. *J. Climate.*, 3, 1129-1152.
- Geise, G. S., and R. B. Hollander, 1987: The Relationship between Coastal Seiches at Palawan Island and Tide-Generated Internal Waves in the Sulu Sea. *Journal of Geophysical Research*, 92 (C 5), 5151-5156.
- Goerss, J. S., and P. A. Phoebus, 1992: The Navy's Operational Atmospheric Analysis. *Wea. Forecasting*, 7, 232-249.
- Goroch, A.K. and T. Brown, 1980: Frequency of Adverse Weather Conditions Affecting High Energy Laser Systems Operations. NAVENVPREDRSCHFAC Technical Report TR 80-06, Naval Research Laboratory, Monterey, CA 93943-5502.
- Guard, C. P., 1985: An Observational Assessment of the Southwest Monsoon East of East Asia. Presented at the International Conference on Climatology and Applied Meteorology. Manila, Republic of Philippines, 17 pp.
- Guard, C. P., 1986: Local and Regional Influences on the Meteorology of Central America. Air Weather Service Forecaster Memo (AWS/FM-86/002), 23 pp.
- Guard, C. P., L. E. Carr, F. H. Well, R. A. Jeffries, N. D. Gural and D. K. Edson, 1992: Joint Typhoon Warning Center and the Challenges of Multibasin Tropical Cyclone Forecasting. *Wea. Forecasting*, 7, 328-352.

- He, Y., and W. B. White, 1987: Interannual Variability of the Kuroshio Frontal Structure along its western boundary in the N. Pacific Ocean associated with the 1982 ENSO Event. *Journal of Physical Oceanography*, 17(9), 1494-1506.
- Helvey, R.A. and J.S. Rosenthal, 1983: Guide for Inferring Refractive Conditions from Synoptic Parameters. Pacific Missile Test Center, Tech. Paper TP000005, 36 pp.
- Hogan, T. F., and T. E. Rosmond, 1991: The Description of the Navy Operational Global Atmospheric Prediction System's spectral forecast model. *Mon. Wea. Rev.*, 119, 1786-1815.
- Huang, R., and C.-C. Huang, 1987: Plankton Communities in the Surface Waters of Taiwan Strait. *Acta Oceanog. Taiw.*, 18, 16-23.
- Hufford, G. L., 1991: Some Items of Interest from the First Symposium on Volcanic Ash and Aviation Safety. Western Region Technical Attachment, No. 91-32. Western Region Headquarters of the National Weather Service, Salt Lake City, UT, 4 pp.
- Hung, T.-C., C. C. H. Tsai, and N.-C. Chen, 1986: Chemical and Biomass Studies: (1) Evidence of Upwelling off the Southwestern Coast of Taiwan. *Acta Oceanog. Taiw.*, 17, 19-44.
- Hung, T.-C., B.-C. Han, and D.-S. Hsu, 1987: Chemical and Biomass Studies: (2) Biological Activities in Upwelling off the Southwestern Coast of Taiwan Including the Penghu Area. *Acta Oceanog. Taiw.*, 18, 62-74.
- Ingmanson, D. E., and W. J. Wallace, 1973: *Oceanology, An Introduction*. Wadsworth Publishing Co., Inc., Belmont CA, pp. 51, 55.
- Kanari, S-I., and T. Teramoto, 1981: Bashi Channel, Luzon Strait: A Hydraulic Model Experiment of the Tidal Current. *J. Oceanog. Soc.*, Japan, 37, 31-48.
- Kendall, T. R., 1969: Net Transports in the Western Equatorial Pacific Ocean. *Journal of Geophysical Research*, 74(6), 1388-1396.
- Krause, D. C., 1966: Tectonics, Marine Geology, and Bathymetry of the Celebes Sea - Sulu Sea Region. *Bull. Geological Society of America*. 77(8), 813-832.
- LaFond, E. C., 1966: South China Sea. *Encyclopedia of Oceanography*, R. W. Fairbridge, Ed., Reinhold Publishing Corp. NY, 829-837.
- Levitus, S., 1982: *Climatological Atlas of the World Ocean*. NOAA Professional Paper 13. Environmental Research laboratories, Geophysical Fluid Dynamics Laboratory, Princeton, NJ, 173 pp.

- Li, H.-W., and K.-H. Su, 1987: A Numerical Model of Typhoon Surges and Tides in the Seas Adjacent to Taiwan. *Acta Oceanog. Taiw.*, 18, 39-48.
- Liu, C.-T., S.-G. Liau, S.-C. Pai, and K.-K. Liu, 1986: Water Masses in the Western Philippine Sea-Physical Aspects. *Acta Oceanog. Taiw.*, 17, 1-17.
- Lukas, R., 1988: Interannual Fluctuations of the Mindanao Current Inferred from Sea Level. *Journal of Geophysical Research*, 93(C 6), 6744-6748.
- Matsuzawa, J., 1968: Second Cruise for CSK RYOFU MARO, Jan. - Mar. 1968. *The Oceanographical Magazine*, 20(2), 173-185.
- McCoy, F. L., and C. Sancetta, 1985: North Pacific Sediments. *The Ocean Basins and Margins* Vol. 7A, The Pacific Ocean, A. E. M. Nairn, F. G. Stehli, and S. Uyeda, Eds. Plenum Press, New York & London, 1-64.
- Miller, R. J., T. L. Tsui and A. J. Schrader, 1988: Climatology of North Pacific Tropical Cyclone Tracks. Technical Report TR 88-10, Naval Research Laboratory, Monterey, CA, 93943-5502, 511 pp.
- Miller, R. J., A. J. Schrader and T. Tsui, 1989: Automated Tropical Cyclone Forecasting System Version 2.6 (Users Guide), Naval Research Laboratory, Monterey, CA, 93943-5502, 57 pp.
- Murdock, J. M., 1980: The Transparency of Southeast Asian and Indonesian Waters. Master's Thesis. Naval Postgraduate School, Monterey, CA, 161 pp.
- National Geographic Society, 1981: *National Geographic Atlas of the World*. 5th ed. Washington, DC, 383 pp.
- Naval Oceanography Command Facility (NOCF), Cubi Point, R.P., 1984: Forecaster's Handbook, NAS Cubi Point, R.P. Commander, Naval Oceanography Command, NSTL Station, Bay St. Louis, MS 39529.
- Ortenburger, L.N., S. B. Lawson, and G. K. Miller, 1978: Optimum Electromagnetic Energy/Ducting Coupling Height. GTE, Sylvania, Electronic Systems Group, Western Division, Mountain View, California.
- PAGASA, 1987: Climatological Normals/Averages of the Philippines (1951-1985). Philippine Atmospheric, Geophysical and Astronomical Services Administration, Quezon City, Republic of Philippines, 64 pp.

- Petit, P, and H. Hamilton, 1984: Assessing and Displaying the Effects of Elevated Trapping Layers in Support of Navy Command and Control. NEPRF CR 84-01, Naval Research Laboratory, Monterey, CA, 93943-5502, 82 pp.
- Ramage, C. S., 1971: *Monsoon Meteorology*. Academic Press, New York, 296 pp.
- Ross, M. A., and G. Hodgson, 1981: A Quantitative Study of Hermatypic Coral University and Zonation at Apo Reef, Philippines. *THE REEF AND MAN*, Vol. 2 (Gomez, E. L. et al., Editors). University of the Philippines, Quezon City, Philippines, p. 283.
- Sadler, J. C. and T. C. Wann, 1984: Mean Upper Tropospheric Flow over the Global Tropics, Volume II. AWS/TR-83/002 Air Weather Service (MAC), Scott AFB, Illinois 62225, 48 pp.
- Sadler, J. C., M. A. Lander, M. A. Hori and L. K. Oda, 1987a: Tropical Marine Climatic Atlas. Vol. I (Indian Ocean and Atlantic Ocean). Dept. Met., U. of Hawaii. Tropical Oceans Global Atmosphere (TOGA) and Equatorial Pacific Ocean Climatic Studies (EPOCS). UHMET Report 87-01, 51 pp.
- Sadler, J.C., M. A. Lander, M. A. Hori and L. K. Oda, 1987b: Tropical Marine Climatic Atlas. Vol. II (Pacific Ocean). Dept. Met., U. of Hawaii. Tropical Oceans Global Atmosphere (TOGA) and Equatorial Pacific Ocean Climatic Studies (EPOCS). UHMET Report 87-02, 27 pp.
- Schramm, W. G., 1979: Airborne Expendable Bathythermograph (AXBT) Observations Immediately Before and After Passage of Typhoon Phyllis in August of 1975. TR-79-05, Naval Research Laboratory, Monterey, CA, 93943-5502, 48 pp.
- Shepard, F. A., P. A. McLaughlin, N. F. Marshall, and G. G. Sullivan, 1977: Current-meter Recordings of Low-speed Turbidity Currents. *Geology*, 5, 297-301.
- Shevtosov, V. P., A. S. Salomatin, and V. I. Yusupov, 1985: Investigation of the Volume Scattering of 12- and 30-kHz Frequency Sound in the Pacific Ocean. *Izvestiya, Atmospheric and Oceanic Physics*, 21(6), 489-494.
- Shoemaker, D. N., 1991: Characteristics of Tropical Cyclones Affecting the Philippine Islands (draft). Naval Oceanography Command Center/Joint Typhoon Warning Center Technical Note 91-01, 35 pp.
- Sweet, W., 1980 Meteorological factors Affecting Evaporation Duct Height Climatologies. NAVENVPREDRSCHFAC Technical Report TR 80-02, Naval Research Laboratory, Monterey, CA, 93943-5502, 33 pp.

- Tjia, H. D., 1966: Sulawesi (Celebes) and Sulu Seas. *The Encyclopedia of Oceanography*, R. W. Fairbridge, Ed., Reinhold Publishing Corp., NY, 885-890.
- Toksoz, M. N., 1975: The Subduction of the Lithosphere. *Continents Adrift and Continents Aground*. W. H. Freeman & Co., San Francisco, 114-115.
- Toole, J. M., E. Zou, and R. C. Millard, 1988: On the Circulation of the Upper Waters in the western equatorial Pacific Ocean. *Deep-Sea Research*, 35(9), 1451-1482.
- Uda, M., 1966: Philippine Sea and Waters South of Japan. *The Encyclopedia of Oceanography*, R. W. Fairbridge, Ed., Reinhold Publishing Corp., NY, 705-712.
- United States Air Force Environmental Technical Applications Center (USAFETAC), 1985: Situation Climatic Briefs. USAFETAC/DS-85/030. Scott Air Force Base, Illinois 62225-5438, Asia: pp. C-56-2 through C-56-5.
- U.S. Department of Commerce, National Oceanic and Atmospheric Administration, National Ocean Service, 1989: Tide Tables, 1990: High and Low Water Predictions: Central and Western Pacific Ocean and Indian Ocean, pp. 144-167.
- U.S. Naval Oceanography Command Center/Joint Typhoon Warning Center 1991: 1990 Annual Tropical Cyclone Report. NAVOCEANCOMCEN/JTWC, COMNAVMARIANAS, PSC 489, Box 12, FPO AP 96540-0051, 278 pp.
- U.S. Naval Oceanography Command Center/Joint Typhoon Warning Center, 1992: 1991 Annual Tropical Cyclone Report. NAVOCEANCOMCEN/JTWC, COMNAVMARIANAS, PSC 489, Box 12, FPO AP 96540-0051, 238 pp.
- Wang, J., 1986: Observation of Abyssal Flows in the Northern South China Sea. *Acta Oceanog. Taiw.*, 16, 36-45.
- Wang, J., and C.-S. Chern, 1988: on the Kuroshio Branch in the Taiwan Strait during Wintertime. *Progress in Oceanography*, 21(3-4), 469-491.
- Western Region Headquarters of the National Weather Service, 1992: The Volcanic Ash Forecast Transport and Dispersion (VAFTAD) Model. Western Region Technical Attachment, No. 92031, Salt Lake City, UT, 5 pp.
- Williams, F. R., G. H. Jung and R. J. Renard, 1989: Forecasters Handbook for Central America and Adjacent Waters. Naval Research Laboratory, Monterey, CA, 93943-5502, TR-89-08, 508 pp.
- Wilson, J. T., 1963: Continents Adrift. *Continents Adrift and Continents Aground*. W. H. Freeman & Co., San Francisco, 22-23.

Woodruff, S. D., R. J. Slutz, R. L. Jenne and P. M. Steurer, 1987: A Comprehensive Ocean-Atmosphere Data Set. *Bull. Amer. Meteor. Soc.*, 68, 1239-1250.

Xiang, H. Y., 1988: Temperature and Salinity Distributions in the South China Sea and Adjacent Waters. *Progress in Oceanography*, 21(3-4), 493-501.

Yin, F., 1988: Seawater Variation east of Taiwan. *Progress in Oceanography*, 21(3-4), 457-467.

Appendix A

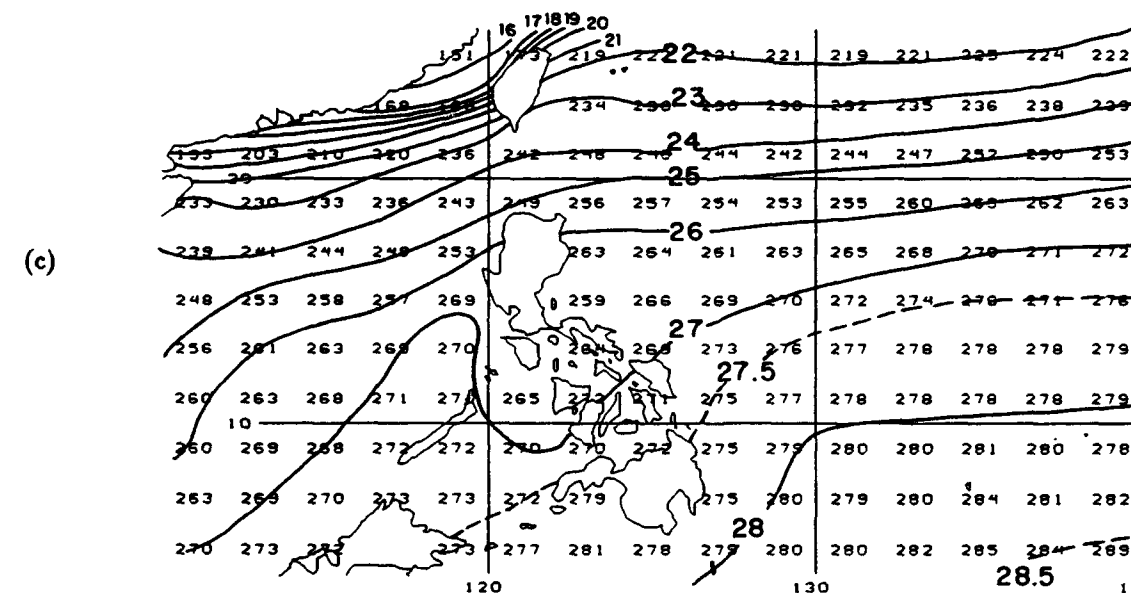
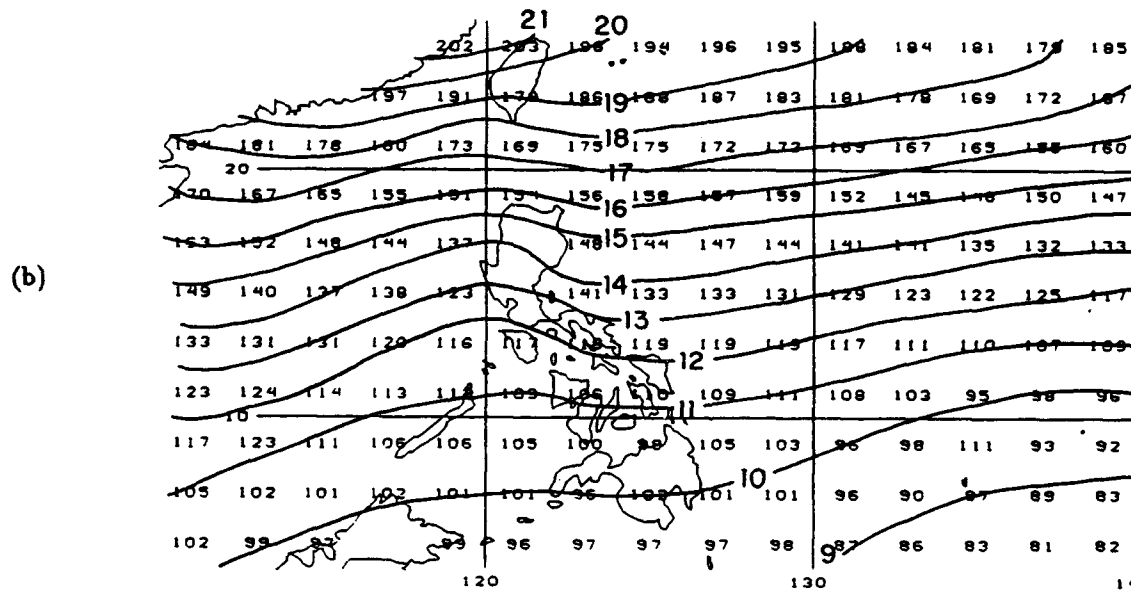
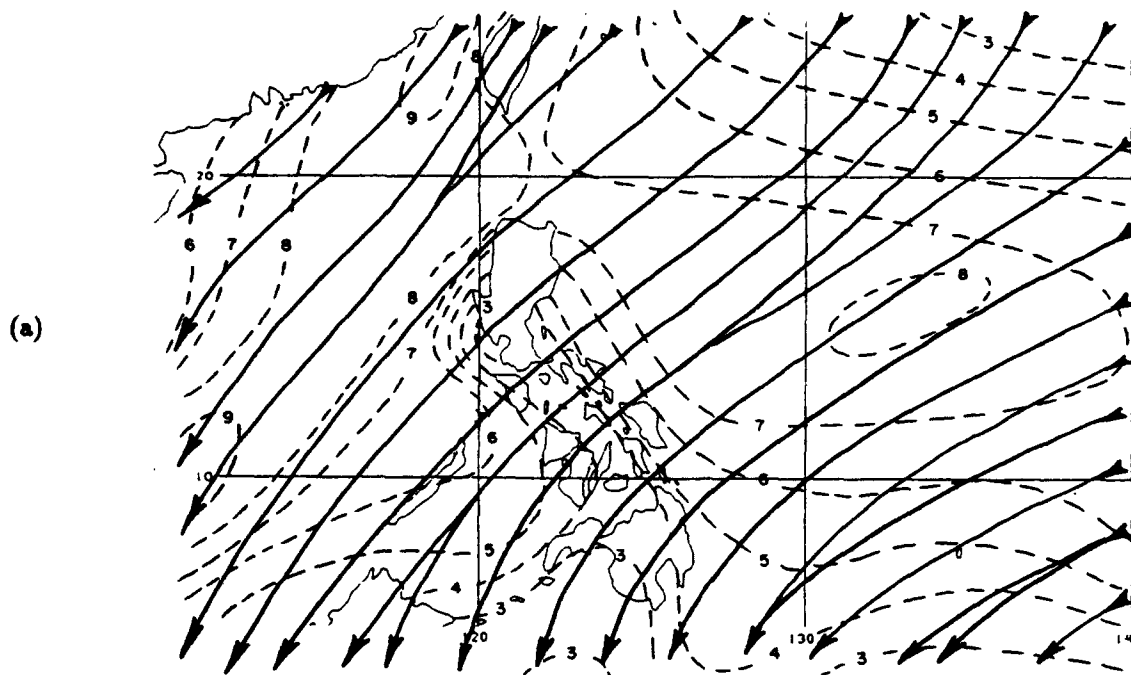
Comprehensive Ocean-Atmosphere Data Set

During the 1970s and 1980s many programs set out to improve the atmospheric and oceanic data bases. The Equatorial Pacific Ocean Climate Studies (EPOCS) conceived a large joint effort to compile global ship observations by the Environmental Research Laboratories of NOAA; the Cooperative Institute for Research in Environmental Sciences (CIRES) of NOAA and the University of Colorado; the National Center for Atmospheric Research (NCAR); and the National Climatic Data Center (NCDC) of NOAA. The product of the endeavor was the Comprehensive Ocean-Atmosphere Data Set (COADS) for the period 1850-1979. Details of the collection, evaluation and compilation of the ship observations are contained in Woodruff et al. (1987).

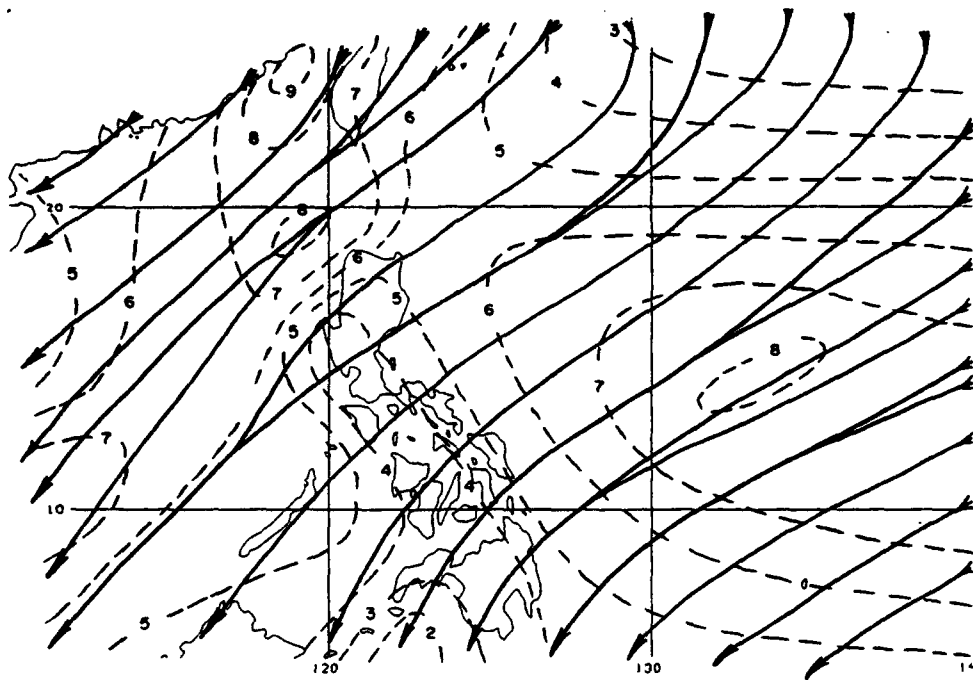
Data density is three times greater in the Atlantic Ocean basin than in the Pacific Ocean basin, and greater along shipping lanes. Presented on 2° by 2° grids in two volumes (Sadler et al. 1987a and Sadler et al. 1987b), COADS, while being the best data base yet assembled, displays large areas, especially in the tropics and the Southern Hemisphere, with inadequate data for analysis. Since the Philippine Islands were plotted on the margins of both of the original volumes, the data was replotted over a single chart covering the South China Sea, the Philippine Islands and the Philippine Sea. While the reader must refer to Sadler et al. (1987a/b) to determine the number of observations in each 2° by 2° grid, generally there are >30 ship observations per month in the northwest sector of the following charts, 2-10 ship observations per month near Visayas and Mindanao, but only 1-2 ship observations per month in the southeast region (east of 130°E and south of 10°N.). Therefore the analyses of the southeastern corner of the charts in this appendix were performed on a very inadequate data base.

This inadequate and uneven distribution of data, as well as large gradients and relatively small atmospheric systems in the tropics dictated a manual analysis. Thus, in contrast to machine analysis—with which it differs significantly—, the manual analysis permits a variable radius of data influence and the incorporation of auxiliary information and experience.

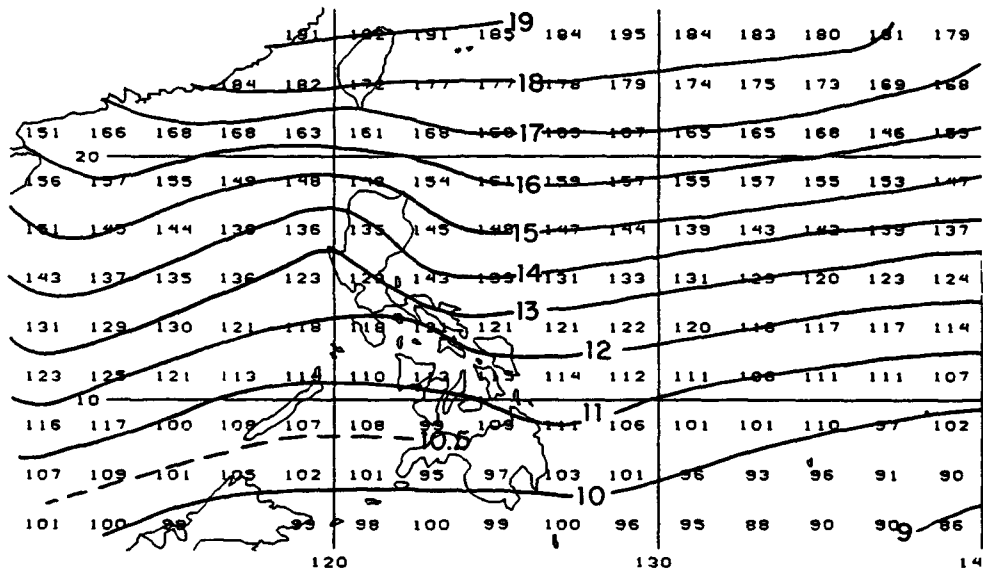
The authors selected the 80-year period, 1900-1979 for their atlases. In this appendix, the averages for the following three elements are presented for each month of the year: surface wind (streamlines and resultant wind speeds in m/s), sea level pressure in hectopascals (hPa or millibars) minus a thousand, and sea surface temperature (in degrees Celsius).



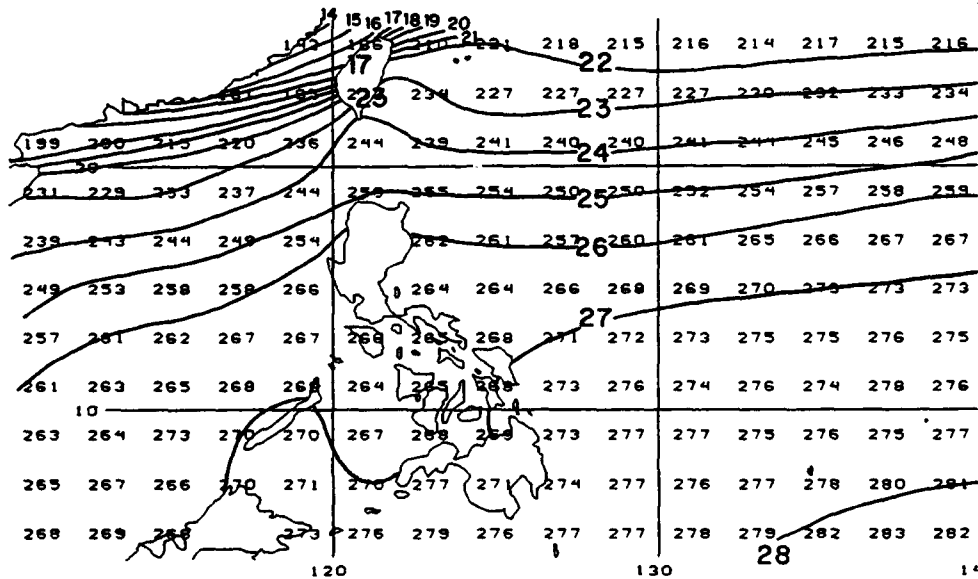
JANUARY: Surface wind (m/s) (a), Sea level pressure (hPa) (b) and Sea surface temperature ($^{\circ}$ C) (c)



(a)



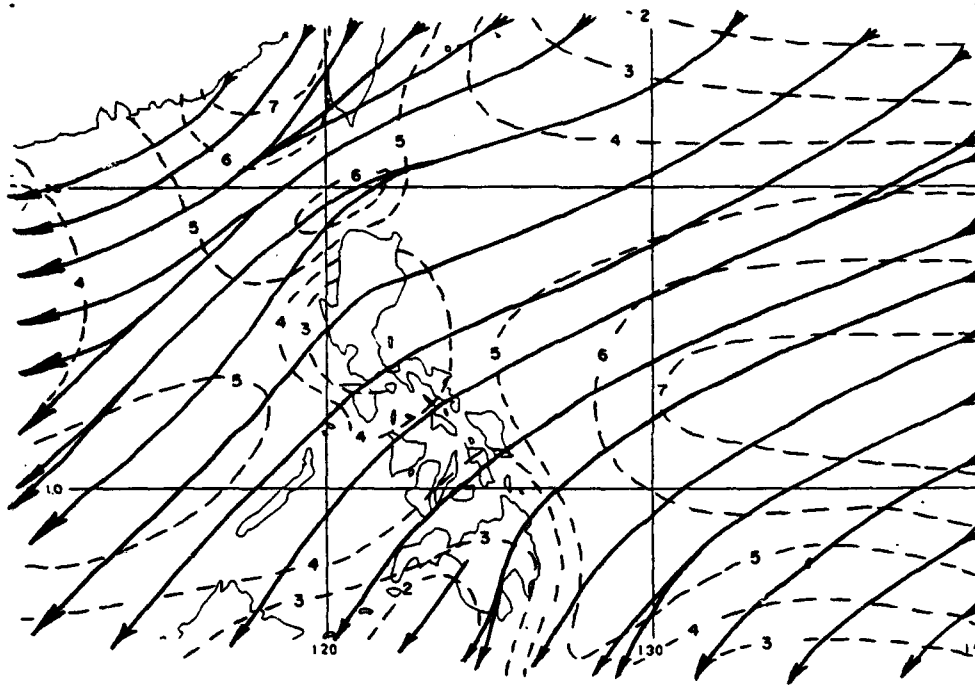
(b)



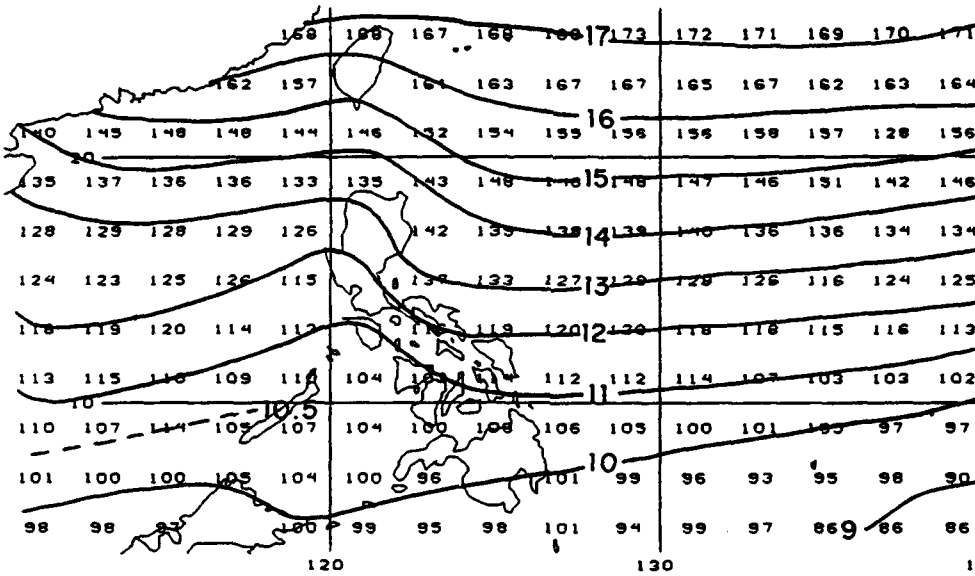
(c)

FEBRUARY: Surface wind (m/s) (a), Sea level pressure (hPa) (b) and Sea surface temperature (°C) (c)

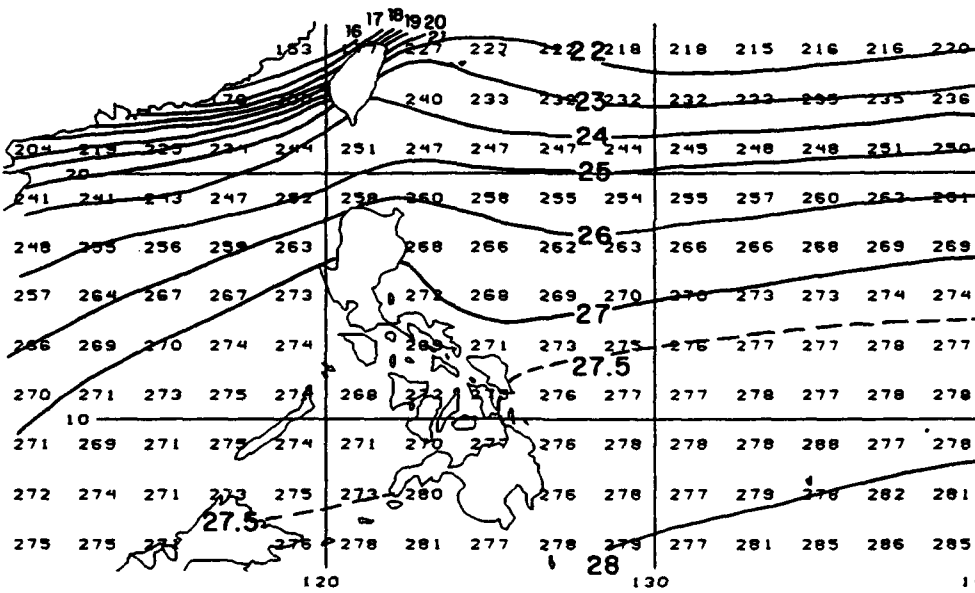
(a)



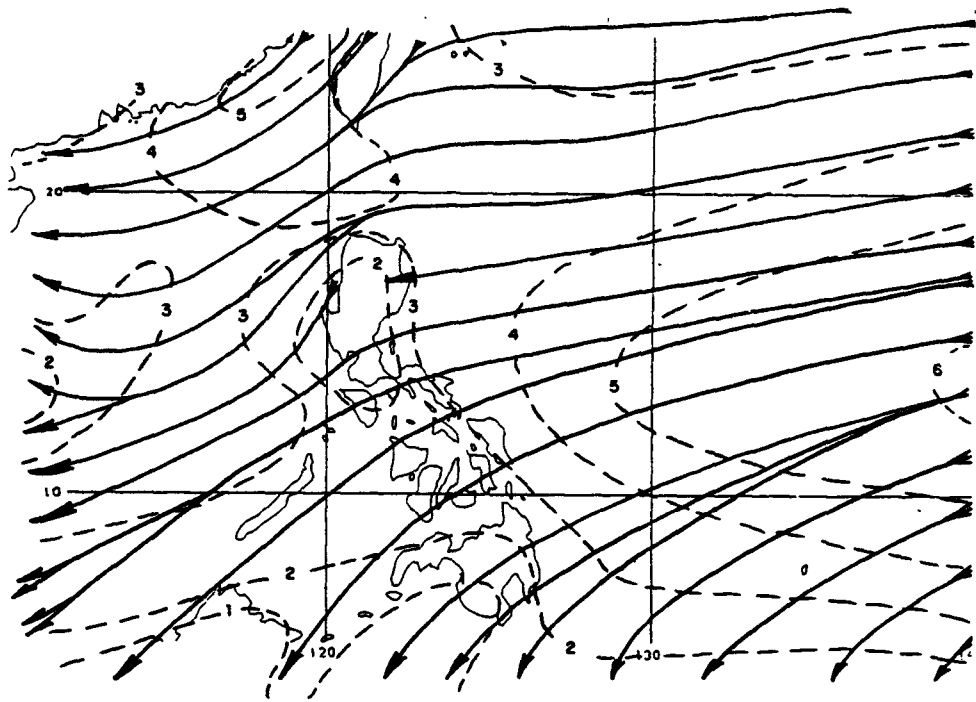
(b)



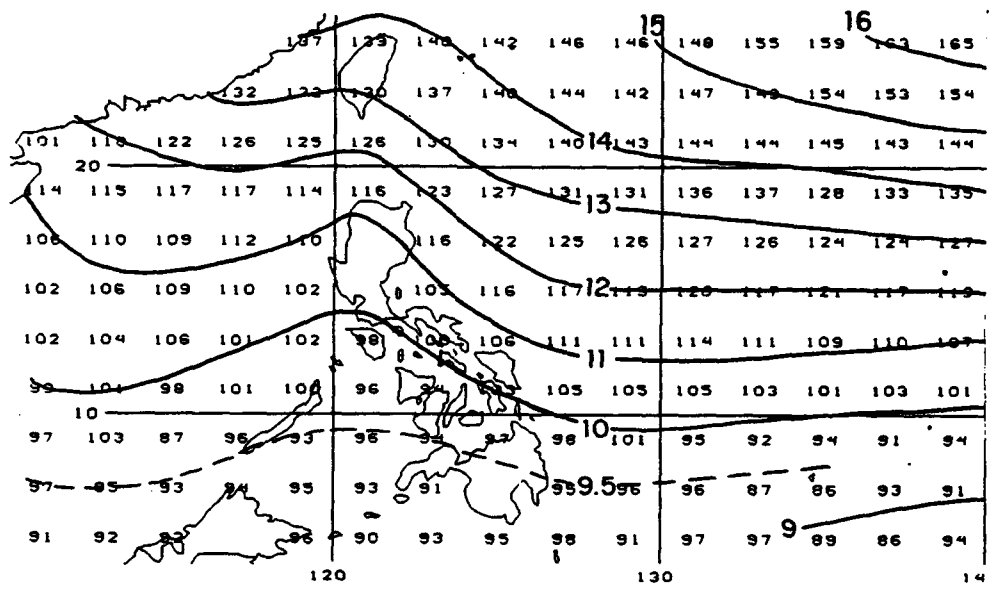
(c)



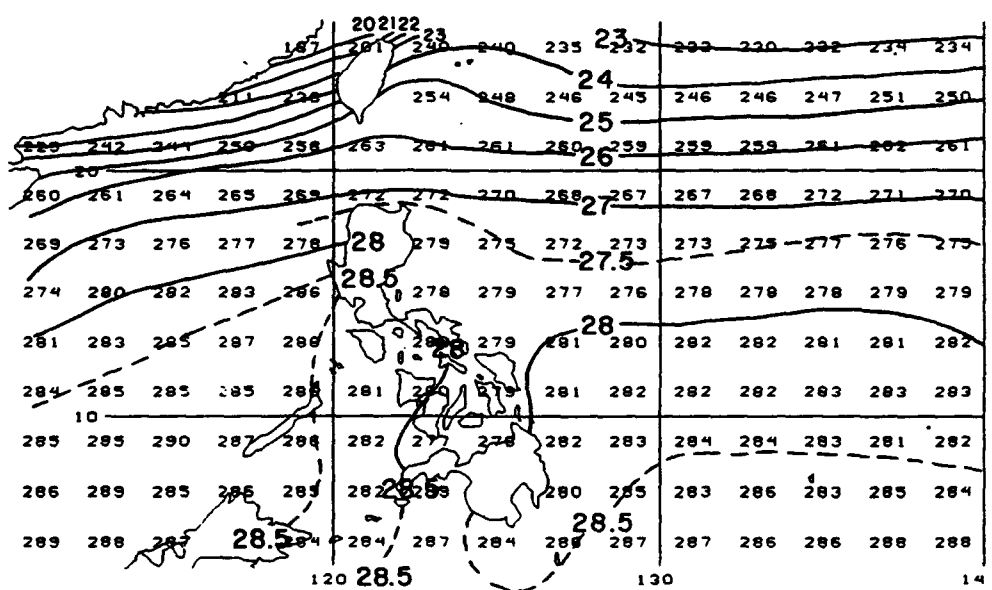
MARCH: Surface wind (m/s) (a), Sea level pressure (hPa) (b) and Sea surface temperature (°C) (c)



(a)



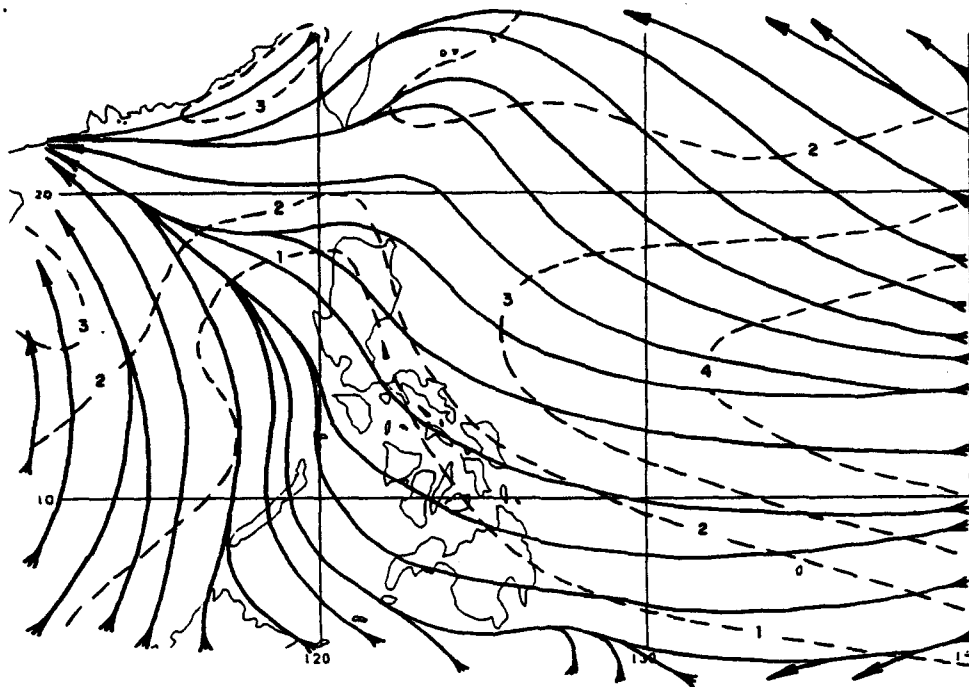
(b)



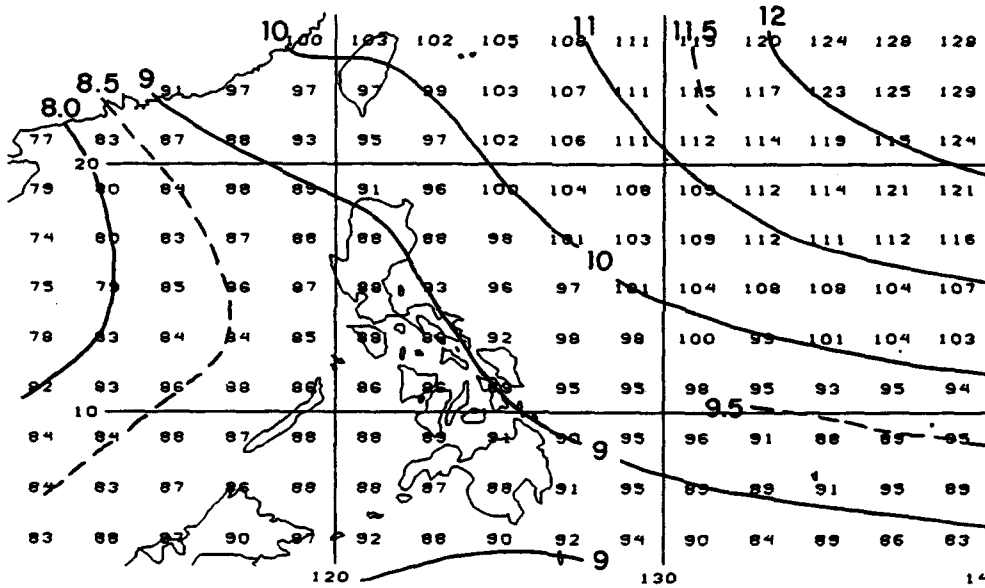
(c)

APRIL: Surface wind (m/s) (a), Sea level pressure (hPa) (b) and Sea surface temperature (°C) (c)

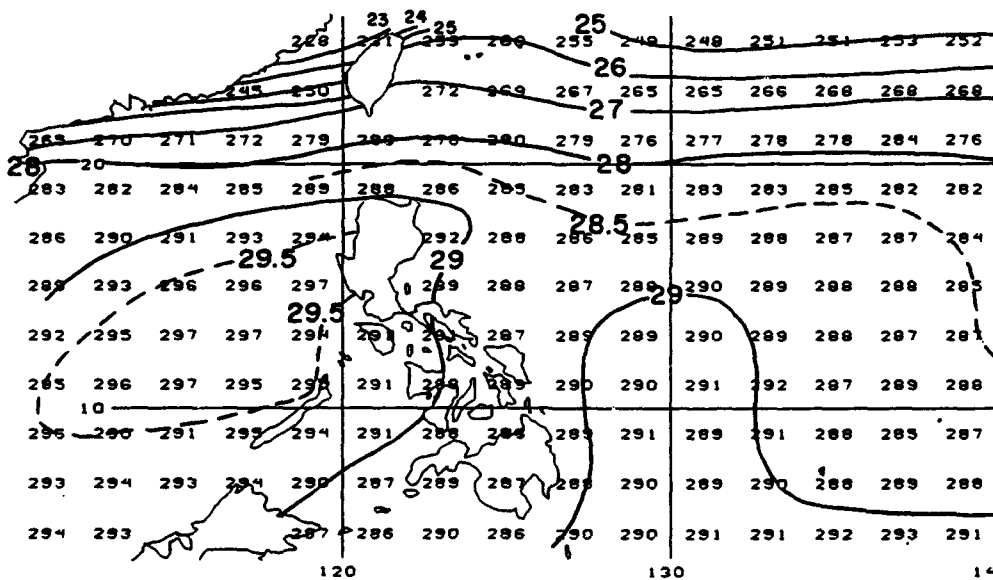
(a)



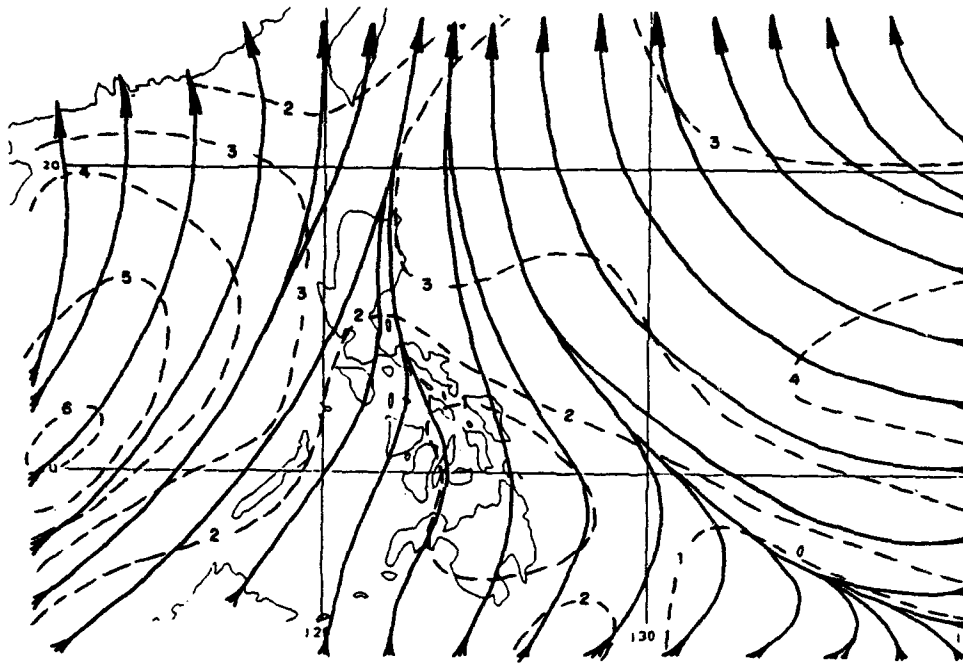
(b)



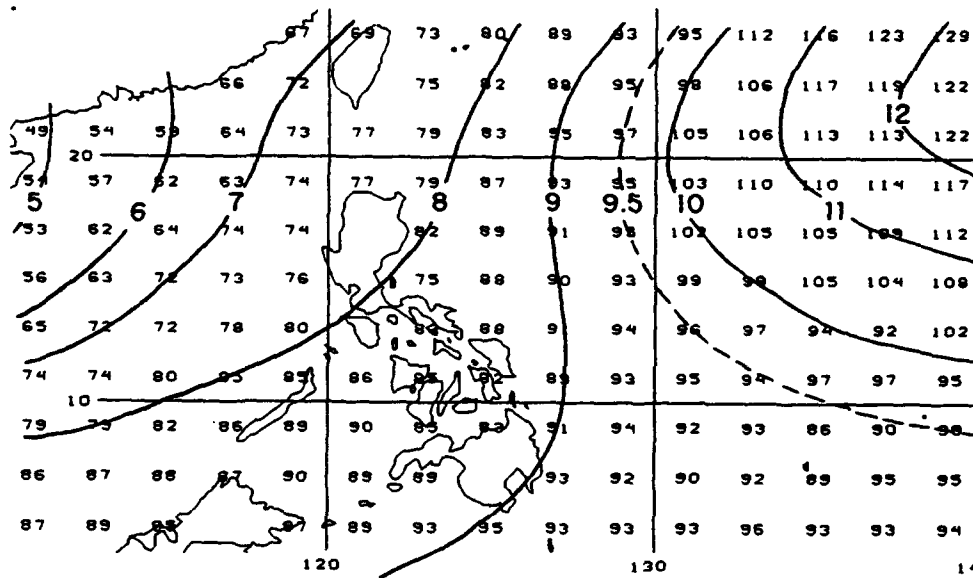
(c)



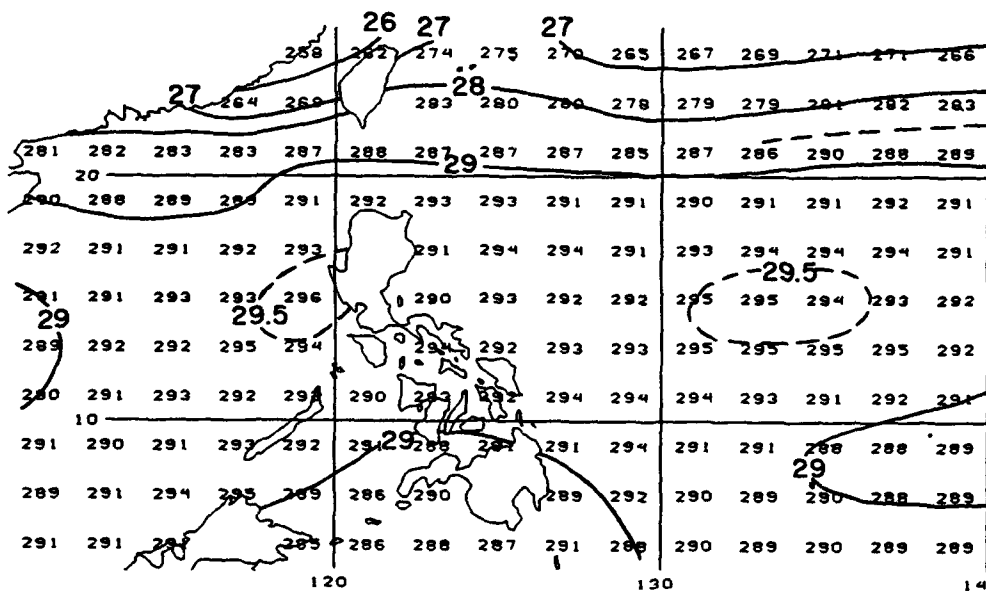
MAY: Surface wind (m/s) (a), Sea level pressure (hPa) (b) and Sea surface temperature (°C) (c)



(a)

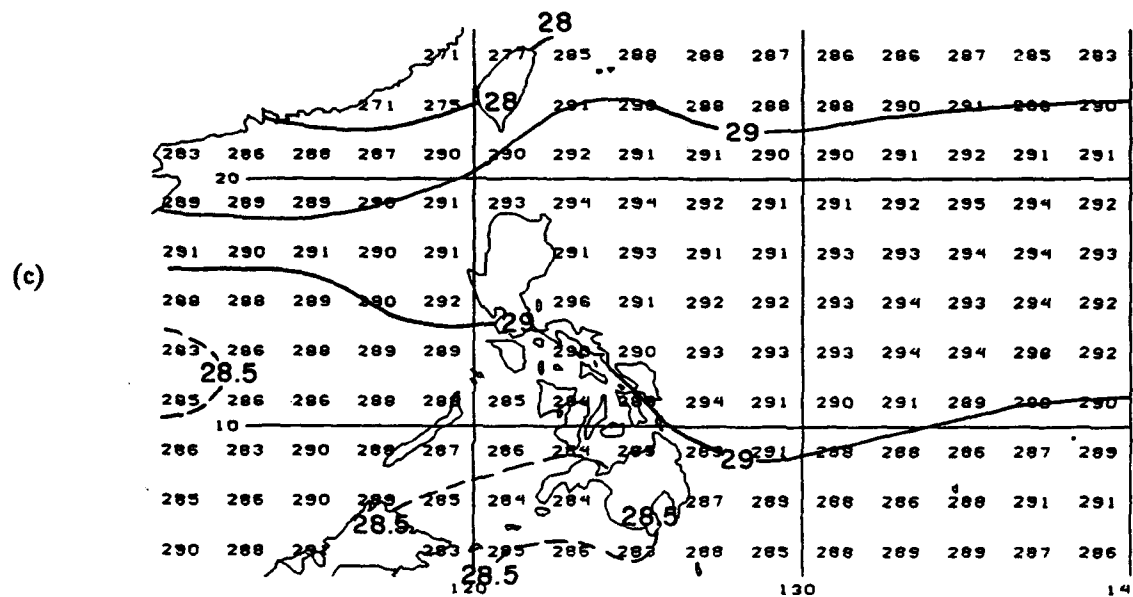
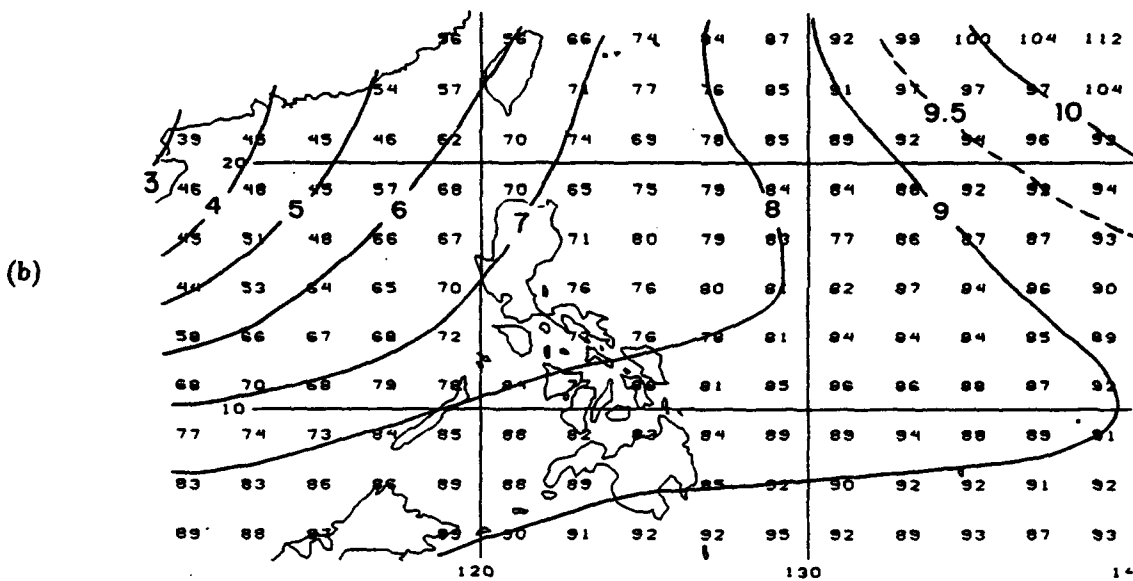
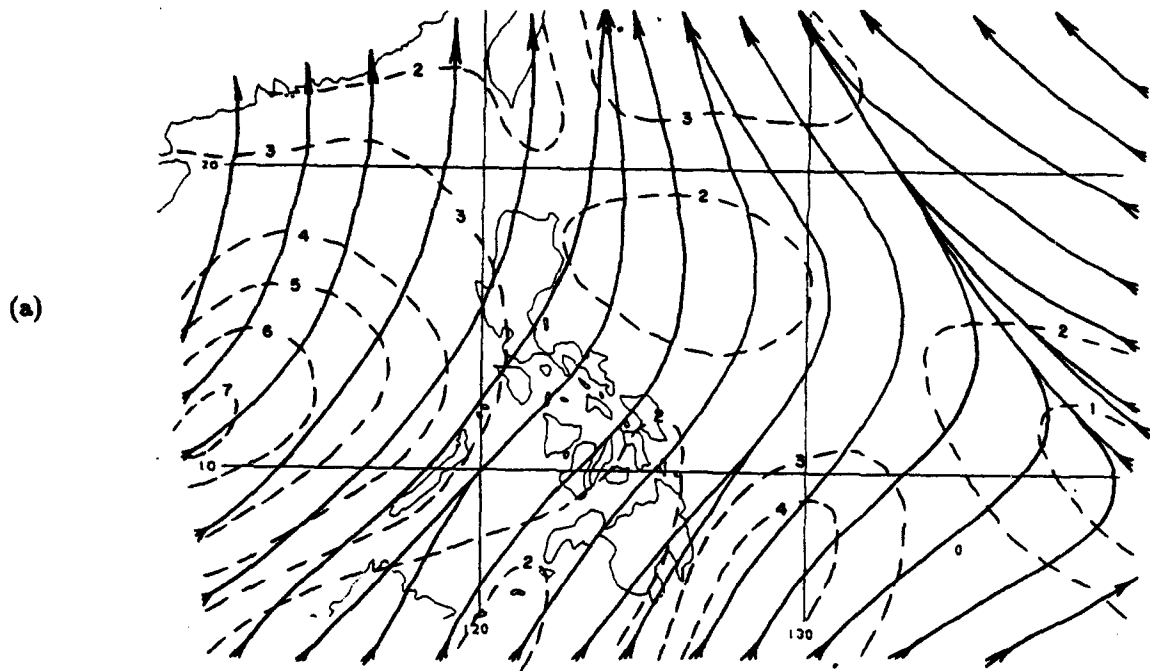


(b)

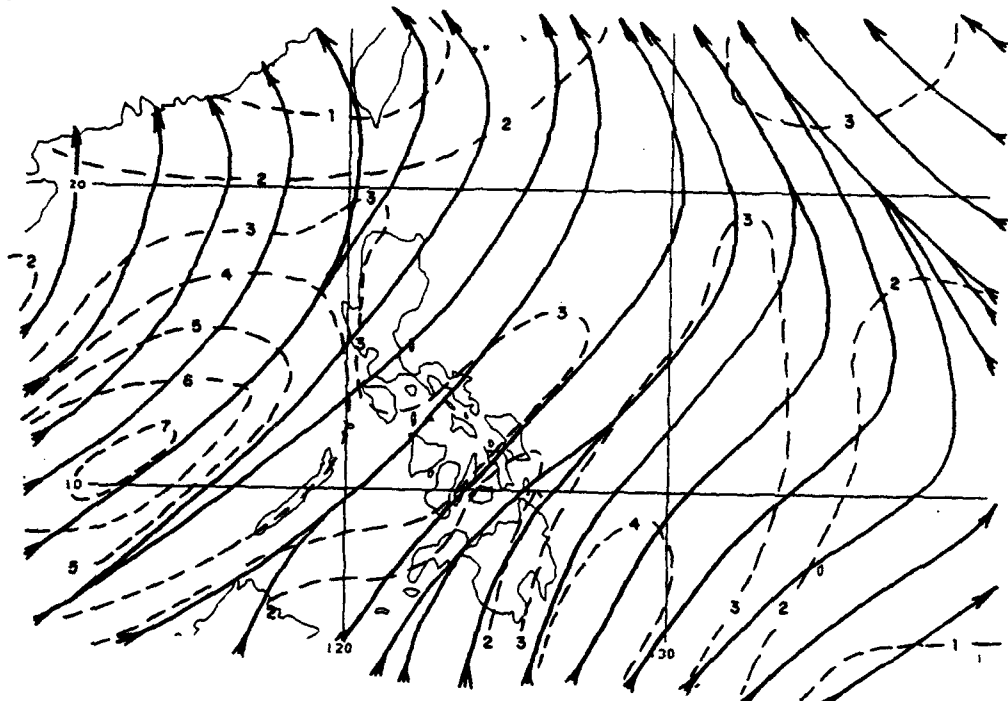


(c)

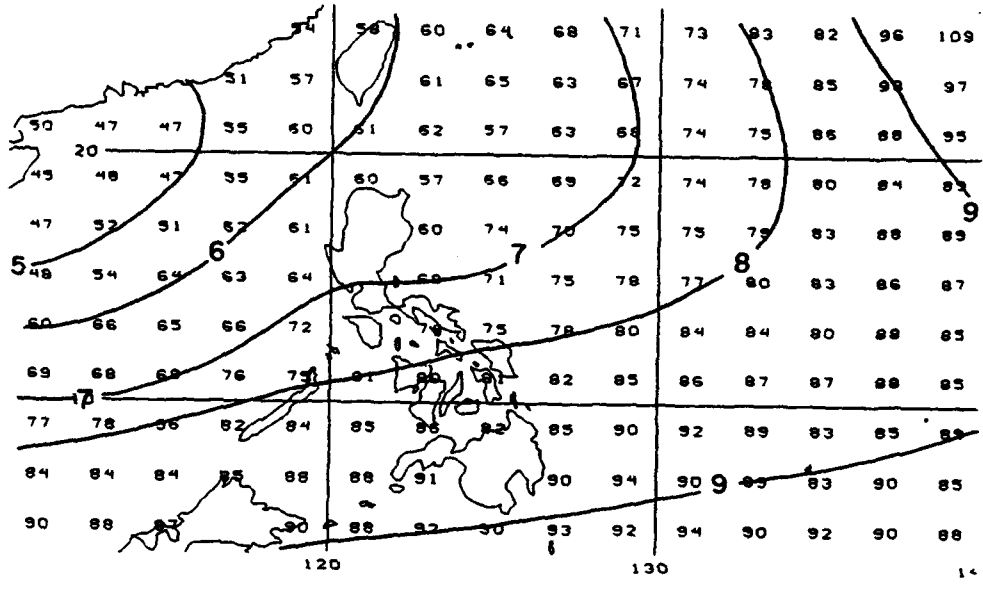
JUNE: Surface wind (m/s) (a), Sea level pressure (hPa) (b) and Sea surface temperature (°C) (c)



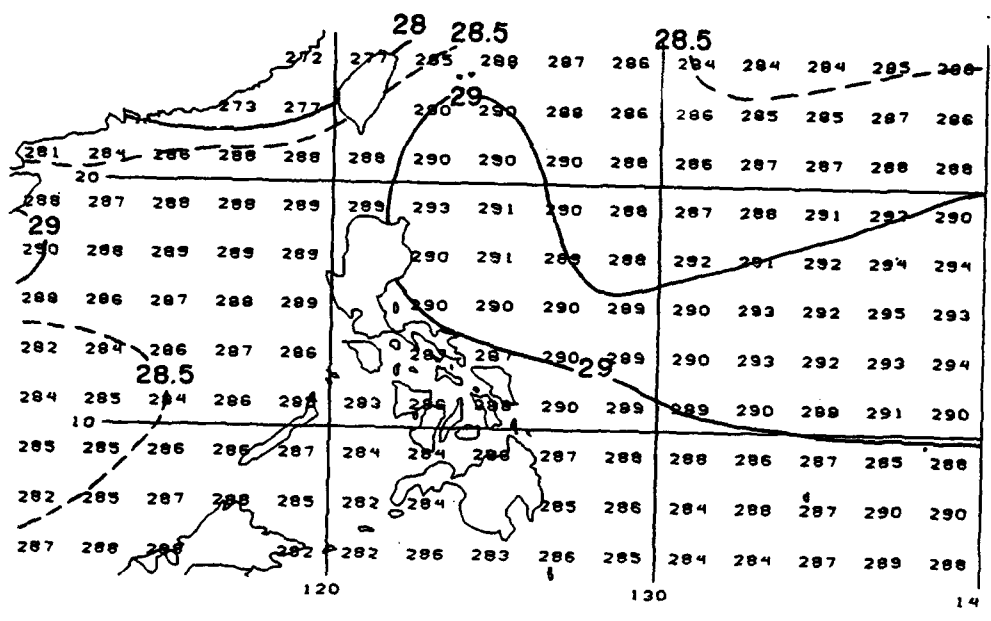
JULY: Surface wind (m/s) (a), Sea level pressure (hPa) (b) and Sea surface temperature (°C) (c)



(a)



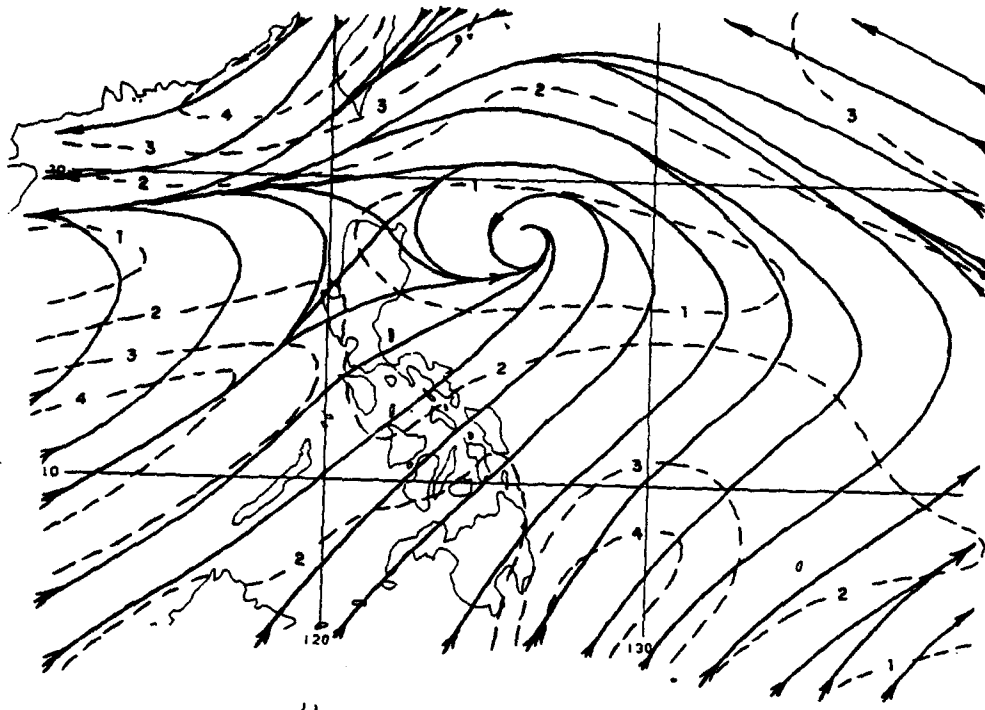
(b)



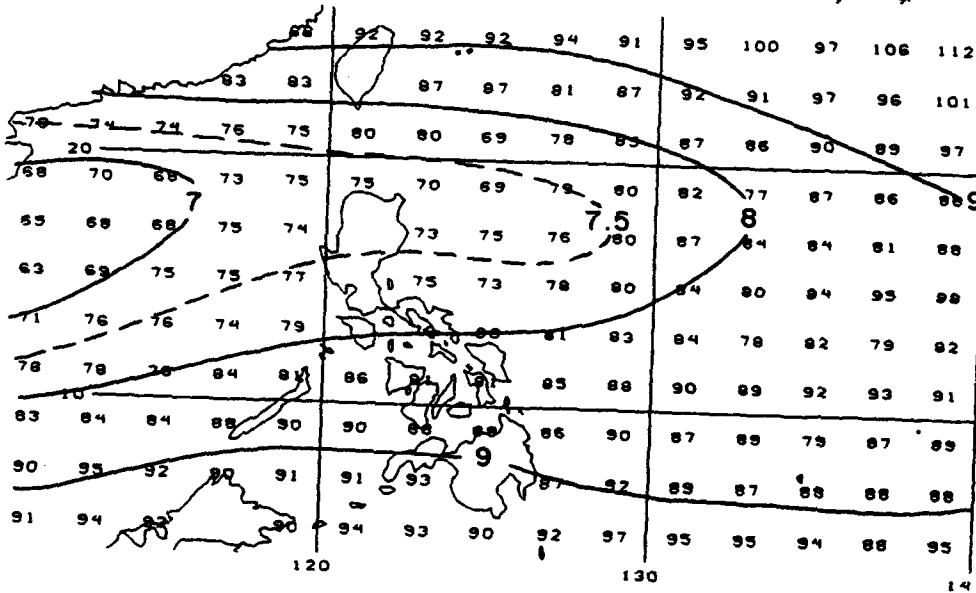
(c)

AUGUST: Surface wind (m/s) (a), Sea level pressure (hPa) (b) and Sea surface temperature (°C) (c)

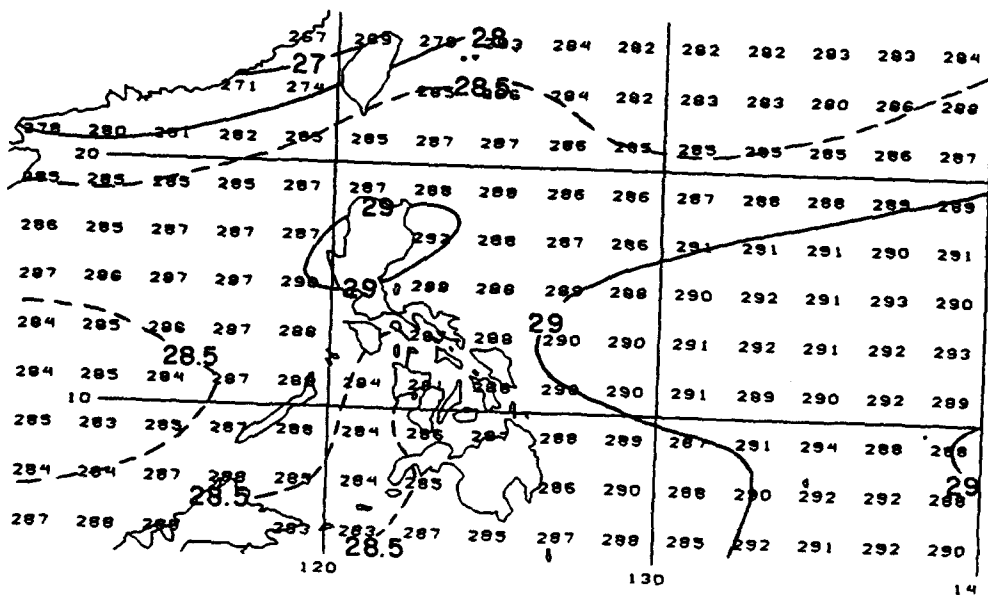
(a)



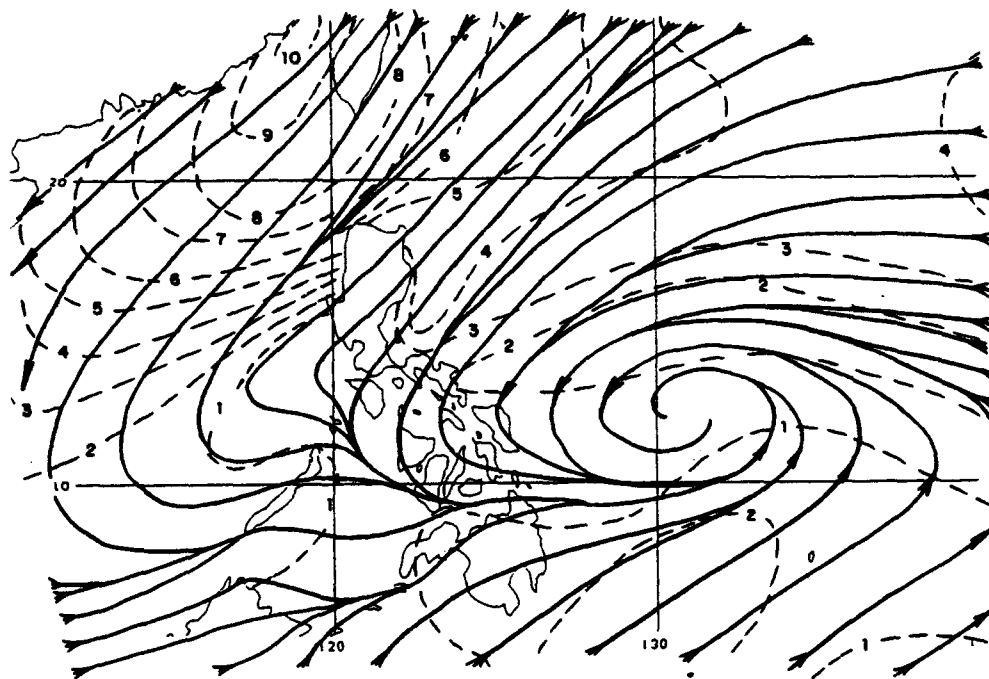
(b)



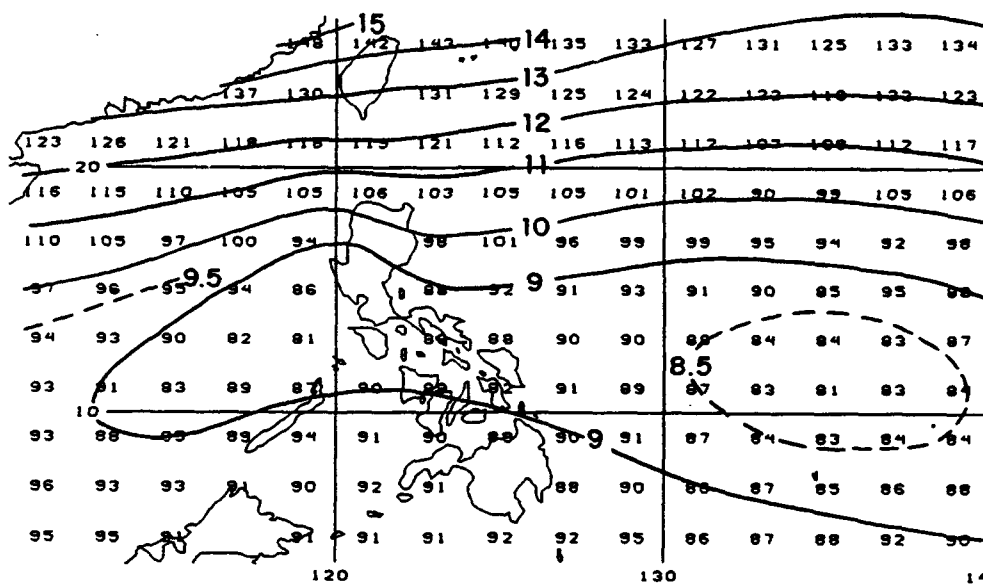
(c)



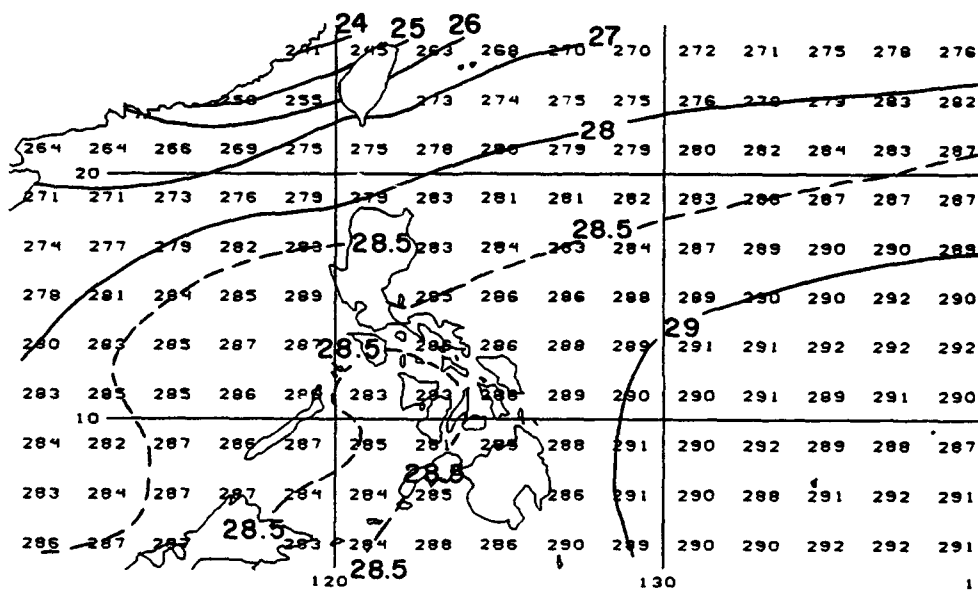
SEPTEMBER: Surface wind (m/s) (a), Sea level pressure (hPa) (b) and Sea surface temperature (°C) (c)



(a)



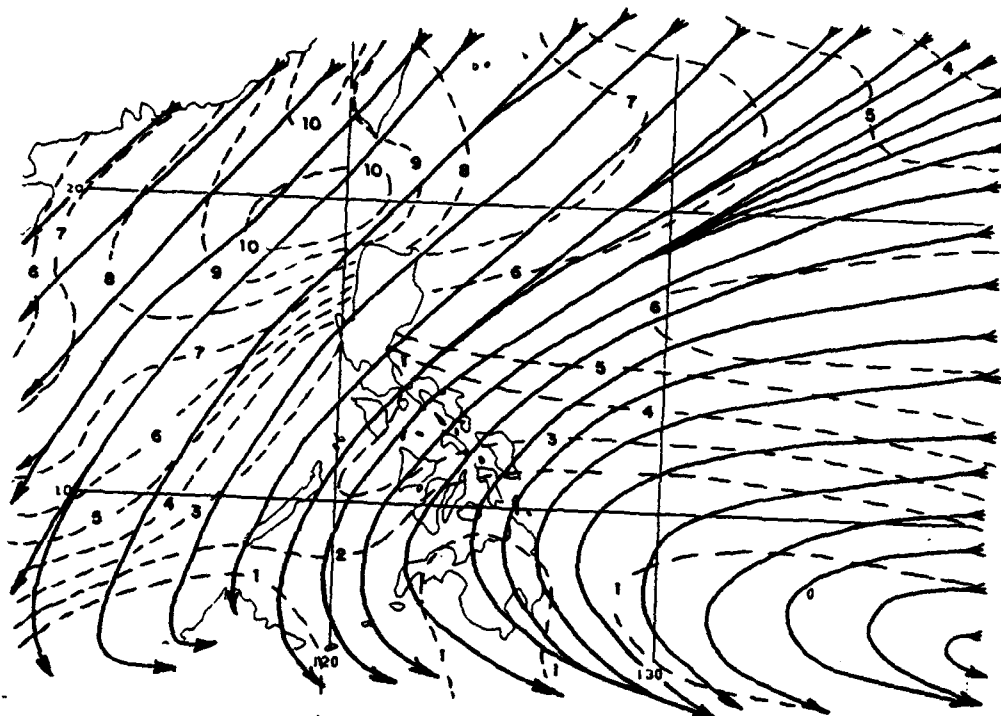
(b)



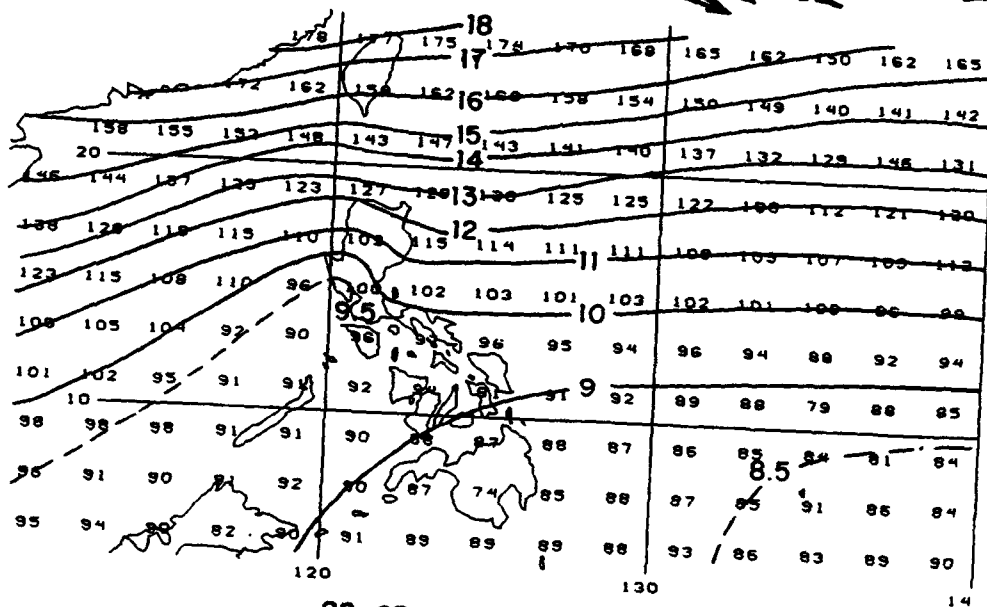
(c)

OCTOBER: Surface wind (m/s) (a), Sea level pressure (hPa) (b) and Sea surface temperature (°C) (c)

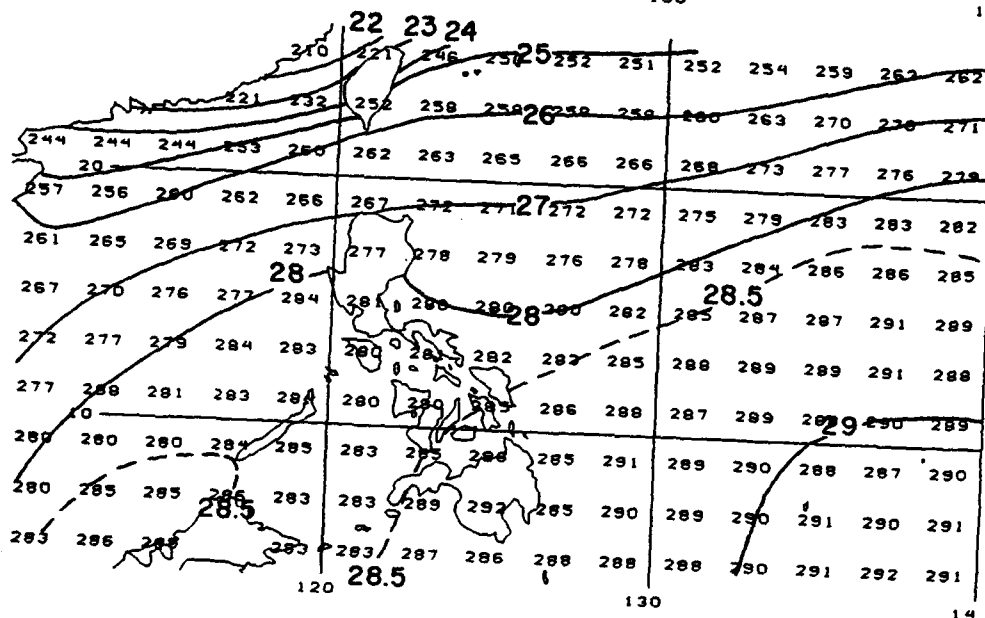
(a)



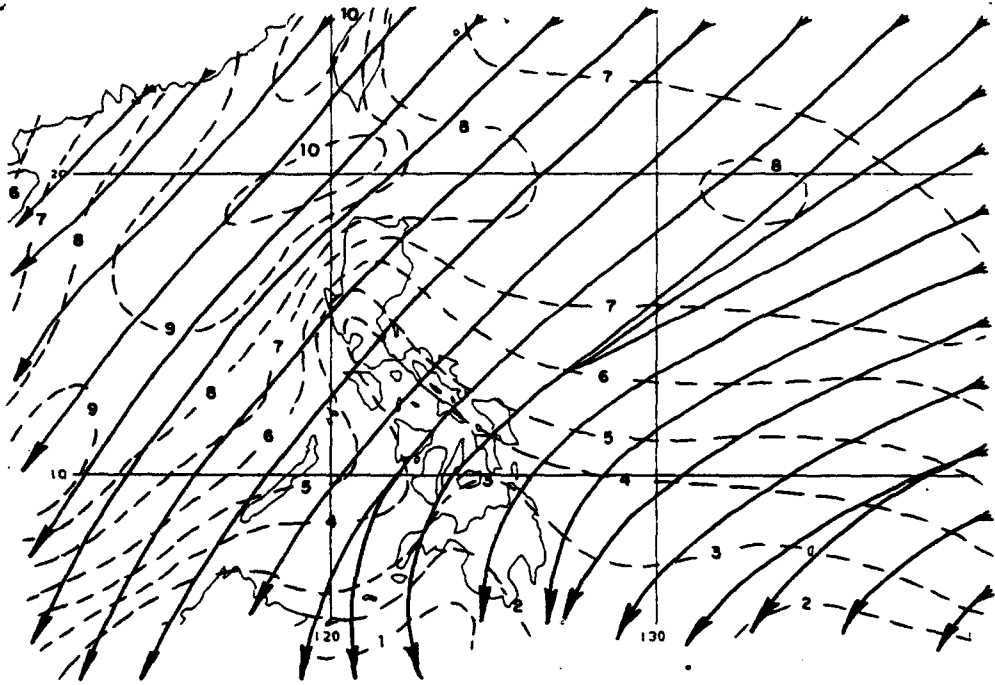
(b)



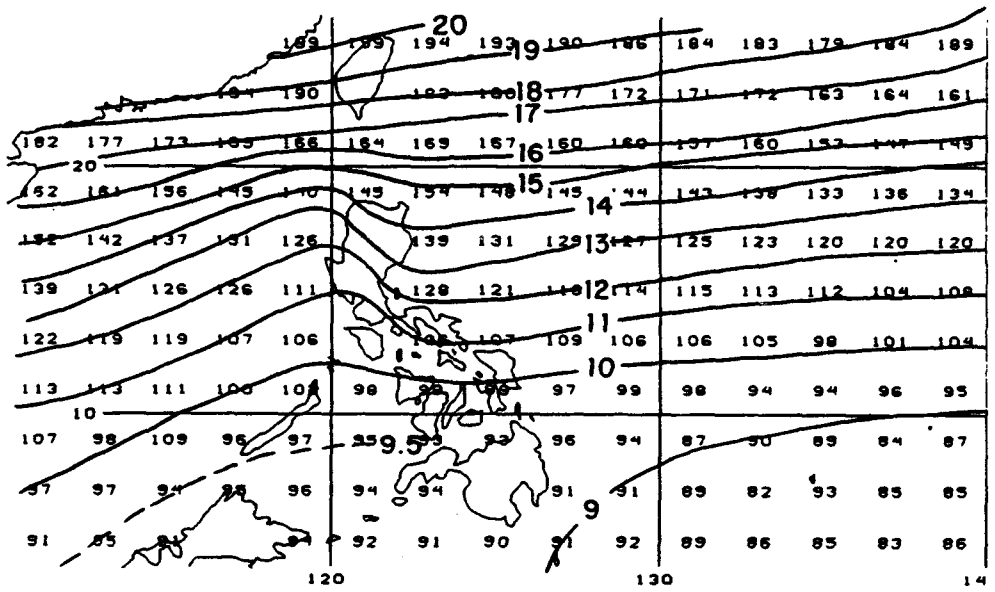
(c)



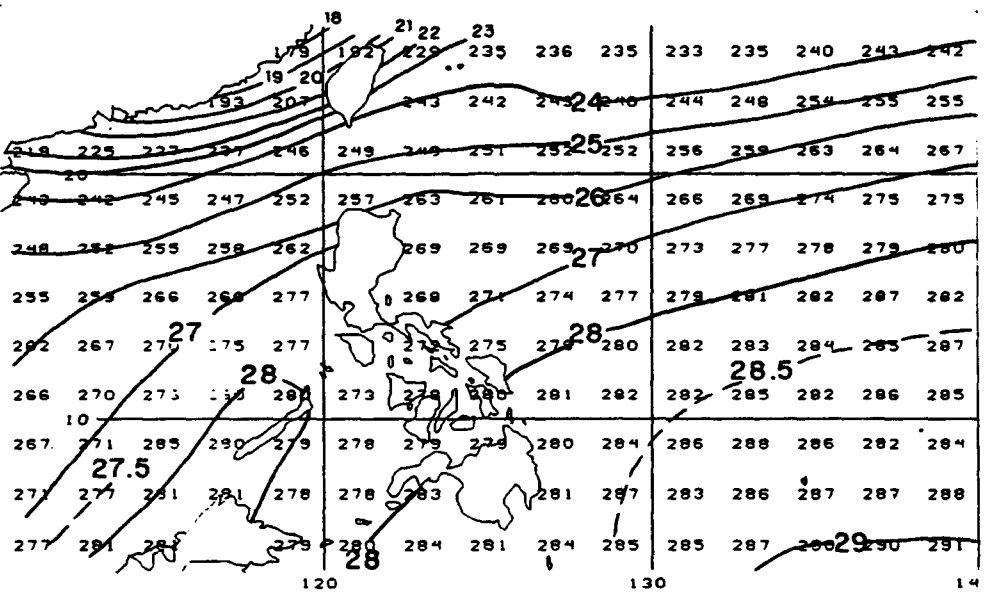
NOVEMBER: Surface wind (m/s) (a), Sea level pressure (hPa) (b) and Sea surface temperature (°C) (c)



(a)



(b)



(c)

DECEMBER: Surface wind (m/s) (a), Sea level pressure (hPa) (b) and Sea surface temperature (°C) (c)

Appendix B

Characteristics of Tropical Cyclones Affecting the Philippine Islands (Shoemaker 1991)

Using a powerful desktop computer and computerized data bases available at the Naval Oceanography Command Center/Joint Typhoon Warning Center (NAVOCEANCOMCEN/JTWC), Shoemaker (1991) presents a climatology of tropical cyclones (TCs) approaching or crossing the Philippine Islands.

The data base for examining TC intensity, direction and speed includes all six-hourly best track positions from 45 years (1945-1989). However due to the lack of satellite coverage the earlier portion of the record identified fewer weak TCs and lowered the number of TCs which hit the PI by more than one per year (20%). Therefore the climatology section is based on 20 years (1970-1989) to preclude lowering the numbers of weaker systems.

The September-November period has the maximum potential for TCs to hit the Philippine Islands. The average time over land is 11 hours north of 14.5° contrasted to 20 hours south of 14.5°.

The average latitude of landfall has an annual cycle, similar to the monsoon trough, with a latitude maximum during August (~15.5°N) and a latitude minimum during February (~9.0°N).

TCs of intensity >65 knots just prior to landfall reach peak intensity 6 to 12 hours prior to landfall whereas storms 65 knots or less prior to landfall peak only 0 to 6 hours before landfall. TCs of typhoon intensity generally weaken as they cross the PI, but TCs with intensity less than 50 knots at landfall do not weaken significantly. The amount of weakening is proportional to intensity, and weakening is less for TCs south of 14.5°.

The average speed in the 12 hours prior to landfall for TCs hitting the PI south of 14.5°N is 13.3 knots with a standard deviation of 4.2 knots. North of 14.5°N, the average speed is 11.8 knots with a standard deviation of 3.2 knots. Accordingly, the average time over land is 20 hours south of 14.5°N, but only 11 hours north of 14.5°N (due to the narrow E-W dimension of Luzon).

TCs moving faster than 15 knots tend to slow down after making landfall; however, TCs moving 15 knots or less experience little velocity change.

The mean direction of motion just before first landfall is west-northwestward; only two storms in 45 years have first hit the PI with an eastward velocity component, (i.e., coming from the South China Sea), and both were weak systems.

TCs moving south of west tend to turn more westward after landfall; however, TCs moving west-northwestward show little change in direction. TCs moving more north than west (320°-360°) tend to recurve before hitting the Philippine Islands (Shoemaker 1991).

ANNUAL CLIMATOLOGY(1970-1989)

The Philippine Islands (0° to 20°N, 118° to 128°E) are hit by an average of 6.5 TCs per year. Only three TCs struck the PI during two of the 20 years; whereas, the maximum occurred in two years when 12 TCs struck the PI. With a standard deviation of 2.6, approximately 70% of the time between 4 and 9 TCs strike annually.

The average intensity at landfall ("just before landfall") for TCs striking the PI is 66.9 knots. With a standard deviation of 34.4 knots, approximately 70% of the TCs have an intensity between 30 and 100 knots. 10% have ≥ 120 knots intensity. During the 20-year period, seven (7) super typhoons (≥ 130 knots) struck the PI (see Fig. B.1).

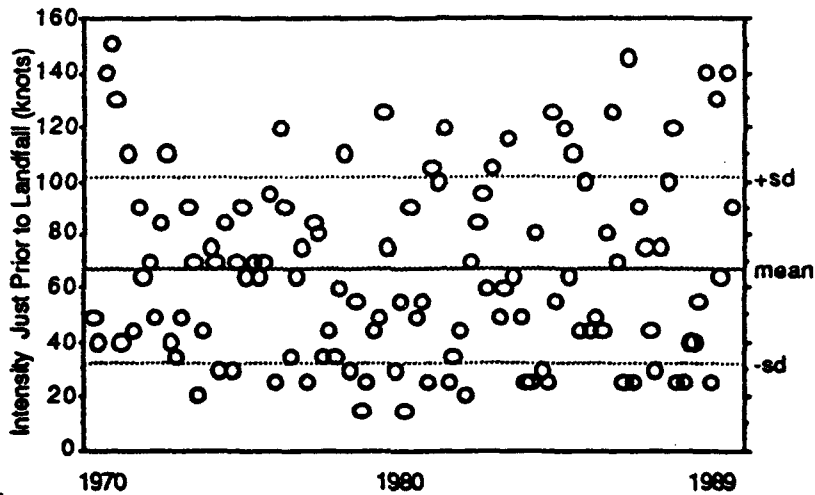


Figure B.1: Average Intensity of TCs Hitting the PI (adapted from Shoemaker (1991)).

TCs that miss the PI (but are located for at least 24 hours in the latitude/longitude box defined above) are significant because they still threaten the PI, causing preparations to be made and impacting operations. The average number of TCs which miss the PI is 4.0 with a standard deviation of 1.6 (see Fig. B.2).

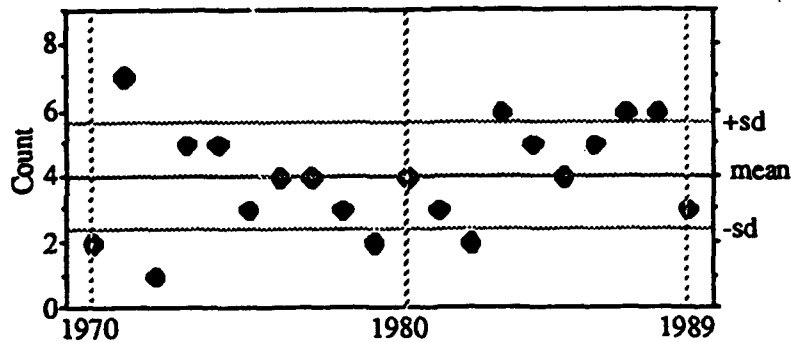


Figure B.2: Annual Climatology of TCs in the Area of Interest but Missing the PI (adapted from Shoemaker (1991)).

The annual mean latitude of landfall is 13.9°N. The standard deviation of 2.7° places the center in the area which is most likely to affect Manila as well as Subic Bay.

MONTHLY CLIMATOLOGY(1970-1989)

Figure B.3 shows the distribution of PI tropical cyclones by month (darkest shade ≡ super typhoon). The lack of February TCs corresponds to the peak of the northeast monsoon when TCs are sheared apart before reaching the PI. The relative minimum in August occurs when the southwest monsoon trough is farthest north and the TCs form on the trough too far north to impact the PI (Atkinson 1971).

The annual distribution is bi-modal, coinciding with the monsoon transition seasons of June-July and October-November. TCs forming close to the islands impact at tropical depression or tropical storm intensity, while those forming farther east in the Philippine Sea are likely to impact at typhoon intensity. In December the number of recurvers and sheared systems increase, and fewer TCs hit the PI.

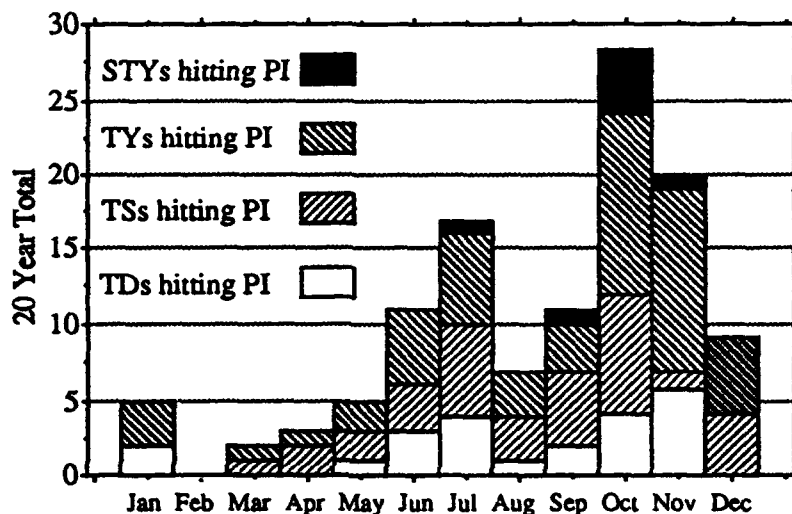


Figure B.3: TCs Hitting the PI during the 20 Years 1970-1989 (adapted from Shoemaker (1991)).

Figure B.4 reveals that while June TCs have the weakest average intensity, November (during the peak season) has the highest average intensity. March with only two TCs, one intense (105 knots) and one moderate (60 knots), ranks surprisingly high. Standard deviations are in the 20 to 30 knot range.

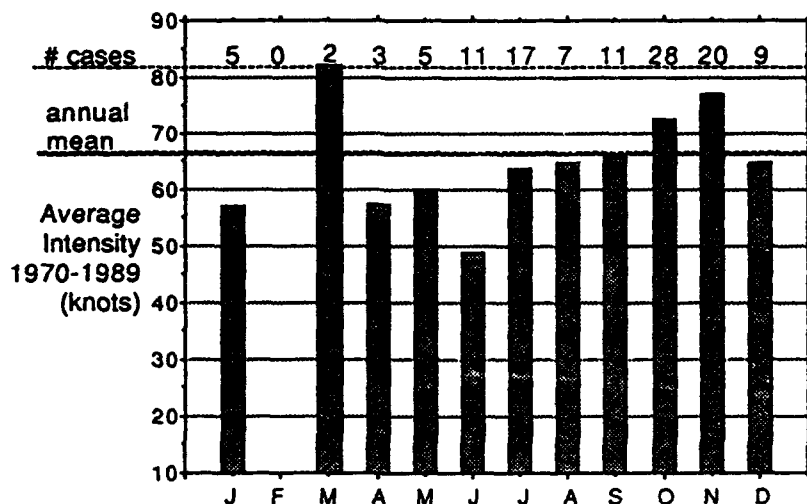


Figure B.4: Monthly Climatology of Intensity for TCs Hitting the PI (adapted from Shoemaker (1991)).

Figure B.5 shows the latitude of landfall following a cycle similar to the monsoon trough cycle, with a latitude maximum occurring during August and a minimum during February (Shoemaker 1991).

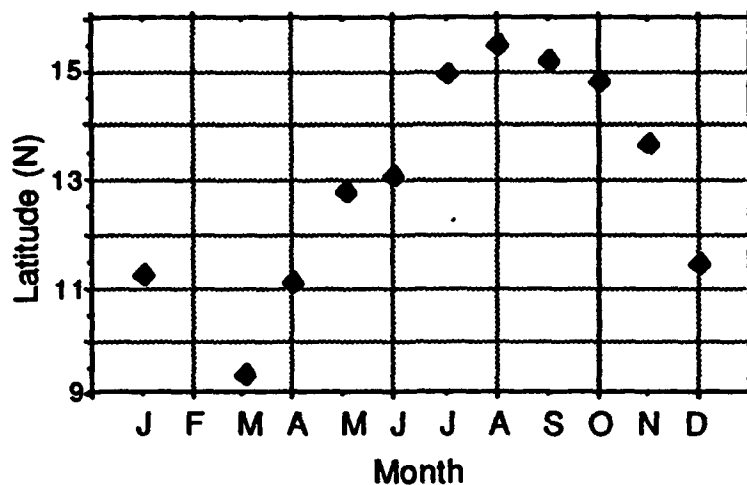
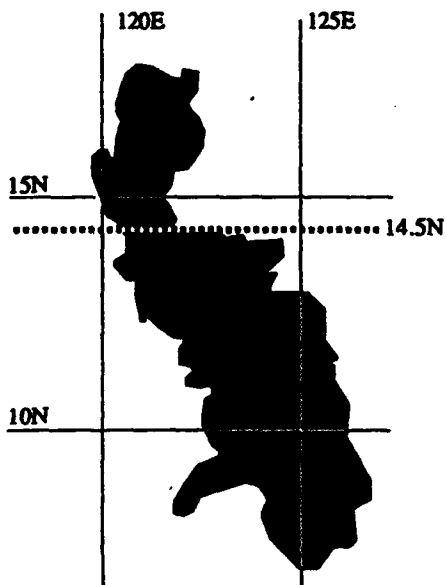


Figure B.5: Monthly Climatology of Landfall Latitude of TCs hitting PI (adapted from Shoemaker (1991)).

INTENSITY CHANGES(1945-1989)



Intensity change statistics utilize the entire 45-year data set and will contain tropical depressions and tropical storms, as well as typhoons. As depicted at left in Fig. B.6, the Philippine Islands are divided into two regions—south and north of 14.5°N. The area encompassed by the island is about twice as wide south of 14.5°N, where there are smaller islands. The northern region, primarily *narrow* northern Luzon, consists of many mountains, while only a smaller portion of the southern region includes Mindanao with its mountainous terrain.

Figure B.6: The Philippines separated by 14.5°N. Transition time was based on entering and exiting the gray area (adapted from Shoemaker 1991)).

Tropical Depressions (25–30 kt) do not present a wind threat, but can still cause heavy rainfall. Tropical depressions actually tend to increase slightly in intensity while transiting the Philippines (see Table B.1). This increase, despite the frictional effects of land, may occur since tropical depressions have normally formed just east of the islands and are responding to the dynamics increasing their intensity to a tropical storm.

Tropical Storms (35–62 kt) are subdivided into weak (35–45 kt) and strong (50–60 kt) tropical storms. While both weaken slightly, strong tropical storms weaken more than the weak ones (Table B.1).

Typhoons are subdivided into weak (65–80 kt), moderate (85–100 kt) and strong (≥ 100 kt). As reported in earlier studies, the more intense the typhoon, the larger the intensity decrease while transiting the islands (Table B.1).

Note that the standard deviations shown in Table B.1 indicate that the most variability occurs with moderate typhoons. Possibly some have peaked before landfall, while others intensify. Variability may also be due to the speed of transition, since slower-moving typhoons experience land effects longer. Further stratification is included in Tables B.2–B.3.

Table B.1: Intensity Change for Tropical Cyclones Crossing the Philippines (Intensity, Change and Std. Dev. in Knots)(adapted from Shoemaker (1991)).

South of 14.5°				North of 14.5°		
Intensity at Landfall	Intensity Change	Std Dev	# of Cases	Intensity Change	Std Dev	# of Cases
25 - 30	5.8	11.3	19	3.0	7.5	10
35 - 45	-2.5	9.6	22	-2.0	11.4	10
50 - 60	-5.8	9.7	18	-6.7	9.9	15
65 - 80	-17.5	13.3	18	-13.5	12.5	26
85 - 100	-20.3	26.4	15	-25.0	25.8	21
> 100	-49.4	16.6	16	-43.5	19.3	23

Tables B.2 through B.3 provide a stratification by intensity trend prior to landfall. Tropical cyclones that weaken in the 12 hours prior to landfall show less variability in their intensity change than those that are intensifying.

Tropical cyclones are also stratified by time over land in Tables B.2 through B.3. Note that for moderate typhoons (85–100 kt) the faster the system moves, the less variable (smaller standard deviations) the expected intensity change (Shoemaker 1991).

Table B.2: Intensity Change for Tropical Cyclones Which Were (a) Weakening
(b) Strengthening Prior to Landfall (South of 14.5°N)(Intensity in Knots)
(adapted from Shoemaker (1991)).

(a)

Intensity	Crossing Time 6 - 12 hours			18 - 24 hours			30 - 36 hours		
	Ins Chg	Std Dev	Count	Ins Chg	Std Dev	Count	Ins Chg	Std Dev	Count
25-30	-5.0	n/a	1	n/a	n/a	0	n/a	n/a	0
35-45	n/a	n/a	0	-10.0	0	2	n/a	n/a	0
50-60	n/a	n/a	0	n/a	n/a	0	n/a	n/a	0
65-80	-26.7	2.8	3	-12.5	31.8	2	-15.0	n/a	1
85-100	-12.5	10.6	2	-10.0	n/a	1	-22.5	53.0	2
> 100	-45	n/a	1	-42.5	9.5	4	-80.0	n/a	1

(b)

Intensity	Crossing Time 6 - 12 hours			18 - 24 hours			30 - 36 hours		
	Ins Chg	Std Dev	Count	Ins Chg	Std Dev	Count	Ins Chg	Std Dev	Count
25-30	5.0	14.1	6	6.7	8.2	6	-10.0	n/a	1
35-45	2.5	5	4	0.0	10.5	10	-5.0	5.0	3
50-60	-1.0	6.5	5	-5.0	10.0	10	-15.0	7.1	2
65-80	-13.3	10.4	3	-15.6	13.2	8	n/a	n/a	0
85-100	22.5	3.5	2	-36.2	13.2	4	-17.5	10.6	2
> 100	-39.0	17.8	5	-65.7	4.8	4	-45.0	n/a	1

Table B.3: Intensity Change for Tropical Cyclones Which Were (a) Weakening
(b) Strengthening Prior to Landfall (North of 14.5°N)(Intensity in Knots)
(adapted from Shoemaker (1991)).

(a)

Intensity	Crossing Time 6 hours			12 hours			18 hours		
	Ins Chg	Std Dev	Count	Ins Chg	Std Dev	Count	Ins Chg	Std Dev	Count
25-30	-10.0	n/a	1	n/a	n/a	0	n/a	n/a	0
35-45	-5.0	n/a	1	n/a	n/a	0	n/a	n/a	0
50-60	-10.0	5.0	3	n/a	n/a	0	n/a	n/a	0
65-80	-16.7	30.5	3	-10.0	7.1	2	-30.0	n/a	1
85-100	-23.3	11.5	3	-10.0	9.1	4	-25.0	30	3
> 100	-43.3	10.3	6	-45.0	n/a	1	-75.0	n/a	1

(b)

Intensity	Crossing Time 6 hours			12 hours			18 hours		
	Ins Chg	Std Dev	Count	Ins Chg	Std Dev	Count	Ins Chg	Std Dev	Count
25-30	0.0	0.0	2	4.0	6.5	5	n/a	n/a	0
35-45	-5.0	7.1	2	-0.7	13.3	7	n/a	n/a	0
50-60	-11.2	6.3	4	-5.0	10.0	4	7.5	17.6	2
65-80	-16.7	5.2	6	-10.5	10.6	11	-15.0	n/a	1
85-100	-26.7	2.9	3	-26.7	13.7	6	60.0	n/a	1
> 100	-37.9	27.5	7	-44.2	16.9	6	-30.0	n/a	1

DIRECTION CHANGES

Using a small data base, Brand and Belloch (1972) reported that TCs crossing the Philippine Islands tend to move more northward just after landfall, followed by a westward shift after exiting into the South China Sea. In Shoemaker's study, a larger data base is used to examine direction changes of TCs.

Figure B.7 shows the direction of movement of all TCs at the time of landfall. Additionally, direction of movement during six-hourly increments, for 48-hours before and 48-hours after landfall, is presented. The average direction of movement at landfall is found to be toward the northwest (283°). However, in contrast to the earlier study (Brand and Belloch 1972), the TCs are found to move slightly more northwards after exiting into the South China Sea. The increased length of the error bars following landfall indicates the greater variability of the direction of movement following landfall (see Fig. B.7).

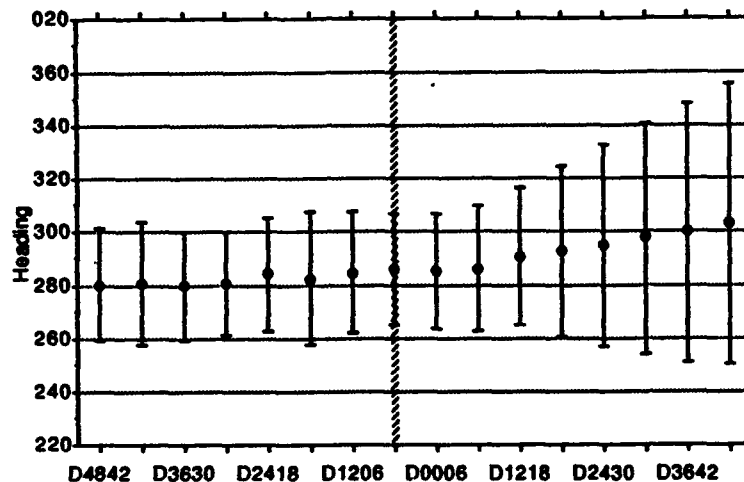


Figure B.7: Average Direction of Movement prior to and after Landfall in the Philippines. Error bars represent one standard deviation. The horizontal axis is in six hourly increments prior to and after landfall (dashed vertical line) (adapted from Shoemaker (1991)).

Figures B.8 through B.11 stratify the TCs that cross the Philippines by the direction of movement and by intensity, just prior to landfall.

- Weak TCs moving toward the west-southwest generally travel more westward 48 hours prior to landfall, and after landfall. More intense TCs moving toward the west-southwest have a greater tendency, than the weaker TCs, to turn toward the northwest (see Figs. B.8(a) and (b)).
- More intense TCs moving toward the west have less directional variability and tend to turn more toward the northwest than do weaker TCs (see Figs. B.9(a) and (b)).
- TCs moving toward the west-northwest exhibit less directional variability. In the late calendar year, the winter monsoon, with low level flow from the northeast can shear a system apart and force a more southward movement—thus the large standard deviation after exiting into the South China Sea (see Figs. B.10(a) and (b)).
- TCs moving northwestward exhibit great variability in direction after landfall indicating that many recurve—especially the stronger TCs. Northwestward moving TCs tend to move more westward after landfall (while crossing the PI), then resume their northwestward movement—again, especially the stronger TCs (see Figs. B.11(a) and (b) (Shoemaker 1991)).

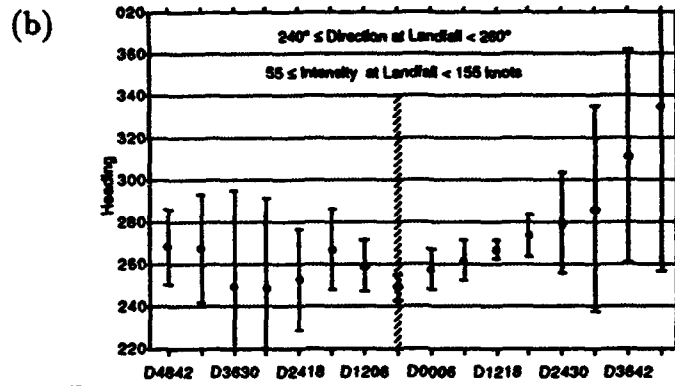
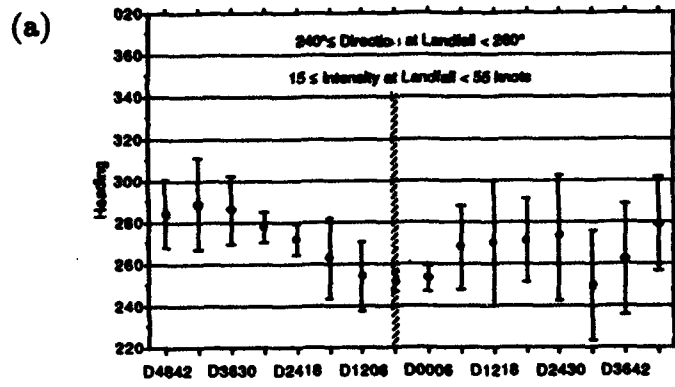


Figure B.8: Average Direction of Movement of Weaker (a) and More Intense (b) TCs Moving West-southwest at Landfall. Error bars represent one standard deviation (adapted from Shoemaker (1991)).

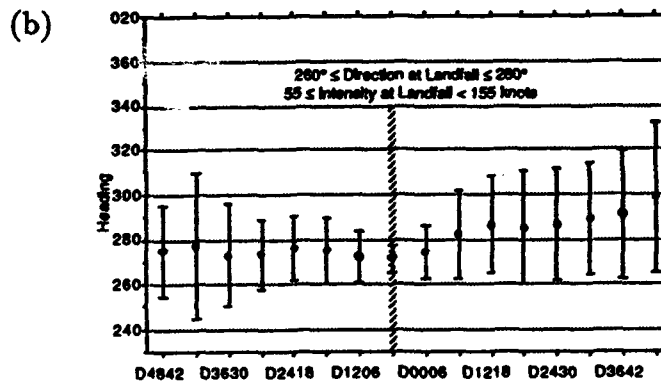
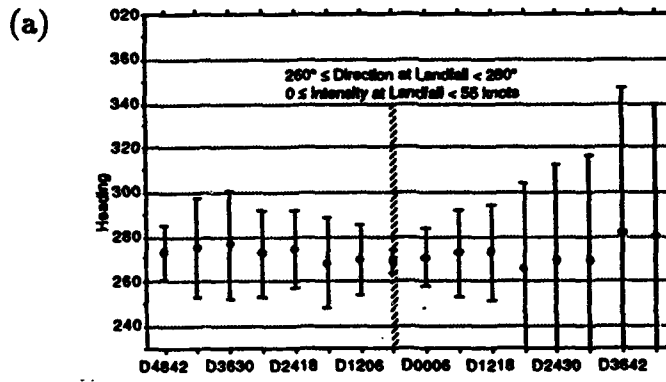


Figure B.9: Same as Fig. B.8 except for TCs Moving Westward (adapted from Shoemaker (1991)).

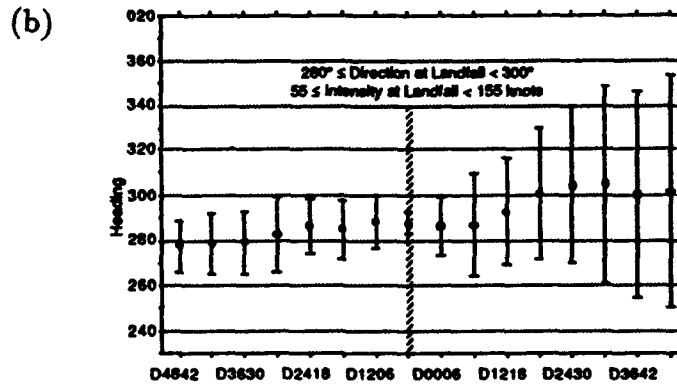
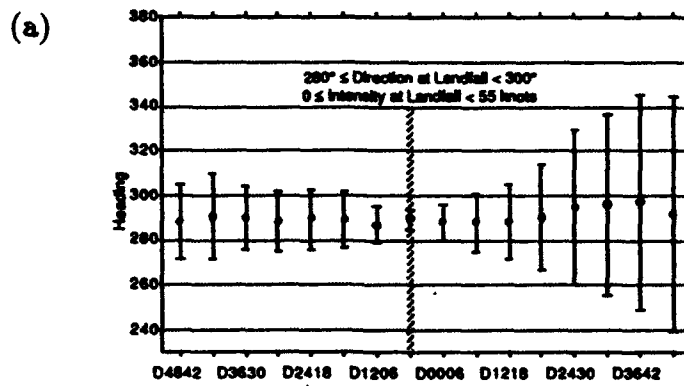


Figure B.10: Average Direction of Movement of Weaker (a) and More Intense (b) TCs Moving West-northwest at Landfall. Error bars represent one standard deviation (adapted from Shoemaker (1991)).

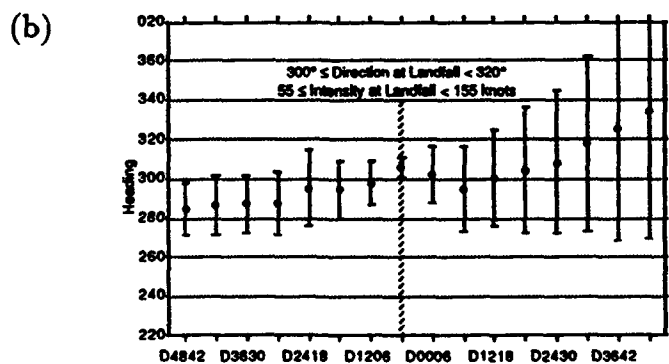
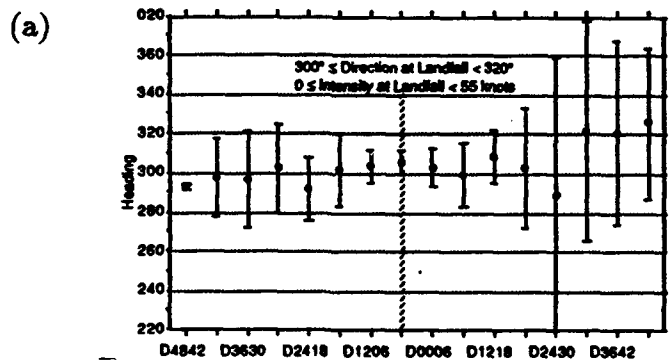


Figure B.11: Same as Fig. B.10 except for TCs Moving Northwestward (adapted from Shoemaker (1991)).

SPEED

The forecasting of the speed of movement of TCs approaching the Philippine Islands affects setting of Conditions of Readiness (CORs), as well as the time of onset and cessation of damaging winds.

Brand and Brelloch (1972), using a small sample of 30 typhoons (only), observed that these typhoons slowed until 18 hours prior to landfall, accelerated until landfall and then slowed while exiting into the South China Sea. Speed of movement differences, for typhoons averaging 12 knots at landfall, were less than two knots. Shoemaker (1991), using a much larger data base, reexamines TCs speed, presenting a detailed stratification and standard deviation statistics.

In Figure B.12, the TCs moving westward or west-northwestward ($260^{\circ} - 300^{\circ}$) during the six hours prior to landfall are presented. Six-hourly speeds are computed using adjacent best track positions.

In Figs. B.13-B.16, the TCs are stratified into categories of tropical depressions, tropical storms, typhoons ≤ 100 knots and typhoons > 100 knots. These categories are further subdivided by speed of movement (slow, moderate and rapid). A further stratification across $14.5^{\circ}N$ had no effect and was not presented.

Results reveal a slight tendency for systems to move gradually faster until landfall, with an increased tendency for TCs with a larger speed at landfall. TCs tend to slow down after landfall and during exit into the South China Sea. Individual TC speed differences may be caused by synoptic factors, since most speed differences lie within one standard deviation of the mean.

In the following figures, categories were omitted when the sample size was one or less (Shoemaker 1991).

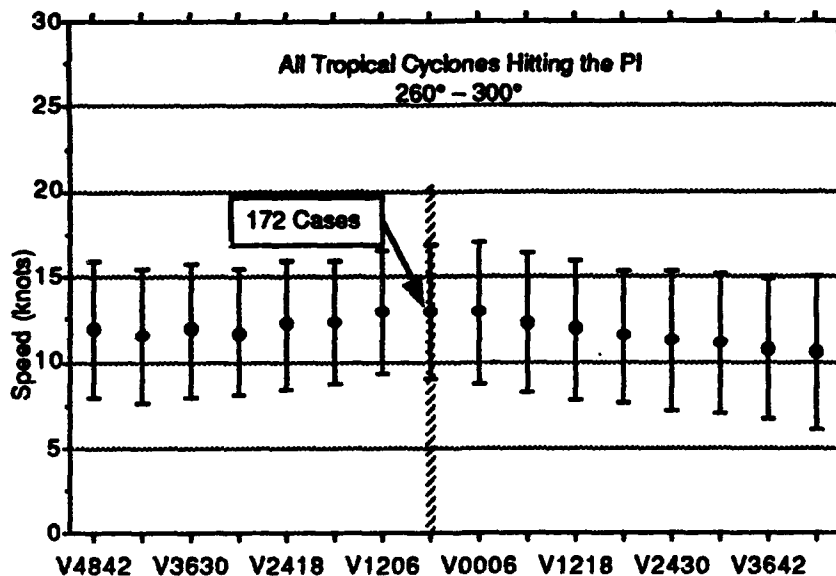


Figure B.12: Six Hourly Average Speed for All Tropical Cyclones moving Westward or West-northwestward in the Six Hours prior to Landfall. Error bars indicate one standard deviation. The dashed vertical line represents landfall (adapted from Shoemaker (1991)).

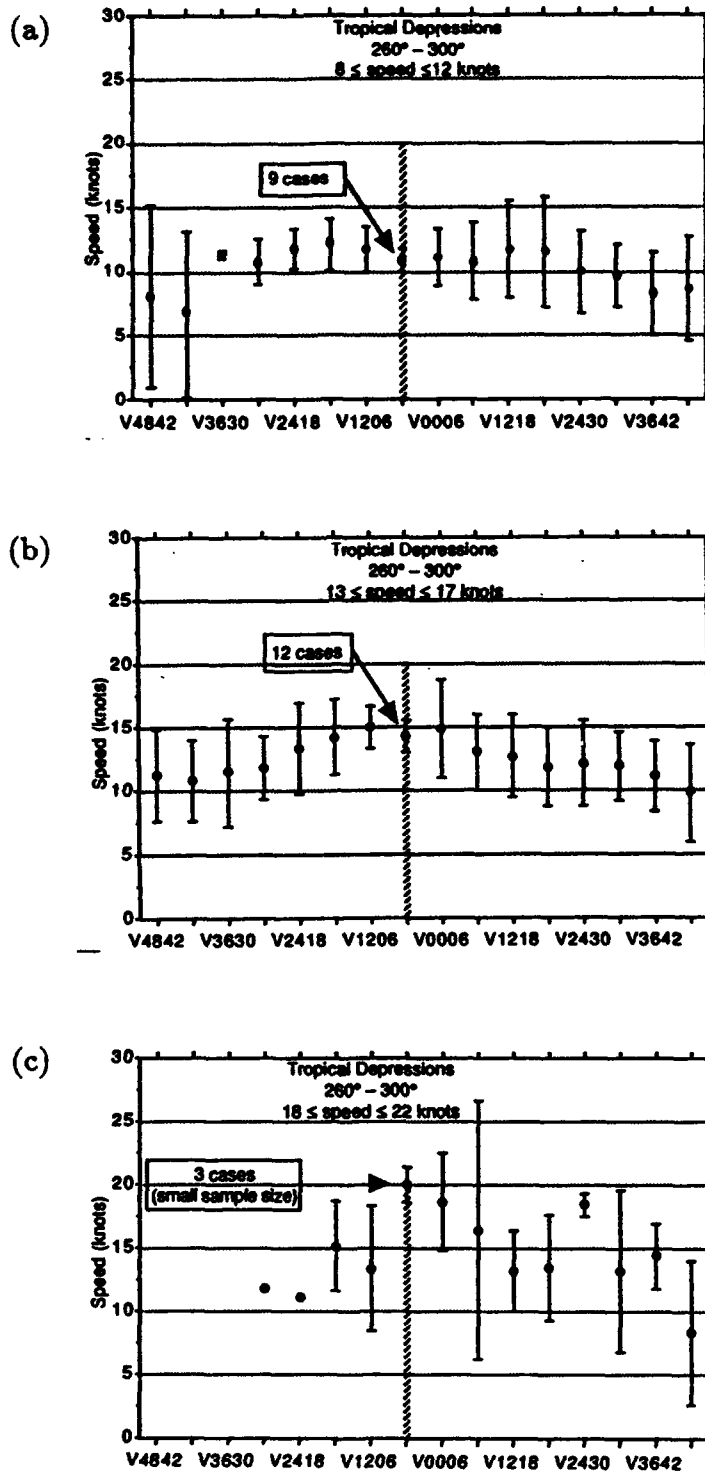


Figure B.13: Six Hourly Average Speed for Tropical Depressions (Intensity 25–30 knots) Moving at (a) 8 to 12 knots (b) 13 to 17 knots and (c) 18 to 22 knots Prior to Landfall. Error bars represent one standard deviation. Note the small sample size and large standard deviations in (c) (adapted from Shoemaker (1991)).

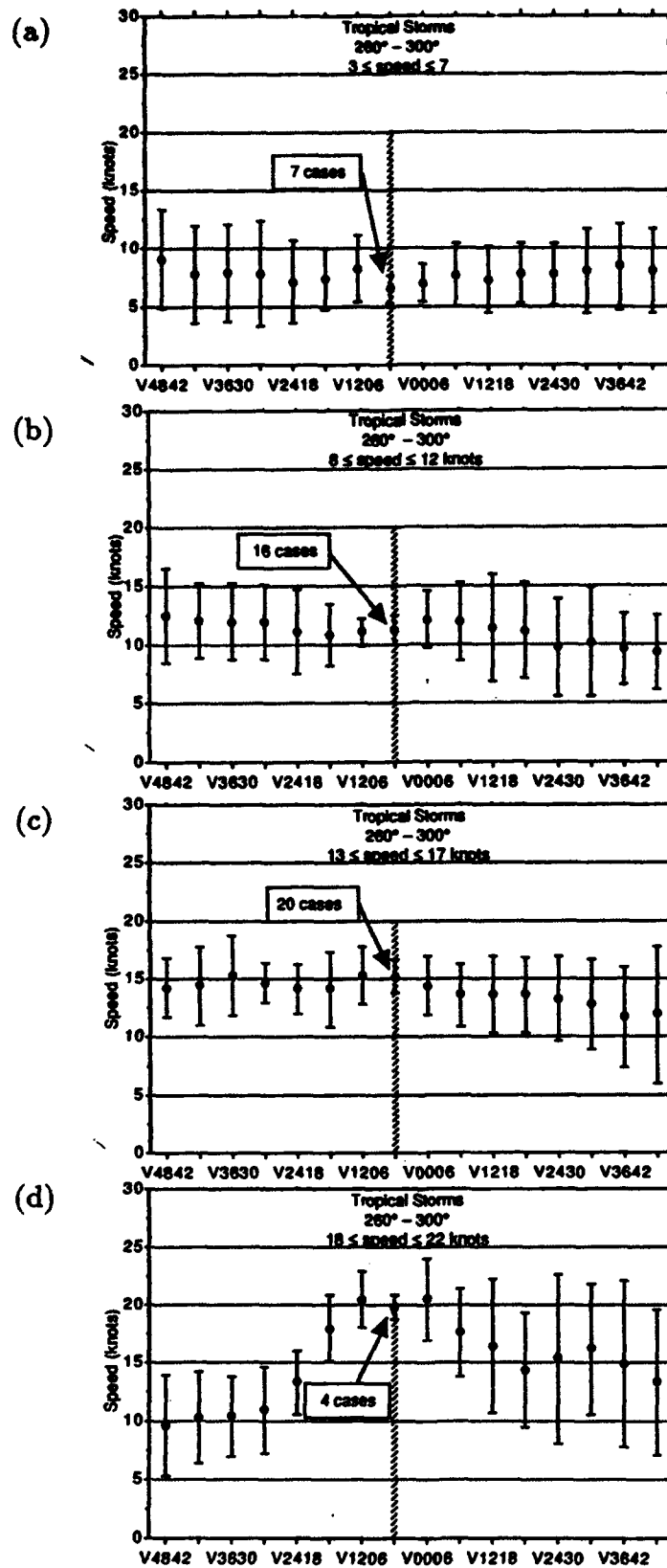


Figure B.14: Six Hourly Average Speed for Tropical Storms (Intensity 35-60 knots) Moving at (a) 3 to 7 knots (b) 8 to 12 knots (c) 13 to 17 knots and (d) 18 to 22 knots Prior to Landfall. Error bars represent one standard deviation. Again, note the small sample size in the most rapidly moving tropical storms in (d) (adapted from Shoemaker (1991)).

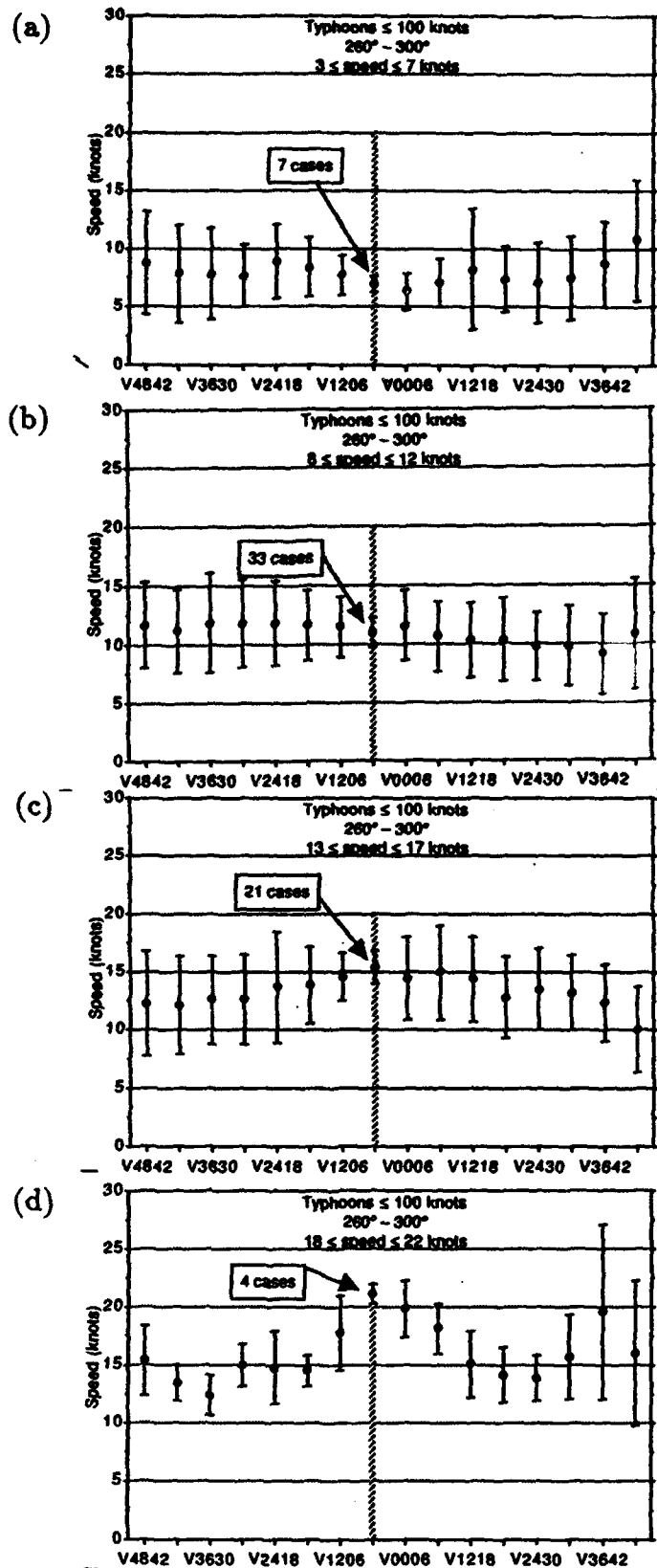


Figure B.15: Six Hourly Average Speed for Typhoons (Intensity ≤ 100 knots) Moving at (a) 3 to 7 knots (b) 8 to 12 knots (c) 13 to 17 knots and (d) 18 to 22 knots Prior to Landfall. Error bars represent one standard deviation. Again, note the small sample size in the very fast moving typhoons in (d) (adapted from Shoemaker (1991)).

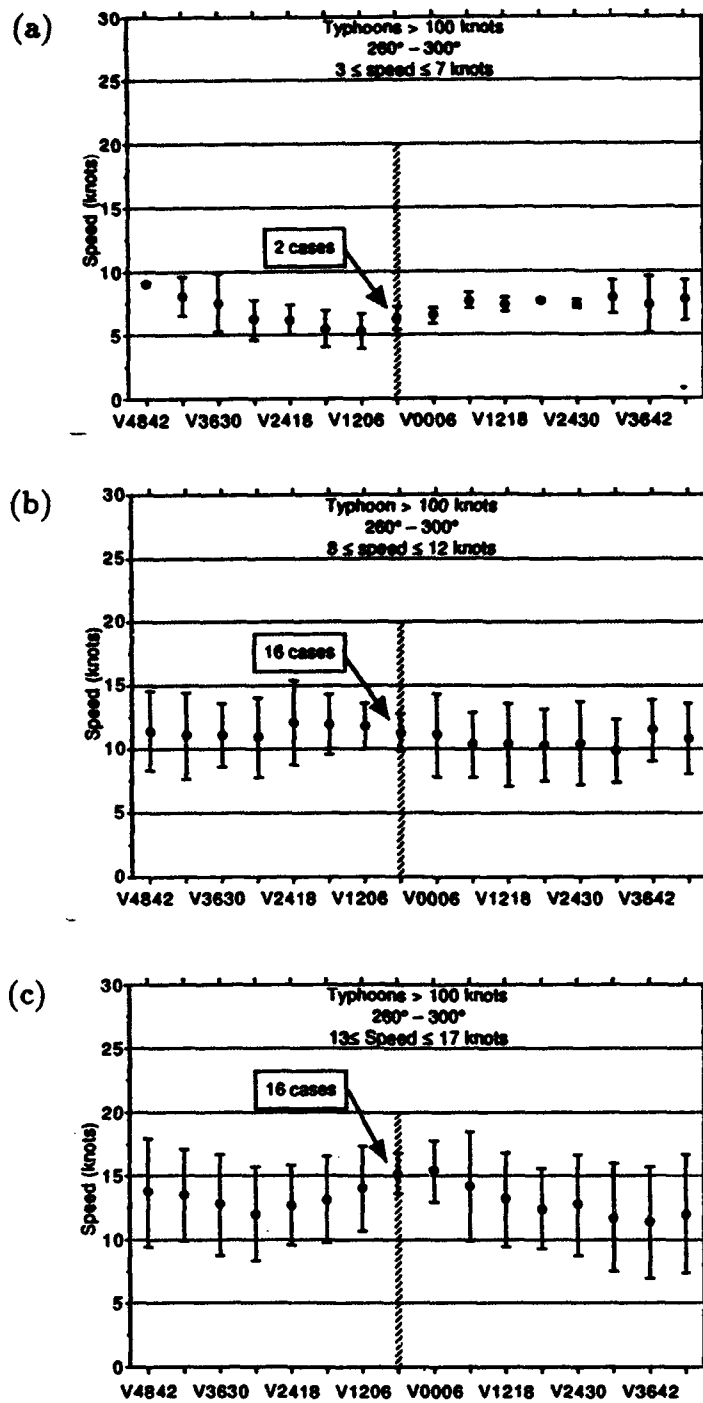


Figure B.16: Six Hourly Average Speed for Typhoons (Intensity >100 knots) Moving at (a) 3 to 7 knots (b) 8 to 12 knots and (c) 13 to 17 knots Prior to Landfall. Error bars represent one standard deviation. Note the small sample size in the slow moving strong typhoons in (a); no strong typhoons made landfall moving faster than 17 knots. Such speed are generally caused by a strong environmental wind envelope, which tends to shear the TCs apart vertically (adapted from Shoemaker (1991)).

Appendix C

Climatic Normals of the Philippines (1951-1985) (PAGASA 1987)

PAGE	STATION	PAGE	STATION
C-3	ALABAT	C-10	INFANTA
C-3	AMBULONG	C-10	ITBAYAT
C-3	APARRI	C-11	JOLO
C-3	BAGUIO	C-11	LAOAG
C-4	BALER	C-11	LEGASPI
C-4	BASCO	C-11	LUCENA
C-4	BORONGAN	C-12	LUMBIA AP CAGAYAN
C-4	BUTUAN CITY	C-12	MAASIN, S.LEYTE
C-5	CABANATUAN	C-12	MACTAN AIRPORT
C-5	CAGAYAN DE ORO	C-12	MALAYBALAY
C-5	CAGAYAN DE SULU	C-13	MANILA INT. AIRPORT
C-5	CALAPAN	C-13	MASBATE
C-6	CALAYAN	C-13	MUNOZ, N. ECIJA
C-6	CASIGURAN	C-13	PAGASA, PALAWAN
C-6	CATARMAN	C-14	PORT AREA MANILA
C-6	CATBALOGAN	C-14	PUERTA PRINCESA
C-7	CEBU CITY	C-14	ROMBLON
C-7	CORON	C-14	ROXAS CITY
C-7	COTABATO	C-15	SAN FRANCISCO
C-7	CUYO	C-15	SANGLEY POINT
C-8	DAET	C-15	SAN JOSE, OCC. MINDORO
C-8	DAGUPAN	C-15	SCIENCE GARDEN
C-8	DAVAO CITY	C-16	TACLOBAN CITY
C-8	DIPOLOG	C-16	TAGBILARAN CITY
C-9	DUMAGUETE CITY	C-16	TAYABAS
C-9	GENERAL SANTOS	C-16	TUGUEGARAO
C-9	GUIUAN	C-17	VIGAN
C-9	HINATUAN	C-17	VIRAC SYNOP
C-10	IBA	C-17	VIRAC RADAR
C-10	ILOILO	C-17	ZAMBOANGA

CLARIFICATION ON THE TERMS USED IN THE TABULATION

CLIMATOLOGICAL NORMALS:	Period averages computed for a uniform and relatively long period comprising at least 3 consecutive 10-year periods.
RAINFALL: (COL. 2)	The amount of precipitation (rain, hail, etc.), expressed in millimeter depth, of the layer of water which has fallen.
RAINY DAYS: (COL. 3)	A rainy day is defined as a period of 24 hours beginning at 8AM to 8AM of the next day during which 0.1 mm of rain is recorded
MAXIMUM TEMPERATURE: (COL. 4)	The maximum temperature recorded for the day. Usually occurs in the afternoon.
MINIMUM TEMPERATURE: (COL. 5)	The minimum temperature recorded for the day. Usually occurs during the early hours of the morning, before sunrise.
MEAN TEMPERATURE: (COL. 6)	Mean temperature = $\frac{\text{Max Temp} + \text{Min Temp}}{2}$
DRY BULB TEMPERATURE: (COL. 7)	Gives the air temperature at the time of observation.
WET BULB TEMPERATURE: (COL. 8)	Gives the temperature that an air parcel would have if cooled adiabatically to saturation at constant pressure by evaporating water into it.
DEW POINT TEMPERATURE: (COL. 9)	The temperature, at a given pressure, to which air must be cooled to become saturated.
RELATIVE HUMIDITY:	The ratio of the amount of water vapor actually in the air to the maximum amount the air can hold at that temperature.
MEAN SEA LEVEL PRESSURE: (COL. 11)	The force exerted by the weight of the atmosphere on a unit area at the mean sea level. The atmospheric pressure at the mean sea level.
PREVAILING WIND: (COLs. 12 & 13)	The wind direction most frequently observed during a given period. The average wind speed is the arithmetic average.
CLOUD: (COL. 14)	The amount of cloud present in the sky, expressed in oktas of the sky cover.
OKTA:	The fraction equal to 1/8 used in coding of cloud amount.
DAYS WITH THUNDERSTORM: (COL. 15)	A "thunderstorm day" is defined as an observational day during which thunder is heard at the station.
DAYS WITH LIGHTNING (COL. 16)	A day with lightning is reported whenever lightning is observed.

Station: ALABAT Posit.: 14°06'N 122°01'E Elev. 1 m. Per. of records: 1961-1985

MO.	RAIN-FALL (mm)	RAIN DAYS	TEMPERATURE (°C)					DRY BULB	WET BULB	DEW PT.	RH (%)	MN. SEA LEVEL PRESS (mbs)	PREVAILING WIND			DAYS WITH	
			MAX	MIN	MEAN	DIREC-TION	SPD (mps)						CLD (octa)	TRW	LGTN		
JAN	280.8	20	30.4	21.9	26.2	25.0	23.1	22	85	1014.0	NE	4	6	0	0		
FEB	133.5	14	30.9	22.1	26.5	25.5	23.3	23	83	1013.8	NE	4	6	0	0		
MAR	99.3	10	32.7	22.7	27.7	26.3	23.9	23	82	1013.6	NE	3	5	0	0		
APR	81.5	9	33.5	23.6	28.6	27.6	23.0	24	81	1012.1	NE	3	5	1	1		
MAY	109.5	9	34.9	24.1	29.6	28.7	23.8	25	79	1010.0	NE	2	5	5	3		
JUN	280.2	14	34.7	24.1	29.4	28.2	23.8	25	82	1009.0	SW	2	6	5	3		
JUL	226.4	17	34.2	23.9	29.1	27.8	23.5	25	83	1008.5	SW	3	6	5	2		
AUG	174.9	15	33.9	23.9	29.0	27.8	23.5	25	83	1008.1	SW	2	6	3	2		
SEP	263.4	17	33.7	23.6	28.6	27.4	23.2	25	84	1008.9	SW	2	6	4	2		
OCT	510.1	24	33.1	23.3	28.2	26.9	24.8	24	84	1010.4	NE	3	6	5	2		
NOV	530.9	22	32.1	23.2	27.6	26.5	24.5	24	85	1011.2	NE	5	6	1	1		
DEC	571.4	24	30.9	22.6	26.8	25.6	23.8	23	86	1012.9	NE	4	6	0	0		
ANN	3221.9	196	32.9	23.3	28.1	26.9	24.7	24	83	1011.0	NE	3	6	29	16		

Station: AMBULONG BATANGAS Posit.: 14°05'N 121°04'E Elev. Unk. Per. of records: 1961-1985

MO.	RAIN-FALL (mm)	RAIN DAYS	TEMPERATURE (°C)					DRY BULB	WET BULB	DEW PT.	RH (%)	MN. SEA LEVEL PRESS (mbs)	PREVAILING WIND			DAYS WITH	
			MAX	MIN	MEAN	DIREC-TION	SPD (mps)						CLD (octa)	TRW	LGTN		
JAN	22.1	5	30.3	21.5	26.0	25.3	22.2	21	78	1013.1	NE	2	4	0	0		
FEB	9.9	3	31.7	21.4	26.6	25.8	22.2	21	73	1012.9	NE	2	4	0	0		
MAR	16.3	3	33.5	22.2	27.9	27.2	22.9	21	69	1012.4	NE	2	3	1	1		
APR	37.4	5	34.8	23.4	29.2	28.6	24.2	23	69	1010.8	NE	2	3	4	6		
MAY	105.3	10	34.3	23.9	29.2	28.8	25.0	24	73	1009.3	SW	2	4	12	18		
JUN	237.5	16	31.6	24.0	27.9	27.9	23.2	24	80	1008.7	SW	2	6	14	16		
JUL	289.9	19	31.4	23.6	27.5	27.2	24.9	24	83	1008.4	SW	2	6	16	16		
AUG	323.7	19	30.8	23.8	27.3	27.1	24.8	24	83	1008.2	SW	2	6	9	9		
SEP	259.7	18	31.3	23.4	27.3	26.9	24.8	24	84	1009.1	SW	2	6	14	16		
OCT	234.1	16	31.5	23.0	27.3	26.7	24.4	24	83	1009.7	NE	2	5	8	12		
NOV	156.6	13	31.1	22.8	27.0	26.5	23.8	23	80	1010.6	NE	2	5	3	6		
DEC	97.6	10	30.0	22.2	26.2	25.6	22.9	22	79	1012.1	NE	2	5	1	2		
ANN	1790.1	137	31.9	22.9	27.5	27.0	23.9	23	78	1010.4	NE	2	5	82	102		

Station: APARRI Posit.: 18°22'N 121°38'E Elev. 4 m. Per. of records: 1951-1985

MO.	RAIN-FALL (mm)	RAIN DAYS	TEMPERATURE (°C)					DRY BULB	WET BULB	DEW PT.	RH (%)	MN. SEA LEVEL PRESS (mbs)	PREVAILING WIND			DAYS WITH	
			MAX	MIN	MEAN	DIREC-TION	SPD (mps)						CLD (octa)	TRW	LGTN		
JAN	141.1	15	26.4	20.4	23.4	23.1	21.2	20	84	1016.0	NE	4	6	0	0		
FEB	76.0	9	27.6	20.7	24.1	23.8	21.7	21	83	1015.2	NE	4	5	0	0		
MAR	45.6	6	29.3	22.0	25.7	25.3	23.0	22	82	1014.2	NE	3	4	1	1		
APR	35.4	5	31.6	23.6	27.6	27.1	24.4	24	80	1011.9	NE	3	3	3	3		
MAY	100.6	8	33.3	24.6	29.0	28.3	25.4	25	79	1009.4	NE	3	4	7	9		
JUN	164.1	13	33.3	24.8	29.2	28.5	25.7	26	80	1007.9	S	3	5	11	14		
JUL	183.2	12	32.9	24.8	28.9	28.3	25.7	25	81	1007.5	S	3	6	8	13		
AUG	225.5	15	32.4	24.6	28.5	27.9	25.5	25	82	1006.5	S	3	6	6	9		
SEP	274.7	15	31.6	24.3	27.9	27.5	25.3	25	84	1008.2	NE	3	5	6	8		
OCT	343.0	18	30.2	23.7	26.9	26.8	24.6	24	83	1011.0	NE	4	6	3	6		
NOV	396.0	21	28.2	22.8	25.5	25.4	23.6	23	86	1013.3	NE	4	6	1	1		
DEC	208.7	19	26.8	21.4	24.1	23.8	22.2	22	87	1015.3	NE	4	6	0	0		
ANN	2213.9	156	30.3	23.1	26.7	26.3	24.0	23	83	1011.4	NE	3	5	46	64		

Station: BAGUIO Posit.: 16°25'N 120°36'E Elev. 1501 m. Per. of records: 1951-1985

MO.	RAIN-FALL (mm)	RAIN DAYS	TEMPERATURE (°C)					DRY BULB	WET BULB	DEW PT.	RH (%)	MN. SEA LEVEL PRESS (mbs)	PREVAILING WIND			DAYS WITH	
			MAX	MIN	MEAN	DIREC-TION	SPD (mps)						CLD (octa)	TRW	LGTN		
JAN	12.1	4	22.6	12.9	17.8	16.6	14.5	13	80	1012.1	SE	2	4	0	0		
FEB	35.8	2	23.6	13.1	18.4	17.2	14.8	13	78	1011.6	SE	2	4	1	0		
MAR	55.9	4	24.7	14.3	19.6	18.4	16.0	15	78	1010.8	SE	2	4	2	1		
APR	102.9	9	25.1	15.5	20.4	19.4	17.2	16	80	1009.4	SE	2	5	9	3		
MAY	331.1	19	24.6	16.2	20.5	19.4	17.8	17	86	1007.9	SE	2	6	18	10		
JUN	480.6	22	23.6	16.2	20.0	19.0	17.7	17	88	1007.3	SE	3	6	15	8		
JUL	670.8	28	23.0	16.0	19.6	18.6	17.5	17	90	1006.6	SE	3	7	14	6		
AUG	847.9	27	22.0	15.9	18.9	18.2	17.4	17	92	1006.2	SE	3	8	11	4		
SEP	582.3	25	22.9	15.7	19.3	18.5	17.4	17	90	1007.1	NW	2	7	13	5		
OCT	262.4	17	23.5	15.4	19.5	18.6	17.2	17	87	1008.1	SE	3	6	8	5		
NOV	152.3	9	23.2	14.8	19.0	18.1	16.3	15	83	1009.5	SE	3	5	2	1		
DEC	28.8	5	22.8	14.0	18.4	17.4	15.3	14	80	1010.9	SE	2	4	1	0		
ANN	3562.9	169	23.5	15.0	19.3	18.3	16.6	16	84	1009.0	SE	2	6	94	43		

Station: **BALER QUEZON** Posit.: 15°45'N 121°34'E Elev. 6 m. Per. of records: 1951-1985

MO.	RAIN-FALL (mm)	RAIN DAYS	TEMPERATURE (°C)						DEW PT.	RH (%)	MN. SEA LEVEL PRESS (mbs)	PREVAILING WIND			DAYS WITH	
			MAX	MIN	MEAN	DRY BULB	WET BULB	DIRC-TION				SPD (mps)	CLD (octa)	TRW	LGTN	
JAN	188.1	18	28.3	20.3	24.4	24.0	21.7	31	82	1018.1	E	2	6	0	0	
FEB	180.8	18	29.0	20.6	24.8	24.2	21.9	31	82	1014.9	E	2	6	0	0	
MAR	213.1	17	30.1	21.4	25.7	26.3	22.8	32	81	1014.2	E	2	5	0	2	
APR	232.4	19	31.5	22.6	27.0	26.5	24.1	33	82	1012.5	E	2	5	3	7	
MAY	301.4	19	32.7	23.4	28.0	27.5	25.0	34	82	1010.1	E	2	5	12	17	
JUN	272.3	17	33.0	23.7	28.3	27.8	25.1	34	80	1008.8	SW	2	6	11	17	
JUL	240.5	18	32.8	23.6	28.2	27.6	24.8	34	80	1007.9	W	2	6	11	16	
AUG	218.6	18	32.5	23.7	28.1	27.5	24.7	34	80	1007.1	W	3	6	8	13	
SEP	300.6	18	32.3	23.4	27.8	27.2	24.6	34	81	1006.5	SW	2	6	9	15	
OCT	416.0	18	31.5	22.6	27.0	26.5	24.3	34	83	1010.5	E	2	6	6	11	
NOV	444.4	18	30.2	21.9	26.0	25.7	23.5	33	83	1012.0	E	2	6	2	3	
DEC	327.9	16	29.1	21.1	25.1	24.8	22.5	32	82	1013.9	E	2	6	0	0	
ANN	3311.1	206	31.1	22.4	26.7	26.2	23.8	33	82	1011.3	E	2	6	62	101	

Station: **BASCO** Posit.: 20°27'N 121°58'E Elev. 11 m. Per. of records: 1951-1985

MO.	RAIN-FALL (mm)	RAIN DAYS	TEMPERATURE (°C)						DEW PT.	RH (%)	MN. SEA LEVEL PRESS (mbs)	PREVAILING WIND			DAYS WITH	
			MAX	MIN	MEAN	DRY BULB	WET BULB	DIRC-TION				SPD (mps)	CLD (octa)	TRW	LGTN	
JAN	183.9	18	24.7	19.2	22.0	22.0	19.8	19	82	1016.8	NE	5	6	0	0	
FEB	126.1	18	25.7	19.8	22.7	22.7	20.5	20	82	1016.9	NE	5	6	0	1	
MAR	102.6	13	27.5	21.2	24.3	24.2	21.9	21	82	1014.8	NE	5	5	0	0	
APR	83.1	10	29.2	23.8	26.3	26.2	23.8	23	82	1012.6	SE	4	5	2	2	
MAY	138.4	11	30.9	24.7	27.8	27.9	25.6	25	83	1008.7	SE	4	5	3	7	
JUN	278.3	18	31.4	25.2	28.3	28.5	26.1	26	83	1007.9	SE	4	6	3	9	
JUL	289.2	17	31.6	25.1	28.4	28.6	26.4	26	84	1007.1	SE	5	5	3	9	
AUG	430.2	21	30.9	24.8	27.9	28.1	26.1	26	85	1006.4	SW	5	6	4	7	
SEP	370.1	20	30.9	24.4	27.6	27.8	25.6	26	84	1006.2	NE	4	6	3	7	
OCT	330.1	20	29.5	23.5	26.5	26.7	24.3	24	82	1010.1	NE	4	6	3	7	
NOV	317.1	21	27.5	22.3	24.9	24.9	22.6	20	82	1013.9	NE	6	6	0	1	
DEC	289.9	21	25.7	20.3	22.9	23.0	21.0	20	84	1014.1	NE	6	6	0	0	
ANN	2679.0	203	28.8	22.8	25.8	25.9	23.6	23	83	1011.4	NE	5	6	21	50	

Station: **BORONGAN SAMAR** Posit.: 11°36'N 125°26'E Elev. 6 m. Per. of records: 1951-1985

MO.	RAIN-FALL (mm)	RAIN DAYS	TEMPERATURE (°C)						DEW PT.	RH (%)	MN. SEA LEVEL PRESS (mbs)	PREVAILING WIND			DAYS WITH	
			MAX	MIN	MEAN	DRY BULB	WET BULB	DIRC-TION				SPD (mps)	CLD (octa)	TRW	LGTN	
JAN	625.3	25	29.0	22.1	26.5	25.3	23.5	23	86	1012.3	NE	3	6	0	0	
FEB	414.1	22	29.5	22.3	25.9	26.4	23.5	23	85	1012.3	NE	3	6	0	0	
MAR	306.9	21	30.3	22.5	26.4	26.1	23.9	23	83	1012.5	NE	2	5	0	1	
APR	256.1	21	31.4	23.1	27.2	27.0	24.7	24	83	1011.2	NE	2	5	2	3	
MAY	296.9	18	32.1	23.4	27.7	27.4	25.1	24	83	1010.0	E	2	5	6	6	
JUN	232.0	18	32.2	23.2	27.7	27.3	25.1	24	84	1009.6	W	2	5	6	9	
JUL	198.8	17	32.3	23.1	27.7	27.2	24.8	24	82	1009.0	W	2	6	7	8	
AUG	182.0	15	32.7	23.1	27.9	27.3	24.7	24	81	1008.6	W	2	6	6	10	
SEP	204.5	16	32.6	23.0	28.8	27.2	24.8	24	82	1008.9	W	2	6	7	9	
OCT	312.7	20	31.8	22.8	27.3	26.8	24.7	24	84	1009.5	W	2	6	6	8	
NOV	555.4	23	30.7	22.8	26.7	26.3	24.5	24	86	1010.2	NE	2	6	3	4	
DEC	663.3	27	29.7	22.7	26.2	25.9	24.1	23	86	1011.2	NE	2	6	1	2	
ANN	4248.0	243	31.2	22.8	27.0	26.6	24.5	24	84	1010.4	NE	2	6	44	60	

Station: **BUTUAN CITY** Posit.: 08°56'N 125°41'E Elev. 46 m. Per. of records: 1981-1985

MO.	RAIN-FALL (mm)	RAIN DAYS	TEMPERATURE (°C)						DEW PT.	RH (%)	MN. SEA LEVEL PRESS (mbs)	PREVAILING WIND			DAYS WITH	
			MAX	MIN	MEAN	DRY BULB	WET BULB	DIRC-TION				SPD (mps)	CLD (octa)	TRW	LGTN	
JAN	436.9	19	30.0	21.8	25.9	25.6	24.1	24	88	1013.4	NW	1	6	2	14	
FEB	205.4	13	31.5	21.1	26.3	25.9	23.9	23	85	1011.2	NW	1	5	1	6	
MAR	100.1	13	32.1	21.8	26.9	26.8	24.3	23	81	1013.4	SE	1	5	3	6	
APR	63.49	10	33.5	22.8	28.1	27.9	25.1	24	80	1011.4	ESE	1	4	9	11	
MAY	124.6	13	34.1	23.3	28.7	28.3	25.5	25	80	1010.4	ESE	1	5	16	21	
JUN	124.4	13	33.1	23.3	28.2	27.8	25.2	24	81	1010.0	ESE	2	6	10	22	
JUL	161.2	15	32.5	22.6	27.5	27.4	25.3	25	84	1010.9	NW	2	6	12	26	
AUG	73.3	9	32.9	23.0	27.9	27.8	25.2	24	81	1011.3	ESE	2	6	11	20	
SEP	182.1	16	32.5	22.9	27.7	27.3	25.1	24	84	1011.6	VRBL	1	6	10	19	
OCT	181.1	17	32.0	22.7	27.3	27.1	25.1	24	85	1011.8	NW	1	6	14	24	
NOV	158.7	15	32.0	22.5	27.2	27.0	25.0	24	85	1011.9	VRBL	1	6	11	22	
DEC	223.5	18	30.7	22.3	26.5	26.8	24.5	24	83	1012.9	NW	1	5	4	19	
ANN	2033.7	171	32.2	22.5	23.4	27.1	24.9	24	83	1011.7	NW	1	6	103	210	

Station: CABANATUAN Posit.: 15°29'N 120°58'E Elev. 31 m. Per. of records: 1951-1976

MO.	RAIN-FALL (mm)	RAIN DAYS	TEMPERATURE (°C)					DRY BULB	WET BULB	DEW PT.	RH (%)	MN. SEA LEVEL PRESS (mbs)	PREVAILING WIND			DAYS WITH	
			MAX	MIN	MEAN	DIREC-TION	SPD (mps)						CLD (octa)	TRW	LGTN		
JAN	7.5	2	31.5	20.0	28.8	25.0	21.3	20	73	1013.7	NE	2	4	0	0		
FEB	4.9	1	32.6	20.1	26.4	25.6	21.4	19	69	1013.6	NE	2	4	0	0		
MAR	16.4	3	34.0	21.1	27.6	27.0	22.3	20	66	1013.0	SE	2	4	1	1		
APR	19.7	3	35.5	22.8	29.2	28.7	23.5	21	64	1011.4	SE	2	4	3	4		
MAY	150.1	11	35.3	23.7	29.5	28.8	24.7	23	71	1009.6	SE	2	5	10	10		
JUN	267.6	9	33.4	23.6	28.5	27.7	25.0	24	80	1009.2	SE	1	6	11	9		
JUL	340.8	20	32.4	23.4	27.9	27.1	24.9	24	84	1008.7	SW	2	6	12	8		
AUG	395.8	24	31.5	23.4	27.5	26.7	24.8	24	86	1008.2	S	2	6	10	6		
SEP	305.2	21	31.9	23.3	27.6	26.8	24.8	24	85	1009.0	VAR	1	6	10	5		
OCT	190.8	12	32.5	22.8	27.7	26.9	24.4	23	81	1010.3	NE	2	5	5	5		
NOV	134.8	9	31.8	21.9	26.9	26.3	23.3	22	78	1011.4	NE	2	5	1	1		
DEC	39.9	6	31.5	20.9	26.2	25.6	22.2	21	74	1012.7	NE	2	5	0	0		
ANN	1873.5	121	32.8	22.3	27.6	25.0	23.6	22	76	1010.9	NE	2	5	63	49		

Station: CAGAYAN DE ORO CITY Posit.: 08°24'N 124°36'E Elev. Unk. Per. of records: 1951-1985

MO.	RAIN-FALL (mm)	RAIN DAYS	TEMPERATURE (°C)					DRY BULB	WET BULB	DEW PT.	RH (%)	MN. SEA LEVEL PRESS (mbs)	PREVAILING WIND			DAYS WITH	
			MAX	MIN	MEAN	DIREC-TION	SPD (mps)						CLD (octa)	TRW	LGTN		
JAN	107.4	10	30.6	21.5	28.0	25.7	23.4	23	82	1010.7	SW	1	5	1	2		
FEB	64.7	8	30.8	21.6	26.2	25.9	23.3	22	80	1010.6	SW	1	5	2	1		
MAR	56.7	7	31.7	21.7	26.7	26.6	23.6	23	78	1010.5	SW	1	5	2	3		
APR	38.4	6	32.7	22.7	27.7	27.7	24.3	23	76	1009.7	SW	1	4	4	8		
MAY	102.7	11	33.2	23.4	28.3	28.1	24.9	24	77	1008.9	SW	1	5	11	19		
JUN	198.8	18	32.7	23.0	27.8	27.4	24.8	24	81	1009.3	SW	1	6	13	13		
JUL	214.0	18	32.5	22.6	27.5	27.0	24.4	24	81	1009.1	SW	1	6	11	11		
AUG	199.1	17	32.7	22.6	27.6	27.1	24.4	24	80	1009.1	SW	1	6	10	11		
SEP	216.7	17	32.5	22.7	27.6	27.0	24.4	24	81	1009.4	SW	1	6	13	12		
OCT	178.2	16	32.3	22.6	27.4	27.1	24.4	24	83	1009.2	SW	1	6	10	13		
NOV	128.0	13	32.1	22.4	27.2	26.9	24.3	23	81	1009.2	SW	1	5	7	12		
DEC	116.3	12	31.1	22.1	26.6	26.3	24.1	23	83	1009.6	SW	1	5	3	7		
ANN	1618.0	153	32.1	22.4	27.2	26.9	24.2	23	80	1009.6	SW	1	5	87	112		

Station: CAGAYAN DE SULU Posit.: 07°00'N 118°05'E Elev. Unk. Per. of records: 1975-1980

MO.	RAIN-FALL (mm)	RAIN DAYS	TEMPERATURE (°C)					DRY BULB	WET BULB	DEW PT.	RH (%)	MN. SEA LEVEL PRESS (mbs)	PREVAILING WIND			DAYS WITH	
			MAX	MIN	MEAN	DIREC-TION	SPD (mps)						CLD (octa)	TRW	LGTN		
JAN	194.4	17	28.6	23.4	26.0	26.1	24.3	24	86	1009.9	NE	3	6	1	6		
FEB	118.1	13	28.9	23.9	26.4	26.5	24.4	24	86	1011.3	E	3	6	1	0		
MAR	23.3	4	30.5	26.7	27.1	27.4	24.6	24	79	1010.4	E	3	5	0	3		
APR	50.1	7	31.3	23.9	27.6	28.0	25.0	24	78	1010.3	SE/E	2	5	3	11		
MAY	103.7	10	31.1	24.6	27.8	28.3	25.3	24	78	1010.1	SE/E	2	5	11	18		
JUN	218.9	17	29.9	23.9	26.9	27.2	24.9	24	83	1010.7	SSW	2	6	9	17		
JUL	267.6	18	30.1	23.4	26.7	27.0	24.6	24	83	1010.6	S/SSW	2	6	8	20		
AUG	192.2	17	29.6	23.5	26.5	26.9	24.6	24	83	1009.4	S	2	6	9	20		
SEP	242.8	16	30.3	23.5	26.9	27.0	24.8	24	84	1009.8	N/SSW	2	6	11	11		
OCT	300.2	19	30.0	23.3	26.6	27.0	25.0	24	85	1009.7	VRBL	2	6	7	15		
NOV	308.1	20	29.6	23.3	26.4	26.5	24.6	24	86	1008.6	N	2	6	8	19		
DEC	272.8	17	29.5	23.7	26.6	26.6	24.6	24	85	1010.0	VRBL	3	6	6	8		
ANN	2286.2	175	30.0	23.7	26.8	27.0	24.7	24	83	1009.3	E	2	6	74	148		

Station: CALAPAN Posit.: 13°25'N 121°11'E Elev. 40 m. Per. of records: 1951-1985

MO.	RAIN-FALL (mm)	RAIN DAYS	TEMPERATURE (°C)					DRY BULB	WET BULB	DEW PT.	RH (%)	MN. SEA LEVEL PRESS (mbs)	PREVAILING WIND			DAYS WITH	
			MAX	MIN	MEAN	DIREC-TION	SPD (mps)						CLD (octa)	TRW	LGTN		
JAN	91.4	17	28.4	22.2	25.3	24.7	22.4	22	82	1013.8	NE	2	6	1	0		
FEB	54.8	11	29.0	22.5	25.8	25.2	22.6	22	80	1013.5	NE	3	5	1	0		
MAR	52.7	10	30.3	23.3	26.8	26.4	23.3	22	78	1013.4	E	3	5	1	1		
APR	90.2	10	31.6	24.0	27.7	27.7	24.4	23	76	1011.8	E	3	4	6	6		
MAY	159.4	12	32.2	24.1	28.2	27.9	24.9	24	78	1009.8	E	2	5	16	14		
JUN	200.9	15	31.8	23.7	27.8	27.4	24.8	24	81	1009.0	E	2	6	17	16		
JUL	183.4	16	31.2	23.4	27.3	26.9	24.5	24	82	1008.6	NW	2	6	13	13		
AUG	199.5	17	31.1	23.6	27.4	26.9	24.5	24	82	1008.2	NW	2	6	11	9		
SEP	189.9	16	31.2	23.3	27.3	26.8	24.5	24	83	1008.8	NW	2	6	13	11		
OCT	296.3	19	30.8	23.3	27.1	26.6	24.3	24	82	1009.1	NE	2	6	10	10		
NOV	237.5	19	29.9	23.3	26.6	26.1	23.9	23	84	1011.2	NE	3	6	5	5		
DEC	172.4	19	28.7	22.8	25.8	25.1	22.4	21	79	1012.8	NE	3	6	5	5		
ANN	1930.4	181	30.5	23.3	26.9	26.5	23.9	23	81	1010.8	NE	2	6	96	87		

Station: CALAYAN Posit.: 19°16'N 121°28'E Elev. 12 m. Per. of records: 1951-1985

MO.	RAIN-FALL (mm)	RAIN DAYS	TEMPERATURE (°C)					DRY BULB	WET BULB	DEW PT.	RH (%)	MN. SEA LEVEL PRESS (mbs)	PREVAILING WIND			DAYS WITH	
			MAX	MIN	MEAN	DIREC-TION	SPD (mps)						CLD (octa)	TRW	LGTN		
JAN	188.8	19	26.4	20.0	23.3	23.8	20.8	20	84	1014.9	NE	3	6	0	0		
FEB	109.7	12	27.5	20.3	25.9	23.4	21.8	20	83	1018.5	E	3	5	0	0		
MAR	73.3	9	29.0	21.5	25.2	24.9	22.7	22	83	1014.6	E	3	4	0	0		
APR	46.2	6	30.9	23.0	26.9	26.7	24.3	23	82	1012.5	E	3	4	1	2		
MAY	107.0	7	32.7	24.0	28.3	28.3	25.6	25	80	1009.9	E	2	4	5	11		
JUN	196.1	10	32.4	24.5	28.4	28.5	26.1	25	83	1008.5	W	2	5	6	14		
JUL	242.8	11	32.3	24.7	28.5	28.3	26.1	25	84	1007.9	E/W	3	5	4	11		
AUG	323.0	17	31.4	24.5	27.9	27.8	25.8	25	85	1007.0	W	3	6	4	8		
SEP	330.0	16	31.4	24.1	27.7	27.5	25.6	25	86	1008.5	E	3	6	3	8		
OCT	349.0	19	30.5	23.5	27.0	26.7	24.6	24	84	1011.5	NE	3	5	3	4		
NOV	394.3	21	28.6	22.5	25.5	26.3	23.2	22	84	1013.7	NE	4	6	0	1		
DEC	317.7	22	26.9	21.1	24.0	23.7	21.8	21	85	1015.8	NE	4	6	0	0		
ANN	2676.4	169	30.0	22.8	26.4	26.3	24.0	23	84	1011.7	E	3	5	26	59		

Station: CASIGURAN Posit.: 16°17'N 122°07'E Elev. 4 m. Per. of records: 1951-1985

MO.	RAIN-FALL (mm)	RAIN DAYS	TEMPERATURE (°C)					DRY BULB	WET BULB	DEW PT.	RH (%)	MN. SEA LEVEL PRESS (mbs)	PREVAILING WIND			DAYS WITH	
			MAX	MIN	MEAN	DIREC-TION	SPD (mps)						CLD (octa)	TRW	LGTN		
JAN	217.2	18	27.8	19.4	23.7	22.9	21.8	21	89	1014.8	N	2	6	0	0		
FEB	157.5	14	26.7	19.3	24.0	23.3	21.8	21	88	1014.5	N	2	5	0	0		
MAR	192.8	14	29.9	20.0	24.9	24.3	22.8	22	88	1013.7	N	2	5	0	1		
APR	136.9	13	31.8	21.3	26.5	26.0	24.3	24	87	1012.0	N	2	4	2	4		
MAY	235.6	16	32.8	22.3	27.6	27.3	25.4	25	86	1009.6	S	2	4	9	13		
JUN	237.9	15	33.3	22.9	28.1	27.7	25.8	25	86	1008.2	S	2	5	8	14		
JUL	261.2	16	32.6	22.8	27.8	27.3	25.5	25	86	1007.4	S	2	5	9	14		
AUG	236.2	17	32.6	22.9	27.7	27.1	25.5	25	88	1006.6	S	2	6	8	10		
SEP	294.9	18	32.3	22.4	27.4	26.7	25.2	25	88	1008.0	S	2	6	8	11		
OCT	422.3	18	31.3	21.8	26.5	25.9	24.3	24	88	1010.0	N	2	5	5	7		
NOV	601.7	20	29.7	21.3	25.5	24.9	23.4	23	88	1011.9	N	2	6	3	2		
DEC	437.2	19	28.5	20.3	24.5	23.9	22.4	22	88	1013.8	N	2	6	0	1		
ANN	3427.4	198	31.0	21.4	26.2	25.6	24.0	24	88	1010.9	N	2	5	52	77		

Station: CATARMAN SAMAR Posit.: 12°30'N 124°38'E Elev. 6 m. Per. of records: 1951-1985

MO.	RAIN-FALL (mm)	RAIN DAYS	TEMPERATURE (°C)					DRY BULB	WET BULB	DEW PT.	RH (%)	MN. SEA LEVEL PRESS (mbs)	PREVAILING WIND			DAYS WITH	
			MAX	MIN	MEAN	DIREC-TION	SPD (mps)						CLD (octa)	TRW	LGTN		
JAN	417.4	22	28.4	22.1	25.2	25.1	23.4	23	87	1011.9	NE	3	6	1	0		
FEB	260.8	19	28.8	21.8	25.3	25.2	23.3	23	85	1012.0	NE	3	5	1	0		
MAR	215.2	16	29.8	22.0	25.9	25.8	23.7	23	84	1012.1	NE	3	4	1	1		
APR	146.7	14	30.9	22.4	26.6	26.5	24.5	24	85	1010.9	NE	2	4	5	4		
MAY	149.8	13	31.9	23.0	27.4	27.4	25.2	24	84	1009.2	NE	2	4	14	11		
JUN	179.3	15	32.1	23.3	27.7	27.3	25.1	24	84	1008.7	NE	2	5	15	15		
JUL	208.8	16	31.6	23.4	27.5	27.1	24.9	24	84	1008.1	SW	2	6	11	14		
AUG	157.8	13	32.0	23.6	27.8	27.3	24.9	24	82	1007.9	SW	2	6	9	11		
SEP	212.0	16	31.6	23.2	27.4	26.9	24.8	24	84	1008.5	SW	2	6	11	13		
OCT	372.5	21	30.7	23.0	26.8	26.6	24.8	24	86	1009.2	NE	2	5	10	12		
NOV	525.8	23	29.9	22.9	26.4	26.1	24.5	24	88	1009.4	NE	3	6	6	6		
DEC	493.0	26	28.8	22.7	25.7	25.6	24.1	24	88	1010.6	NE	3	6	3	2		
ANN	3329.1	214	30.5	22.8	26.6	26.4	24.4	24	85	1009.9	NE	2	5	87	69		

Station: CATBALOGAN SAMAR Posit.: 11°47'N 124°53'E Elev. 5 m. Per. of records: 1951-1985

MO.	RAIN-FALL (mm)	RAIN DAYS	TEMPERATURE (°C)					DRY BULB	WET BULB	DEW PT.	RH (%)	MN. SEA LEVEL PRESS (mbs)	PREVAILING WIND			DAYS WITH	
			MAX	MIN	MEAN	DIREC-TION	SPD (mps)						CLD (octa)	TRW	LGTN		
JAN	225.3	17	30.1	21.9	26.0	25.4	23.1	22	82	1012.0	NE	2	6	1	1		
FEB	144.8	16	30.6	21.8	26.2	25.6	23.1	22	81	1012.1	NE	2	6	0	0		
MAR	129.8	14	31.6	22.2	26.9	26.4	23.5	22	78	1012.0	NE	2	5	1	1		
APR	102.6	14	32.7	23.2	27.9	27.5	24.5	24	78	1010.8	NE	2	4	5	4		
MAY	170.1	15	33.1	24.1	28.6	28.2	25.1	24	78	1009.5	NE	2	5	12	11		
JUN	200.0	17	32.7	24.1	28.4	28.0	25.2	24	80	1009.1	SW	2	6	14	13		
JUL	243.7	18	32.1	24.1	28.1	27.8	25.1	24	80	1008.7	SW	2	6	13	12		
AUG	224.9	17	32.3	24.4	28.3	28.0	25.1	24	79	1008.5	SW	2	6	10	11		
SEP	263.0	19	32.1	24.1	28.1	27.3	25.0	24	83	1008.9	SW	2	6	11	11		
OCT	301.5	21	31.7	23.5	27.6	27.0	24.7	24	83	1009.3	N/VAR	2	6	11	12		
NOV	321.4	22	31.1	23.0	27.0	26.5	24.4	24	84	1009.7	NE	1	6	6	7		
DEC	309.6	22	30.3	22.5	26.4	25.9	23.8	23	84	1010.8	NE	2	6	2	3		
ANN	2636.7	212	31.7	23.2	27.5	27.0	24.4	23	81	1010.1	NE	2	6	86	86		

Station: CEBU CITY Posit.: 10°20'N 123°54'E Elev. 33 m. Per. of records: 1951-1983

MO.	RAIN-FALL (mm)	RAIN DAYS	TEMPERATURE (°C)					DRY BULB	WET BULB	DEW PT.	RH (%)	MN. SEA LEVEL PRESS (mbs)	PREVAILING WIND			DAYS WITH	
			MAX	MIN	MEAN	DIREC-TION	SPD (mps)						CLD (octa)	TRW	LGTN		
JAN	106.5	12	30.3	22.6	26.4	26.0	23.2	22	79	1011.4	NE	3	6	1	0		
FEB	67.6	10	30.6	22.6	26.6	26.2	23.2	22	78	1011.6	NE	3	6	1	1		
MAR	54.4	9	31.7	23.0	27.3	27.0	23.6	22	75	1011.5	NE	3	5	1	1		
APR	50.4	7	33.0	23.9	28.4	28.3	24.3	24	72	1010.5	NE	3	5	3	3		
MAY	107.6	11	33.2	24.5	28.8	28.7	25.2	24	75	1009.4	NE	2	5	10	7		
JUN	183.5	16	32.4	24.1	28.2	27.9	25.1	24	80	1009.4	SW	2	6	13	7		
JUL	206.5	16	31.5	23.7	27.6	27.3	24.8	24	82	1009.0	SW	2	6	13	7		
AUG	184.4	16	31.7	23.8	27.7	27.5	24.7	24	80	1008.8	SW	2	6	12	7		
SEP	196.7	16	31.7	23.7	27.7	27.3	24.8	24	81	1009.2	SW	2	7	13	6		
OCT	195.5	19	31.5	23.5	27.5	27.1	24.7	24	82	1009.4	SW	2	6	13	8		
NOV	187.8	15	31.3	23.4	27.3	27.0	24.5	24	81	1009.6	N	2	6	7	6		
DEC	127.3	15	30.6	23.0	26.8	26.4	23.9	23	81	1010.5	NE	3	6	2	3		
ANN	1638.2	162	31.6	23.5	27.5	27.2	24.3	23	79	1010.0	NE	2	6	89	56		

Station: CORON Posit.: 12°00'N 120°12'E Elev. 14 m. Per. of records: 1951-1985

MO.	RAIN-FALL (mm)	RAIN DAYS	TEMPERATURE (°C)					DRY BULB	WET BULB	DEW PT.	RH (%)	MN. SEA LEVEL PRESS (mbs)	PREVAILING WIND			DAYS WITH	
			MAX	MIN	MEAN	DIREC-TION	SPD (mps)						CLD (octa)	TRW	LGTN		
JAN	25.7	3	31.5	22.0	26.8	26.9	23.9	23	78	1012.1	E	2	3	0	1		
FEB	8.0	2	31.9	22.2	27.1	27.0	23.8	23	76	1011.8	E	2	3	0	0		
MAR	5.7	1	32.5	22.7	27.7	27.6	24.2	23	75	1011.8	E	2	2	0	1		
APR	30.4	2	33.2	23.6	28.4	28.5	24.9	24	74	1009.3	E	2	2	1	4		
MAY	184.4	9	32.9	24.2	28.6	28.5	25.5	25	78	1010.0	E	1	4	8	12		
JUN	378.6	19	31.3	23.3	27.3	27.4	23.4	22	71	1008.5	SW	1	5	9	9		
JUL	480.1	22	30.3	22.6	26.5	26.6	24.8	24	86	1009.9	SW	2	6	7	9		
AUG	551.4	22	30.2	22.8	26.5	26.5	24.8	24	87	1008.1	SW	1	6	7	7		
SEP	436.6	20	30.5	22.9	26.8	26.6	24.8	24	86	1009.9	SW	1	6	7	8		
OCT	288.9	16	31.3	22.7	27.0	26.7	24.9	24	86	1009.9	E	1	5	5	9		
NOV	135.2	10	31.7	22.5	27.1	27.2	24.8	24	82	1010.4	E	1	4	2	6		
DEC	82.1	6	31.6	22.2	26.9	26.9	24.4	24	81	1009.8	E	2	3	1	2		
ANN	2607.1	132	31.6	22.8	27.2	27.2	24.5	24	80	1010.1	E	2	4	47	68		

Station: COTABATO MAGUINDANAO Posit.: 07°13'N 124°15'E Elev. 17 m. Per. of records: 1951-1965

MO.	RAIN-FALL (mm)	RAIN DAYS	TEMPERATURE (°C)					DRY BULB	WET BULB	DEW PT.	RH (%)	MN. SEA LEVEL PRESS (mbs)	PREVAILING WIND			DAYS WITH	
			MAX	MIN	MEAN	DIREC-TION	SPD (mps)						CLD (octa)	TRW	LGTN		
JAN	71.3	10	32.6	21.2	26.9	26.3	23.6	23	80	1010.3	SE	2	6	6	3		
FEB	90.9	11	33.0	21.4	27.2	26.5	23.7	23	79	1010.2	SE	2	6	8	4		
MAR	95.3	10	33.8	21.8	27.8	27.2	24.0	23	77	1010.4	SE	2	6	9	7		
APR	131.8	14	34.0	22.4	28.2	27.7	24.7	24	78	1009.8	SE	2	6	14	13		
MAY	257.2	20	33.2	22.6	27.9	27.4	25.0	24	82	1009.6	VRBL	2	6	19	16		
JUN	251.4	19	32.5	22.3	27.4	26.8	24.6	24	83	1010.2	NW	2	6	13	10		
JUL	248.9	21	31.9	22.1	27.0	26.5	24.4	24	84	1010.3	VRBL	2	6	10	8		
AUG	323.7	20	31.9	21.9	26.9	26.3	24.3	24	85	1010.0	VRBL	2	6	10	6		
SEP	238.3	19	32.0	22.0	27.0	26.5	24.4	24	84	1010.3	VRBL	2	6	10	6		
OCT	253.6	21	32.5	22.1	27.3	26.7	24.6	24	84	1010.2	VRBL	2	6	15	9		
NOV	176.7	19	32.5	21.9	27.2	26.8	26.5	24	83	1009.7	SE	2	6	13	8		
DEC	98.7	14	32.6	21.6	27.1	26.5	24.1	23	82	1009.9	SE	2	6	6	3		
ANN	2237.8	198	32.7	21.9	27.3	26.8	24.5	24	82	1010.1	SE	2	6	133	93		

Station: CUYO Posit.: 10°51'N 121°02'E Elev. 4 m. Per. of records: 1951-1985

MO.	RAIN-FALL (mm)	RAIN DAYS	TEMPERATURE (°C)					DRY BULB	WET BULB	DEW PT.	RH (%)	MN. SEA LEVEL PRESS (mbs)	PREVAILING WIND			DAYS WITH	
			MAX	MIN	MEAN	DIREC-TION	SPD (mps)						CLD (octa)	TRW	LGTN		
JAN	13.2	2	29.0	24.8	26.9	26.6	24.0	23	80	1011.6	NE	9	5	0	1		
FEB	2.5	1	29.4	24.8	27.1	26.7	24.0	23	80	1011.7	NE	8	5	0	0		
MAR	8.2	1	30.5	25.1	27.8	27.4	24.6	24	79	1011.2	NE	6	4	0	1		
APR	44.1	3	31.8	25.9	28.8	28.6	25.6	25	79	1010.5	NE	5	4	1	5		
MAY	187.3	13	32.4	25.5	28.9	28.8	26.0	25	80	1009.5	NE	2	6	7	16		
JUN	376.2	20	31.6	24.8	28.2	28.0	25.7	25	83	1009.5	SW	2	7	8	15		
JUL	437.7	22	30.9	24.5	27.7	27.4	25.5	25	86	1009.3	SW	3	7	6	12		
AUG	409.7	21	31.0	24.5	27.7	27.6	25.5	25	84	1009.2	SW	4	8	6	10		
SEP	375.0	20	30.9	24.5	27.7	27.4	25.5	25	86	1009.6	SW	3	7	6	11		
OCT	272.1	17	30.8	24.9	27.8	27.8	25.5	25	83	1009.8	NE	5	6	6	12		
NOV	148.2	9	30.5	25.4	27.9	27.8	25.3	25	82	1009.5	NE	7	6	2	7		
DEC	55.1	4	29.5	25.4	27.4	27.2	24.8	24	82	1010.3	NE	9	6	0	2		
ANN	2329.3	133	30.7	25.0	27.3	27.6	25.2	25	82	1010.1	NE	5	6	42	92		

Station: DAET Posit.: 14°07'N 122°57'E Elev. 4 m. Per. of records: 1951-1985

MO.	RAIN-FALL (mm)	RAIN DAYS	TEMPERATURE (°C)						DEW PT.	RH (%)	MN. SEA LEVEL PRESS (mbs)	PREVAILING WIND			DAYS WITH	
			MAX	MIN	MEAN	DRY BULB	WET BULB	DIREC-TION				SPD (mps)	CLD (octa)	TRW	LGTN	
JAN	313.0	25	28.8	22.3	25.5	25.0	22.9	23	84	1014.1	NE	3	5	0	0	
FEB	175.0	16	28.9	22.3	25.6	25.3	22.9	22	82	1014.0	NE	3	4	0	0	
MAR	183.9	13	30.0	22.6	26.3	26.1	23.5	23	80	1013.6	NE	3	4	1	0	
APR	126.1	12	31.4	23.5	27.4	27.3	24.6	24	81	1011.9	NE	3	4	4	3	
MAY	139.1	12	32.8	24.0	28.4	28.0	25.3	24	80	1010.0	ENE	2	5	12	14	
JUN	173.9	16	32.8	24.0	28.4	28.0	25.3	24	80	1009.2	S	2	5	14	17	
JUL	235.7	17	32.2	23.9	28.0	27.4	25.1	24	83	1008.6	S	2	6	14	16	
AUG	222.3	17	32.1	24.0	28.0	27.4	25.0	24	82	1007.9	S/SSW	2	6	11	12	
SEP	267.6	19	31.8	23.6	27.7	27.0	24.9	24	84	1008.9	NE	2	6	12	13	
OCT	518.6	23	30.9	23.5	27.2	26.7	24.8	24	86	1010.1	NE	2	5	10	12	
NOV	590.2	24	29.9	23.6	26.7	26.4	24.4	24	85	1011.1	NE	4	6	5	4	
DEC	591.9	26	28.7	23.1	26.9	26.6	23.7	23	85	1012.8	NE	4	6	1	1	
ANN	3506.3	218	30.9	23.4	27.1	26.7	24.4	24	83	1011.0	NE	3	5	84	92	

Station: DAGUPAN Posit.: 16°03'N 120°20'E Elev. 2 m. Per. of records: 1951-1985

MO.	RAIN-FALL (mm)	RAIN DAYS	TEMPERATURE (°C)						DEW PT.	RH (%)	MN. SEA LEVEL PRESS (mbs)	PREVAILING WIND			DAYS WITH	
			MAX	MIN	MEAN	DRY BULB	WET BULB	DIREC-TION				SPD (mps)	CLD (octa)	TRW	LGTN	
JAN	6.2	2	30.9	20.9	25.9	25.4	22.0	20	74	1013.2	NNW	3	3	0	0	
FEB	6.2	2	31.8	21.4	26.6	26.1	22.3	20	72	1013.2	SSE	3	3	0	0	
MAR	17.6	3	33.5	22.7	28.1	27.5	23.3	21	70	1012.6	NNW	4	3	2	2	
APR	73.2	5	34.9	24.2	29.5	28.9	24.6	23	70	1011.1	NNW	4	3	6	9	
MAY	216.1	13	34.3	24.6	29.4	28.9	25.3	24	73	1009.4	SE	3	5	17	19	
JUN	346.6	17	32.9	24.4	28.6	28.1	25.3	24	81	1008.6	SE	3	6	16	15	
JUL	462.1	22	32.0	24.2	28.1	27.6	25.3	24	82	1008.0	SE	3	6	17	15	
AUG	608.4	24	31.1	24.0	27.5	27.1	25.1	24	85	1007.7	SE	3	6	15	10	
SEP	324.8	20	31.7	24.1	27.9	27.4	25.2	24	84	1008.6	SE	3	6	13	13	
OCT	188.8	12	32.2	23.8	28.0	27.6	24.8	24	80	1009.8	SE	3	5	8	11	
NOV	63.1	5	31.7	22.8	27.2	27.0	23.9	22	77	1011.0	SE/NNW	3	4	2	3	
DEC	13.8	2	31.2	21.7	26.4	26.0	22.8	21	75	1012.6	SE/SSE	3	4	0	0	
ANN	2296.6	127	32.4	23.2	27.8	27.3	24.2	23	77	1010.5	SE	3	5	96	97	

Station: DAVAO CITY Posit.: 07°05'N 125°37'E Elev. 25 m. Per. of records: 1951-1985

MO.	RAIN-FALL (mm)	RAIN DAYS	TEMPERATURE (°C)						DEW PT.	RH (%)	MN. SEA LEVEL PRESS (mbs)	PREVAILING WIND			DAYS WITH	
			MAX	MIN	MEAN	DRY BULB	WET BULB	DIREC-TION				SPD (mps)	CLD (octa)	TRW	LGTN	
JAN	114.7	17	30.9	21.9	26.4	26.0	23.5	23	81	1010.6	N	3	6	2	3	
FEB	99.0	14	31.3	22.0	26.6	26.2	23.6	23	80	1010.8	N	3	6	2	2	
MAR	77.9	12	32.3	22.3	27.3	26.9	23.9	23	78	1010.8	N	3	5	3	3	
APR	144.9	11	33.0	23.0	28.0	27.6	24.6	24	78	1009.0	N	2	5	9	6	
MAY	206.7	15	33.0	23.0	28.0	27.6	25.0	24	81	1009.4	N	2	6	16	9	
JUN	190.1	19	31.6	22.9	27.2	27.1	24.6	24	81	1009.7	N	2	6	13	9	
JUL	175.9	18	31.4	22.7	27.0	26.9	24.5	24	82	1009.6	N	2	6	12	9	
AUG	173.2	17	31.6	22.7	27.1	27.0	24.5	24	81	1009.6	S	2	6	12	10	
SEP	180.1	17	31.8	22.8	27.3	27.1	24.5	24	81	1009.7	N	2	6	13	9	
OCT	174.8	19	32.1	22.8	27.4	27.2	24.5	24	80	1009.7	N	2	6	14	8	
NOV	145.7	20	32.1	22.7	27.4	27.0	24.5	24	81	1009.6	N	2	6	10	8	
DEC	109.7	20	31.4	22.4	26.9	26.5	24.1	23	82	1010.7	N	2	6	5	6	
ANN	1792.7	199	31.9	22.6	27.2	26.9	24.3	24	81	1009.9	N	2	6	111	82	

Station: DIPOLOG Posit.: 08°35'N 123°20'E Elev. 5 m. Per. of records: 1951-1985

MO.	RAIN-FALL (mm)	RAIN DAYS	TEMPERATURE (°C)						DEW PT.	RH (%)	MN. SEA LEVEL PRESS (mbs)	PREVAILING WIND			DAYS WITH	
			MAX	MIN	MEAN	DRY BULB	WET BULB	DIREC-TION				SPD (mps)	CLD (octa)	TRW	LGTN	
JAN	158.8	14	30.5	23.1	26.8	26.3	24.2	24	84	1011.1	NE	2	6	1	1	
FEB	72.2	10	31.0	23.1	27.0	26.5	24.3	24	83	1011.1	NE	2	6	1	1	
MAR	75.7	8	32.0	23.5	27.7	27.3	24.5	24	79	1011.1	NE	2	5	2	2	
APR	97.9	8	33.3	23.7	28.5	28.0	25.1	24	79	1010.1	NE	2	5	5	6	
MAY	185.0	12	33.2	23.5	28.3	27.8	25.4	25	82	1009.4	NE	2	5	13	12	
JUN	254.1	17	32.7	23.3	28.0	27.3	25.2	25	84	1009.5	SE	2	6	13	10	
JUL	239.8	15	32.5	23.0	27.7	27.0	24.9	24	84	1009.5	SE	2	6	8	8	
AUG	225.8	14	32.7	23.0	27.8	27.2	25.0	24	84	1009.4	SE	2	6	9	8	
SEP	234.1	14	32.5	23.0	27.7	27.1	25.0	24	84	1009.7	SW	2	6	9	10	
OCT	297.2	17	32.6	22.9	27.7	27.1	25.0	24	84	1009.8	SE	2	6	10	11	
NOV	356.1	17	32.1	23.1	27.6	27.0	25.0	24	85	1009.8	NE	2	6	8	9	
DEC	280.8	15	31.3	23.2	27.2	26.7	24.8	24	86	1009.7	NE	2	6	4	4	
ANN	2477.5	161	32.2	23.2	27.7	27.1	24.9	24	83	1010.0	NE	2	6	83	82	

Station: DUMAGUETE Posit.: 09°19'N 123°19'E Elev. 6 m. Per. of records: 1951-1985

MO.	RAIN-FALL (mm)	RAIN DAYS	TEMPERATURE (°C)					DRY BULB	WET BULB	DEW PT.	RH (%)	MN. SEA LEVEL PRESS (mbs)	PREVAILING WIND			DAYS WITH	
			MAX	MIN	MEAN	DIREC-TION	SPD (mps)						CLD (octa)	TRW	LGTN		
JAN	80.8	13	29.8	23.8	26.6	26.4	23.9	23	81	1011.4	NE	2	5	0	2		
FEB	54.3	10	29.7	23.8	26.7	26.6	23.9	23	80	1011.5	NE	2	5	0	1		
MAR	54.3	8	30.7	24.3	27.5	27.4	24.3	23	77	1011.5	NE	2	4	1	2		
APR	49.5	6	31.9	25.1	28.5	28.4	25.1	24	76	1010.4	NE	2	4	3	7		
MAY	75.6	8	32.4	25.1	28.7	28.7	25.4	24	77	1009.4	NE	1	5	8	19		
JUN	134.3	15	32.2	24.3	28.2	28.2	25.1	24	78	1009.4	NE	2	6	10	18		
JUL	139.6	14	32.0	23.8	27.9	27.7	24.9	24	80	1009.2	SW	1	5	8	15		
AUG	123.5	14	32.2	23.8	28.0	27.8	24.8	24	79	1009.1	SW	2	6	7	14		
SEP	137.4	15	32.1	23.8	27.9	27.7	24.8	24	79	1009.4	SW	1	6	8	17		
OCT	183.1	17	31.6	23.9	27.7	27.6	24.9	24	80	1009.5	NE	2	5	10	18		
NOV	162.8	15	31.2	24.1	27.6	27.5	24.8	24	80	1009.7	NE	2	5	7	15		
DEC	113.7	16	30.3	24.1	27.2	27.1	24.5	24	81	1010.5	NE	2	5	2	8		
ANN	1308.9	151	31.3	24.2	27.7	27.6	24.7	24	79	1010.1	NE	2	5	64	136		

Station: GENERAL SANTOS Posit.: 06°07'N 125°11'E Elev. 14 m. Per. of records: 1951-1985

MO.	RAIN-FALL (mm)	RAIN DAYS	TEMPERATURE (°C)					DRY BULB	WET BULB	DEW PT.	RH (%)	MN. SEA LEVEL PRESS (mbs)	PREVAILING WIND			DAYS WITH	
			MAX	MIN	MEAN	DIREC-TION	SPD (mps)						CLD (octa)	TRW	LGTN		
JAN	64.1	9	32.6	21.5	27.0	26.7	23.5	22	76	1010.4	N	3	5	1	4		
FEB	73.2	8	32.9	21.6	27.2	26.9	23.6	22	76	1010.3	N	3	6	2	5		
MAR	39.5	7	33.6	21.8	27.7	27.5	24.0	23	75	1010.5	N	3	5	2	5		
APR	50.5	8	33.7	22.4	28.0	27.8	24.6	23	77	1009.8	N	3	5	4	9		
MAY	87.5	12	32.7	22.7	27.7	27.4	24.7	24	80	1009.7	N	3	6	6	13		
JUN	112.5	14	31.4	22.3	26.8	26.8	24.4	24	82	1010.2	S	3	6	4	11		
JUL	104.3	13	31.0	22.0	26.5	26.4	24.2	23	83	1010.0	S	2	6	4	8		
AUG	87.2	13	31.0	21.9	26.4	26.5	24.2	23	83	1010.3	S	3	6	4	9		
SEP	80.6	12	31.4	21.9	26.6	26.6	24.2	23	82	1010.2	S	3	6	4	9		
OCT	94.4	12	31.8	22.0	26.9	26.8	24.3	23	81	1010.1	S	3	6	4	10		
NOV	87.0	12	32.4	21.9	27.1	26.9	24.3	23	81	1009.7	N	3	6	4	10		
DEC	74.1	11	32.5	21.7	27.1	26.8	24.0	23	79	1009.7	N	3	6	3	7		
ANN	954.9	131	32.3	22.0	27.1	26.9	24.2	23	80	1010.1	N	3	6	42	106		

Station: GUIUAN E. SAMAR Posit.: 11°02'N 125°44'E Elev. 2 m. Per. of records: 1973-1985

MO.	RAIN-FALL (mm)	RAIN DAYS	TEMPERATURE (°C)					DRY BULB	WET BULB	DEW PT.	RH (%)	MN. SEA LEVEL PRESS (mbs)	PREVAILING WIND			DAYS WITH	
			MAX	MIN	MEAN	DIREC-TION	SPD (mps)						CLD (octa)	TRW	LGTN		
JAN	255.7	21	28.8	23.2	26.0	25.9	23.9	23	85	1011.0	NE	3	6	0	1		
FEB	284.7	17	28.9	23.2	26.0	26.0	23.9	23	84	1011.5	NE	3	6	0	0		
MAR	152.9	16	29.6	23.9	26.7	26.5	24.2	23	83	1011.8	NE	3	6	0	1		
APR	161.6	17	30.6	24.5	27.5	27.5	24.9	24	81	1010.4	NE	3	6	2	4		
MAY	121.3	12	31.6	25.0	28.3	28.0	25.8	25	84	1009.3	NE	2	6	3	9		
JUN	278.4	21	31.3	24.4	27.8	27.7	25.4	25	83	1009.1	E/N	2	6	8	13		
JUL	185.5	16	31.1	24.2	27.6	27.4	25.4	25	85	1008.7	SW	2	6	8	17		
AUG	153.1	13	31.7	24.7	28.2	27.9	25.3	24	81	1008.4	SW	2	6	6	16		
SEP	212.3	18	31.4	24.3	27.8	27.6	25.1	24	82	1009.2	SW	2	6	7	17		
OCT	180.3	18	31.1	24.5	27.8	27.6	25.4	25	84	1009.4	NE	2	6	5	13		
NOV	321.5	23	30.1	24.2	27.1	27.1	25.1	24	85	1009.1	NE	2	6	4	11		
DEC	368.5	24	29.0	23.7	26.3	26.3	24.3	24	85	1010.4	NE	3	6	3	6		
ANN	2635.8	216	30.4	24.2	27.3	27.1	24.9	24	84	1009.9	NE	2	6	46	113		

Station: HINATUAN Posit.: 08°22'N 126°20'E Elev. 3 m. Per. of records: 1951-1985

MO.	RAIN-FALL (mm)	RAIN DAYS	TEMPERATURE (°C)					DRY BULB	WET BULB	DEW PT.	RH (%)	MN. SEA LEVEL PRESS (mbs)	PREVAILING WIND			DAYS WITH	
			MAX	MIN	MEAN	DIREC-TION	SPD (mps)						CLD (octa)	TRW	LGTN		
JAN	730.3	24	29.2	21.9	25.5	25.2	23.8	23	89	1010.6	W	2	6	2	3		
FEB	523.1	23	29.2	21.8	25.5	25.2	23.9	23	90	1010.8	W	2	6	1	2		
MAR	434.8	23	29.9	21.9	25.9	25.8	24.3	24	88	1010.9	W	2	6	1	4		
APR	320.5	21	30.8	22.5	26.6	26.6	24.8	24	86	1010.0	W	2	6	4	8		
MAY	275.3	18	31.6	23.0	27.3	27.2	25.3	25	86	1009.1	W	2	6	9	15		
JUN	257.6	18	31.7	22.8	27.2	27.0	25.0	24	85	1009.0	W	2	6	11	17		
JUL	214.4	17	32.0	22.4	27.2	26.9	24.9	24	85	1008.7	W	2	6	11	18		
AUG	190.1	15	32.3	22.5	27.4	27.1	25.0	24	84	1008.5	W	2	6	11	18		
SEP	213.3	15	32.1	22.5	27.3	27.0	25.0	24	85	1008.8	W	2	6	12	19		
OCT	232.5	18	31.8	22.5	27.1	26.9	25.0	24	86	1008.8	W	2	6	11	19		
NOV	350.1	20	31.1	22.4	26.7	26.5	24.8	24	87	1008.9	W	2	6	7	13		
DEC	586.4	25	30.0	22.3	26.1	25.7	24.3	24	89	1009.5	W	2	6	4	7		
ANN	4328.4	237	31.0	22.4	26.7	26.4	24.7	24	87	1009.5	W	2	6	84	143		

Station: IBA ZAMBALES Posit.: 15°20'N 119°58'E Elev. 5 m. Per. of records: 1951-1985

MO.	RAIN-FALL (mm)	RAIN DAYS	TEMPERATURE (°C)					DRY BULB	WET BULB	DEW PT.	RH (%)	MN. SEA LEVEL PRESS (mbs)	PREVAILING WIND			DAYS TRSW	WITH LGTN
			MAX	MIN	MEAN	DIREC-TION	SPD (mps)						CLD (octa)				
JAN	8.0	1	31.0	20.3	25.6	25.3	22.0	21	75	1013.1	E	2	2	0	0		
FEB	3.7	2	31.3	20.4	25.8	25.6	22.3	21	74	1012.9	NW	3	2	0	0		
MAR	12.1	2	32.3	21.7	27.0	27.0	23.3	22	73	1012.4	NW/W	3	2	1	1		
APR	26.6	4	33.3	23.3	28.3	28.4	24.6	23	73	1011.0	E	3	2	5	8		
MAY	280.7	12	32.9	23.8	28.3	28.5	25.3	24	77	1009.3	E/W	2	4	13	15		
JUN	579.0	18	31.5	23.6	27.5	27.5	25.2	24	83	1008.6	E	3	5	13	13		
JUL	763.1	24	30.7	23.3	27.0	26.7	24.9	24	86	1008.3	SW	2	6	13	14		
AUG	1186.9	25	29.9	23.3	26.5	26.1	24.8	24	90	1007.8	SW	3	6	10	9		
SEP	615.8	21	30.7	23.3	26.9	26.6	24.8	24	86	1008.7	E	2	6	10	12		
OCT	308.9	14	31.6	23.1	27.3	27.0	24.6	24	82	1009.5	E	2	5	7	10		
NOV	80.9	7	31.7	22.5	27.1	26.7	23.8	23	78	1010.6	E	2	4	2	5		
DEC	25.6	4	31.3	21.4	26.3	26.1	22.8	22	75	1012.0	E	2	3	0	1		
ANN	3701.5	134	31.5	22.5	27.0	26.8	24.0	23	79	1010.4	E	2	4	74	88		

Station: ILOILO Posit.: 10°42'N 122°35'E Elev. 8 m. Per. of records: 1951-1985

MO.	RAIN-FALL (mm)	RAIN DAYS	TEMPERATURE (°C)					DRY BULB	WET BULB	DEW PT.	RH (%)	MN. SEA LEVEL PRESS (mbs)	PREVAILING WIND			DAYS TRSW	WITH LGTN
			MAX	MIN	MEAN	DIREC-TION	SPD (mps)						CLD (octa)				
JAN	42.8	8	29.1	22.6	25.9	25.5	23.2	22	82	1011.9	NE	6	5	1	1		
FEB	25.3	6	29.7	22.7	26.2	25.8	23.3	22	81	1011.8	NE	6	5	0	1		
MAR	34.3	8	30.9	23.3	27.1	26.9	23.7	23	76	1011.7	NE	5	4	1	1		
APR	52.4	5	32.2	24.5	28.4	28.2	24.6	23	74	1010.5	NE	5	4	4	6		
MAY	115.1	10	32.5	24.8	28.7	28.5	25.3	24	77	1009.5	NE	4	5	10	17		
JUN	271.6	18	31.2	24.5	27.8	27.8	25.2	24	81	1009.5	SW	3	6	13	16		
JUL	300.8	20	30.4	24.3	27.3	27.2	25.1	24	84	1009.4	SW	4	6	10	13		
AUG	348.0	20	30.1	24.4	27.2	27.2	25.1	24	84	1009.1	SW	4	6	7	9		
SEP	276.4	19	30.3	24.2	27.3	27.1	25.0	24	84	1009.5	SW	3	6	9	13		
OCT	281.1	18	30.6	24.0	27.3	27.0	24.9	24	84	1009.7	SW	3	5	11	15		
NOV	179.7	14	30.3	23.9	27.1	26.7	24.7	24	85	1010.1	NE	4	5	6	10		
DEC	96.9	12	29.6	23.5	26.5	26.1	24.1	23	85	1010.9	NE	5	5	2	4		
ANN	1994.4	155	30.6	23.9	27.2	27.0	24.5	23	81	1010.3	NE	4	5	73	106		

Station: INFANTA Posit.: 14°45'N 121°39'E Elev. 5 m. Per. of records: 1951-1985

MO.	RAIN-FALL (mm)	RAIN DAYS	TEMPERATURE (°C)					DRY BULB	WET BULB	DEW PT.	RH (%)	MN. SEA LEVEL PRESS (mbs)	PREVAILING WIND			DAYS TRSW	WITH LGTN
			MAX	MIN	MEAN	DIREC-TION	SPD (mps)						CLD (octa)				
JAN	353.8	23	27.0	21.9	24.5	24.2	22.5	22	86	1014.7	N	3	6	0	0		
FEB	220.1	17	27.9	21.9	24.9	24.6	22.7	22	85	1014.3	N	3	6	0	0		
MAR	187.3	15	29.3	22.5	25.9	25.6	23.4	23	83	1013.9	N	3	5	0	1		
APR	179.7	16	30.8	23.6	27.2	26.9	24.5	24	82	1012.2	N	2	5	2	6		
MAY	228.2	15	32.1	24.2	28.2	27.9	25.3	24	81	1009.9	N	2	5	13	20		
JUN	249.4	17	32.4	24.4	28.5	28.2	25.3	24	79	1008.8	SW	2	6	12	20		
JUL	258.7	17	32.0	24.2	28.2	27.7	25.0	24	80	1008.2	SW	2	6	11	19		
AUG	196.4	17	31.9	24.5	28.2	27.7	24.8	24	79	1007.5	SW	2	6	8	12		
SEP	325.2	20	31.4	23.9	27.7	27.2	24.8	24	82	1008.6	SW	2	6	11	16		
OCT	607.8	24	30.1	23.6	26.9	26.5	24.6	24	86	1010.2	N	2	6	8	13		
NOV	597.4	24	29.0	23.5	26.3	26.1	24.2	24	85	1011.2	N	4	7	2	1		
DEC	597.2	25	27.6	22.8	25.2	25.1	23.3	23	86	1013.4	N	4	7	1	1		
ANN	3998.2	230	30.1	23.4	26.8	26.5	24.2	24	83	1011.1	N	3	6	68	109		

Station: ITBAYAT Posit.: 20°45'N 121°48'E Elev. 124 m. Per. of records: 1951-1985

MO.	RAIN-FALL (mm)	RAIN DAYS	TEMPERATURE (°C)					DRY BULB	WET BULB	DEW PT.	RH (%)	MN. SEA LEVEL PRESS (mbs)	PREVAILING WIND			DAYS TRSW	WITH LGT
			MAX	MIN	MEAN	DIREC-TION	SPD (mps)						CLD (octa)				
JAN	240.6	14	23.9	19.0	21.5	21.4	19.9	19	87	1018.5	NE	3	6	0	0		
FEB	135.1	12	24.4	19.6	22.0	22.1	20.6	20	87	1018.5	NE	4	5	0	0		
MAR	111.1	8	26.2	20.8	23.5	23.4	22.0	21	88	1016.7	E	3	5	0	0		
APR	82.9	6	28.0	22.6	25.3	25.3	23.7	23	87	1015.0	E	3	5	1	1		
MAY	297.3	10	30.0	24.1	27.1	26.8	25.3	25	88	1011.9	E	2	5	2	3		
JUN	785.7	11	30.1	24.8	27.5	27.6	26.1	26	89	1010.0	W	3	5	1	4		
JUL	669.5	13	30.5	25.0	27.8	27.7	26.3	26	90	1008.1	W	3	5	3	3		
AUG	935.0	20	29.3	24.6	27.0	27.2	25.8	25	89	1008.4	W	3	6	2	3		
SEP	482.1	15	29.8	24.6	27.2	27.0	25.6	25	89	1010.5	E	3	6	2	4		
OCT	722.2	14	28.5	23.7	26.1	26.3	24.6	24	87	1012.0	E	3	6	1	2		
NOV	464.4	16	26.5	22.5	24.5	24.4	22.8	22	87	1015.8	NE	4	6	0	0		
DEC	311.1	16	24.0	19.8	21.9	22.1	20.5	20	86	1018.9	NE	4	6	0	0		
ANN	5237.0	155	27.6	22.6	25.1	25.1	23.6	23	88	1013.5	E	3	6	12	20		

Station: JOLO Posit.: 06°03'N 121°00'E Elev. 11 m. Per. of records: 1951-1980

MO.	RAIN-FALL (mm)	RAIN DAYS	TEMPERATURE (°C)					DEW PT.	RH (%)	MN. SEA LEVEL PRESS (mbs)	PREVAILING WIND			DAYS WITH	
			MAX	MIN	MEAN	DRY BULB	WET BULB				DIREC-TION	SPD (mps)	CLD (octa)	TRW	LGTN
JAN	104.1	10	29.7	22.6	26.2	26.2	24.4	24	86	1010.8	N	2	6	2	2
FEB	94.5	8	29.7	22.7	26.2	26.2	24.4	24	86	1011.1	N	2	6	2	2
MAR	85.8	8	30.4	22.5	26.5	26.4	24.6	24	86	1010.8	N	2	6	3	3
APR	145.1	10	31.3	22.3	26.8	26.8	25.0	24	86	1010.5	N	1	6	7	8
MAY	226.4	15	31.9	22.8	27.4	27.1	25.2	24	86	1009.9	SE	1	6	10	11
JUN	242.4	16	31.6	22.8	27.2	26.8	24.9	24	86	1010.2	SE	1	6	5	7
JUL	187.1	15	31.7	23.2	27.5	26.7	24.9	24	86	1010.1	S	2	6	4	5
AUG	161.6	14	31.6	23.0	27.3	26.8	24.8	24	85	1010.2	S	2	6	4	5
SEP	194.1	14	31.4	22.8	27.1	26.8	24.8	24	85	1009.9	S/W	2	6	6	8
OCT	264.1	17	30.9	22.7	26.8	26.5	24.7	24	86	1010.0	W	2	6	8	9
NOV	194.7	17	30.4	22.7	26.6	26.4	24.7	24	87	1010.2	VRBL	2	6	6	8
DEC	150.1	8	30.1	22.7	26.4	26.3	24.7	24	86	1010.3	VRBL	2	6	3	5
ANN	2650.0	152	30.9	22.7	26.8	26.6	24.8	24	86	1010.3	N	2	6	60	73

Station: LAOAG Posit.: 18°11'N 120°32'E Elev. 5 m. Per. of records: 1951-1985

MO.	RAIN-FALL (mm)	RAIN DAYS	TEMPERATURE (°C)					DEW PT.	RH (%)	MN. SEA LEVEL PRESS (mbs)	PREVAILING WIND			DAYS WITH	
			MAX	MIN	MEAN	DRY BULB	WET BULB				DIREC-TION	SPD (mps)	CLD (octa)	TRW	LGTN
JAN	11.8	1	30.0	18.8	24.4	24.0	20.5	19	75	1014.1	N	3	3	0	0
FEB	1.1	1	30.8	19.2	25.0	24.8	21.1	20	72	1013.6	N	3	2	0	0
MAR	2.5	1	32.0	20.9	26.5	26.6	22.7	21	72	1012.6	NW	3	3	1	1
APR	19.8	2	33.4	23.1	28.2	28.5	24.7	23	73	1011.3	NW	3	3	8	4
MAY	125.1	8	33.8	24.4	29.1	29.1	25.4	24	74	1009.5	W/WWSW	3	4	15	12
JUN	376.8	15	32.5	24.3	28.4	28.1	25.6	25	82	1008.2	SW	3	6	17	14
JUL	386.4	17	31.8	24.0	27.8	27.7	25.3	25	82	1006.9	E/SW	3	6	17	13
AUG	547.3	20	31.0	23.9	27.4	27.0	25.1	25	86	1006.3	SW	3	6	14	10
SEP	324.1	15	31.3	23.6	27.5	27.1	25.1	24	85	1006.3	E	3	6	12	10
OCT	86.1	8	31.9	22.9	27.4	27.1	24.2	23	79	1010.0	N	3	4	5	6
NOV	48.1	5	31.2	21.9	26.5	26.3	22.9	22	75	1011.4	N	4	4	1	2
DEC	10.2	2	30.5	20.2	25.4	25.1	21.4	20	72	1013.0	N	4	4	0	0
ANN	1836.3	96	31.7	22.3	27.0	26.8	23.7	23	77	1010.4	N	3	4	80	72

Station: LEGASPI Posit.: 13°09'N 123°43'E Elev. 17 m. Per. of records: 1951-1985

MO.	RAIN-FALL (mm)	RAIN DAYS	TEMPERATURE (°C)					DEW PT.	RH (%)	MN. SEA LEVEL PRESS (mbs)	PREVAILING WIND			DAYS WITH	
			MAX	MIN	MEAN	DRY BULB	WET BULB				DIREC-TION	SPD (mps)	CLD (octa)	TRW	LGTN
JAN	296.9	20	28.6	22.1	26.3	25.1	23.0	22	84	1012.9	NE	4	6	1	0
FEB	195.6	17	29.1	22.2	26.6	25.4	23.1	22	82	1013.1	NE	4	6	0	0
MAR	192.6	17	29.9	22.8	26.3	26.1	23.7	23	82	1012.8	NE	4	5	0	0
APR	152.1	16	31.1	23.5	27.3	27.2	24.7	24	81	1011.6	NE	4	5	2	1
MAY	181.3	14	32.1	24.1	28.1	28.0	25.4	25	81	1009.8	NE	3	5	7	9
JUN	240.9	16	32.2	24.0	28.1	27.8	25.4	25	82	1009.1	NE	3	5	11	12
JUL	251.3	19	31.8	23.7	27.7	27.3	25.1	24	84	1008.6	SW	3	6	10	10
AUG	264.2	20	31.6	23.7	27.6	27.2	25.1	24	84	1008.2	SW	3	6	10	8
SEP	259.9	20	31.5	23.5	27.5	27.0	25.0	24	85	1008.9	W	3	6	11	11
OCT	325.5	21	31.1	23.3	27.2	26.8	24.7	24	84	1009.4	NE	3	6	9	10
NOV	483.7	22	30.1	23.1	26.6	26.4	24.4	24	85	1010.2	NE	4	6	6	5
DEC	456.0	23	29.0	22.9	25.9	25.7	23.8	23	85	1011.7	NE	4	6	2	2
ANN	3500.0	225	30.7	23.2	26.9	26.7	24.5	24	83	1010.5	NE	4	6	69	68

Station: LUCENA QUEZON Posit.: 13°56'N 121°37'E Elev. 11 m. Per. of records: 1951-1970

MO.	RAIN-FALL (mm)	RAIN DAYS	TEMPERATURE (°C)					DEW PT.	RH (%)	MN. SEA LEVEL PRESS (mbs)	PREVAILING WIND			DAYS WITH	
			MAX	MIN	MEAN	DRY BULB	WET BULB				DIREC-TION	SPD (mps)	CLD (octa)	TRW	LGTN
JAN	89.3	16	29.0	21.8	26.4	24.8	23.0	22	86	1014.3	NE	3	6	0	0
FEB	60.3	10	29.8	21.8	25.8	25.1	22.6	22	81	1014.2	NE	3	5	0	0
MAR	42.5	9	31.1	22.5	26.8	26.2	23.4	22	79	1013.7	NE	3	4	0	0
APR	54.6	7	32.7	23.6	28.1	27.7	24.5	23	77	1012.3	NE	3	4	4	2
MAY	90.0	8	33.4	26.4	29.9	28.5	25.3	24	77	1014.6	NE	3	5	6	10
JUN	160.3	14	32.8	26.1	29.4	28.1	25.3	24	82	1009.9	SW	3	6	13	13
JUL	184.6	16	32.1	23.7	27.9	27.3	24.9	24	82	1009.4	SW	3	6	10	10
AUG	198.9	17	31.9	23.7	27.8	27.2	24.8	24	82	1008.8	SW	3	6	7	6
SEP	225.5	17	31.7	23.5	27.6	26.9	24.5	24	82	1009.4	SW	3	6	7	7
OCT	336.2	20	31.2	23.3	27.2	26.6	24.2	23	82	1010.9	NE	3	6	6	8
NOV	305.3	18	30.3	23.1	26.7	26.2	24.1	23	84	1011.7	NE	3	6	2	3
DEC	235.2	21	29.3	22.5	25.9	25.3	23.3	22	84	1013.2	NE	3	6	0	1
ANN	1962.7	173	31.3	23.5	27.4	26.7	24.2	23	82	1011.9	NE	3	6	57	60

Station: LUMBIA AP CAGAYAN Posit.: 08°26'N 124°17'E Elev. 188 m. Per. of records: 1976-1985

MO.	RAIN-FALL (mm)	RAIN DAYS	TEMPERATURE (°C)					DRY BULB	WET BULB	DEW PT.	RH (%)	MN. SEA LEVEL PRESS (mbs)	PREVAILING WIND			DAYS WITH	
			MAX	MIN	MEAN	DIREC-TION	SPD (mps)						CLD (octa)	TRW	LGTN		
JAN	83.7	10	29.2	21.3	25.3	25.0	22.9	22	84	1010.9	S	3	6	4	1		
FEB	62.4	6	29.9	20.7	25.3	25.5	22.8	22	79	1011.3	S	3	5	1	1		
MAR	29.8	3	31.1	21.1	26.1	26.2	23.1	22	77	1010.7	S	3	5	2	1		
APR	24.6	5	32.1	22.0	27.0	27.4	24.1	23	76	1009.6	N,S	3	5	4	4		
MAY	98.5	8	32.4	23.3	27.8	27.6	24.0	23	74	1009.4	S	3	5	13	13		
JUN	209.0	16	31.3	22.8	27.0	26.4	24.1	23	68	1009.2	S	2	6	17	13		
JUL	230.5	16	30.6	22.2	26.4	26.1	23.7	23	62	1009.7	SE/S	2	6	15	9		
AUG	221.4	14	31.6	22.1	26.8	26.3	23.5	23	79	1009.5	S	2	7	15	10		
SEP	181.2	15	31.2	22.0	26.6	26.1	23.6	23	81	1009.8	S	2	6	16	13		
OCT	206.9	16	30.8	22.1	26.4	25.9	23.6	23	82	1009.6	S	2	6	15	12		
NOV	91.0	8	30.8	22.0	26.4	26.0	23.7	23	82	1010.0	S	2	6	11	14		
DEC	100.0	11	29.9	21.6	25.7	25.5	23.4	23	84	1010.6	S	3	6	4	5		
ANN	1849.0	126	30.9	21.9	26.4	26.2	23.5	23	80	1010.0	S	3	6	117	86		

Station: MAASIN S. LEYTE Posit.: 10°08'N 124°50'E Elev. 19 m. Per. of records: 1972-1985

MO.	RAIN-FALL (mm)	RAIN DAYS	TEMPERATURE (°C)					DRY BULB	WET BULB	DEW PT.	RH (%)	MN. SEA LEVEL PRESS (mbs)	PREVAILING WIND			DAYS WITH	
			MAX	MIN	MEAN	DIREC-TION	SPD (mps)						CLD (octa)	TRW	LGTN		
JAN	186.5	14	29.1	21.7	25.4	26.0	23.1	22	78	1010.3	NE	1	5	1	14		
FEB	145.4	11	29.4	22.2	25.8	26.1	23.2	22	78	1010.9	NE	2	5	0	10		
MAR	109.9	9	30.3	22.7	26.5	27.1	23.7	23	75	1010.6	E	2	4	1	11		
APR	60.3	7	30.5	23.8	27.1	27.8	24.1	23	74	1009.2	E	2	4	1	13		
MAY	64.9	6	31.3	23.6	27.4	28.2	24.5	23	74	1009.0	E/SE	2	4	4	20		
JUN	106.5	12	30.5	23.3	26.9	27.7	24.4	23	76	1008.3	SE	2	5	7	26		
JUL	170.3	13	30.1	23.4	26.7	27.5	24.2	23	76	1008.4	SW	2	6	6	27		
AUG	161.5	13	30.2	23.7	26.9	27.5	24.5	23	78	1008.3	SW	2	5	8	24		
SEP	163.8	15	30.2	22.9	26.5	27.3	23.8	23	75	1008.6	SW	2	6	12	25		
OCT	202.4	16	30.3	23.0	26.6	27.2	23.4	22	72	1008.4	SW	2	6	10	26		
NOV	168.2	15	30.2	23.4	26.8	27.1	23.8	23	76	1008.9	E	2	5	4	20		
DEC	230.7	18	29.3	22.0	25.6	26.4	23.5	22	78	1008.5	NE	2	6	2	16		
ANN	1772.4	149	30.1	23.0	26.5	27.2	23.9	23	76	1008.2	E/SW	2	5	68	230		

Station: MACTAN AIRPORT Posit.: 10°18'N 124°52'E Elev. 9 m. Per. of records: 1972-1985

MO.	RAIN-FALL (mm)	RAIN DAYS	TEMPERATURE (°C)					DRY BULB	WET BULB	DEW PT.	RH (%)	MN. SEA LEVEL PRESS (mbs)	PREVAILING WIND			DAYS WITH	
			MAX	MIN	MEAN	DIREC-TION	SPD (mps)						CLD (octa)	TRW	LGTN		
JAN	96.5	9	31.2	21.6	26.4	26.5	23.7	23	79	1011.3	NE	3	6	1	1		
FEB	78.6	9	31.6	22.2	26.9	26.8	23.8	23	78	1011.3	NE	3	5	0	0		
MAR	46.8	6	32.5	22.6	27.5	27.6	24.3	23	76	1012.0	NE	3	5	0	0		
APR	34.3	4	33.7	23.9	28.8	28.8	25.1	24	74	1010.1	NE	3	4	2	3		
MAY	66.4	6	34.5	23.8	29.1	29.2	25.7	25	76	1009.0	NE	2	5	6	6		
JUN	181.9	14	33.9	23.6	28.7	28.5	25.5	25	78	1008.8	SW	2	6	10	11		
JUL	187.3	15	33.7	23.2	28.4	27.9	25.1	24	80	1008.7	SW	2	6	13	12		
AUG	194.9	12	34.2	22.8	28.5	28.3	25.1	24	77	1008.4	SW	3	6	10	9		
SEP	189.1	15	33.6	23.0	28.3	28.0	25.2	24	80	1009.3	SW	2	6	16	12		
OCT	137.6	13	33.3	22.7	28.0	28.0	25.1	24	79	1009.4	NE	2	6	12	13		
NOV	150.9	13	32.8	23.2	28.0	27.8	25.2	24	81	1009.4	NE	2	6	5	10		
DEC	145.6	13	32.0	22.7	27.3	27.1	24.5	24	81	1010.2	NE/N	3	6	2	3		
ANN	1481.9	129	33.1	22.9	28.0	27.9	24.9	24	78	1009.9	NE	3	6	77	80		

Station: MALAYBALAY Posit.: 08°10'N 125°08'E Elev. 627 m. Per. of records: 1951-1985

MO.	RAIN-FALL (mm)	RAIN DAYS	TEMPERATURE (°C)					DRY BULB	WET BULB	DEW PT.	RH (%)	MN. SEA LEVEL PRESS (mbs)	PREVAILING WIND			DAYS WITH	
			MAX	MIN	MEAN	DIREC-TION	SPD (mps)						CLD (octa)	TRW	LGTN		
JAN	124.5	15	27.9	17.8	22.8	22.1	20.1	19	83	1007.1	N	1	6	1	2		
FEB	95.9	13	28.3	17.5	22.9	22.2	20.1	19	82	1007.0	N	2	6	2	2		
MAR	103.2	11	29.4	17.5	23.4	23.0	20.4	19	79	1007.1	NW	1	6	3	2		
APR	104.4	12	30.4	18.2	24.3	23.8	21.0	20	78	1006.1	NW/VAR	1	5	5	6		
MAY	222.5	19	30.2	19.1	24.6	23.9	21.5	20	81	1005.6	S/SE	1	6	13	10		
JUN	307.1	23	28.8	19.2	24.0	23.2	21.1	20	83	1006.2	SE	1	6	13	8		
JUL	315.9	24	28.0	19.0	23.5	22.7	20.9	20	85	1006.3	SE	1	7	13	7		
AUG	300.3	23	28.1	19.0	23.5	22.7	20.9	20	85	1006.2	S	1	7	13	7		
SEP	327.0	24	28.3	19.0	23.6	22.8	21.0	20	85	1006.4	SE	1	6	15	10		
OCT	299.4	22	28.5	18.8	23.6	22.8	20.9	20	84	1006.3	SE	1	6	14	9		
NOV	187.3	18	28.8	18.6	23.4	22.9	20.9	20	84	1006.1	VAR	2	6	7	7		
DEC	149.8	17	28.3	18.2	23.2	22.5	20.5	20	83	1006.5	NW	1	6	3	4		
ANN	2837.3	221	28.8	18.5	23.6	22.9	20.9	20	83	1006.4	SE	1	6	102	74		

Station: MANILA INT. AIRPORT Posit.: 14°31'N 121°00'E Elev. 15 m. Per. of records: 1951-1985

MO.	RAIN-FALL (mm)	RAIN DAYS	TEMPERATURE (°C)						DEW PT.	RH (%)	MN. SEA LEVEL PRESS (mbs)	PREVAILING WIND			DAYS WITH	
			MAX	MIN	MEAN	DRY BULB	WET BULB	DIREC-TION				SPD (mps)	CLD (octa)	TRW	LGTN	
JAN	12.3	3	30.2	20.7	25.5	24.9	21.7	20	78	1013.4	SE	5	5	0	0	
FEB	3.6	2	31.3	20.9	26.1	25.8	21.7	20	70	1013.2	SE	4	4	0	0	
MAR	13.4	2	32.8	22.0	27.4	27.2	22.6	21	67	1012.6	SE	4	4	0	0	
APR	15.9	2	34.2	23.7	28.9	28.8	23.7	22	65	1011.1	SE	4	3	1	4	
MAY	109.4	8	34.2	24.6	29.4	29.1	24.7	23	70	1009.5	SE	4	5	6	9	
JUN	258.6	14	32.5	24.3	28.4	28.0	24.9	24	78	1008.8	SE	3	6	9	12	
JUL	332.6	18	31.3	24.0	27.6	27.3	24.7	24	81	1008.2	SW	3	6	10	10	
AUG	417.0	21	30.7	23.9	27.3	26.9	24.5	24	82	1007.9	SW	3	7	7	6	
SEP	304.7	18	30.9	23.8	27.3	26.8	24.6	24	83	1008.8	SW	3	7	8	8	
OCT	180.5	14	31.1	23.3	27.2	26.7	24.2	23	81	1009.7	SE	2	6	6	5	
NOV	116.7	10	30.7	22.5	26.6	26.1	23.5	23	80	1010.9	E	2	6	2	1	
DEC	54.1	7	30.2	21.3	25.7	25.3	22.5	21	78	1012.3	SE	3	5	0	0	
ANN	1822.8	119	31.7	22.9	27.3	26.9	23.6	22	76	1010.5	SE	3	5	49	58	

Station: MASBATE Posit.: 12°22'N 123°37'E Elev. 11 m. Per. of records: 1951-1985

MO.	RAIN-FALL (mm)	RAIN DAYS	TEMPERATURE (°C)						DEW PT.	RH (%)	MN. SEA LEVEL PRESS (mbs)	PREVAILING WIND			DAYS WITH	
			MAX	MIN	MEAN	DRY BULB	WET BULB	DIREC-TION				SPD (mps)	CLD (octa)	TRW	LGTN	
JAN	163.2	16	29.8	23.1	26.3	26.8	23.7	23	84	1012.5	NE	3	5	0	0	
FEB	80.3	12	30.1	22.9	26.5	26.0	23.7	23	82	1012.6	NE	3	5	0	0	
MAR	68.5	11	31.4	23.5	27.4	26.9	24.3	23	81	1012.4	NE	3	4	0	0	
APR	54.9	6	32.7	24.5	28.6	28.2	25.3	24	79	1011.1	NE	2	4	1	2	
MAY	134.0	8	33.5	25.3	29.4	28.9	25.9	23	79	1009.6	SE/E	3	4	6	10	
JUN	158.4	14	33.1	25.2	29.1	28.6	25.9	23	81	1009.1	SW	3	5	10	13	
JUL	191.2	17	32.3	24.9	28.6	28.0	25.7	23	83	1008.6	SW	3	6	9	11	
AUG	180.3	17	32.2	24.8	28.5	27.9	25.6	23	83	1008.3	SW	3	6	7	9	
SEP	218.8	16	32.1	24.7	28.4	27.8	25.5	23	83	1008.7	SW	3	6	8	11	
OCT	212.8	17	31.8	24.6	28.2	27.8	25.4	23	82	1009.4	NE	3	6	7	10	
NOV	232.7	17	31.0	24.2	27.6	27.2	25.0	24	84	1010.1	NE	3	6	2	5	
DEC	257.1	18	29.9	23.7	26.8	26.4	24.4	24	85	1011.3	NE	3	6	1	2	
ANN	1949.2	169	31.6	24.3	28.0	27.5	25.0	24	82	1010.3	NE	3	5	51	73	

Station: MUNOZ NUEVA ECLJA Posit.: 15°43'N 120°54'E Elev. 74 m. Per. of records: 1981-1985

MO.	RAIN-FALL (mm)	RAIN DAYS	TEMPERATURE (°C)						DEW PT.	RH (%)	MN. SEA LEVEL PRESS (mbs)	PREVAILING WIND			DAYS WITH	
			MAX	MIN	MEAN	DRY BULB	WET BULB	DIREC-TION				SPD (mps)	CLD (octa)	TRW	LGTN	
JAN	9.4	1	30.2	21.4	25.8	25.0	21.4	20	73	1013.2	NE	4	4	0	0	
FEB	1.7	1	30.9	21.3	26.1	26.0	22.2	21	72	1010.5	ENE	4	3	0	0	
MAR	8.5	2	32.1	21.8	26.9	26.9	23.2	22	73	1012.0	ENE	3	3	1	2	
APR	55.4	5	33.6	23.1	28.3	28.2	24.2	23	72	1010.3	E	3	3	9	11	
MAY	88.9	10	33.0	23.8	29.4	28.9	24.8	23	72	1008.5	E	2	5	15	16	
JUN	385.3	18	32.6	23.6	28.1	27.7	25.0	24	80	1006.7	VRBL	2	6	12	13	
JUL	299.6	19	31.9	23.4	27.6	27.1	24.9	24	84	1007.4	S	2	6	14	13	
AUG	466.2	25	30.6	23.2	26.9	26.3	24.3	24	85	1006.3	S	2	7	11	7	
SEP	258.7	18	31.7	23.1	27.4	27.0	24.8	24	84	1008.5	E/ENE	2	6	13	14	
OCT	169.7	15	31.8	22.2	27.0	26.7	24.3	24	82	1009.0	ENE	3	6	6	9	
NOV	90.6	6	31.6	21.9	26.7	26.4	23.2	22	76	1009.9	NE	3	5	2	2	
DEC	15.6	2	30.9	21.1	26.0	25.6	21.7	20	71	1011.9	NE	3	4	2	1	
ANN	1849.8	122	31.9	22.5	27.2	26.8	23.7	23	77	1009.5	ENE	3	5	45	58	

Station: PAGASA PALAWAN Posit.: 07°00'N 118°05'E Elev. Unk. Per. of records: 1974-1985

MO.	RAIN-FALL (mm)	RAIN DAYS	TEMPERATURE (°C)						DEW PT.	RH (%)	MN. SEA LEVEL PRESS (mbs)	PREVAILING WIND			DAYS WITH	
			MAX	MIN	MEAN	DRY BULB	WET BULB	DIREC-TION				SPD (mps)	CLD (octa)	TRW	LGTN	
JAN	127.3	11	29.9	23.0	26.4	26.6	24.4	24	83	1010.6	NNE	4	5	0	0	
FEB	28.2	3	29.5	22.6	26.0	26.3	24.2	23	84	1011.1	NE	5	4	0	0	
MAR	25.0	3	32.0	24.7	28.3	27.9	25.2	24	80	1010.0	NE	3	3	1	1	
APR	36.8	5	33.2	25.5	29.3	28.9	25.9	25	79	1008.7	ENE	3	4	2	3	
MAY	118.4	12	33.0	25.8	29.4	29.2	26.4	26	80	1007.7	SW	4	5	5	8	
JUN	315.7	17	31.1	25.3	28.2	28.4	26.2	25	84	1007.0	SW	4	6	5	7	
JUL	280.5	16	31.4	25.0	28.2	28.1	26.0	25	86	1007.4	SW	5	6	5	6	
AUG	282.9	15	30.9	25.0	27.9	28.2	26.0	25	84	1007.3	SW	6	6	4	4	
SEP	254.8	17	32.1	24.5	28.3	28.1	26.0	25	85	1008.2	S	4	6	6	11	
OCT	399.0	20	31.2	24.4	27.8	27.7	25.7	25	85	1007.8	NE	4	6	6	11	
NOV	289.9	17	30.8	24.7	27.7	27.7	25.5	25	84	1008.9	NE/NNE	4	6	5	8	
DEC	303.4	17	29.5	23.7	26.6	26.9	24.9	24	86	1010.3	NNE	5	6	3	3	
ANN	2461.9	153	31.2	24.5	27.8	27.8	25.5	25	83	1008.8	NE/SW	4	5	42	62	

Station: PORT AREA MANILA Posit.: 14°35'N 120°35'E Elev. 18 m. Per. of records: 1951-1985

MO.	RAIN-FALL (mm)	RAIN DAYS	TEMPERATURE (°C)					DRY BULB	WET BULB	DEW PT.	RH (%)	MN. SEA LEVEL PRESS (mbs)	PREVAILING WIND			DAYS WITH	
			MAX	MIN	MEAN	DIREC-TION	SPD (mps)						CLD (octa)	TRW	LGTN		
JAN	13.3	4	28.5	23.3	25.9	26.6	21.9	20	72	1013.3	NE	3	4	0	0		
FEB	7.3	2	30.2	23.4	26.3	26.1	22.0	20	73	1012.3	SE	3	4	0	0		
MAR	21.4	3	31.9	23.6	27.7	27.6	22.7	21	66	1012.8	SE	4	3	0	1		
APR	18.7	3	33.3	25.0	29.1	29.0	23.7	22	64	1011.3	SE	4	3	1	6		
MAY	126.6	10	33.4	25.7	29.5	29.5	24.8	23	68	1009.7	SE	4	4	9	21		
JUN	283.8	16	32.1	25.3	28.7	28.6	25.2	24	76	1009.0	SW	4	5	13	16		
JUL	364.1	22	31.2	24.8	28.0	27.8	25.0	24	80	1008.6	SW	4	6	14	16		
AUG	476.3	22	30.4	24.4	27.4	27.3	25.0	24	83	1008.0	SW	5	6	11	10		
SEP	334.1	20	30.6	24.5	27.5	27.4	24.8	24	81	1008.8	SW	4	6	12	15		
OCT	200.5	18	30.9	24.3	27.6	27.4	24.4	23	78	1009.8	NE	3	5	9	13		
NOV	111.4	14	30.5	23.8	27.1	27.0	23.7	23	76	1010.8	NE	3	5	3	4		
DEC	86.0	9	29.6	22.9	26.3	26.1	22.7	21	75	1012.5	NE	3	5	0	1		
ANN	2025.7	143	31.1	24.1	27.6	27.5	23.8	22	74	1010.7	VRBL	4	5	72	103		

Station: PUERTO PRINCESA Posit.: 09°45'N 118°44'E Elev. 16 m. Per. of records: 1951-1985

MO.	RAIN-FALL (mm)	RAIN DAYS	TEMPERATURE (°C)					DRY BULB	WET BULB	DEW PT.	RH (%)	MN. SEA LEVEL PRESS (mbs)	PREVAILING WIND			DAYS WITH	
			MAX	MIN	MEAN	DIREC-TION	SPD (mps)						CLD (octa)	TRW	LGTN		
JAN	30.7	4	30.7	22.7	26.3	26.1	23.9	23	83	1011.8	NE	2	5	0	1		
FEB	16.7	2	31.2	22.6	26.9	26.4	23.9	23	81	1011.8	NE	2	5	0	0		
MAR	37.2	4	32.0	23.2	27.7	27.1	24.3	23	79	1011.7	NE	2	5	1	1		
APR	42.4	5	32.9	24.2	28.6	27.9	25.1	24	80	1010.6	NE	2	4	3	5		
MAY	142.4	12	32.5	24.5	28.5	27.9	25.5	25	82	1009.7	W	1	6	9	13		
JUN	184.2	15	31.3	23.9	27.6	27.0	25.0	24	85	1009.7	S	1	6	7	8		
JUL	177.6	16	30.9	23.4	27.2	26.5	24.7	24	86	1009.5	S	1	6	6	6		
AUG	183.6	17	30.9	23.4	27.2	26.6	24.7	24	86	1009.5	S	1	6	6	7		
SEP	196.4	16	30.9	23.4	27.2	26.4	24.6	24	86	1009.9	S/W	1	6	6	6		
OCT	210.0	16	31.0	23.4	27.2	26.4	24.7	24	87	1010.1	W	1	6	6	9		
NOV	205.2	14	30.9	23.4	27.2	26.5	24.7	24	86	1010.2	NE	2	6	5	8		
DEC	137.4	9	30.7	23.3	27.1	26.4	24.5	24	86	1010.9	NE	2	6	2	5		
ANN	1663.8	130	31.3	23.5	27.4	26.8	24.6	24	84	1010.3	NE	2	6	51	69		

Station: ROMBLON Posit.: 12°35'N 122°16'E Elev. 47 m. Per. of records: 1951-1985

MO.	RAIN-FALL (mm)	RAIN DAYS	TEMPERATURE (°C)					DRY BULB	WET BULB	DEW PT.	RH (%)	MN. SEA LEVEL PRESS (mbs)	PREVAILING WIND			DAYS WITH	
			MAX	MIN	MEAN	DIREC-TION	SPD (mps)						CLD (octa)	TRW	LGTN		
JAN	114.4	15	28.4	23.3	25.8	26.4	23.2	22	83	1013.2	NE	4	5	0	0		
FEB	48.3	10	29.1	23.4	26.2	26.7	23.3	22	82	1013.1	NE	4	4	0	0		
MAR	48.3	10	30.2	24.0	27.1	26.6	23.9	23	80	1012.8	ENE	4	4	0	0		
APR	71.4	8	31.6	25.1	28.3	27.9	24.8	24	78	1011.4	ENE	3	3	1	4		
MAY	125.4	11	32.5	25.4	28.9	28.5	25.5	25	78	1009.9	E/ENE	3	5	6	13		
JUN	206.7	16	32.0	24.9	28.4	28.1	25.4	25	80	1008.4	SSW	3	6	8	16		
JUL	249.5	19	31.2	24.4	27.8	27.5	25.1	24	82	1009.1	SSW	3	6	8	13		
AUG	227.9	17	30.8	24.6	27.7	27.4	25.1	24	83	1008.9	SSW	4	6	5	10		
SEP	252.4	18	30.9	24.4	27.6	27.3	25.0	24	83	1009.5	SSW	3	6	6	10		
OCT	323.1	21	30.7	24.4	27.5	27.2	25.0	24	84	1010.1	NE	3	6	7	12		
NOV	284.3	18	29.8	24.3	27.0	26.9	24.6	24	83	1010.8	NE	4	6	4	7		
DEC	204.6	17	28.8	23.9	26.3	26.1	24.0	23	84	1012.0	NE	4	6	1	2		
ANN	2106.3	180	30.5	24.3	27.4	27.1	24.6	24	82	1010.8	NE	4	5	46	67		

Station: ROXAS Posit.: 11°35'N 122°45'E Elev. 6 m. Per. of records: 1951-1985

MO.	RAIN-FALL (mm)	RAIN DAYS	TEMPERATURE (°C)					DRY BULB	WET BULB	DEW PT.	RH (%)	MN. SEA LEVEL PRESS (mbs)	PREVAILING WIND			DAYS WITH	
			MAX	MIN	MEAN	DIREC-TION	SPD (mps)						CLD (octa)	TRW	LGTN		
JAN	115.9	14	29.2	23.6	26.4	26.3	23.5	23	79	1013.0	NE	4	5	1	1		
FEB	50.4	10	29.5	23.5	26.5	26.4	23.6	23	79	1013.1	NE	3	4	1	2		
MAR	56.7	7	30.5	24.0	27.2	26.5	24.1	23	82	1012.7	NE	3	4	1	3		
APR	57.7	5	32.0	25.1	28.5	27.3	25.0	24	83	1011.6	NE	3	3	3	6		
MAY	146.2	10	32.7	25.1	28.9	28.5	25.5	25	78	1010.1	NE	3	4	14	21		
JUN	253.0	16	32.6	24.3	28.4	28.8	25.3	24	78	1009.7	S	2	5	19	19		
JUL	246.9	17	32.2	23.9	28.0	28.1	25.0	24	78	1009.3	S	2	5	18	19		
AUG	232.6	17	32.3	23.9	28.1	27.7	24.9	24	80	1008.9	S	2	5	16	19		
SEP	240.4	17	32.1	23.8	27.9	27.6	24.9	24	80	1009.6	S	2	5	16	18		
OCT	321.6	19	31.6	24.0	27.8	27.6	25.0	24	81	1010.2	NE	3	5	17	18		
NOV	228.0	17	30.8	24.4	27.6	27.5	24.9	24	81	1010.7	NE	3	5	8	15		
DEC	172.4	17	29.8	24.1	26.9	26.9	24.2	23	80	1011.6	NE	4	5	2	6		
ANN	2118.8	166	31.3	24.1	27.7	27.4	24.7	24	80	1010.9	NE	3	5	118	149		

Station: SAN FRANCISCO QUEZON Posit.: 13°21'N 122°31'E Elev. UNK. Per. of records: 1951-1970

MO.	RAIN-FALL (mm)	RAIN DAYS	TEMPERATURE (°C)					DRY BULB	WET BULB	DEW PT.	RH (%)	MN. SEA LEVEL PRESS (mbs)	PREVAILING WIND			DAYS WITH	
			MAX	MIN	MEAN	DIREC-TION	SPD (mps)						CLD (octa)	TRW	LGTN		
JAN	49.3	10	29.4	21.4	25.4	24.9	22.8	22	84	1013.5	NE	3	5	0	6		
FEB	17.9	7	30.1	21.4	25.7	25.2	23.0	22	83	1013.2	NE	3	5	0	6		
MAR	27.1	7	31.2	22.0	26.6	26.4	23.4	22	78	1012.8	NE	2	5	1	1		
APR	28.1	4	32.2	22.7	27.4	27.4	24.1	23	76	1011.5	SW	2	5	3	3		
MAY	88.9	8	32.6	23.6	28.1	28.0	24.5	23	75	1010.0	SW	2	5	10	10		
JUN	162.7	14	31.8	24.0	27.9	27.8	24.4	23	76	1009.4	SW	3	6	13	10		
JUL	222.2	19	31.2	23.9	27.5	27.3	24.1	23	77	1008.9	SW	3	6	14	10		
AUG	187.5	16	30.8	24.2	27.5	27.4	24.1	23	76	1008.2	SW	3	6	10	7		
SEP	179.2	17	30.9	23.8	27.3	27.2	24.1	23	77	1008.9	SW	3	6	12	9		
OCT	220.2	18	31.1	22.9	27.0	26.8	23.8	23	78	1009.9	NE	2	6	11	9		
NOV	173.9	15	30.7	22.8	26.7	26.3	23.7	23	80	1010.4	NE	3	6	5	4		
DEC	126.4	14	29.8	22.1	25.9	25.5	23.3	23	83	1012.0	NE	3	6	1	1		
ANN	1480.4	149	31.0	22.9	26.9	26.7	23.8	23	79	1010.7	NE/SW	3	6	80	64		

Station: SANGLEY PT., CAVITE Posit.: 14°30'N 120°55'E Elev. 4 m. Per. of records: 1974-1985

MO.	RAIN-FALL (mm)	RAIN DAYS	TEMPERATURE (°C)					DRY BULB	WET BULB	DEW PT.	RH (%)	MN. SEA LEVEL PRESS (mbs)	PREVAILING WIND			DAYS WITH	
			MAX	MIN	MEAN	DIREC-TION	SPD (mps)						CLD (octa)	TRW	LGTN		
JAN	25.3	3	29.5	22.0	25.7	25.5	23.4	22	77	1012.8	E	2	5	0	1		
FEB	2.1	2	30.5	22.3	26.4	27.2	23.5	22	73	1013.2	ESE	2	5	0	0		
MAR	7.4	1	32.4	23.4	27.9	28.7	24.5	23	71	1012.3	ESE	2	4	0	1		
APR	13.6	1	34.4	24.7	29.5	30.2	25.8	24	70	1011.0	ESE	2	5	2	4		
MAY	102.2	6	34.1	25.7	29.9	30.2	25.9	24	71	1008.8	ESE	2	6	8	14		
JUN	289.3	15	32.6	24.6	28.6	29.2	26.1	25	78	1007.8	SW	2	7	12	16		
JUL	289.5	17	31.6	24.4	28.0	28.9	25.7	25	77	1007.7	SW	2	6	14	15		
AUG	460.5	20	30.6	24.5	27.5	28.0	25.5	25	82	1007.0	SW	2	7	8	8		
SEP	243.8	16	31.3	24.6	27.9	28.5	25.8	25	80	1008.3	SW	2	6	14	13		
OCT	185.6	14	31.1	24.3	27.7	28.3	25.5	25	80	1008.5	ESE	2	6	9	12		
NOV	91.7	8	30.5	23.9	27.2	27.8	24.9	24	79	1010.2	N	2	6	2	4		
DEC	32.8	4	29.8	23.0	26.4	27.2	23.9	23	76	1011.6	N	2	6	0	0		
ANN	1683.3	107	31.5	24.0	27.7	28.4	25.0	24	78	1009.9	ESE	2	6	69	88		

Station: SAN JOSE OCC. MINDORO Posit.: 12°21'N 121°02'E Elev. 3 m. Per. of records: 1981-1985

MO.	RAIN-FALL (mm)	RAIN DAYS	TEMPERATURE (°C)					DRY BULB	WET BULB	DEW PT.	RH (%)	MN. SEA LEVEL PRESS (mbs)	PREVAILING WIND			DAYS WITH	
			MAX	MIN	MEAN	DIREC-TION	SPD (mps)						CLD (octa)	TRW	LGTN		
JAN	3.1	3	31.3	21.5	26.4	26.6	22.8	21	75	1010.8	E	2	5	0	0		
FEB	2.3	1	32.2	21.6	26.9	27.3	22.7	21	68	1009.9	E	3	4	0	0		
MAR	18.7	2	33.5	23.0	28.2	28.4	23.6	22	67	1010.3	E	2	3	1	1		
APR	140.5	7	33.1	23.2	28.1	28.8	24.8	23	72	1008.4	E	3	4	5	6		
MAY	88.9	6	33.1	23.7	28.4	28.9	25.3	24	78	1008.0	E	2	5	12	20		
JUN	343.4	15	32.1	23.3	27.7	28.0	25.4	25	80	1007.8	SW	2	5	12	18		
JUL	433.1	16	30.7	23.1	26.9	27.2	25.2	24	85	1007.0	SW	1	6	12	17		
AUG	589.3	23	31.0	23.7	27.3	26.9	25.2	25	87	1006.7	SW	2	7	10	12		
SEP	391.8	17	30.5	22.8	26.6	26.9	25.1	25	87	1008.0	SW	1	6	11	15		
OCT	245.2	16	30.8	22.7	26.7	27.0	25.0	25	84	1008.2	E	1	6	11	16		
NOV	55.4	6	31.9	22.6	27.2	27.4	24.5	23	79	1008.4	E	2	5	4	9		
DEC	8.7	2	31.9	22.0	26.9	27.2	23.5	22	73	1009.2	E	2	5	1	2		
ANN	2290.4	114	31.8	22.8	27.3	27.6	24.4	23	78	1008.6	E	2	5	79	118		

Station: SCI. GARDEN DILIMAN Posit.: 14°39'N 121°03'E Elev. 46 m. Per. of records: 1961-1985

MO.	RAIN-FALL (mm)	RAIN DAYS	TEMPERATURE (°C)					DRY BULB	WET BULB	DEW PT.	RH (%)	MN. SEA LEVEL PRESS (mbs)	PREVAILING WIND			DAYS WITH	
			MAX	MIN	MEAN	DIREC-TION	SPD (mps)						CLD (octa)	TRW	LGTN		
JAN	17.2	4	29.9	20.0	25.1	24.8	21.5	20	75	1012.6	NE	2	5	0	0		
FEB	9.7	2	31.2	20.0	25.6	25.4	21.4	20	70	1012.4	NE	2	4	0	0		
MAR	22.1	3	33.0	21.3	27.2	27.1	22.5	21	67	1012.1	SE	2	4	1	1		
APR	28.3	4	34.6	22.9	28.8	28.7	23.6	22	66	1010.6	SE	2	3	3	4		
MAY	172.7	12	34.2	23.8	29.0	28.8	24.8	23	72	1008.9	VRBL	2	5	12	14		
JUN	339.6	18	32.2	23.7	28.0	27.5	24.9	24	81	1008.3	SW	2	6	15	13		
JUL	448.1	22	31.1	23.4	27.3	26.9	24.7	24	84	1007.7	SW	2	6	15	12		
AUG	504.8	23	30.5	23.4	27.0	26.5	24.5	24	86	1007.5	SW	2	6	13	8		
SEP	381.8	21	30.9	23.2	27.1	26.5	24.6	24	86	1008.1	SW	2	6	13	11		
OCT	234.0	18	31.0	22.6	26.8	26.5	24.6	24	86	1008.7	NE	2	6	9	8		
NOV	144.0	14	30.7	21.7	26.2	25.9	23.5	23	82	1010.7	NE	2	5	4	3		
DEC	53.8	8	30.2	20.8	25.5	25.3	22.5	21	78	1011.9	NE	2	5	1	0		
ANN	2386.1	149	31.6	22.2	27.0	26.7	23.5	22	77	1010.0	NE	2	5	86	74		

Station: TACLOBAN CITY Posit.: 11°15'N 125°00'E Elev. 21 m. Per. of records: 1951-1985

MO.	RAIN-FALL (mm)	RAIN DAYS	TEMPERATURE (°C)					DRY BULB	WET BULB	DEW PT.	RH (%)	MN. SEA LEVEL PRESS (mbs)	PREVAILING WIND			DAYS WITH	
			MAX	MIN	MEAN	DIREC-TION	SPD (mps)						CLD (octa)	TRW	LGTN		
JAN	281.8	20	28.8	22.8	25.8	25.3	23.3	22	84	1011.9	NW	3	6	1	1		
FEB	208.3	18	29.1	22.7	25.9	25.4	23.1	22	82	1012.0	NW	3	6	1	1		
MAR	137.6	16	30.0	23.2	26.5	26.0	23.5	23	82	1012.0	NW	3	5	2	1		
APR	121.2	15	30.8	24.1	27.4	27.0	24.5	24	81	1010.8	NW	3	5	6	6		
MAY	146.1	15	31.1	24.8	27.9	27.7	25.1	24	81	1009.6	SE	3	5	13	15		
JUN	184.7	16	31.2	24.6	27.9	27.5	25.1	24	82	1009.2	SE/SSE	3	6	15	19		
JUL	167.0	17	31.1	24.4	27.7	27.3	24.8	24	82	1008.7	NW	3	6	16	19		
AUG	129.1	15	31.4	24.5	27.9	27.5	24.8	24	80	1008.5	NW	3	6	15	15		
SEP	146.8	16	31.3	24.5	27.9	27.4	24.8	24	81	1008.9	NW	3	6	15	19		
OCT	184.4	19	31.0	24.2	27.6	27.0	24.7	24	83	1009.2	NW	3	6	16	19		
NOV	244.8	20	30.3	23.9	27.1	26.5	24.4	24	84	1009.3	NW	3	6	10	11		
DEC	316.9	23	29.5	23.4	26.5	25.8	23.9	23	85	1010.7	NW	3	6	6	5		
ANN	2215.6	210	30.5	23.9	27.2	26.7	24.3	24	82	1010.1	NW	3	6	116	131		

Station: TAGBILARAN CITY Posit.: 09°39'N 123°51'E Elev. 6 m. Per. of records: 1961-1985

MO.	RAIN-FALL (mm)	RAIN DAYS	TEMPERATURE (°C)					DRY BULB	WET BULB	DEW PT.	RH (%)	MN. SEA LEVEL PRESS (mbs)	PREVAILING WIND			DAYS WITH	
			MAX	MIN	MEAN	DIREC-TION	SPD (mps)						CLD (octa)	TRW	LGTN		
JAN	108.0	14	30.4	21.7	26.0	25.6	23.4	23	83	1011.5	NE	2	6	1	2		
FEB	78.5	11	30.6	21.5	26.1	25.8	23.3	22	81	1011.6	NE	2	6	1	1		
MAR	71.8	10	31.7	21.8	26.7	26.5	23.8	23	80	1011.6	NE	2	6	2	2		
APR	57.8	9	32.7	22.6	27.6	27.6	24.4	23	77	1010.6	NE	2	8	6	6		
MAY	80.3	10	33.1	23.5	28.2	28.1	25.3	24	80	1009.6	NE	1	6	14	18		
JUN	131.0	15	32.5	23.7	28.1	27.8	25.3	24	82	1009.5	VAR/NE	1	6	15	21		
JUL	134.8	14	32.3	23.7	28.0	27.7	25.1	24	81	1009.2	SW	2	6	11	15		
AUG	107.8	13	32.6	23.9	28.2	28.0	25.1	24	79	1009.3	SW	2	6	9	15		
SEP	136.0	15	32.3	23.7	28.0	27.6	25.1	24	82	1009.5	SW/WSW	2	6	13	18		
OCT	212.8	17	32.1	23.3	27.6	27.2	25.0	24	84	1009.8	NE	1	6	14	18		
NOV	190.5	17	31.8	22.8	27.3	26.8	24.8	24	85	1010.1	NE	1	6	11	14		
DEC	117.2	16	31.2	22.5	26.8	26.3	24.2	23	84	1010.4	NE	2	6	4	7		
ANN	1423.5	161	32.0	22.9	27.4	27.1	24.6	24	82	1010.2	NE	2	6	101	137		

Station: TAYABAS QUEZON Posit.: 14°03'N 121°35'E Elev. 158 m. Per. of records: 1970-1985

MO.	RAIN-FALL (mm)	RAIN DAYS	TEMPERATURE (°C)					DRY BULB	WET BULB	DEW PT.	RH (%)	MN. SEA LEVEL PRESS (mbs)	PREVAILING WIND			DAYS WITH	
			MAX	MIN	MEAN	DIREC-TION	SPD (mps)						CLD (octa)	TRW	LGTN		
JAN	188.1	19	27.2	21.4	24.3	23.7	21.9	21	85	1012.5	N/NE	3	6	0	1		
FEB	72.3	13	27.7	21.6	24.6	24.0	22.0	21	86	1011.9	NE	3	5	0	0		
MAR	72.3	10	29.2	22.2	25.7	25.0	22.6	21	81	1011.6	NE	3	5	1	1		
APR	103.2	9	30.9	23.3	27.1	26.5	24.0	23	81	1010.7	NE	2	4	4	6		
MAY	227.5	14	31.8	23.7	27.7	27.2	24.8	24	82	1009.3	NE	2	5	17	23		
JUN	257.9	17	31.2	23.6	27.4	26.9	24.8	24	84	1009.9	SW	1	6	19	25		
JUL	260.6	19	30.7	23.1	26.9	26.5	23.9	23	95	1006.5	SW	1	6	16	23		
AUG	172.6	17	30.8	23.0	26.9	26.3	24.4	23	86	1006.9	SW	2	7	13	17		
SEP	316.1	20	30.6	22.7	26.6	26.0	23.6	23	97	1007.9	SW	1	6	18	25		
OCT	512.7	24	29.6	23.1	26.3	25.8	24.1	23	87	1008.6	NE	2	6	14	21		
NOV	519.9	23	28.7	22.8	25.7	25.3	23.7	23	87	1009.2	NE	3	6	1	2		
DEC	413.7	24	27.5	22.2	24.8	24.3	22.9	22	89	1010.8	NE	3	6	1	2		
ANN	3083.9	209	29.7	22.7	26.2	25.6	23.9	23	87	1009.5	NE	2	6	104	146		

Station: TUGUEGARAO Posit.: 17°37'N 121°44'E Elev. 24 m. Per. of records: 1951-1985

MO.	RAIN-FALL (mm)	RAIN DAYS	TEMPERATURE (°C)					DRY BULB	WET BULB	DEW PT.	RH (%)	MN. SEA LEVEL PRESS (mbs)	PREVAILING WIND			DAYS WITH	
			MAX	MIN	MEAN	DIREC-TION	SPD (mps)						CLD (octa)	TRW	LGTN		
JAN	21.4	6	29.1	19.3	24.3	23.1	20.7	20	80	1015.3	N	2	6	0	0		
FEB	16.5	4	31.3	19.4	25.4	24.2	21.1	20	76	1014.7	N	2	4	0	0		
MAR	57.2	5	33.7	20.8	27.3	26.2	22.3	21	71	1013.3	N	2	3	1	1		
APR	73.6	5	35.9	22.6	29.3	28.2	23.7	22	68	1011.5	N	2	3	4	3		
MAY	172.1	10	36.7	23.7	30.3	29.0	24.5	23	69	1009.2	S	2	4	8	8		
JUN	161.6	13	35.6	23.8	29.7	28.6	24.7	23	73	1008.0	S	2	5	9	11		
JUL	192.8	14	34.8	23.6	29.2	28.0	24.7	24	76	1007.6	S	2	5	9	10		
AUG	246.5	16	34.1	23.6	28.9	27.7	24.6	24	78	1007.6	S	2	6	8	7		
SEP	209.1	15	33.6	23.3	28.5	27.3	24.4	23	79	1007.9	N	2	6	4	7		
OCT	252.9	14	32.2	22.6	27.4	26.3	23.7	23	80	1010.4	N	2	5	2	4		
NOV	274.2	15	30.1	21.6	25.9	24.8	22.6	22	83	1012.6	N	2	6	1	1		
DEC	93.9	11	28.8	20.2	24.5	23.5	21.5	21	84	1014.7	N	2	6	0	0		
ANN	1771.8	128	33.0	22.0	27.6	26.4	23.2	22	76	1011.1	N	2	5	46	52		

Station: VIGAN Posit.: 17°34'N 120°23'E Elev. 31 m. Per. of records: 1951-1985

MO.	RAIN-FALL (mm)	RAIN DAYS	TEMPERATURE (°C)					DRY BULB	WET BULB	DEW PT.	RH (%)	MN. SEA LEVEL PRESS (mbs)	PREVAILING WIND			DAYS WITH	
			MAX	MIN	MEAN	DIREC-TION	SPD (mps)						CLD (octa)	TRW	LGTN		
JAN	2.3	1	29.7	21.0	26.3	25.2	22.2	21	77	1014.1	N	4	2	0	0		
FEB	3.3	1	30.1	21.5	25.8	25.5	22.5	21	77	1013.5	N	4	2	0	0		
MAR	5.0	2	31.3	22.9	27.1	26.9	23.7	23	76	1013.3	NNW	3	2	0	0		
APR	17.4	2	32.5	24.3	28.4	28.3	25.0	24	76	1012.1	N	3	2	1	4		
MAY	145.9	9	32.8	24.8	28.8	28.8	25.8	25	79	1010.1	VAR	3	3	5	10		
JUN	404.3	17	31.4	24.0	27.7	27.9	25.6	25	83	1008.8	SSE	3	5	7	9		
JUL	483.3	19	30.7	23.8	27.2	27.3	25.3	25	85	1008.3	SSE	3	6	7	8		
AUG	738.9	22	30.0	23.4	26.7	26.8	25.1	24	87	1007.8	SSE	3	6	6	6		
SEP	365.7	15	30.3	23.5	26.9	26.9	25.1	24	86	1008.9	SE/SSE	3	6	5	7		
OCT	112.5	7	31.1	23.4	27.2	27.2	24.8	24	82	1010.2	N	3	3	4	4		
NOV	35.1	4	30.9	22.9	26.9	26.8	24.3	23	87	1010.5	N	4	3	1	1		
DEC	9.1	2	30.4	22.0	26.2	26.1	23.1	23	78	1012.9	N	3	3	0	0		
ANN	2312.8	101	30.9	23.1	27.0	27.0	24.4	23	81	1010.9	N	3	4	36	49		

Station: VIRAC Posit.: 13°35'N 124°14'E Elev. 6 m. Per. of records: 1951-1985

MO.	RAIN-FALL (mm)	RAIN DAYS	TEMPERATURE (°C)					DRY BULB	WET BULB	DEW PT.	RH (%)	MN. SEA LEVEL PRESS (mbs)	PREVAILING WIND			DAYS WITH	
			MAX	MIN	MEAN	DIREC-TION	SPD (mps)						CLD (octa)	TRW	LGTN		
JAN	219.9	19	29.3	22.1	26.7	25.4	22.9	22	81	1011.5	NE	3	6	0	0		
FEB	132.2	15	29.8	21.8	25.8	25.5	22.8	22	79	1011.6	NE	3	6	0	0		
MAR	119.2	14	30.6	22.2	26.4	26.2	23.3	22	78	1012.7	E	3	6	0	0		
APR	128.6	15	31.5	23.0	27.3	27.2	24.3	23	79	1011.3	E	3	5	1	3		
MAY	185.6	15	32.0	23.9	28.0	28.0	25.2	24	80	1009.6	E	3	6	5	10		
JUN	325.2	16	32.2	24.1	28.2	28.1	25.4	25	80	1007.6	SE	3	6	6	13		
JUL	323.8	17	31.8	23.9	27.9	27.7	25.2	24	82	1008.1	SW	3	6	7	12		
AUG	174.1	15	32.0	24.1	28.1	27.7	25.1	24	81	1006.4	SW	3	6	4	8		
SEP	248.8	17	31.8	23.7	27.8	27.4	25.0	24	82	1006.5	W	3	6	7	6		
OCT	373.9	21	31.3	23.2	27.3	26.9	24.7	24	84	1007.9	E	3	6	5	9		
NOV	486.4	23	30.7	23.3	27.0	26.7	24.4	24	83	1008.7	NE	3	6	3	4		
DEC	412.5	22	29.8	22.8	26.3	26.1	23.8	23	82	1010.2	NE	3	6	1	2		
ANN	2930.2	209	31.1	23.2	27.2	26.9	24.3	23	81	1009.3	NE/E	3	6	39	67		

Station: VIRAC RADAR Posit.: 13°59'N 124°19'E Elev. Unk. Per. of records: 1968-1985

MO.	RAIN-FALL (mm)	RAIN DAYS	TEMPERATURE (°C)					DRY BULB	WET BULB	DEW PT.	RH (%)	MN. SEA LEVEL PRESS (mbs)	PREVAILING WIND			DAYS WITH	
			MAX	MIN	MEAN	DIREC-TION	SPD (mps)						CLD (octa)	TRW	LGTN		
JAN	360.3	21	28.3	20.8	23.5	23.7	22.1	22	87	1012.6	NE	5	6	0	1		
FEB	209.1	18	26.5	21.0	23.7	23.9	22.2	22	86	1012.1	NE	4	6	0	0		
MAR	160.5	16	27.6	21.8	24.7	24.7	22.9	22	86	1010.5	NE	4	6	0	0		
APR	175.2	16	28.6	22.6	25.6	25.7	23.9	23	86	1009.3	NE	4	5	2	2		
MAY	184.8	15	29.3	23.4	26.3	26.5	24.7	24	86	1008.9	NE	4	6	11	6		
JUN	225.9	16	29.5	23.6	26.5	26.8	24.9	24	86	1006.3	SW	3	6	7	16		
JUL	245.7	16	29.4	22.9	26.1	26.2	24.5	24	87	1007.0	SW	4	6	8	12		
AUG	164.2	16	29.2	23.1	26.1	26.3	24.4	24	86	1005.2	SW	4	7	6	12		
SEP	273.9	18	29.2	22.8	26.0	26.0	24.4	24	88	1006.8	SW	3	6	9	13		
OCT	377.3	22	29.1	22.7	25.9	25.9	24.3	24	88	1008.5	NE	4	6	8	11		
NOV	549.5	24	28.0	22.3	25.1	25.3	23.9	23	89	1008.8	NE	4	6	3	4		
DEC	544.1	25	27.1	21.7	24.4	24.5	23.3	23	90	1010.3	NE	4	7	1	1		
ANN	3470.7	223	28.3	22.4	25.3	25.5	23.8	23	87	1008.8	NE	4	6	55	78		

Station: ZAMBOANGA CITY Posit.: 06°55'N 122°04'E Elev. 6 m. Per. of records: 1951-1985

MO.	RAIN-FALL (mm)	RAIN DAYS	TEMPERATURE (°C)					DRY BULB	WET BULB	DEW PT.	RH (%)	MN. SEA LEVEL PRESS (mbs)	PREVAILING WIND			DAYS WITH	
			MAX	MIN	MEAN	DIREC-TION	SPD (mps)						CLD (octa)	TRW	LGTN		
JAN	43.9	7	31.5	21.8	26.6	26.2	23.6	23	80	1010.2	SW	2	5	3	6		
FEB	44.2	6	31.7	22.0	26.8	26.3	23.6	23	80	1010.2	SW	2	5	3	5		
MAR	37.7	6	32.2	22.4	27.3	27.0	24.0	23	78	1010.3	W	2	5	6	6		
APR	51.0	8	32.2	23.0	27.6	27.4	24.5	24	79	1009.8	W	2	5	10	12		
MAY	94.8	12	31.9	23.5	27.7	27.3	24.9	24	82	1009.4	W	2	5	14	18		
JUN	142.3	15	31.2	23.3	27.2	26.9	24.6	24	83	1009.8	W	2	6	9	12		
JUL	135.1	14	30.9	22.9	26.8	26.6	24.4	24	83	1009.9	W	2	6	8	9		
AUG	128.5	13	31.2	23.0	27.1	26.7	24.4	24	83	1009.9	W	2	6	8	9		
SEP	145.1	13	31.3	23.0	27.1	26.7	24.4	24	83	1010.0	W	2	6	8	10		
OCT	192.4	15	31.3	22.8	27.0	26.6	24.4	24	83	1009.1	W	2	6	12	13		
NOV	108.7	13	31.7	22.6	27.1	26.7	24.4	24	83	1009.6	W	2	5	10	11		
DEC	88.1	10	31.6	22.3	26.9	26.5	24.1	23	82	1009.8	W	2	5	6	8		
ANN	1211.8	132	31.6	22.7	27.1	26.7	24.3	24	82	1009.8	W	2	5	97	119		

Appendix D

Percent Frequencies of Wave Heights (CNOC 1989)

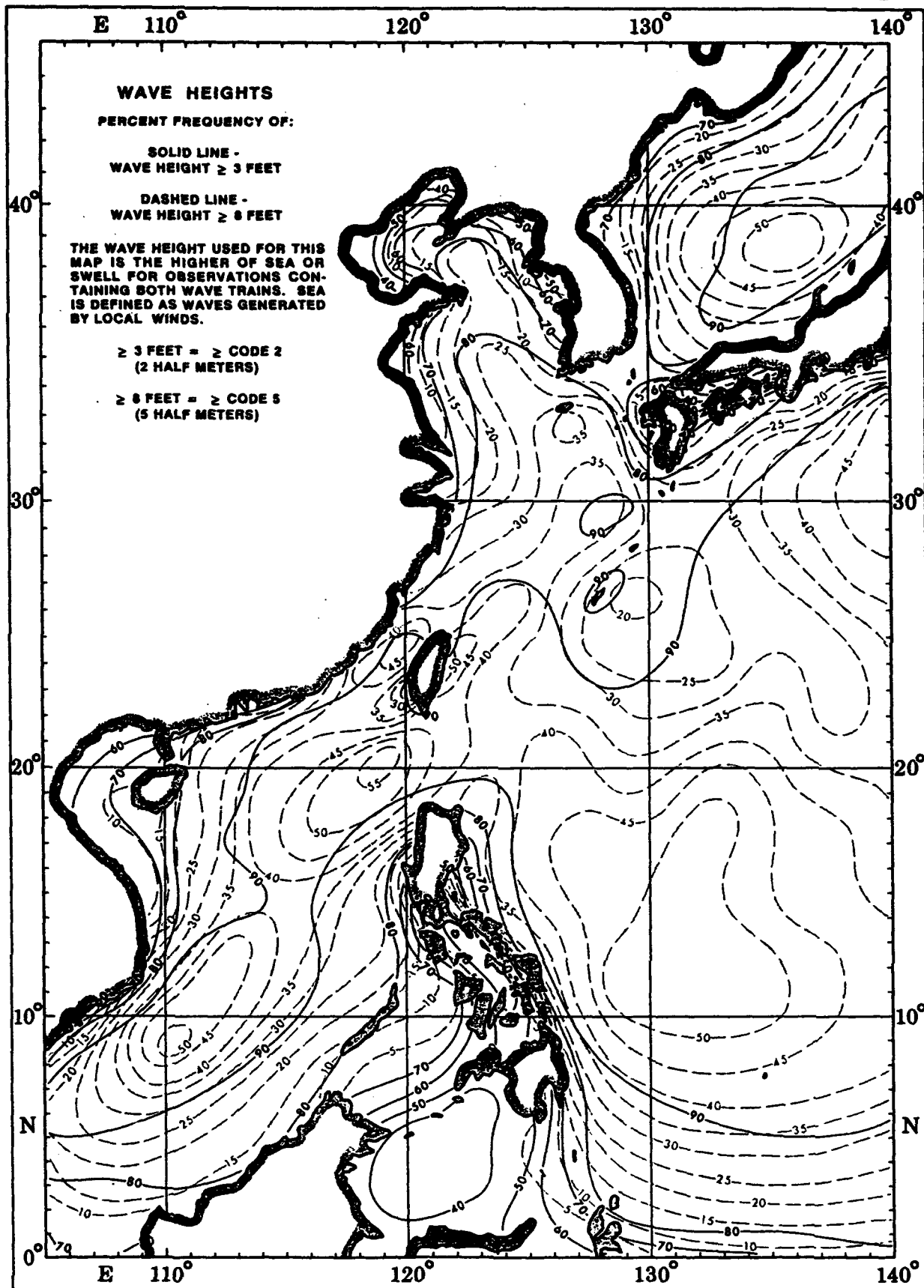
This Appendix is made available to assist in operational planning. As defined on the legends on the upper-left portion of each figure, percent frequency of ≥ 3 -foot (solid) and ≥ 8 -foot (dashed) wave heights are shown for each month. (The wave height used is the higher of sea or swell for observations containing both wave trains.) The analyses were produced by the National Climatic Data Center using data from the period (1948-1987).

Wave observations are one of the least commonly observed elements. In earlier years, many observers were reluctant to take wave observations, due to the difficulty in estimating waves, especially in confused seas.

The observations were subject to biases, generally with heights too low, periods too short and poor sea-swell discrimination. The observations were not adjusted for the suspected biases, but were subjected to a quality control procedure, where an internal check was made between wind speed and sea height (CNOC 1989).

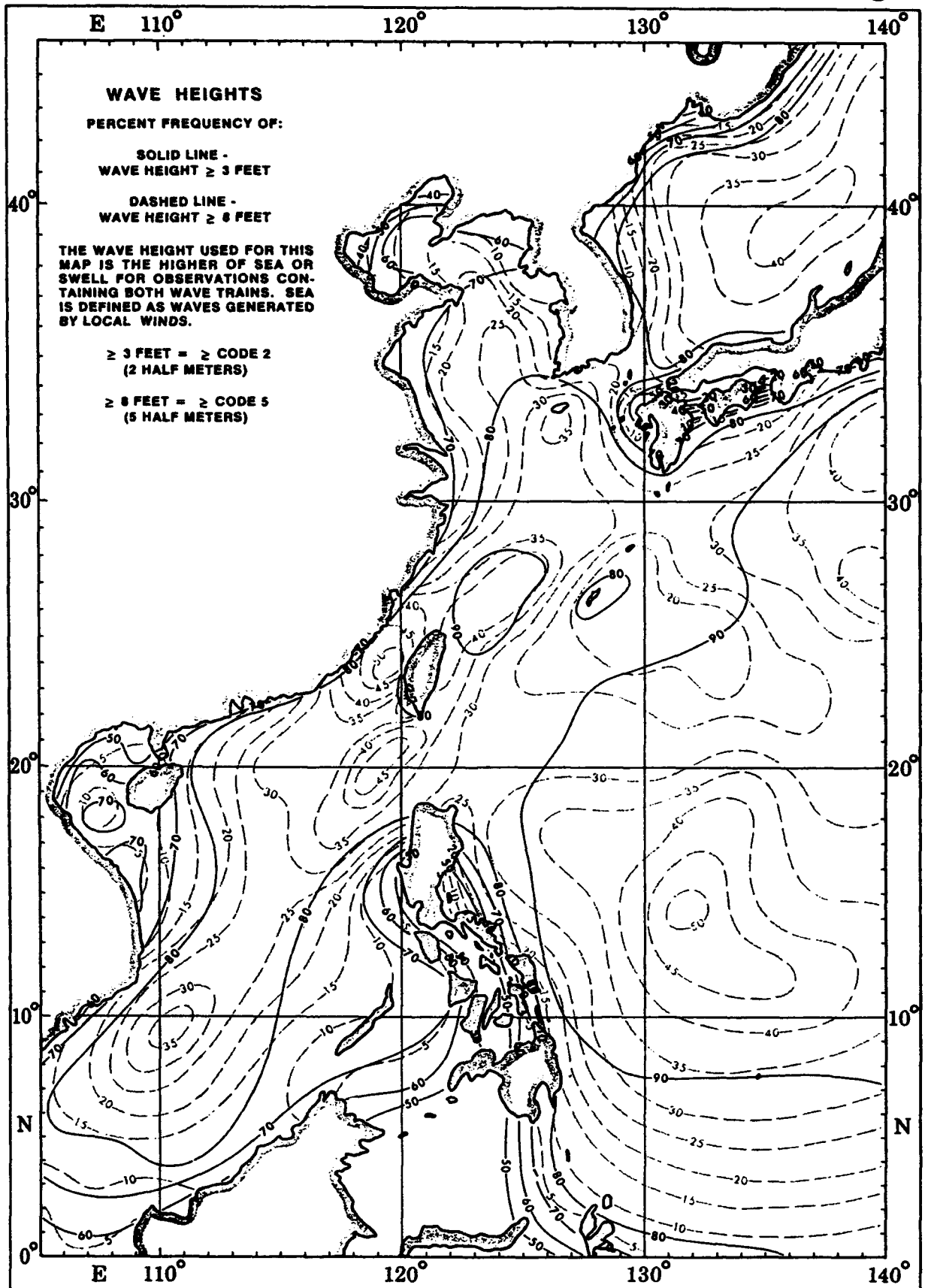
January

Wave Height



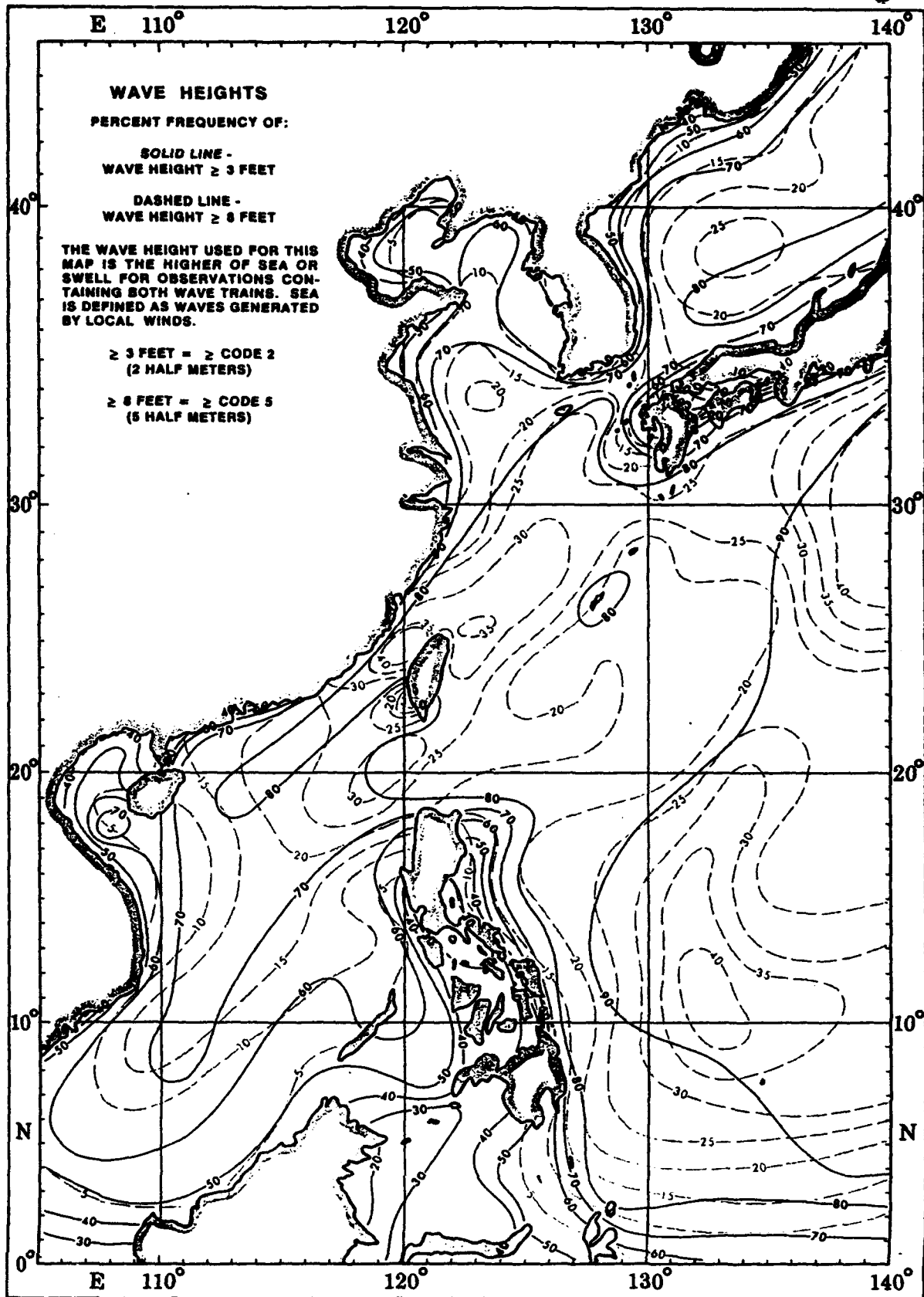
February

Wave Height



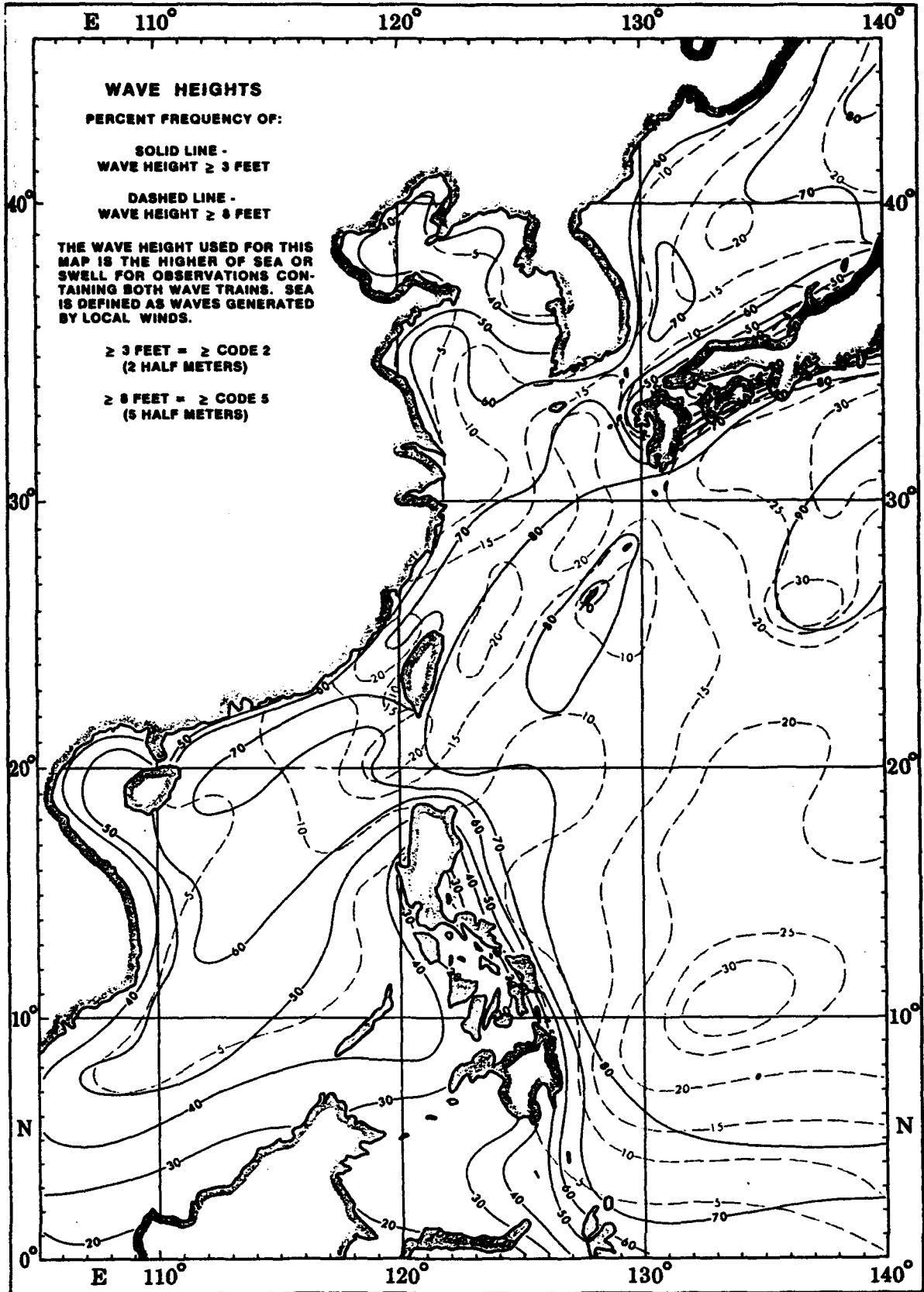
March

Wave Height



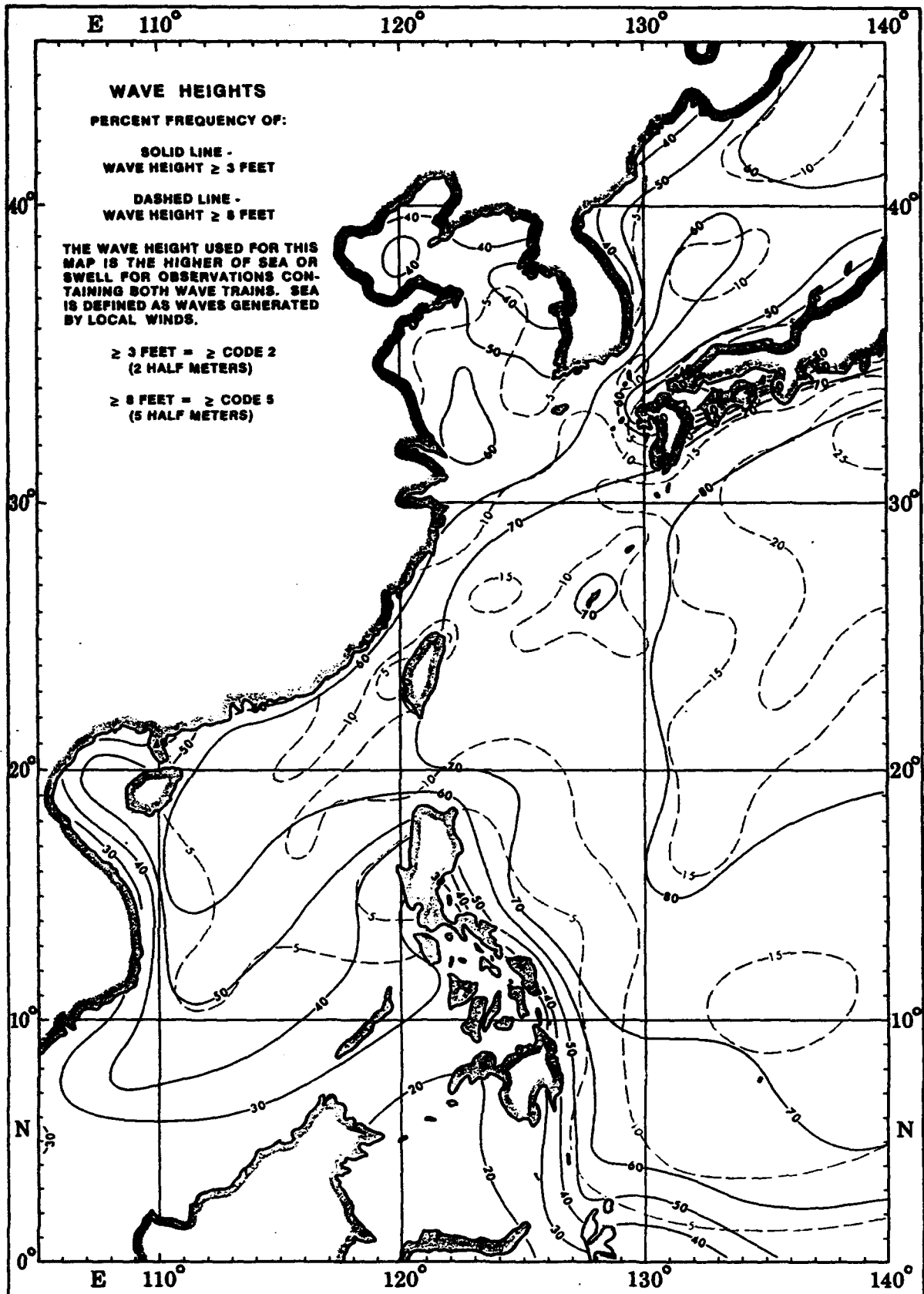
April

Wave Height



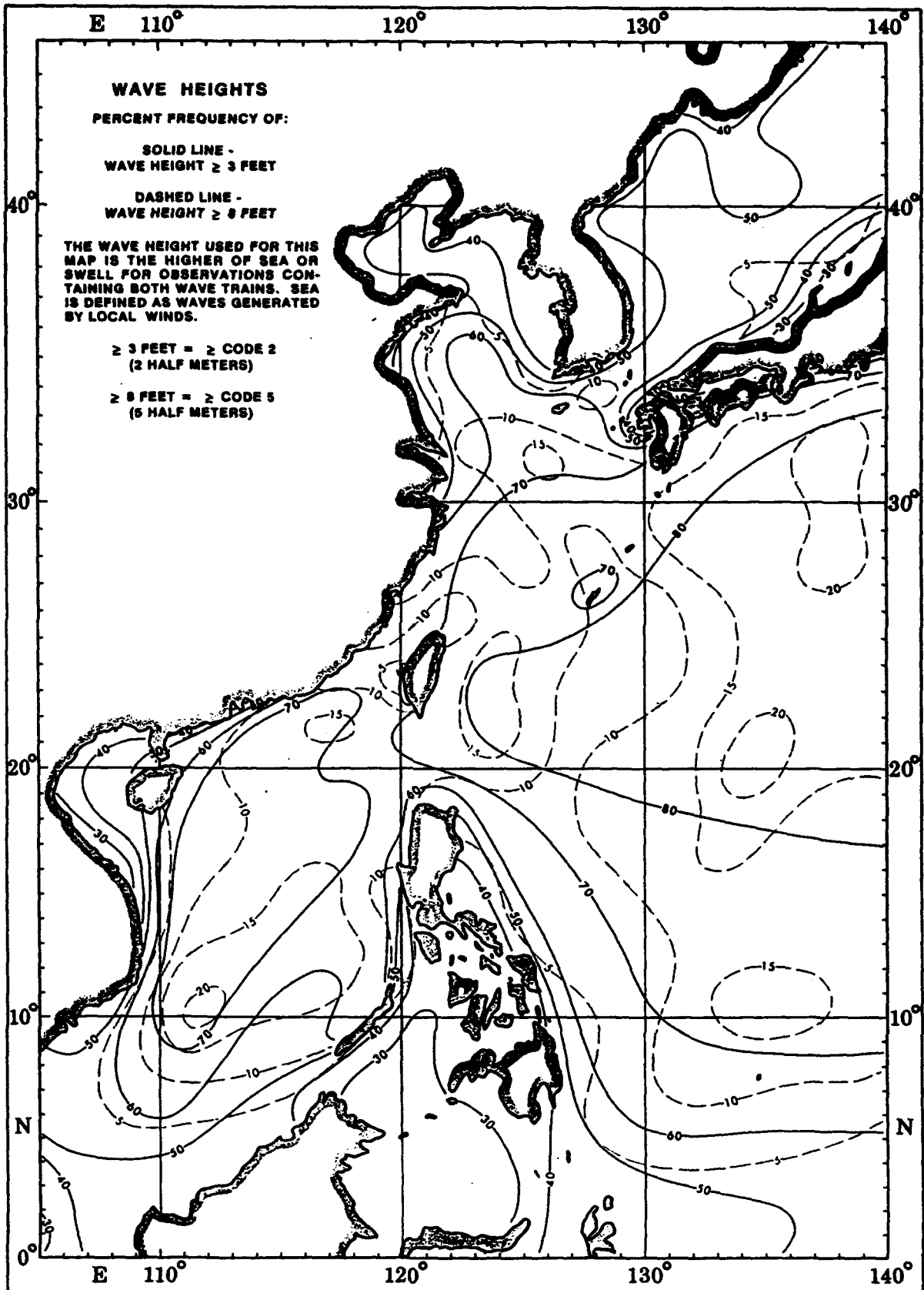
May

Wave Height



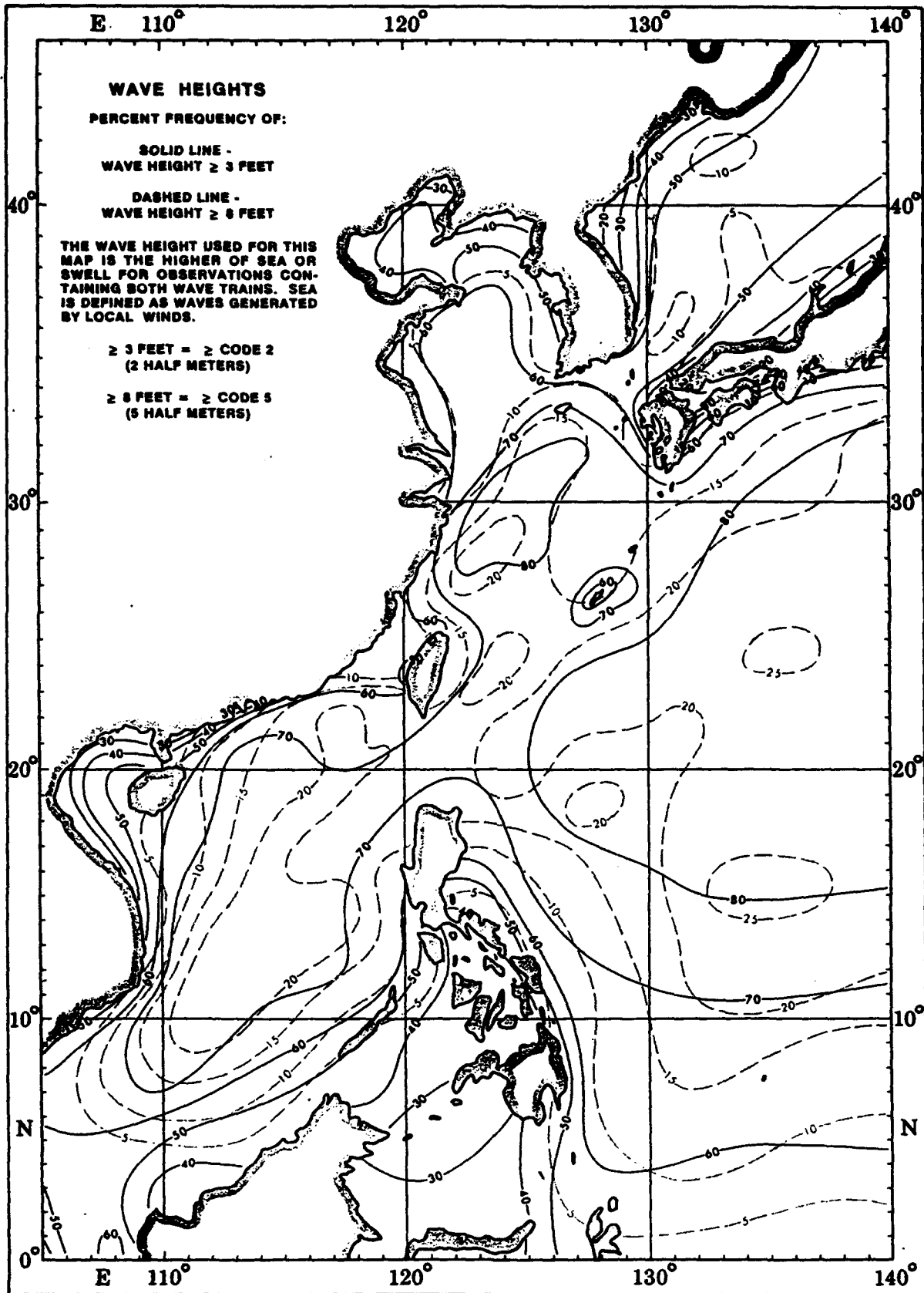
June

Wave Height



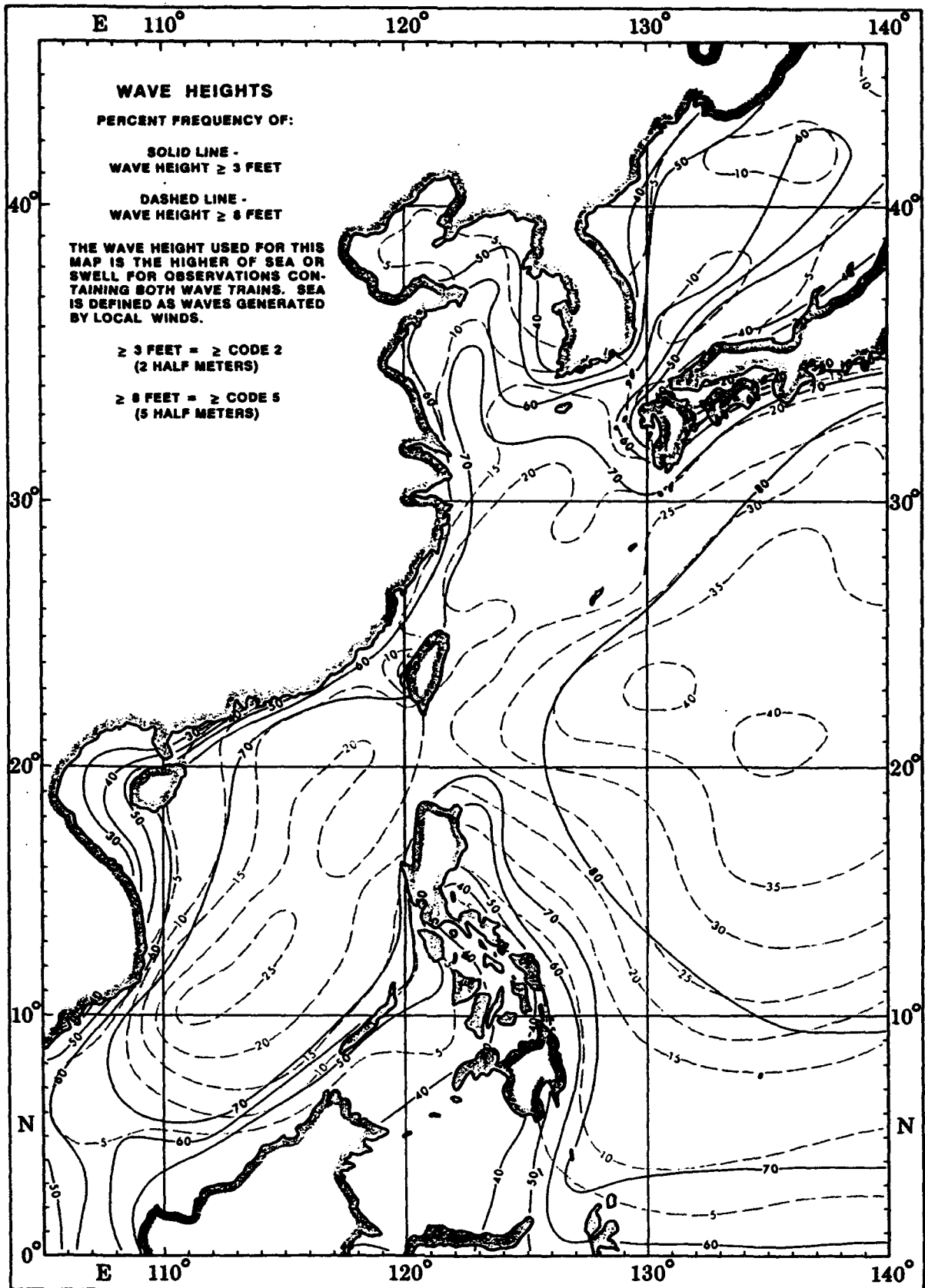
July

Wave Height



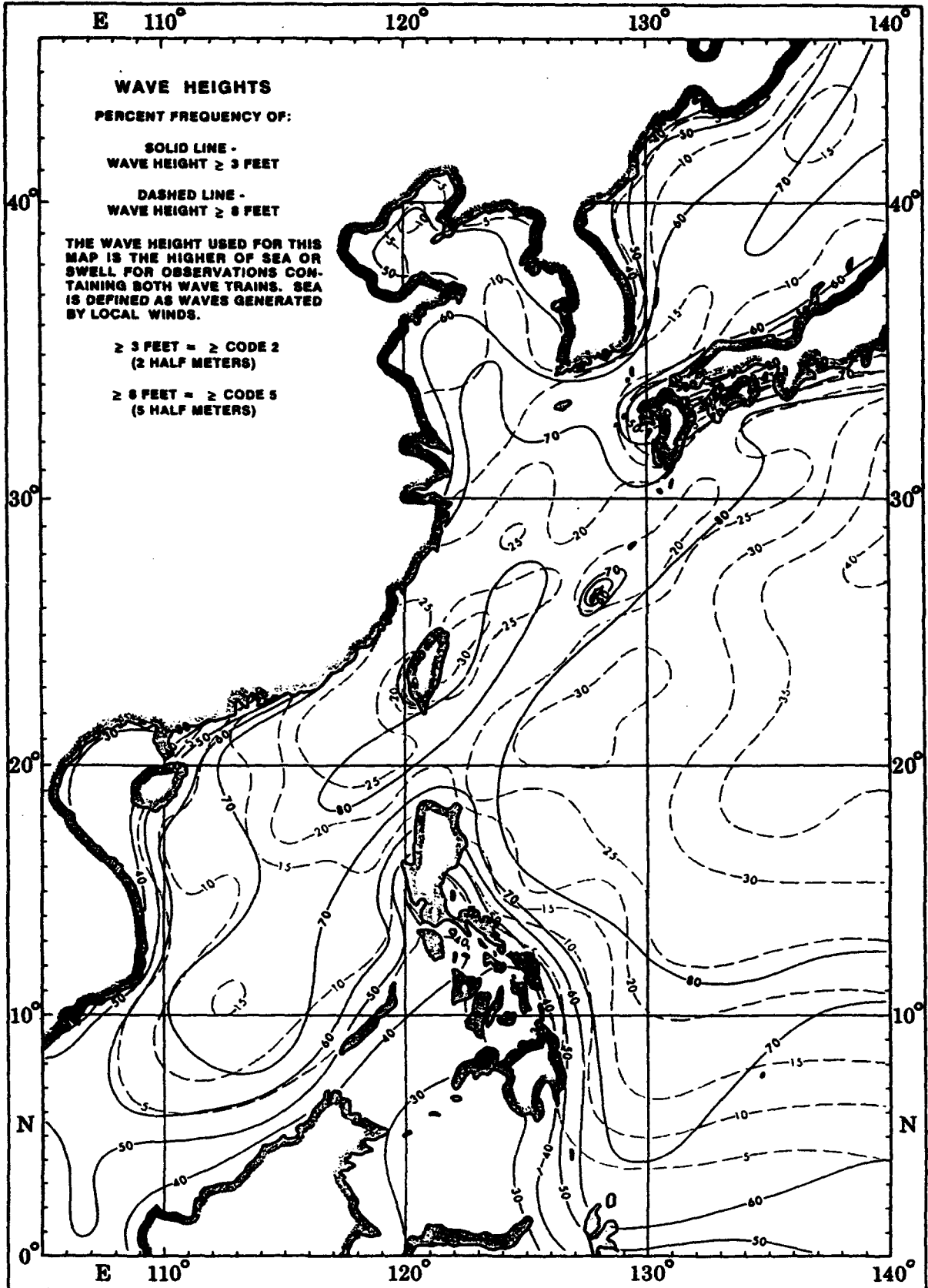
August

Wave Height



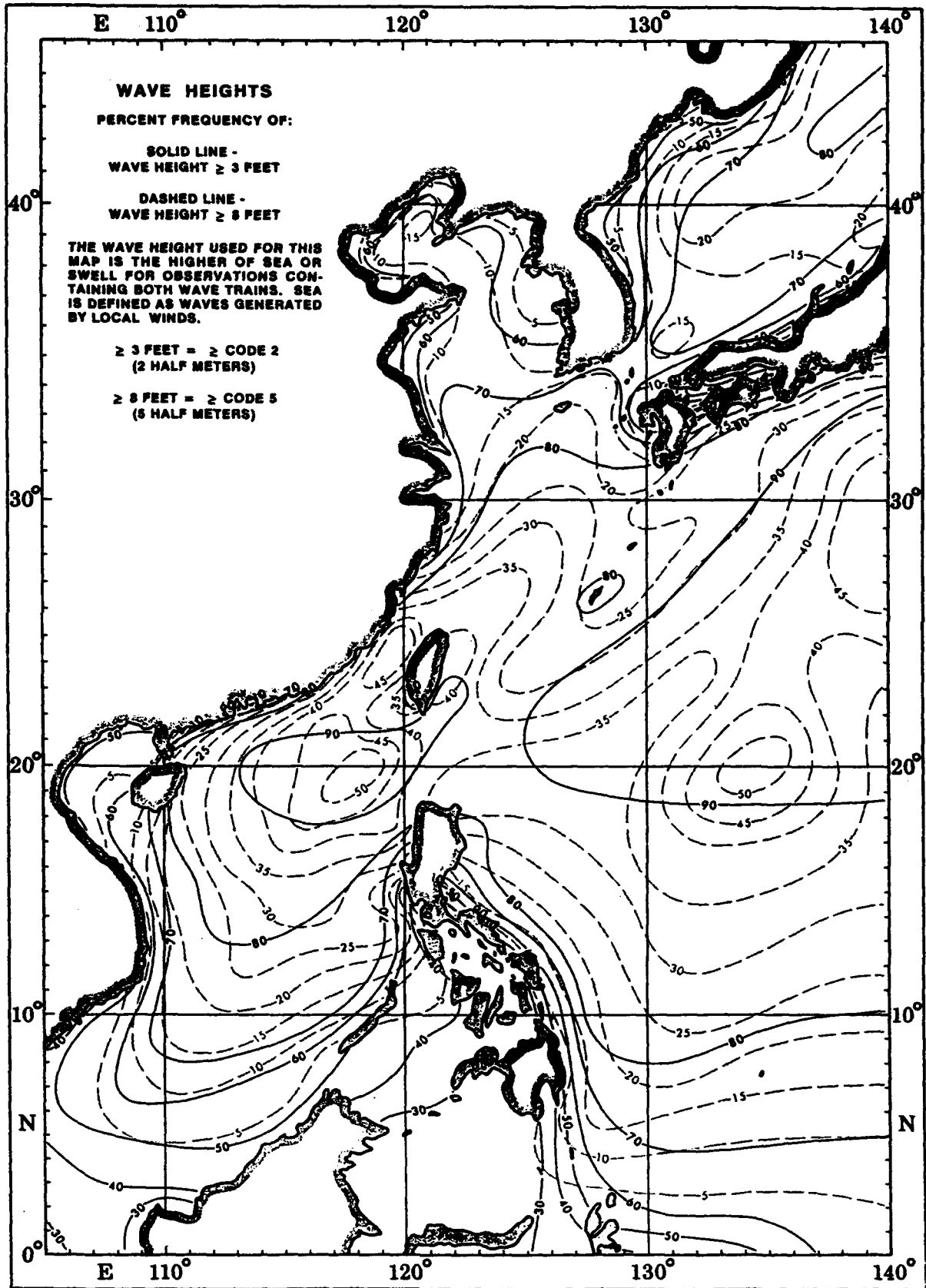
September

Wave Height



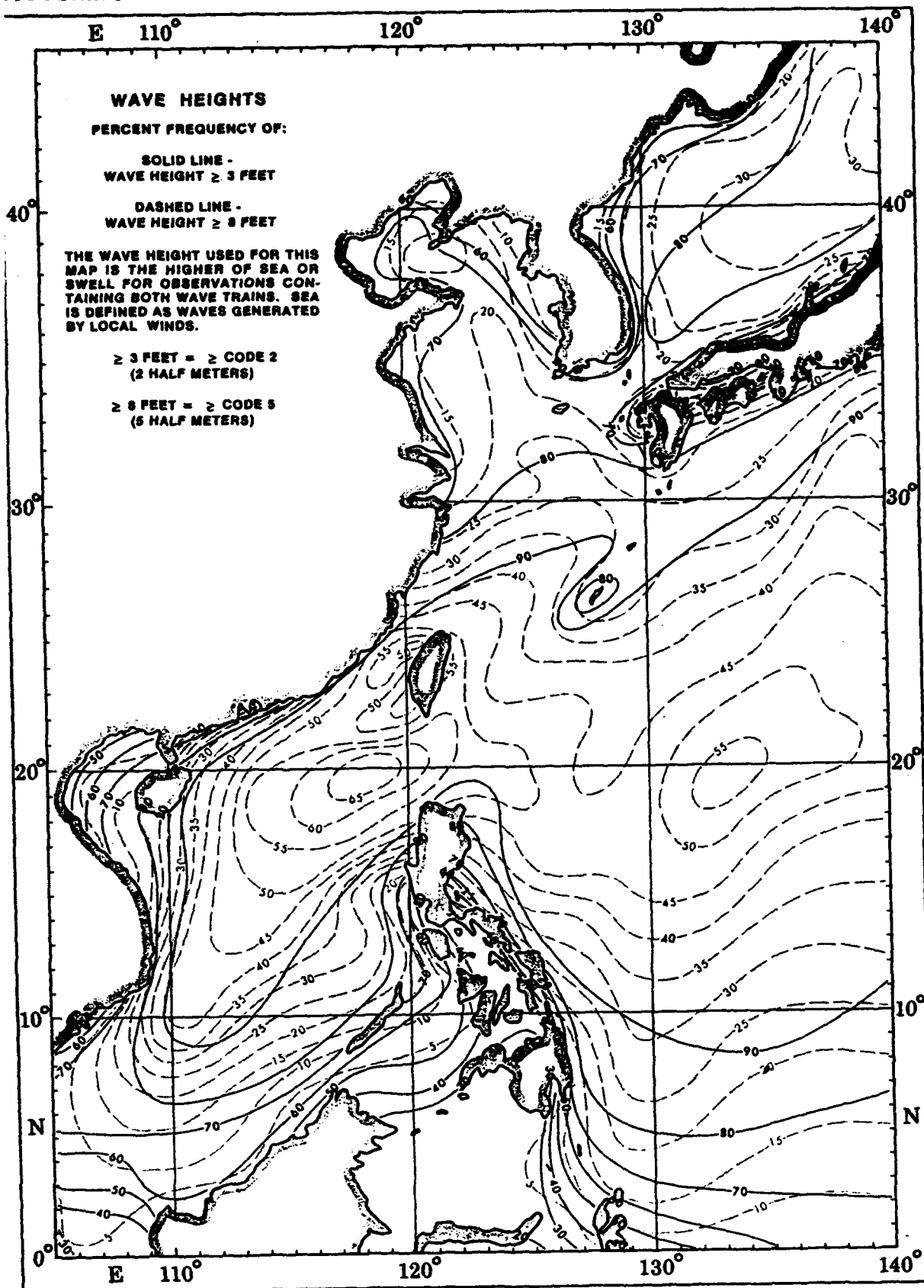
October

Wave Height



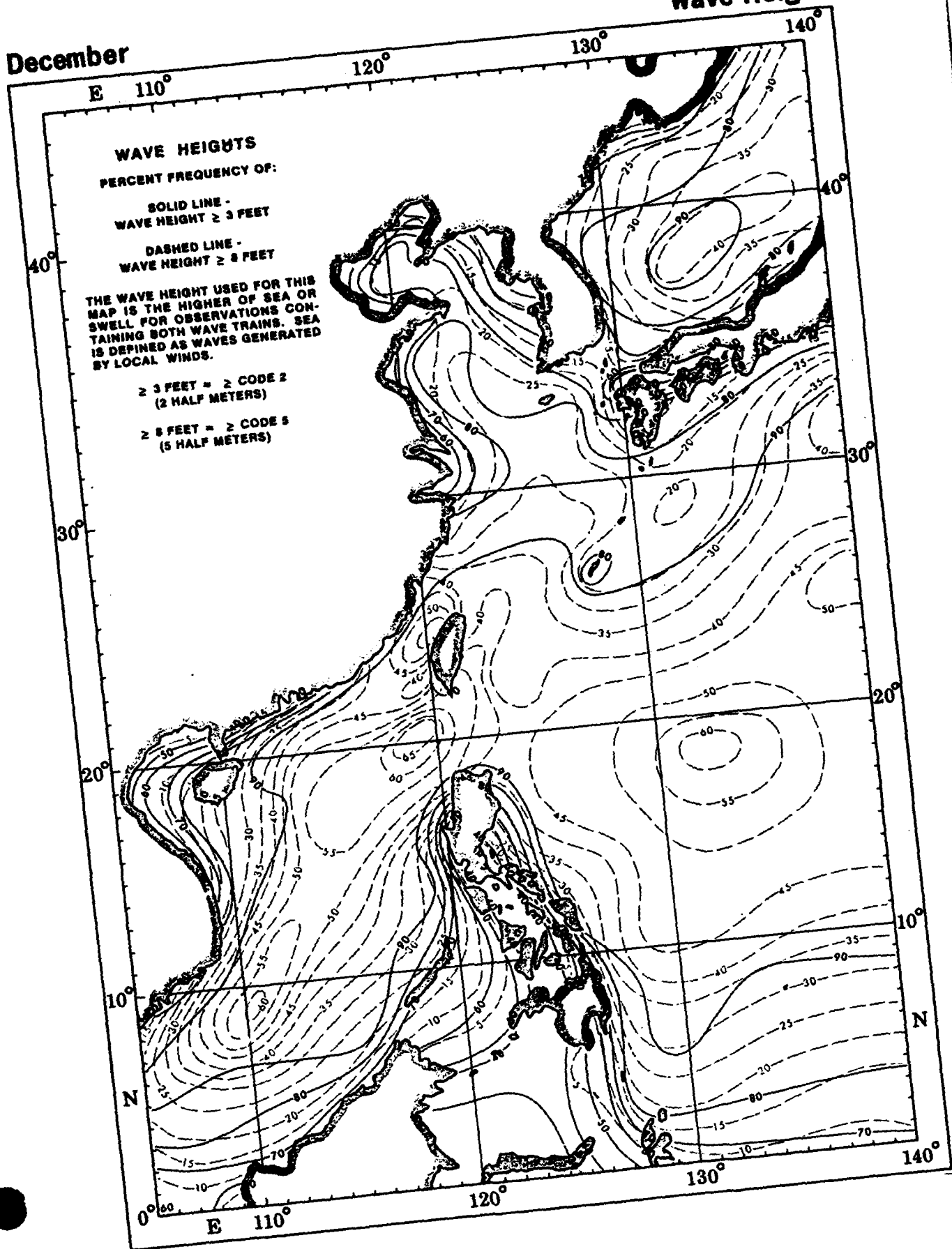
November

Wave Height



December

Wave Height



DISTRIBUTION LIST

CINCPACFLT
ATTN CODE 02M
PEARL HARBOR HI 96860-7000

COMMANDER
ATTN FLT METEOROLOGIST
SEVENTH FLEET
FPO AP 96601-6003

COMMANDER
ATTN FLT METEOROLOGIST
THIRD FLEET
FPO AP 96601-6001

COMMANDER
U S NAVAL FORCES
PSC 473 BOX 12
FPO AP 96349-0051

COMMANDER
US NAVAL FORCES KOREA
UNIT 15250
APO AP 96301-0023

COMMANDER
US NAVFOR MARIANAS
PSC 455 BOX 14
FPO AP 96540-0051

COMNAVAIRPAC
NAS NORTH ISLAND
PO BOX 357051
SAN DIEGO CA 92135-705

COMNAVSURFPAC
2421 VELLA LAVELLA RD
SAN DIEGO CA 92155-5490

COMSUBFORPAC
ATTN CODE N216
PEARL HARBOR HI 96860-6550

COMPHIBGRU ONE
ATTN METEORO OFFICER
UNIT 25093
FPO AP 96601-6006

DEPCOMOPTEVFOR PAC
NAS NORTH ISLAND
PO BOX 357061
SAN DIEGO CA 92135-7061

COMMANDING OFFICER
ATTN METEORO OFFICER
USS A LINCOLN (CVN 72)
FPO AP 96612-2872

COMMANDING OFFICER
ATTN METEORO OFFICER
USS CARL VINSON (CVN 70)
FPO AP 96629-2840

COMMANDING OFFICER
ATTN METEORO OFFICER
USS CONSTELLATION (CV 64)
FPO AP 96635-2780

COMMANDING OFFICER
ATTN METEORO OFFICER
USS INDEPENDENCE (CV 62)
FPO AP 96618-2760

COMMANDING OFFICER
ATTN METEORO OFFICER
USS KITTY HAWK (CV 63)
FPO AP 96634-2770

COMMANDING OFFICER
ATTN METEORO OFFICER
USS NIMITZ (CVN 68)
FPO AP 98780-2820

COMMANDING OFFICER
ATTN METEORO OFFICER
USS BLUE RIDGE (LCC 19)
FPO AP 96628-3300

COMMANDING OFFICER
ATTN METEORO OFFICER
USS BELLEAU WOOD (LHA 3)
FPO AP 96623-1610

COMMANDING OFFICER
ATTN METEORO OFFICER
USS NEW ORLEANS (LPH 11)
FPO AP 96627-1650

COMMANDING OFFICER
ATTN METEORO OFFICER
USS TARAWA (LHA 1)
FPO AP 96622-1600

COMMANDING OFFICER
USS PELELIU (LHA 5)
FPO AP 96624-1620

COMMANDING OFFICER
ATTN METEORO OFFICER
USS TRIPOLI (LPH 10)
FPO AP 96626-1645

COMMANDING OFFICER
ATTN OA DIVISION
USS CORONADO (AGF 11)
FPO AP 96662-3330

1ST MARINE AIRCRAFT WING
UNIT 37101
FPO AP 96603-7101

COMMANDER IN CHIEF
U S PACIFIC COMMAND
BOX 28
CAMP H M SMITH HI 96861-5025

CHIEF OF NAVAL OPERATIONS
ATTN OP 987
WASHINGTON DC 20350-2000

DEFENSE TECH INFO CENTER 2
CODE DTIC-FD DOC PROC DIV
BLDG 5 CAMERON STATION
ALEXANDRIA VA 22304-6145

COMMANDING OFFICER 12
ATTN CODE 5227 DOCS SEC
NAVRSCHLAB
WASHINGTON DC 20375-5000

COMMANDING OFFICER
ATTN CODE 1221 CLASSIF MGT
NAVRSCHLAB
WASHINGTON DC 20375-5000

NAVRSCHLAB
ATTN CODE 70353 LIBRARY
JCSSC MS 39529-5004

OFFICER IN CHARGE
US NAVOCEANCOMDET
PSC 456 BOX 81
FPO AP 96540-1281

OFFICER IN CHARGE
US NAVOCEANCOMDET
FLEET ACTIVITIES
FPO AP 96370-0051

OFFICER IN CHARGE
US NAVOCEANCOMDET
UNIT 5052
APO AP 96319-5000

OFFICER IN CHARGE
NAVOCEANCOMDET
686 CUSHING ROAD
NEWPORT RI 02841-1207

NAVAL OCEANOGRAPHIC OFFICE
ATTN CODE HBAC
1002 BALCH BOULEVARD
JCSSC MS 39529-5001

COMMANDING OFFICER
NAVEASTOCEANCEN
9141 THIRD AVE
NORFOLK VA 23511-2394

COMMANDING OFFICER
NAVWESTOCEANCEN
BOX 113
PEARL HARBOR HI 96860-5050

US NAVAL ACADEMY
ATTN LIBRARY REPORTS
121 BLAKE RD
ANNAPOLIS MD 21405000

US NAVAL ACADEMY
ATTN OCEANOGRAPHY DEPT
121 BLAKE RD
ANNAPOLIS MD 21402-5000

NAVPGSCOL 20
ATTN CODE MR
MONTEREY CA 93943-5000

NAVPGSCOL
ATTN CODE OC
MONTEREY CA 93943-5000

NAVPGSCOL
ATTN CODE MR WF
MONTEREY CA 93943-5000

NAVPGSCOL
ATTN LIBRARY CODE 524
MONTEREY CA 93943-5000

HQ 1ST WEATHER WING DN
HICKAM AFB HI 96853

USAFETAC TS 10
ATTN TECH LIBRARY
SCOTT AFB IL 62225

20 VS DON
APO AP 96328 5000

DET 8 20 VS
APO AP 96239

USAF ETAC
ATTN KENNETH WALTERS
SCOTT AFB IL 92225-5483

COMMANDANT
US COAST GUARD
WASHINGTON DC 20226

NOAA NESDIS LIAISON
ATTN CODE SC2
NASA JOHNSON SPACE CENTER
HOUSTON TX 77058

CHIEF SCIENTIFIC SERVICES
NWS PACIFIC REGION NOAA
PO BOX 50027
HONOLULU HI 96850-4993

DIRECTOR NMC
NWS NOAA
WWB W32 RM 204
WASHINGTON DC 20233

NATIONAL WEATHER SERVICE
WORLD WEATHER BLDG RM 307
5200 AUTH ROAD
CAMP SPRINGS MD 20023

DIRECTOR JTWC 5
BOX 17
FPO AP 96630

COLORADO STATE UNIVERSITY
ATTN DR WILLIAM GRAY
ATMOSPHERIC SCIENCES DEPT
FT COLLINS CO 80523

UNIVERSITY OF HAWAII
ATTN METEOROLOGY DEPT
2525 CORREA ROAD
HONOLULU HI 96822

SCIENCE APPLICATIONS
INTERNATIONAL CORP
205 MONTECITO AVE
MONTEREY CA 93940

MARITIME METEOROLOGY DIV
JAPAN METEOROL AGENCY
OTE MACHI 1 3 4 CHIYODA KU
TOKYO JAPAN

COORDINATOR NATIONAL
ATMOS RESEARCH PROGRAM
INSTITUTE OF PHYSICS
ACADEMIA SINICA
TAIPEI TAIWAN

CENTRAL WX BUREAU
64 KUNG YUAN RD
TAIPEI TAIWAN 100

DIRECTOR PAGASA 5
ASIATRUST BANK BLDG
1424 QUEZON AVE
QUEZON CITY 1104 PHILIPPINES